UNIVERSITY OF SOUTHAMPTON

FACULTY OF NATURAL AND ENVIRONMENTAL SCIENCES

Chemistry

Complexes of Group V and VI metals with soft donor ligands - towards reagents for early metal chalcogenide thin films

by

Yao-Pang Chang

Thesis for the degree of Doctor of Philosophy

October 2017

UNIVERSITY OF SOUTHAMPTON

ABSTRACT

FACULTY OF NATURAL AND ENVIRONMENTAL SCIENCES

Chemistry

Doctor of Philosophy

COMPLEXES OF GROUP V AND VI METALS WITH SOFT DONOR LIGANDS - TOWARDS REAGENTS FOR EARLY METAL CHALCOGENIDE THIN FILMS

Yao-Pang Chang

Preparations of NbX_4 (X = Cl, Br) have been developed in good yield, leading to the formation of a series of 2:1 and 1:1 adducts upon reaction with neutral diphosphine ligands. The 2:1 ligand:metal complexes $[NbX_4(P–P)_2]$ (X = Cl, Br; P–P = $Me_2P(CH_2)_2PMe_2$, $Et_2(CH_2)_2PEt_2$, *o*-$C_6H_4(PMe_2)_2$) were characterised by IR and UV-visible spectroscopies, their purities determined by microanalysis and the solid-state structures confirmed by X-ray crystallography to be that of eight coordinate dodecahedra or square antiprisms. The dimeric 1:1 complexes $[Nb_2X_4(P–P)_2(\mu\text{-}X)_4]$ (P–P = $Me_2P(CH_2)_2PMe_2$, $Et_2P(CH_2)_2PEt_2$, $Ph_2P(CH_2)_3PPh_2$, $Cy_2P(CH_2)_2PCy_2$, *o*-$C_6H_4(PPh_2)_2$) were also characterised by ^1H and $^{31}P\{^1H\}$ NMR spectroscopy.

A series of six-coordinate monomeric complexes, $[NbCl_4(L–L)]$ (L–L = $MeS(CH_2)_2SMe$, $^iPrS(CH_2)_2S^iPr$, $MeS(CH_2)_3SMe$, *o*-$C_6H_4(CH_2SEt)_2$, $MeSe(CH_2)_2SeMe$, $MeSe(CH_2)_3SeMe$ and $^nBuSe(CH_2)_3Se^nBu$) and $[NbCl_4(ER_2)_2]$ (ER_2 = SMe_2, $SeMe_2$, Se^nBu_2 and $TeMe_2$) were prepared from $NbCl_4$ and the ligand in CH_2Cl_2 solution. X-ray structures show that most of them form six-coordinate octahedral complexes, whereas $[NbCl_4(SeMe_2)_2]$ and $[NbCl_4(TeMe_2)_2]$ are thought to be dimeric from X-ray crystallography of the latter. The Nb(IV) complexes were unsuitable as CVD precursors.

Monomeric $[NbSCl_3(L–L)]$ (L–L = $MeS(CH_2)_2SMe$, $^iPrS(CH_2)_2S^iPr$, $MeS(CH_2)_3SMe$, $^nBuS(CH_2)_3S^nBu$ and $MeSe(CH_2)_3SeMe$) and dimeric $[NbSCl_3(SR_2)]$ (R = Me and ^{n}Bu) were prepared from reaction of $[NbSCl_3(NCCH_3)_2]$ with the ligand in CH_2Cl_2 solution or reaction of $[NbCl_5(SR_2)]$ with $S(SiMe_3)_2$ in CH_2Cl_2 solution and characterised by IR, ^1H NMR and ^{93}Nb NMR spectroscopies, X-ray crystallography and microanalysis. Isolated complexes $[NbSe_nCl_3(L)]$ (n = 1, L = CH_3CN; n = 2, L = $^nBu_2Se$) were identified by IR spectroscopy and microanalysis. $[NbSCl_3(S^nBu_2)]$, $[NbSCl_3(^nBuS(CH_2)_3S^nBu)]$ and $[NbSe_2Cl_3(Se^nBu_2)]$ were used as single source precursors in LPCVD. The resulting NbS_2 and $NbSe_2$ thin films were characterised *via* X-ray diffraction, SEM and EDX spectroscopy.

Isolated complexes of the form, $[MBr_5(E^nBu_2)]$ (M = Nb, Ta; E = S, Se), were identified *via* IR and multinuclear NMR spectroscopies and the Nb complexes were used as single source precursors in LPCVD to deposit NbS_2 and $NbSe_2$ thin films. The growth of 2H-/3R-$NbSe_2$ thin films was controlled by varying the temperature used in LPCVD. All NbS_2 and 2H-/3R-$NbSe_2$ thin films were characterised using X-ray diffraction, SEM and EDX spectroscopies.

A series of new $MoCl_4$ complexes, $[MoCl_4(ER_2)_2]$ (ER_2 = Me_2S, Me_2Se, $^nBu_2S$, $^nBu_2Se$) and $[MoCl_4(L–L)]$ (L–L = $MeS(CH_2)_2SMe$, $^iPrS(CH_2)_2S^iPr$, $MeS(CH_2)_3SMe$, and $MeSe(CH_2)_3SeMe$), were made using $MoCl_5$ or $[MoCl_4(NCCH_3)_2]$ as the Mo source and characterised using IR and UV-visible spectroscopies, X-ray crystallography and microanalysis. Single source LPCVD precursors, $[MoCl_4(S^nBu_2)_2]$ and $[MoCl_4(Se^nBu_2)_2]$, deposited MoS_2 or $MoSe_2$ thin films which were characterised *via* X-ray diffraction, SEM and EDX spectroscopy.

Table of Contents

List of Tables

List of Figures

DECLARATION OF AUTHORSHIP

I, Yao-Pang Chang, declare that this thesis and the work presented in it are my own and has been generated by me as the result of my own original research.

Group V and VI complexes with soft neutral donor ligands and applications single source precursors for low-pressure chemical vapour deposition of metal chalcogenide thin films

I confirm that:

1. This work was done wholly or mainly while in candidature for a research degree at this University;
2. Where any part of this thesis has previously been submitted for a degree or any other qualification at this University or any other institution, this has been clearly stated;
3. Where I have consulted the published work of others, this is always clearly attributed;
4. Where I have quoted from the work of others, the source is always given. With the exception of such quotations, this thesis is entirely my own work;
5. I have acknowledged all main sources of help;
6. Where the thesis is based on work done by myself jointly with others, I have made clear exactly what was done by others and what I have contributed myself;
7. Parts of this work have been published as:

'Chalcogenoether complexes of Nb(V) thio- and seleno-halides as single source precursors for low pressure chemical vapour deposition of NbS_2 and $NbSe_2$ thin films' Y.-P. Chang, A. L. Hector, W. Levason and G. Reid, *Dalton Trans.*, 2017, **46**, 9824.

'Developments in the chemistry of the hard early metals (Groups 1-6) with thioether, selenoether and telluroether ligands' Y.-P. Chang, W. Levason and G. Reid, *Dalton Trans.*, 2016, **45**, 18393.

'Niobium tetrachloride complexes with thio-, seleno- and telluro-ether coordination - synthesis and structures' Y.-P. Chang, W. Levason, M. E. Light and G. Reid, *Dalton Trans.*, 2016, **45**, 16262.

'**Niobium tetrahalide complexes with neutral diphosphine ligands'** S. L. Benjamin, Y.-P. Chang, A. L. Hector, M. Jura, W. Levason, G. Reid and G. Stenning, *Dalton Trans.*, 2016, **45**, 8192.

Signed: .....

Date:.....

Acknowledgements

I would like to thank Prof. Gillian Reid and Em. Prof. William Levason for their supervision and support over my 3 years PhD research (in addition to my M.Sc year) and for imparting their scientific knowledge, especially their expertise in Group V, VI, XV and XVI chemistry. I would like to thank Em. Prof. William Levason for collecting all of the multinuclear and low temperature NMR spectra for this work. I would like to thank Prof. Andrew L. Hector for his support and knowledge of materials chemistry, including phase matching suggestions and lattice parameter refinements. I would like to thank Dr. Mark Light for single crystal X-ray data solution and refinement on two tricky structures and for maintaining all of X-ray diffractometer. I would like to thank Dr. Wenjian Zhang for his suggestions for X-ray single crystal structure data solution and refinements. I would also like to thank Josh Whittam for collecting Raman data. I would like to thank Dr. Stephen P. Richards and Dr. Victoria K. Greenacre for proof reading. I would like to thank all of the members in Levason/Reid, Hyett and Hector groups, past and present, for their help in the laboratory. I would also like to thank the University of Southampton for awarding me Vice-Chancellor's Scholarship during my PhD. Finally, I would like to thank my family for all their support.

Definitions and Abbreviations

δ	Chemical shift (ppm)
ν	Wavelength (cm^{-1})
Å	10^{-10} m (Å ngström)
exo-	Outer
endo-	Inner
fac-	Facial
mer-	Meridional
κ	Denticity
μ_{eff}	Magnetic moment value
[9]aneS_3	1,4,7-trithiacyclononane
[9]aneN_2S	1,4-Diaza-7-thiacyclononane
[9]aneOS_2	1-oxa-4,7-dithianonane
[10]aneS_3	1,4,7-Trithiacyclodecane
[12]aneS_4	1,4,7,10-Tetrathiacyclododecane
[15]aneO_3S_2	1,4,10-Trioxa-10,13-dithiacyclopentadecane
[15]aneS_5	1,4,7,10,13-Pentathiacyclopentadecane
[18]aneO_4S_2	1,4,10,13-Tetraoxa-7,16-dithiacyclooctadecane
[18]aneO_4Se_2	1,4,10,13-Tetraoxa-7,16-diselenocyclooctadecane
[18]aneO_4Te_2	1,4,10,13-Tetraoxa-7,16-ditellurocyclooctadecane
[18]aneS_6	1,4,7,10,13,16-Hexathiacyclooctadecane
AACVD	Aerosol-Assisted Chemical Vapour Deposition
ALD	Atomic Layer Deposition
APCVD	Atmospheric Pressure Chemical Vapour Deposition
Ar	Aryl group
^{n}Bu	*n*-butyl
COD	Cycloocta-1,5-diene
CVD	Chemical Vapour Deposition
CVT	Chemical Vapour Transport

Cy	Cyclohexyl
EDX	Energy-Dispersive X-ray Spectroscopy
EXAFS	Extended X-ray Absorption Fine Structure
ER_2	Chalcogenoether (E = S, Se, Te)
Et	Ethyl
FET	Field-Effect Transistors
FWHM	Full width at half maximum
GIXRD	Grazing Incidence X-ray Diffraction
HSAB	Hard and Soft Lewis Acid and Base
IPXRD	In-Plane X-ray Diffraction
IR	Infrared
L–L	Bidentate ligand
LPCVD	Low Pressure Chemical Vapour Deposition
Me	Methyl
mmHg	Millimetres of mercury
NMR	Nuclear Magnetic Resonance
o-C_6H_4	*Ortho*-phenyl
P–P	Generic diphosphine ligand
PACVD	Photo-Assisted Chemical Vapour Deposition
PECVD	Plasma Enhanced Chemical Vapour Deposition
Ph	Phenyl
^{i}Pr	Isopropyl
PVD	Physical vapour deposition
ppm	Parts Per Million
PXRD	Powder X-ray Diffraction
Q	Quadropolar
R	Alkyl groups
SEM	Scanning Electronic Microscopy
TACVD	Thermally Activated Chemical Vapour Deposition
TGA	Thermogravimetric Analysis

THF	Tetrahydrofuran
THT	Tetrahydrothiophene
TMD	Transition Metal Dichalcogenide
ttob	2,5,8-Trithia[9]-o-benzophane
UHVCVD	Ultra-High Vacuum Chemical Vapour Deposition
UV-vis	UV-visible
XRD	X-ray diffraction

Chapter 1: Introduction and background

1.1 The behaviour of neutral chalcogenoether ligands

1.1.1 General neutral chalcogenoether chemistry

The coordination chemistry of chalcogenoethers (thio-, seleno- and telluroethers) to transition metals has been the focus of considerable attention during the last twenty years, although transition metal complexes with neutral chalcogenoethers remain relatively rare.[1, 2] While steric effects are considered important for group 15 ligands such as phosphines, this is not the case for group 16 ligands as they only have two substituents. The neutral chalcogenoether (ER_2) has two lone pairs on the chalcogen atom, with one typically forming a bond to a σ-acceptor (metal centre). In some cases, the second lone pair can form a σ-bond to a second metal centre to result in a bridging ER_2 group, *i.e.* $[Nb_2Cl_4(S^nBu_2)_2(\mu\text{-}Cl)_2(\mu\text{-}S^nBu_2)]$ (Figure 1.1).[3] The second lone pair may also form a π-bond onto the metal acceptor, however, usually the second lone pair remains non-bonding and is a source of π-repulsion in $M–ER_2$.[1]

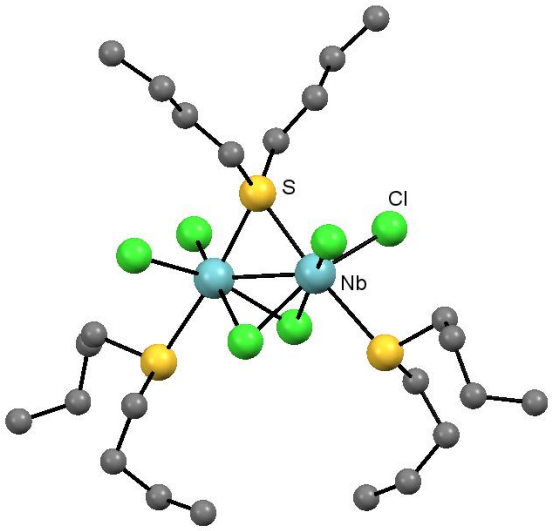

Figure 1.1 An example of the bridging binding mode of thioether, $[Nb_2Cl_4(S^nBu_2)_2(\mu\text{-}Cl)_2(\mu\text{-}S^nBu_2)]$.[3]

Chalcogenoethers can also carry the two different R groups. The coordination of one lone pair to an acceptor leads to chirality. Monodentate chalcogenoethers used in this project have the same R groups to prevent forming a chiral centre on the chalcogen atoms (S, Se or Te). However, dichalcogenoethers, such as $MeS(CH_2)_2SMe$ and $o\text{-}C_6H_4(CH_2SEt_2)_2$, inherently have two different alkyl groups on the chalcogen atoms and are therefore likely to give rise to a *meso* form and a pair of enantiomeric *DL* isomers (Figure 1.2), because there are two lone pairs to coordinate to accepters. The interconversion of diastereoisomers often occurs on the NMR time-scale by pyramidal inversion,

leading to a slight difference in the chemical shifts observed.[1, 3-7] Bidentate chalcogenoethers tend to be chelating ligands in most examples, although sometimes they act as a bridged ligand, such as in $[\{Nb_2Cl_4(\mu\text{-}Cl)_2(\mu\text{-}SMe_2)\}_2(\mu\text{-}MeSe(CH_2)_3SeMe)_2]$ (Figure 1.3).[3]

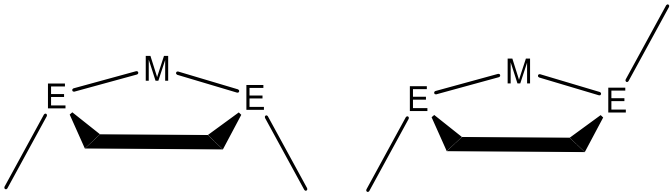

Figure 1.2 *meso* (left) and *DL* (right) isomzers.

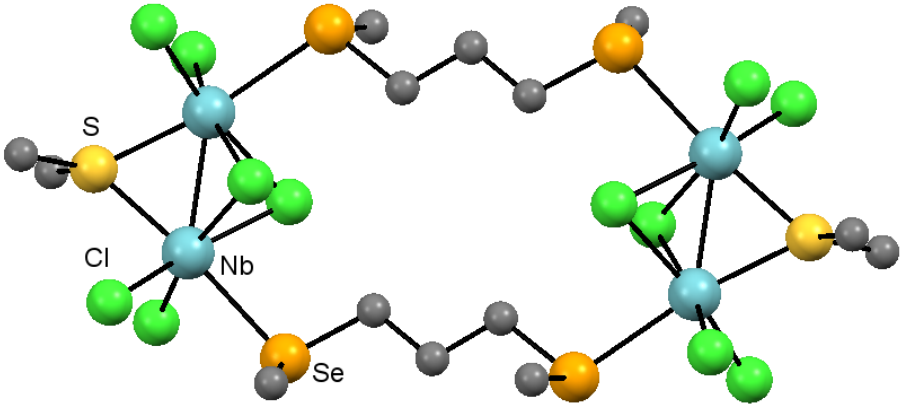

Figure 1.3 An example of bridging thioether, $[\{Nb_2Cl_4(\mu\text{-}Cl)_2(\mu\text{-}SMe_2)\}_2(\mu\text{-}MeSe(CH_2)_3SeMe)_2]$.[3]

Macrocyclic chalcogenoethers are able to coordinate toward a metal centre in different ways; [9]andS_3, for example, is reported to be a monodentate ligand, ($[AuCl([9]aneS_3)]$),[8] a bidentate ligand, ($[Mo(CO)_2(Cp)([9]aneS_3)]^+$),[9] or a facially coordinating ligand, ($[Mo(CO)_3([9]aneS_3)]$)[10] (Figure 1.4). The *tetra*- and *penta*-thia macrocycles could also coordinate metal ion either *exo* ($[SnBr_4([12]aneS_4)]$)[11] or *endo* ($[Pt([12]aneS_4)]^{2+}$)[12] fashion (Figure 1.5).[13, 14]

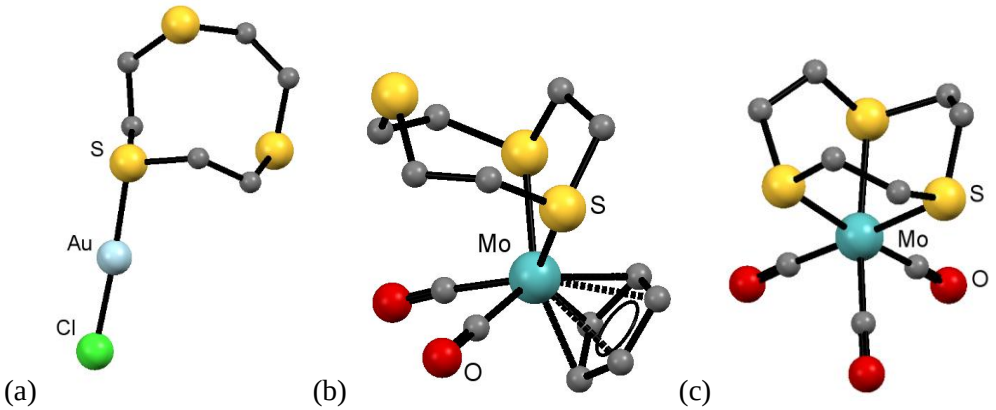

(a) (b) (c)

Figure 1.4 Examples of using *tri*-thia macrocycles coordinated to metal ions. (a) $[AuCl([9]aneS_3)]$;[8] (b) $[Mo(CO)_2(Cp)([9]aneS_3)]^+$;[9] (c) $([Mo(CO)_3([9]aneS_3)])$.[10]

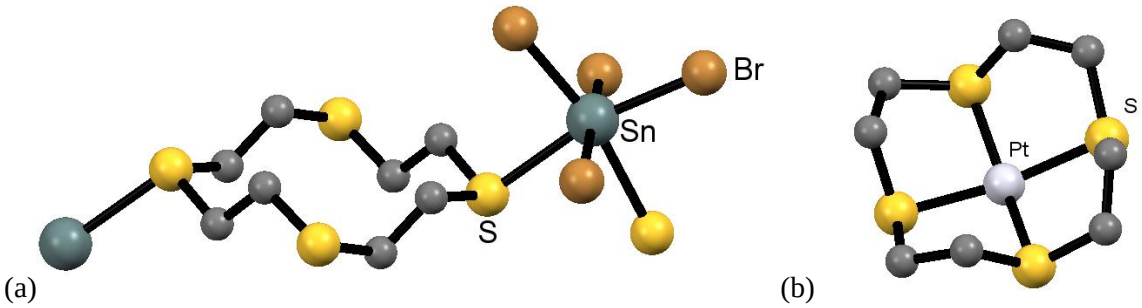

Figure 1.5 Examples of *tetra*-thia macrocycles coordinated to metal ions. (a) $[SnBr_4([12]aneS_4)]$[11] and (b) $[Pt([12]aneS_4)]^{2+}$.[12]

In this research project, monodentate chalcogenoethers, ER_2 (E = S, Se or Te; R_2 = Me_2 or $^nBu_2$) were used to avoid forming enantiomers. Chalcogenoethers with a methyl group were chosen to form the simplest molecular species in each case and to encourage crystal growth, whereas ligands with *n*-butyl groups were selected for LPCVD to enable β-hydride elimination, in order to provide a low energy decomposition pathway.[15] Dichalcogenoethers, $RE(CH_2)_2ER$ (E = S, Se; R = Me or ^iPr), $RE(CH_2)_3ER$ (E = S, Se; R = Me or ^nBu or E = Te; R = ^tBu) and *o*-$C_6H_4(CH_2SEt_2)_2$, were used to attempt to form chelating ligand complexes. Increasing the size of the linking groups to form five-, six- or seven-ring chelates provide good comparisons, and complexes with bidentate ligands, such as $[TiCl_4\{o\text{-}C_6H_4(CH_2EMe)_2\}]$ (E =S, Se)[16] and $[SnCl_4\{^nBuSe(CH_2)_nSe^nBu\}]$ (n = 2 or 3),[15] were prepared as potential suitable single source LPCVD precursors. $RTe(CH_2)_2TeR$ are unknown due to their tendency to eliminate the backbone, leading to the formation Te_2R_2 and ethylene (detail in next section). Polychalcogenoethers (containing three or more chalcogen atoms in the ligand) or cyclic-chalcogenoethers are not used in this project because the resulting complexes would be expected to be involatile and contain the wrong M:E ratio to deposit ME_2 thin films using LPCVD.

1.1.2 Synthesis of chalcogenoethers

Although some of the more frequently used thio- and selenoethers are now commercially available (SMe_2, SEt_2, S^nPr_2, S^nBu_2, [9]aneS$_3$, $SeMe_2$, $SeEt_2$, $SePh_2$ *etc*.), dichalcogenoethers are typically made in the laboratory when required. Since macrocyclic chalcogenoethers ligands were not used in this project, although their preparation has been developed over many years,[14, 17] and will not be included in this section. This section will include the common preparation routes of acyclic-chalcogenoethers, and the most relevant syntheses in this project will be explored in further detail.

1.1.2.1 Thioether preparation

The bi- and poly-dentates with aliphatic backbones are usually prepared using RSNa with an appropriate haloalkane (Scheme 1.1), to form $RS(CH_2)_nSR$,[18] $MeC(CH_2SR)_3$,[19, 20] $RS(CH_2)_nS(CH_2)_nSR$ and $RS(CH_2)_nS(CH_2)_nS(CH_2)_nSR$ (n = 2 or 3).[20, 21] The new ligand, $^nBuS(CH_2)_3S^nBu$, was prepared from a modified literature method,[18] detailed in Appendix 1.

o-$C_6H_4(SR)_2$ can be obtained by several methods, for example, CuSPh reacts with *o*-$C_6H_4Br_2$ to form *o*-$C_6H_4(SPh)_2$.[18] However, the reaction by *o*-$C_6H_4(SMe)(SH)$ with MeI in Na/EtOH can avoid the copper reagents.[18] *o*-$C_6H_4(CH_2SR')_2$ (R' = Me, Et) are also made by the nucleophilic attack of $R'S^-$ on *o*-$C_6H_4(CH_2Br)_2$, in this case, $S_2R'_2$ was added slowly into sodium/liquid-ammonia with stirring at -78 ℃. Ammonia was removed and the remaining white solid was reacted with *o*-$C_6H_4(CH_2Br)_2$ in boiling EtOH (Scheme 1.1).[22]

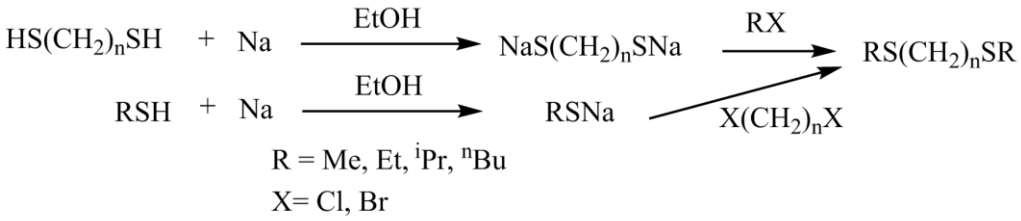

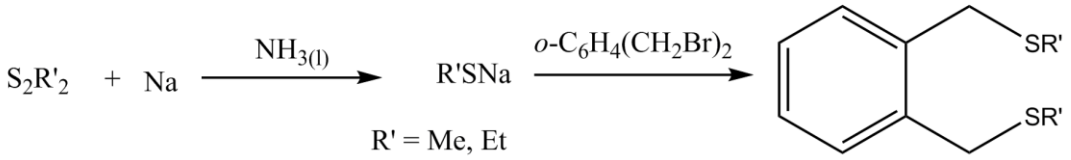

Scheme 1.1 Synthesis of thioethers used in this project.[18, 22]

1.1.2.2 Selenoether and telluroether preparation

Seleno- and telluroethers are made from elemental Se or Te powder frozen in tetrahydrofuran (THF) under a nitrogen atmosphere, before the addition of an ethereal solution of alkyl lithium. The solution is allowed to warm to ambient temperature as RLi (R = Me, ^{n}Bu) reacts with E powder to form RSeLi or RTeLi. Finally, RX is added to produce SeR_2 or TeR_2 (Scheme 1.2).[22-27] Both selenoethers (SeR_2) and telluroethers (TeR_2) are malodorous yellow/orange oils. The former are air/moisture stable but the latter are air/light sensitive.[1, 28]

The synthesis of diselenoethers tend to start from elemental Se, converting to RSeLi before adding dihalide alkanes. The bidentate ligands, $MeSe(CH_2)_2SeMe$, $MeSe(CH_2)_3SeMe$ and ^{n}BuSe$(CH_2)_3$Se^{n}Bu are prepared using this method (Scheme 1.2).[22-27] Tripodal $MeC(CH_2SeR)_3$ are prepared in a similar fashion, from RSeLi with $MeC(CH_2Br)_3$ in THF.[23] *Tri*- or *tetra*-selenoethers such as $MeSe(CH_2)_nSe(CH_2)_nSeMe$ (n = 2, 3) use similar methods from MeSeLi, but with $X(CH_2)_nOH$ to form $MeSe(CH_2)_nOH$. Then, the alcohol group is converted to $MeSe(CH_2)_nOTs$ by using *p*-$MeC_6H_4SO_2Cl$ before reacting this with Na_2Se to form $MeSe(CH_2)_nSe(CH_2)_nSeMe$ (n = 2, 3).[23, 29]

The preparation of di- and polytelluroethers are not as simple as diselenoethers because the instability of the Te–C bond usually leads to Te–C fission during the ligands synthesis.[1, 24] Ditelluroether ligands, $RTe(CH_2)_nTeR$, are much more difficult to prepare than corresponding diselenoethers,

although they use a similar method, and only ditelluroethers with certain number of n are known (n = 1, 3).[24] The successful synthesises of $RTeCH_2TeR$ include reaction of Te_2R_2 with diazomethane,[30] or using RTe^- with CH_2X_2 (R = Me, Ph; X = Cl, Br).[24, 31] The synthesis of $RTe(CH_2)_3TeR$ at controlled temperatures using $X(CH_2)_3X$ and RTeLi lead to different products.[28] Preparation in ambient temperature gives Te_2R_2 and olefin, however, using low temperature (-50 °C) results high yields of $RTe(CH_2)_3TeR$ (R = Me, ^{t}Bu, ^{n}Bu) (Scheme 1.2).[28] *o*-$C_6H_4(TeR)_2$ are made using Te_2R_2 with benzyne or RTeLi with *o*-$C_6H_4Br_2$.[27, 32]

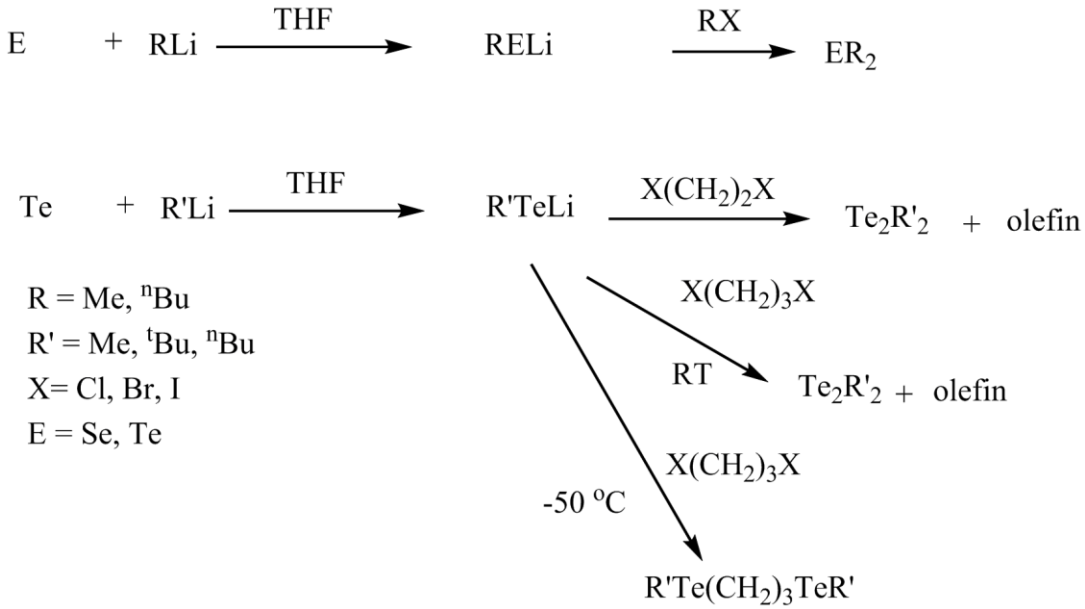

Scheme 1.2 Synthesis of seleno- and telluroethers used in this project.[22-26, 28]

1.1.3 Transition metal complexes with chalcogenoether ligands

Early transition metal halide complexes with neutral thio- and selenoether ligands are relatively uncommon.[2] Traditional inorganic chemistry, Hard and Soft Lewis Acid and Base theory (HSAB), predicts hard metals (high valent) preferentially bind to hard ligands (*e.g.* halide ions, water and oxide), while soft metals (in lower oxidation states) tend to form more stable complexes with soft ligands (including chalcogenoethers, phosphines, *etc.*).[33] Therefore, transition metal halides in their middle or high oxidation state are less likely to coordinate well with neutral soft donors such as SR_2, SeR_2 or TeR_2.

However, when considering the coordination chemistry from a donor/acceptor viewpoint, d-block metal halides are good accepters, whereas neutral donor ligands such as chalcogenoethers are ideal σ-donors. This would mean transition metal halide complexes with soft neutral donors are accessible. As described earlier, neutral soft donors, such as chalcogenoethers, have the ability to be σ/π-donors when coordinating toward electron-poor metals.[33]

When chalcogenoethers coordinate to a transition metal, they are considered to form a coordination bond. When the transition metal is in its higher or highest oxidation states, the d-orbitals are very contracted, making it a 'hard metal', which increases the difficulty to overlap with the σ-donor (p-orbital) on the E (E = S, Se, Te) in chalcogenoether. Whereas when the transition metal is in medium oxidation states, its d-orbitals are more extended than those in higher oxidation states, which increases the overlap with the p-orbital from the E in ER_2 ligands.

For low oxidation state metals, studies of the NMR chemical shifts (^{55}Mn, ^{77}Se and ^{125}Te) of coordinated chalcogenoethers show the stability of the M–E bond follows the order Te >> Se > S.[34, 35] The same order was found for the stability for Fe–E bonds from $[Fe(CO)_2(Cp)L]$ complexes where L = group 15 or 16 donor ligands.[36] A density functional theory study was undertaken by Ziegler and co-workers to examine the π-acceptor ability from a series of $[Cr(CO)_5L]$ species where L included chalcogenoethers. Thio- and selenoether were found to be moderate σ-donors and weak π-acceptors based on the energies from calculated molecular orbital models.[37] Interestingly, studying ^{77}Se and ^{125}Te NMR chemical shifts on M^I and M^{III} complexes shows that telluroethers are stronger donors than selenoethers when forming M^I compounds $[M(COD)\{MeC(CH_2EMe)_3\}]^+$ (M = Rh or Ir; E = Se or Te; COD = cycloocta-1,5-diene), however, the ligand donation ability switches to Se > Te when the metal centres are M^{III} such as $[M(Cp)\{MeC(CH_2EMe)_3\}]^{2+}$.[38] Therefore, the relative donor strength varies with the metal acceptor to become S < Se > Te when the metal is in its medium or high oxidation state, and S < Se < Te while the metal is in its low oxidation state.

1.2 Literature survey of chalcogenoethers with metal Group III to VI metal ions

Although there are a significant number of reported complexes containing transition metals in their medium or high oxidation state with neutral chalcogenoether ligands, these compounds are still relatively unusual. This section will discuss Group III to VI metals in their high oxidation states using acyclic or cyclic chalcogenoether ligands.

1.2.1 Group III (Sc, Y)

There are no Group III metal complexes with simple mono- or bidentate chalcogenoethers. $[Sc(CH_2SiMe_3)_3([9]aneS_3)]$ with a thio-macrocyclic ligand was made using $[9]aneS_3$ and $[Sc(CH_2SiMe_3)_3(THF)_2]$ in toluene and forms a *fac*-octahedral structure (Figure 1.6).[39, 40] Using similar conditions, the yttrium analogue has been prepared in solution, but was not isolated.[39, 40]

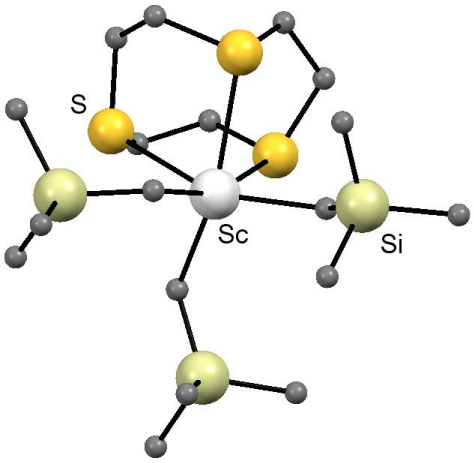

Figure 1.6 The structure of $[Sc(CH_2SiMe_3)_3([9]aneS_3)]$.[40]

The five-coordinate complex, $[Sc(CH_2SiMe_3)_2([9]aneS_3)]^+$ was prepared by treating $[Sc(CH_2SiMe_3)_3([9]aneS_3)]$ with $[CPh_3][B(C_6H_5)_4]$ in CH_2Cl_2 solution, which also forms a byproduct, $[Sc(CH_2SiMe_3)_2([9]aneS_3)(THF)]^+$; $[Sc(CH_2SiMe_3)_2([9]aneS_3)]^+$ is also an active ethlyene and α-olefin polymerisation catalyst.[39, 40] The yttrium cation was not isolated, but its seven-coordinate cation, $[Y(CH_2SiMe_3)_2([9]aneS_3)(THF)_2]^+$, was detected from solution NMR measurements.[39, 40]

Scandium halides with heterocrown complexes were made either by reaction of $[ScCl_3(THF)_3]$ with $[15]aneO_3S_2$, $[18]aneO_4S_2$ or $[18]aneO_4Se_2$ in dry CH_3CN solution with one equivalent of $FeCl_3$ as a chloride abstractor to form $[ScCl_2(heterocrown)][FeCl_4]$ or by reaction of ScI_3 with corresponding heterocrown ligands in anhydrous CH_3CN to afford $[ScI_2(heterocrown)]I$.[41, 42] Resulting crystal structures show both complexes are eight-coordinate and the two halides in $[ScX_2([18]aneO_4S_2)]^+$

are in mutually *cis* positions (Figure 1.7 a).[42] The multinuclear (^{1}H, ^{13}C, ^{45}Sc and ^{77}Se) NMR spectra of the [18]aneO_4Se_2 complexes in CD_3CN/CH_3CN solution suggest the soft iodides are displaced by the acetonitrile solvent.[42] The attempted reaction of $[ScCl_3(THF)_3]$, $FeCl_3$ and [18]aneO_4Te_2 were carried on a CH_3CN solution and gave a brown solid, believed to be $[ScCl_2([18]aneO_4Te_2)][FeCl_4]$ based on NMR spectroscopic evidence on its fresh solution sample, however the complex rapidly decomposes and deposits black elemental Te.[42]

The yttrium halides with heterocrowns were made using similar methods to the scandium analogues mentioned above and characterised with crystal structure evidence and multinuclear NMR analysis.[42] $[YCl_2(heterocrown)][FeCl_4]$ was made from $[YCl_2(THF)_5][YCl_4(THF)_2]$, $FeCl_3$ and heterocrown in CH_3CN solution.[42] The crystal structure of $[YCl_2([18]aneO_4S_2)]^+$ shows an eight-coordinate metal centre with two *cis* disposed chlorides, the same as its Sc analogue (Figure 1.7 b).[42]

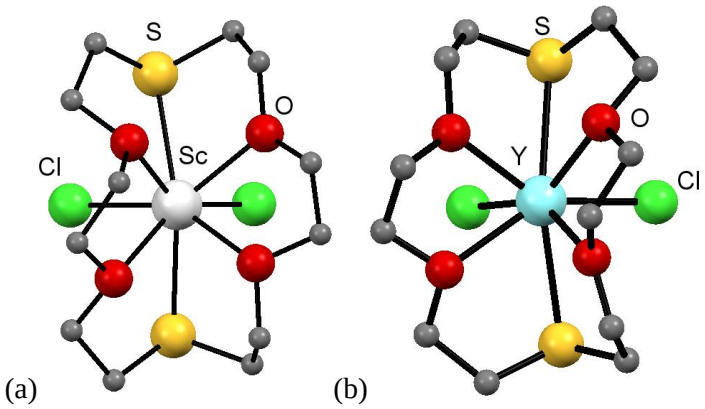

Figure 1.7 The structure of (a) $[ScCl_2([18]aneO_4S_2)]^+$ and (b) $[YCl_2([18]aneO_4S_2)]^+$.[42]

1.2.2 Group IV

1.2.2.1 Titanium

Complexes of tetravalent Group IV metal (titanium, zirconium and hafnium) halides with thio- and selenoether have been known for many years.[7, 43] There are no examples of the equivalent telluroether complexes.

Complexes of the form *cis*-$[TiX_4(ER_2)_2]$ (X = Cl, Br; ER_2 = SMe_2, SEt_2, $SeMe_2$, THT *etc.*) were made from $TiCl_4$ with the corresponding ligands in *n*-hexane, resulting in very moisture sensitive yellow or orange products.[15, 44-46] The preference for *cis* over *trans* isomers in these complexes are due to the more favourable X(π)–Ti(d) bonding in the former, as shown by electronic spectral studies of the complexes.[44-46] Those complexes were studied for potential single source precursors for LPCVD. Complexes $[TiCl_4(SR_2)_2]$ (R_2 = Me_2, $(CH_2)_4$, $(CH_2)_5$) were used as single source precursors in LPCVD, however, only $[TiCl_4(SMe_2)_2]$ deposited TiS_2 thin films at temperature 400–600 °C.[44] The *cis*-$[TiCl_4(SeR_2)_2]$ (R = Et or ^{n}Bu) were prepared from the reaction of $TiCl_4$ and SeR_2 in *n*-

hexane, followed by vacuum sublimation, before it was used to deposit $TeSe_2$ using LPCVD at 500–600 ℃ (Figure 1.8 a).[15]

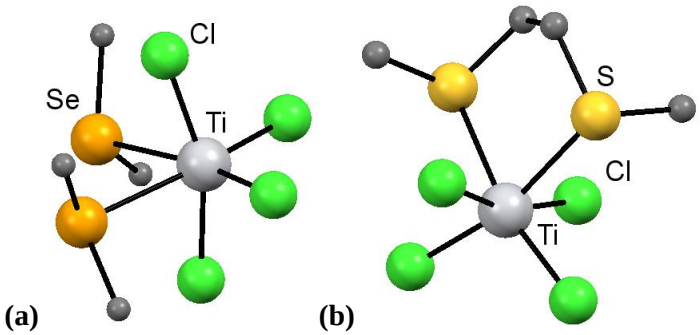

Figure 1.8 The structure of (a) *cis*-$[TiCl_4(SeMe_2)_2]$[15] and (b) $[TiCl_4\{MeS(CH_2)_2SMe\}]$.[47]

A series of $[TiX_4(L–L)]$ complexes (E = S, Se; X = Cl, Br; L–L = $MeE(CH_2)_nEMe$; n = 2, 3; $PhE(CH_2)_2EPh$; *o*-$C_6H_4(EMe)_2$; *o*-$C_6H_4(CH_2EMe_2)_2$) were made from a similar method using $TiCl_4$ and corresponding dichalcogenoethers in hexane (Figure 1.8 b).[16, 47] They were identified by IR, UV-visible, multinuclear (^1H, ^{13}C, ^{77}Se) NMR spectroscopies and X-ray crystallography.[16, 47] Interestingly, these Ti(IV) complexes are unable to form eight-coordinate compounds, which is different to those with diphosphine ligands.[48] The variable temperature solution NMR data show $TiCl_4$ complexes undergo some ligand dissociation in low temperatures, whereas $TiBr_4$ analogues are mostly dissociated, suggesting that Lewis acid strength in these system is $TiCl_4$ > $TiBr_4$.[16, 47] $[TiCl_4\{o\text{-}C_6H_4(CH_2EMe)_2\}]$ were used as single source precursor in LPCVD at *ca.* 500 ℃ and deposited TiE_2 thin film successfully.[16]

The TiI_4 analogues, $[TiI_4\{MeSe(CH_2)_2SeMe\}]$ and $[TiI_4\{o\text{-}C_6H_4(SeMe)_2\}]$ were successfully characterised *via* IR, UV-visible and NMR spectra.[47] Tripodal $MeC(CH_2EMe)_3$ (E = S, Se) reacted with $TiCl_4$ or $TiBr_4$ to give $[TiX_4\{\kappa^2\text{-}MeC(CH_2EMe)_3\}]$ identified from NMR analysis.[49] Trithia macrocycles, [9]aneS_3 and [10]aneS_3, formed 1:1 complexes with TiX_4, and unfortunately solution NMR spectroscopic and single crystal X-ray diffraction data were not provided due to the insolubility of the complexes.[49, 50] Hydrolysis usually completely decomposes these compounds, but a trace of water can slowly generate bridging-oxide species, such as $[Cl_3(Me_2S)_2Ti(\mu\text{-}O)Ti(SMe_2)_2Cl_3]$ (Figure 1.9),[51] similar hydrolysis of $[TiCl_4\{MeS(CH_2)_2SMe\}]$ also forms $[Ti_2Cl_6(\mu\text{-}O)\{MeS(CH_2)_2SMe\}]$.[47]

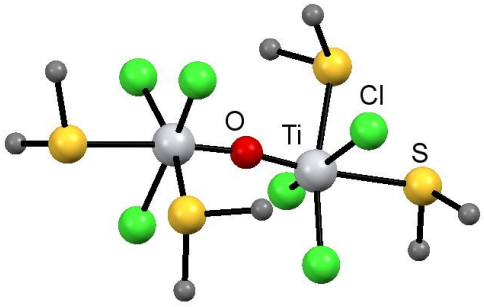

Figure 1.9 The structure of $[Cl_3(Me_2S)_2Ti(\mu\text{-}O)Ti(SMe_2Cl_3)]$.[51]

Ti(III) halides complexes with chalcogenoether ligands are rare, but $[TiX_3(ER_2)_3]$ (X = Cl, Br; ER_2 = SMe_2, $SeMe_2$ or THT), $[TiCl_3([9]aneS_3)]$ have been reported using TiX_3 with corresponding ligands although with limited characterisation data.[52, 53]

1.2.2.2 Zirconium and hafnium

Zirconium and hafnium halide complexes are relatively less common compared to titanium species.[4] The attempted synthesis of $[ZrCl_4\{PhSe(CH_2)_2SePh\}]$ was carried out using $ZrCl_4$ or $[ZrCl_4(THF)_2]$ with $PhSe(CH_2)_2SePh$ in dry CH_2Cl_2 solution and only resulted in Se_2Ph_2.[4] However, MCl_4 (M = Zr, Hf) rapidly coordinate with SMe_2 in anhydrous CH_2Cl_2 to form *cis*-$[MCl_4(SMe_2)_2]$ in high yield.[4] Other complexes are made by the substitution of SMe_2 from *cis*-$[MCl_4(SMe_2)_2]$ using dichalcogenoethers ($MeE(CH_2)_nEMe$, n = 2, 3, *o*-$C_6H_4(CH_2EMe)_2$; E = S, Se).[4] The direct reaction of $ZrCl_4$ or MI_4 with $SeEt_2$ in dry CH_2Cl_2 was also reported to produce *cis*-$[MX_4(SeEt_2)]$.[16] In some cases, the ligand may undergo quaternization, such as $[Et_3Se]_2[ZrI_6]$ and $[Me_2SCH_2Cl]_2[Zr_2Cl_{10}]$; both were identified from X-ray crystallography.[4, 16]

Unlike the titanium system where only six-coordinate complexes have been reported with dichalcogenoether ligands,[16, 47] zirconium and hafnium tetrachloride can form 1:1 or 1:2 complexes with dichalcogenoethers; the former were made by controlling one equivalent of ligand with metal chlorides, whereas the latter required a 1:3 metal:ligand molar ratio. Both were reported as highly moisture sensitive and poorly soluble in weakly coordinating solvents.[4] The complexes with ligands $MeE(CH_2)_2EMe$ which form five membered chelate rings were reported to be six- or eight-coordinate compounds (Figure 1.10 a and b), however, compounds using $MeS(CH_2)_3SMe$ were found to be dimeric with bridging ligands (Figure 1.11 a) and six-coordinate metal ions.[4]

Tripodal $MeC(CH_2EMe)_3$ (E = S, Se) were also reported and form 1:1 complexes, made by substitution from $[MCl_4(SMe_2)_2]$ (M = Zr or Hf), however, these complexes are too insoluble to grow single crystals or for NMR studies and no further evidence was provided to show if the resulting complexes are six or seven-coordinate.[49] Macrocyclic $[9]aneS_3$ and $[10]aneS_3$ also form poorly soluble $[MCl_4(macrocyclic)]$ complexes, and the crystal structure, $[ZrCl_4([9]aneS_3)]$, was obtained and shown a seven-coordination metal centre with the macrocycle (Figure 1.11 b), and NMR spectroscopic data is also consistent with a seven-coordinate complexes.[4, 16, 49]

In contrast to the titanium analogues, $[TiCl_4\{o\text{-}C_6H_4(CH_2EMe)_2\}]$, mentioned above, these zirconium and hafnium complexes were not suitable as to be single source precursor in LPCVD for the deposition ZrE_2 or HfE_2 thin films.[4, 16]

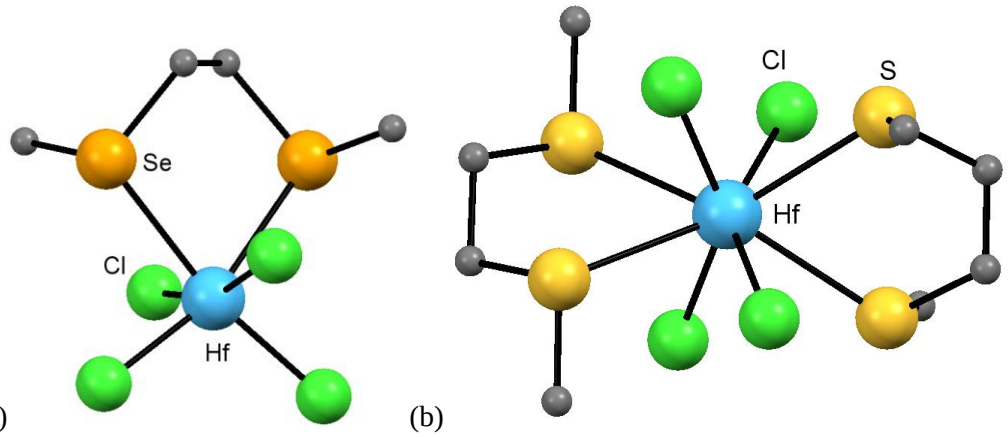

(a) (b)

Figure 1.10 The structures of (a) $[HfCl_4\{MeSe(CH_2)_2SeMe\}]$ and (b) $[HfCl_4\{MeS(CH_2)_2SMe\}_2]$.[4]

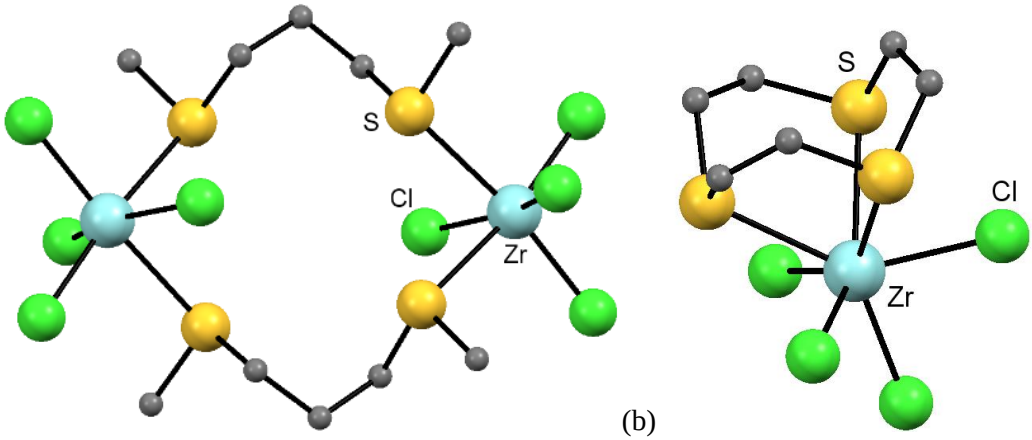

(a) (b)

Figure 1.11 (a) The dimer structure present in $[ZrCl_4\{MeS(CH_2)_3SMe\}]$ and (b) The structure of $[ZrCl_4([9]aneS_3)]$.[4]

1.2.3 Group V

1.2.3.1 Vanadium (V)

The high oxidation state vanadium ions are hard Lewis acids and easily reduced by soft donor ligands. It is unusual to find V^VX_5 or $V^{IV}X_4$ (X = halides) complexes with chalcogenoether ligands. $VOCl_3$ was reported to be immediately reduced by most of the neutral chalcogenoethers, such as SMe_2, SPh_2, $SeMe_2$, $MeS(CH_2)_3SMe$ or $MeSe(CH_2)_2SeMe$, and resulted in unisolated V(IV) or V(III) species.[54] Complexes $[VOCl_3\{RS(CH_2)_2SR\}]$ (R = Me, Et, ^{i}Pr) were made directly from $VOCl_3$ and the corresponding dithioether in dry CH_2Cl_2 and was reported to decompose in a few hours.[55]

Unstable complexes $[VOF_3(SMe_2)_2]$ and $[VOF_3\{RS(CH_2)_2SR\}]$ were also made from the substitution of $NCCH_3$ from $[VOF_3(NCCH_3)]$, and confirmed by IR and multinuclear (^{1}H, ^{19}F and ^{51}V) NMR spectroscopies using fresh samples.[56]

$[VOCl_3([9]aneS_3)]$ and $[(VOCl_3)_n(1,4\text{-dithiane})]$ were also made by reacting $VOCl_3$ and ligands in anhydrous CH_2Cl_2 solution. The latter was reported to form 1:1 or 1:2 complexes.[55] There is also no evidence reported of chalcogenoether reacting with VO_2F or VO_2Cl.

1.2.3.2 Vanadium(IV)

A series of $[VCl_4\{L–L\}]$ (L–L = $RS(CH_2)_2SR$, $MeS(CH_2)_3SMe$ or 1,4-thiane; R = Me, Et, ^iPr) complexes were made by adding one equivalent of ligand to a solution of VCl_4 and dry CH_2Cl_2.[55] However, using excess thioether or heating the solution caused a reduction of the metal to form V(III) complexes. Once isolated, these VCl_4 complexes are not as sensitive as VOX_3 species and they could be stored under inert conditions for several weeks. These $[VCl_4\{RS(CH_2)_2SR\}]$ complexes are identified to be in their *cis* form by their UV-visible and IR spectra.[55] Complexes of the form $[VCl_4(L–L)]$ were also reported using VCl_4 and diselenoether ligands, ($RSe(CH_2)_2SeR$; R = Me, ^nBu; $MeSe(CH_2)_3SeMe$) in anhydrous CH_2Cl_2, but using monodentate selenoether caused a metal reduction to V(III).[57]

$[VOCl_2(SMeEt)_2]$ was synthesised from VCl_3, SMeEt and dry CH_2Cl_2, although this product presumably was the result of air-oxidation or hydrolysis.[58] $[VOCl_2\{RS(CH_2)_2SR\}]$ were reported by controlling O/Cl exchange using $O(SiMe_3)_2$ or trace amounts of water from $[VCl_4\{RS(CH_2)_2SR\}]$ in CH_2Cl_2/CH_3CN solutions, as mentioned above. The crystal structure of $[VOCl_2\{MeS(CH_2)_2SMe\}]$ was collected and contains a V_4O_4 core (Figure 1.12).[55] $[VOCl_2([9]aneS_3)]$ was formed by oxidation/hydrolysis of $[VCl_3([9]aneS_3)]$ and shows a distorted octahedral geometry (Figure 1.13 a).[59] The similar complex, $[VOCl_2(ttob)]$ (ttob = 2,5,8,trithia[9]-*o*-benzophane), was obtained from the substitution of $NCCH_3$ from $[VOCl_2(NCCH_3)_2]$ using ttob.[60, 61] The solid state structure of heterocrowns $[VOCl_2([9]aneN_2S)]$ was collected and shows a distorted octahedron with the S *trans* to the V═O bond (Figure 1.13 b).[62]

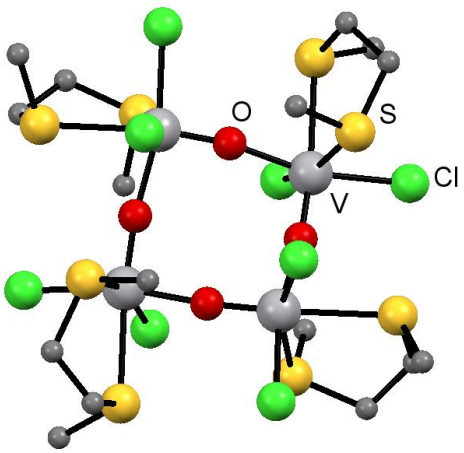

Figure 1.12 Structures of $[VOCl_2\{MeS(CH_2)_2SMe\}]$.[55]

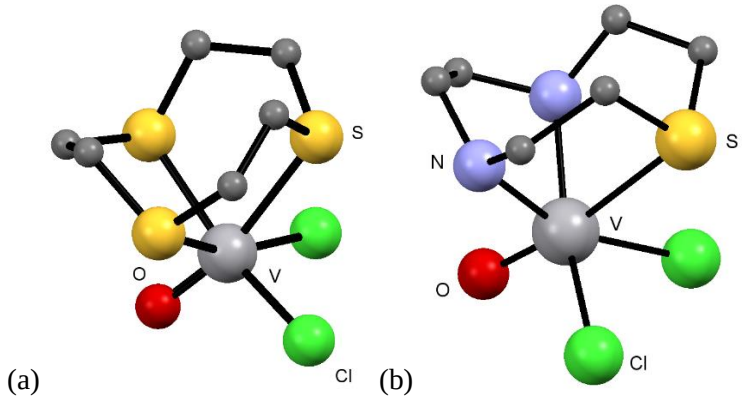

(a) (b)

Figure 1.13 Structures of (a) $[VOCl_2([9]aneS_3)]$[59] and (b) $[VOCl_2([9]aneN_2S)]$.[62]

Although a series of $[VOF_2L_n]$ (L = N- and O-donor neutral ligands) complexes were made using VF_4, H_2O and various ligands in an autoclave, similar reactions using chalcogenoethers as ligands in an autoclave were unsuccessful.[63]

1.2.3.3 Vanadium(III)

Vanadium(III) is a common oxidation state and the first vanadium(III) thioether compounds were reported many years ago.[7] $[VX_3(SR_2)_2]$ (SR_2 = SMe_2, SEt_2, S^nPr_2, S^nBu_2 or THT) were made using VX_3 and thioether in dry benzene and reported as five-coordinate complexes.[64, 65] A series of $[VCl_3(selenoether)_n]$ (selenoether = $SeMe_2$, $RSe(CH_2)_3SeR$, R = Me, ^nBu; *o*-$C_6H_4(CH_2SeMe)_2$) were also reported and were reduced by heating their $[VCl_4(SeR_2)_n]$ analogues.[57] These $[VCl_3(SeR_2)_n]$ complexes were identified as six coordinate d^2 ions from IR and UV-visible spectroscopies which suggests they contain a chloride bridged, although there is no X-ray data to confirm this.[57] LPCVD using $[VCl_3(SeMe_2)_2]$ was demonstrated to deposit VSe_2 thin films.[57] Several $[VX_3(macrocyclic)]$ (X = Cl, Br; macrocyclic = $[9]aneS_3$, $[10]aneS_3$, $[9]aneOS_2$ or ttob) were also reported to be formed from VCl_3 with ligands in dry CH_2Cl_2 solution or substitution from $[VBr_3(THF)_3]$.[60, 61, 66-69] The solid state structure of $[VCl_3([9]aneS_3)]$ and $[(VCl_3)_2([18]aneS_6)]$ show a *fac*-octahedron (Figure 1.14), and other $[VX_3(thia\text{-}macrocycle)]$ complexes are assigned as V(III) octahedron from UV-visible spectra.[60, 61, 66-69]

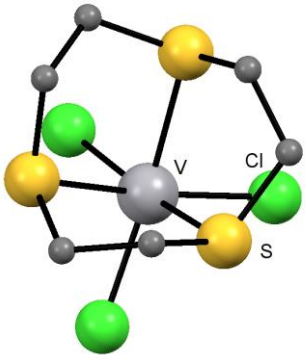

Figure 1.14 The structure of $[VCl_3([9]aneS_3)]$.[61]

1.2.3.4 Niobium(V) and tantalum(V)

1.2.3.4.1 Niobium(V) and tantalum(V) fluoride complexes

NbX_5 and TaX_5 (X = F, Cl, Br, I) are the most common niobium or tantalum halides and are commercially available. They exist as dimeric M_2X_{10} (M = Nb, Ta; X = Cl, Br, I) systems or tetrameric $[MF_5]_4$ with bridging halides in the solid state.[70, 71]

The MF_5 are very strong, hard Lewis acids, but dissolve readily in neat SMe_2 or SEt_2 to form moisture sensitive colourless products $[MF_5L]$ and their multinuclear (^1H, ^{19}F and ^{93}Nb) NMR studies show reversible dissociation of the SR_2 in solution.[5, 6] $[MF_5(SeMe_2)]$ were made by a similar method but are less stable and decomposed within a few days in the solid state.[5, 6] $[TaF_5(TeMe_2)]$ was identified from NMR studies at 0 °C with a fresh sample, and was rapidly decomposed to Me_2TeF_2 and $[Ta_2F_{11}]^-$ based on NMR spectroscopic data.[5, 6] The attempted formation of $[NbF_5(TeMe_2)]$ was unsuccessful and formed a black tar immediately after $TeMe_2$ was added to a CH_2Cl_2 suspension with NbF_5.[6]

A solution with excess SMe_2 and $[MF_5(SMe_2)]$ in CH_2Cl_2 was stored at -18 °C for several days and deposited extremely moisture sensitive, colourless crystals of $[MF_4(SMe_2)_4][MF_6]$ confirmed by its crystal structures shows octahedral anions ($[MF_6]^-$) and eight-coordinate distorted dodecahedral cations ($[MF_4(SMe_2)_4]^+$, Figure 1.15 a).[5, 6] $[NbF_4(THT)_2][NbF_6]$ and $[NbF_4(THT)_4][NbF_6]$ were also reported made by controlling the ligand stoichiometry.[72] The former used 1:1 ratio and confirmed as six-coordinate cation and anion, whereas the latter used 1:2 ratio and has an eight-coordinate cation and a six-coordinate anion, and both were identified with multinuclear (^1H, ^{19}F) NMR data.[72] The formation of $[TaF_4(SEt_2)_4][TaF_6]$ was identified by NMR studies, but could not be isolated. Interestingly, the selenoether analogues are not reported to form cationic complexes.

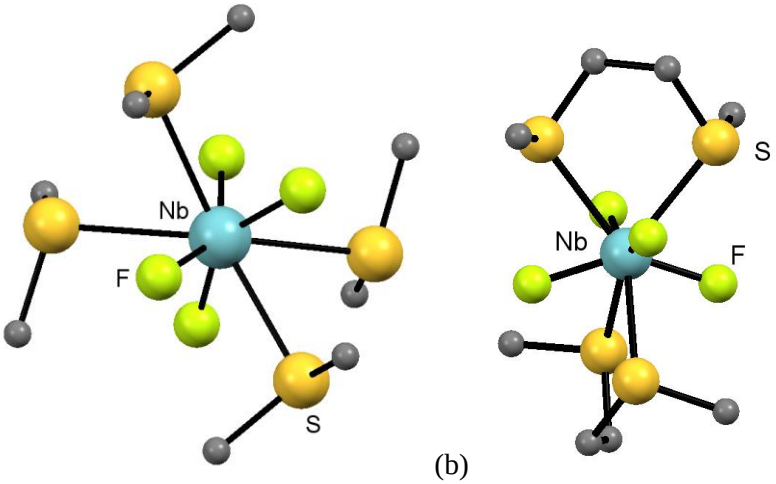

(a) (b)

Figure 1.15 The structure of (a) $[NbF_4(SMe_2)_4]^+$ and (b) $[NbF_4\{MeS(CH_2)_2SMe\}_2]^+$.[6]

The reaction of MF_5 with the dithioether in anhydrous CH_2Cl_2 resulted in formation of $[MF_4(L–L)_2][MF_6]$ (L–L = $RS(CH_2)_2SR$, R = Me, Et, ^{i}Pr). The crystal structure of $[MF_4\{^iPrS(CH_2)_2S^iPr\}_2][MF_6]$ shows the chelating ligand in the *meso* form, whereas the two

dithioethers in $[MF_4\{MeS(CH_2)_2SMe\}_2][MF_6]$ have *DL* forms (Figure 1.15 b).[5, 6] The reaction of NbF_5 with *o*-$C_6H_4(CH_2SMe)_2$ in dry CH_2Cl_2 solution also resulted in eight coordinate cations, but rather than a monomeric seven-membered ring, it formed a chain polymer (Figure 1.16).[73]

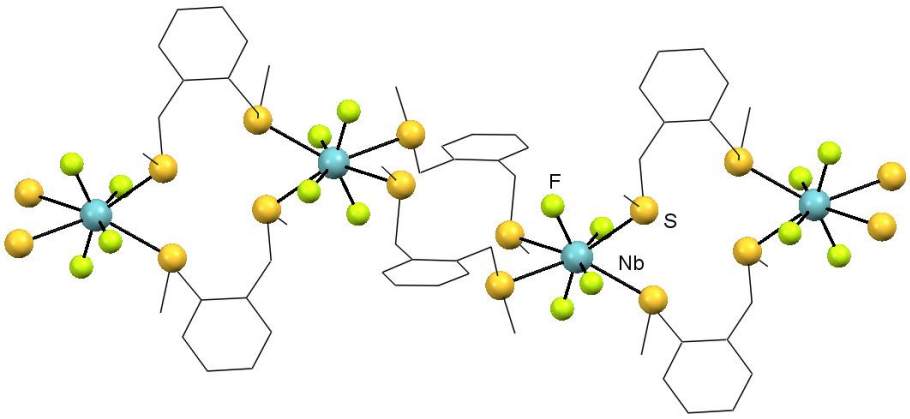

Figure 1.16 The structure of $[NbF_4\{o\text{-}C_6H_4(CH_2SMe)\}]^+$.[73]

1.2.3.4.2 Niobium(V) and tantalum(V) chloride, bromide and iodide complexes

MCl_5 and MBr_5 (M = Nb, Ta) complexes with thioether or selenoether are more stable than their fluoride analogues and some of them were initially studied in 1962.[5, 6, 74-76] Complexes $[MX_5L]$ (M = Nb, Ta; X = Cl, Br; L = SMe_2, SEt_2, S^nBu_2, $SeMe_2$, Se^nBu_2 etc.) were made by using MX_5 with corresponding ligands in anhydrous CH_2Cl_2 solution and reacted almost immediately.[5, 6, 74-76] Dichalcogenoethers tend to form a bridged-ligand dimers of form $[(MCl_5)_2\{L–L\}]$ (L–L = $RE(CH_2)_nER$, *o*-$C_6H_4(CH_2SR')_2$; R = Me; R' = Me, Et) (Figure 1.17 a).[5, 6, 76] These compounds form six-coordinate distorted octahedrons, as identified *via* IR, UV-visible, multinuclear (^1H, ^{13}C, ^{77}Se, ^{93}Nb) NMR spectroscopies alongside single crystal solid state structures.[5, 6, 76]

The reaction of the telluroethers, $TeMe_2$ or Te^nBu_2, with NbX_5 resulted in very unstable $[NbX_5(TeR_2)]$ compounds, but surprisingly, $[TaX_5(TeMe_2)]$ was found to be stable over a long period of time under inert conditions.[76] Both niobium and tantalum complexes were identified by IR, multinuclear (^1H, ^{13}C, ^{93}Nb, ^{125}Te) NMR spectroscopies on a fresh sample and the crystal structure of $[TaCl_5(TeMe_2)]$ was collected (Figure 1.17 b).[76]

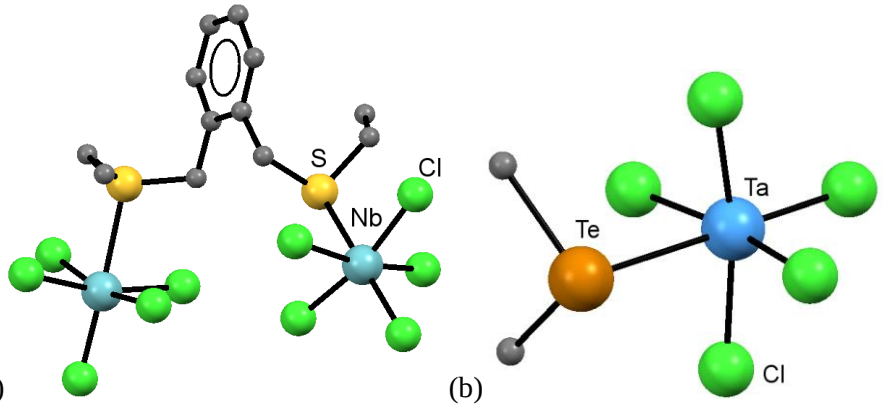

(a) (b)

Figure 1.17 The structure of (a) $[(NbCl_5)_2\{o\text{-}C_6H_4(CH_2SEt)_2\}]$ and (b) $[TaCl_5(Me_2Te)]$.[76]

Unlike the reaction of MF_5 with excess SMe_2, resulting in $[MF_4(SMe_2)_4][MF_6]$,[5, 6] there are no reports of complexes of the form $[MX_4(ER_2)_4][MX_6]$ with Cl or Br analogues. However, using excess dichalcogenoether, such as $MeS(CH_2)_2SMe$, could form $[MX_4\{MeS(CH_2)_2SMe\}_2][MX_6]$ (X = Cl, Br) with the same geometry of their fluoride analgoues $[MF_4\{MeS(CH_2)_2SMe\}_2][MF_6]$.[5, 6] The use of macrocyclic ligands is also reported with $NbCl_5$ in the resulting complex, the ligands tend to be *exodentate* as shown by IR and multinuclear NNR studies (Figure 1.18).[77-82]

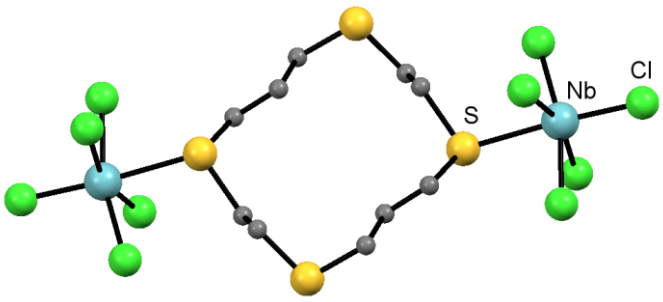

Figure 1.18 The structure of $[(NbCl_5)_2([14]aneS_4)]$.[78]

The tantalum complexes proved to be unsuitable as LPCVD precursors. However, the LPCVD application using single source precursors, $[NbCl_5(S^nBu_2)]$ and $[NbCl_5(Se^nBu_2)]$, successfully deposited continuously NbE_2 thin films at 650 to 750 °C.[76] Further research of LPCVD application by using weaker Lewis acid (Br^-) to metal centre will be discussed in Chapter 5.

1.2.3.4.3 Other niobium(V) and tantalum(V) species

Other high oxidation state Nb(V) or Ta(V) materials, MEX_3 (M = Nb, Ta; E = O, S, Se; X = F, Cl ,Br), are stable polymers and are difficult to react with soft neutral donors. The formation of $[MEX_3L_n]$ (E = O, S, Se; X = Cl, Br; L = clalcogenoether; n = 1 or 2) were reported, but they were usually made from other MX_5 or MX_5 complexes with further process.

The $[NbOF_3L]$ species were only reported to form with some N- and O-donor neutral ligands. Attempts to prepare thioether complexes were unsuccessful.[83] $[NbOCl_3(SMe_2)]$ (Figure 1.19a) and $[NbOCl_3\{MeS(CH_2)_2SMe\}]$ were obtained by 'accident' as products of the oxidation/hydrolysis of $[NbCl_4(chalcogenoether)]$.[84] The crystal structure of $[NbOCl_3(SMe_2)]$ contains a μ-O bridge linked with two Nb(V) centres, and its preparation from $[NbCl_5(SMe_2)]$ with $O(SiMe_3)_2$ in CH_2Cl_2 is described in Appendix 5. It is possible that other $[NbOX_3(chalcogenoether)]$ complexes could also be prepared using this method. In contrast, the hydrolysis of $[(TaCl_5)_2\{^iPrS(CH_2)_2S^iPr\}]$ resulted in the formation of the dimer, $[Cl_5Ta(\mu\text{-}O)TaCl_3\{^iPrS(CH_2)_2{}^iPr\}]$ (Figure 1.19b).[85]

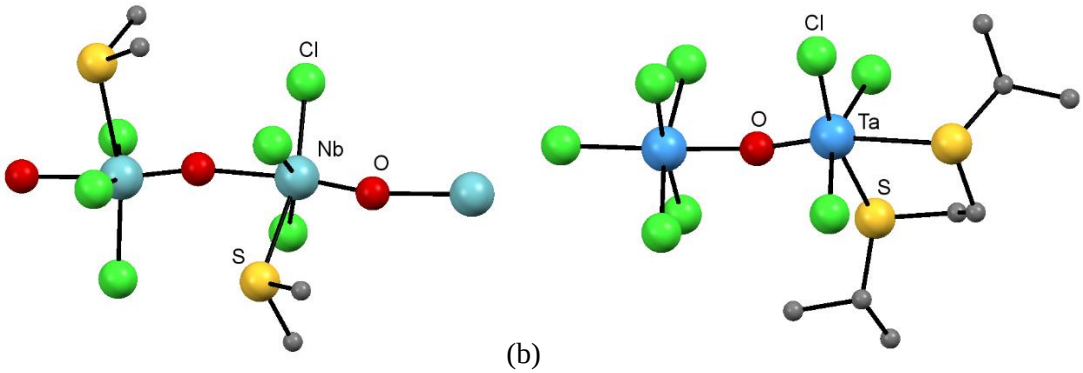

(a) (b)

Figure 1.19 Structure of (a) $[NbOCl_3(SMe_2)]$[84] and (b) $[Cl_5Ta(\mu\text{-}O)TaCl_3\{^iPrS(CH_2)_2{}^iPr\}]$.[85]

The complexes $[MEX_3(chalcogenoether)_n]$ (M = Nb, Ta; E = S, Se; X = Cl, Br) reported in the literature are usually made by the direct reaction of MSX_3 with chalcogenoethers, such as (SEt_2, $SPPh_3$, THT, $PhS(CH_2)_2SPh$ *etc.*), in CS_2 solution.[86-94] The reaction of MEX_3 with monodentate chalcogenoether (SEt_2, $SPPh_3$, THT) were reported with different coordination numbers, including 1:1 ($[NbSCl_3(SPPh_3)]$[91] and $[NbSCl_3(SEt_2)]$),[94] and 1:2 ($[NbSBr_3(THT)_2]$).[87] The crystal structure of $[NbSBr_3(THT)_2]$ shows a distorted octahedral geometry with two THT units placed in the *cis*-positions with one of the THT *trans* to the Nb═S bond (Figure 1.20 a).[87] Interestingly, the crystal structure of $[NbSCl_3(SPPh_3)]$ forms both a monomer and a dimer in its unit cell. The dimer has two Nb═S bonds in terminal positions, two bridged-chlorides and the two $SPPh_3$ are *anti*, whereas the monomer is a five-coordinate compound (Figure 1.20 b).[91] The reactions of dithioether $PhS(CH_2)_2SPh$ with $TaSX_3$ resulted in dimeric $[TaSX_3\{PhS(CH_2)_2SPh\}]$ with the solid state structure provided. The dithioether forms a five-membered ring with one of the S atoms *trans* to Ta═S bond.[89]

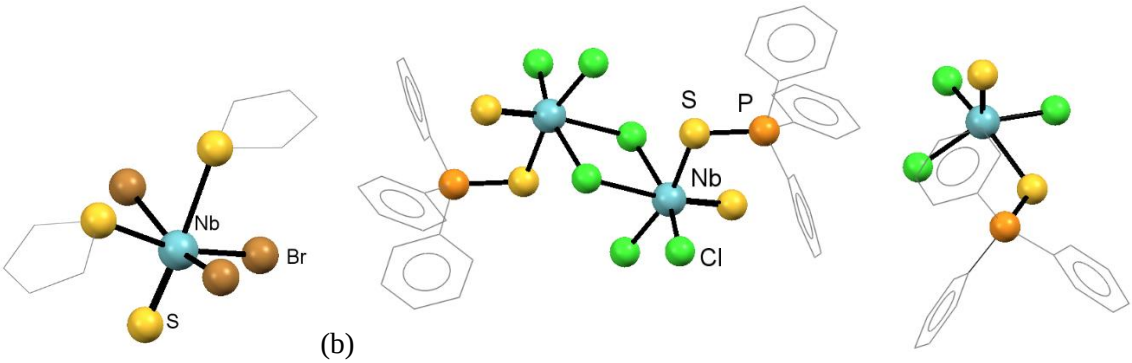

(a) (b)

Figure 1.20 The structure of (a) $[NbSBr_3(THT)_2]$[87] and (b) $[NbSCl_3(SPPh_3)]$ (monomer and dimer in a unit cell).[91]

The starting material MEX_3 was used to make all complexes mentioned above, this is usually prepared by the reaction of MX_5 with Sb_2E_3 but this method also forms SbX_3, which is very difficult to separate.[87-93] The clean preparation of $NbSCl_3$ was reported by Gibson and co-workers,[95, 96] but there has been no further exploration based on this method. Chapter 4 will discuss further detail of harnessing S/Cl exchange to afford a series of $[NbSCl_3(chalcogenoether)_n]$ and $[NbSe_nCl_3L]$ complexes.

1.2.3.5 Niobium(IV) and tantalum(IV)

In contrast to the abundant literature reports of Nb(V) and Ta(V) complexes, there are only a few examples of $[Nb^{IV}X_4L]$ complexes, even including the more common N-, O-, P-donor neutral ligands.[97-99] There are no oxygen free Nb(IV) or Ta(IV) starting materials available commercially. $[NbCl_4(THF)_2]$ is the only product available from Sigma-Aldrich Ltd. However, there is not successful substitution reaction reported by using chalcogenoether with $[NbCl_4(THF)_2]$. The pure MX_4 (M = Nb, Ta; X = Cl, Br) compound was made from a temperature gradient method, however, this preparation is difficult to repeat.[100] More efficient NbX_4 preparations were explored in this project and the results will be discussed in Chapter 2.

$[NbX_4(thioether)_n]$ (X = Cl, Br; thioether = SMe_2, $MeS(CH_2)_2SMe$) are usually made by the direct reaction from NbX_4 with corresponding ligands. All those complexes were reported to be paramagnetic and had IR and UV-visible analysis, but without solid state structure data.[101-103]

Interestingly, the complex $[NbCl_4(SMe_2)]$ was reported with IR and UV-visible data and thought to be a dimer, but the geometry of this complex was a mystery.[103] No other examples of NbX_4 with seleno- or telluroethers have been reported in literature search.

A series of $[M_2X_4(L)(\mu\text{-}E)_n(\mu\text{-}E_2)_n]$ (M = Nb, Ta; X = Cl, Br; E = S, Se) were reported and synthesised from different methods. Complexes $[M_2Cl_4(SMe_2)_4(\mu\text{-}S)_2]$ were made by the slow diffusion of SMe_2, S_2Me_2 in hexane with $[M_2Cl_4(SMe_2)(\mu\text{-}Cl)_2(\mu\text{-}SMe_2)]$ for over two weeks.[104] Compounds $[M_2Cl_4\{EtS(CH_2)_2SEt\}_2(\mu\text{-}S)_2]$ (M = Cl, Br) were made in a similar fashion to $[M_2Cl_4(SMe_2)_4(\mu\text{-}S)_2]$ which were initially determined to form bridged-chloride M(III) complexes.[104, 105] Other dimeric $[Nb_2X_4(THT)_4(\mu\text{-}S)_2]$ (X = Cl, Br) complexes with bridging-sulfide were made from a self-redox reaction by an excess of $[NbSX_3(THT)_2]$ in CS_2 solution for 24 hours.[90] $[NbSX_3(L)(\mu\text{-}S)(\mu\text{-}S_2)]$ (X = Cl, Br; E = S, Se; L = SMe_2, THT, $PhS(CH_2)_2SPh$) were made from NbX_5, Sb_2E_3 and corresponding ligands in CS_2 solution.[90] A bridged-selenide complex $[Ta_2Cl_4\{o\text{-}C_6H_4(CH_2SeMe)_2\}(\mu\text{-}Se)_2]$ was reported as an unexpected product; the $\mu\text{-}Se^{2-}$ groups are assumed to originate from the C–Se cleavage from the ligands (Figure 1.21).[3] Complexes $[Nb_2X_4(L)_4(\mu\text{-}Se_2)_2]$ (X = Cl, Br; L = SMe_2, THT) were made using NbX_5, Sb_2Se_3 and ligands.[86, 88] The bridged-chloride complex $[Ta_2Cl_6(SMe_2)_2(\mu\text{-}Cl)_2]$ was obtained by accident and the condition of preparation remains unclear.[3]

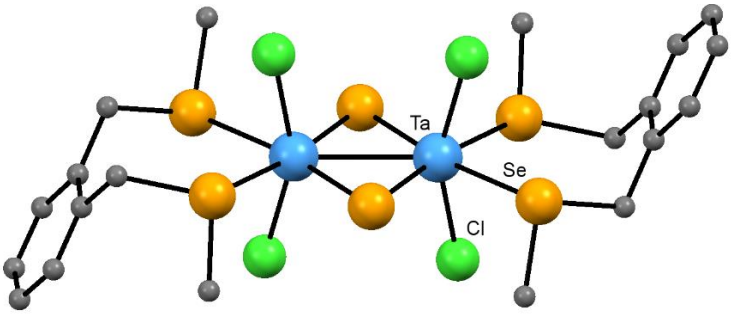

Figure 1.21 The structrue of $[Ta_2Cl_4\{o\text{-}C_6H_4(CH_2SeMe)_2\}(\mu\text{-}Se)_2]$[3]

1.2.3.6 Niobium(III) and tantalum(III)

Simple niobium(III) and tantalum(III) halides of the form MX_3 have not been isolated, instead they form clusters of M_3X_8 (or $MX_{2.66}$). While there is no commercial source for oxygen free $[MCl_3(L)_n]$ compounds, niobium(III) or tantalum(III) halides with chalcogenoether ligands have been reported and form face sharing dimeric structures, such as $[M_2Cl_4(SR_2)_2(\mu\text{-}Cl)_2(\mu\text{-}SR_2)]$ (R = Me, ^{n}Bu) (Figure 1.1, as above).[3, 104, 106] There are three common methods used to prepare Nb(III) or Ta(III) halide complexes with neutral chalcogenoethers. The first is the reduction of the metal centre from M(V) to M(III) using magnesium powder in a diethyl ether solution.[3] The second is using Na/Hg as a reducing agent, but this preparation is more commonly used for the formation of M(IV) complexes, especially for M(IV) phosphine compounds (*i.e.* $[TaCl_4\{Me_2P(CH_2)_2PMe\}_2]$).[104, 106] The third method is the substitution of SMe_2 from $[M_2Cl_4(SMe_2)_2(\mu\text{-}Cl)_2(\mu\text{-}SMe_2)]$ using bidentate chalcogenoethers.[3, 104, 105]

Products obtained from substitution reactions typically form edge-sharing dimers with bridged-chlorides using dichalcogenoether, such as $[M_2Cl_4(L\text{–}L)(\mu\text{-}Cl)_2]$ (L–L = $MeE(CH_2)_2EMe$, $MeSe(CH_2)_3SeMe$, ^{n}BuSe$(CH_2)_3$Se^{n}Bu; E = S, Se). The oxidation state on the metal centre for these complexes is challenging to determine by X-ray crystallography because bridging S^{2-} is very difficult to distinguish from bridging Cl^-. The more likely solution in each case, is determined based on the oxidation state consistent with the M–M bond distance.[3, 104, 105] However, there are no examples of the coordination of telluroethers to Nb(III) or Ta(III) halides. Dimers for dimer complexes, such as $[\{Nb_2Cl_4(\mu\text{-}Cl)_2(\mu\text{-}SMe_2)\}_2(\mu\text{-}MeSe(CH_2)_3SeMe)_2]$, is an unusual examples of the bridged-dichalcogenoether and linked to dimers (Figure 1.3, at above).[3]

1.2.4 Group VI

1.2.4.1 Chromium

Group VI metals in their higher oxidation states are relatively unstable, especially chromium which is immediately reduced in the presence of thioether. In the medium oxidation state, chromium(III) complexes have been reported to coordinate with thioether. Complexes of the form $[CrX_3(SR_2)_3]$ (X = Cl, Br; R = Me, Et) were prepared from the direct reaction CrX_3 and Zn powder resulting with IR and UV-visible spectra data supporting. Unfortunately, the expected formulation not provide a solid state structural data of these complexes.[107] *fac*- and *mer*-$[CrCl_3(THT)_3]$ isomers were reported using a large excess of THT to substitute NMe_3 from $[CrCl_3(NMe_3)_2]$ in benzene and demonstrates the isomerisation can proceed in benzene solution. Although the report mentioned crystals were obtained, there is no solid state crystal structure reported.[108]

Many $[CrX_3L]$ complexes with thia-macrocycle, tri- or polydentate thioether or seleno-macrocycle ligands have been reported using in different methods. These preparations include the substitution

from $[CrX_3(THF)_3]$ using neutral macrocyclic or tripod thioether, such as $S(CH_2CH_2CH_2SMe)_2$, $CMe(CH_2SMe)_3$,[67, 109-111] $MeC(CH_2SeMe)_3$ and $Se(CH_2CH_2CH_2SeMe)_2$,[112, 113] and the reaction of $CrCl_3{\cdot}6H_2O$ in $NCCH_3$ solution heated to reflux in the presence of ligands ([9]aneS_3, [10]aneS_3, $S(CH_2CH_2SMe)_2$ *etc.*).[69, 114]

The complexes $[Cr(L)_n][BF_4]_3$ (n = 3 , L = *cis*-MeSCH═CHSMe; n = 2, L = $S(CH_2CH_2CH_2SMe)_2$), were made by the substitution of THF from $[Cr(THF)_6][BF_4]_3$ by ligands in THF solution and the resulting UV-visible data studied to show octahedral structures.[115] Most of complexes provided valuable IR, UV-visible and Extended X-ray Absorption Fine Structure (EXAFS) data and form distorted octahedrons, however, only a few X-ray structures were reported such as $[CrCl_3(\kappa^3$-[15]ane$S_5)]$ (Figure 1.22).[67]

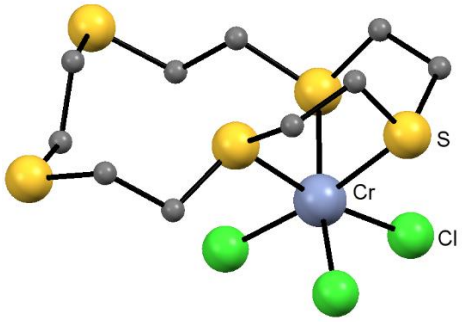

Figure 1.22 The structure of $[CrCl_3(\kappa^3$-[15]ane$S_5)]$.[67]

1.2.4.2 Molybdenum and tungsten in their high oxidation state (V to VI)

Molybdenum and tungsten halides are unstable in their high oxidation states. $MoCl_6$ in particular is very unstable, and readily decomposes to $MoCl_5$ and Cl_2 at ambient temperature.[116] WX_6 (X = Cl, Br) species are more stable and are reported to coordinate with thioethers to form $[WCl_6(SR_2)_2]$ (SR_2 = SMe_2, SEt_2, S^iPr_2, THT and $MeS(CH_2)_2SMe$) under certain conditions, or by adding WCl_6 to ligands in CCl_4.[117] However, WX_6 complexes are also reduced when there is a minor change in reaction conditions (*i.e.* solvents) to form W(V), W(IV), a salt such as $[R_3S][WCl_6]$ or non-stoichiometric materials.[117, 118]

Other Mo(VI) and W(VI) complexes containing chalcogenoethers, such as $[WOCl_4(MeS(CH_2)_2SMe)]$[119] and $[(WSCl_4)_2(MeS(CH_2)_2SMe)]$,[119, 120] were afforded using dithioether and $WECl_4$ (E = O, S), with their ^{1}H NMR spectra studied to show distorted octahedra. $[MO_2X_2(L–L)]$ (X = Cl, Br) were made either using MO_2X_2 with L–L (L–L = $RS(CH_2)_2SR$, R = Me, Et, ^{i}Pr, *o*-$C_6H_4(CH_2SMe)_2$, $MeSe(CH_2)_2SeMe$)[121, 122] in CH_2Cl_2 solution or by using WX_6 with L–L (L–L = 1,4-dithiane, $RS(CH_2)_2SR$, R = Me, ^{i}Pr) before they undergo O/Cl exchange by $O(SiMe_3)_2$ in Et_2O solution.[122] These $[MO_2X_2(L–L)]$ have been identified as six-coordinate distorted octahedral by crystal structures, in addition to IR, UV-visible and multinuclear (^{1}H, ^{13}C, ^{95}Mo) NMR spectroscopies (Figure 1.23).[121, 122]

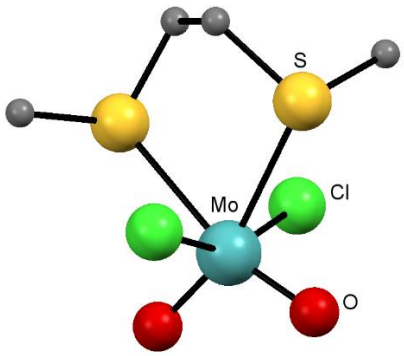

Figure 1.23 The structure of $[MoO_2Cl_2\{MeS(CH_2)_2SMe\}]$.[121]

Molybdenum(V) and tungsten(V) halides remain unstable in many reactions toward soft neutral donor ligands or in solvents. Molybdenum(V) chloride is commercially available but unstable and has been reported to rapidly reduce in the presence of solvents (CH_2Cl_2, *n*-hexane, benzene *etc.*).[123, 124]

$[MoOCl_3(SR_2)_2]$ (SR_2 = SMe_2, SEt_2, S^nPr_2, S^nBu_2, THT) are made from direct reaction $MoOCl_3$ and neat ligands.[125] $[MoOCl_3(L–L)]$ (L–L = $RS(CH_2)_2SR$, R = Me, Et) were made using $MoOCl_3$ and ligands in benzene with reported IR and UV-visible analysis and are paramagnetic complexes.[126] Both $[MoOCl_3(SR_2)_2]$ and $[MoOCl_3(L–L)]$ were assigned six-coordinate complexes from their IR and Uv-visible analysis and their magnetic moment value (μ_{eff}) agree with d^1 paramagnetic system.[125, 126] The tungsten analogues $[WOCl_3(1,4\text{-dithiane})]$ was made by heating $WOCl_3$ and 1,4-dithiane in a CH_2Cl_2 solution for 3 weeks and afforded a grey-green insoluble product. This compound was characterised from IR and UV-visible spectra and magnetic moment experiments.[127] A series of $[MOCl_3(\text{tripod-thioether})]$ complexes have also been reported by ligand substitution from $[MOCl_3(THF)_2]$ by tripod-thioether and identified as having a six-coordinate geometry *via* IR and UV-visible spectra.[128] Crystals of $[WSCl_3\{MeS(CH_2)_2SMe\}]$ were obtained by reaction of $WSCl_4$ and one equivalent of $MeS(CH_2)_2SMe$ in $CHCl_3$ solution for 3 weeks; its X-ray crystal structure was reported as a distorted octahedron.[129]

1.2.4.3 Molybdenum and tungsten in their medium oxidation state (III to IV)

Molybdenum tetrachloride complexes with thioethers have been recently investigated but only the formation of $[MoCl_4(THT)_2]$, $[MoCl_4(SMe_2)_2]$ and $[MoCl_4(SEt_2)_2]$ has been reported.[123, 130-132] These *trans*-$[MoCl_4(SR_2)_2]$ complexes were made by the substitution of CH_3CN from $[MoCl_4(NCCH_3)_2]$ or by a direct reaction from $MoCl_5$ and THT in CH_2Cl_2 solution. The geometry was confirmed from *trans*-$[MoCl_4(THT_2)_2]$ crystal structure and IR data.[123, 130-132] There were no examples of $MoCl_4$ coordinating with selenoether or telluroether.

A few $[MoCl_3(SR_2)_3]$ (SR_2 = SMe_2 or THT) complexes were reported and the X-ray crystal structures show the structures to be either $[Mo_2Cl_3(\text{thioether})_3(\mu\text{-}Cl)_3]$ or

$[Mo_2Cl_4(thioether)_2(\mu\text{-}Cl)_2(\mu\text{-}thioether)]$.[132] This species were made by reducing $[MoCl_4(SR_2)_2]$ using excess ligands or Sn powder.[132] The MoX_3 complexes with macrocyclic chalcogenoethers also were reported and usually made by the reaction of $[MoX_3(THF)_3]$ and macrocyclic thioether in a THF solution. This complex was reported forming a monomeric six-coordinate geometry.[133] However, there are no examples of MoX_3 with selenoethers or telluroethers.

1.3 Thin film transition metal dichalcogenides

1.3.1 The background of 2D materials

Nanomaterials is a branch of materials science where at least one dimension of the material is on the nanometre scale. The materials' properties are strongly influenced by the arrangement of atoms or molecules at this scale.[134] Graphene is one of the earliest studied materials on the nanometre scale, which can be traced back to the 1960s, and consists of a single layer of carbon atoms with a two-dimensional (2D) honeycomb structure.[134, 135] Nanoscale sp^2 carbon materials could be fullerenes (0D), nanotubes (1D), graphene (2D) and graphite (3D).[134, 135] All of these give rise to special properties and have been widely studied. Graphite has been known since the sixteenth century and is widely used in industry for steel-making. Fullerenes, first discovered in 1985,[136] lead to a series of research studies both on these and on nanotubes in 1991.[137] Monolayer graphene sheets were first isolated in 2004 by Geim and co-workers.[134, 135, 138]

Graphene has strong bonding across the layer, due to the strong sp^2 carbon bonds, but has weak interlayer interactions, allowing separation into individual thin layers. The exploration of graphene has uncovered some unusual electronic properties.[134, 135] The absence of a band gap makes graphene able to absorb a wide range of light from IR to UV region of spectrum and has a huge number of possible electronic transitions.[139] This provides a large number of applications in electronic-photonic devices. When graphene is very thin, such as single layer, the light absorption rate is reduced to 2.3 %.[140] Further applications for graphene include solar cells,[141] liquid crystals,[142] high-speed electronic[143] and optical devices,[144] energy generation and store,[144-146] hybrid materials[147, 148] and chemical sensors.[149] However, the absence of a tuneable band gap also makes graphene not suitable for some applications such as operators, although the solution is using a small current on/off ratio.[135, 150]

After the discovery of graphene, the interest in other 2D materials increased, and a significant number of 2D materials were subsequently reported, such as *h*-BN (*h* = hexagonal), transition metal dichalcogenide (TMD) and Group IV and III metal chalcogenides.[134, 135] Interestingly, it is not necessary to have a substrate when depositing other 2D materials, in contrast to graphene, where a substrate is essential in its preparation.[134, 135] 2D materials are able to deposit very thin film (less than 10 atoms).[134] The non-bonding bands of these 2D materials are located within the gap between the bonding (σ) and antibonding (σ*) bands, which are also called band gaps. The different band gaps allow the materials to absorb different parts of the electromagnetic spectrum and make them conducting, semiconducting or insulating. *h*-BN materials have the highest band gaps (*ca.* 6.00 eV) and are considered as insulating.[135] The band gap range for TMD is 1.3 eV to 2.0 eV (MoS_2) which is ideal for optoelectronic applications. Group IV metal chalcogenide materials (SnE, GeE; E = S,

Se) have band gaps in the range of 0.5 to 1.6 eV, which overlaps with the solar spectrum, and gives them optoelectronic properties.[135]

This project focuses on the deposition of TMD materials (ME_2), where M covers a series of transition metals (Nb, Ta or Mo) and E is chalcogen (S, Se or Te). TMD materials stack with strong bonds across the plane but with weak force between the layers, which is similar to other 2D materials. These materials form layered structures of the form X–M–X, with the chalcogen atoms in two hexagonal planes, separated by the plane of the metal atoms'.[151, 152] The weak interaction between each ME_2 layer also results in bulk crystals in variety of polytypes, caused by the different stacking orders. In general, the packing sequences could be AA (1T), AB (2H) or ABC (3R) (T = tetragonal, H = hexagonal, R = rhombohedral), whereas the number represents the packing layers (Figure 1.24).[153] The packed layers also affect the materials' properties. For example, 2H-NbE_2 (E = S, Se) are superconductive but 3R-NbE_2 is not due to the larger Nb distance in the *c* direction in the 3R-stacking sequence.[154, 155]

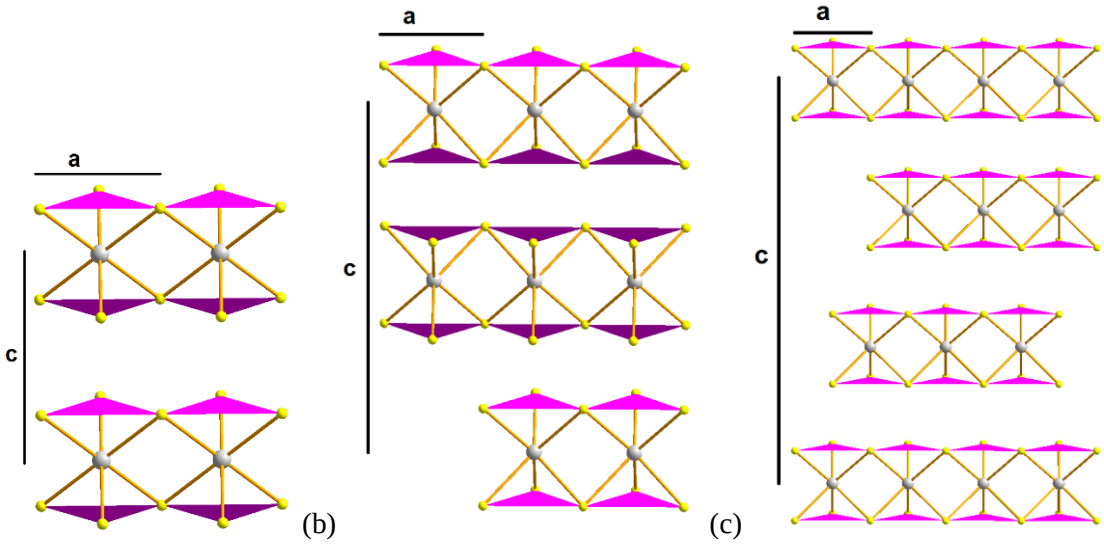

(a) (b) (c)

Figure 1.24 Examples of NbS_2 in its (a) 1T,[156] (b) 2H[156] and (c) 3R[157] packing sequence.

The band gap in TMD decreases when the size of the chalcogen atom increases, but changing the transition metal ion size has less of an effect on the band gap. For example, the band gaps for MoS_2 (1.9 eV) is larger than $MoSe_2$ (1.65 eV), whereas WS_2 (2 eV) has a bigger band gap than WSe_2 (1.7 eV).[134, 135, 158, 159] As mentioned above, band gaps in TMD tend to lie within the region 1.0 to 2.0 eV, allowing these materials have important properties such as thermoelectricity,[160] semiconductivity,[152] half-metallic magnetism,[161] superconductivity,[162] or charge density wave[163] and have applications in many areas such as lubrication,[164] catalysis,[165] photovoltaics,[166] supercapacitors,[167] and rechargeable battery systems,[168, 169] electrocatalysts for hydrogen evolution,[170, 171] high performance materials for optoelectronics[172] or as sensors for environmental applications.[173]

1.3.2 Literature survey of synthesis TMD material and purpose

Some of the TMD materials are widely used in industry and within daily life, but these tend to involve the preparation of large scale materials. For example, molybdenite (MoS_2) is a mineral and is widely used as a lubricant and in catalysis.[174] This section mainly focus on the synthesis and application of thin Group IV to VI transition metal dichalcogenide (E = S, Se or Te) films. Common synthetic routes will be described, while some special methods will be included in this section.

1.3.2.1 Group IV transition metal dichalcogenide

These Group IV transition metal dichalcogenides are reported to be semiconductors and are diamagnetic.[134, 135, 152] Applications of titanium disulfide (Eg = 1.03 eV)[175] include cathode materials for Li secondary batteries,[152, 176-178] solid state lubricants capable of withstanding high temperatures[179] and catalysts for the removal of impurities from crude oil in the petroleum industry.[180] Titanium diselenide has properties such as charge density waves at low temperature[181, 182] and superconductivity with Cu intercalation.[183] $TiTe_2$ is studied for its superconductivity at high pressure[184] and field-effect transistors (FET) ability.[185] These TiE_2 materials are air sensitive and react with oxygen, gradually forming TiO_2.[186] ZrE_2 and HfE_2 have been studied for their electrical transport properties[187-189] and are one of the candidates for large-area solar cell applications with high short-circuit currents.[190]

1.3.2.1.1 Titanium dichalcogenide (TiE_2) thin films

TiS_2 could be formed by reaction of Ti or TiI_4 with S under vacuum at 800 ℃.[186] Another preparation for TiS_2 uses a vapour transport method, where titanium and H_2S react under vacuum at 625 ℃.[175] Chemical vapour deposition (CVD) methods using dual source precursors were also reported to deposit TiS_2 thin films, using $TiCl_4$ and $S_2{}^tBu_2$ at 300 ℃ in ultra-high vacuum CVD (UHVCVD)[191] or $TiCl_4$ and H_2S *via* plasma enhanced CVD (PECVD).[192, 193] Dual source precursor CVD methods were further studied by controlling the amount of precursors used and temperature (400–1000 ℃) conditions, this led to the deposition of deposited thin films with 2.5–32 μm thickness, as determined by scanning electronic microscopy (SEM).[176]

Examples of dual source precursors used in CVD have been increased by the research of Carmalt, Parkin and co-workers, who used ambient pressure CVD (APCVD) with $[Ti(NMe_2)_4]$ and ^{t}BuSH, $S_2{}^tBu_2$ or $S(SiMe_3)_2$ at 300–600 ℃.[180] The titanium complex was also used in aerosol-assisted CVD (AACVD) with ^{t}BuSH at 150–300 ℃ and successfully deposited TiS_2 thin films.[194] Another titanium complex, $[Ti(S^tBu)_4]$, was also used with ^{t}BuSH in AACVD at 150–300 ℃ and deposited TiS_2 thin film.[194]

Complexes of the form $[TiCl_4(SR_2)_2]$ (SR_2 = SMe_2, THT, $S(CH_2)_5$) were tested as single source precursors for APCVD at 400–600 ℃, and the research concluded that precursors $[TiCl_4(THT)_2]$ and

$[TiCl_4(S(CH_2)_5)_2]$ were unsuitable for CVD because the cyclic group slows down the rate of C–S cleavage.[44] Most recently, $[TiCl_4\{o\text{-}C_6H_4(CH_2SMe)_2\}]$ was used in LPCVD as a single source precursor and was found to deposit TiS_2 onto silica substrates at 500 ℃.[16] TiS_2 also reported to be deposited by the sol-gel method, using $[Ti(O^iPr)_4]$ and $^nBuNH_2$ with bubbled H_2S gas before sulfidisation with H_2S.[195]

Compared to many successful TiS_2 precursor research, only a few publications explore the specific deposition method of $TiSe_2$. $TiSe_2$ could be prepared from the vapour transport method.[196] Some thin films studies obtained $TiSe_2$ by the exfoliation of bulk $TiSe_2$ crystals.[182] Others were done by CVD methods using Ti and Se powder and successfully depositing these onto a substate.[197] Dual source precursors using the titanium source, ($TiCl_4$) and selenium source ($SeEt_2$ or Se^tBu_2) in APCVD at 250–600 ℃ also successfully deposited $TiSe_2$ on a glass substrate.[198] Single source precursors $[TiCl_4(SeR_2)_2]$ (R = Et or ^nBu),[15] $[(Cp)_2Ti(Se^tBu)_2]$[199] or $[TiCl_4\{o\text{-}C_6H_4(CH_2SeMe)_2\}]$[16] were also used in LPCVD at 500–600 ℃ and were found to successfully deposit $TeSe_2$ on SiO_2 substrates. Unfortunately, $TiTe_2$ thin film is only reported from exfoliated $TiTe_2$.[185]

1.3.2.1.2 Zirconium dichalcogenide (ZrE_2) and hafnium dichalcogenide (HfE_2) thin films

ZrS_2 and HfS_2 could be made by the reaction of M or MI_4 (M = Zr or Hf) with S under vacuum.[186] CVD methods were reported using $ZrCl_4$ and S powder as precursors and deposited onto *h*-BN or Si/SiO_2 substrates at 600–800 ℃ with 1–3 μm (*h*-BN substrates) or 7–330 μm (Si/SiO_2 substrates) thickness.[200-203]

$ZrSe_2$ and $HfSe_2$ have been synthesised using vapour transport methods, where metal powder was mixed with Se powder and heated to 700–900 ℃ with iodine as a transporting agent.[204-206] Single source precursors, $[(Cp)_2M(Se^tBu)_2]$ (M = Zr or Hf), for the deposition of MSe_2 at 450–600 ℃ were also reported using LPCVD,[199] while MTe_2 (M = Zr, Hf) films made by vapour transport method, using metal powders and tellurium with iodine and CBr_4 as transport agents.[207-209]

1.3.2.2 Group V transition metal dichalcogenide

Thin films of ME_2 (M = V, Nb, Ta; E = S, Se, Te) are of interest due to their superconductive properties.[167] Further research into their properties focuses on charge density wave transition,[210-212] magnetism[213] and intercalation properties.[214]

1.3.2.2.1 Vanadium dichalcogenide (VE_2) thin films

VS_2 was first reported as $LiVS_2$ made in 1977 using $LiCO_3$, V_2O_5 and H_2S in a CVD application.[213, 215-217] Later, it is reported that simply washing $LiVS_2$ with deionized water and ethanol results in the formation of VS_2.[218] Dual source precursors consisting of a vanadium source (VCl_3) and sulfur was found to produce films of VS_2 using APCVD at 500 ℃.[212] A special method was performed with

$VS_2{\cdot}NH_3$ by hydrothermal reaction with $Na_3VO_4.12\ H_2O$ and thioacetamide. Then $VS_2{\cdot}NH_3$ was reacted with degassed water to deposited VS_2.[167]

VSe_2 thin films were grown by the reaction of vanadium and selenium metal powder at 700–800 ℃ and crystals have been grown with the addition of iodine as a transporting agents.[211-213] Parkin and co-workers used the vanadium sources, ($VOCl_3$ or $V(NMe_2)_4$) and selenium source (Se^tBu_2) as dual source precursors for APCVD at 250–600 ℃; these deposited non-stoichiometrically pure VSe_n (n = 0.7–2.1) thin films, as identified from EDX and Raman data. The results which were closer to the formulation, VSe_2, were produced using $V(NMe_2)_4$ and Se^tBu_2.[219] $[VCl_3(SeMe_2)_2]$ (600 ℃) and $[(Cp)_2V(Se^tBu_2)_2]$ (500 and 600 ℃) were used as single source precursor in LPCVD and were found to deposit VSe_2 thin films. The former deposit very low density films with a morphology $VSe_{0.9}$ as identified from EDX spectra, whereas the latter resulted in thicker films (~2 μm) as shown by SEM while its morphology was found to be $VSe_{1.16}$ as determined by EDX spectra.[57]

1.3.2.2.2 Niobium dichalcogenide (NbE_2) and tantalum dichalcogenide (TaE_2) thin films

Crystals of NbE_2 and TaE_2, suitable for single crystal X-ray diffraction, were grown by the vapour transport method[157, 220, 221] or recrystallization.[222] 2H-NbS_2 thin films have only been reported when using dual source precursors $[Nb(NMe_2)_5]$ and ^{t}BuSH using AACVD from a CH_2Cl_2 or *n*-hexane solution,[223] while 1T- or 3R-NbS_2 thin films were prepared *via* the reaction of elemental Nb and S powder or *via* dual source APCVD using $NbCl_5$ with $HSCH_2CH_2SH$ or ^{t}BuSH.[156, 224-228] 3R-NbS_2 is also deposited using a single source precursor $[NbCl_4(S_2R_2)_2][NbCl_6]$ in LPCVD at 500 ℃ and identified *via* its XRD pattern and X-ray photoelectron spectrum.[229]

In contrast, 2H-$NbSe_2$ thin films were made *via* chemical vapour transport with elemental Nb and Se powders or from dual source APCVD using $NbCl_5$ and Se^tBu_2.[223, 230-233] However, thus far, there is only one literature report of 3R-$NbSe_2$ thin film deposition, which used the single source precursor, $[NbCl_5(Se^nBu_2)_2]$ in LPCVD at 650 ℃ to form a $NbSe_2$ thin film.[76, 234]

The crystal structures of TaS_2 and $TaSe_2$ have been reported, from crystals deposited by temperature gradient using sintered powder at 900 ℃ under vacuum.[212] Precursors of the type $[TaCl_5(E^nBu_2)]$ (E = S, Se, Te) failed to deposit TaE_2 thin films,[76] and interestingly, there is only one literature report of TaS_2 thin films using $[Ta(NMe_2)_5]$ and ^{t}BuSH in AACVD with CH_2Cl_2 or *n*-hexane,[223] whereas 2H-$TaSe_2$ is only reported to be prepared from the chemical vapour transport (CVT) method.[235, 236]

Unfortunately, there are no reports of the successful deposition of $NbTe_2$ or $TaTe_2$ thin films. One attempted LPCVD deposition was carried out using $[MCl_5(Te^nBu_2)]$ (M = Nb, Ta) at 475–550 ℃ but only deposited tellurium mixed with some niobium-containing (M = Nb) compound.[76, 234]

1.3.2.3 Group VI transition metal dichalcogenide

MoE_2 thin films are probably the most explored TMD material. 2D-ME_2 (M = Mo, W; E = S, Se) thin films are highly promising candidates for a variety of applications such as spintronics,[237] electrocatalysts for hydrogen evolution,[170, 238] high performance materials for optoelectronics[172] and as sensors for environmental applications.[173] More recently, MoS_2 has also been studied for its thermoelectric properties.[160]

1.3.2.3.1 Molybdenum dichalcogenide (MoE_2) and tungsten dichalcogenide (WE_2) thin films

In general, ME_2 (E = Mo, W; E = S, Se) films or powders are prepared by MO_3 with elemental chalcogen powders at high temperature (*ca.* 800 ℃ for MoE_2 or *ca.* 925 ℃ for WE_2) under vacuum.[239-262] Some reports claim to have deposited very thin films (*ca.* 0.7 nm)[239, 242] or a monolayer of MoE_2.[240, 246] Other methods of producing these films include reducing $[NH_4]_2[MoS_4]$ with dihydrogen gas in the gas-phase to deposit a MoS_2 thin film,[263, 264] while $MoSe_2$ thin films were also reported to be deposited by CVD method using $MoSe_2$ powder[265] or *via* APCVD using $MoCl_5$ and Se^tBu_2 as dual source precursors at 450–650 ℃.[266] However, there are no reports of MoE_2 films produced from a single source precursor in LPCVD.

There have been a few studies focusing on MTe_2 (M = Mo, W). This is likely to be because the precursors are less stable and the materials decompose rapidly at high temperature to release Te vapour.[267] MTe_2 thin films have been prepared by the reaction of Mo/W and Te in their metal form using CVD methods at 650–700 ℃ ($MoTe_2$)[268, 269] or 1000 ℃ (WTe_2).[270] Very recently, dual source precursor CVD using metal oxide (WO_3 or MoO_3), metal halides (WCl_6 or $MoCl_5$) and Te powder in 1:1:1 ratio were found to successfully deposit MTe_2 thin films at 700–800 ℃ which were identified *via* Raman spectroscopy.[267]

1.4 Thin film coating techniques

1.4.1 Different coating techniques

The most common approaches to coat thin films use sol-gel, Physical Vapour Deposition (PVD) and Chemical Vapour Deposition (CVD) techniques. The sol-gel dip coating method involves hydrolysing the precursors in aqueous or organic solvents to form the intermediate $[M(OR)_n]$ (M = desired metal; R = alkyl), which is called the 'gel'. The 'gel' is shaped to the required form and then is dried or heated to convert it to the desired materials.[271] PVD methods begin with a pure source of material, and involves vaporizing the material by heating under vacuum or by laser ablation before the vapour is deposited on the substrate.[272] This means PVD results in high purity film, but cannot be used to coat complex structures and requires high purity starting materials. In contrast, the CVD process involves one or more molecular sources which undergo chemical reactions in order to deposit the desired films on the substrate.[273]

Other deposition methods widely used in material science includes atomic layer deposition (ALD) and chemical vapour transportation (CVT). ALD is a technique to deposit thin films, grown later-by-layer, and usually required two steps. The first step is the first precursor forming a film, before using a second precursor to react with the first layer to grow the desired material.[274] In TMD material syntheses, the first coating of films tend to be metal oxides (*i.e.* MoO_3) while the second precursors are chalcogen sources (H_2S, S or Se).[239-262]

CVT is a crystal growth method for deposited metal dichalcogenides. The synthesis involves loading high purity metal and chalcogen into an ampoule with a transport agent, which is then heated in a furnace. After increasing the temperature, the bulk material vaporizes, and is then transported to the cold end and recrystallizes on the cold surface.[275]

1.4.2 Chemical Vapour Deposition

The deposition method used in this project is chemical vapour deposition (CVD). CVD is a thermally-driven technique that allows formation of a stable solid product, usually as a powder or thin film. Precursor compounds containing the relevant elements are decomposed in an activated (heat, light or plasma) environment. The products are formed under a homogeneous phase, such as vapour and/or heterogeneous phase and react on or near the heated surface.

The first CVD application was recorded in the 1860s by de Lodyguine, depositing tungsten on lamp filaments using WCl_5 and H_2 as precursors.[273, 276] Initially, CVD was developed for metal purification, extraction or refinement of elements such as titanium, nickel, zirconium and tantalum.[273] Exploration of CVD and investigations into the mechanisms involved did not begin until 1970s.[276] Today, CVD technology not only has potential in several modern technological areas such as aerospace and engineering, but is also suitable to form thin films for various coatings.[273]

The mechanism in a CVD reaction is complex. In general, dual source precursors are generated and moved as a vapour to the substrate area. The precursors are thought to 'preform' a compound which upon contact with the substrate, results in adsorption, surface diffusion, nucleation and growth of the desired material (Figure 1.25). Single source precursors have already 'preformed' a compound, so begin with contact to the substrate and deposition.[273, 276] The substrates used can vary from insulator (SiO_2) to semiconductor (Si) to metallic (TiN), depending on the desired use of the material.[273, 276]

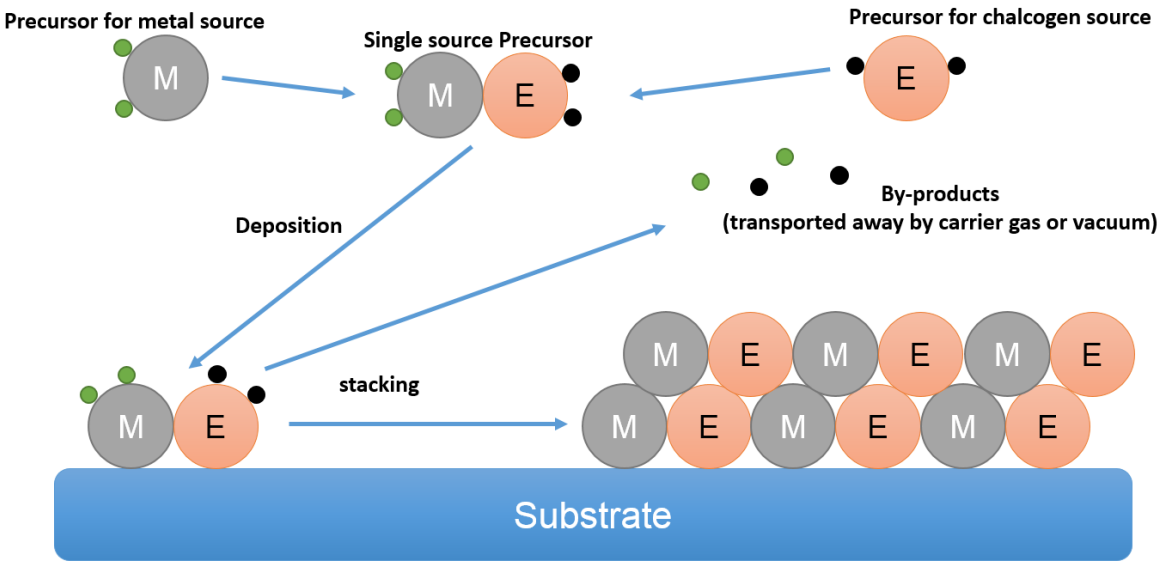

Figure 1.25 General schematic representation of the metal-organic CVD process.[273, 276]

The advantages for using CVD include the resulting high purity films and being able to deposit films onto any shape of surface, in addition to the uniform materials being coated in a single experiment. The CVD method is also easy to control and is readily reproducible, as well as being easily scalable to cover large surface areas.[273, 276] However, some of the starting materials (*i.e.* metal halides, H_2S *etc.*) are toxic, corrosive or flammable (pyrophoric).[273]

1.4.3 Different types of CVD methods

In general, specific types of CVD application are named from the energy source provided for the chemical reaction to occur. The most traditional CVD method is using thermal energy and is called Thermally Activated CVD (TACVD). Other methods, such as Plasma Enhanced CVD (PECVD) and Photo-Assisted CVD (PACVD), using plasma or light to activate the deposition, usually these have the advantage of requiring a lower deposition temperature. [273, 276] Aerosol Assisted CVD (AACVD) uses a solvent to help transport less-volatile precursors.[273, 276] While varying pressures can be used in TACVD, Ambient Pressure CVD (APCVD) application is done under ambient pressure, whereas Low-Pressure CVD (LPCVD) tends to use a working pressure at 0.01–1.33 kPa.[273, 276]

1.4.4 CVD precursor selection

As mentioned above, CVD applications can use dual source precursors, using two or more starting materials in the same time, or single source precursors, using only one compound in an application. Dual source precursors tend to be simple molecules such as metal halides, alkyls or hydrides, which have low molecular weight and hence are volatile. These simple molecules have easily breakable bonds, facilitating the chemical reaction required. Dual source precursors are usually commercially available and cheap. However, these compounds can also be toxic and/or pyrophoric.[273, 276]

Single source precursors ideally have a direct bond linking the target elements, while the alkyl groups in a single source precursor are often selected to enable β-hydride elimination in order to provide a low energy decomposition pathway.[15] The bond types between the desired elements for the thin films could include a covalent or coordination bond. This preformed intermolecular M–E bond means the energy required for CVD is typically reduced. A single source precursor requires many steps to make but ultimately tend to be less toxic or pyrophoric. It can be very challenging to make a single source precursor with all of the required properties. Transition metal halides are often air and moisture sensitive, as are their derivatives, while the ligands are often not commercially available, so can require syntheses. Therefore, the effective design of suitable single source precursor is of particular importance. [273, 276]

1.5 Characterisation techniques and sample preparations

1.5.1 Molecular characterisation

1.5.1.1 Infrared spectroscopy

Infrared (IR) spectroscopy is a very useful tool for the characterisation of new precursors, where the key vibrational bands lie in the 'fingerprint' region (1500–200 cm^{-1}). Generally, the absorption for ν(M–X) (M = metals; X = halides) of transition metal halide complexes also lie around this region (600 to 200 cm^{-1}).[70, 76, 97, 101, 102, 277-284] The position of the ν(M–X) bands can provide valuable information about the oxidation state of the metal centre, nature of the halides and geometry of these complexes *via* group theory.[70]

For example, the symmetry of $[MX_5L]$ (M = metals, X = halides, L = ligands) is C_{4v} and its IR spectrum exhibits three peaks contributed by M–X bands ($2A_1 + E$).[278, 283] The symmetry operation of *cis*-$[MX_4L_2]$ is C_{2v} and of *trans*-$[MX_4L_2]$ is D_{4h}; the M–X stretches number are four for C_{2v} ($2A_1 + B_1 + B_2$) or one for D_{4h} (E_u).[97, 101] Eight-coordinate complexes $[MX_4(L–L)_2]$ could be dodecahedral (D_{2d}: $B_2 + E$) or square antiprismic (D_2: $B_1 + B_2 + B_3$) but these are usually difficult to distinguish due to their structure being distorted from the ideal geometry.[102, 279-282] The number of absorptions can therefore indicate the point group and consequently the geometry of the complex. Table 1.1 lists a series M–X bands related to this project, where M is Nb, Ta or Mo; X is Cl or Br. The oxidation states are from +4 to +5.

Characteristic IR stretches of metal–oxides can indicate if highly sensitive compounds have undergone oxidation or hydrolysis by adventitious oxygen or water.[83, 285] IR spectroscopy can also identify certain ligands, for example, a band *ca.* 2290 cm^{-1} may be indicative of acetonitrile in the sample,[283, 284] whereas a band at *ca.* 550 cm^{-1} could be assigned as ν(Nb═S).[94]

Complexes with the same metal centre, ligands, coordination numbers and geometry but with different oxidation states can be distinguished from their IR spectra, as the absorptions are shifted to high wavenumber if the oxidation state of the metal is increased. Different halide analogues can also be identified, as higher frequency is consistent with a lighter halide atom.[70, 277, 278]

Table 1.1 Selected IR absorption ν(M–X) (cm^{-1}) related to this project alongside theoretical number of bands assigned

Complexes	**ν(M–X)**	**Complexes**	**ν(M–X)**
$[NbCl_5L]$[6, 76] L = *a, b, c*	400–330 (3 bands)	$[NbCl_4(L–L)]$[286, 287] L–L = *g*	340–290 (4 bands)
$[NbBr_5L]$[6] L = *b*	300–230 (3 bands)	$[NbSCl_3L_2]$[94] L = *h*	340–300 (3 bands)
cis-$[NbCl_4L_2]$[101, 103] L = *e* L = *f*	400–340 (4 bands) 370–288 (4 bands)	$[TaCl_5L]$[5, 76] L = *a, b, c*	400–300 (3 bands)
		$[TaBr_5L]$[5, 76] L = *c*	260–210 (3 bands)
$[NbCl_4(L–L)_2]$[102] L–L = *d*	310–260 (2 bands)	*trans*-$[MoCl_4L_2]$[288] L = *i*	350–310 (1 band)

a = SEt_2, S^nBu_2, *o*-$C_6H_4(CH_2SEt)_2$, Se^nBu_2, Te^nBu_2; *b* = *o*-$C_6H_4(CH_2SMe)_2$, *o*-$C_6H_4(CH_2SeMe)_2$, $MeSe(CH_2)_2SeMe$; *c* = SMe_2, $SeMe_2$ $TeMe_2$; *d* = $MeS(CH_2)_2SMe$; *e* = THT, SEt_2; *f* = 2,2'-bipyridine, $NCCH_3$, THF, $O(CH_2)_5$; *g* = $Ph_2P(CH_2)_nPPh_2$ (n = 1, 2, 3, 4, ,5 ,6),[286] $(P^tBu_3)_4$, $(PCy_3)_4$;[287] *h* = $NCCH_3$, $OPPh_3$; *i* = $NCCH_3$, bipyridine, PPh_3.[288]

1.5.1.2 UV-Visible spectroscopy

UV-visible spectroscopy is routinely used to collect information about the electronic transitions from the ground state to the excited state in the molecular orbitals from a complex. There are three major transitions which can be observed in UV-visible spectra, these are ligand–ligand transitions, metal–metal (d–d) transitions and charge transfer transitions.[289, 290]

Ligand–ligand transitions are the electronic transitions in the ligand's molecular orbitals, and usually occurs in organic ligands containing π-systems, such as aromatic groups or pyridine.[289, 290] Metal–metal transitions can be observed when transition metal complexes have partially filled *d*-orbitals, *i.e.* $Nb^{IV}Cl_4$ species. In an octahedral environment, the *d*-orbitals spilt into t_{2g} and e_g orbitals and the electronic transitions from t_{2g} to e_g, but this is usually weak in spectra due to this transition being forbidden by both the $g \rightarrow u$ and Laporte selection rules.[289, 290] In a distorted octahedral system with lower symmetry, the *d–d* orbitals separate into a more complex model and the energy of each transition is affected by the surrounding ligands.[289, 290] Charge transfer bands represent the metal to ligand or ligand to metal transitions, which are observed in second or third row transition metal complexes. Charge transfer transitions tend to be much stronger than *d–d* or ligand–ligand transitions due to charge transfer transitions being allowed transitions.[289, 290]

In this work, there are no ligand–ligand transitions due to the selected ligands not containing π-systems. There are no free electrons in *d*-orbitals when the transition metal is in its highest oxidation

state, such as in $NbCl_5$, $NbBr_5$, $TaCl_5$, $TaBr_5$ and $NbSCl_3$ species, so *d*–*d* transitions are not observed in UV-visible spectra. The d^1 $NbCl_4$ complexes are reported to be eight coordinate or six coordinate complexes and have been studied for many years, but with limited assignment of the electronic spectra.[97, 102, 103, 291-293] The d^2 distorted octahedral $MoCl_4$ systems have also been studied and their electronic transitions were found to be at *ca*. 20 000 and. 25 000 cm^{-1} and assigned as $^3T_{1g} \rightarrow {}^3T_{2g}$ and $^3T_{1g} \rightarrow {}^3T_{1g}(P)$, respectively.[288, 289, 294] These metal centres are in their high oxidation and therefore it is very difficult to observe metal to ligand charge transfer bands. The ligands in these complexes are soft neutral ligands, σ donors and/or π-donors, and therefore the ligand to metal transitions are described as $L(\sigma) \rightarrow M$ or $L(\pi) \rightarrow M$.[289, 290] This work aims to use UV-visible spectra to characterise the complexes by comparison to these literature values, rather than to explore the theoretical molecular orbital structure.

1.5.1.3 Nuclear Magnetic Resonance spectroscopy

Nuclear magnetic resonance (NMR) is a powerful technique that can be used to provide important insights into M–E interactions. However, ligand dissociation in solution can occur during an experiment and resulting in fast exchange in solution. The properties of NMR active-nuclei relevant to this work are found in Table 1.2.[295] A nucleus with a spin > 1/2 has a quadrupole moment (Q) and lower symmetry. This makes the NMR signals broader than those of spin = 1/2 nuclei due to quadrupolar relaxation.[295]

A common use for ^1H NMR spectroscopy at room temperature in the present work is to observe the difference in frequency of free ligand relative to coordinated ligand. ^1H NMR spectra taken at low temperature (253 K or 183 K) can allow observation of *DL* and *meso* isomers present in solution in dithioether complexes and allows the confirmation of any ligand dissociation mentioned previously.[3, 296] Multinuclear NMR spectra ($^{31}P\{^1H\}$ and $^{77}Se\{^1H\}$) are also used to indicate the presence of free or coordinated ligands where these additional nuclei are present. The coordination chemical shift expressed as the difference in the shift between coordinated ligands and free ligands have been studied in detail.[297]

Table 1.2 Nuclear properties of the metals and donor atoms relevant to this work

Nucleus	**Spin**	**Abundance (%)**	**MHz**	**Q (10^{-28} m^2)**
^1H	**1/2**	**100**	**100**	**–**
^{13}C	**1/2**	**1.11**	**25.15**	**–**
^{31}P	**1/2**	**100**	**40.48**	**–**
^{77}Se	**1/2**	**7.58**	**19.07**	**–**
^{93}Nb	**9/2**	**100**	**24.55**	**-0.32**
^{95}Mo	**5/2**	**15.72**	**6.547**	**-0.015**

^{93}Nb NMR spectra has been widely studied together with Nb chemistry in its oxidation state +5.[295] The external reference of ^{93}Nb NMR is $[Et_4N][NbCl_6]$ in CH_3CN ($\delta = 0$ ppm); previous to this, spectra were referenced to $NbOCl_4^-$. The ^{93}Nb NMR resonances corresponding to this project are listed in Table 1.3, alongside the solvent used. In general, the ^{93}Nb NMR resonances in $[NbCl_5L]$ species (169–80 ppm) are lower in frequency than those of $[NbBr_5L]$ (775–722 ppm) or $[NbSCl_3L_2]$ (400 ppm), which indicates $NbCl_5$ is a stronger Lewis acid than $NbSCl_3$ or $NbBr_5$.[33] This literature data is based on highly symmetric Nb complexes, whereas Nb complexes with lower symmetry are more challenging to obtain ^{93}Nb NMR spectra, due to ^{93}Nb's highly quadrupolar nature. ^{95}Mo NMR spectroscopy has not been used in this work because they are molybdenum (IV) complexes and therefore they are paramagnetic.

Table 1.3 Selected ^{93}Nb NMR resonances (ppm) from Nb(V) systems

Complexes	**^{93}Nb**	**Solvents**	**Complexes**	**^{93}Nb**	**Solvents**
$[NbCl_6]^-$ [298]	0	CD_3CN	$[NbSCl_4]^-$ [299]	499	CD_3CN
$[NbCl_5L]$[6, 76] L = *a*, *b*, *c*	169–80 (L = *a*, *b*) 49 (L = *c*)	CD_2Cl_2 CD_3CN (L = *c*)	$[NbSCl_3L_2]$[299] L = *c*	400	CD_3CN
$[NbBr_6]^-$ [298]	731	CD_3CN	$[NbSeCl_4]^-$ [299]	970	CD_3CN
$[NbBr_5L]$[6] L = *b*, *c*	775–722 640 (L = *c*)	CD_2Cl_2 CD_3CN (L = *c*)	$[NbSeCl_3L_2]$[299] L = *c*	845	CD_3CN
$[NbOCl_4]^-$ [300]	460	CD_3CN			
$[NbOCl_3L_2]$[298, 300] L = *c*	483	CD_3CN			

a = SMe_2, SEt_2, S^nBu_2, *o*-$C_6H_4(CH_2SEt)_2$, $SeMe_2$, Se^nBu_2, $TeMe_2$, Te^nBu_2; *b* = *o*-$C_6H_4(CH_2SMe)_2$, *o*-$C_6H_4(CH_2SeMe)_2$, $MeSe(CH_2)_2SeMe$; *c* = CH_3CN.

The NMR spectroscopy of paramagnetic systems usually results in line broadening, the chemical shifts vary greatly and is sometimes offset by the spectral expansion. The changes in nuclear shielding arising from the interaction with unpaired electron spin density are called paramagnetic shifts or Knight shifts. These are observed for nuclei in a paramagnetic molecule such as a ligand coordinated to a metal ion.[295, 301]

1.5.1.4 Thermogravimetric Analysis

Thermogravimetric analysis (TGA) is a characterisation method which records the weight of the sample at increasing or decreasing temperature. This analysis of the weight usually represented as weight percentage, can help to work out the proposed intermediate in each weight loss step. The identification of the proposed intermediate in each weight loss step will require additional techniques, such as TGA/MS, TGA/FTIR, differential thermal analysis and differential scanning calorimetry.[302]

TGA also provides the temperature when the thermal decomposition begins and ends. This is useful for a CVD precursor research, because it provides the ideal heating temperature for CVD at ambient pressure (TGA experiments are usually undertaken at ambient pressure).[15, 303, 304] In a low-pressure CVD application, it is expected that the thermal evaporation/deposition temperature is lower than at ambient pressure. Hence, an estimated range of temperatures can be tested in LPCVD, based on the precursor's TGA data.

1.5.1.5 Single Crystal X-ray Diffraction

Single crystal XRD is a very useful technique in coordination chemistry, although it does require the growth of high quality single crystals. Common techniques of crystallisation include solvent evaporation, cooling, solvent diffusion *etc*.[305]

When an X-ray beam is directed at a crystal consisting of a regular array of atoms, a pattern of reflection can be recorded. The patterns are dependent on the orientation of the crystal and the direction of the beam. A single crystal X-ray diffraction experiment will collect all the reflection patterns by rotating the orientation of the crystal sample and the beam direction.[290] After collecting the diffraction pattern, the software integrates the signals in each pattern and constructs the electron density map. Then, another program is used to simulate the electronic density map based on the elements present as well as their relative position and compares this to the experimental data. After repeating refinements the simulated and experimental data, the final structure of the molecule in the single crystal is given.[290]

A solid state X-ray structure provides evidence of the geometry of the compound, and the presence of any isomers in the sample such as *cis*- or *trans*-isomers in $[MX_4L_2]$ species and *DL*- or *meso*-isomers for species containing chelating ligands, as long as the isomers are present in the single crystal lattice. The eight-coordinate geometries, dodecahedron and square antiprism, can also identified from single crystal X-ray structures. Distances calculated from X-ray data provide information about the oxidation of metal centre by comparing d(M–X) or d(M–M).

1.5.1.6 Powder X-ray Diffraction

Powder X-ray Diffraction (PXRD) collects 1D X-ray data, in contrast to single crystal X-ray diffraction, which produces a series of 2D X-ray patterns to build 3D electronic density maps. Powder X-ray Diffraction is used to identify samples of crystalline compounds such as metal halide starting materials, and to determine their purity. The analysis of the diffraction data usually involves comparison to standard PXRD patterns (for compounds already reported with their crystal information file in a database) and Rietveld refinement.

1.5.2 Materials characterisation

1.5.2.1 Grazing Incidence X-ray Diffraction

While the angle of the X-ray beam changes in a typical PXRD experiment, grazing incidence XRD (GIXRD) uses a very low fixed incident angle (1° or lower) to reduce the X-ray scattering (diffraction) from substrates when examining thin films. During a GIXRD experiment, only the detector moves across the sample at an angle of 2θ (Figure 1.26).[306]

The data analysis for PXRD and GIXRD follows a similar process. The thin film samples usually have a preferred orientation, which means there are inconsistent intensities of each peaks when comparing to a bulk PXRD pattern. Therefore, the diffraction pattern profile fitting refinement for thin film XRD data often uses Le Bail fitting. Rietveld refinement uses the structure factor to calculate the intensity of the profiles in refinements so it cannot easily recognise the intensities that are an effect of the preferred orientation. Le Bail fitting uses arbitrary values of the intensity for fitting the diffraction XRD pattern. Although Le Bail fitting results in the loss of information on atom position, it is an effective refining method for thin film samples to obtain lattice parameters.[307]

1.5.2.2 In-plane X-ray Diffraction

The XRD reflections from the substrate seen in GIXRD due to ultra-thin films can be avoided in in-plane XRD by offsetting the angle of the detector by 2θχ.[306] This means that in-plane XRD only collects the scattered diffraction rather than the direct diffraction, making the signal strength much weaker than in grazing incidence XRD (Figure 1.26). In-plane XRD gives a diffraction pattern from 2θχ to compare with the preferred orientation.

1.5.2.3 X-ray Pole Figures

X-ray pole-figure experiment moves the sample surface α angle and the β angle (ϕ rotation angle around sample surface normal direction, Figure 1.26).[308] A series of data across α = 0° to 90° is collected to give the information for the crystalline films to confirm the material stacking sequence by measuring the angle between the selected angle 2θ corresponding to the orientation plane. Pole Figure XRD is mainly used to explore the crystal packing sequences of the thin films and compare with the single crystal structure in order to confirm the material's packing sequence.

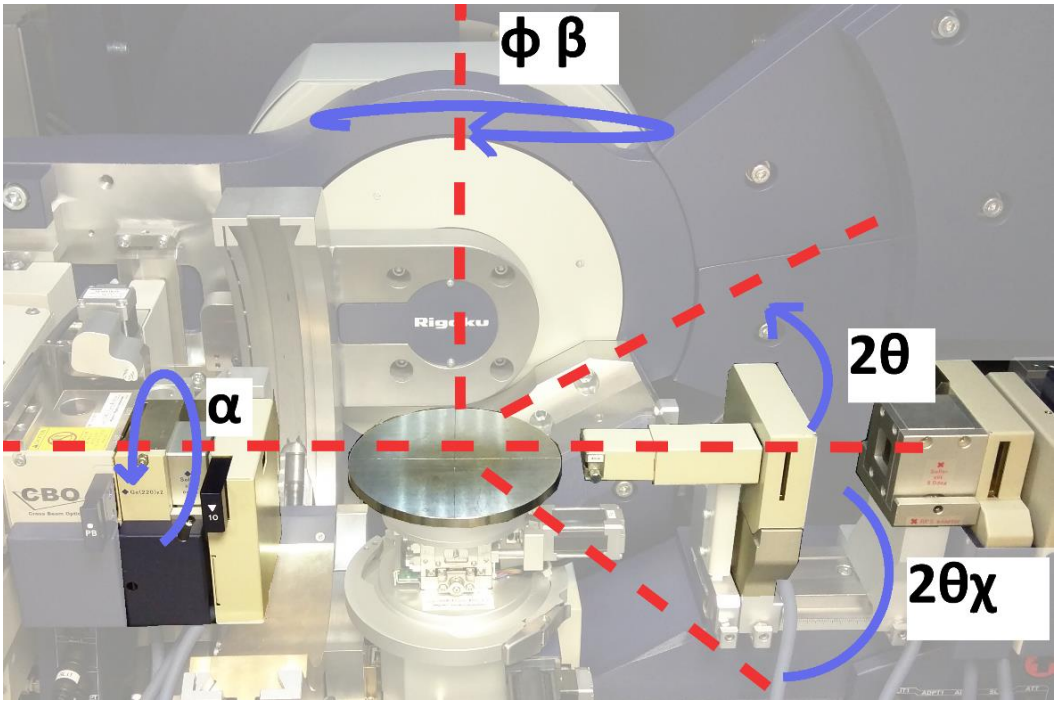

Figure 1.26 Detector movement in a Smartlab X-ray diffractometer. Detector moves 2θ for a grazing incidence XRD experiment and 2θχ for an in-plane XRD measurement. Sample position(β) and the sample/detector(α) rotate during pole figure XRD experiments.

1.5.2.4 Raman Spectroscopy

The theory of Raman spectroscopy is very similar to that of IR spectroscopy. Both techniques are used to observe vibrational modes in a system. The main difference between IR and Raman is that Raman spectra are scattering spectra; in contrast, IR spectra are absorption spectra.

In a Raman instrument, the detector is ideally set up at an angle (often 90°) to avoid picking up the signal directly from the beam source.[70, 302] It also uses excitation wavelengths which avoid generating fluorescence. Although the signal from Raman scattering is very weak, the advantage is that Raman scattering generally occur in the visible or near-IR region for which more sensitive detectors are available.[70, 302] Transition metal dichalcogenide materials, such as NbS_2, $NbSe_2$, MoS_2 and $MoSe_2$, have been widely studied in recent years using Raman spectroscopy, providing a useful database to identify different materials.[226, 233, 263, 309-312]

1.5.2.5 Scanning Electron Microscope

Scanning electron microscopy (SEM) uses a narrow focused beam of electrons to stimulate the surface of a sample. Some electrons are back-scattered by the atoms on the top of the surface. Others excite the electrons in inner shells of the atoms, called secondary electrons. Back-scattered and secondary electrons are the two principal signals detected in SEM and this data is transformed into images. These electrons are mainly emitted from the atoms near to the surface.[313] The material on

the surface should be metallic or conducting. If the sample is a semiconductor or insulator, only the X-ray generating area is charged. This causes the irregular release of electrons and reduces the clarity of the images.[313]

1.5.2.6 Energy-Dispersive X-ray Spectroscopy

When an electron beam strikes an element, electrons in the inner shell are excited to higher energy shells. This causes the electron to emit a quantum of radiation and relax back to a low energy shell. The energy emitted by an electron moving from the L shell to the K shell is called K_α, while the emission from the M shell to the L shell is called L_α.

Energy-dispersive X-ray spectroscopy (EDX) records the energies emitted, due to each element having unique K_α and L_α energies, the resulting information can be used to distinguish between different elements.[302, 313] EDX is a relatively quick material characterisation method, because it can scan the whole spectrum at once. Lighter elements (lighter than Na)[302, 313] can be identified, but are unquantifiable due to low fluorescence yield as well as their K absorption peaks overlapping with the L, M and N lines of heavier elements.[302, 313] EDX also struggles with two overlapping peaks. For example, the energy of Mo L_α (2.293 eV) is similar to the energy of S K_α (2.306 eV).[314]

The detector in wavelength-dispersive X-ray spectroscopy (WDX) collects the same signals as EDX. However, WDX is based on a similar theory to X-ray diffraction. A known crystal is placed on the detector. The collecting wavelength (λ) is determined using Bragg's Law ($n\lambda = 2d\ sin\theta$). Unlike EDX, which collects all signals at once, WDX scans each wavelength in turn. In addition, it can integrate the signals from each wavelength to give more accurate quantification of the elements present.[302, 313]

1.6 Project aim

Hard and Soft Lewis Acid and Base (HSAB) theory suggests that soft acids form stronger bonds with soft bases, while hard acids form stronger bands with hard bases. This project focuses on the coordination of soft neutral ligands such as thioether, selenoether, telluroether and diphosphine ligands, to hard metal halides such as NbX_4, NbX_5 (X = Cl, Br), $NbSCl_3$, $MoCl_4$. This combination of hard metals and soft ligands will explore the scope of HSAB theory. This work will involve developing the synthetic route for the starting materials and the resulting complexes. The characterisation of these compounds will include infrared, multinuclear NMR and UV-visible spectroscopies, single crystal and powder X-ray diffraction.

Similar complexes with hard metal halides and soft donors have been reported as potential single source LPCVD precursors. Recently, compounds of the type $[NbCl_5(E^nBu_2)]$ (E = S, Se) have been tested for their LPCVD properties as single source precursors and have been found to successfully deposit NbE_2 thin films.[76] Therefore, the second part of the project will aim to synthesise a range of suitable single source precursors based upon *n*-butyl containing ligands. This *n*-butyl group will allow the precursors to undergo facile β-hydride elimination allowing a low energy decomposition pathway to form ME_2 thin films. These single source precursors will be tested in LPCVD, and the resulting thin films identified *via* X-ray diffraction techniques (grazing incidence, in-plane and pole-figure), scanning electronic microscopy (SEM), energy-dispersive X-ray (EDX) and Raman spectroscopies.

1.7 References

1. W. Levason and G. Reid, *Comprehensive Coordination Chemistry II*, ed. J. A. McCleverty and T. J. Meyer, Elsevier, Oxford, 2003, **1**, 391.
2. Y.-P. Chang, W. Levason and G. Reid, *Dalton Trans.*, 2016, **45**, 18393.
3. S. L. Benjamin, Y.-P. Chang, M. Huggon, W. Levason and G. Reid, *Polyhedron*, 2015, **99**, 230.
4. R. Hart, W. Levason, B. Patel and G. Reid, *J. Chem. Soc., Dalton Trans.*, 2002, 3153.
5. S. L. Benjamin, A. Hyslop, W. Levason and G. Reid, *J. Fluorine Chem.*, 2012, **137**, 77.
6. M. Jura, W. Levason, R. Ratnani, G. Reid and M. Webster, *Dalton Trans.*, 2010, **39**, 883.
7. S. G. Murray and F. R. Hartley, *Chem. Rev.*, 1981, **81**, 365.
8. D. Parker, P. S. Roy, G. Ferguson and M. M. Hunt, *Inorg. Chim. Acta*, 1989, **155**, 227.
9. C. A. Gamelas, N. A. Bandeira, C. C. Pereira, M. J. Calhorda, E. Herdtweck, M. Machuqueiro, C. C. Romao and L. F. Veiros, *Dalton Trans.*, 2011, **40**, 10513.
10. M. T. Ashby and D. L. Lichtenberger, *Inorg. Chem.*, 1985, **24**, 636.
11. W. Levason, M. L. Matthews, R. Patel, G. Reid and M. Webster, *New J. Chem.*, 2003, **27**, 1784.
12. M. A. Watzky, D. Waknine, M. J. Heeg, J. F. Endicott and L. A. Ochrymowyzc, *Inorg. Chem.*, 1993, **32**, 4882.
13. A. J. Blake and M. Schröder, *Adv. Inorg. Chem.*, 1990, **35**, 1.
14. W. Levason and G. Reid, *Comprehensive Coordination Chemistry II*, ed. J. A. McCleverty and T. J. Meyer, Elsevier, Oxford, 2003, **1**, 399.
15. S. L. Benjamin, C. H. de Groot, C. Gurnani, A. L. Hector, R. Huang, K. Ignatyev, W. Levason, S. J. Pearce, F. Thomas and G. Reid, *Chem. Mater.*, 2013, **25**, 4719.
16. S. D. Reid, A. L. Hector, W. Levason, G. Reid, B. J. Waller and M. Webster, *Dalton Trans.*, 2007, 4769.
17. K. Travis and D. H. Busch, *Inorg. Chem.*, 1974, **13**, 2591.
18. F. R. Hartley, S. G. Murray, W. Levason, H. E. Soutter and C. A. McAuliffe, *Inorg. Chim. Acta*, 1979, **35**, 265.
19. K. Brodersen, W. Rölz, G. Jordan, R. Gerbeth and J. Ellermann, *Chem. Ber.*, 1978, **111**, 132.
20. R. Ali, S. J. Higgins and W. Levason, *Inorg. Chim. Acta*, 1984, **84**, 65.
21. W. Levason, C. A. McAuliffe and S. G. Murray, *Inorg. Chim. Acta*, 1976, **17**, 247.
22. W. Levason, M. Nirwan, R. Ratnani, G. Reid, N. Tsoureas and M. Webster, *Dalton Trans.*, 2007, 439.
23. D. J. Gulliver, E. G. Hope, W. Levason, S. G. Murray, D. M. Potter and G. L. Marshall, *J. Chem. Soc., Perkin Trans. II*, 1984, 429.
24. E. G. Hope, T. Kemmitt and W. Levason, *Organometallics*, 1988, **7**, 78.

25. K. George, C. H. de Groot, C. Gurnani, A. L. Hector, R. Huang, M. Jura, W. Levason and G. Reid, *Chem. Mater.*, 2013, **25**, 1829.

26. N. Kuhn, P. Faupel and E. Zauder, *J. Organomet. Chem.*, 1986, **302**, C4.

27. T. Kemmitt and W. Levason, *Organometallics*, 1989, **8**, 1303.

28. E. G. Hope, T. Kemmitt and W. Levason, *Organometallics*, 1987, **6**, 206.

29. E. W. Abel, K. Kite and P. S. Perkins, *Polyhedron*, 1986, **5**, 1459.

30. C. H. W. Jones and R. D. Sharma, *Organometallics*, 1986, **5**, 805.

31. K. G. K. De Silva, Z. Monsef-Mirzai and W. R. McWhinnie, *J. Chem. Soc., Dalton Trans.*, 1983, 2143.

32. N. Petragnani and V. G. Toscano, *Chem. Ber.*, 1970, **103**, 1652.

33. G. L. Miessler, P. J. Fischer and D. A. Tarr, *Inorganic Chemistry* Pearson, London, 2014.

34. J. Connolly, A. R. J. Genge, W. Levason, S. D. Orchard, S. J. A. Pope and G. Reid, *J. Chem. Soc., Dalton Trans.*, 1999, 2343.

35. W. Levason, S. D. Orchard and G. Reid, *Organometallics*, 1999, **18**, 1275.

36. H. Schumann, A. M. Arif, A. L. Rheingold, C. Janiak, R. Hoffmann and N. Kuhn, *Inorg. Chem.*, 1991, **30**, 1618.

37. H. B. Kraatz, H. Jacobsen, T. Ziegler and P. M. Boorman, *Organometallics*, 1993, **12**, 76.

38. W. Levason, S. D. Orchard, G. Reid and J. M. Street, *J. Chem. Soc., Dalton Trans.*, 2000, 2537.

39. C. S. Tredget, F. Bonnet, A. R. Cowley and P. Mountford, *Chem. Commun.*, 2005, 3301.

40. C. S. Tredget, E. Clot and P. Mountford, *Organometallics*, 2008, **27**, 3458.

41. M. D. Brown, W. Levason, D. C. Murray, M. C. Popham, G. Reid and M. Webster, *Dalton Trans.*, 2003, 857.

42. M. J. D. Champion, P. Farina, W. Levason and G. Reid, *Dalton Trans.*, 2013, **42**, 13179.

43. E. G. Hope and W. Levason, *Coord. Chem. Rev.*, 1993, 109.

44. T. S. Lewkebandara, P. J. McKarns, B. S. Haggerty, G. P. A. Yap, A. L. Rheingold and C. H. Winter, *Polyhedron*, 1998, **17**, 1.

45. E. Turin, R. M. Nielson and A. E. Merbach, *Inorg. Chim. Acta*, 1987, **134**, 79.

46. K. Baker and G. W. A. Fowles, *J. Less-Common. Met.*, 1965, **8**, 47.

47. W. Levason, B. Patel, G. Reid, V. A. Tolhurst and M. Webster, *J. Chem. Soc., Dalton Trans.*, 2000, 3001.

48. R. Hart, W. Levason, B. Patel and G. Reid, *Eur. J. Inorg. Chem.*, 2001, 2927.

49. W. Levason, B. Patel and G. Reid, *Inorg. Chim. Acta*, 2004, **357**, 2115.

50. G. R. Willey, J. Palin, M. T. Lakin and N. W. Alcock, *Transition Met. Chem.*, 1994, **19**, 187.

51. M. Schormann, *Acta Cryst.*, 2003, **E59**, m674.

52. G. W. A. Fowles, T. E. Lester and R. A. Walton, *J. Chem. Soc. (A)*, 1968, 198.

53. R. N. Pandey, R. K. Singh and K. Shahi, *Asian J. Chem.*, 2011, **23**, 2739.

54. C. D. Beard, R. J. Barrie, J. Evans, W. Levason, G. Reid and M. D. Spicer, *Eur. J. Inorg. Chem.*, 2006, 4391.

55. A. L. Hector, W. Levason, A. J. Middleton, G. Reid and M. Webster, *Eur. J. Inorg. Chem.*, 2007, 3655.

56. M. F. Davis, W. Levason, J. Paterson, G. Reid and M. Webster, *Eur. J. Inorg. Chem.*, 2008, 802.

57. A. L. Hector, M. Jura, W. Levason, S. D. Reid and G. Reid, *New J. Chem.*, 2009, **33**, 641.

58. M. Matsuura, T. Fujihara and A. Nagasawa, *Acta Cryst.*, 2013, **E69**, m209.

59. G. R. Willey, M. T. Lakin and N. W. Alcock, *J. Chem. Soc., Chem. Commun.*, 1991, 1414.

60. M. C. Durrant, S. C. Davies, D. L. Hughes, C. Le Floc'h, R. L. Richards, J. R. Sanders, N. R. Champness, S. J. Pope and G. Reid, *Inorg. Chim. Acta*, 1996, **251**, 13.

61. S. C. Davies, M. C. Durrant, D. L. Hughes, C. Le Floc'h, S. J. A. Pope, G. Reid, R. L. Richards and J. R. Sanders, *J. Chem. Soc., Dalton Trans.*, 1998, 2191.

62. M. C. Cornock and T. A. Stephenson, *J. Chem. Soc., Dalton Trans.*, 1977, 501.

63. Y.-P. Chang, L. Furness, W. Levason, G. Reid and W. Zhang, *J. Fluorine Chem.*, 2016, **191**, 149.

64. M. W. Duckworth, G. W. A. Fowles and P. T. Greene, *J. Chem. Soc. (A)*, 1967, 1592.

65. J. S. Wood, *Inorg. Chem.*, 1968, **7**, 852.

66. D. Rehder, H. Nekola, A. Behrens, S. P. Cramer and T. Funk, *Z. Anorg. Allg. Chem.*, 2013, **639**, 1401.

67. C. D. Beard, L. Carr, M. F. Davis, J. Evans, W. Levason, L. D. Norman, G. Reid and M. Webster, *Eur. J. Inorg. Chem.*, 2006, 4399.

68. D. Rehder, H. Nekola, A. Behrens, S. P. Cramer and T. Funk, *Z. Anorg. Allg. Chem.*, 2013, **639**, 1401.

69. G. J. Grant, K. E. Rogers, W. N. Setzer and D. G. VanDerveer, *Inorg. Chim. Acta*, 1995, **234**, 35.

70. K. Nakamoto, *Infrared and Raman Spectra of Inorganic and Coordination Compounds*, Wiley, New York, 1986.

71. R. D. Werder, *J. Chem. Phys.*, 1967, **47**, 4159.

72. F. Marchetti, G. Pampaloni and S. Zacchini, *J. Fluorine Chem.*, 2010, **131**, 21.

73. M. Jura, W. Levason, G. Reid and M. Webster, *Dalton Trans.*, 2009, 7610.

74. F. Fairbrother, K. H. Grundy and A. Thompson, *J. Chem. Soc.*, 1965, 765.

75. F. Fairbrother and J. F. Nixon, *J. Chem. Soc.*, 1962, 150.

76. S. L. Benjamin, Y.-P. Chang, C. Gurnani, A. L. Hector, M. Huggon, W. Levason and G. Reid, *Dalton Trans.*, 2014, **43**, 16640.

77. R. E. DeSimone and T. M. Tighe, *J. Inorg. Nucl. Chem.*, 1976, **38**, 1623.

78. R. E. DeSimone and M. D. Glick, *J. Coord. Chem.*, 1976, **5**, 181.

79. R. E. DeSimone and M. D. Glick, *J. Am. Chem. Soc.*, 1975, **97**, 942.

80. S. R. Wade and G. R. Willey, *Inorg. Chim. Acta*, 1983, **72**, 201.

81. J. D. Wilkins, *J. Inorg. Nucl. Chem.*, 1975, **37**, 2095.

82. G. W. A. Fowles, D. A. Rice and J. D. Wilkins, *J. Chem. Soc., Dalton Trans.*, 1973, 961.

83. W. Levason, G. Reid, J. Trayer and W. Zhang, *Dalton Trans.*, 2014, **43**, 3649.

84. Y.-P. Chang, W. Levason, M. E. Light and G. Reid, *Dalton Trans.*, 2016, **45**, 16262.

85. S. L. Benjamin, A. Hyslop, W. Levason and M. Webster, *Acta Cryst.*, 2011, **C67**, m221.

86. M. G. B. Drew, D. A. Rice and D. M. Williams, *Acta Cryst.*, 1984, **C40**, 1547.

87. M. G. B. Drew, D. A. Rice and D. M. Williams, *J. Chem. Soc., Dalton Trans.*, 1983, 2251.

88. M. G. B. Drew, D. A. Rice and D. M. Williams, *J. Chem. Soc., Dalton Trans.*, 1984, 1087.

89. M. G. B. Drew, D. A. Rice and D. M. Williams, *J. Chem. Soc., Dalton Trans.*, 1984, 845.

90. M. G. B. Drew, D. A. Rice and D. M. Williams, *J. Chem. Soc., Dalton Trans.*, 1985, 417.

91. M. G. B. Drew and R. J. Hobson, *Inorg. Chim. Acta*, 1983, **72**, 233.

92. M. G. B. Drew, G. W. A. Fowles and R. J. R. Hobson, D. A., *Inorg. Chim. Acta*, 1976, **20**, L35.

93. G. W. A. Fowles, R. J. Hobson, D. A. Rice and K. J. Shanton, *J. Chem. Soc., Chem. Commun.*, 1976, **14**, 552.

94. K. Behzadi, A. O. Baghlaf and A. Thompson, *J. Less-Common. Met.*, 1987, **128**, 195.

95. V. C. Gibson, T. P. Kee and A. Shaw, *Polyhedron*, 1990, **9**, 2293.

96. V. C. Gibson, A. Shaw and D. N. Williams, *Polyhedron*, 1989, **8**, 549.

97. G. W. A. Fowles, D. J. Tidmarsh and R. A. Walton, *Inorg. Chem.*, 1969, **8**, 631.

98. F. A. Cotton, S. A. Duraj and W. J. Roth, *Inorg. Chem.*, 1984, **23**, 4046.

99. F. A. Cotton, L. R. Falvello and R. C. Najjar, *Inorg. Chem.*, 1983, **22**, 770.

100. R. E. McCarley and B. A. Torp, *Inorg. Chem.*, 1963, **2**, 540.

101. J. B. Hamilton and R. E. McCarley, *Inorg. Chem.*, 1970, **9**, 1333.

102. J. B. Hamilton and R. E. McCarley, *Inorg. Chem.*, 1970, **9**, 1339.

103. G. W. A. Fowles, D. J. Tidmarsh and R. A. Walton, *J. Inorg. Nucl. Chem.*, 1969, **31**, 2373.

104. J. A. M. Canich and F. A. Cotton, *Inorg. Chem.*, 1987, **26**, 3473.

105. E. Babaian-Kibala, F. A. Cotton and P. A. Kibala, *Inorg. Chem.*, 1990, **29**, 4002.

106. F. A. Cotton and R. C. Najjar, *Inorg. Chem.*, 1981, **20**, 2716.

107. R. J. H. Clark and G. Natile, *Inorg. Chim. Acta*, 1970, **4**, 533.

108. J. Hughes and G. R. Willey, *Inorg. Chim. Acta*, 1974, **11**, L25.

109. S. J. A. Pope, N. R. Champness and G. Reid, *J. Chem. Soc., Dalton Trans.*, 1997, 1639.

110. L. R. Gray, A. L. Hale, W. Levason, F. P. McCullough and M. Webster, *J. Chem. Soc., Dalton Trans.*, 1984, 47.

111. J. O. Moulin, J. Evans, D. S. McGuinness, G. Reid, A. J. Rucklidge, R. P. Tooze and M. Tromp, *Dalton Trans.*, 2008, 1177.

112. W. Levason, J. M. Manning, G. Reid, M. Tuggey and M. Webster, *Dalton Trans.*, 2009, 4569.

113. W. Levason, G. Reid and S. M. Smith, *Polyhedron*, 1997, **16**, 4253.

114. H.-J. Küppers and K. Wieghardt, *Polyhedron*, 1989, **8**, 1770.

115. A. L. Hale and W. Levason, *J. Chem. Soc., Dalton Trans.*, 1983, **12**, 2569.

116. F. Tamadon and K. Seppelt, *Angew. Chem. Int. Ed.*, 2013, **52**, 767.

117. P. M. Boorman, M. Islip, M. M. Reimer and K. J. Reimer, *J. Chem. Soc., Dalton Trans.*, 1972, 890.

118. P. M. Boorman, T. Chivers and K. N. Mahedev, *Can. J. Chem.*, 1975, **53**, 383.

119. G. A. W. Fowles, D. A. Rice and K. J. Shanton, *J. Chem. Soc., Dalton Trans.*, 1978, 1658.

120. D. Britnell, M. G. B. Drew, G. W. A. Fowles and D. A. Rice, *Inorg. Nucl. Chem. Letters*, 1973, **9**, 501.

121. M. D. Brown, M. B. Hursthouse, W. Levason, R. Ratnani and G. Reid, *Dalton Trans.*, 2004, 2487.

122. M. F. Davis, W. Levason, M. E. Light, R. Ratnani, G. Reid, K. Saraswat and M. Webster, *Eur. J. Inorg. Chem.*, 2007, 1903.

123. J. R. Dilworth and R. L. Richards, *Inorg. Synth.*, 1990, **28**, 33.

124. E. L. McCann III and T. M. Brown, *Inorg. Synth.*, 1970, **12**, 181.

125. K. Feenan and G. W. A. Fowles, *Inorg. Chem.*, 1965, **4**, 310.

126. C. A. McAuliffe and B. J. Sayle, *Inorg. Chim. Acta*, 1978, **30**, 35.

127. P. C. Crouch, G. W. A. Fowles, P. R. Marshall and R. A. Walton, *J. Chem. Soc. (A)*, 1968, 1634.

128. W. Levason, C. A. McAuliffe, F. P. McCullough, S. G. Murray and C. A. Rice, *Inorg. Chim. Acta*, 1977, **22**, 227.

129. M. G. B. Drew, G. F. Griffin and D. A. Rice, *Inorg. Chim. Acta*, 1979, **34**, L192.

130. P. Dierkes, G. Frenzen, S. Wocadlo, W. Massa, S. Berger, J. Pebler and K. Dehnicke, *Z. Naturforsch., B: Chem. Sci.*, 1995, **50**, 159.

131. L. Favero, F. Marchetti, G. Pampaloni and S. Zacchini, *Dalton Trans.*, 2014, **43**, 495.

132. K. J. Moynihan, X. Gao, P. M. Boorman, J. F. Fait, G. K. W. Freeman, P. Thornton and D. J. Ironmonger, *Inorg. Chem.*, 1990, **29**, 1648.

133. S. A. Bartlett, P. P. Wells, M. Nachtegaal, A. J. Dent, G. Cibin, G. Reid, J. Evans and M. Tromp, *J. Catal.*, 2011, **284**, 247.

134. R. Mas-Balleste, C. Gomez-Navarro, J. Gomez-Herrero and F. Zamora, *Nanoscale*, 2011, **3**, 20.

135. M. Xu, T. Liang, M. Shi and H. Chen, *Chem. Rev.*, 2013, **113**, 3766.

136. H. W. Kroto, J. R. Heath, S. C. O'Brien, R. F. Curl and R. E. Smalley, *Nature*, 1985, **318**, 162.

137. S. Iijima, *Nature*, 1991, **354**, 56.

138. K. S. Novoselov, A. K. Geim, S. V. Morozov, D. Jiang, Y. Zhang, S. V. Dubonos, I. V. Grigorieva and A. A. Firsov, *Science*, 2004, **306**, 666.

139. F. Wang, Y. Zhang, C. Tian, C. Girit, A. Zettl, M. Crommie and Y. R. Shen, *Science*, 2008, **320**, 206.

140. R. R. Nair, P. Blake, A. N. Grigorenko, K. S. Novoselov, T. J. Booth, T. Stauber, N. M. Peres and A. K. Geim, *Science*, 2008, **320**, 1308.

141. X. Wang, L. Zhi and K. Mullen, *Nano Lett.*, 2008, **8**, 323.

142. G. Eda, G. Fanchini and M. Chhowalla, *Nat. Nanotechnol.*, 2008, **3**, 270.

143. Y. M. Lin, C. Dimitrakopoulos, K. A. Jenkins, D. B. Farmer, H. Y. Chiu, A. Grill and P. Avouris, *Science*, 2010, **327**, 662.

144. M. Liu, X. Yin, E. Ulin-Avila, B. Geng, T. Zentgraf, L. Ju, F. Wang and X. Zhang, *Nature*, 2011, **474**, 64.

145. K. S. Kim, Y. Zhao, H. Jang, S. Y. Lee, J. M. Kim, K. S. Kim, J. H. Ahn, P. Kim, J. Y. Choi and B. H. Hong, *Nature*, 2009, **457**, 706.

146. Y. Zhu, S. Murali, M. D. Stoller, K. J. Ganesh, W. Cai, P. J. Ferreira, A. Pirkle, R. M. Wallace, K. A. Cychosz, M. Thommes, D. Su, E. A. Stach and R. S. Ruoff, *Science*, 2011, **332**, 1537.

147. M. F. El-Kady, V. Strong, S. Dubin and R. B. Kaner, *Science*, 2012, **335**, 1326.

148. X. Yang, M. Xu, W. Qiu, X. Chen, M. Deng, J. Zhang, H. Iwai, E. Watanabe and H. Chen, *J. Mater. Chem.*, 2011, **21**, 8096.

149. A. K. Geim and K. S. Novoselov, *Nat. Mater.*, 2007, **6**, 183.

150. K. Kim, J. Y. Choi, T. Kim, S. H. Cho and H. J. Chung, *Nature*, 2011, **479**, 338.

151. Q. H. Wang, K. Kalantar-Zadeh, A. Kis, J. N. Coleman and M. S. Strano, *Nat. Nanotechnol.*, 2012, **7**, 699.

152. M. Chhowalla, H. S. Shin, G. Eda, L. J. Li, K. P. Loh and H. Zhang, *Nat. Chem.*, 2013, **5**, 263.

153. T. Heine, *Acc. Chem. Res.*, 2015, **48**, 65.

154. A. Niazi and A. K. Rastogi, *J. Phys.: Condens. Matter*, 2001, **13**, 6786.

155. M. B. Alemayehu, M. Falmbigl, K. Ta and D. C. Johnson, *Chem. Mater.*, 2015, **27**, 2158.

156. C. J. Carmalt, T. D. Manning, I. P. Parkin, E. S. Peters and A. L. Hector, *J. Mater. Chem.*, 2004, **14**, 290.

157. B. Morosin, *Acta Cryst.*, 1974, **B30**, 551.

158. M. Bernardi, C. Ataca, M. Palummo and J. C. Grossman, *Nanophotonics*, 2017, **6**, 111.

159. F. A. Rasmussen and K. S. Thygesen, *J. Phys. Chem. C*, 2015, **119**, 13169.

160. G. Zhang and Y.-W. Zhang, *J. Mater. Chem. C*, 2017, **5**, 7684.

161. T. Shishidou, A. J. Freeman and R. Asahi, *Phys. Rev. B*, 2001, **64**, 180401.

162. K. Takada, H. Sakurai, E. Takayama-Muromachi, F. Izumi, R. A. Dilanian and T. Sasaki, *Nature*, 2003, **422**, 53.

163. R. L. Withers and J. A. Wilson, *J. Phys. C Solid. State Physi.*, 1986, **19**, 4809.

164. C. Lee, Q. Li, W. Kalb, X. Z. Liu, H. Berger, R. W. Carpick and J. Hone, *Science*, 2010, **328**, 76.

165. A. B. Laursen, S. Kegnaes, S. Dahl and I. Chorkendorff, *Energy Environ. Sci.*, 2012, **5**, 5577.

166. J. Puthussery, S. Seefeld, N. Berry, M. Gibbs and M. Law, *J. Am. Chem. Soc.*, 2011, **133**, 716.

167. J. Feng, X. Sun, C. Wu, L. Peng, C. Lin, S. Hu, J. Yang and Y. Xie, *J. Am. Chem. Soc.*, 2011, **133**, 17832.

168. S. Ding, D. Zhang, J. S. Chen and X. W. Lou, *Nanoscale*, 2012, **4**, 95.

169. J. Liu and X.-W. Liu, *Adv. Mater.*, 2012, **24**, 4097.

170. Q. Xiang, J. Yu and M. Jaroniec, *J. Am. Chem. Soc.*, 2012, **134**, 6575.

171. I. Roger, M. A. Shipman and M. D. Symes, *Nature Reviews Chemistry*, 2017, **1**, 0003.

172. J. Pu, Y. Yomogida, K.-K. Liu, L.-J. Li, Y. Iwasa and T. Takenobu, *Nano. Lett.*, 2012, **12**, 4013.

173. K. Lee, R. Gatensby, N. McEvoy, T. Hallam and G. S. Duesberg, *Adv. Mater.*, 2013, **25**, 6699.

174. F. S. Dovell and H. Greenfield, *J. Org. Chem.*, 1964, **29**, 1265.

175. P. B. Perry, *Phys. Rev. B*, 1976, **13**, 5211.

176. K. Kanehori, *J. Electrochem. Soc.*, 1989, **136**, 1265.

177. M. S. Whittingham, *Chem. Rev.*, 2004, **104**, 4271.

178. J. E. Trevey, C. R. Stoldt and S. H. Lee, *J. Electrochem. Soc.*, 2011, **158**, A1282.

179. R. C. Bill, *Wear*, 1985, **106**, 283.

180. E. S. Peters, C. J. Carmalt and I. P. Parkin, *J. Mater. Chem.*, 2004, **14**, 3474.

181. J. Wang, H. Zheng, G. Xu, L. Sun, D. Hu, Z. Lu, L. Liu, J. Zheng, C. Tao and L. Jiao, *J. Am. Chem. Soc.*, 2016, **138**, 16216.

182. D. L. Duong, G. Ryu, A. Hoyer, C. Lin, M. Burghard and K. Kern, *ACS Nano*, 2017, **11**, 1034.

183. E. Morosan, H. W. Zandbergen, B. S. Dennis, J. W. G. Bos, Y. Onose, T. Klimczuk, A. P. Ramirez, N. P. Ong and R. J. Cava, *Nature Physics*, 2006, **2**, 544.

184. R. C. Xiao, W. J. Lu, D. F. Shao, J. Y. Li, M. J. Wei, H. Y. Lv, P. Tong, X. B. Zhu and Y. P. Sun, *J. Mater. Chem. C*, 2017, **5**, 4167.

185. J. Khan, C. M. Nolen, D. Teweldebrhan, D. Wickramaratne, R. K. Lake and A. A. Balandin, *Appl. Phys. Lett.*, 2012, **100**, 043109.

186. L. E. Conroy and R. J. Bouchard, *Inorg. Synth.*, 1970, **12**, 158.

187. G. Fiori, F. Bonaccorso, G. Iannaccone, T. Palacios, D. Neumaier, A. Seabaugh, S. K. Banerjee and L. Colombo, *Nat. Nanotechnol.*, 2014, **9**, 768.

188. Y. Li, J. Kang and J. Li, *RSC Advances*, 2014, **4**, 7396.

189. L. Li, X. Fang, T. Zhai, M. Liao, U. K. Gautam, X. Wu, Y. Koide, Y. Bando and D. Golberg, *Adv. Mater.*, 2010, **22**, 4151.

190. P. E. Blöchl, *Phys. Rev. B*, 1994, **50**, 17953.

191. D. Tonti, C. Pettenkofer and W. Jaegermann, *Ionics*, 2000, **6**, 196.

192. S. Kikkawa, M. Miyazaki, Y. Liu and F. Kanamaru, *Solid State Ionics*, 1990, **40-41**, 553.

193. R. Shimanouchi, T. Yamamoto, S. Kikkawa and M. Koizumi, *Chem. Lett.*, 1985, **14**, 1323.

194. C. J. Carmalt, S. A. O'Neill, I. P. Parkin and E. S. Peters, *J. Mater. Chem.*, 2004, **14**, 830.

195. A. L. Let, D. E. Mainwaring, C. Rix and P. Murugaraj, *J. Non-Cryst. Solids*, 2008, **354**, 1801.

196. K. Rossnagel, L. Kipp and M. Skibowski, *Phys. Rev. B*, 2002, **65**, 235101.

197. K. Sugawara, Y. Nakata, R. Shimizu, P. Han, T. Hitosugi, T. Sato and T. Takahashi, *ACS Nano*, 2016, **10**, 1341.

198. N. D. Boscher, C. J. Carmalt and I. P. Parkin, *Chem. Vap. Dep.*, 2006, **12**, 54.

199. A. L. Hector, W. Levason, G. Reid, S. D. Reid and M. Webster, *Chem. Mater.*, 2008, **20**, 5100.

200. Y. Zhu, X. Wang, M. Zhang, C. Cai and L. Xie, *Nano Research*, 2016, **9**, 2931.

201. M. Zhang, Y. Zhu, X. Wang, Q. Feng, S. Qiao, W. Wen, Y. Chen, M. Cui, J. Zhang, C. Cai and L. Xie, *J. Am. Chem. Soc.*, 2015, **137**, 7051.

202. W. Zhang, Z. Huang, W. Zhang and Y. Li, *Nano Research*, 2014, **7**, 1731.

203. X. Wang, L. Huang, X.-W. Jiang, Y. Li, Z. Wei and J. Li, *J. Mater. Chem. C*, 2016, **4**, 3143.

204. X.-g. Zheng, H. Kuriyaki and K. Hirakawa, *J. Phys. Soc. Jpn.*, 1989, **58**, 622.

205. M. Amberg and J. R. Guenter, *Solid State Ionics*, 1996, **84**, 313.

206. M. J. Mleczko, C. Zhang, H. R. Lee, H. H. Kuo, B. Magyari-Kope, R. G. Moore, Z. X. Shen, I. R. Fisher, Y. Nishi and E. Pop, *Sci. Adv.*, 2017, **3**, e1700481.

207. Y. Aoki, T. Sambongi, F. Levy and H. Berger, *J. Phys. Soc. Jpn.*, 1996, **65**, 2590.

208. B. Harbrecht, M. Conrad, T. Degen and R. Herbertz, *J. Alloys Compd.*, 1997, **255**, 178.

209. D. N. Bhavsar and A. R. Jani, *J. Optoelectronics Adv. Mat.*, 2014, **16**, 215.

210. K. Terashima, T. Sato, H. Komatsu, T. Takahashi, N. Maeda and K. Hayashi, *Phys. Rev. B*, 2003, **68**, 155108.

211. D. J. Eaglesham, R. L. Withers and D. M. Bird, *J. Phys. C Solid. State Physi.*, 1986, **19**, 359.

212. B. Giambattista, C. G. Slough, W. W. McNairy and R. V. Coleman, *Phys. Rev. B*, 1990, **41**, 10082.

213. F. J. DiSalvo and J. V. Waszczak, *Phys. Rev. B*, 1981, **23**, 457.

214. H. E. Brauer, I. Ekvall, H. Olin, H. I. Starnberg, E. Wahlström, H. P. Hughes and V. N. Strocov, *Phys. Rev. B*, 1997, **55**, 10022.

215. D. W. Murphy, C. Cros, F. J. Di Salvo and J. V. Waszczak, *Inorg. Chem.*, 1977, **16**, 3027.

216. H. A. Therese, F. Rocker, A. Reiber, J. Li, M. Stepputat, G. Glasser, U. Kolb and W. Tremel, *Angew. Chem. Int. Ed.*, 2004, **44**, 262.

217. M. Homyonfer, B. Alperson, Y. Rosenberg, L. Sapir, S. R. Cohen, G. Hodes and R. Tenne, *J. Am. Chem. Soc.*, 1997, **119**, 2693.

218. J. Feng, L. Peng, C. Wu, X. Sun, S. Hu, C. Lin, J. Dai, J. Yang and Y. Xie, *Adv. Mater.*, 2012, **24**, 1969.

219. N. D. Boscher, C. S. Blackman, C. J. Carmalt, I. P. Parkin and A. G. Prieto, *Appl. Surf. Sci.*, 2007, **253**, 6041.

220. B. E. Brown and D. J. Beerntsen, *Acta Cryst.*, 1965, **18**, 31.

221. J. K. Dash, L. Chen, P. H. Dinolfo, T.-M. Lu and G.-C. Wang, *J. Phys. Chem. C*, 2015, **119**, 19763.

222. A. Jobst and S. van Smaalen, *Acta Cryst.*, 2002, **B58**, 179.

223. E. S. Peters, C. J. Carmalt, I. P. Parkin and D. A. Tocher, *Eur. J. Inorg. Chem.*, 2005, 4179.

224. S. Zhao, T. Hotta, T. Koretsune, K. Watanabe, T. Taniguchi, K. Sugawara, T. Takahashi, H. Shinohara and R. Kitaura, *2D Materials*, 2016, **3**, 025027.

225. T. Yanase, S. Watanabe, M. Weng, M. Wakeshima, Y. Hinatsu, T. Nagahama and T. Shimada, *Cryst. Growth Des.*, 2016, **16**, 4467.

226. W. Ge, K. Kawahara, M. Tsuji and H. Ago, *Nanoscale*, 2013, **5**, 5773.

227. C. J. Carmalt, E. S. Peters, I. P. Parkin, T. D. Manning and A. L. Hector, *Eur. J. Inorg. Chem.*, 2004, 4470.

228. C. J. Carmalt, T. D. Manning, I. P. Parkin, E. S. Peters and A. L. Hector, *Thin Solid Films*, 2004, **469**, 495.

229. P. J. McKarns, M. J. Heeg and C. H. Winter, *Inorg. Chem.*, 1998, **37**, 4743.

230. E. Hitz, J. Wan, A. Patel, Y. Xu, L. Meshi, J. Dai, Y. Chen, A. Lu, A. V. Davydov and L. Hu, *ACS Appl. Mater. Interfaces*, 2016, **8**, 11390.

231. Y. H. Huang, R. S. Chen, J. R. Zhang and Y. S. Huang, *Nanoscale*, 2015, **7**, 18964.

232. N. D. Boscher, C. J. Carmalt and I. P. Parkin, *Appl. Surf. Sci.*, 2010, **256**, 3178.

233. N. D. Boscher, C. J. Carmalt and I. P. Parkin, *Eur. J. Inorg. Chem.*, 2006, 1255.

234. Y.-P. Chang, M.Sc Thesis, University of Southampton, 2014.

235. J. Renteria, R. Samnakay, C. Jiang, T. R. Pope, P. Goli, Z. Yan, D. Wickramaratne, T. T. Salguero, A. G. Khitun, R. K. Lake and A. A. Balandin, *J. Appl. Phys.*, 2014, **115**, 034305.

236. D. C. Papageorgopoulos, V. Saltas, C. A. Papageorgopoulos, D. Tonti, C. Pettenkofer and W. Jaegermann, *Appl. Surf. Sci.*, 2000, **161**, 347.

237. H. Zeng, J. Dai, W. Yao, D. Xiao and X. Cui, *Nat. Nanotechnol.*, 2012, **7**, 490.

238. J. Wang, J. Liu, B. Zhang, X. Ji, K. Xu, C. Chen, L. Miao and J. Jiang, *Phys. Chem. Chem. Phys.*, 2017, **19**, 10125.

239. Y.-H. Chang, W. Zhang, Y. Zhu, Y. Han, J. Pu, J.-K. Chang, W.-T. Hsu, J.-K. Huang, C.-L. Hsu, M.-H. Chiu, T. Takenobu, H. Li, C.-I. Wu, W.-H. Chang, A. T. S. Wee and L.-J. Li, *ACS Nano*, 2014, **8**, 8582.

240. X. Wang, Y. Gong, G. Shi, W. L. Chow, K. Keyshar, G. Ye, R. Vajtai, J. Lou, Z. Liu, E. Ringe, B. K. Tay and P. M. Ajayan, *ACS Nano*, 2014, **8**, 5125.

241. A. Bachmatiuk, R. F. Abelin, H. T. Quang, B. Trzebicka, J. Eckert and M. H. Rummeli, *Nanotechnology*, 2014, **25**, 365603.

242. X. Lu, M. I. Utama, J. Lin, X. Gong, J. Zhang, Y. Zhao, S. T. Pantelides, J. Wang, Z. Dong, Z. Liu, W. Zhou and Q. Xiong, *Nano Lett.*, 2014, **14**, 2419.

243. C. Jung, S. M. Kim, H. Moon, G. Han, J. Kwon, Y. K. Hong, I. Omkaram, Y. Yoon, S. Kim and J. Park, *Sci. Rep.*, 2015, **5**, 15313.

244. J. C. Shaw, H. Zhou, Y. Chen, N. O. Weiss, Y. Liu, Y. Huang and X. Duan, *Nano Research*, 2015, **7**, 511.

245. W. Zhang, X. Li, T. Jiang, J. Song, Y. Lin, L. Zhu and X. Xu, *Nanoscale*, 2015, **7**, 13554.

246. J. Krustok, T. Raadik, R. Jaaniso, V. Kiisk, I. Sildos, M. Marandi, H. P. Komsa, B. Li, X. Zhang, Y. Gong and P. M. Ajayan, *Appl. Phys. Lett.*, 2016, **109**, 253106.

247. A. A. Mitioglu, K. Galkowski, A. Surrente, L. Klopotowski, D. Dumcenco, A. Kis, D. K. Maude and P. Plochocka, *Phys. Rev. B*, 2016, **93**, 165412.

248. M. O'Brien, N. McEvoy, D. Hanlon, T. Hallam, J. N. Coleman and G. S. Duesberg, *Sci. Rep.*, 2016, **6**, 19476.

249. A. S. Pawbake, M. S. Pawar, S. R. Jadkar and D. J. Late, *Nanoscale*, 2016, **8**, 3008.

250. B. B. Wang, K. Ostrikov, T. van der Laan, K. Zheng, R. Shao, M. K. Zhu and S. S. Zou, *RSC Adv.*, 2016, **6**, 37236.

251. J. Chen, X. Zhao, S. J. Tan, H. Xu, B. Wu, B. Liu, D. Fu, W. Fu, D. Geng, Y. Liu, W. Liu, W. Tang, L. Li, W. Zhou, T. C. Sum and K. P. Loh, *J. Am. Chem. Soc.*, 2017, **139**, 1073.

252. S. Umrao, J. Jeon, S. M. Jeon, Y. J. Choi and S. Lee, *Nanoscale*, 2017, **9**, 594.

253. B. B. Wang, K. Zheng, X. X. Zhong, D. Gao and B. Gao, *J. Alloys Compd.*, 2017, **695**, 27.

254. W. Park, J. Baik, T. Y. Kim, K. Cho, W. K. Hong, H. J. Shin and T. Lee, *ACS Nano*, 2014, **8**, 4961.

255. Y. H. Lee, X. Q. Zhang, W. Zhang, M. T. Chang, C. T. Lin, K. D. Chang, Y. C. Yu, J. T. Wang, C. S. Chang, L. J. Li and T. W. Lin, *Adv. Mater.*, 2012, **24**, 2320.

256. A. M. van der Zande, P. Y. Huang, D. A. Chenet, T. C. Berkelbach, Y. You, G.-H. Lee, T. F. Heinz, D. R. Reichman, D. A. Muller and J. C. Hone, *Nat. Mater.*, 2013, **12**, 554.

257. H. Schmidt, S. Wang, L. Chu, M. Toh, R. Kumar, W. Zhao, A. H. Neto, J. Martin, S. Adam, B. Ozyilmaz and G. Eda, *Nano Lett.*, 2014, **14**, 1909.

258. J. Wu, H. Schmidt, K. K. Amara, X. Xu, G. Eda and B. Ozyilmaz, *Nano Lett.*, 2014, **14**, 2730.

259. A. Zafar, H. Nan, Z. Zafar, Z. Wu, J. Jiang, Y. You and Z. Ni, *Nano Research*, 2017, **10**, 1608.

260. Y. Gao, Z. Liu, D. M. Sun, L. Huang, L. P. Ma, L. C. Yin, T. Ma, Z. Zhang, X. L. Ma, L. M. Peng, H. M. Cheng and W. Ren, *Nat. Commun.*, 2015, **6**, 8569.

261. S. Najmaei, Z. Liu, W. Zhou, X. Zou, G. Shi, S. Lei, B. I. Yakobson, J. C. Idrobo, P. M. Ajayan and J. Lou, *Nat. Mater.*, 2013, **12**, 754.

262. J. K. Huang, J. Pu, C. L. Hsu, M. H. Chiu, Z. Y. Juang, Y. H. Chang, W. H. Chang, Y. Iwasa, T. Takenobu and L. J. Li, *ACS Nano*, 2014, **8**, 923.

263. K. K. Liu, W. Zhang, Y. H. Lee, Y. C. Lin, M. T. Chang, C. Y. Su, C. S. Chang, H. Li, Y. Shi, H. Zhang, C. S. Lai and L. J. Li, *Nano Lett.*, 2012, **12**, 1538.

264. Y. Shi, W. Zhou, A. Y. Lu, W. Fang, Y. H. Lee, A. L. Hsu, S. M. Kim, K. K. Kim, H. Y. Yang, L. J. Li, J. C. Idrobo and J. Kong, *Nano Lett.*, 2012, **12**, 2784.

265. J. S. Rhyee, J. Kwon, P. Dak, J. H. Kim, S. M. Kim, J. Park, Y. K. Hong, W. G. Song, I. Omkaram, M. A. Alam and S. Kim, *Adv. Mater.*, 2016, **28**, 2316.

266. N. D. Boscher, C. J. Carmalt, R. G. Palgrave, J. J. Gil-Tomas and I. P. Parkin, *Chem. Vap. Dep.*, 2006, **12**, 692.

267. J. Zhou, F. Liu, J. Lin, X. Huang, J. Xia, B. Zhang, Q. Zeng, H. Wang, C. Zhu, L. Niu, X. Wang, W. Fu, P. Yu, T. R. Chang, C. H. Hsu, D. Wu, H. T. Jeng, Y. Huang, H. Lin, Z. Shen, C. Yang, L. Lu, K. Suenaga, W. Zhou, S. T. Pantelides, G. Liu and Z. Liu, *Adv. Mater.*, 2017, **29**, 1603471.

268. D. H. Keum, S. Cho, J. H. Kim, D.-H. Choe, H.-J. Sung, M. Kan, H. Kang, J.-Y. Hwang, S. W. Kim, H. Yang, K. J. Chang and Y. H. Lee, *Nature Physics*, 2015, **11**, 482.

269. J. C. Park, S. J. Yun, H. Kim, J. H. Park, S. H. Chae, S. J. An, J. G. Kim, S. M. Kim, K. K. Kim and Y. H. Lee, *ACS Nano*, 2015, **9**, 6548.

270. C. H. Naylor, W. M. Parkin, J. Ping, Z. Gao, Y. R. Zhou, Y. Kim, F. Streller, R. W. Carpick, A. M. Rappe, M. Drndic, J. M. Kikkawa and A. T. Johnson, *Nano Lett.*, 2016, **16**, 4297.

271. S. M. Attia, J. Wang, G. Wu, J. Shen and J. Ma, *J. Mater. Sci. Technol.*, 2002, **18**, 211.

272. N. Selvakumar and H. C. Barshilia, *Sol. Energy Mater. Sol. Cells*, 2012, **98**, 1.

273. K. L. Choy, *Prog. Mater Sci.*, 2003, **48**, 57.

274. E. Ahvenniemi, A. R. Akbashev, S. Ali, M. Bechelany, M. Berdova, S. Boyadjiev, D. C. Cameron, R. Chen, M. Chubarov, V. Cremers, A. Devi, V. Drozd, L. Elnikova, G. Gottardi, K. Grigoras, D. M. Hausmann, C. S. Hwang, S.-H. Jen, T. Kallio, J. Kanervo, I. Khmelnitskiy, D. H. Kim, L. Klibanov, Y. Koshtyal, A. O. I. Krause, J. Kuhs, I. Kärkkänen, M.-L. Kääriäinen, T. Kääriäinen, L. Lamagna, A. A. Łapicki, M. Leskelä, H. Lipsanen, J. Lyytinen, A. Malkov, A. Malygin, A. Mennad, C. Militzer, J. Molarius, M. Norek, Ç. Ö zgit-Akgün, M. Panov, H. Pedersen, F. Piallat, G. Popov, R. L. Puurunen, G.

Rampelberg, R. H. A. Ras, E. Rauwel, F. Roozeboom, T. Sajavaara, H. Salami, H. Savin, N. Schneider, T. E. Seidel, J. Sundqvist, D. B. Suyatin, T. Törndahl, J. R. van Ommen, C. Wiemer, O. M. E. Ylivaara and O. Yurkevich, *J. Vac. Sci. Technol. A*, 2017, **35**, 010801.

275. M. Binnewies, R. Glaum, M. Schmidt and P. Schmidt, *Z. Anorg. Allg. Chem.*, 2013, **639**, 219.

276. A. C. Jones and M. L. Hitchman, *Chemical Vapour Deposition*, Royal Society of Chemistry, Cambridge, 2009.

277. I. R. Beattie, T. R. Gilson and G. A. Ozin, *J. Chem. Soc. (A)*, 1968, **11**, 2765.

278. I. R. Beattie, K. M. S. Livingston, G. A. Ozin and D. J. Reynolds, *J. Chem. Soc. (A)*, 1969, **6**, 958.

279. W. Levason, M. L. Matthews, B. Patel, G. Reid and M. Webster, *Dalton Trans.*, 2004, 3305.

280. S. J. Lippard and B. J. Russ, *Inorg. Chem.*, 1968, **7**, 1686.

281. J. K. Burdett, R. Hoffmann and R. C. Fay, *Inorg. Chem.*, 1978, **17**, 2553.

282. A. Vincent, *Molecular Symmetry and Group Theory*, Wiley, New York, 1977.

283. G. A. Ozin and R. A. Walton, *J. Chem. Soc. (A)*, 1970, **13**, 2236.

284. D. L. Kepert and R. S. Nyholm, *J. Chem. Soc.*, 1965, 2871.

285. M. F. Davis, W. Levason, R. Ratnani, G. Reid, T. Rose and M. Webster, *Eur. J. Inorg. Chem.*, 2007, 306.

286. S. Sharma, S. Gupta, A. K. Narula, O. P. Vermani and P. N. Kapoor, *Ind. J. Chem. A*, 1995, **34**, 66.

287. J. L. Morancais and L. G. Hubert-Pfalzgraf, *Trans. Mat. Chem.*, 1984, **9**, 130.

288. E. A. Allen, K. Feenan and G. W. A. Fowles, *J. Chem. Soc.*, 1965, 1636.

289. A. B. P. Lever, *Inorganic Electronic Spectroscopy*, Elsevier, New York, 1984.

290. E. A. V. Ebsworth, D. W. H. Rankin and S. Cradock, *Structural Methods in Inorganic Chemistry*, Blackwell Scientific, Oxford, 1986.

291. D. L. Kepert and K. R. Trigwell, *J. Chem. Soc., Dalton Trans.*, 1975, 1903.

292. R. L. Deutscher and D. L. Kepert, *Inorg. Chem.*, 1970, **9**, 2305.

293. R. J. H. Clark, D. L. Kepert, J. Lewis and R. S. Nyholm, *J. Chem. Soc.*, 1965, 2865.

294. W. M. Carmichael, D. A. Edwards and R. A. Walton, *J. Chem. Soc. (A)*, 1966, **1**, 97.

295. J. Mason, *Multinuclear NMR*, Plenum Press, New York, 1987.

296. E. W. Abel, S. K. Bhargava and K. G. Orrell, *Prog. Inorg. Chem.*, 1984, **32**, 1.

297. P. E. Garrou, *Chem. Rev.*, 1981, **81**, 229.

298. R. G. Kidd and H. G. Spinney, *Inorg. Chem.*, 1973, **12**, 1967.

299. V. P. Tarasov, S. M. Sinitsyna, V. D. Kopanev, V. G. Khlebodarov and Y. A. Buslaev, *Russ. J. Coord. Chem.*, 1980, **6**, 1568.

300. Y. A. Buslaev, V. P. Tarasov, S. M. Sinitsyna, V. G. Khlebodarov and V. D. Kopanev, *Russ. J. Coord. Chem.*, 1979, **5**, 189.

301. W. D. Knight, *Phys. Rev.*, 1949, **76**, 1259.

302. D. A. Skoog, F. J. Holler and S. R. Crouch, *Principles of Instrumental Analysis*, Thomson Brooks/Cole, Belmont, CA, 2007.

303. C. J. Carmalt, C. W. Dinnage, I. P. Parkin, A. J. White and D. J. Williams, *Inorg. Chem.*, 2002, **41**, 3668.

304. S. L. Benjamin, C. H. de Groot, C. Gurnani, A. L. Hector, R. Huang, E. Koukharenko, W. Levasona and G. Reid, *J. Mater. Chem. A*, 2014, **2**, 4865.

305. W. Clegg, *Comprehensive Coordination Chemistry II*, ed. J. A. McCleverty and T. J. Meyer, Elsevier, Oxford, 2003, **1**, 579.

306. S. Kobayashi, *The Rigaku Journal*, 2010, **26**, 3.

307. S. Grazulis, D. Chateigner, R. T. Downs, A. F. Yokochi, M. Quiros, L. Lutterotti, E. Manakova, J. Butkus, P. Moeck and A. Le Bail, *J. Appl. Cryst.*, 2009, **42**, 726.

308. K. Nagao and E. Kagami, *The Rigaku Journal*, 2011, **27**, 6.

309. C. S. Wang and J. M. Chen, *Solid State Commun.*, 1974, **14**, 1145.

310. S. Onari, T. Arai, R. Aoki and S. Nakamura, *Solid State Commun.*, 1979, **31**, 577.

311. W. G. McMullan and J. C. Irwin, *Solid State Commun.*, 1983, **45**, 557.

312. J. L. Verble and T. J. Wieting, *Phys. Rev. Lett.*, 1970, **25**, 362.

313. J. I. Goldstein, *Scanning Electron Microscopy and X-ray Microanalysis*, Plenum Press, New York, 2003.

314. A. C. Thompson and D. Vaughan, *X-ray data booklet*, Lawrence Berkeley National Laboratory, University of California, Berkeley, Calif., 2001.

Chapter 2: Niobium tetrahalide complexes with neutral diphosphine ligands

2.1 Introduction

This chapter focuses on the use of neutral diphosphine (P–P) ligands in order to explore their coordination chemistry and to provide a basis for the chemistry with chalcogenoethers, due to the failure of ligand substitution from $[NbCl_4L_2]$ (L = CH_3CN or THF) with thioethers to produce potential single source precursors from $NbCl_4$ complexes (as presented in Chapter 3). Therefore, this chapter aims to understand the reactions of NbX_4 with stronger donors (diphosphine ligands) before exploring $[NbCl_4(chalcogenoether)_n]$ chemistry.

There are three main methods to prepare $[MCl_4(phosphine)_n]$ (M = Nb, Ta) or $[NbCl_4(arsine)_n]$ complexes. Dimeric $[Nb_2Cl_4(PMe_3)_4(\mu\text{-}Cl)_4]$,[1] $[Ta_2Cl_4(PMe_3)_4(\mu\text{-}Cl)_4]$,[2] monomeric *trans*-$[NbCl_4(PEtPh_2)_2]$,[1] unusual seven-coordinated $[NbCl_4(PMe_2Ph)_3]$,[3] and eight coordinated $[TaCl_4\{Me_2P(CH_2)_2PMe_2\}_2]$[4] complexes were made using a Nb/Hg reduction from MCl_5. Whereas *trans*-$[NbCl_4(PEt_3)_2]$,[1, 5] seven-coordinated $[NbCl_4(PMe_3)_3]$,[2] eight-coordinated $[NbC1_4(P–P)_2]$ (P–P = $R_2P(CH_2)_2PR_2$, R = Me, Et)[5] as well as dimeric $[Nb_2Cl_8\{Ph_2P(CH_2)_nPPh_2\}_2]$ (n = 1 to 6)[6] and $[Nb_2Cl_8(PR'_3)_4]$ (R' = ^{t}Bu or Cy)[7] complexes were prepared *via* the substitution of tetrahydrofuran (THF) from $[NbCl_4(THF)_2]$. $[NbCl_4\{o\text{-}C_6H_4(AsMe_2)_2\}_2]$[8, 9] and $[NbX_4\{o\text{-}C_6H_4(AsEt_2)_2\}_2]$ (X = Cl, Br I)[8] were made from substitution CH_3CN from $[NbCl_4(NCCH_3)_2]$.

Although many $[MCl_4(phosphine)_n]$ and $[NbCl_4(arsine)_n]$ were mentioned above, there are limited $[NbCl_4(P–P)_n]$ (n = 1 or 2) complexes (*i.e.* $[NbC1_4(P–P)_2]$ (P–P = $R_2P(CH_2)_2PR_2$, R = Me, Et) and $[Nb_2Cl_8\{Ph_2P(CH_2)_nPPh_2\}_2]$) reported in the literature and none of these have been structurally characterised.[5, 6] Therefore, the chemistry of Nb(IV) chloride with bidentate Group 15 ligands has also proven to be complex and requiring further investigation. In contrast, the structure of $[TaCl_4\{Me_2P(CH_2)_2PMe_2\}_2]$ has been published and the complex is shown to exist in a square antiprismatic geometry. This is particularly intriguing as Nb(V) phosphine complexes have a dodecahedral geometry.[4, 10, 11]

This Chapter describes the preparation and characterisation of the starting materials NbX_4 (X = Cl, Br) using metal reduction or halide exchange and their subsequent reaction with CH_3CN and substitution using diphosphine ligands. These diphosphine adducts form either 1:1 dimers or 2:1 ligand:metal monomers, the evidence for this will be discussed using solid state X-ray structures, IR and UV-visible spectroscopy. As dimeric Nb(IV) complexes are no longer paramagnetic, multinuclear (^{1}H, ^{31}P) NMR spectroscopic data will be also discussed.

2.2 Result and Discussion

2.2.1 The preparation of NbX_4 (X = Cl, Br)

2.2.1.1 $NbCl_4$

The purity of the starting material, $NbCl_4$, is essential for the formation of $[NbCl_4(diphosphine)_2]$. The reduction of $NbCl_4$ has been described and the analysis of the reaction system and stability have been studied previously.[12-18] Most of the reported methods use a temperature gradient with the starting materials in opposite ends of a tube and each end independently heated to different temperatures (Figure 2.1). However, these reports only provide the temperature both ends were heated to, and do not record the temperature for the deposited region or provide more detail of the gradient setup.[12-18]

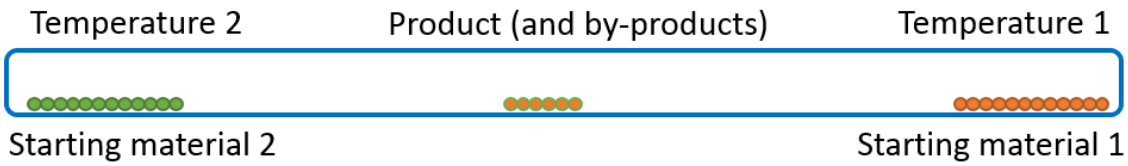

Figure 2.1 Schematic showing the general setup of gradient temperature used in previous reports.[15]

In this project, $NbCl_4$ was prepared *via* the reduction of $NbCl_5$ by niobium powder in a sealed tube under low pressure (*ca.* 10^{-2} mmHg). The tube was placed at the centre of a furnace and heated to 350 ℃ for 2 days. After slowly cooling down, black needle crystals formed at one end and a small amount of yellow needle crystals and white needle crystals had sublimed at the other end (Figure 2.2). The tube was cutter using a glass cuter from its neck and black crystals, yellow crystals and white crystals were separated manually. It is assumed the yellow crystals were unreacted $NbCl_5$ and white crystals were Nb_2O_5. The black needle crystals were identified as $NbCl_4$ *via* powder X-ray diffraction (PXRD) and infrared spectroscopy and compare favourably to literature results (Figure 2.3 and A6.1).[17, 18] Rietveld refinement of the PXRD data gave lattice parameters a = 8.1431(6), b = 6.8405(4), c = 8.8854(8) Å ; β = 91.667(4)° (R_{wp} = 6.92 %, R_p = 5.35 %), which are comparable with literature values of a = 8.140(5), b = 6.823(4), c = 8.852(6) Å, β = 91.92(5)°.[17]

Figure 2.2 The product of $NbCl_5$ reduction in sealed tubes at 350 ℃. The black needle crystals and brown powder at the right side are $NbCl_4$ identified *via* PXRD analysis and from IR spectroscopy. The white powder assumed to be Nb_2O_5 and the yellow solid is $NbCl_5$.

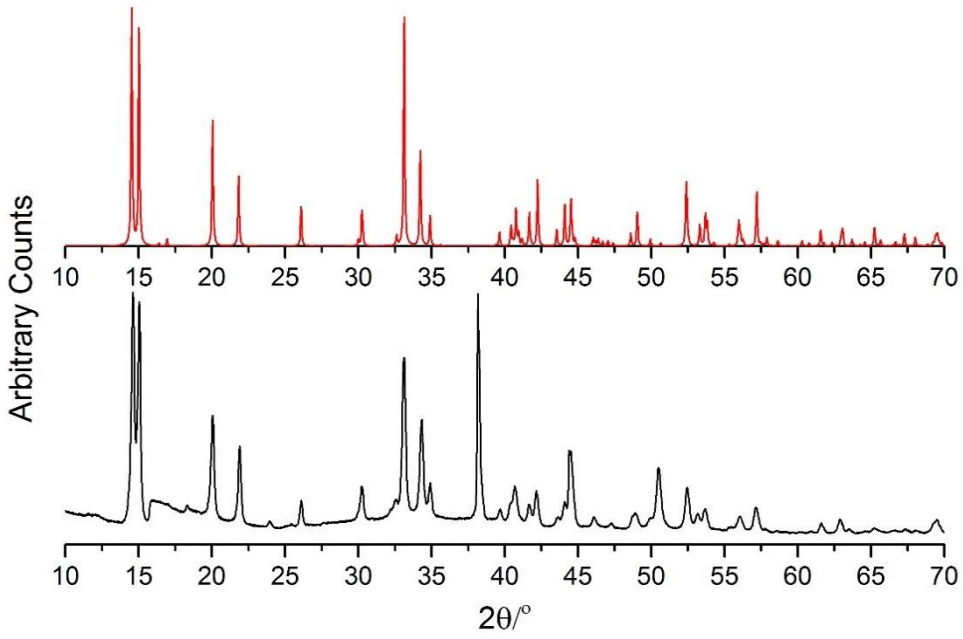

Figure 2.3 PXRD pattern from the synthesis of $NbCl_4$ (black) compared with standard $NbCl_4$ PXRD pattern (red).[17] The two strong diffraction peaks at 2θ = *ca.* 37° and 44° are from the aluminium powder sample holder.

2.2.1.2 $NbBr_4$

$NbBr_4$ was prepared from an analogous method to $NbCl_4$. $NbBr_5$ and niobium metal powder were loaded in a thick glass walled tube and sealed *in vacuo* (*ca*. 0.01 mmHg). The tube was placed in the centre of a furnace and heated to 370 ℃ overnight. After slowly cooling down, black block crystals deposited with black powder/crystals (Figure 2.4). The single crystal structure was determined and is presented below in Figure 2.5.

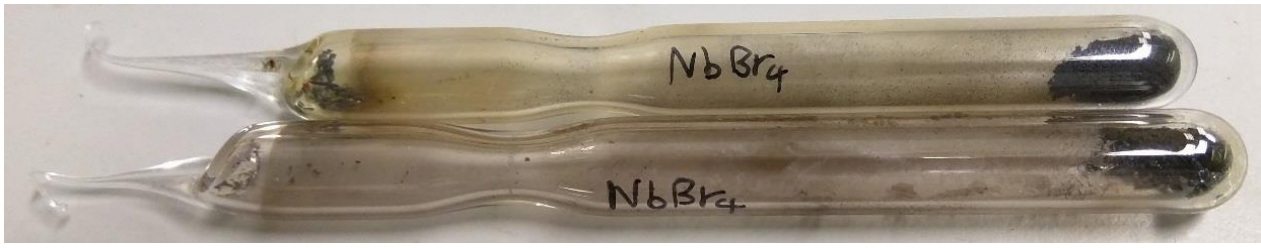

Figure 2.4 The product of $NbBr_5$ reduction in sealed tubes at 370 ℃. The black crystals and brown powder at the right hand side of the glass tube are $NbBr_4$ identified *via* a single crystal X-ray diffraction structure and confirmed as uniphase *via* PXRD analysis and IR spectra**.**

The $NbBr_5$–Nb reduction system has been studied and the temperature range for deposition of $NbBr_4$ is reported to be 257–388 ℃ at ambient pressure; once the temperature is over 388 ℃, it starts to form Nb_3Br_8.[19] Therefore the synthesis of $NbBr_4$ is only attempted at temperatures up to 370 ℃.

The structure of $NbBr_4$ is isomorphous with $NbCl_4$,[17] and consists of chains of edge-linked $NbBr_6$ in an octahedral geometry (Figure 2.5 and Table 2.1). These chains contain alternating long (4.030(2) Å) and short (3.156(2) Å) Nb–Nb distances, with the latter ascribed to metal-metal bonding between the d^1 Nb^{4+} centres.[17] The metal-metal bond distance is 3.029(2) Å in $NbCl_4$.[17] The powder X-ray diffraction pattern has confirmed that the products form a single phase (Figure 2.6).

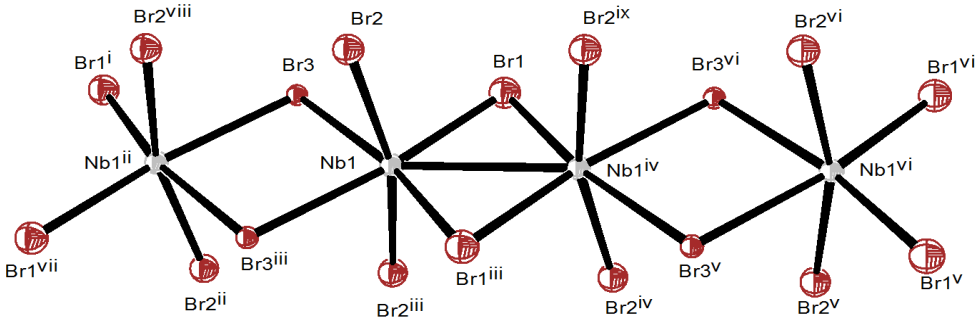

Figure 2.5 The crystal structure of $NbBr_4$ showing the atom numbering scheme and with ellipsoids drawn at the 50 % probability level. Symmetry operation: i = x, 1 + y, z; ii = -x, 1 - y, -z; iii = -x, y, -z; iv = -x, -y, -z; v = -x, -1 + y; vi = x, -1 + y, z; viii = x, 1 - y, z; ix = x, -y, z.

Table 2.1 Selected bond lengths (Å) and angles (°)for $NbBr_4$

Bond lengths		**Bond angles**	
Nb1–Br1	**2.5771(8)**	**Br1–Nb1–Br1^{iii}**	**104.50(5)**
Nb1–Br2	**2.4622(8)**	**Br1–Nb1–Br2**	**92.54(3)**
Nb1–Br3	**2.6921(9)**	**Br1–Nb1–Br2^{ii}**	**92.51(3)**
Nb1–Nb1^{iv}	**3.156(2)**	**Br1–Nb1–Br3**	**169.29(4)**
		Br1–Nb1–Br3^{iii}	**86.21(2)**
		Br2–Nb–Br2^{iii}	**171.75(5)**
		Br2–Nb–Br3	**86.81(3)**
		Br3–Nb–Br3^{iii}	**83.08(5)**
		Nb–Br1–Nb^{iv}	**75.50(5)**
		Nb–Br3–Nb^{ii}	**96.92(5)**

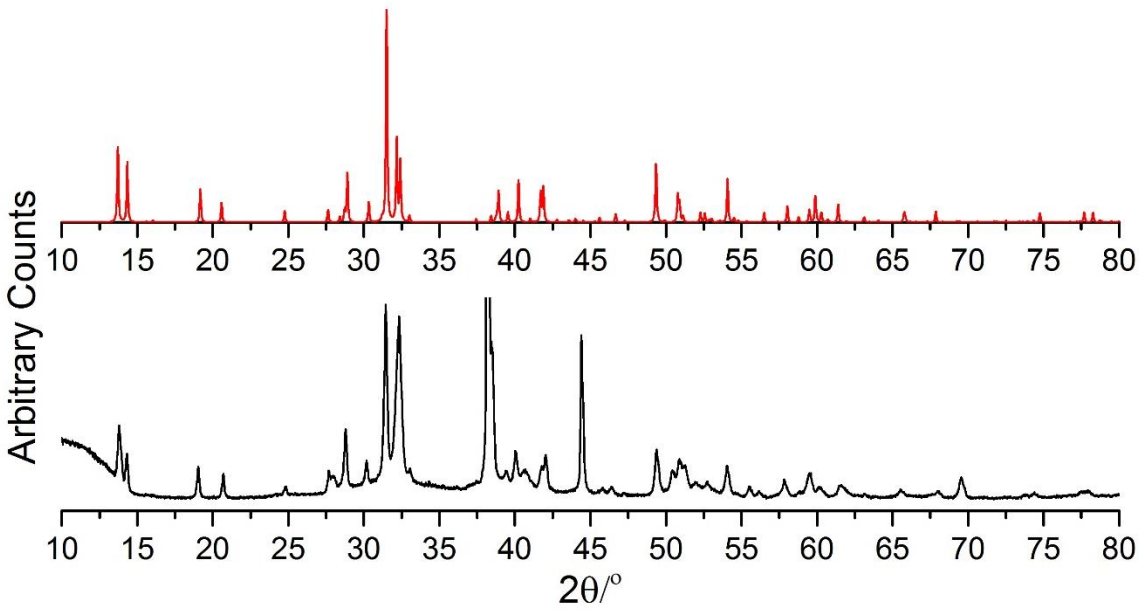

Figure 2.6 PXRD pattern from the synthesis of $NbBr_4$ from a metal reduction (black) compared with standard PXRD pattern (red). The two strong diffraction peaks at 2θ = *ca.* 37° and 44° are from the aluminium sample holder. The red line corresponds to the simulated PXRD pattern from $NbBr_4$ single crystal structure in Figure 2.5.

$NbBr_4$ can also be prepared from a halogen exchange reaction. Halogen exchange has been established for many anhydrous metal chlorides, and yields are usually high (usually 90 % or higher).[20]

Niobium tetrachloride was suspended in boron tribromide (BBr_3) and refluxed for 4 days under a nitrogen atmosphere. The excess BBr_3 solution was decanted before the dark solid was dried *in vacuo* and a dark red powder remained. The synthesis of $NbBr_4$ has been confirmed from both the IR spectrum and PXRD pattern (Experimental section and Figure 2.7).

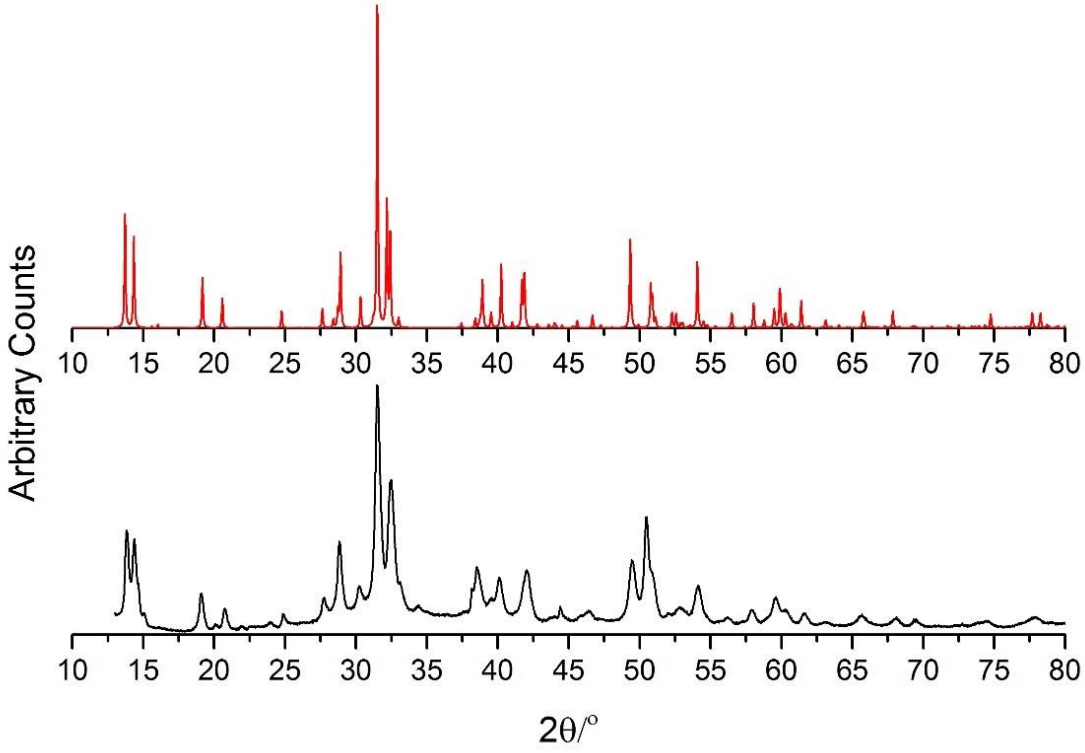

Figure 2.7 PXRD pattern from the synthesis of $NbBr_4$ *via* halide exchange (black) compared with standard PXRD pattern (red). The red line corresponds to the generated PXRD pattern from $NbBr_4$ single crystal structure in Figure 2.5.

2.2.2 2:1 Nb(IV) diphosphine monomeric complexes

Complexes of $[NbX_4(P–P)_2]$ (P–P = $Me_2P(CH_2)_2PMe_2$, $Et_2P(CH_2)_2PEt_2$ or *o*-$C_6H_4(PMe_2)_2$; X = Cl, Br) have been made by ligand substitution from $[NbX_4(NCCH_3)_2]$. NbX_4 was refluxed in acetonitrile for 30 minutes and filtered to remove unreacted NbX_4 and/or Nb powder, which is not easily separated after the metal reduction. The solution was then added to a solution of the ligand in acetonitrile. The colour of the isolated complexes varied from blue green to yellow green (Scheme 2.1).

Crystals of $[NbCl_4\{Me_2P(CH_2)_2PMe_2\}_2]$, $[NbCl_4\{Et_2P(CH_2)_2PEt_2\}_2]$ and $[NbBr_4\{Me_2P(CH_2)_2PMe_2\}_2]$ formed from storing the filtrates at 5 ℃ or -18 ℃, and blue crystals of each were isolated after a week. Crystals of $[NbX_4\{o\text{-}C_6H_4(PMe_2)_2\}_2]$ were grown by dissolving the complex in CH_3CN and allowing slow diffusion of diethyl ether; blue crystals were grown after few days.

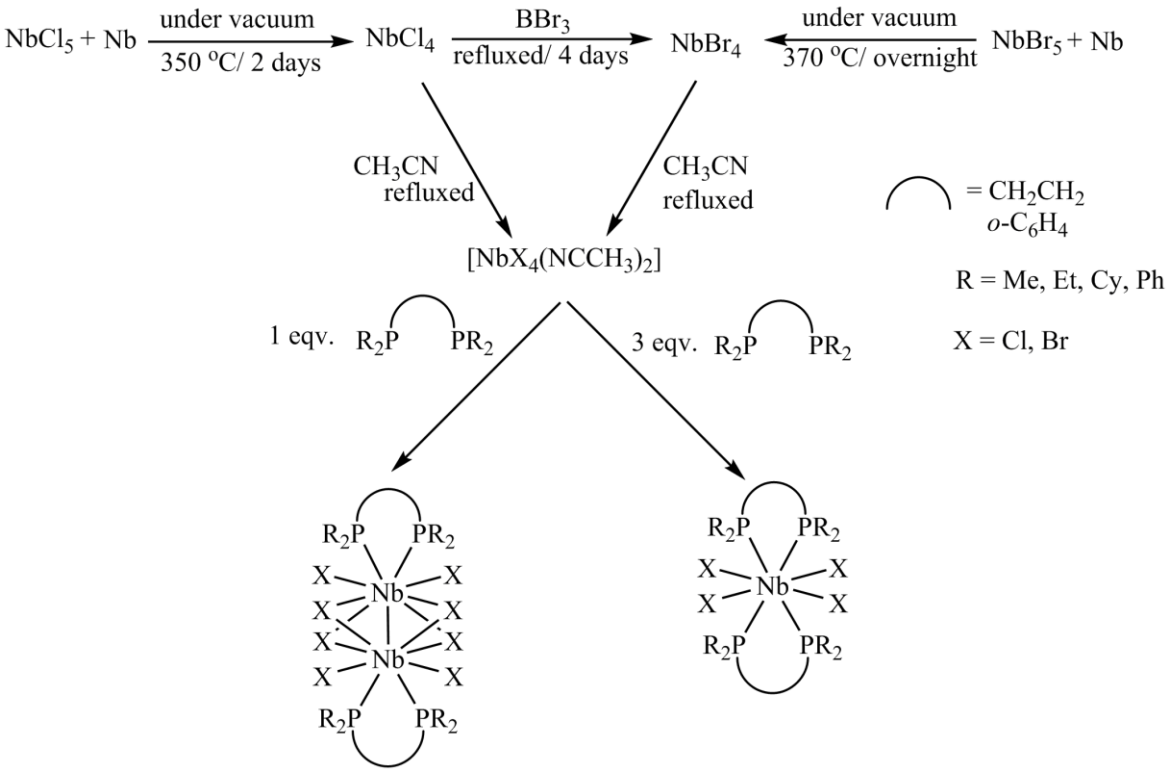

Scheme 2.1 Reaction from NbX_5 and substitution from $[NbX_4(NCCH_3)_2]$ (X = Cl, Br).

These eight coordinated $[NbX_4(P–P)_2]$ complexes form either distorted dodecahedra or distorted square antiprismatic species and the electron state energy in both geometries are difficult to distinguish.[21] Lippard and Russ suggest measuring the angle between two planes intersecting the metal centre, if the value is close to 90°, then the geometry is dodecahedron, whereas the angle in a square antiprism is *ca.* 77.4°.[22] Taking $[NbCl_4\{Me_2P(CH_2)_2PMe_2\}_2]$ for example (Figure 2.8), the planes are defined by $P1^i$, $P2^i$, Nb1, Cl1, $Cl2^i$ and P1, P2, Nb1, $Cl1^i$, Cl2. Unfortunately, most of the eight coordinated complexes in this work do not follow this rule (Table 2.2). This is because

complexes with ethylene backbones ([$NbCl_4\{Me_2P(CH_2)_2PMe_2\}_2$], [$NbCl_4\{Et_2P(CH_2)_2PEt_2\}_2$], [$NbBr_4(Me_2PCH_2CH_2PMe_2)_2$]) are much more distorted when compared to the examples in the proposed method.[22]

Table 2.2 The result of the geometry calculation on [$NbX_4(P–P)_2$] complexes

Complexes	Angle (°)	Complexes	Angle (°)
[$NbCl_4\{Me_2P(CH_2)_2PMe_2\}_2$]	88.08	[$NbCl_4\{Me_2P(CH_2)_2PMe_2\}_2$]	90
[$NbCl_4\{Et_2P(CH_2)_2PEt_2\}_2$]	87.95	[$NbCl_4\{Me_2P(CH_2)_2PMe_2\}_2$]	90
[$NbBr_4\{Me_2P(CH_2)_2PMe_2\}_2$]	88.05		

Cotton and co-workers concluded the different between dodecahedron and square antiprism can be identified from symmetry groups. Considering the NbX_4P_4 (X = Cl, Br) cluster, D_{2d} symmetry can be found in a dodecahedron, whereas D_2 symmetry is existing in a square antiprism.[4] Based on the proposal method from Cotton and co-workers, [$NbX_4\{Me_2P(CH_2)_2PMe_2\}_2$], and [$NbCl_4\{Et_2P(CH_2)_2PEt_2\}_2$] (Figure 2.8–2.10 and Table 2.3–2.5) form as distorted square antiprismatic species (D_2), which is the same as that reported for [$TaCl_4\{Me_2P(CH_2)_2PMe_2\}_2$].[4] In contrast, the structures of [$NbX_4\{o\text{-}C_6H_4(PMe_2)_2\}_2$] (X = Cl, Br) (Figure 2.11–2.12 and Table 2.6–2.7) are distorted dodecahedra (D_{2d}) at the niobium, similar to the Nb(V) analogues, [$NbX_4\{o\text{-}C_6H_4(PMe_2)_2\}_2]^+$,[10, 11] and [$NbCl_4\{o\text{-}C_6H_4(AsMe_2)_2\}_2]^+$.[9] Cotton and co-workers suggest that the different structures of [$TaCl_4\{Me_2P(CH_2)_2PMe_2\}_2$] (distorted square antiprismatic) and [$TaCl_4\{Me_2P(CH_2)_2PMe_2\}_2]^+$ (distorted dodecahedral) might be due to the presence of π-bonding of the metal with the phosphine in the Ta^{IV} (d^1) complex.[4] However, this does not account for the observation that both [$NbX_4\{o\text{-}C_6H_4(PMe_2)_2\}_2$] (X = Cl, Br) (Figure 2.11–2.12) exhibit a dodecahedral geometry, which indicates that π-bonding is not the only factor in determining geometry.

Overall, the Nb–P distances in [$NbCl_4(P–P)_2$] complexes are shorter than that in [$NbBr_4(P–P)_2$]. In contrast, the Nb–Cl distances in the square antiprismatic complexes are longer than those in the dodecahedral complexes by *ca.* 0.1 Å. The chelate angle 'P–Nb–P' is very slightly smaller (71.8°) for the rigid aromatic backboned ligand ($o\text{-}C_6H_4(PMe_2)_2$), compared to the more flexible, $R_2PCH_2CH_2PR_2$ (72.3–73.8°). These are unlikely to be significant enough to explain the change in geometry.

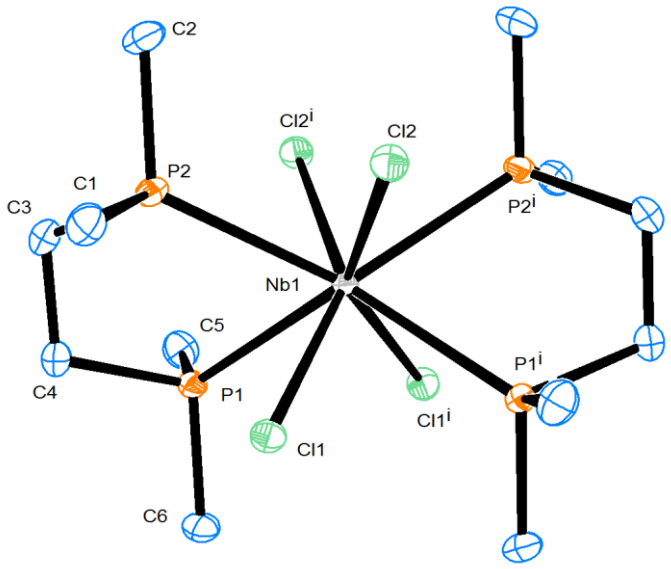

Figure 2.8 The structure of $[NbCl_4\{Me_2P(CH_2)_2PMe_2\}_2]$ showing the atom numbering scheme and with ellipsoids drawn at the 50 % probability level. Hydrogen atoms are omitted for clarity. Symmetry operators: i = -x, 2 - y, z.

Table 2.3 Selected bond lengths (Å) and angles (°) for $[NbCl_4\{Me_2P(CH_2)_2PMe_2\}_2]$

Bond lengths		**Bond angles**	
Nb1–Cl1	**2.5224(8)**	**Cl1–Nb1–Cl1^i**	**105.15(4)**
Nb1–Cl2	**2.5195(8)**	**Cl1–Nb1–Cl2**	**85.59(3)**
Nb1–P1	**2.6553(8)**	**Cl2–Nb1–Cl1^i**	**144.86(2)**
Nb1–P2	**2.6581(8)**	**Cl2–Nb1–Cl2^i**	**104.89(4)**
		P1–Nb1–P2	**73.81(3)**

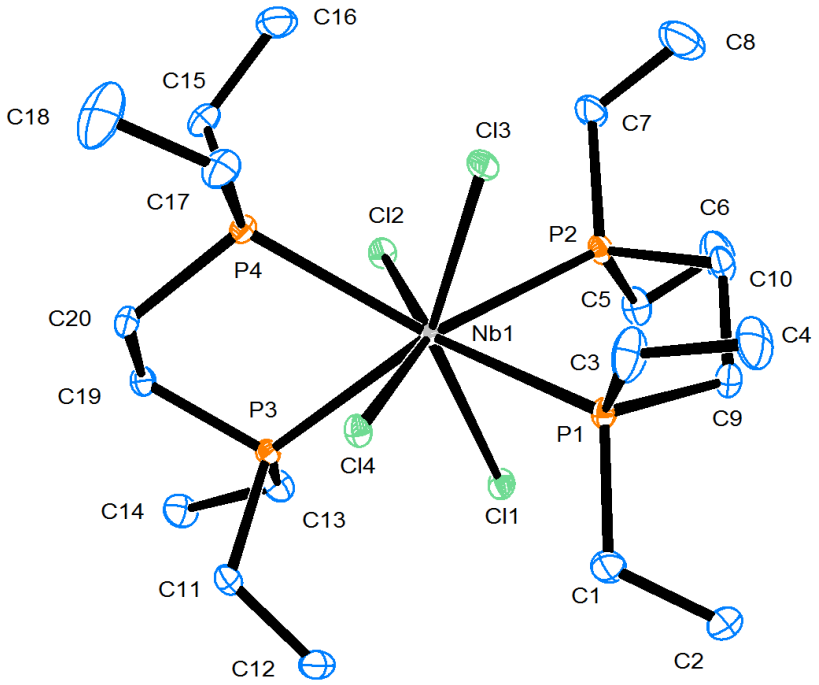

Figure 2.9 The structure of $[NbCl_4\{Et_2P(CH_2)_2PEt_2\}_2]$ showing the atom numbering scheme and with ellipsoids drawn at the 50 % probability level. The ethyl chain is disordered and only the major component is shown. Hydrogen atoms are omitted for clarity.

Table 2.4 Selected bond lengths (Å) and angles (°) for $[NbCl_4\{Et_2P(CH_2)_2PEt_2\}_2]$

Bond lengths		**Bond angles**	
Nb1–Cl1	**2.5235(7)**	**Cl1–Nb1–Cl2**	**87.85(2)**
Nb1–Cl2	**2.5228(7)**	**Cl1–Nb1–Cl3**	**143.79(2)**
Nb1–Cl3	**2.5273(7)**	**Cl1–Nb1–Cl4**	**102.83(2)**
Nb1–Cl4	**2.5240(7)**	**Cl2–Nb1–Cl3**	**100.59(2)**
Nb1–P1	**2.6818(7)**	**Cl2–Nb1–Cl4**	**146.19(2)**
Nb1–P2	**2.6785(8)**	**Cl3–Nb1–Cl4**	**89.57(2)**
Nb1–P3	**2.7157(7)**	**P1–Nb1–P2**	**73.41(2)**
Nb1–P4	**2.7111(7)**	**P3–Nb1–P4**	**72.95(2)**

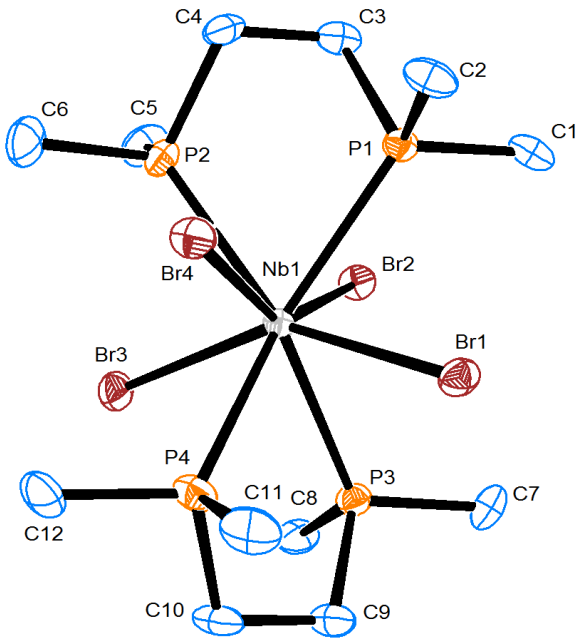

Figure 2.10 The structure of $[NbBr_4\{Me_2P(CH_2)_2PMe_2\}_2]$ showing the atom numbering scheme and with ellipsoids drawn at the 50 % probability level. Hydrogen atoms are omitted for clarity.

Table 2.5 Selected bond lengths (Å) and angles (°) for $[NbBr_4\{Me_2P(CH_2)_2PMe_2\}_2]$

Bond lengths		**Bond angles**	
Nb1–Br1	**2.6975(7)**	**Br1–Nb1–Br2**	**85.40(2)**
Nb1–Br2	**2.7116(7)**	**Br1–Nb1–Br3**	**146.92(2)**
Nb1–Br3	**2.6883(7)**	**Br1–Nb1–Br4**	**104.80(2)**
Nb1–Br4	**2.6916(7)**	**Br2–Nb1–Br3**	**103.28(2)**
Nb1–P1	**2.706(2)**	**Br2–Nb1–Br4**	**146.55(2)**
Nb1–P2	**2.691(2)**	**Br3–Nb1–Br4**	**85.56(2)**
Nb1–P3	**2.697(2)**	**P1–Nb1–P2**	**72.89(4)**
Nb1–P4	**2.693(2)**	**P3–Nb1–P4**	**72.30(4)**

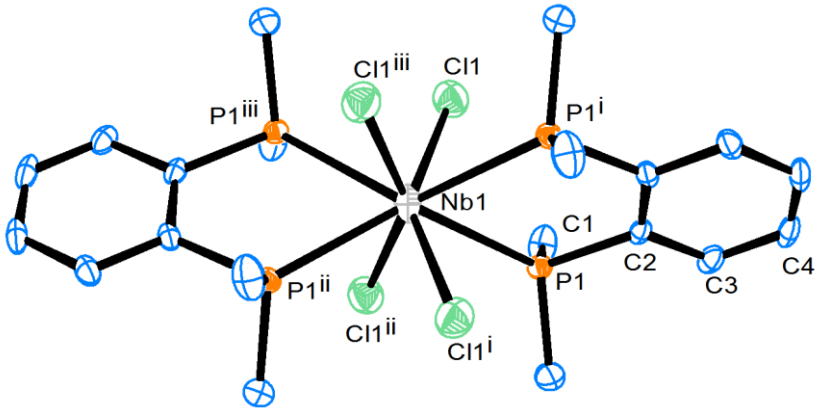

Figure 2.11 The structure of $[NbCl_4\{o\text{-}C_6H_4(PMe_2)_2\}_2]$ showing the atom numbering scheme and with ellipsoids drawn at the 50 % probability level. Hydrogen atoms are omitted for clarity. Symmetry operation: i = -1 + y, 1 + x, z; ii = -x, 2 - y, z; iii = 1 - y, 1 + x, 2 - z.

Table 2.6 Selected bond lengths (Å) and angles (°) for $[NbCl_4\{o\text{-}C_6H_4(PMe_2)_2\}_2]$

Bond lengths		**Bond angles**	
Nb1–Cl1	**2.441(3)**	**Cl1–Nb1–Cl1^i**	**94.91(4)**
Nb1–P1	**2.703(2)**	**P1–Nb1–P1^i**	**71.9(1)**

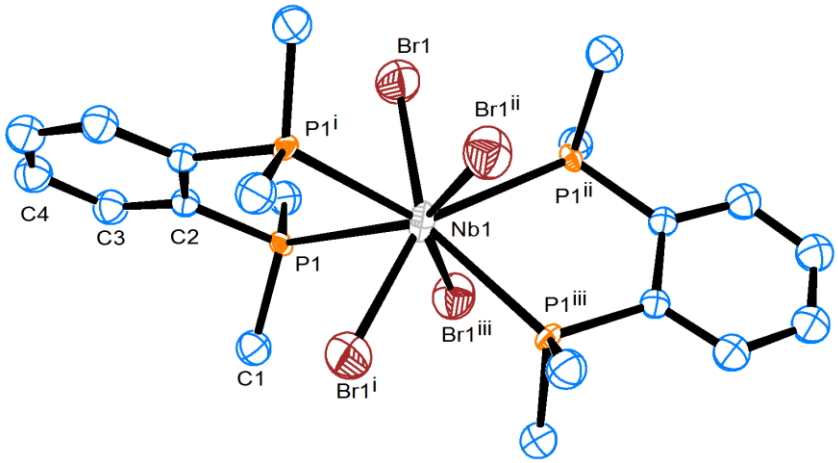

Figure 2.12 The structure of $[NbBr_4\{o\text{-}C_6H_4(PMe_2)_2\}_2]$ showing the atom numbering scheme and with ellipsoids drawn at the 50 % probability level. Hydrogen atoms are omitted for clarity. Symmetry operation: i = -x, -y, z, ii = -y, x, 1 - z; iii = y, -x, 1 - z.

Table 2.7 Selected bond lengths (Å) and angles (°) for $[NbBr_4\{o\text{-}C_6H_4(PMe_2)_2\}_2]$

Bond lengths		**Bond angles**	
Nb1–Br1	**2.679(9)**	**Br1–Nb1–Br1^i**	**95.5(2)**
Nb1–P1	**2.719(3)**	**P1–Nb1–P1^i**	**71.9(1)**

After examination of the literature data, all known eight-coordinate d-block halides with *o*-phenylene backboned (*o*-C_6H_4) diphosphines or diarsines (L–L) are found to be dodecahedral. These are $[ZrX_4(L–L)_2]$,[23] $[HfX_4(L–L)_2]$,[23] $[TiX_4(L–L)_2]$,[24] $[VCl_4\{o\text{-}C_6H_4(AsMe_2)_2\}_2]$,[25] $[TaCl_4\{o\text{-}C_6H_4(AsMe_2)_2\}_2]$,[26] $[MoCl_4\{o\text{-}C_6H_4(AsMe_2)_2\}_2]^+$,[27] $[TaBr_4\{o\text{-}C_6H_4(AsMe_2)_2\}_2]^+$,[28] $[TcCl_4\{o\text{-}C_6H_4(AsMe_2)_2\}_2]^+$,[29] $[NbX_4\{o\text{-}C_6H_4(PMe_2)_2\}_2]^+$[10, 11], $[NbCl_4\{o\text{-}C_6H_4(AsMe_2)_2\}_2]^+$,[9] $[UCl_4\{o\text{-}C_6H_4(PMe_2)_2\}_2]$ and $[UCl_4\{o\text{-}C_6H_4(AsMe_2)_2\}_2]$.[30] There are limited X-ray structures which have been reported for $[MX_4(L'–L')_2]$ where L'–L' is a PCH_2CH_2P backboned diphosphine. These show that $[TiCl_4\{Me_2P(CH_2)_2PMe_2\}_2]$[31] and $[TaCl_4\{Me_2P(CH_2)_2PMe_2\}_2]$[4] are distorted square antiprismatic, whereas $[WCl_4\{Me_2P(CH_2)_2PMe_2\}_2]^+$,[32] $[UCl_4\{Me_2P(CH_2)_2PMe_2\}_2]$[33] and $[TaCl_4\{Me_2P(CH_2)_2PMe_2\}_2]^+$ are dodecahedral.[4] Thus, all cases with *o*-phenylene backboned ligands are shown to be dodecahedral, but for $R_2P(CH_2)_2PR_2$ backbones the pattern is unclear.

All complexes show varying degrees of distortion from a regular polyhedron, this is unavoidable given the short chelate 'bites' of the diphosphines. No clear explanation emerges from consideration of these data. It seems probable that the energy differences between square antiprismatic and dodecahedral geometries are very small, and the shape adopted in practice may be the result of several small factors which are not easy to identify.[21, 34]

The IR spectra of the chloro-complexes show strong ν(Nb–Cl) bands in the regions 320–290 cm^{-1}, but there is no significant difference between the two geometries (D_{2d}: b_2 + e and D_2: $b_1 + b_2 + b_3$) (Figure A6.4–A6.6 and Table 2.9).

In the solid state UV-visible spectra, there are intense bands at *ca.* 330 and *ca.* 425 nm which could be assigned as P(σ) → Nb and Cl(π) → Nb transitions (Figure 2.13). These are consistent with the charge transfer energies in the Nb(V) complexes[10, 11] and six-coordinate $[NbCl_6]^{2-}$.[35] There are three weak overlapping bands in the region 600–1200 nm which could be assigned as *d*–*d* transitions, this agrees with results reported for $[NbCl_4(diarsine)_2]$ complexes.[8, 36] Solution state data are unavailable as the species rapidly decompose in solution.

These monomer complexes are paramagnetic making NMR analysis uninformative. Due to the limited amount of the respective sample, only magnetic data for $[NbCl_4\{Me_2P(CH_2)_2PMe_2\}_2]$ was collected, giving μ_{eff} = 1.74 B.M. at 295 K, as expected for a d^1 system.[8, 9, 36]

The synthesis of $[NbF_4(diphosphine)_2]$ has been attempted by dissolving $[NbCl_4\{Me_2P(CH_2)_2PMe_2\}_2]$ in CH_3CN and adding a mixture of CH_3CN and Me_3SnF and allowing the mixture to stir overnight. Use of Me_3SnF to achieve Cl/F exchange has been used in other systems.[37] However, in this case free $Me_2P(CH_2)_2PMe_2$ was observed in the $^{31}P\{^1H\}$ NMR spectrum, which indicates possible dissociation of the ligand during the attempted halogen-exchange. However, the ^1H NMR spectrum shows the chemical shift of Me_3SnCl (δ = 0.58 ppm), showing that halide exchange has happened. The failure to make $[NbF_4(diphosphine)_2]$ is a similar result to that found

for the corresponding Zr and Hf systems which result in phosphine dissociation.[38] It is likely that the formation of polymeric NbF_4 is preferred over coordination of the phosphine.

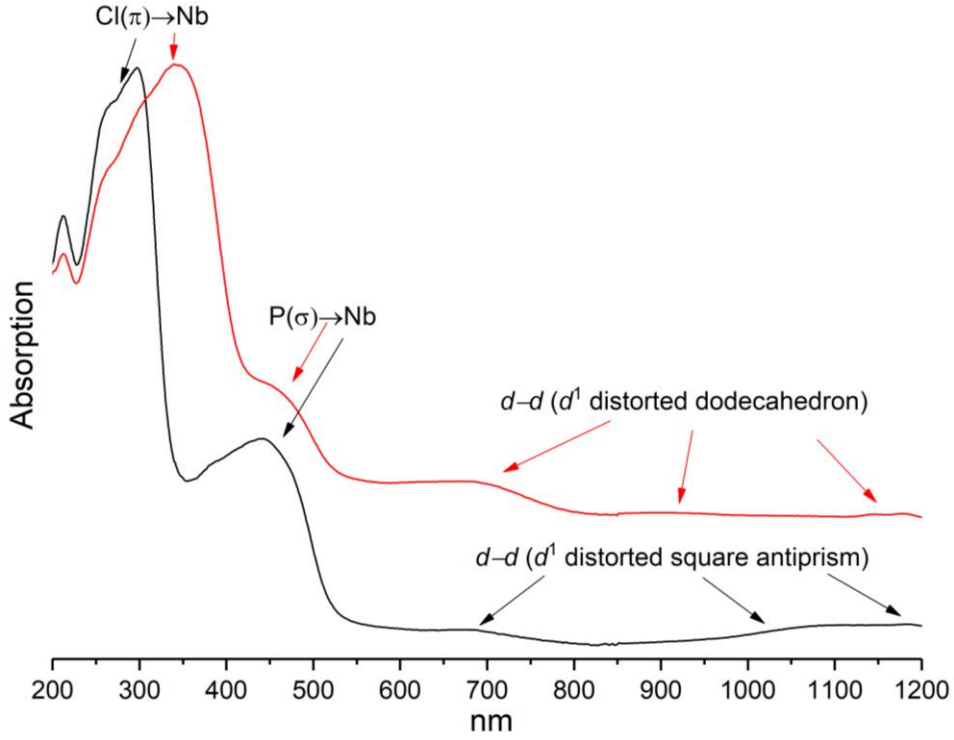

Figure 2.13 UV-visible spectra of solid $[NbCl_4\{Me_2P(CH_2)_2PMe_2\}_2]$ (black) and $[NbCl_4\{o\text{-}C_6H_4(PMe_2)_2\}_2]$ (red).

2.2.3 1:1 Nb(IV) diphosphine dimeric complexes

$[Nb_2X_8\{R_2P(CH_2)_2PR_2\}_2]$ (X = Cl, Br; R = Me, Et, Cy), $[Nb_2Cl_8\{Ph_2P(CH_2)_3PPh_2\}_2]$ and $[Nb_2Cl_8\{o\text{-}C_6H_4(PPh_2)_2\}_2]$ were synthesised from the substitution of $[NbCl_4(NCCH_3)_2]$. Controlling the substitution in a 1:1 molar ratio gives green or yellow-green powders with the composition $[NbCl_4(\text{diphosphine})]$ shown by elemental analysis. The attempt to isolate 1:1 complexes with $o\text{-}C_6H_4(PMe_2)_2$ failed and resulted in a mixture containing 2:1 complexes (discussed in Section 2.2.2 and Figure 2.11).

These complexes of $[Nb_2X_8\{R_2P(CH_2)_2PR_2\}_2]$ are unstable in dry CH_2Cl_2 or CH_3CN and repeated attempts to obtain crystals have been unsuccessful and result in only 2:1 complexes crystallizing from solution. However, these 1:1 dimeric complexes are no longer paramagnetic so ^1H and $^{31}P\{^1H\}$ NMR data have been obtained. The niobium environment would generate a high efg and ^{93}Nb resonances would not be expected due to fast quadrupolar relaxation (and were not observed).

The resulting NMR spectra show this kind of species is diamagnetic and features a metal-metal bond. The ^1H NMR spectra show a significant coordinated ligand shift from the free ligands and show a single phosphorus environment in each case. The $^{31}P\{^1H\}$ NMR spectra each show a single

phosphorus resonance with a significant high frequency coordination shift compared to free ligand, suggesting the formation of five-membered chelate rings (Table 2.8).[39]

Table 2.8 ^{1}H and $^{31}P\{^{1}H\}$ NMR data (CD_3CN, 298 K) of $[NbX_4(diphosphine)]$ complexes

Complexes	^{1}H NMR	Free Ligand ^{1}H NMR	$^{31}P\{^{1}H\}$ NMR	Free Ligand $^{31}P\{^{1}H\}$ NMR
$[Nb_2Cl_4\{Me_2P(CH_2)_2PMe_2\}_2(\mu\text{-}Cl)_4]$	1.73, 2.23	0.81, 1.30	8.5	-48.8
$[Nb_2Br_4\{Me_2P(CH_2)_2PMe_2\}_2(\mu\text{-}Br)_4]$	1.97, 2.73	0.81, 1.30	8.7	-48.8
$[Nb_2Cl_4\{Et_2P(CH_2)_2PEt_2\}_2(\mu\text{-}Cl)_4]$	1.2br, 2.2br	0.96, 1.23, 1.43	45.0	-18.8
$[Nb_2Cl_4\{Cy_2P(CH_2)_2PCy_2\}_2(\mu\text{-}Cl)_4]$	1.35-1.83, 2.32br		42.7	0
$[Nb_2Cl_4\{o\text{-}C_6H_4(PPh_2)_2\}_2(\mu\text{-}Cl)_4]$	7.1-7.7		1.8	-13

IR spectra also show the Nb–Cl absorption bands are very different from the 2:1 complexes discussed above. These dimer complexes have broad absorptions at *ca.* 300 cm^{-1} and *ca.* 200 cm^{-1}, the latter could be assigned to the bridging halide (Figure A6.8–A6.12 and Table 2.9). In contrast, those monomers in Section 2.2.2 have two sharp absorption bands.

The analogous crystal structures of $[Nb_2Cl_4(PR_3)_4(\mu\text{-}Cl)_4]$ (R = Me, or Me_2Ph) have been reported to contain four bridging chlorides, sharing a common square face and with a metal–metal bond (Figure 2.14).[1, 3, 40] Complexes of the type $[Nb_2Cl_4(P–P)_2(\mu\text{-}X)_4]$ are expected to have the same geometry as $[Nb_2Cl_4(PR_3)_4(\mu\text{-}Cl)_4]$ based on the IR and NMR spectroscopic data.

Table 2.9 Far infrared absorption (cm^{-1}) of $[NbCl_4(diphosphine)_n]$ (n = 1 or 2)

Monomer Complexes	ν(Nb–Cl)	Dimer Complexes	ν(Nb–Cl)
$[NbCl_4\{Me_2P(CH_2)_2PMe_2\}_2]$	322, 290	$[Nb_2Cl_4\{Me_2P(CH_2)_2PMe_2\}_2(\mu\text{-}Cl)_4]$	326sh, 301, 275sh, 203
$[NbCl_4\{Et_2P(CH_2)_2PEt_2\}_2]$	303, 280	$[Nb_2Cl_4\{Et_2P(CH_2)_2PEt_2\}_2(\mu\text{-}Cl)_4]$	301, 275
$[NbCl_4\{o\text{-}C_6H_4(PMe_2)_2\}_2]$	318, 307	$[Nb_2Cl_4\{o\text{-}C_6H_4(PPh_2)_2\}_2(\mu\text{-}Cl)_4]$	324br
		$[Nb_2Cl_4\{Cy_2P(CH_2)_2PCy_2\}_2(\mu\text{-}Cl)_4]$	301, 294sh, 206
		$[Nb_2Cl_4\{Ph_2P(CH_2)_3PPh_2\}_2(\mu\text{-}Cl)_4]$	318, 205

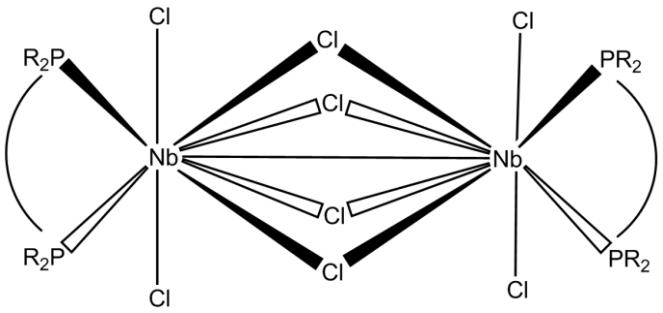

Figure 2.14 Proposed structure of the $[Nb_2Cl_4(RP–PR)_2(\mu\text{-}Cl)_4]$ complexes. R = Me, Et, Ph, Cy.

2.2.4 A Nb^{IV} diphosphine compound with unusual bridging $[Me_2C_2N_2]^{2-}$

Yellow crystals of $[\{\{Cy_2P(CH_2)_2PCy_2\}NbCl_3\}_2\{\mu\text{-}(Me_2C_2N_2)_2\}]$ (Figure 2.16 and Table 2.10) grew during recrystallization from a solution of $[NbCl_4\{Cy_2P(CH_2)_2PCy_2\}]$. $[NbCl_4\{Cy_2P(CH_2)_2PCy_2\}]$ was dissolved in CH_3CN and dried under nitrogen environment. The diffraction data shows each metal centre is coordinated by three halides, a diphosphine ligand and a bridging $[Me_2C_2N_2]^{2-}$ group. The unusual bridging group is from the solvent (CH_3CN) and provides stability to the complex. Similar bridging complexes have been described by Cotton[41] and McCarley[42] and co-workers. Cotton explains the combination of two acetonitrile units can form a cationic bridging unit (Figure 2.15 a). They also suggest the structure for the bridge should contain a Nb≡N bond and with a C═C bond between two acetonitrile units (Figure 2.15 b).[41] Each nitrogen atom contributes two pairs of electrons and uses its lone pair to coordinate to the metal centre. The average Nb–N bond length in this complex is 1.782(6) Å, which corresponds with other Nb≡N bond length in literature examples (Nb≡N = *ca.* 1.78 Å).[43, 44] The central C═C distance in this crystal structure is 1.38(1) Å which is slightly longer than the standard C═C distance (1.335 Å), but is significantly shorter than normal C–C bond (*ca.* 1.5 Å). The C–CH_3 distance is 1.49(1) Å and remains a single bond.

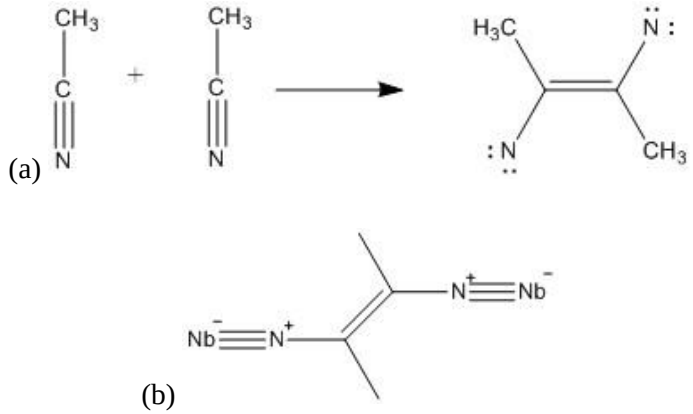

Figure 2.15 (a) The mechanism of acetonitrile cation bridge formation and (b) the bonding environment when the bridge coordinates with Nb(IV) centres.

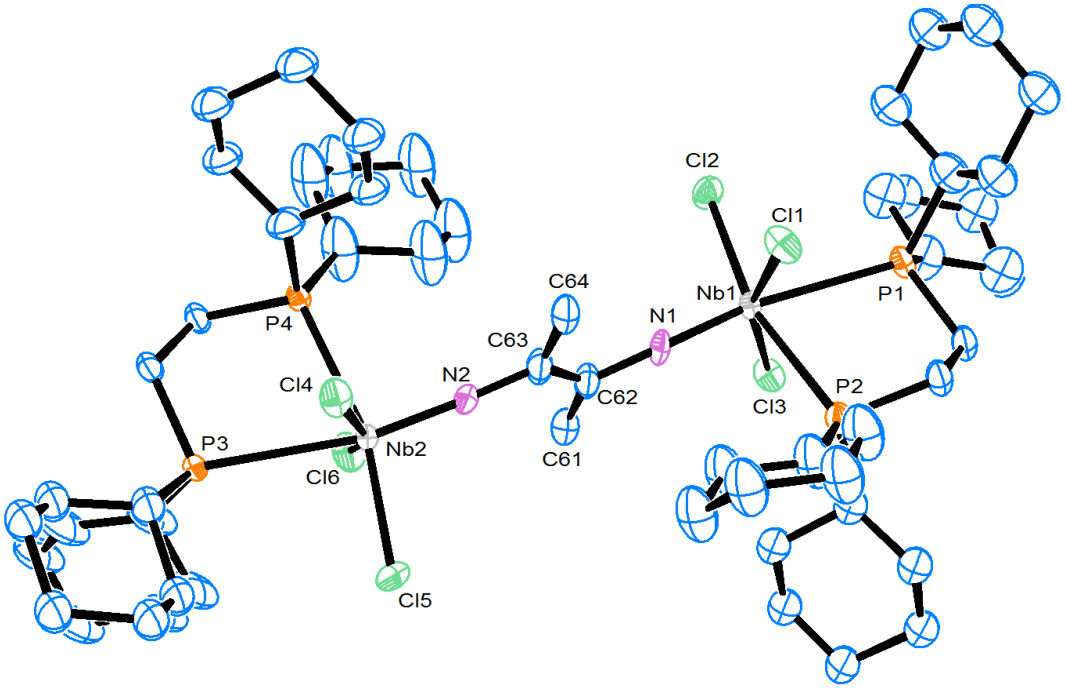

Figure 2.16 The structure of [{{$Cy_2P(CH_2)_2PCy_2$}$NbCl_3$}$_2${μ-$Me_2C_2N_2$}] showing the atom numbering scheme and with ellipsoids drawn at the 50 % probability level. Hydrogen atoms are omitted for clarity.

Table 2.10 Selected bond lengths (Å) and angles (°) for [{{$Cy_2P(CH_2)_2PCy_2$}$NbCl_3$}$_2${μ-$Me_2C_2N_2$}]

Bond lengths		**Bond angles**	
Nb1–Cl1	**2.401(2)**	**P1–Nb1–P2**	**75.91(6)**
Nb1–Cl2	**2.388(2)**	**N1–Nb1–Cl**	**98.8(2)**
Nb1–Cl3	**2.396(2)**	**N1–Nb1–Cl2**	**99.6(2)**
Nb1–N1	**1.778(6)**	**N1–Nb1–Cl3**	**96.5(2)**
Nb1–P1	**2.843(2)**	**N1–Nb1–P2**	**95.9(2)**
Nb1–P2	**2.690(2)**	**P3–Nb2–P4**	**74.68(6)**
Nb2–Cl4	**2.396(2)**	**N2–Nb2–Cl4**	**96.1(2)**
Nb2–Cl5	**2.379(2)**	**N2–Nb2–Cl5**	**100.3(2)**
Nb2–Cl6	**2.382(2)**	**N2–Nb2–Cl6**	**98.6(2)**
Nb2–N2	**1.785(6)**	**N2–Nb2–P4**	**94.7(2)**
Nb2–P3	**2.897(2)**		
Nb2–P4	**2.705(2)**		
C62–C63	**1.38(1)**		

2.3 Conclusion

The convenient preparation method of $NbCl_4$ from a metal reduction has been developed and the resulting $NbCl_4$ characterised *via* PXRD and IR spectroscopies. $NbBr_4$ has been synthesised *via* a metal reduction and the resulting $NbBr_4$ has been characterised from a single crystal structure, PXRD and IR data. A new solution based route for the synthesis of $NbBr_4$ *via* a halide exchange from $NbCl_4$ and BBr_3 has also been developed and the PXRD data compares favourably with $NbBr_4$ single crystal structure.

Several eight-coordinate $[NbX_4(P–P)_2]$ (X = Cl, Br) complexes have been synthesised with full solid-state characterisation. These complexes are shown to feature either a dodecahedral (D_{2d}) or square antiprismatic (D_2) geometry, unfortunately no explanation for the different geometries has been found.

A series of unstable 1:1 diphosphine complexes has also been prepared. Although there is no supporting structural evidence, their geometries are believed to be an eight coordinate bimetallic species, featuring a Nb–Nb bond and four halide bridges.

2.4 Experimental

Starting materials

2.4.1 $NbCl_4$

$NbCl_5$ (540 mg, 2.0 mmol) and niobium powder (92 mg, 1.0 mmol) were loaded in a thick walled glass tube and the tube sealed *in vacuo.* The tube was placed in a furnace and heated to 350 ℃ for 2 days. After cooling down, the tube was opened in a glove box and the crystals removed (small amounts of yellow $NbCl_5$ were found at the cooler end of the tube). The brown-black crystals were characterised by powder X-ray diffraction and IR spectra as $NbCl_4$. Yield: 505 mg, 86 %. IR (Nujol, cm^{-1}): 429, 388, 356, 265 (Nb–Cl). Rietveld refinement of the PXRD pattern gave lattice parameters a = 8.1431(6) Å, b = 6.8405(4) Å, c = 8.8854(8) Å, β = 91.667(4)° (R_{wp} = 6.92 %, R_p = 5.35 %) which compare to literature values of a = 8.140(5) Å, b = 6.823(4) Å, c = 8.852(6) Å, β = 91.92(5)°.[17]

2.4.2 $NbBr_4$

$NbBr_5$ (250 mg, 0.5 mmol) and niobium powder (50 mg, 0.5 mmol) were loaded in a thick walled glass tube and the tube sealed *in vacuo.* The tube was place in a furnace and heated to 370 ℃ overnight. After slowly cooling down, black block crystals and black powder were deposited. The Black crystals have been identified as $NbBr_4$ from single crystal X-ray diffraction data. The black powder was confirmed as $NbBr_4$ being demonstrated by comparing PXRD pattern with reference to a simulated pattern from single crystal X-ray diffraction data. Yield: 240 mg, 93 %. IR (Nujol, cm^{-1}): 309, 287 (Nb–Br).

Alternative method:

BBr_3 (5 mL) was added to finely powdered $NbCl_4$ (200 mg, 0.851 mmol), and the solution was refluxed under a slow stream of nitrogen for four days. After cooling down, a black solid precipitated from the solution. The supernatent liquid was decanted by syringe, and the solid was dried *in vacuo* at 50 ℃, producing a dark red powder. Yield: 295 mg, 84 %. IR (Nujol, cm^{-1}): 309, 287 (Nb–Br).

Monomers

2.4.3 $[NbCl_4(NCCH_3)_2]$

The complex was prepared using a published procedure method.[35] $NbCl_4$ (100 mg, 0.426 mmol) was stirred in CH_3CN (20 mL). The solution was heated to reflux (100 ℃) for 30 minutes. Most of the solid dissolved and the solution colour changed to brown-green. After allowing the mixture to cool down to ambient temperature, the solution was filtered and the solvent was removed *in vacuo* to

reveal a pale yellow powder. Yield: 0.045 mg, 33 %. IR (Nujol, cm^{-1}): 413, 400 (Nb–N), 370, 356, 335 (Nb–Cl).

2.4.4 $[NbCl_4\{Me_2P(CH_2)_2PMe_2\}_2]$

$NbCl_4$ (70 mg, 0.3 mmol) was dissolved in CH_3CN (20 mL). The solution was heated to reflux until all solid had dissolved. The pale green solution was filtered before a solution of $Me_2P(CH_2)_2PMe_2$ (60 mg, 0.3 mmol) in CH_3CN (1 mL) was added. A light green precipitate formed immediately upon addition and then redissolved. The solution was stirred for 1 hour, and the solvent was reduced to ca. 5 mL *in vacuo* and then filtered. The solid collected was dried *in vacuo* and left a yellow green powder. Yield: 67 mg, 42 %. Required for $C_{12}H_{32}Cl_4NbP_4$ (535.00 g/mol): C, 26.9; H, 6.0. Found: C, 27.0; H, 5.9. IR (Nujol, cm^{-1}): 322, 290s, 277sh (Nb–Cl). UV-vis/cm^{-1}: 33 670, 29 000, 22 700, 15 150, 12 580, 11 430. μ_B = 1.74 B.M. The filtrate was stored in the fridge (5 ℃) for 2 days before being stored in a freezer (-18 ℃) for a week. Blue crystals formed and crystallographic data has been collected.

2.4.5 $[NbCl_4\{Et_2P(CH_2)_2PEt_2\}_2]$

This complex was made in a similar fashion to $[NbCl_4\{Me_2P(CH_2)_2PMe_2\}_2]$, and purified to a green powder. Yield: 49.5 %. Required for $C_{20}H_{48}Cl_4NbP_4$ (647.20 g/mol): C, 37.1; H, 7.5. Found: C, 37.4; H, 7.5. IR (Nujol, cm^{-1}): 303s, 280s (Nb–Cl). UV-vis/cm^{-1}: 30 865, 22 950, 14 080, 11 615. Blue crystals grew from the mother liquor at -18 ℃ over a few days.

2.4.6 $[NbCl_4\{o\text{-}C_6H_4(PMe_2)_2\}_2]$

This complex was made in a similar fashion to $[NbCl_4\{Me_2P(CH_2)_2PMe_2\}_2]$, and isolated as a green powder. Yield: 44.5 %. Required for $C_{20}H_{32}Cl_4NbP_4$ (631.08 g/mol): C, 38.06; H, 5.1. Found: C, 38.2; H, 5.3. IR (Nujol, cm^{-1}): 318sh, 307vs (Nb–Cl). UV-vis/cm^{-1}: 29 410, 22 700, 15 060, 11 560. Recrystallisation of a portion of the sample from CH_3CN/diethyl ether gave a green powder and some blue crystals.

2.4.7 $[NbBr_4\{Me_2P(CH_2)_2PMe_2\}_2]$

$NbBr_4$ (82.5 mg, 0.2 mmol) was dissolved in CH_3CN (20 mL) and the mixture heated to reflux. The solution was cooled, filtered, and to the yellow-orange filtrate a solution of $Me_2P(CH_2)_2PMe_2$ (90 mg, 0.6 mmol) in CH_3CN (1 mL) was added. After stirring for 30 minutes, the solution was evaporated to dryness, and the powder rinsed with CH_3CN (5 mL), before the solid was dried *in vacuo*. Yield: 40 mg, 28 %. Required for $C_{12}H_{32}Br_4NbP_4$ (712.8 g/mol): C, 20.2; H, 4.5. Found: C, 20.4; H, 4.4. IR (Nujol, cm^{-1}): 245sh, 231s (Nb–Br). UV-vis/cm^{-1}: 33 500, 26 650, 21 300, 16 950,

14 500, 12 500. Some dark blue crystals were obtained by storing a CH_3CN solution of the complex in a fridge (5 ℃).

2.4.8 [$NbBr_4${*o*-$C_6H_4(PMe_2)_2$}$_2$]

$NbBr_4$ (57 mg, 0.14 mmol) was dissolved in CH_3CN (15 mL) and the mixture heated to reflux until the majority part of the solid had dissolved. The solution was cooled and filtered before a solution of *o*-$C_6H_4(PMe_2)_2$ (82 mg, 0.41 mmol) in CH_3CN (ca. 1 mL) was added to the filtrate. After stirring for 30 minutes, the solution was taken to dryness *in vacuo*. The resulting solid was dissolved in CH_3CN (10 mL) and the solution filtered. The green filtrate was stored in a freezer (-18 ℃) for a week when light green powder precipitated, which was filtered off and dried *in vacuo*. Yield: 10 mg, 9 %. Required for $C_{20}H_{32}Br_4NbP_4$ (808.9 g/mol): C, 29.7; H, 4.0. Found: C, 29.7; H, 4.1. UV-vis/cm^{-1}: 33 560, 27 780, 21 300, 11 560. Crystals were obtained by allowing CH_3CN solution to slowly evaporate under a nitrogen atmosphere. The X-ray crystal structure refinement appears to contain some chloride and hence the bond length data is not reliable.

Dimer complexes

2.4.9 [$NbCl_4${$Me_2P(CH_2)_2PMe_2$}]

$NbCl_4$ (93 mg, 0.4 mmol) was dissolved in hot CH_3CN (20 mL). The pale green solution was filtered before a solution of $Me_2P(CH_2)_2PMe_2$ (64 mg, 0.4 mmol) in CH_3CN (1 mL) was added, resulting in the formation of a light green precipitate. The solution was stirred for 5 minutes and the solid filtered off and dried *in vacuo*, giving a blue green powder. Yield: 69 mg, 45 %. Required for $C_6H_{16}Cl_4NbP_2$ (384.86 g/mol): C, 18.7; H, 4.2. Found: C, 18.8; H, 4.3. IR (Nujol, cm^{-1}): 326sh, 301br, 275sh, 203 (Nb–Cl). ^{1}H NMR (CD_3CN, 298 K): δ = 1.73 (br s, [12H], CH_3), 2.23 (br, [4H], CH_2). $^{31}P\{^1H\}$ NMR (CD_3CN, 298 K): δ = 8.53. UV-vis/cm^{-1}: 34 800, 22 200, 19 800, 15 250, 11 620. μ_{eff} = diamagnetic.

2.4.10 [$NbCl_4${$Et_2P(CH_2)_2PEt_2$}]

This complex was made in a similar fashion to [$NbCl_4${$Me_2P(CH_2)_2PMe_2$}] and purified to a green powder. Yield: 26.5 %. Required for $C_{10}H_{24}Cl_4NbP_2$ (440.96 g/mol): C, 27.2; H, 5.5. Found: C, 27.4; H, 5.6. IR (Nujol, cm^{-1}): 301s, 275s (Nb–Cl). ^{1}H NMR (CD_3CN, 298 K): δ = 1.2 (br s, [12H], CH_3), 2.2 (br, [12H], PCH_2CH_2P and $\underline{CH_2}CH_3$). $^{31}P\{^1H\}$ NMR (CD_3CN, 298 K): δ = 45.0. UV-vis/cm^{-1}: 31 850, 22 940, 17 180, 13 990, 11 750.

2.4.11 [$NbCl_4${$Cy_2P(CH_2)_2PCy_2$}]

This complex was obtained similarly as a yellow-green powder by reaction of $NbCl_4$ and 2 in a 1: 2 mol ratio. Yield: 55 %. Required for $C_{26}H_{44}Cl_4NbP_2$ (653.30 g/mol): C, 47.8; H, 6.8. Found: C, 47.5; H, 6.6. IR (Nujol, cm^{-1}): 301s, 294sh, 206s (Nb–Cl). ^{1}H NMR (CD_3CN, 298 K): δ = 1.35–1.83 (m,

cyclohexyl), 2.32 (br, PCH_2CH_2P). $^{31}P\{^1H\}$ NMR (CD_3CN, 298 K): δ = 42.7. UV-vis/cm^{-1}: 32 050, 23 260, 14 085, 11 750. μ_{eff} = diamagnetic.

2.4.12 [$NbCl_4${*o*-$C_6H_4(PPh_2)_2$}]

This complex was made similarly to [$NbCl_4\{Me_2P(CH_2)_2PMe_2\}$] and isolated as a green powder. Yield: 65 %. Required for $C_{30}H_{24}Cl_4NbP_2$ (681.18 g/mol): C, 52.9; H, 3.6. Found: C, 53.0; H, 3.5. IR (Nujol, cm^{-1}): 324br (Nb–Cl). ^1H NMR (CD_3CN, 298 K): δ = 7.1~7.7 (br m). $^{31}P\{^1H\}$ NMR (CD_3CN, 298 K): δ = 1.8. UV-vis/cm^{-1}: 30 300, 25 000, 16 660, 11 700. μ_{eff} = diamagnetic.

2.4.13 [$NbCl_4\{Ph_2P(CH_2)_3PPh_2\}$]

$NbCl_4$ (70 mg, 0.3 mmol) was dissolved in CH_3CN (15 mL) and the solution heated to reflux until all solids had dissolved. The resulting green solution was filtered and added to a solution of $Ph_2P(CH_2)_3PPh_2$ (124 mg, 0.3 mmol) in CH_2Cl_2 (10 mL) and left to stir for 20 minutes. The solution changed colour from green to yellow green without any precipitation. The solution was evaporated *in vacuo* leaving a combination of yellow green and white solids. The solid was washed with CH_2Cl_2 (2 mL), before being isolated and dried *in vacuo*. Yield: 16 mg, 8.2 %. Required for $C_{27}H_{26}Cl_4NbP_2$ (647.16 g/mol): C, 50.1; H, 4.1. Found: C, 50.3; H, 3.9. IR (Nujol, cm^{-1}): 318, 205 (Nb–Cl). UV-vis/cm^{-1}: 33 900, 31 750, 23 360, 14 300, 11 760.

2.4.14 [$NbBr_4\{Me_2P(CH_2)_2PMe_2\}$]

$NbBr_4$ (62 mg, 0.15 mmol) was dissolved in CH_3CN (15 mL) and the solution heated to reflux until all solid had dissolved. The solution was cooled and filtered before the addition of a solution of $Me_2P(CH_2)_2PMe_2$ (13 mg, 0.09 mmol) in CH_3CN (ca. 2 mL), when a dark green powder formed immediately. After stirring for 30 minutes, the solvent was removed *in vacuo*, and the isolated green solid was washed with 3 mL CH_3CN, filtered and dried *in vacuo*. Yield: 28 mg, 57%. Required for $C_6H_{16}Br_4NbP_2$ (562.66 g/mol): C, 12.8; H, 2.9. Found: C, 12.7; H, 2.9. IR (Nujol, cm^{-1}): 230s (Nb–Br). ^1H NMR (CD_3CN, 298 K): δ = 1.97(br, [12H], CH_3), 2.73(br, [4H], CH_2). $^{31}P\{^1H\}$ NMR (CD_3CN, 298 K): δ = 8.7. UV-vis/cm^{-1}: 29 400, 14 240, 11 550.

2.5 References

1. F. A. Cotton, S. A. Duraj and W. J. Roth, *Inorg. Chem.*, 1984, **23**, 3592.
2. F. A. Cotton, M. P. Diebold and W. J. Roth, *Polyhedron*, 1985, **4**, 1103.
3. F. A. Cotton and W. J. Roth, *Inorg. Chem.*, 1984, **23**, 945.
4. F. A. Cotton, L. R. Falvello and R. C. Najjar, *Inorg. Chem.*, 1983, **22**, 770.
5. L. E. Manzer, *Inorg. Chem.*, 1977, **16**, 525.
6. S. Sharma, S. Gupta, A. K. Narula, O. P. Vermani and P. N. Kapoor, *Ind. J. Chem. A*, 1995, **34**, 66.
7. J. L. Morancais and L. G. Hubert-Pfalzgraf, *Trans. Mat. Chem.*, 1984, **9**, 130.
8. R. L. Deutscher and D. L. Kepert, *Inorg. Chem.*, 1970, **9**, 2305.
9. D. L. Kepert, B. W. Skelton and A. H. White, *J. Chem. Soc., Dalton Trans.*, 1981, 652.
10. W. Levason, M. E. Light, G. Reid and W. Zhang, *Dalton Trans.*, 2014, **43**, 9557.
11. W. Levason, G. Reid and W. Zhang, *J. Fluorine Chem.*, 2015, **172**, 62.
12. L. M. Bazhanova, A. S. Izmailovich and V. I. Tsirel'nikov, *Russ. J. Inorg. Chem.*, 1986, **31**, 1824.
13. L. M. Bazhanova, A. S. Izmailovich and V. I. Tsirel'nikov, *Russ. J. Inorg. Chem.*, 1986, **31**, 1832.
14. P. Frere, *Ann. Chim.*, 1962, **7**, 85.
15. R. E. McCarley and B. A. Torp, *Inorg. Chem.*, 1963, **2**, 540.
16. G. Brauer, *Handbook of Preparative Inorganic Chemistry*, ed. G. Brauer, Academic Press, London, 1965, **2**, 1252.
17. D. R. Taylor, J. C. Calabrese and E. M. Larsen, *Inorg. Chem.*, 1977, **16**, 721.
18. E. A. Pisarev, D. V. Drobot and I. V. Makarchuk, *Zh. Neorg. Khim.*, 1982, **21**, 19.
19. O. I. Vlaskina, A. S. lzmailovich and V. I. Tsirelnikov, *J. Therm. Anal.*, 1996, **46**, 85.
20. P. M. Druce and M. F. Lappert, *J. Chem. Soc. (A)*, 1971, **22**, 3595.
21. J. K. Burdett, R. Hoffmann and R. C. Fay, *Inorg. Chem.*, 1978, **17**, 2553.
22. S. J. Lippard and B. J. Russ, *Inorg. Chem.*, 1968, **7**, 1686.
23. W. Levason, M. L. Matthews, B. Patel, G. Reid and M. Webster, *Dalton Trans.*, 2004, 3305.
24. R. Hart, W. Levason, B. Patel and G. Reid, *Eur. J. Inorg. Chem.*, 2001, 2927.
25. B. M. Gray, A. L. Hector, W. Levason, G. Reid, M. Webster, W. Zhang and M. Jura, *Polyhedron*, 2010, **29**, 1630.
26. J. C. Dewan, D. L. Kepert, C. L. Raston and A. H. White, *J. Chem. Soc., Dalton Trans.*, 1975, 2031.
27. M. G. B. Drew, G. M. Egginton and J. D. Wilkins, *Acta Cryst.*, 1974, **B30**, 1895.

28. M. G. B. Drew, A. P. Wolters and J. D. Wilkins, *Acta Cryst.*, 1975, **B31**, 324.

29. K. A. Glavan, R. Whittle, J. F. Johnson, R. C. Elder and E. Deutsch, *J. Am. Chem. Soc.*, 1980, **102**, 2103.

30. S. S. Rozenel, P. G. Edwards, M. A. Petrie and R. A. Andersen, *Polyhedron*, 2016, **116**, 122.

31. F. A. Cotton, J. H. Matonic, C. A. Murillo and M. A. Petrukhina, *Inorg. Chim. Acta*, 1998, **267**, 173.

32. V. Saboonchian, G. Wilkinson, B. Hussain-Bates and M. B. Hursthouse, *Polyhedron*, 1991, **10**, 595.

33. B. S. Newell, T. C. Schwaab and M. P. Shores, *Inorg. Chem.*, 2011, **50**, 12108.

34. F. A. Cotton and W. J. Roth, *Inorg. Chem.*, 1983, **22**, 2654.

35. G. W. A. Fowles, D. J. Tidmarsh and R. A. Walton, *Inorg. Chem.*, 1969, **8**, 631.

36. D. L. Kepert and K. R. Trigwell, *J. Chem. Soc., Dalton Trans.*, 1975, 1903.

37. A. Dimitrov, D. Heidemann and E. Kemnitz, *Inorg. Chem.*, 2006, **45**, 10807.

38. S. L. Benjamin, W. Levason, D. Pugh, G. Reid and W. Zhang, *Dalton Trans.*, 2012, **41**, 12548.

39. P. E. Garrou, *Chem. Rev.*, 1981, **81**, 229.

40. P. D. W. Boyd, A. J. Nielson and C. E. F. Rickard, *J. Chem. Soc., Dalton Trans.*, 1987, 307.

41. F. A. Cotton and W. T. Hall, *Inorg. Chem.*, 1978, **17**, 3525.

42. P. A. Finn, M. S. King, P. A. Kilty and R. E. McCarley, *J. Am. Chem. Soc.*, 1975, **97**, 220.

43. Cambridge Crystallographic Data Base accessed August 2017.

44. C. R. Groom and F. H. Allen, *Angew. Chem. Int. Ed.*, 2014, **53**, 662.

Chapter 3: Niobium tetrachloride complexes with neutral chalcogenoethers

3.1 Introduction

The preparation of the clean starting materials NbX_4 (X = Cl, Br) has been described in Chapter 2, alongside successful substitutions of CH_3CN in $[NbX_4(NCCH_3)_2]$ with diphosphine ligands. This chapter continues the work of Chapter 2, but using much weaker donor chalcogenoether ligands to coordinate to $NbCl_4$.

There are few reports which mention $[NbX_4(\text{chalcogenoether})]$ complexes. Compounds with monodentate ligands (dimethyl sulfide or tetrahydrothiophene) could form monomeric complexes and are often described in the form as $[NbX_4(SR_2)_2]$ (X = Cl or Br; SR_2).[1] 1:1 dimeric $[Nb_2Cl_8(ER_2)_2]$ complexes have been reported but their solid-state geometry remains unknown.[2] Compounds with the bidentate ligand $MeS(CH_2)_2SMe$ of the form $[NbX_4(MeS(CH_2)_2SMe)_2]$ have been described although there is no solid-state structural data.[3] There are no reports of seleno- or telluroether analogues.

Some of the Nb(IV) complexes are potential single source precursors in low pressure chemical vapour deposition (LPCVD) applications. Ideal single source niobium dichalcogenide precursors are thought to include the tetravalent oxidation state in line with that of NbE_2 (E = S, Se), and for the compounds to have a direct M–E bonds.[4] Besides this, the alkyl group in these chalcogenoether complexes could be modified to enable them to undergo facile β-hydride elimination. This can also be a key feature for ideal CVD precursors.[4-7]

This chapter will describe a series of bidentate chalcogenoethers that have been used in direct reactions with $NbCl_4$ to form either 1:1 monomers or 2:1 ligand:metal monomers. Their crystallographic data, IR and UV-visible spectra will be discussed. Additionally, the synthesis of complexes of $NbCl_4$ with monodentate chalcogenoethers will be discussed with crystallographic data and IR spectra. These complexes can form either a 2:1 monomer $[NbCl_4(ER_2)_2]$, a 2:1 dimer $[Nb_2Cl_4(ER_2)_4(\mu\text{-}Cl)_4]$ or a 1:1 dimer $[Nb_2Cl_6(ER_2)_2(\mu\text{-}Cl)_2]$. Some of these chalcogenoether complexes have been demonstrated to undergo ligand fragmentation. Finally, the complexes $[NbCl_4\{^iPrS(CH_2)_2S^iPr\}]$, $[NbCl_4\{^nBuSe(CH_2)_3Se^nBu\}]$ and $[NbCl_4(Se^nBu_2)_2]$ which are able to undergo β-hydride elimination have been identified as potential LPCVD single source precursors. These complexes have been tested in LPCVD, and the results will be discussed.

3.2 Result and Discussion

3.2.1 Substitution of THF from [$NbCl_4(THF)_2$] using thioethers

The complex [$NbCl_4(THF)_2$] (THF = tetrahydrofuran) was initially thought to be a suitable starting material to allow the substitution of THF by chalcogenoethers. Excess dimethyl sulfide was added to a suspension of [$NbCl_4(THF)_2$] in both toluene and benzene. In each case, the resulting brown solid was identified as unreacted [$NbCl_4(THF)_2$] using IR spectroscopy, while the purple filtrate was evaporated to dryness *in vacuo*. Recrystallization of the purple solid afforded single crystals suitable for X-ray diffraction.

The crystal structure shows the resulting complex to be the Nb(III) dimer, [$Nb_2Cl_4(THF)_2(\mu\text{-}Cl)_2(\mu\text{-}SMe_2)$] (Figure 3.1 and Table 3.1), featuring two metal centres with a Nb═Nb metal bond. Each metal is an octahedral centre, with three terminal ligands (THF and Cl) and three bridging ligands (Cl and SMe_2). Terminal chlorides are *trans* to the bridging chlorides. The Nb-Cl_{bridge} distance is longer than that of Nb-$Cl_{terminal}$.

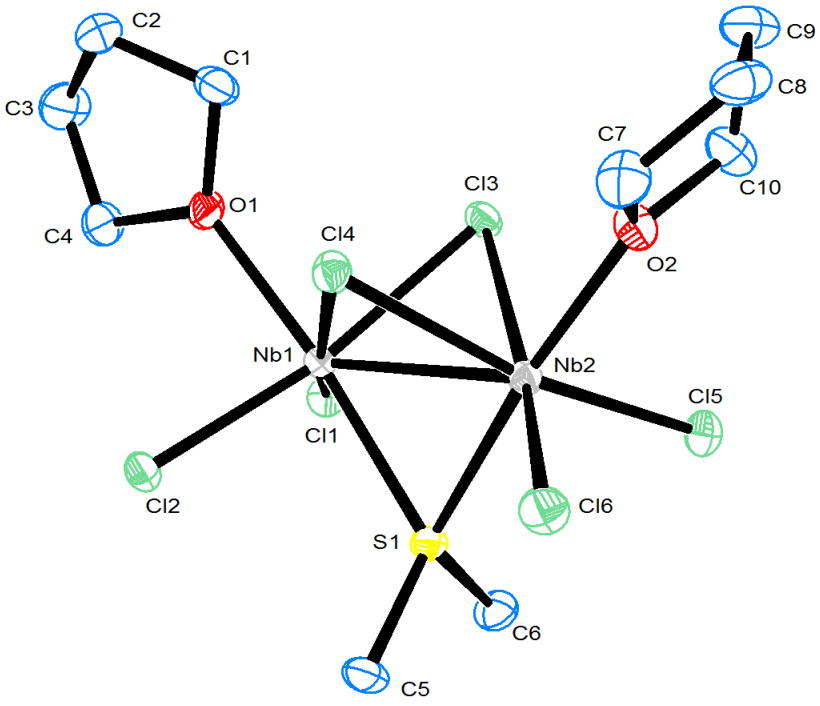

Figure 3.1 Asymmetric unit of [$Nb_2Cl_4(THF)_2(\mu\text{-}Cl)_2(\mu\text{-}SMe_2)]\cdot 2[C_6H_6]$. Ellipsoids are drawn at the 50 % probability level. H atoms and two benzene solvent molecules are omitted for clarity.

Table 3.1 Selected bond lengths (Å) and angles (°) for $[Nb_2Cl_4(THF)_2(\mu\text{-}Cl)_2(\mu\text{-}SMe_2)]\cdot 2[C_6H_6]$

Bond length		**Bond Angles**			
Nb1–Cl1	**2.3925(7)**	**Cl1–Nb1–Cl2**	**98.62(2)**	**Cl3–Nb2–Cl4**	**77.87(2)**
Nb1–Cl2	**2.3839(7)**	**Cl1–Nb1–Cl3**	**90.46(2)**	**Cl3–Nb2–Cl5**	**91.68(3)**
Nb1–Cl3	**2.4976(7)**	**Cl1–Nb1–O1**	**87.99(5)**	**Cl3–Nb2–O2**	**83.79(5)**
Nb1–Cl4	**2.5150(7)**	**Cl1–Nb1–S1**	**88.97(2)**	**Cl3–Nb2–S2**	**100.63(2)**
Nb1–O1	**2.242(2)**	**Cl2–Nb1–Cl4**	**91.88(2)**	**Cl4–Nb2–Cl6**	**89.21(3)**
Nb1–S1	**2.4130(7)**	**Cl2–Nb1–O1**	**87.75(5)**	**Cl4–Nb2–O2**	**85.73(5)**
Nb2–Cl3	**2.5065(7)**	**Cl2–Nb1–S1**	**87.35(2)**	**Cl4–Nb2–S2**	**98.64(2)**
Nb2–Cl4	**2.5260(7)**	**Cl3–Nb1–Cl4**	**78.23(2)**	**Cl5–Nb2–Cl6**	**100.55(3)**
Nb2–Cl5	**2.3948(8)**	**Cl3–Nb1–O1**	**84.90(5)**	**Cl5–Nb2–O2**	**88.47(5)**
Nb2–Cl6	**2.4020(7)**	**Cl3–Nb1–S1**	**100.55(2)**	**Cl5–Nb2–S2**	**87.84(3)**
Nb2–O2	**2.218(2)**	**Cl4–Nb1–O1**	**85.36(5)**	**Cl6–Nb2–O2**	**88.66(5)**
Nb2–S1	**2.4008(7)**	**Cl4–Nb1–S1**	**98.62(2)**	**Cl6–Nb2–S2**	**87.78(3)**

Previously reported by Cotton and co-workers, the layering of a *n*-hexane solution of $[Nb_2Cl_4(SMe_2)_2(\mu\text{-}Cl)_2(\mu\text{-}SMe_2)]$ with THF also affords $[Nb_2Cl_4(THF)_2(\mu\text{-}Cl)_2(\mu\text{-}SMe_2)]$.[8] This method allows the niobium metal centre to retain its oxidation state (Nb(III)). In contrast, the starting material $[NbCl_4(THF)_2]$ contains Nb(IV) and the metal centre is possibly being reduced by SMe_2 to form the volatile by-product Me_2SCl_2, although this was not identified.

The addition of $MeS(CH_2)_2SMe$ to $[NbCl_4(THF)_2]$ in toluene, unfortunately, results in unreacted $[NbCl_4(THF)_2]$ after isolation. This suggests that THF is a stronger donor to Nb(IV) than the soft chalcogenoether. The substitution of acetonitrile in $[NbCl_4(NCCH_3)_2]$ using excess thioether ($MeS(CH_2)_2SMe$) was also carried in CH_2Cl_2 solution but resulted in a mixture containing residual $[NbCl_4(NCCH_3)_2]$, as identified by its infrared spectrum, and unknown $NbCl_4$ complexes, which proved difficult to isolate. This suggests that chalcogenoethers are weaker donors, compared to acetonitrile when coordinated to $NbCl_4$; therefore, the preparation of $[NbCl_4(\text{chalcogenoether})]$ was modified to include the direct reaction from $NbCl_4$.

3.2.2 Niobium tetrachloride complexes with bidentate chalcogenoethers

A series of oxygen and moisture sensitive niobium complexes were prepared by stirring $NbCl_4$ with a CH_2Cl_2 solution of $RE(CH_2)_nER$ (R = Me, ^{i}Pr, ^{n}Bu; E = S, Se; n = 2, 3), *o*-$C_6H_4(CH_2SEt)_2$ or ^{t}Bu$Te(CH_2)_3Te^t$Bu for a few days (Scheme 3.1). The resulting solutions were either red (thioether) or orange (selenoether) with some residual brown precipitate, identified by IR spectroscopy as unreacted $NbCl_4$.

After filtration, the isolated solutions were taken to dryness *in vacuo*, before being washed with *n*-hexane to afford a red-orange solid. Crystals of $[NbCl_4\{MeS(CH_2)_2SMe\}_2]$, $[NbCl_4\{MeS(CH_2)_2SMe\}]$, $[NbCl_4\{^iPrS(CH_2)_2S^iPr\}]$, $[NbCl_4\{MeS(CH_2)_3SMe\}]$, $[NbCl_4\{o\text{-}C_6H_4(CH_2SEt)_2\}]$ and $[NbCl_4\{MeSe(CH_2)_2SeMe\}]$ were obtained by the slow evaporation of saturated solutions in CH_2Cl_2.

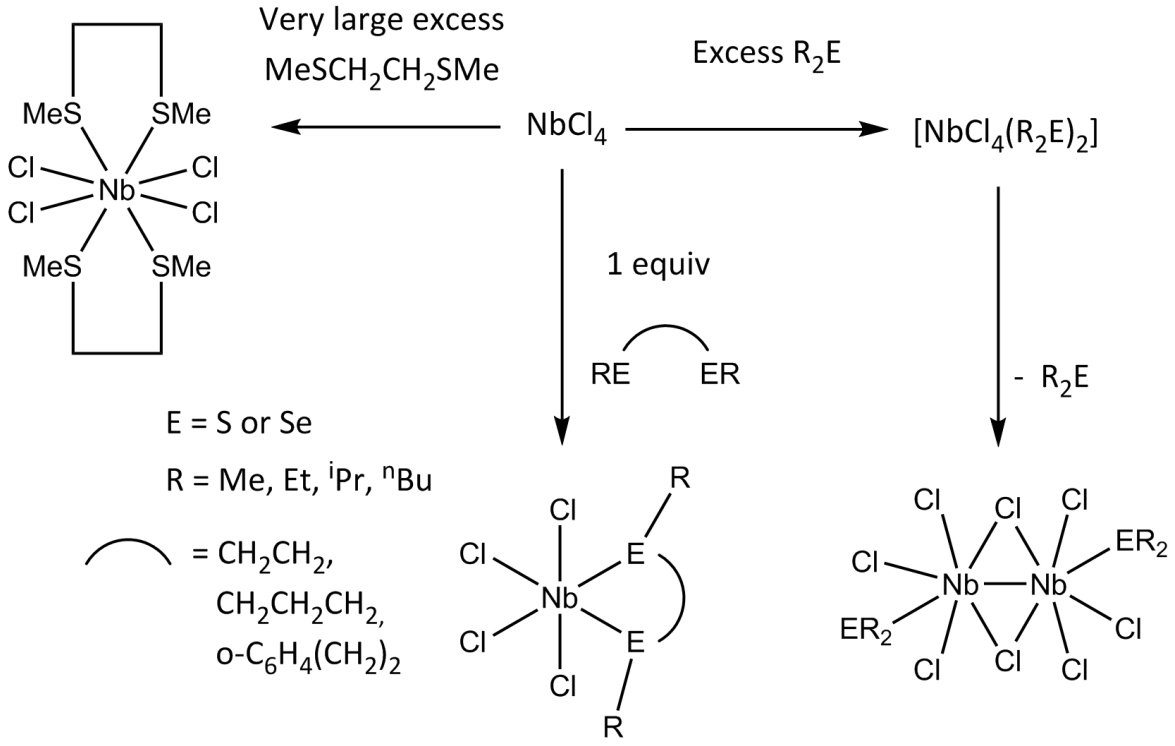

Scheme 3.1 Reactions of $NbCl_4$ with chalcogenoethers

Most of the reactions of $NbCl_4$ with excess bidentate chalcogenoether compounds result in the addition of a single equivalent of ligand, except in the case of $MeS(CH_2)_2SMe$, where a large excess of ligand affords $[NbCl_4\{MeS(CH_2)_2SMe\}_2]$. Microanalysis data show that $[NbCl_4\{MeS(CH_2)_2SMe\}]$ was not pure due to the persistent formation of a product mixture also containing $[NbCl_4\{MeS(CH_2)_2SMe\}_2]$. The latter is described by Hamilton and McCarley without solid-state structural data,[3] but examples of 1:1 complexes have not been identified previously. The structure of $[NbCl_4\{MeS(CH_2)_2SMe\}_2]$ is similar to the eight coordinate Nb(V) cation in $[NbCl_4\{MeS(CH_2)_2SMe\}_2][NbCl_6]$.[9] The successful isolation of the eight-coordinate

$[NbCl_4\{MeS(CH_2)_2SMe\}_2]$ complex is probably due to the five-membered chelate ring and small steric demands of the methyl groups. There is a series of eight coordinate $[NbCl_4(P–P)_2]$ complexes which also require a five-membered ring and small terminal groups for their formation, as discussed in Chapter 2.

The geometry of $[NbCl_4\{MeS(CH_2)_2SMe\}_2]$ is that of a distorted square antiprism (Figure 3.2 and Table 3.2), and is similar to the geometry of $[NbCl_4\{Me_2P(CH_2)_2PMe_2\}_2]$ (Chapter 2). The determining factors between the niobium complexes crystallising to form either a square antiprism or a dodecahedral geometry remain unclear, but that is thought to be due to subtle electronic effects, and it is probable that the energy difference between the two is small.[10-12] Both $MeS(CH_2)_2SMe$ ligands have the *DL* conformation, and the average Nb–Cl bond lengths (2.494(1) Å) are slightly shorter than those reported for $[NbCl_4\{R_2P(CH_2)_2PR_2\}_2]$ (R = Me, Et) (2.5224(8), 2.5195(8) Å) (Chapter2).

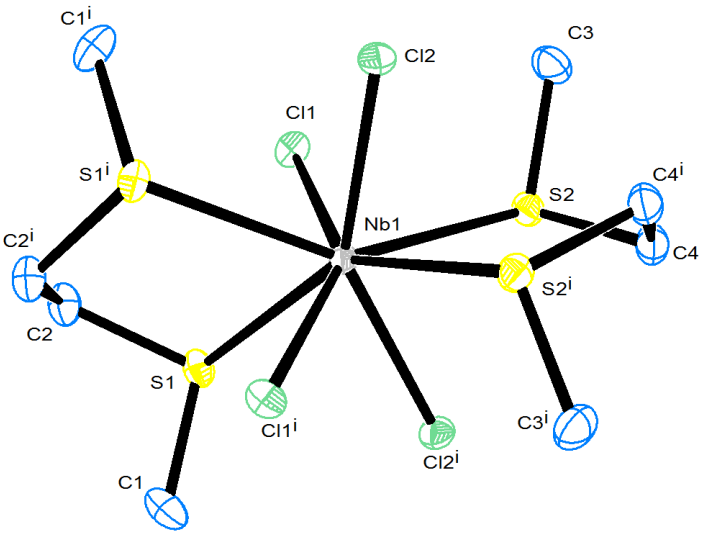

Figure 3.2 The structure of $[NbCl_4\{MeS(CH_2)_2SMe\}_2]$ showing the atom numbering scheme and with ellipsoids drawn at the 50 % probability level. Hydrogen atoms are omitted for clarity. Symmetry operation: i = -1 + y, 1 + x, -z.

Table 3.2 Selected bond lengths (Å) angles (°) for $[NbCl_4\{MeS(CH_2)_2SMe\}_2]$

Bond lengths		**Bond angles**	
Nb1–Cl1	**2.493(1)**	**Cl1–Nb1–Cl1^i**	**144.78(6)**
Nb1–Cl2	**2.495(1)**	**Cl2–Nb1–Cl2^i**	**144.58(6)**
Nb1–S1	**2.686(1)**	**Cl1–Nb1–Cl2**	**82.58(4)**
Nb1–S2	**2.674(1)**	**Cl1–Nb1–Cl2^i**	**108.26(3)**
		S1–Nb1–S1^i	**76.89(5)**
		S2–Nb1–S2^i	**76.94(5)**

The six-coordinate complex, [$NbCl_4${$MeS(CH_2)_2SMe$}], is a distorted octahedron with Cl–Nb–Cl angles > 90° and S–Nb–S = 81.85(3)° (Figure 3.3 and Table 3.3). The Nb–S bond length (2.625(1) and 2.652(1) Å) are slightly shorter than those found in [$NbCl_4${$MeS(CH_2)_2SMe$}$_2$] (2.686(1) and 2.674(1) Å), whereas the Nb–Cl bond lengths are on average (*ca.* 0.15 Å) shorter in the six-coordinate complex. This is due to the dominant Nb–Cl bonding and the lower coordination number.

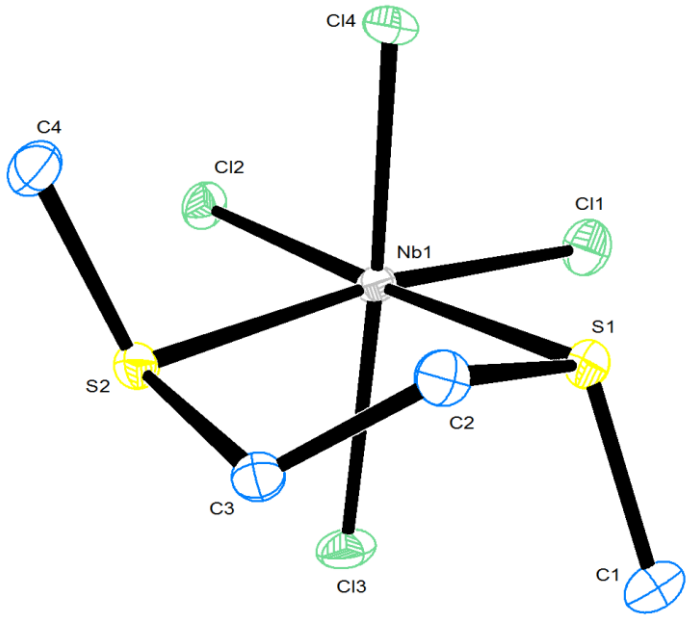

Figure 3.3 The structure of [$NbCl_4${$MeS(CH_2)_2SMe$}] showing the atom numbering scheme and with ellipsoids drawn at the 50 % probability level. Hydrogen atoms are omitted for clarity.

Table 3.3 Selected bond lengths (Å) angles (°) for [$NbCl_4${$MeS(CH_2)_2SMe$}]

Bond lengths		**Bond Angles**			
Nb1–Cl1	**2.333(1)**	**Cl1–Nb1–Cl2**	**96.11(4)**	**Cl2–Nb1–S2**	**94.20(3)**
Nb1–Cl2	**2.359(1)**	**Cl1–Nb1–Cl3**	**97.51(4)**	**Cl3–Nb1–S1**	**88.47(3)**
Nb1–Cl3	**2.330(1)**	**Cl1–Nb1–Cl4**	**95.93(4)**	**Cl3–Nb1–S2**	**78.98(4)**
Nb1–Cl4	**2.340(1)**	**Cl1–Nb1–S1**	**88.10(3)**	**Cl4–Nb1–S1**	**79.48(3)**
Nb1–S1	**2.625(1)**	**Cl2–Nb1–Cl3**	**96.03(4)**	**Cl4–Nb1–S2**	**85.55(3)**
Nb1–S2	**2.652(1)**	**Cl2–Nb1–Cl4**	**94.96(3)**	**S1–Nb1–S2**	**81.85(3)**

Crystallographic data for [$NbCl_4${$^iPrS(CH_2)_2S^iPr$}], [$NbCl_4${$MeE(CH_2)_3EMe$}] (E = S, Se) and [$NbCl_4${o-$C_6H_4(CH_2SEt)_2$}] have been collected and they confirm the presence of 5-, 6- and 7-membered chelate rings (Figure 3.4–3.6). The increasing chelate ring-size results in the increase of the S–Nb–S angles (81.28(4) → 85.4(1) → 101.50(5)°). In contrast, there is little difference between

the Nb–Cl and Nb–S bond lengths between each structure. Only the [$NbCl_4${*o*-$C_6H_4(CH_2SEt)_2$}] structure demonstrate the ligands existing in the *meso* form, while the others contain *DL*-invertomers.

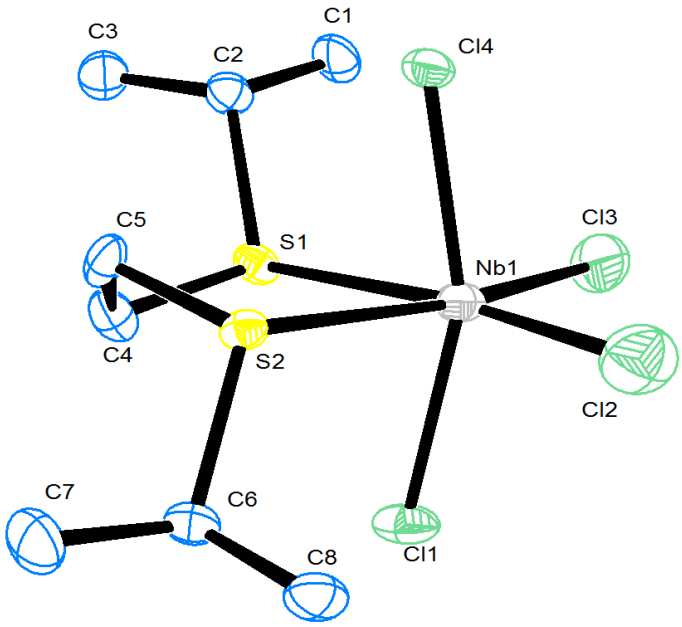

Figure 3.4 The structure of [$NbCl_4$\{^{i}PrS$(CH_2)_2$S^{i}Pr\}] showing the atom numbering scheme and with ellipsoids drawn at the 50 % probability level. Hydrogen atoms are omitted for clarity.

Table 3.4 Selected bond lengths (Å) angles (°) for [$NbCl_4$\{^{i}PrS$(CH_2)_2$S^{i}Pr\}]

Bond lengths		**Bond Angles**			
Nb1–Cl1	**2.351(2)**	**Cl1–Nb1–Cl2**	**96.72(7)**	**Cl2–Nb1–S2**	**94.55(7)**
Nb1–Cl2	**2.250(2)**	**Cl1–Nb1–Cl3**	**96.20(6)**	**Cl3–Nb1–Cl4**	**97.95(6)**
Nb1–Cl3	**2.305(2)**	**Cl1–Nb1–S1**	**78.44(5)**	**Cl3–Nb1–S1**	**89.54(6)**
Nb1–Cl4	**2.341(1)**	**Cl1–Nb1–S2**	**85.18(5)**	**Cl4–Nb1–S1**	**86.44(5)**
Nb1–S1	**2.702(2)**	**Cl2–Nb1–Cl3**	**94.86(8)**	**Cl4–Nb1–S2**	**78.36(5)**
Nb1–S2	**2.675(2)**	**Cl2–Nb1–Cl4**	**97.24(6)**	**S1–Nb1–S2**	**81.28(4)**

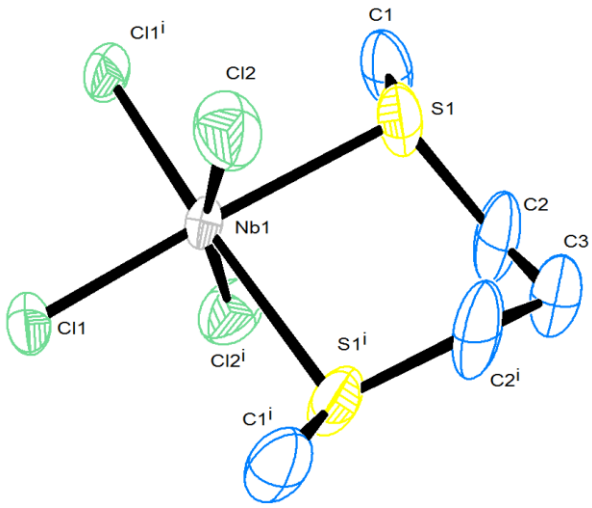

Figure 3.5 The structure of [$NbCl_4${$MeS(CH_2)_3SMe$}] showing the atom numbering scheme and with ellipsoids drawn at the 50 % probability level. Hydrogen atoms are omitted for clarity. Symmetry operation: i = -x, 1 - y, z.

Table 3.5 Selected bond lengths (Å) angles (°) for [$NbCl_4${$MeS(CH_2)_3SMe$}]

Bond lengths		**Bond Angles**			
Nb1–Cl	**2.349(3)**	**Cl1–Nb1–Cl1^i**	**94.1(2)**	**Cl1^i–Nb1–S1**	**90.4(1)**
Nb1–Cl	**2.332(4)**	**Cl1–Nb1–Cl2**	**92.8(2)**	**Cl2–Nb1–S1**	**82.5(1)**
Nb1–S1	**2.630(3)**	**Cl1–Nb1–Cl2^i**	**97.(2)**	**Cl2–Nb1–S1^i**	**86.71)**
		Cl1–Nb1–S1^i	**90.4(1)**	**Cl2^i–Nb1–S1**	**86.7(1)**
		Cl1^i–Nb1–Cl2	**97.2(2)**	**Cl2^i–Nb1–S1^i**	**82.5(1)**
		Cl1^i–Nb1–Cl2^i	**92.8(2)**	**S1–Nb1–S1^i**	**85.4(2)**

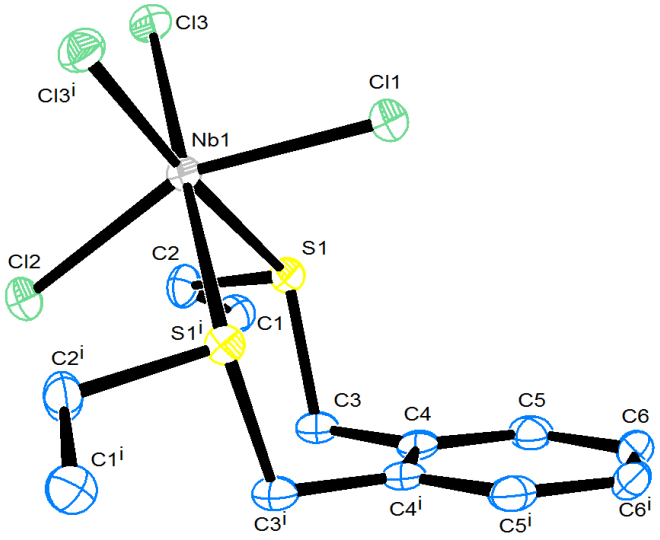

Figure 3.6 The structure of [$NbCl_4${o-$C_6H_4(CH_2SEt)_2$}] showing the atom numbering scheme and with ellipsoids drawn at the 50 % probability level. Hydrogen atoms are omitted for clarity. Symmetry operation: i = x, ½ - y, z.

Table 3.6 Selected bond lengths (Å) angles (°) for [$NbCl_4${*o*-$C_6H_4(CH_2SEt)_2$}]

Bond lengths		**Bond Angles**			
Nb1–Cl1	**2.331(2)**	**Cl1–Nb1–Cl3**	**97.07(4)**	**Cl2–Nb1–S1**	**84.17(4)**
Nb1–Cl2	**2.327(1)**	**Cl1–Nb1–Cl3^i**	**97.07(4)**	**Cl2–Nb1– S1^i**	**84.17(4)**
Nb1–Cl3	**2.376(1)**	**Cl1–Nb1–S1**	**81.41(3)**	**Cl3–Nb1–Cl3^i**	**92.05(5)**
Nb1–S1	**2.652(1)**	**Cl1–Nb1–S1^i**	**81.41(3)**	**Cl3–Nb1–S1**	**83.18(4)**
		Cl2–Nb1–Cl3	**98.77(4)**	**Cl3^i–Nb1–S1^i**	**83.18(4)**
		Cl2–Nb1–Cl3^i	**98.77(4)**	**S1–Nb1–S1^i**	**101.50(5)**

The six- and eight-coordinate niobium complexes are distinguished by Nb–Cl stretches in far IR spectra. The six-coordinate complexes tend to exhibit Nb–Cl stretching bands in the range 360–320 cm^{-1} (Figure A6.16–A6.22), while the eight-coordinate complex shows two bands at 305 and 282 cm^{-1} (Figure A6.15 and Table 3.7). Similar shifts were observed in the eight-coordinate complexes in [MCl_4{$MeS(CH_2)_2SMe$}] (M = Zr or Hf), reflecting the higher coordination number.[12, 13]

Table 3.7 Far infrared spectroscopic data (cm^{-1}) of [$NbCl_4$(chalcogenoether)$_n$] (n = 1 or 2)

Complexes	**ν(Nb-Cl)**	**Complexes**	**ν(Nb-Cl)**
[$NbCl_4${$MeS(CH_2)_2SMe$}$_2$]	305, 282	[$NbCl_4${^{n}BuSe$(CH_2)_3$Se^{n}Bu}]	376, 344
[$NbCl_4${$MeS(CH_2)_2SMe$}]	350, 335, 325, 312	[$NbCl_4(SMe_2)_2$]	380, 362, 343, 321
[$NbCl_4${^{i}PrS$(CH_2)_2$S^{i}Pr}]	368, 353, 339, 319	[$Nb_2Cl_6(SMe_2)_2(\mu$-Cl$)_4$]	375, 351, 336
[$NbCl_4${$MeS(CH_2)_3SMe$)]	356, 350, 340, 325	[$NbCl_4(SeMe_2)_2$]	341, 314, 286, 255
[$NbCl_4${*o*-$C_6H_4(CH_2SEt)_2$}]	365, 341	[$NbCl_4$(Se^{n}Bu$_2)_2$]	378, 343, 320
[$NbCl_4${$MeSe(CH_2)_2SeMe$}]	382, 372, 337	[$Nb_2Cl_4(TeMe_2)_4(\mu$-Cl$)_4$]	358, 326, 276, 250
[$NbCl_4${$MeSe(CH_2)_3SeMe$}]	359, 345, 323	[$NbCl_4${^{t}BuTe$(CH_2)_3$Te^{t}Bu}$_2$]	355, 336, 320

The UV-visible spectra of the six-coordinate complexes in the solid-state show strong absorptions < 400 nm, which could be assigned as S(π) → Nb and Cl(π) → Nb charge transfer transitions. The broad band in the range 500–900 nm can be assigned to *d*–*d* transitions (Figure 3.7).[1-3, 14] The small difference in charge transfer transition energies and *d*–*d* transition energies of six- and eight-coordinate niobium complexes is expected and attributed to the subtle difference in electronics of the systems.[3, 10, 12] However, the small differences do not allow the coordination number of the Nb centre to be identified with certainty from UV-visible data alone.

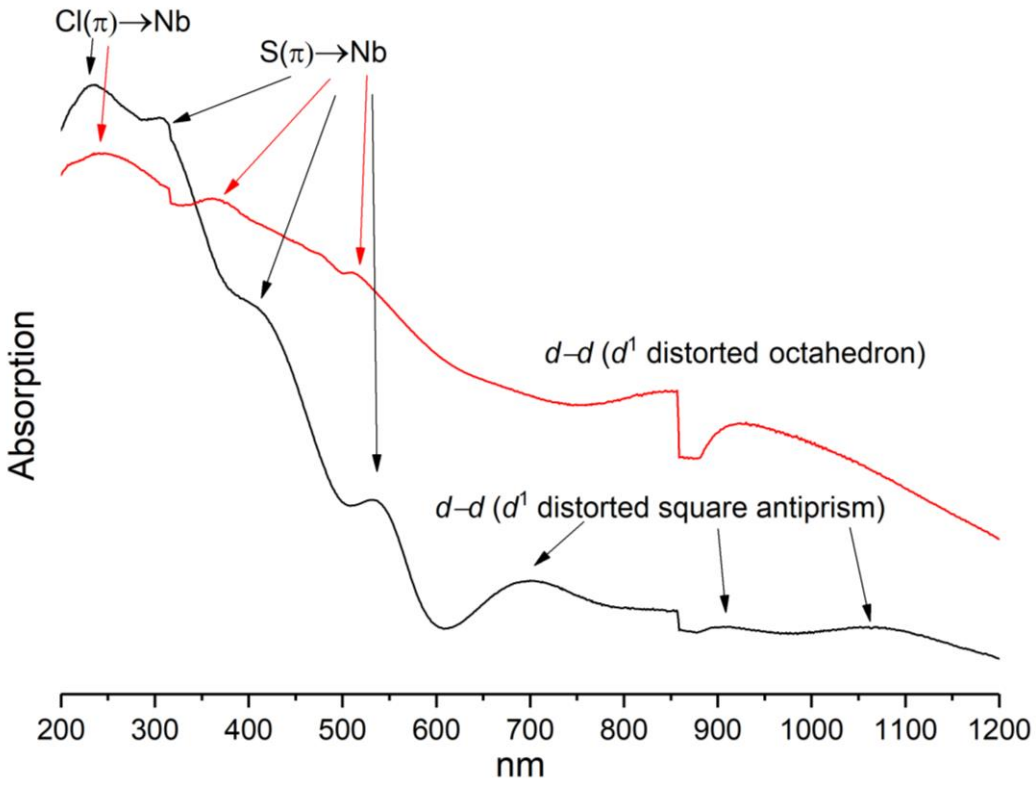

Figure 3.7 UV-visible spectra of solid $[NbCl_4\{MeS(CH_2)_2SMe_2\}_2]$ (black) and $[NbCl_4\{MeS(CH_2)_2SMe_2\}]$ (red). The feature at *ca.* 875 nm is a detector change in the spectrometer.

These Nb(IV) complexes are paramagnetic. Unfortunately, due to the low amount on the sample, only magnetic data for $[NbCl_4\{^iPrS(CH_2)_2S^iPr\}]$ was collected and this has μ_{eff} = 1.69 B.M. at 298 K, and $[NbCl_4\{MeS(CH_2)_2SMe\}_2]$ was reported previously (μ = 1.69 B.M.).[3] Both of them are as expected for a d^1 system.[15-17]

Other bidentate selenoethers ($RSe(CH_2)_nSeR$, R = Me, ^{n}Bu; n = 2 or 3) have been coordinated to $NbCl_4$. The formation of $[NbCl_4\{MeSe(CH_2)_2SeMe\}]$, $[NbCl_4\{MeSe(CH_2)_3SeMe\}]$ and $[NbCl_4\{^nBuSe(CH_2)_3Se^nBu\}]$ has been confirmed by IR spectra (Table 3.7) and elemental analysis (See Experimental section). Additionally, the crystal structure of $[NbCl_4\{MeSe(CH_2)_2SeMe\}]$ is displayed (Figure 3.8 and Table 3.8).

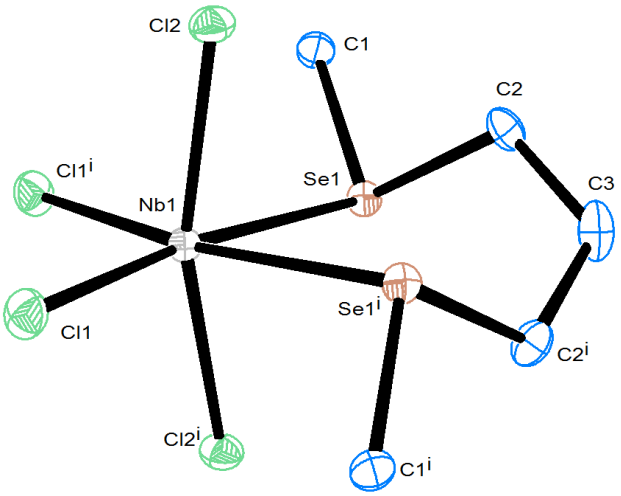

Figure 3.8 The structure of $[NbCl_4\{MeSe(CH_2)_3SeMe\}]$ showing the atom numbering scheme and with ellipsoids drawn at the 50 % probability level. Hydrogen atoms are omitted for clarity. Symmetry operation: i = 1 - x, 1.5 - y, z.

Table 3.8 Selected bond lengths (Å) and angles (°) for $[NbCl_4\{MeSe(CH_2)_3SeMe\}]$

Bond lengths		**Bond Angles**			
Nb1–Cl1	**2.360(1)**	**Cl1–Nb1–Cl1^i**	**95.39(7)**	**Cl1^i–Nb1–Se1**	**90.47(3)**
Nb1–Cl2	**2.339(1)**	**Cl1–Nb1–Cl2**	**97.67(4)**	**Cl2–Nb1–Se1**	**86.43(4)**
Nb1–Se1	**2.7648(7)**	**Cl1–Nb1–Cl2^i**	**93.49(4)**	**Cl2–Nb1–Se1^i**	**81.25(3)**
		Cl1–Nb1–Se1^i	**90.47(3)**	**Cl2–Nb1–Se1**	**81.25(3)**
		Cl1^i–Nb1–Cl2	**93.49(4)**	**Cl2^i–Nb1–Se1^i**	**86.43(4)**
		Cl1^i–Nb1–Cl2^i	**97.67(4)**	**Se1–Nb1–Se1^i**	**84.07(3)**

Attempted coordination of *o*-$C_6H_4(CH_2SeMe)_2$ to $NbCl_4$ showed fragmentation of the diselenoether and will be discussed in Section 3.2.4. The attempted reaction of ditelluroethers such as *o*-$C_6H_4(TeMe)_2$ with $NbCl_4$ were unsuccessful and resulted in C–Te cleavage. The addition of ^{t}BuTe$(CH_2)_3$Te^{t}Bu to $NbCl_4$ resulted in the formation of a brown solid, and while IR and UV-visible spectra and elemental analysis data are not inconsistent with the formation of $[NbCl_4\{^t$BuTe$(CH_2)_3$Te^{t}Bu$\}_2]$ attempts to crystallize the complex were ultimately unsuccessful.

3.2.3 Niobium tetrachloride complexes with monodentate chalcogenoethers

The $[NbCl_4(ER_2)_2]$ (E = S, Se, Te) complexes were prepared by the direct reaction of $NbCl_4$ and chalcogenoether ligands (Scheme 3.1). These complexes are very sensitive and unstable and rapidly decompose to a sticky black oil during attempts to isolate product from excess solvent (either under vacuum or by distillation under a nitrogen atmosphere). Successful isolation was ultimately achieved by maintaining a low temperature (0 °C) while removing the solvent under vacuum.

Single crystals of $[NbCl_4(TeMe_2)_2]$ were grown by the slow evaporation of a CH_2Cl_2 solution under a nitrogen atmosphere and confirm the presence of 2:1 dimer, which is the first Nb(IV) telluroether complex. Similar attempts with $[NbCl_4(SMe_2)_2]$ and $[NbCl_4(SeMe_2)_2]$ were unsuccessful as the ligands are lost to afford 1:1 $[NbCl_4(EMe_2)]$ complexes (E = S ,Se) (discussed below).

As described above, the very unstable complex $[NbCl_4(SMe_2)_2]$ has been isolated, and it is likely to be *cis*-$[NbCl_4(SMe_2)_2]$ because its far-IR absorption is very similar to those of the six-coordinated complexes reported in Section 3.2.2 (Figure A6.24 and Table 3.7) and other *cis*-$[NbCl_4L_2]$ in the literature.[1, 18]

The complex $[NbCl_4(SMe_2)_2]$ is very unstable and loses SMe_2 rapidly in solid state or in solution. The slow evaporation of a saturated CH_2Cl_2 solution afforded yellow-brown crystals of the bimetallic complex and shows a 1:1 dimeric structure. The 1:1 complex was isolated in low yield by layering a solution of $[NbCl_4(SMe_2)_2]$ and CH_2Cl_2 with *n*-hexane. The structure shows a centrosymmetric $[Nb_2Cl_6(SMe_2)_2(\mu\text{-}Cl)_2]$ dimer with a single Nb–Nb bond (3.1094(5) Å) (Figure 3.9 and Table 3.9).[19] Unfortunately, because the product is poorly soluble in non-coordinating NMR solvents, such as $CDCl_3$ and CD_2Cl_2, solution-state NMR spectra were not able to be obtained.

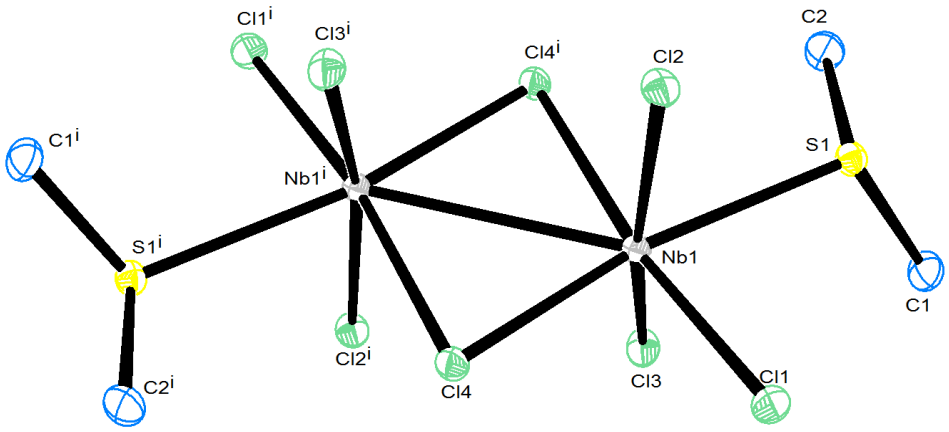

Figure 3.9 The structure of $[Nb_2Cl_6(SMe_2)_2(\mu\text{-}Cl)_2]$ showing the atom numbering scheme and with ellipsoids drawn at the 50 % probability level. Hydrogen atoms are omitted for clarity. Symmetry operation: i = + 2, - y, z + 1.

Table 3.9 Selected bond lengths (Å) angles (°) for $[Nb_2Cl_6(SMe_2)_2(\mu\text{-}Cl)_2]$

Bond lengths		**Bond Angles**			
Nb1–Cl1	**2.3768(7)**	**Cl1–Nb1–Cl2**	**92.93(2)**	**Cl2–Nb1–S1**	**80.52(2)**
Nb1–Cl2	**2.3110(6)**	**Cl1–Nb1–Cl3**	**94.50(2)**	**Cl3–Nb1–Cl4**	**97.48(2)**
Nb1–Cl3	**2.3149(6)**	**Cl1–Nb1–Cl4**	**86.37(2)**	**Cl3–Nb1–Cl4^{i}**	**85.82(2)**
Nb1–Cl4	**2.4205(6)**	**Cl1–Nb1–S1**	**81.94(2)**	**Cl3–Nb1–S1**	**85.61(2)**
Nb1–Cl4^{i}	**2.5107(6)**	**Cl2–Nb1–Cl4**	**98.03(2)**	**Cl4–Nb1–Cl4^{i}**	**101.84(2)**
Nb1–Nb1^{i}	**3.1094(5)**	**Cl2–Nb1–Cl4^{i}**	**84.68(2)**	**Cl4^{i}–Nb1–S1**	**89.80(2)**
Nb1–S1	**2.6207(7)**				

Two selenoether complexes $[NbCl_4(SeR_2)_2]$ (R = Me, ^{n}Bu) were isolated using a similar method to $[NbCl_4(SMe_2)_2]$, the resulting selenoether species were found to be more stable than the SMe_2 complex. The complex $[NbCl_4(Se^{n}Bu_2)_2]$ is found to be spectroscopically similar to previous $[NbCl_4(\text{dithioether})]$ complexes, suggesting a *cis*-octahedral structure (Table 3.7). In contrast, far IR data for $[NbCl_4(SeMe_2)_2]$ ν(Nb–Cl, cm^{-1}) = 341, 314, 286, 255 (Figure A6.26), with the Nb–Cl stretches at lower frequencies, than shown for a *cis*-octahedral structure. This is likely to reflect a higher coordinated geometry, suggesting it might contain eight-coordinate niobium in a dimeric structure with a similar geometry to $[Nb_2Cl_8(TeMe_2)_4]$ (see below).The measured magnetic moment for $[NbCl_4(SeMe_2)_2]$ at 295 K is μ_{eff} = 1.15 B. M., which is difficult to rationalise. However, the value does lie in the range reported by Hamilton and McCarley for $[NbX_4(SMe_2)_2]$ (X = Br or I) and $[NbX_4(THT)_2]$ (X = Cl, Br or I) (μ = 1.05–1.38 B.M. at 297 K).[1] Detailed variable temperature magnetic studies will be required to explain these strange magnetic moments.

Attempts to grow crystals of $[NbCl_4(SeMe_2)_2]$ were ultimately unsuccessful and only resulted in yellow $[Nb_2Cl_6(SeMe_2)_2(\mu\text{-}Cl)_2]$ crystals (Figure 3.10 and Table 3.10). The crystal structure of $[Nb_2Cl_6(SeMe_2)_2(\mu\text{-}Cl)_2]$ was found to be similar, but not isomorphous, to $[Nb_2Cl_6(SMe_2)_2(\mu\text{-}Cl)_2]$. The selenium analogue, contains a Nb–Nb single bond (3.0524(9) Å), compared to $[Nb_2Cl_6(SMe_2)_2(\mu\text{-}Cl)_2]$ which has a Nb–Nb bond length of 3.1094(5) Å, showing Nb(IV) dimeric centres.[19]

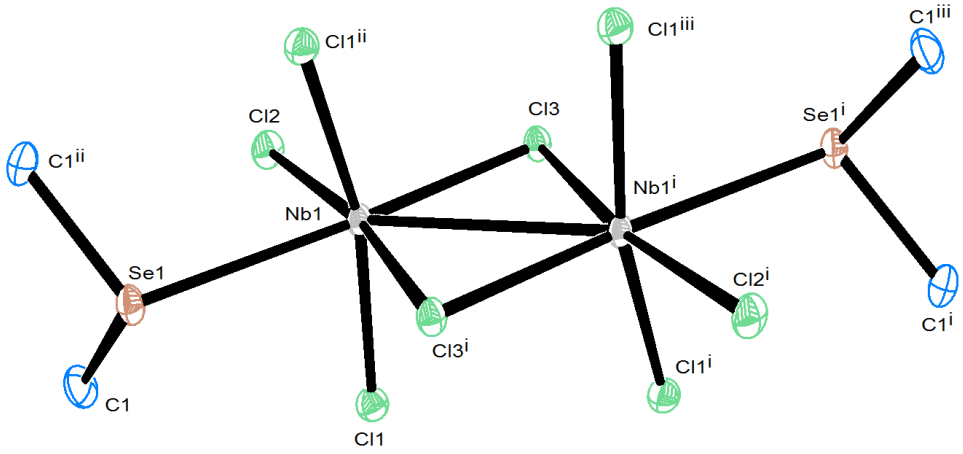

Figure 3.10 The structure of $[Nb_2Cl_6(SeMe_2)_2(\mu\text{-}Cl)_2]$ showing the atom numbering scheme and with ellipsoids drawn at the 50 % probability level. Hydrogen atoms are omitted for clarity. Symmetry operation: i = x, -y, 1 - z; ii = 1 - x, y, z; iii = 1-x, -y, 1 - z.

Table 3.10 Selected bond lengths (Å) angles (°) for $[Nb_2Cl_6(SeMe_2)_2(\mu\text{-}Cl)_2]$

Bond lengths		**Bond Angles**			
Nb1–Cl1	**2.297(1)**	**Cl1–Nb1–Cl2**	**92.04(3)**	**$Cl1^{ii}$–Nb1–$Cl3^{i}$**	**86.67(3)**
Nb1–Cl2	**2.385(1)**	**Cl1–Nb1–Cl3**	**97.83(3)**	**$Cl1^{ii}$–Nb1–Se1**	**82.36(3)**
Nb1–Cl3	**2.405(1)**	**Cl1–Nb1–$Cl3^{i}$**	**86.67(3)**	**Cl2–Nb1–Cl3**	**87.32(5)**
Nb1–$Cl3^{i}$	**2.472(1)**	**Cl1–Nb1–Se1**	**82.36(3)**	**Cl2–Nb1–Se1**	**87.40(4)**
Nb1–$Nb1^{i}$	**3.0524(9)**	**$Cl1^{ii}$–Nb1–Cl2**	**92.04(3)**	**Cl3–Nb1–$Cl3^{i}$**	**102.51(4)**
Nb1–Se1	**2.7518(8)**	**$Cl1^{ii}$–Nb1–Cl3**	**97.83(3)**	**$Cl3^{i}$–Nb1–Se1**	**82.77(4)**

$[Nb_2Cl_8(TeMe_2)_4]$ was prepared by combining $NbCl_4$ and $TeMe_2$ in CH_2Cl_2 solution and stirring for three days at room temperature (see Experimental section). A brown complex with a 2:1 $TeMe_2$:$NbCl_4$ composition was obtained; the red crystals were grown by allowing a saturated CH_2Cl_2 solution of the complex to slowly evaporate under a nitrogen atmosphere. The crystal structure of $[Nb_2Cl_4(TeMe_2)_4(\mu\text{-}Cl)_4]$ (Figure 3.11 and Table 3.11) is very similar to the phosphine analogue $[Nb_2Cl_4(PR_3)_4(\mu\text{-}Cl)_4]$, which displays two eight-coordinate Nb^{4+} centres bonding with a Nb–Nb bond (2.8208(8) Å) to form a dimer.[20-22] There are four Cl bridging ligands arranged in the plane linking to the Nb centres. The far IR spectrum is similar to that described of $[NbCl_4(SeMe_2)_2]$ with ν(Nb–Cl) = 358, 326, 276, 250 cm^{-1} (Figure A6.28). The formation of $[Nb_2Cl_4(TeMe_2)_4(\mu\text{-}Cl)_4]$ is a remarkable and illustrates the complexity of Nb(IV) chalcogenoether chemistry.

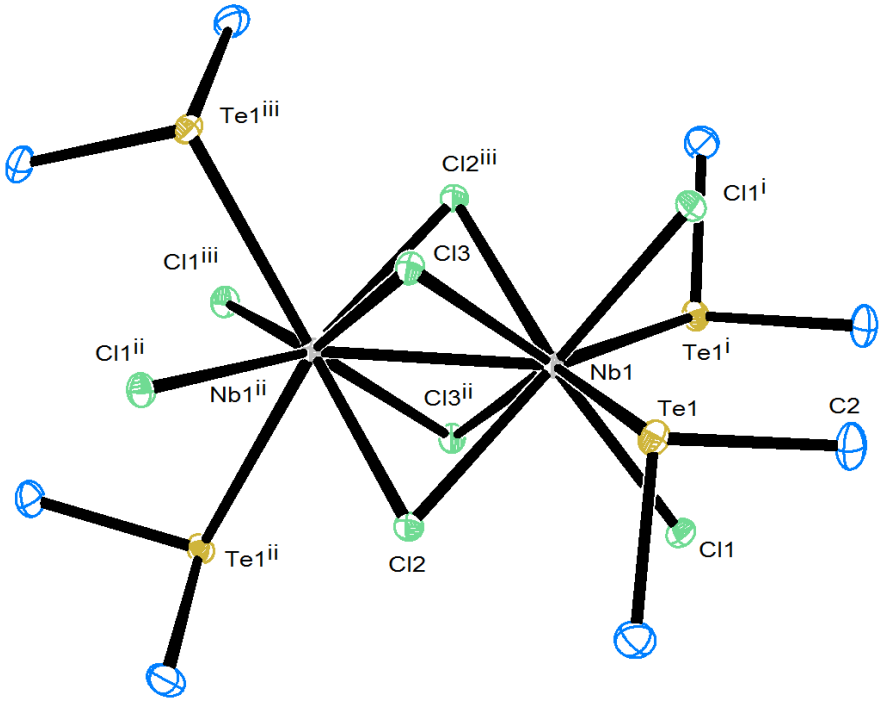

Figure 3.11 The structure of $[Nb_2Cl_4(TeMe_2)_4(\mu\text{-}Cl)_4]$ showing the atom numbering scheme and with ellipsoids drawn at the 50 % probability level. Hydrogen atoms are omitted for clarity. Symmetry operation: i = -y + 1, -x + 1, -z + 2, ii = -x + 1, -y + 1, z, iii = y, x, -z + 2.

Table 3.11 Selected bond lengths (Å) angles (°) for $[Nb_2Cl_4(TeMe_2)_4(\mu\text{-}Cl)_4]$

Bond lengths		**Bond angles**	
Nb1–Cl1	**2.4922(8)**	**Cl1–Nb1–Cl1^{i}**	**105.14(4)**
Nb1–Cl2	**2.5548(9)**	**Cl2–Nb1–Cl2^{iii}**	**112.99(3)**
Nb1–Cl3	**2.5445(9)**	**Cl3–Nb1–Cl3^{ii}**	**112.68(3)**
Nb1–Nb1^{ii}	**2.8208(8)**	**Te1–Nb1–Te1^{i}**	**123.26(2)**
Nb1–Te1	**2.9591(3)**		

3.2.4 Bidentate chalcogenoether fragmentation reactions

It has been reported that chalcogenoether ligands can undergo C–E cleavage in some reactions and the products might contain sulfide or selenide ligands or even RE^- groups.[4, 19, 23] Since Cl^- and S^{2-} ligands are very difficult to distinguish by X-ray crystallography; some examples were initially identified as the wrong structure and subsequently corrected after publication.[19, 23, 24]

Crystals of $[Nb_2Cl_4\{MeS(CH_2)_3SMe\}_2(\mu\text{-}S)_2]$ were obtained as a minor product from a 1:1 mixture of $NbCl_4$ and $MeS(CH_2)_3SMe$ in CH_2Cl_2 over *ca.* 6 weeks. The Nb–Nb distance (2.881(1) Å) is consistent with a single bond and allows the determination of the metal oxidation state as Nb(IV) and confirms the bridge as containing sulfide (S^{2-}) ligands rather than a bridging chloride (Cl^-) (Figure 3.12 and Table 3.12).[19, 23] The bridging sulfur atom must result from C–S cleavage of the $MeS(CH_2)_3SMe$ ligands.

The reaction of $NbCl_4$ with *o*-$C_6H_4(CH_2SeMe)_2$ affords a brown diamagnetic product in low yield. The ^1H and $^{13}C\{^1H\}$ NMR spectra indicate the presence of CH_2Se and the aromatic backbone, but not the presences of SeMe. Crystals grown from the reaction mixture show the presence of free 1,3-dihydro-benzo[*c*]selenophane (*o*-$C_6H_4(CH_2)_2Se$) (Figure 3.13 a). Fragmentation of the ligand *o*-$C_6H_4(CH_2SeMe)_2$ has been reported to occur in other systems and by reaction with $[Ta_2Cl_4(SMe_2)_2(\mu\text{-}Cl)_2(\mu\text{-}SMe_2)]$, to form $[Ta_2Cl_4\{o\text{-}C_6H_4(CH_2SeMe)_2\}_2(\mu\text{-}Se)_2]$ (Figure 3.13 b).[4, 25-27]

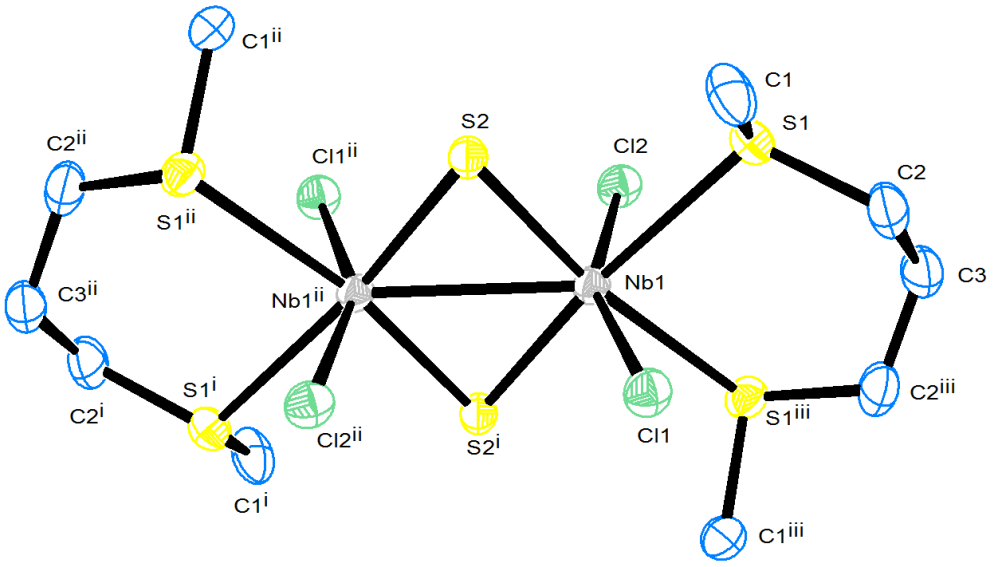

Figure 3.12 The structure of $[Nb_2Cl_4\{MeS(CH_2)_3SMe\}_2(\mu\text{-}S)_2]$ showing the atom numbering scheme and with ellipsoids drawn at the 50 % probability level. Hydrogen atoms are omitted for clarity. Symmetry operation: i = 1 - x, 1 - y, -z; ii = 1 - x, 1 - y, z; iii = x, y, -z.

Table 3.12 Selected bond lengths (Å) angles (°) for $[Nb_2Cl_4\{MeS(CH_2)_3SMe\}_2(\mu\text{-}S)_2]$

Bond lengths		**Bond Angles**			
Nb1–Cl1	**2.374(2)**	**Cl1–Nb1–S1**	**83.70(4)**	**Cl2–Nb1–S2**	**96.76(3)**
Nb1–Cl2	**2.382(1)**	**Cl1–Nb1–S1^{iii}**	**83.70(4)**	**Cl2–Nb1–S2^{i}**	**96.76(3)**
Nb1–Nb1^{ii}	**2.881(1)**	**Cl1–Nb1–S2**	**98.14(3)**	**S1–Nb1–S1^{iii}**	**87.28(5)**
Nb1–S1	**2.677(1)**	**Cl1–Nb1–S2^{i}**	**98.14(3)**	**S1–Nb1–S2**	**84.11(3)**
Nb1–S2	**2.349(1)**	**Cl2–Nb1–S1**	**78.72(4)**	**S1^{iii}–Nb1–S2^{i}**	**84.11(3)**
		Cl2–Nb1–S1^{iii}	**78.72(4)**	**S2–Nb1–S2^{i}**	**104.33(4)**

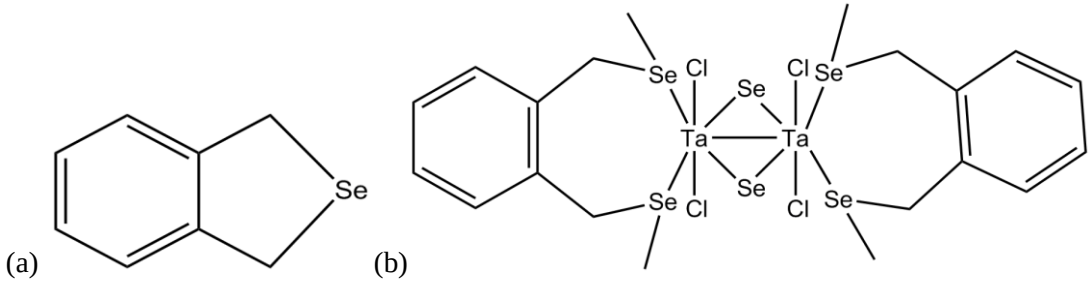

Figure 3.13 (a) 1,3-dihydro-benzo[c]selenophane and (b) the structure of $[Ta_2Cl_4\{o\text{-}C_6H_4(CH_2SeMe)_2\}_2(\mu\text{-}Se)_2]$ from reference 4.

The crystal structure of the present complex contains two superimposed molecules, the major component (occupancy 90 %) is $[Nb_2Cl_4\{o\text{-}C_6H_4(CH_2)_2Se\}_4(\mu\text{-}Se)_2]$ (Figure 3.14 a), while the minor component (occupancy 10 %) is $[Nb_2Cl_4\{o\text{-}C_6H_4(CH_2)_2Se\}_4(\mu\text{-}Se)(\mu\text{-}Se_2)]$ (Figure 3.14 b). The major and minor compounds are the same in numerous single crystals, although the ratio of the two is slightly different in each case. The Se–Se distance in μ-Se_2 is 2.28(2) Å , this indicates a Se_2^{2-} ligand,[28] the Nb–Nb distance is 2.8980(9) Å , suggesting the niobium is in the Nb(IV) oxidation state.[19]

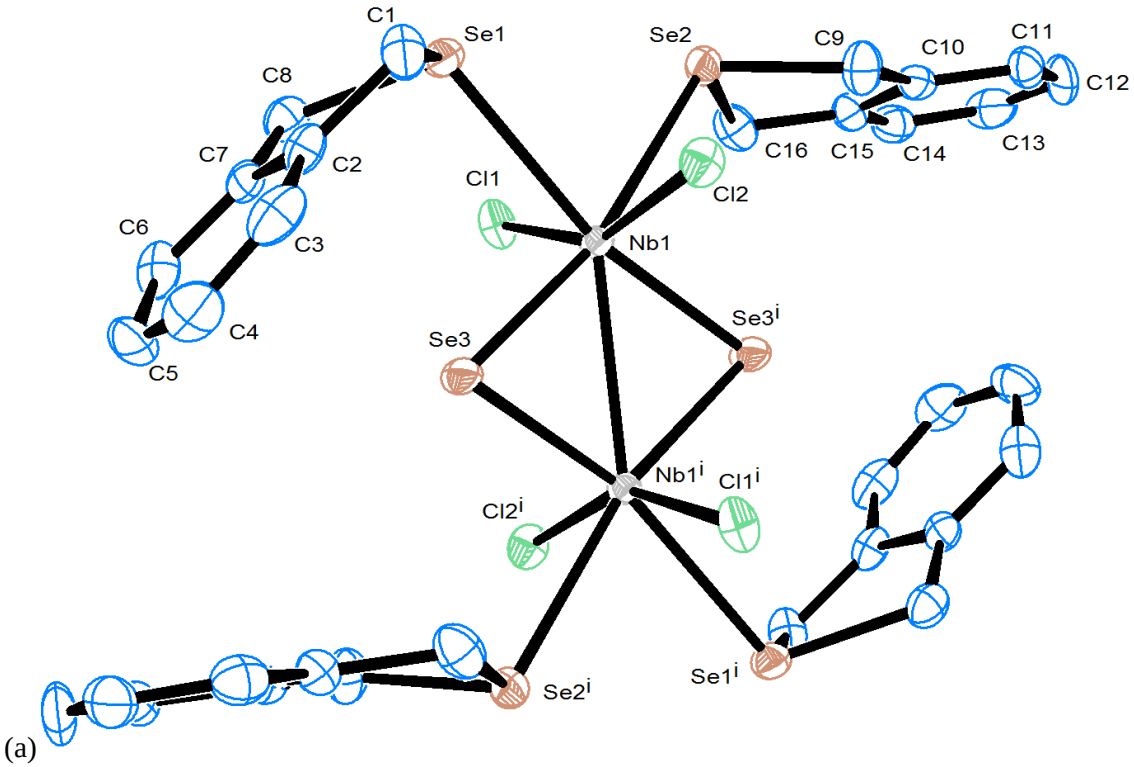

(a)

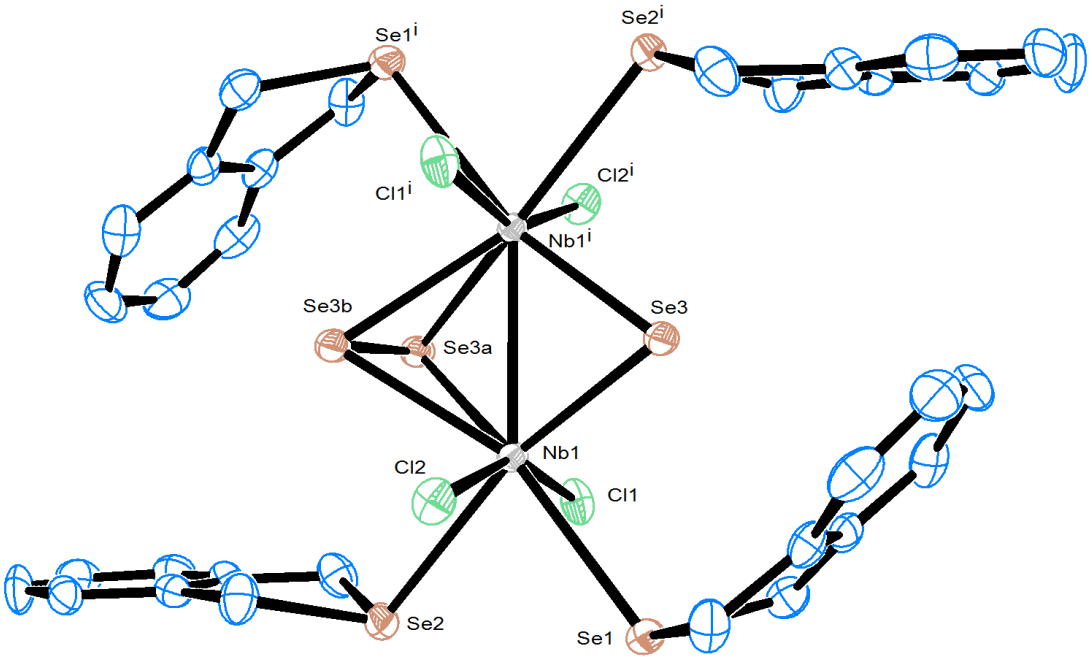

(b)

Figure 3.14 (a) The structure of $[Nb_2Cl_4\{o\text{-}C_6H_4(CH_2)_2Se\}_4(\mu\text{-}Se)_2]$ showing the atom numbering scheme and with ellipsoids drawn at the 50 % probability level. Hydrogen atoms are omitted for clarity. Symmetry operation: i = 1 - x, -y, -z. (b) The structure of $[Nb_2Cl_4\{o\text{-}C_6H_4(CH_2)_2Se\}_4(\mu\text{-}Se)(\mu\text{-}Se_2)]$ showing the atom numbering scheme and with ellipsoids drawn at the 50 % probability level. Hydrogen atoms are omitted for clarity. Symmetry operation: i = 1 - x, -y, -z.

Table 3.13 Selected bond lengths (Å) angles (°) for $[Nb_2Cl_4\{o\text{-}C_6H_4(CH_2)_2Se\}_4(\mu\text{-}Se)_x]$

Bond lengths		**Bond angles**	
Nb1–Cl1	**2.384(1)**	**Cl1–Nb1–Cl2**	**152.68(6)**
Nb1–Cl2	**2.372(2)**	**Se1–Nb1–Se2**	**79.79(2)**
Nb1–Nb1^{ii}	**2.8980(9)**	**Nb1–Se3–Nb1**	**72.36(3)**
Nb1–Se1	**2.8266(8)**	**Nb1–Se3a–Nb1**	**64.3(3)**
Nb1–Se2	**2.8214(7)**	**Nb1–Se3b–Nb1**	**65.3(3)**
Nb1–Se3	**2.4579(8)**		
Nb1–Se3a	**2.73(1)**		
Nb1–Se3b	**2.712(1)**		
Se3a–Se3b	**2.28(2)**		

3.2.5 LPCVD application

$[NbCl_4\{PrS(CH_2)_2S^iPr\}]$, $[NbCl_4\{^nBuSe(CH_2)_3Se^nBu\}]$ and $[NbCl_4(Se^nBu_2)_2]$ were all tested for potential LPCVD application at *ca.* 600–750 ℃ of 0.05 mmHg. However, carbon ($[NbCl_4\{^iPrS(CH_2)_2S^iPr\}]$) or elemental selenium ($[NbCl_4\{^nBuSe(CH_2)_3Se^nBu\}]$ and $[NbCl_4(Se^nBu_2)_2]$) were deposited instead of NbE_2 thin films (E = S, Se). A possible reason for this might be that the ligands in these Nb(IV) complexes readily dissociate and result in formation of the less volatile $NbCl_4$. The free thio- and selenoethers then undergo thermal decomposition to result in either elemental selenium or carbon thin films on substrates.

Such ligand loss is demonstrated in the recrystallization of $[NbCl_4(EMe_2)_2]$ (E = S, Se and Te) in Section 3.2.3. Both $[NbCl_4(SMe_2)_2]$ and $[NbCl_4(SeMe_2)_2]$ decomposed into $[Nb_2Cl_6(EMe_2)_2(\mu\text{-}Cl)_2]$ (E = S, Se) under mild recrystallization conditions, and the third example formed the dimer $[Nb_2Cl_4(TeMe_2)_4(\mu\text{-}Cl)_4]$ (Figure 3.9–3.11). Hence it was concluded that these Nb(IV) complexes were not suitable an single source LPCVD reagents.

3.3 Conclusion

The first series of six- and eight- coordinate $NbCl_4$ complexes featuring neutral sulfur and selenium ligands have been synthesised and characterised. These complexes are generally paramagnetic but the six- and eight- coordinate $[NbCl_4(bidentate)_n]$ (n = 1 or 2) complexes can be distinguished using IR spectroscopy.

Selected monodentate thio- and selenoether ligands form both 1:1 and 2:1 ligand:metal complexes with $NbCl_4$, and it is likely that both forms are present in solution. The 1:1 complexes, such as $[NbCl_6(EMe_2)_2(\mu\text{-}Cl)_2]$ (E = S, Se), are diamagnetic dimers in the solid state, whilst the 2:1 complexes appear to be six-coordinate monomers, demonstrated by $[NbCl_4(SMe_2)_2]$ and $[NbCl_4(Se^nBu_2)_2]$. Crystallographic data of $[Nb_2Cl_4(TeMe_2)_4(\mu\text{-}Cl)_4]$ confirms an unexpected 2:1 dimethyltelluride eight-coordinate dimer complex; it is possible that $[NbCl_4(SeMe_2)_2]$ is also dimeric based upon spectroscopic data.

The complexes, $[NbCl_4\{^iPrS(CH_2)_2S^iPr\}]$, $[NbCl_4\{^nBuSe(CH_2)_3Se^nBu\}]$ and $[NbCl_4(Se^nBu_2)_2]$, are deemed to be unsuitable as single source LPCVD precursors because of insufficient volatility or the facile loss of the chalcogenoether ligands at higher temperature.

3.4 Experimental

3.4.1 $[Nb_2Cl_4(THF)_2(\mu\text{-}Cl)_2(\mu\text{-}SMe_2)]$

$[NbCl_4(THF)_2]$ (189 mg, 0.5 mmol) was suspended in anhydrous toluene (20 mL) at room temperature, and a solution of SMe_2 (0.11 mL, 1.5 mmol) was added. The colour changed to purple after 5 minutes, and after stirring overnight, the solution was filtered. The remaining solid part was dried in *vacuo* and identified as unreacted starting material. (0.063g, 0.33 %). The dark purple solution was dried *in vacuo*. for 5 hours to afford a purple solid. Yield: 15 mg, 10 %. ^{1}H NMR ($CDCl_3$, 298 K): δ 2.13 (t, [4H], $OCH_2\underline{CH_2}$), 3.31 (s, [3H], SCH_3), 4.51 (t, [4H], OCH_2). IR (Nujol, cm^{-1}): 396, 383, 339 (Nb–Cl).

Crystal of $[Nb_2Cl_4(THF)_2(\mu\text{-}Cl)_2(\mu\text{-}SMe_2)]\cdot 2[C_6H_6]$

$[NbCl_4(THF)_2]$ (189 mg, 0.5 mmol) was suspended in anhydrous benzene (10 mL) at room temperature, and added to a stirred solution of SMe_2 (0.15 mL, 2.0 mmol) in benzene (5 mL). After one hour, the purple solution was filtered and evaporated *in vacuo,* to afford a pink sticky solid. *n*-Hexane (5 mL) was added to dissolve pink solid before it was stored in a fridge (0 ℃). Pink crystals were formed after 12 hours.

$NbCl_4$ with bidentate chalcogenoethers

3.4.2 $[NbCl_4\{MeS(CH_2)_2SMe\}_2]$

$NbCl_4$ (82 mg, 0.35 mmol) was suspended in toluene (5 mL) at room temperature. A solution of $MeS(CH_2)_2SMe$ (640 mg, 5.24 mmol) in toluene (5 ml) was added and the resulting solution stirred for 3 days. After filtering off any remaining solid, the filtrate was taken to dryness *in vacuo*, leaving a sticky brown solid. The brown solid was dissolved in CH_2Cl_2 (30 mL), filtered, and the red brown filtrate taken to dryness *in vacuo* to give a brown powder. Yield: 19 mg, 11 %. Required for $C_8H_{20}Cl_4NbS_4$ (479.22 g/mol): C, 20.1; H, 4.2. Found: C, 19.9; H, 4.1. IR (Nujol, cm^{-1}): 305s, 282s (Nb–Cl). UV-vis/cm^{-1}: 42 370, 32 900, 24 940, 18 830, 14 290, 11 050. Red crystals were grown by slow evaporation of a CH_2Cl_2 solution under a nitrogen atmosphere.

3.4.3 $[NbCl_4\{MeS(CH_2)_2SMe\}]$

$NbCl_4$ (71 mg, 0.3 mmol) was suspended in CH_2Cl_2 (10 mL) at room temperature. A solution of $MeS(CH_2)_2SMe$ (36 mg, 0.3 mmol) in CH_2Cl_2 (2 mL) was added and the solution stirred for 3 days. After filtering, the orange solution was evaporated *in vacuo*. *n*-Hexane (10 mL) was added to wash the solid and the washings decanted via a syringe. The dark brown solid was dried *in vacuo*. Yield: 74 mg, 69 %. Microanalyses were typically high in C/H, due to some of the 2:1 complex present. Required for $C_4H_{10}Cl_4NbS_2$ (356.97 g/mol): C, 13.46; H, 2.82. Found from 1st experiments:

C, 15.95; H, 3.56. Found from 2nd experiments: C, 15.95; H, 3.51 (please see section 3.2.2 for detail). IR (Nujol, cm^{-1}): 350, 335, 325sh, 312sh (Nb–Cl). Red crystals were grown by slow evaporation of a CH_2Cl_2 solution under a nitrogen atmosphere.

3.4.4 [$NbCl_4\{^iPrS(CH_2)_2S^iPr\}$]

$NbCl_4$ (70 mg, 0.3 mmol) was suspended in CH_2Cl_2 (15 mL) at room temperature. A solution of $^iPrS(CH_2)_2S^iPr$ (53 mg, 0.3 mmol) in CH_2Cl_2 (2 mL) was added and the solution stirred for 3 days. The colour of the solution changed from colourless to red-brown. The solution was filtered and the solvent removed *in vacuo*, affording a sticky dark brown solid. *n*-Hexane (4 mL) was added, the suspension stirred and the solid filtered off. The solid was dried *in vacuo* leaving a red brown powder. Yield: 65 mg, 52.5 %. Required for $C_8H_{18}Cl_4NbS_2$ (413.08 g/mol): C, 23.3; H, 4.4. Found: C, 23.4; H, 4.5. IR (Nujol, cm^{-1}): 368sh, 353s, 339sh, 319sh (Nb–Cl). UV-vis/cm^{-1}: 34 500, 29 675, 24 270, 19 720, 14 700, 10 730. μ_{eff} = 1.69 B.M. Red crystals were grown by slow evaporation of a CH_2Cl_2 solution under a nitrogen atmosphere.

Alternative method: $NbCl_4$ (70 mg, 0.3 mmol) was suspended in toluene (15 mL) before the addition of $^iPrS(CH_2)_2S^iPr$ (108 mg, 0.6 mmol) at room temperature. After stirring for 5 days, the brown solution was filtered and the filtrate taken to dryness *in vacuo*, affording a sticky red-brown solid. This was washed with *n*-hexane (5 mL) and the solid filtered off and dried *in vacuo* to give a red powder. Yield: 58 mg, 47 %. Required for $C_8H_{18}Cl_4NbS_2$ (413.08 g/mol): C, 23.3; H, 4.4. Found: C, 23.9; H, 4.4. The product was spectroscopically identical to that from the other method.

3.4.5 [$NbCl_4\{MeS(CH_2)_3SMe\}$]

$NbCl_4$ (70 mg, 0.3 mmol) was suspended in CH_2Cl_2 (10 mL) and a CH_2Cl_2 solution (5 mL) of $MeS(CH_2)_3SMe$ (40 mg, 0.3 mmol) was added and stirred for 3 days. After filtering off any remaining solid, the red-yellow filtrate was taken to dryness *in vacuo,* leaving a sticky brown solid. This was washed with *n*-hexane (5 mL), filtered off and dried *in vacuo*, affording a brown powder. Yield: 30 mg, 27 %. Required for $C_5H_{12}Cl_4NbS_2$ (371.0 g/mol): C, 16.2; H, 3.3. Found: C, 16.3; H, 3.3. IR (Nujol, cm^{-1}): 356, 350, 340, 325 (Nb–Cl). UV-vis/cm^{-1}: 43 670, 32 260, 21 000, 19 200, 11 900.

A mixture of yellow (minor) and red (major) crystals were grown from a 1:1 mixture of $NbCl_4$ and $MeS(CH_2)_3SMe$ in CH_2Cl_2 over *ca.* 6 weeks. The red crystals were found to be [$NbCl_4\{MeS(CH_2)_3SMe\}$], whilst the yellow crystals were identified as [$Nb_2Cl_4\{MeS(CH_2)_3SMe\}_2(\mu\text{-}S)_2$].

3.4.6 [$NbCl_4\{o\text{-}C_6H_4(CH_2SEt)_2\}$]

$NbCl_4$ (70 mg, 0.3 mmol) was suspended in CH_2Cl_2 (15 mL) and a CH_2Cl_2 solution (2 mL) of $o\text{-}C_6H_4(CH_2SEt)_2$ (68 mg, 0.3 mmol) was added with continued stirring. After 2 days the yellow-

orange solution was filtered and the filtrate taken to dryness *in vacuo*. The product was washed with *n*-hexane (5 mL) and dried *in vacuo*. Orange solid. Yield: 21 mg, 15 %. Required for $C_{12}H_{18}Cl_4NbS_2$ (461.12 g/mol): C, 31.3; H, 3.9. Found: C, 31.5; H, 4.1. IR (Nujol, cm^{-1}): 365s, 341s (Nb–Cl). UV-vis/cm^{-1}: 43 100, 33 000, 27 020, 18 730, 13 900. Yellow crystals were grown by allowing a CH_2Cl_2 solution to evaporate under a nitrogen atmosphere.

3.4.7 [$NbCl_4${$MeSe(CH_2)_2SeMe$}]

$NbCl_4$ (70 mg, 0.3 mmol) was suspended in CH_2Cl_2 (15 mL) and a solution of $MeSe(CH_2)_2SeMe$ (66 mg, 0.3 mmol) in CH_2Cl_2 (2 mL) was added. After stirring for 3 days the orange solution was filtered, and the remaining orange solid redissolved in CH_2Cl_2 (20 mL). This solution was filtered and taken to dryness *in vacuo*. The product was stirred with *n*-hexane (5 mL), collected by filtration and dried i*n vacuo*, leaving an orange powder. Yield: 16 mg, 12 %. Required for $C_5H_{12}Cl_4NbSe_2$ (450.76 g/mol): C, 10.7; H, 2.2. Found: C, 10.8; H, 2.2. IR (Nujol, cm^{-1}): 382, 372, 337 (Nb–Cl). UV-vis/cm^{-1}: 45 300, 34 250, 23 000, 13 950, 11 250.

3.4.8 [$NbCl_4${$MeSe(CH_2)_3SeMe$}]

$NbCl_4$ (70 mg, 0.3 mmol) was suspended in CH_2Cl_2 (10 mL) and $MeSe(CH_2)_3SeMe$ (67 mg, 0.3 mmol) in CH_2Cl_2 (5 mL) was added and stirred for 2 days affording a green-brown solution. The solution was filtered and the brown filtrate was evaporated to dryness *in vacuo*. The dark brown solid was washed by *n*-hexane (5 mL), and dried *in vacuo*. Yield: 29 mg, 21 %. Required for $C_5H_{12}Cl_4NbSe_2$ (464.79 g/mol): C, 12.92; H, 2.6. Found: C, 13.09; H, 2.69. IR (Nujol, cm^{-1}): 359, 345, 323 (Nb–Cl). UV-vis/cm^{-1}: 44 850, 36 600, 20 700, 19 350, 12 000, 10 950. Red crystals were grown by allowing a CH_2Cl_2 solution to evaporate under a nitrogen atmosphere. The crystals of [$NbCl_4$($MeSe(CH_2)_3SeMe$)] were twinned and this was modelled with a 45 : 55 ratio.

3.4.9 [$NbCl_4${$^nBuSe(CH_2)_3Se^nBu$}]

$NbCl_4$ (70 mg, 0.3 mmol) was suspended in CH_2Cl_2 (10 mL). A solution of $^nBuSe(CH_2)_3Se^nBu$ (93 mg, 0.3 mmol) in CH_2Cl_2 (5 mL) was added and stirred for 3 days giving a yellow solution. This was filtered and the yellow filtrate was evaporated *in vacuo* affording a red-orange oil. *n*-Hexane (4 mL) was added and the mixture stirred. The orange sticky solid was filtered off and dried *in vacuo*. Yield: 29 mg, 18 %. Required for $C_{11}H_{24}Cl_4NbSe_2$ (548.95): C, 24.1; H, 4.4. Found: C, 24.0; H, 4.7. IR (Nujol, cm^{-1}): 376sh, 344 (Nb–Cl). UV-vis/cm^{-1}: 41 000, 34 600, 24 400, 20 400, 11 600.

3.4.10 [$NbCl_4${$^tBuTe(CH_2)_3Te^tBu$}$_2$]

$NbCl_4$ (70 mg, 0.3 mmol) was suspended in CH_2Cl_2 (10 mL). The Schlenk tube was covered with foil to exclude light, before it was cooled in an ice bath. A solution of $^tBuTe(CH_2)_3Te^tBu$ (130 mg,

0.3 mmol) in CH_2Cl_2 (2 mL) was added and the deep brown solution was stirred overnight before being filtered, the solid was washed with *n*-hexane (10 mL) and dried *in vacuo*, leaving a dark powder. Yield: 73 mg, 37 %. Required for $C_{22}H_{48}Cl_4NbTe_4$ (1057.7): C, 25.0; H, 4.6. Found: C, 24.5; H, 4.8. IR (Nujol, cm^{-1}): 355, 336, 320 (Nb–Cl). UV-vis/cm^{-1}: 41 700, 35 200, 28 650, 19 500.

$NbCl_4$ with monodentate chalcogenoethers

3.4.11 $[NbCl_4(SMe_2)_2]$

$NbCl_4$ (70 mg, 0.3 mmol) was suspended in CH_2Cl_2 (10 mL) and SMe_2 (2 mL) was added with stirring for 1 h. The dark purple solution formed was filtered and the filtrate taken to dryness *in vacuo* while in an ice bath to afford a dark purple sticky solid. Yield: 76 mg 70 %. The complex loses SMe_2 on warming or *in vacuo* and a satisfactory microanalysis could not be obtained. IR (Nujol, cm^{-1}): 380, 362, 343, 321 (Nb–Cl).

A CH_2Cl_2 solution of the complex was allowed to evaporate under a nitrogen atmosphere, yielding yellow crystals identified as $[Nb_2Cl_8(SMe_2)_2]$ from an X-ray structure determination.

3.4.12 $[Nb_2Cl_6(SMe_2)_2(\mu\text{-}Cl)_2]$

$NbCl_4$ (105 mg, 0.4 mmol) was stirred with a mixture of SMe_2 (1 mL) and CH_2Cl_2 (10 mL). The solution was stirred for 1 hour, before the dark purple solution was filtered. The brown solid (27 mg) obtained was unreacted $NbCl_4$ identified by its IR spectrum. The dark purple filtrate was diluted by *n*-hexane (50 mL) and stirred overnight under a nitrogen flow, resulting in a brown precipitate. The purple solution was decanted and the brown powder washed with *n*-hexane (10 mL) and dried *in vacuo*. Yield: 27 mg, 23 %. Required for $C_2H_6Cl_4NbS_2$ (296.85 g/mol): C, 8.1; H, 2.0. Found: C, 8.3; H, 1.9. IR (Nujol, cm^{-1}): 375sh, 351, 336sh (Nb–Cl). UV-vis/cm^{-1}: 34 480, 28 900, 21 460, 19 680, 9 900.

3.4.13 $[NbCl_4(SeMe_2)_2]$

$NbCl_4$ (70 mg, 0.3 mmol) was suspended in CH_2Cl_2 (15 mL) before a solution of $SeMe_2$ (100 mg, 0.9 mmol) in CH_2Cl_2 (3 mL) was added and the reaction mixture was stirred overnight. The brownish-green solution was filtered and the filtrate taken to dryness *in vacuo* with cooling to 0 ℃, producing a brown solid. Yield: 73 mg, 54 %. Required for $C_4H_{12}Cl_4NbSe_2$ (452.78 g/mol): C, 10.6; H, 2.7. Found: C, 10.8; H, 2.7. IR (Nujol, cm^{-1}): 341, 314, 286, 255 (Nb–Cl). UV-vis/cm^{-1}: 37 000, 29 500, 20 620, 20 000, 13 700sh, 10 800.

Slow evaporation of a solution of the complex in CH_2Cl_2 under nitrogen produced yellow crystals identified as $[Nb_2Cl_8(SeMe_2)_2]$.

3.4.14 $[NbCl_4(Se^nBu_2)_2]$

Prepared in a similar fashion to $[NbCl_4(SeMe_2)_2]$ from $NbCl_4$ (70 mg, 0.3 mmol) and Se^nBu_2 (116 mg, 0.6 mmol), and isolated as a sticky dark solid, after washing with *n*-hexane. Yield: 36 mg, 19 %. Required for $C_{16}H_{36}Cl_4NbSe_2$ (621.09 g/mol): C, 30.9; H, 5.8. Found: C, 31.1; H, 6.1. IR (Nujol, cm^{-1}): 378, 343, 320sh (Nb–Cl). UV-vis/cm^{-1}: 40 400, 35 000sh, 24 000, 14 200, 11 380.

3.4.15 $[Nb_2Cl_4(TeMe_2)_4(\mu\text{-}Cl)_4]$

$NbCl_4$ (70 mg, 0.3 mmol) was placed in a Schlenk tube before a solution of $TeMe_2$ (142 mg, 0.9 mmol) in CH_2Cl_2 (10 mL) was added. The solution was stirred for 3 days at room temperature and a dark brown solution and dark solid formed. The solution was filtered, giving a dark orange solid which was dried *in vacuo*. Yield: 47 mg, 28 %. Required for $C_8H_{24}Cl_8Nb_2Te_4$ (1100.1 g/mol): C, 8.7; H, 2.2. Found: C, 8.8; H, 2.1. IR (Nujol, cm^{-1}): 358w, 326br, 276, 250w (Nb–Cl). UV-vis/cm^{-1}: 32 260, 28 500, 19 800, 17 240, 9 300.

Red crystals were grown by allowing a CH_2Cl_2 solution to evaporate under a nitrogen atmosphere.

3.4.16 $[Nb_2Cl_4\{o\text{-}C_6H_4(CH_2)_2Se\}_4(\mu\text{-}Se_n)(\mu\text{-}Se)]$ (n = 1 or 2, please see text)

$NbCl_4$ (70 mg, 0.3 mmol) was suspended in CH_2Cl_2 (15 mL) before a solution of $o\text{-}C_6H_4(CH_2SeMe)_2$ (92.0 mg, 0.3 mmol) in CH_2Cl_2 (2 mL) was added and the mixture stirred for 2 days affording a brown suspension. After removal of suspended solids by filtration, the brown solution was taken to dryness *in vacuo*. *n*-Hexane (5 mL) was added and the solid produced filtered off and dried *in vacuo* to afford a dark brown powder. Yield: 70 mg, 34 %. Found: C, 27.0; H, 3.0. IR (Nujol, cm^{-1}): 365sh, 343sh, 330 (Nb–Cl). ^1H NMR ($CDCl_3$, 298 K): δ = 4.35 (s, [4H], CH_2), 7.14–7.26 (m, [4H], Ar). ^1H NMR (CD_2Cl_2, 298 K): δ = 4.22 (s, [4H], CH_2), 7.05–7.18 (m, [4H], Ar). $^{13}C\{^1H\}$ NMR (CD_2Cl_2, 298 K): δ = 30.2 (CH_2), 126.4 (Ar), 126.9 (Ar). Yellow-brown crystals were grown by allowing a CH_2Cl_2 solution to evaporate under a nitrogen atmosphere.

X-ray data of crystals $[Nb_2Cl_4\{o\text{-}C_6H_4(CH_2)_2Se\}_4(\mu\text{-}Se_x)(\mu\text{-}Se)]$ refinement

The molecule exhibits inversion symmetry at the centre of the $Nb_2Cl_2Se_{4+x}$ core. Refinements proceed as expected with the large electron density peak refined as a single Se atom initially, and this is the expected geometry for a species forming a μ^2 bridge such as in $[Ta_2Cl_4\{o\text{-}C_6H_4(CH_2SeMe)_2\}_2(\mu\text{-}Se)_2]$ (Ta–(μ-Se) = 2.489(2) and 2.484(2) Å).[4]

However, two significant electron densities remain asymmetrically above (1.302 Å) and below (0.982 Å) the (μ-Se) and free refinement of the occupancies give the values. The geometry of the two new positions is consistent with a Se_2^{2-} unit (2.73(1) and 2.65(1) Å). The occupancy sum is 1.0 for μ-Se and μ-Se_2 combined and difficult to explain, so that a mixture of Se- and Se_2-bridged Nb Centres

cannot exist without also involving a partially vacant bridging site. The complex $[Nb_2Cl_4(THT)_4(\mu\text{-}S_2)(\mu\text{-}S)]$ is a sulphur bridged analogue[29] of the minor component reported.

An overlay of the crystal structure $[Nb_2Cl_4(THT)_4(\mu\text{-}S)(\mu\text{-}S_2)]$[29] and $[Nb_2Cl_4\{o\text{-}C_6H_4(CH_2)_2Se\}_4(\mu\text{-}Se_2)(\mu\text{-}Se)]$ suggests that these crystal structures have similar geometry in the $M_2Cl_4(\mu\text{-}E)(\mu\text{-}E_2)$ (E = S, Se) core (Figure 3.15).

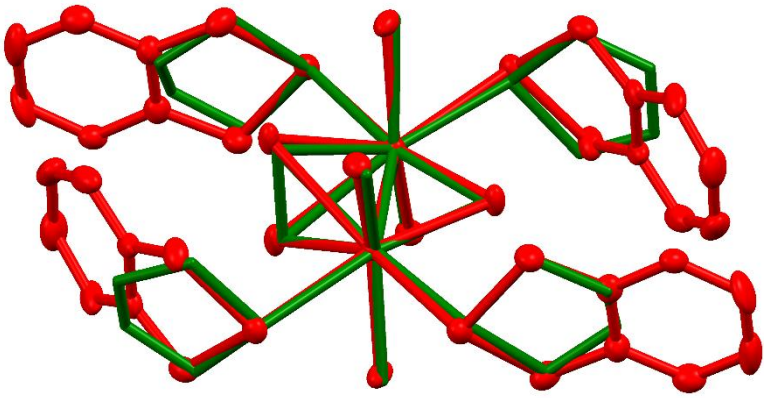

Figure 3.15 Overlay of crystal structures of $[Nb_2Cl_4(THT)_4(\mu\text{-}S)(\mu\text{-}S_2)]$ (green)[29] and $[Nb_2Cl_4\{o\text{-}C_6H_4(CH_2)_2Se\}_4(\mu\text{-}Se_2)(\mu\text{-}Se)]$ (Red, as with Figure 3.14 b).

Attempted LPCVD application

3.4.17 Precursor $[NbCl_4\{^iPrS(CH_2)_2S^iPr\}]$

This precursor (20 mg) was dissolved in CH_2Cl_2 (0.5 mL) and loaded in a LPCVD tube in a glovebox. Silica substrates were loaded after the precursor was loaded and placed end-to-end. The tube was placed in a furnace before being linked to a vacuum pump (0.01 mmHg) which removed the CH_2Cl_2. The temperature in the furnace was increased to 600 ℃ and left for 10 minutes to allow the temperature to equilibrate. The precursor end was moved through the furnace to the opposite edge immediately. No significant change of the precursor was observed. The furnace was then heated to 750 ℃ and the tube remained in the furnace during the temperature increase. The precursor remained at the end of the LPCVD tube. The LPCVD experiment was stopped and the furnace was cooled to ambient temperature. Silica substrates were unloaded under ambient conditions and no deposition was observed on the substrates.

3.4.18 Precursor $[NbCl_4\{^nBuSe(CH_2)_3Se^nBu\}]$

This precursor (*ca.* 10 mg) was dissolved in CH_2Cl_2 (1 mL) and loaded in a LPCVD tube in a glovebox. Silica substrates were loaded after the precursor was loaded and placed end-to-end. The tube was placed in a furnace before being linked to a vacuum pump (0.01 mmHg) which removed

the CH_2Cl_2. The temperature in the furnace was increased to 600 ℃ and stay for 10 minutes to allow the temperature to stabilise. The precursor end of the tube was moved into the furnace gradually until it reached the edge of the furnace. A red film was observed through the open end of the tube. The temperature was increased to 650 ℃ and no changed was observed. The furnace was then cooled to ambient temperature and the substrates were unloaded at ambient conditions. No deposited film was observed on substrates.

3.4.19 Precursor [$NbCl_4(Se^nBu_2)_2$]

This precursor (29 mg) was dissolved in CH_2Cl_2 (1 mL) and loaded in a LPCVD tube in a glovebox. Silica substrates were loaded after the precursor was loaded and placed end-to-end. The tube was placed in a furnace before being linked to a vacuum pump (0.01 mmHg) which removed the CH_2Cl_2. The temperature in the furnace was increased to 550 ℃ and stay for 10 minutes to allow the temperature to stabilise. The precursor end of the tube was moved into the furnace gradually until it reached the edge of the furnace. A red film was observed through the open end of the tube. The temperature was increased to 650 ℃ and no changed was observed. The furnace was then cooled to ambient temperature and the substrates were unloaded at ambient conditions. No deposited film was observed on substrates.

3.5 References

1. J. B. Hamilton and R. E. McCarley, *Inorg. Chem.*, 1970, **9**, 1333.
2. G. W. A. Fowles, D. J. Tidmarsh and R. A. Walton, *J. Inorg. Nucl. Chem.*, 1969, **31**, 2373.
3. J. B. Hamilton and R. E. McCarley, *Inorg. Chem.*, 1970, **9**, 1339.
4. S. L. Benjamin, Y.-P. Chang, M. Huggon, W. Levason and G. Reid, *Polyhedron*, 2015, **99**, 230.
5. S. L. Benjamin, C. H. de Groot, C. Gurnani, A. L. Hector, R. Huang, K. Ignatyev, W. Levason, S. J. Pearce, F. Thomas and G. Reid, *Chem. Mater.*, 2013, **25**, 4719.
6. S. L. Benjamin, Y.-P. Chang, C. Gurnani, A. L. Hector, M. Huggon, W. Levason and G. Reid, *Dalton Trans.*, 2014, **43**, 16640.
7. Y.-P. Chang, M.Sc Thesis, University of Southampton, 2014.
8. F. A. Cotton, S. A. Duraj and W. J. Roth, *Acta Cryst.*, 1985, **C41**, 878.
9. M. Jura, W. Levason, R. Ratnani, G. Reid and M. Webster, *Dalton Trans.*, 2010, **39**, 883.
10. J. K. Burdett, R. Hoffmann and R. C. Fay, *Inorg. Chem.*, 1978, **17**, 2553.
11. F. A. Cotton, L. R. Falvello and R. C. Najjar, *Inorg. Chem.*, 1983, **22**, 770.
12. R. Hart, W. Levason, B. Patel and G. Reid, *J. Chem. Soc., Dalton Trans.*, 2002, 3153.
13. K. Nakamoto, *Infrared and Raman Spectra of Inorganic and Coordination Compounds*, Wiley, New York, 1986.
14. S. L. Benjamin, Y.-P. Chang, A. L. Hector, M. Jura, W. Levason, G. Reid and G. Stenning, *Dalton Trans.*, 2016, **45**, 8192.
15. R. L. Deutscher and D. L. Kepert, *Inorg. Chem.*, 1970, **9**, 2305.
16. D. L. Kepert and K. R. Trigwell, *J. Chem. Soc., Dalton Trans.*, 1975, 1903.
17. D. L. Kepert, B. W. Skelton and A. H. White, *J. Chem. Soc., Dalton Trans.*, 1981, 652.
18. G. W. A. Fowles, D. J. Tidmarsh and R. A. Walton, *Inorg. Chem.*, 1969, **8**, 631.
19. E. Babaian-Kibala, F. A. Cotton and P. A. Kibala, *Inorg. Chem.*, 1990, **29**, 4002.
20. F. A. Cotton, S. A. Duraj and W. J. Roth, *Inorg. Chem.*, 1984, **23**, 3592.
21. F. A. Cotton and W. J. Roth, *Inorg. Chem.*, 1984, **23**, 945.
22. P. D. W. Boyd, A. J. Nielson and C. E. F. Rickard, *J. Chem. Soc., Dalton Trans.*, 1987, 307.
23. J. A. M. Canich and F. A. Cotton, *Inorg. Chem.*, 1987, **26**, 3473.
24. W. Levason and G. Reid, *J. Chem. Res. (S)*, 2002, 467.
25. C. Gurnani, W. Levason, R. Ratnani, G. Reid and M. Webster, *Dalton Trans.*, 2008, 6274.
26. S. D. Reid, A. L. Hector, W. Levason, G. Reid, B. J. Waller and M. Webster, *Dalton Trans.*, 2007, 4769.

27. C. Gurnani, M. Jura, W. Levason, R. Ratnani, G. Reid and M. Webster, *Dalton Trans.*, 2009, 1611.

28. S. Hayashi, K. Matsuiwa, N. Nishizawa and W. Nakanishi, *J. Org. Chem.*, 2015, **80**, 11963.

29. M. G. B. Drew, D. A. Rice and D. M. Williams, *J. Chem. Soc., Dalton Trans.*, 1983, 2251.

Chapter 4: Chalcogenoether complexes of Nb(V) thio- and seleno-halides as single source precursors for LPCVD application

4.1 Introduction

The synthesis of niobium tetrachloride chalcogenoether complexes ([$NbCl_4$(chalcogenoether)]) has been described in Chapter 3 and the complexes able to undergo β-hydride elimination were tested in LPCVD. However, only carbon or elemental selenium films were deposited. Hence, the Nb(IV) precursors in Chapter 3 appear to be unsuitable as single source LPCVD precursors.

A range of [$NbCl_n$(chalcogenoether)] complexes have been tested as single source precursors for LPCVD as part of this project. They are Nb(III) dimers [$Nb_2Cl_4(S^nBu_2)_2(\mu\text{-}Cl)_2(\mu\text{-}S^nBu_2)$], Nb(IV) monomers (in Chapter 3) and Nb(V) monomers [$NbCl_5(E^nBu_2)$] (E = S, Se) (M.Sc work).[1-3] Only [$NbCl_5(E^nBu_2)$] have deposited NbE_2 thin films by LPCVD successfully.[1] The failures using Nb(III) and Nb(IV) precursors in LPCVD are probably because the $NbCl_n$ (n = 3 or 4) are too stable, resulting in distillation of the ligand and leaving behind $NbCl_n$ polymer under LPCVD conditions.

Pentavalent niobium complexes [$NbCl_5(E^nBu_2)$] (E = S, Se) do successfully deposit NbE_2 films, although the Nb(V) metal centre must be reduced in order to deposit the target $Nb^{IV}E_2$ thin films. However, these complexes most likely remain monomeric in LPCVD and transfer into the deposition region. However, those species have a 1:1 ratio of Nb:E, which is not ideal for NbE_2 films (Nb:E = 1:2). Therefore, this chapter starts the search for new possible single source Nb(V) precursor species for LPCVD.

[$NbECl_3(L)_n$] (E = S, Se; L = ligands) species are Nb(V) complexes with a direct Nb═E bond, which is a good starting point for an ideal single source CVD precursor, even without further chalcogenoether ligands. Complexes of $NbSCl_3$ with a range of Lewis bases have been reported, such as $[NbSCl_4]^-$,[4] [$NbSCl_3(SPPh_3)$],[5] $NbSCl_3(OPPh_3)$],[6] [$NbSCl_3(SEt_2)$],[6] and [$NbECl_3(NCCH_3)_2$] (E = S, Se).[6, 7] However, rearrangements occur in some systems to form dichalcogenide bridged dimers [$Nb_2Cl_4(SR_2)_4(\mu\text{-}Se_2)_2$] ($SR_2$ = SMe_2 or THT) and [$Nb_2X_4(THT)_4(\mu\text{-}S)(\mu\text{-}S_2)$] (X = Cl, Br).[8-11]

This chapter will describe different synthetic routes to approach [NbE_nCl_3(chalcogenoethers)$_n$] (E = S, Se) with full physical characterisation. The different chemical environment between Nb═E and Nb–Cl in [$NbSCl_3$(dichalcogenoethers)] will be discussed *via* crystal structures and multinuclear NMR spectroscopy. The dimer complex [$Nb_2Cl_4\{MeS(CH_2)_3SMe\}_2(\mu\text{-}S)(\mu\text{-}S_2)$] has been characterised by single crystal X-ray diffraction. In addition, the synthesis of [$NbSe_nCl_3(L)$] complexes has been explored by similar methods, however, the results are different. Some of the

complexes are potential LPCVD single source precursors for NbE_2 film deposition. They will be tested in LPCVD and the results will be described with scanning electron microscopy (SEM) and energy dispersive X-Ray analysis (EDX) data.

4.2 Result and Discussion

4.2.1 Preparation of niobium thio- and seleno- trihalide complexes

$NbSCl_3$ and $[NbSCl_3(NCCH_3)_2]$ were made by using a literature method.[7] The only difference between these two preparations are the solvents. The former was made in a CH_2Cl_2 solution, while the latter was in a CH_3CN solution (see experimental for detail). $[NbSCl_3(NCCH_3)_2]$ could also be made *via* dissolving $NbSCl_3$ in acetonitrile.

Complexes of $[NbSCl_3(L–L)]$ have been made by ligand substitution from $[NbSCl_3(NCCH_3)_2]$. In a typical experiment, $[NbSCl_3(NCCH_3)_2]$ was dissolved in CH_2Cl_2, and a CH_2Cl_2 solution with three equivalents of L–L ($MeS(CH_2)_2SMe$, $^{i}PrS(CH_2)_2S^{i}Pr$, $MeS(CH_2)_3SMe$, $^{n}BuS(CH_2)_3S^{n}Bu$ or $MeSe(CH_2)_3SeMe$) was added with stirring. The solution colour changed from green to yellow-green. Crystals of $[NbSCl_3\{MeS(CH_2)_2SMe\}]$, $[NbSCl_3\{^{i}PrS(CH_2)_2S^{i}Pr\}]$ and $[NbSCl_3\{MeSe(CH_2)_3SeMe\}]$ were obtained by the slow evaporation from saturated CH_2Cl_2 solutions under a dinitrogen atmosphere.

The $[NbSCl_3(ER_2)]$ (ER_2 = SMe_2, $S^{n}Bu_2$, $Se^{n}Bu_2$) species were prepared *via* a similar method to $[NbSCl_3(NCCH_3)_2]$. The complexes $[NbCl_5(ER_2)]$ were synthesised following a literature method initially,[1] before a solution of one equivalent of $S(SiMe_3)_2$ and CH_2Cl_2 was added with stirring. The solution colour changed from red to dark green. Crystals of $[NbSCl_3(SMe_2)]$ were grown by the slow evaporation of a saturated solution in CH_2Cl_2. The sulfide bridged dimer $[Nb_2Cl_4\{MeS(CH_2)_3SMe\}_2(\mu\text{-}S)(\mu\text{-}S_2)]$ was prepared using the same method as $[NbSCl_3(L)]$; green crystals grew by allowing the CH_2Cl_2 solution to evaporate to dryness in a nitrogen environment.

$[NbSeCl_3(NCCH_3)_2]$ was prepared by adding a solution of $Se(SiMe_3)_2$ and CH_3CN to $NbCl_5$ in acetonitrile. However, when adding $Se(SiMe_3)_2$ to $[NbCl_5(Se^{n}Bu_2)]$ in CH_2Cl_2 solution, black solid $[NbSe_2Cl_3(Se^{n}Bu_2)]$ precipitates (Scheme 4.1).

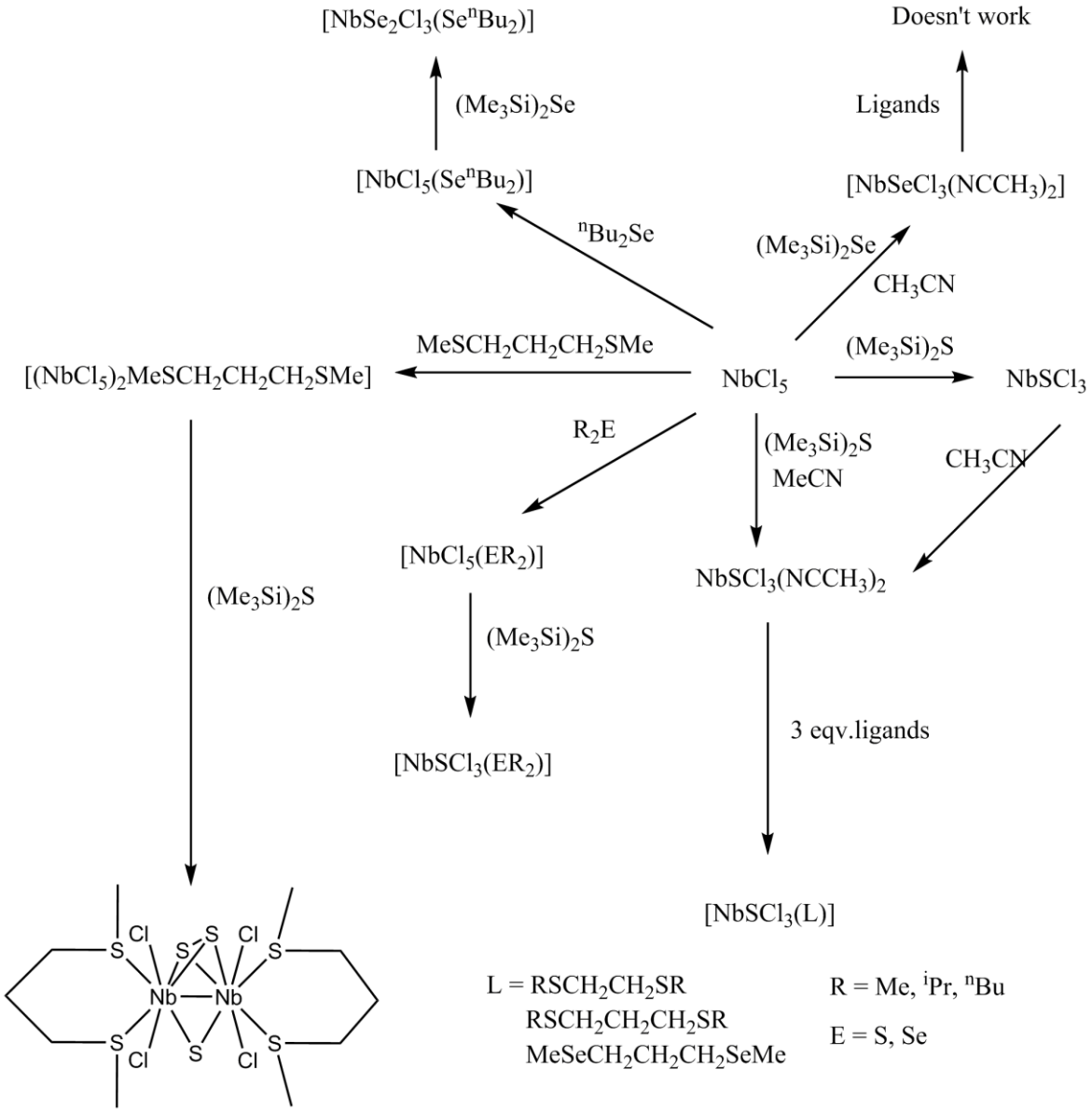

Scheme 4.1 Synthesis of $NbECl_3$ (E = S, Se) and related complexes in this report

4.2.2 Literature known starting material and authentication

$NbSCl_3$ was obtained as a dark green powder.[7] The colour of the product from this work is slightly different to that in the corresponding literature report of a brown solid.[12] The deep colour in our product is probably from $Nb_2S_3Cl_4$ impurities,[12] an over reacted product. Its infrared absorption (ν(Nb═S) = 550 cm^{-1}; Figure A6.30) corresponds to the literature value (550 cm^{-1}).[13] The solid state UV-visible spectrum shows three bands, the band at *ca.* 220 nm presumed to be Cl(π) → Nb charge transfer band, and two bands at *ca.* 290 and 400 nm are S(π) → Nb (Figure 4.1).[14]

The gas phase structure of $NbSCl_3$ has been reported;[12] unfortunately, recrystallization of the solid to produce single crystals has proved ultimately impossible.

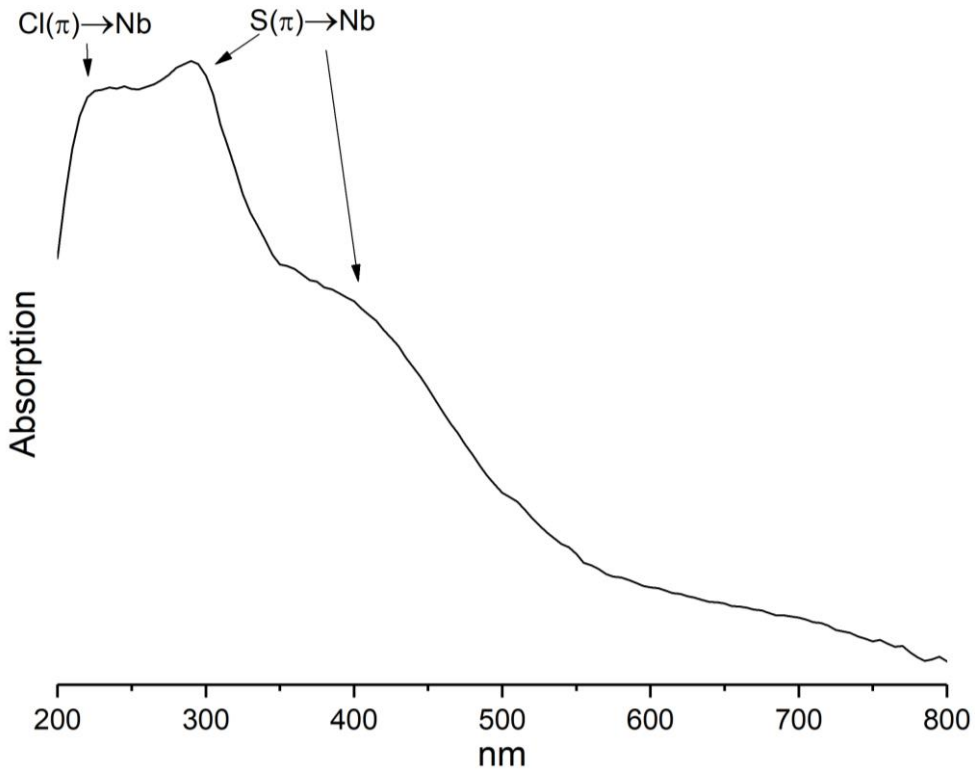

Figure 4.1 UV-visible spectrum of $NbSCl_3$ diffuse reflectance.

$[NbSCl_3(NCCH_3)_2]$ was made by literature method or reacting $NbSCl_3$ with acetonitrile. However, recrystallization of $[NbSCl_3(NCCH_3)_2]$ by allowing the CH_3CN solution to undergo slow evaporation failed.

4.2.3 $NbSCl_3$ dichalcogenoether monomers

The substitution of CH_3CN in $[NbSCl_3(NCCH_3)_2]$ using excess bidentate ligands in CH_2Cl_2 solution was successful, resulting in yellow-green products (dithioethers) or a yellow-brown solid ($MeSeCH_2CH_2CH_2SeMe$).

The structures of $[NbSCl_3\{MeS(CH_2)_2SMe\}]$, $[NbSCl_3\{^iPrS(CH_2)_2S^iPr\}]$ and $[NbSCl_3\{MeSe(CH_2)_3SeMe\}]$ form a typical pseudo octahedral geometries with deviation from ideal 90° and 180° (Fig. 4.2–4.5 and Table 4.1–4.3). All three structures contain the dichalcogenether in the *DL* form. Surprisingly, these crystal structures do not present significant S/Cl disorder. The Nb═S bond distance (*ca.* 2.10 Å) is expected to be shorter than the Nb–Cl distance (*ca.* 2.24 Å). The two Nb–S bonds from the neutral ligands also reflect the different *trans* influences. The Nb–$S_{trans\text{S}}$ distance are slightly longer than the Nb–$S_{trans\text{Cl}}$ distance by *ca.* 0.2–0.3 Å (Table 4.4). However, the S/Cl disorder effects in the crystal structure of $[NbSCl_3\{MeSe(CH_2)_3SeMe\}]$ result in similar Nb–$S_{trans\text{L}}$ distances (Table 4.4 for detail). Distinguishing between S^{2-} and Cl^- in X-ray single crystal data is also a big problem in other systems.[8, 11, 15]

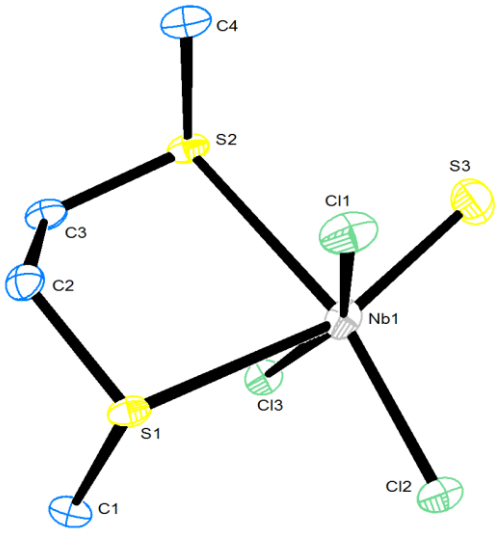

Figure 4.2 The structure of [$NbSCl_3${$MeS(CH_2)_2SMe$}] showing the atom numbering scheme and with ellipsoids drawn at the 50 % probability level. Hydrogen atoms are omitted for clarity.

Table 4.1 Selected bond lengths (Å) and angles (°) for [$NbSCl_3${$MeS(CH_2)_2SMe$}]

Bond lengths		**Bond Angles**			
Nb1–Cl1	**2.354(1)**	**Cl1–Nb1–Cl2**	**97.52(4)**	**Cl2–Nb1–S3**	**106.56(4)**
Nb1–Cl2	**2.242(1)**	**Cl1–Nb1–S1**	**77.05(4)**	**Cl3–Nb1–S1**	**84.15(3)**
Nb1–Cl3	**2.3619(9)**	**Cl1–Nb1–S2**	**86.36(3)**	**Cl3–Nb1–S2**	**76.78(3)**
Nb1–S1	**2.717(1)**	**Cl1–Nb1–S3**	**97.13(4)**	**Cl3–Nb1–S3**	**97.00(4)**
Nb1–S2	**2.739(1)**	**Cl2–Nb1–Cl3**	**95.76(4)**	**S1–Nb1–S2**	**78.18(3)**
Nb1–S3	**2.210(1)**	**Cl2–Nb1–S1**	**90.37(4)**	**S2–Nb1–S3**	**85.33(4)**

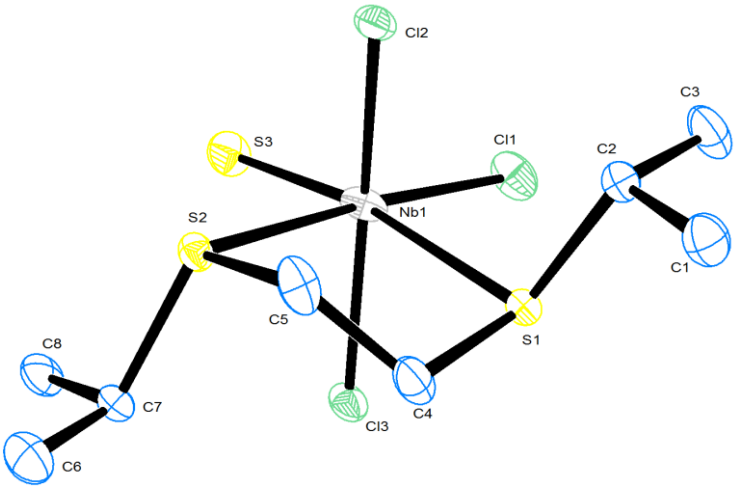

Figure 4.3 The structure of [$NbSCl_3${$^iPrS(CH_2)_2S^iPr$}] showing the atom numbering scheme and with ellipsoids drawn at the 50 % probability level. Hydrogen atoms are omitted for clarity.

Table 4.2 Selected bond lengths (Å) and angles (°) for [$NbSCl_3\{^iPrS(CH_2)_2S^iPr\}$]

Bond lengths		Bond Angles			
Nb1–Cl1	**2.2475(7)**	**Cl1–Nb1–Cl2**	**97.78(2)**	**Cl2–Nb1–S3**	**98.20(2)**
Nb1–Cl2	**2.3588(6)**	**Cl1–Nb1–Cl3**	**97.49(3)**	**Cl3–Nb1–S1**	**76.73(2)**
Nb1–Cl3	**2.3623(6)**	**Cl1–Nb1–S1**	**86.78(2)**	**Cl3–Nb1–S2**	**83.48(2)**
Nb1–S1	**2.7813(6)**	**Cl1–Nb1–S3**	**103.84(3)**	**Cl3–Nb1–S3**	**97.13(3)**
Nb1–S2	**2.7464(6)**	**Cl2–Nb1–S1**	**84.58(2)**	**S1–Nb1–S2**	**78.56(2)**
Nb1–S3	**2.2105(7)**	**Cl2–Nb1–S2**	**76.69(2)**	**S2–Nb1–S3**	**91.14(2)**

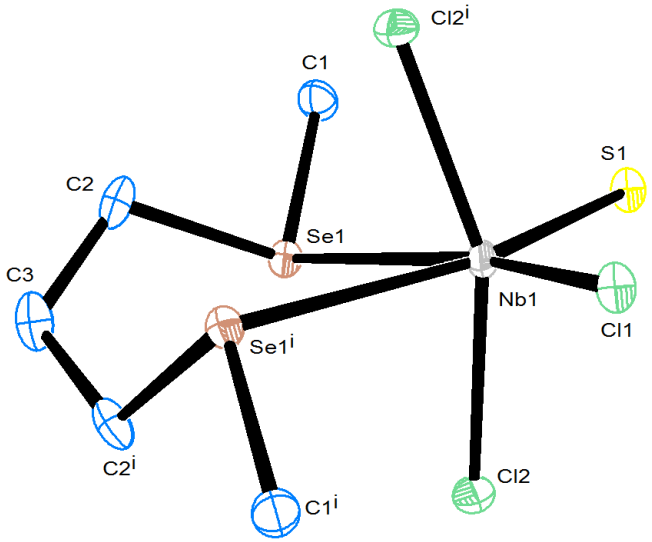

Figure 4.4 The structure of [$NbSCl_3\{MeSe(CH_2)_3SeMe\}$] showing the atom numbering scheme and with ellipsoids drawn at the 50 % probability level. Hydrogen atoms are omitted for clarity. Symmetry operation: i = -x, -y + 3/2, z.

Table 4.3 Selected bond lengths (Å) and angles (°) for [$NbSCl_3\{MeSe(CH_2)_3SeMe\}$]

Bond lengths		Bond Angles			
Nb1–Cl1	**2.308(7)**	**Cl1–Nb1–Cl2**	**96.7(2)**	**Cl2–Nb1–Se1^i**	**83.86(2)**
Nb1–Cl2	**2.3686(6)**	**Cl1–Nb1–Cl2^i**	**96.0(2)**	**Cl2^i–Nb1–S1**	**94.0(2)**
Nb1–S1	**2.197(8)**	**Cl1–Nb1–S1**	**105.73(5)**	**Cl2^i–Nb1–Se1**	**83.86(2)**
Nb1–Se1	**2.8799(4)**	**Cl1–Nb1–Se1^i**	**85.29(6)**	**Cl2^i–Nb1–Se1^i**	**79.07(2)**
		Cl2–Nb1–S1	**100.7(2)**	**S1–Nb1–Se1**	**89.90(8)**
		Cl2–Nb1–Se1	**79.07(2)**	**Se1–Nb1–Se1^i**	**79.27(1)**

Table 4.4 Comparing bond lengths (Å) of [$NbSCl_3$(dichalcogenoether)]

Complexes	Nb=S	Nb–$Cl_{trans E}$	Nb–$E_{trans S}$	Nb–$E_{trans Cl}$	Nb–$Cl_{trans Cl}$
[$NbSCl_3${$MeS(CH_2)_2SMe$}]	**2.210(1)**	**2.242(1)**	**2.739(1)**	**2.717(1)**	**2.352(1)**
[$NbSCl_3${$^iPrS(CH_2)_2S^iPr$}]	**2.2105(7)**	**2.2475(7)**	**2.7813(6)**	**2.7464(6)**	**2.3606(6)**
[$NbSCl_3${$MeSe(CH_2)_3SeMe$}]	**2.197(8)**	**2.308(7)**	**2.8799(4)**	**2.8799(4)**	**2.3686(6)**

4.2.4 Multinuclear NMR spectroscopy

The NMR samples of all three complexes were prepared in CD_2Cl_2 solution, and the ^{93}Nb NMR spectra each exhibit a broad resonance in the region δ = +500 to +550 ppm (Figure A7.11–A7.14), this is significantly shifted to high frequency when compared to [$NbCl_5$(chalcogenoether)] complexes (Chapter 5), but corresponds more closely to the ^{93}Nb NMR spectrum for [$NbSCl_3(NCCH_3)_2$] (δ = 414 ppm in CD_3CN at 298 K).[1, 14]

The ambient temperature ^{1}H NMR spectrum of [$NbSCl_3${$MeS(CH_2)_2SMe$}] in CD_2Cl_2 shows two broad resonances (δ = 2.77 and 2.22 ppm) which are assigned to the δ($SMe_{trans Cl}$) and δ($SMe_{trans S}$) protons, respectively, while the broad weaker resonances at δ = 3.26 and 3.02 ppm correspond to the two SCH_2 units (Figure 4.5). Upon cooling the solution to 183 K, the spectrum shows six main features. The most intense of these signals (δ = 2.06 and 2.63 ppm) are consistent with the methyl and methylene protons of dissociated dithiahexane (Figure 4.6). The remaining four signals are likely to be due to δ($CH_3S_{trans Cl}$), δ($CH_3S_{trans S}$), δ(-$CH_2S_{trans Cl}$) and δ(-$CH_2S_{trans S}$), suggesting slow pyramidal inversion at the sulfur centres; this has been shown in similar systems exhibiting dissociation of the dithioether in solution with fast exchange between coordinated and 'free ligand' at room temperature.[3]

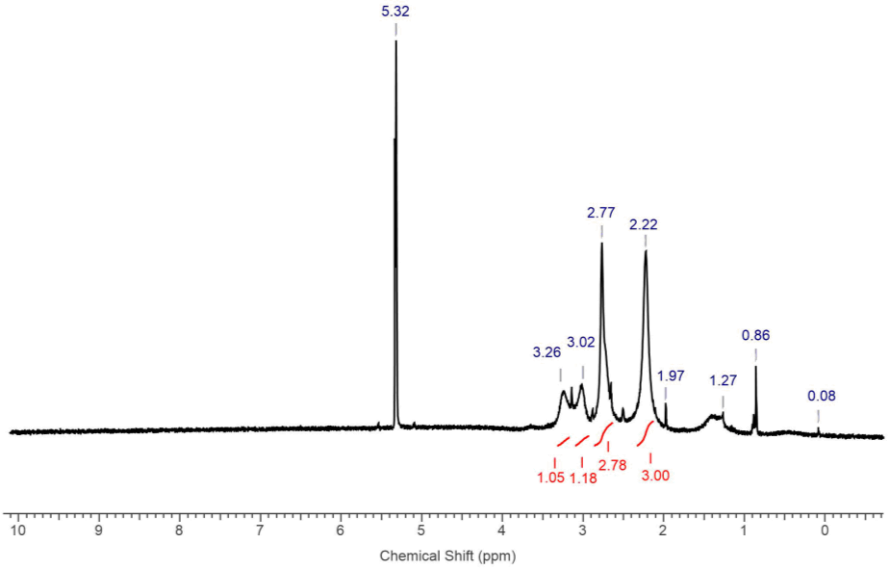

Figure 4.5 ^{1}H NMR spectrum of [$NbSCl_3${$MeS(CH_2)_2SMe$}] in CD_2Cl_2 at 298 K.

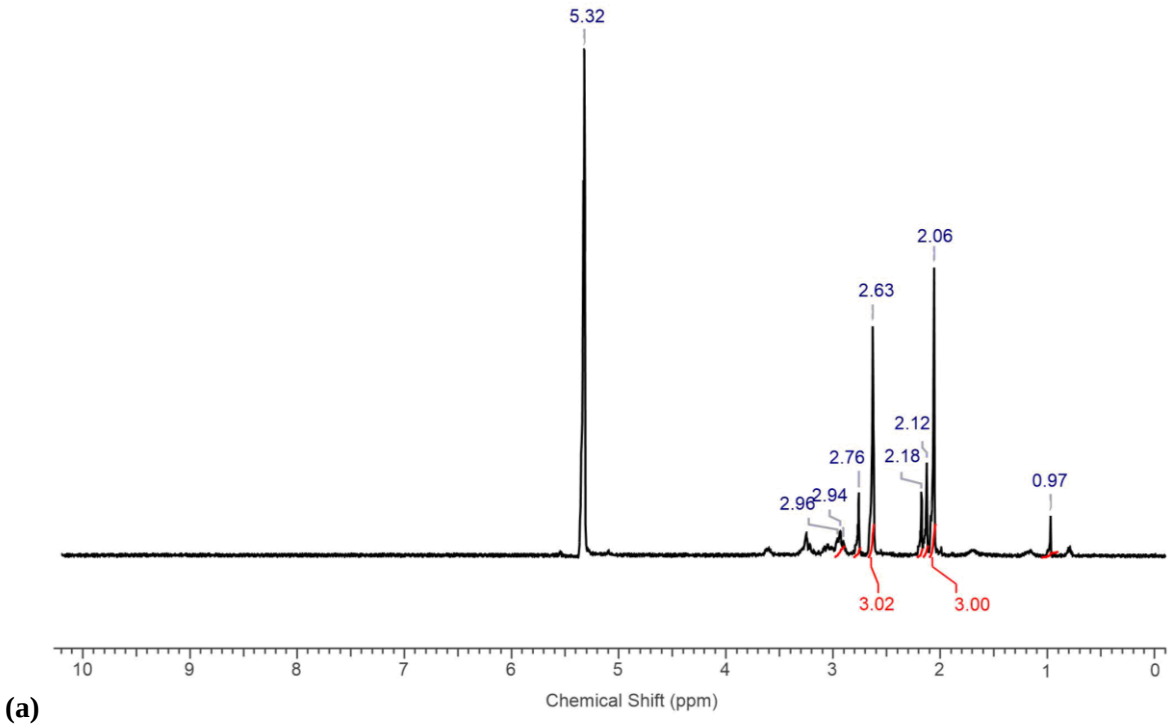

(a)

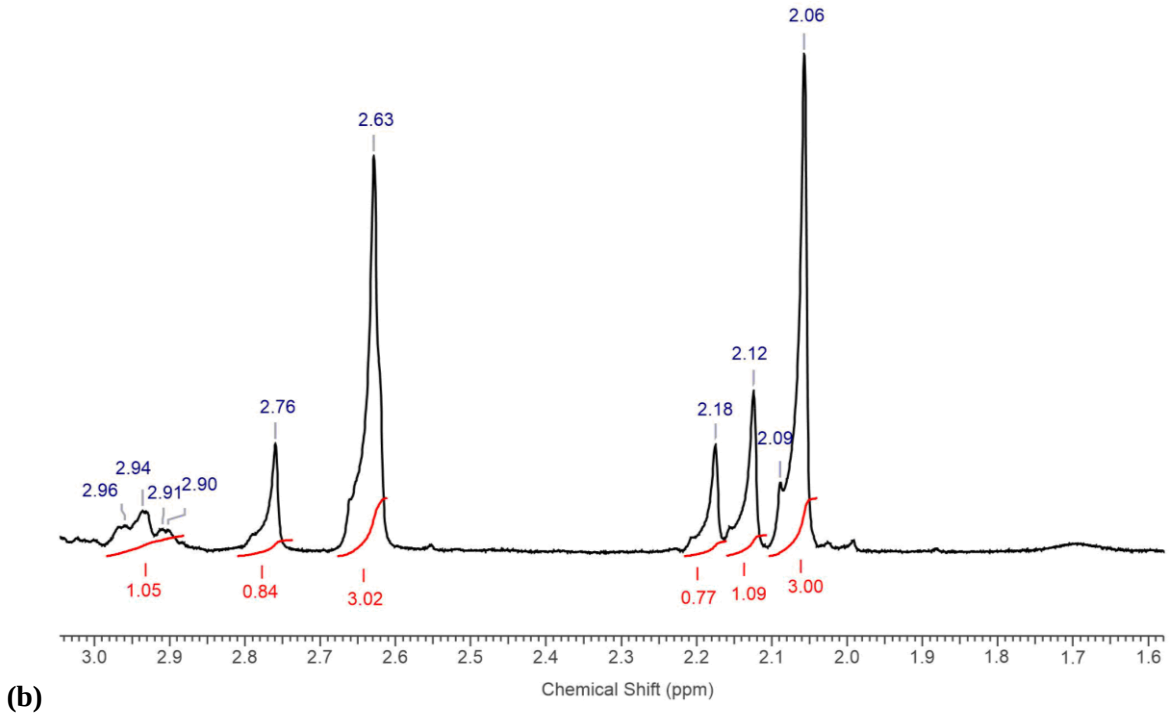

(b)

Figure 4.6 (a) ^{1}H NMR spectrum of $[NbSCl_3\{MeS(CH_2)_2SMe\}]$ in CD_2Cl_2 at 183 K; (b) selected expansion region of Figure 4.6 (a). The resonance at $\delta = 2.12$ is probably acetone impurity.

The ^{1}H NMR spectrum of [$NbSCl_3${$MeSe(CH_2)_3SeMe$}] in CD_2Cl_2 at ambient temperature presents two broad resonances (δ = 2.92 ppm, [4H] and 2.25 ppm, [8H]) (Figure 4.7). Upon cooling the solution to 253 K, these resonances split into two high intensity signals, three weaker signals of medium intensity and four weak and broad signals. The strong signals (δ = 2.59, 1.96 ppm) and the overlapping signal (δ = 2.07 ppm) with an integration ratio of 6:2:4 is consistent with free ligand dissociated from the complex;[16] this is supported by further splitting of the signal at δ = 2.59 at lower temperature (183 K) (Figure 4.8–4.9). The remaining two resonances (δ =2.72 and 2.32 ppm) can be assigned as two MeSe units which are *trans* to Nb═S and Nb–Cl (δ = 2.32 ppm, [3H] and 2.72 ppm, [3H]) and the four weak broad resonances (δ = 2.83–3.21 ppm, [6H]) are from Se*CH₂CH₂CH₂*Se (Figure 4.8–4.9). Such splitting suggest fast dissociation and exchange at ambient temperatures.

There is no observed ^{77}Se{^{1}H} NMR resonance for [$NbSCl_3${$MeSe(CH_2)_3SeMe$}] at ambient temperature, but multiple resonances are observed at δ = 163, 69 and 68 ppm when cooling to 223 K, where the most intensive resonance (δ = 68 ppm) is thought to be dissociated ligand (Figure A7.9). This also corresponds to the free ligand observed in the ^{1}H NMR spectra at low temperature (253 and 183 K).

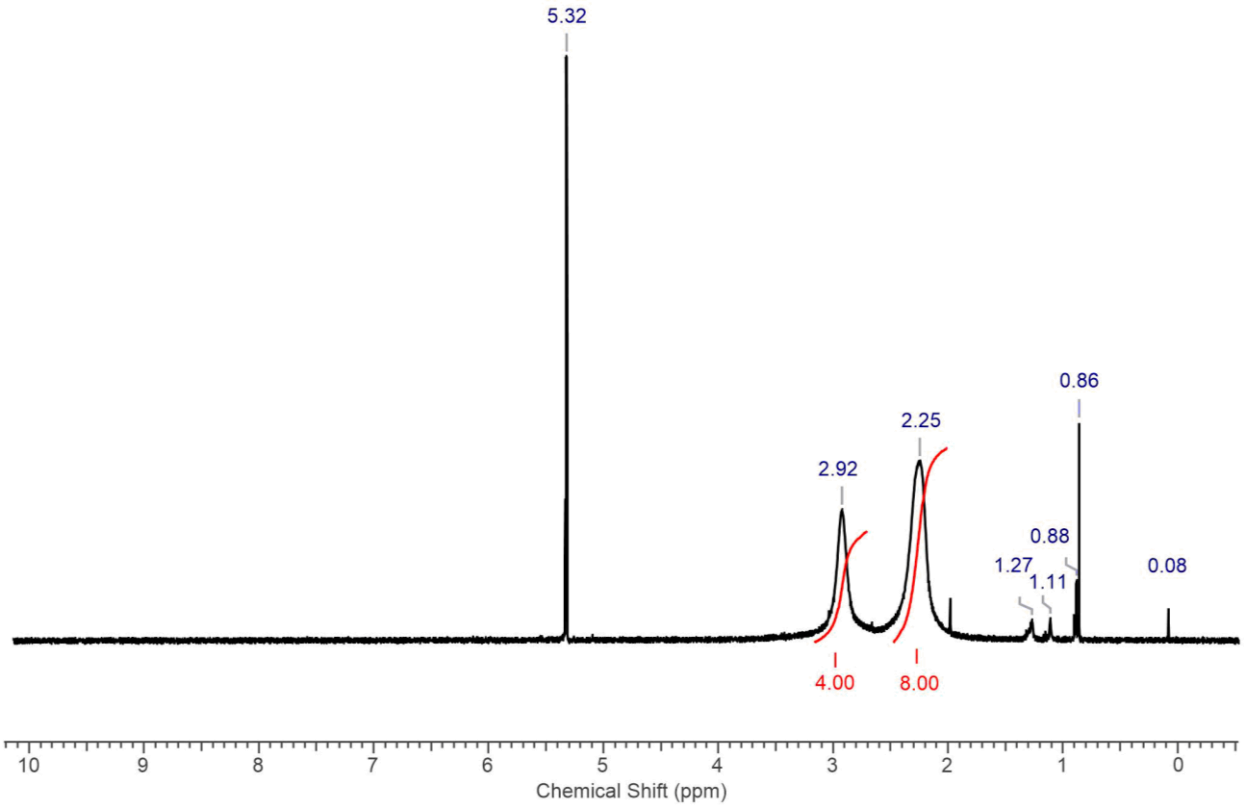

Figure 4.7 ^{1}H NMR spectrum of [$NbSCl_3${$MeSe(CH_2)_3SeMe$}] in CD_2Cl_2 at 298 K.

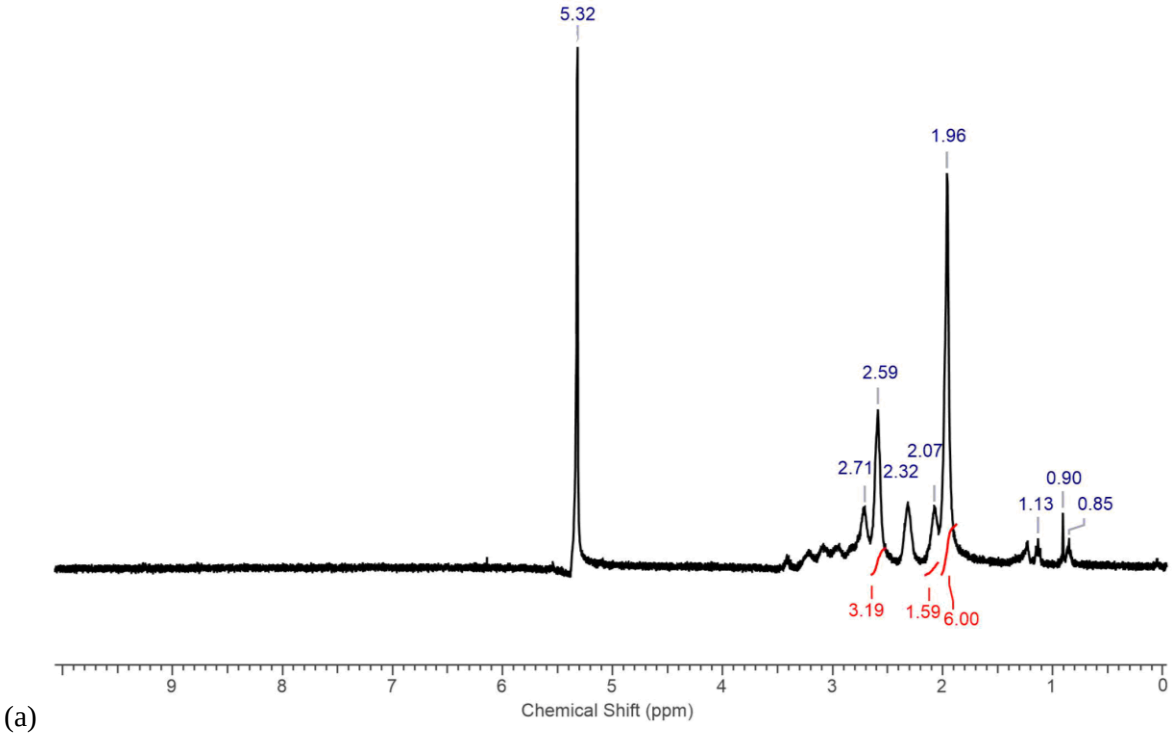

(a)

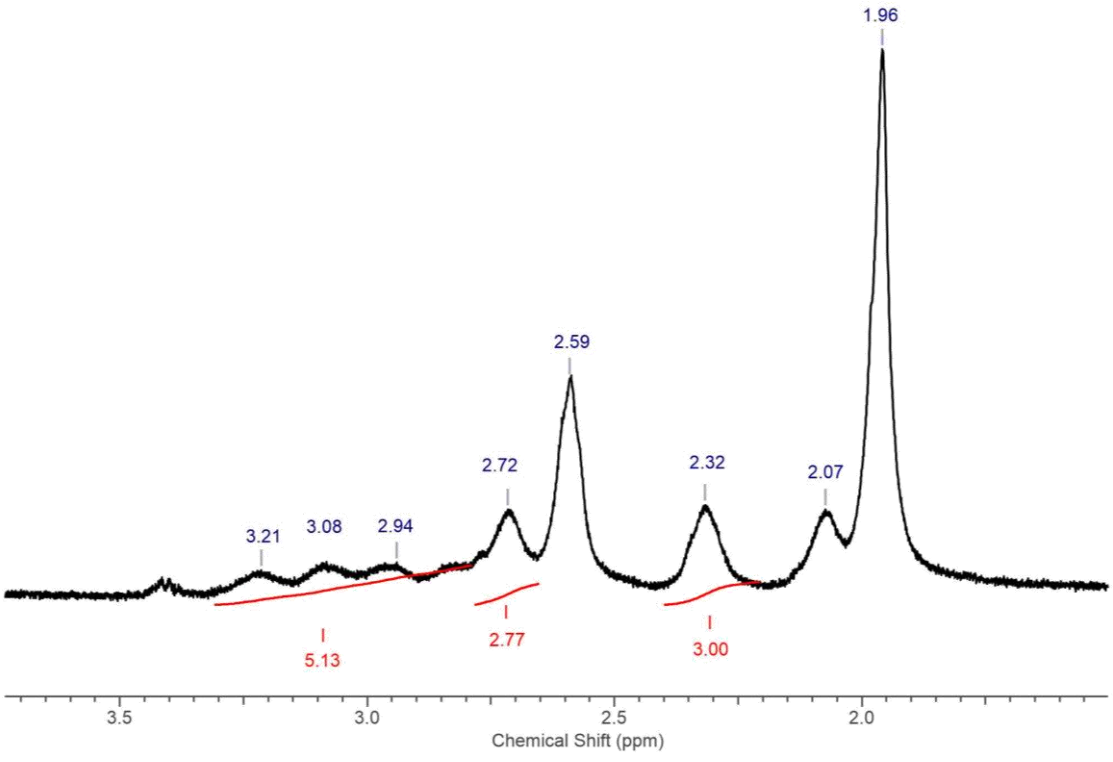

(b)

Figure 4.8 (a) ^{1}H NMR spectrum of [$NbSCl_3${$MeSe(CH_2)_3SeMe$}] in CD_2Cl_2 at 253 K; (b) selected expansion region of Figure 4.8 (a). The resonances at δ = 2.59, 2.07 and 1.96 ppm are from free $MeSe(CH_2)_3SeMe$.

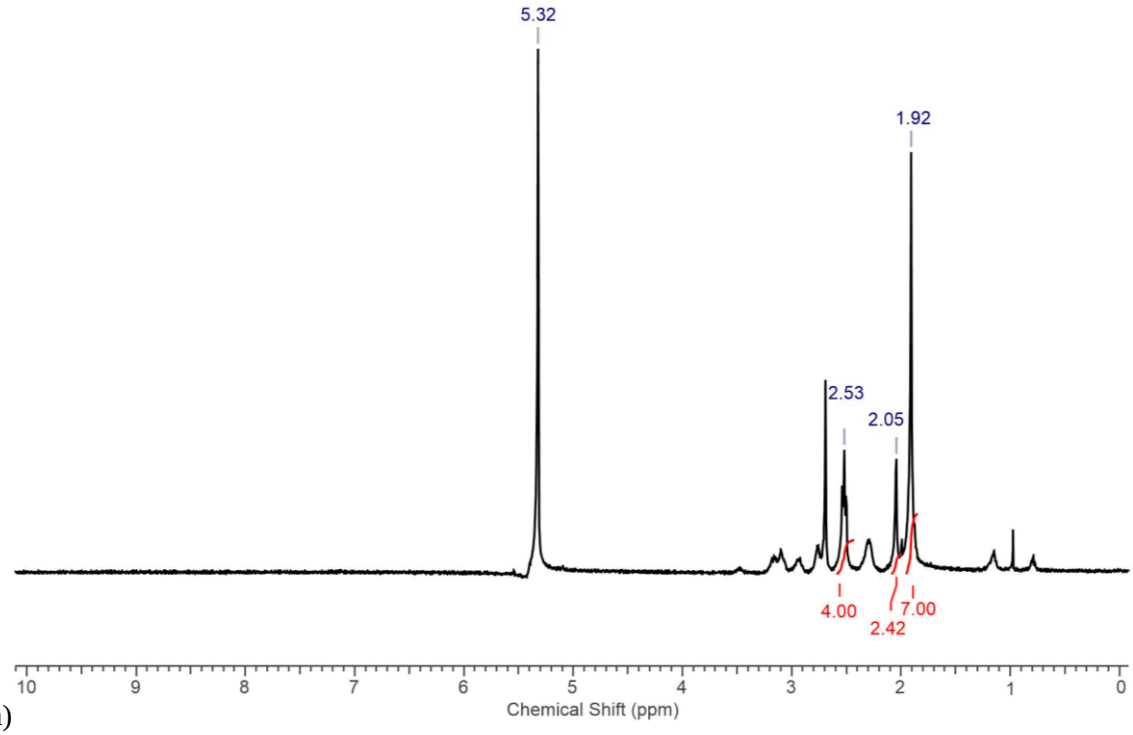

(a)

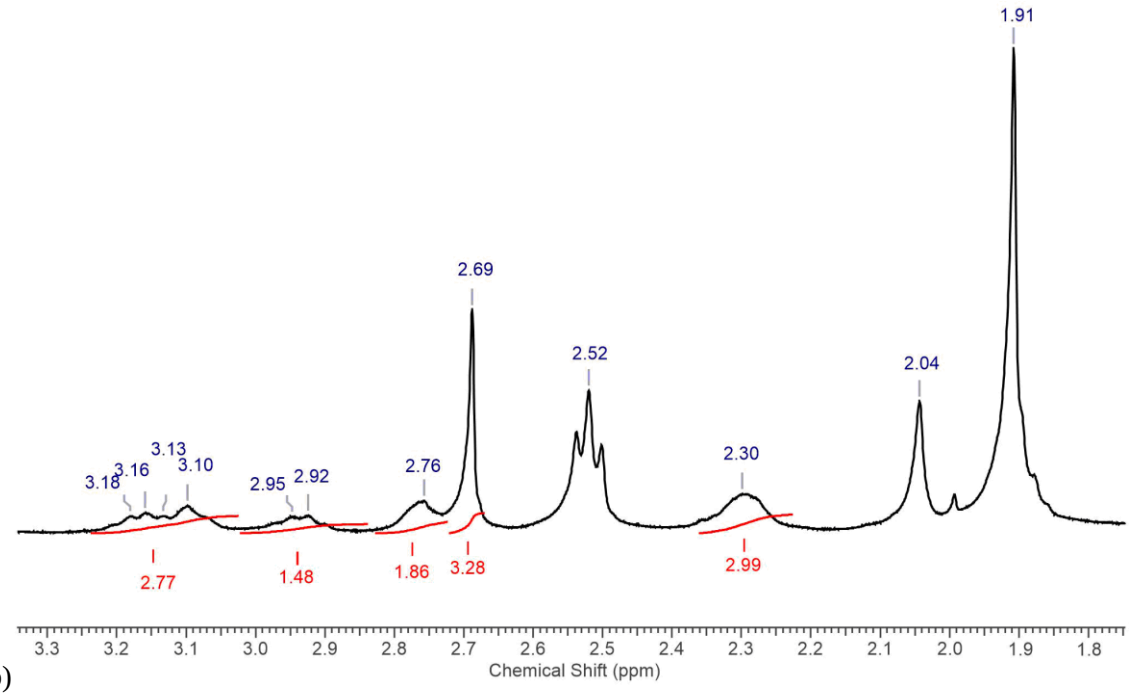

(b)

Figure 4.9 (a) ^{1}H NMR spectrum of [$NbSCl_3${$MeSe(CH_2)_3SeMe$}] in CD_2Cl_2 at 183 K; (b) selected expansion region of Figure 4.9 (a). The resonances at δ = 2.59, 2.07 and 1.96 ppm are from free $MeSe(CH_2)_3SeMe$.

The variable temperature ^{1}H NMR spectra of [$NbSCl_3${$^{i}PrS(CH_2)_2S^{i}Pr$}], [$NbSCl_3${$MeS(CH_2)_3SMe$}] and [$NbSCl_3${$^{n}BuS(CH_2)_3S^{n}Bu$}] also exhibit broad resonances at room temperatures and show similar changes on cooling to lower temperature (Figure A7.2–A7.4). Both the ^{1}H and ^{93}Nb NMR spectra indicate the weaker Lewis acidity of $NbSCl_3$ species compared to $NbCl_5$.

4.2.5 $NbSCl_3$ chalcogenoether dimers

There are a few $NbSX_3$ complexes reported with a monodentate neutral sulfur donor ligand. $[NbSCl_3(SPPh_3)]$ which contains both monomeric and dimeric molecules in the same crystal were obtained using one equivalent of ligand.[5] An excess of THT reacted with $NbSBr_3$, formed $[NbSBr_3(THT)_2]$.[15] However, when using excess diethyl sulfide, only 1:1 $[NbSCl_3(SEt_2)]$ was isolated. The solid state crystal structure has not been determined.[6] The mechanism of forming 1:1 or 2:1 ligand:metal complexes and the geometry of 1:1 are still unclear.

$[NbSCl_3(SMe_2)]$, $[NbSCl_3(S^nBu_2)]$ and $[NbSCl_3(Se^nBu_2)]$ were made from chloride/sulfide substitution. In a typical preparation, $[NbCl_5(ER_2)]$ (ER_2 = SMe_2, S^nBu_2 or Se^nBu_2) complexes were synthesised using the literature method and formed red solutions in CH_2Cl_2 solvent,[1, 14] subsequently, a CH_2Cl_2 solution of one equivalent $S(SiMe_3)_2$ was added. Upon addition the solutions change colour to green (thioether) or black (selenoether), and result in yellow-green solid $[NbSCl_3(SMe_2)]$ or dark oils ($[NbSCl_3(S^nBu_2)]$ and $[NbSCl_3(Se^nBu_2)]$) after removing solvent under vacuum.

All three complexes have satisfactory microanalysis with the respect to carbon:hydrogen ratio and confirm they are 1:1 compounds. Infrared spectra of these complexes show a strong vibration at *ca.* 530 cm^{-1}, assumed to be terminal ν(Nb═S), with a broad absorption at *ca.* 350 cm^{-1} from ν(Nb–Cl) (Figure A6.37–A6.39 and Table 4.5). ^{93}Nb NMR spectra of these three complexes in CD_2Cl_2 have resonances at *ca.* 650–690 ppm (Figure A7.15–A7.17), a higher frequency to $NbCl_5$ complexes, but present a different chemical environment from those monomeric complexes in section 4.2.3. Unfortunately, no ^{77}Se NMR resonance was observed at room temperature or at 223 K for $[NbSCl_3(Se^nBu_2)]$.

Table 4.5 Infrared (cm^{-1}) and ^{93}Nb NMR spectra (CD_2Cl_2, 298 K) of $[NbSCl_3(L)]$ complexes

	$[NbSCl_3(SMe_2)]$	**$[NbSCl_3(S^nBu_2)]$**	**$[NbSCl_3(Se^nBu_2)]$**
ν(Nb–Cl)	369, 356, 322	387, 374, 359	380, 366, 355
ν(Nb═S)	530	554	530
^{93}Nb NMR	651	654	694

Green crystals of $[NbSCl_3(SMe_2)]$ were grown by the slow evaporation of a saturated CH_2Cl_2 solution to undergo slow evaporation under a dinitrogen environment and contain the dimeric structure $[Nb_2S_2Cl_4(SMe_2)_2(\mu\text{-}Cl)_2]$ (Figure 4.10 and Table 4.6). Notably, the two SMe_2 ligands are *syn*-disposed, which is unusual for d-block dimers which commonly form centrosymmetric structure. The distance of S2…S4 is 3.517 Å, which is longer than any reported S–S bond distance and can therefore be concluded to be non-bonding.[17, 18] The distance of Nb–Nb is 4.227(1) Å, which is consistent with non-bonding niobium(V) centres. Again, $Nb{=}S_{terminal}$ distances are slightly shorter than $Nb–Cl_{terminal}$ distances by *ca.* 0.2 Å. The bridge d(Nb–Cl) also reflect *trans* influence from the

other *trans* group; Nb–(μ-Cl)$_{trans\text{S}}$ is longer than Nb–(μ-Cl)$_{trans\text{Cl}}$ by *ca.* 0.52 Å, surprisingly large difference.

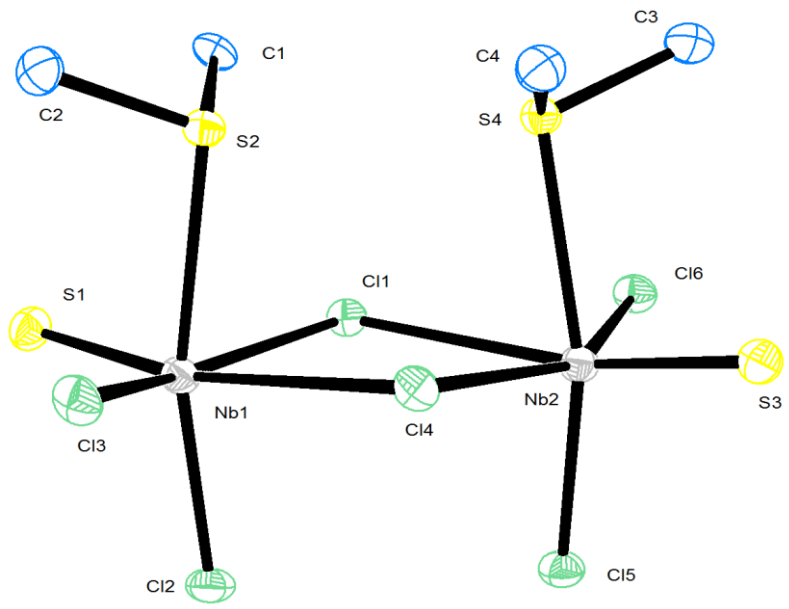

Figure 4.10 The structure of [$Nb_2S_2Cl_4(SMe_2)_2(\mu\text{-}Cl)_2$] showing the atom numbering scheme and with ellipsoids drawn at the 50 % probability level. Hydrogen atoms are omitted for clarity.

Table 4.6 Selected bond lengths (Å) and angles (°) for [$Nb_2S_2Cl_4(SMe_2)_2(\mu\text{-}Cl)_2$]

Bond lengths		**Bond Angles**			
Nb1–Cl1	**2.420(2)**	**Cl1–Nb1–Cl2**	**91.64(8)**	**Cl1–Nb2–Cl4**	**75.03(6)**
Nb1–Cl2	**2.324(2)**	**Cl1–Nb1–Cl4**	**75.16(6)**	**Cl1–Nb2–Cl5**	**88.36(7)**
Nb1–Cl3	**2.305(2)**	**Cl1–Nb1–S1**	**101.37(8)**	**Cl1–Nb2–Cl6**	**78.42(7)**
Nb1–Cl4	**2.921(2)**	**Cl1–Nb1–S2**	**80.64(7)**	**Cl1–Nb2–S4**	**76.75(6)**
Nb1–S1	**2.127(2)**	**Cl2–Nb1–Cl3**	**98.64(8)**	**Cl4–Nb2–Cl5**	**93.43(8)**
Nb1–S2	**2.660(2)**	**Cl2–Nb1–Cl4**	**88.20(7)**	**Cl4–Nb2–S3**	**100.49(8)**
Nb2–Cl1	**2.939(2)**	**Cl2–Nb1–S1**	**103.03(9)**	**Cl4–Nb2–S4**	**82.63(7)**
Nb2–Cl4	**2.405(2)**	**Cl3–Nb1–Cl4**	**77.98(7)**	**Cl5–Nb2–Cl6**	**95.63(8)**
Nb2–Cl5	**2.326(2)**	**Cl3–Nb1–S1**	**102.72(9)**	**Cl5–Nb2–S3**	**103.59(9)**
Nb2–Cl6	**2.323(2)**	**Cl3–Nb1–S2**	**83.11(7)**	**Cl6–Nb2–S3**	**103.38(9)**
Nb2–S3	**2.124(2)**	**Cl4–Nb1–S2**	**78.37(6)**	**Cl6–Nb2–S4**	**81.76(7)**
Nb2–S4	**2.655(2)**	**S1–Nb1–S2**	**90.21(8)**	**S3–Nb2–S4**	**91.27(9)**

4.2.6 Chloride/sulfide substitution in [$(NbCl_5)_2$(dichalcogenoether)]

Chloride/sulfide substitution in [$NbCl_5$(chalcogenoether)] was successful (section 4.2.5). The substitution has also been tested in [$(NbCl_5)_2$(dichalcogenoether)] complexes to attempt to form [$NbSCl_3$(dichalcogenoether)] *via* a different synthetic route. [$(NbCl_5)_2${$MeS(CH_2)_3SMe$}] was prepared using a literature method,[14, 19] before the addition of a CH_2Cl_2 solution of one equivalent $S(SiMe_3)_2$. The solutions changed from red-brown to green. A green powder was isolated after removing solvent and excess ligand under vacuum. Green crystals were grown by allowing the CH_2Cl_2 solution to evaporate to dryness in a nitrogen atmosphere.

The crystal structure of [Nb_2Cl_4{$MeS(CH_2)_3SMe$}$_2$(μ-S)(μ-S_2)] (Figure 4.11 and Table 4.7) is isomorphous with [Nb_2Cl_4{$MeS(CH_2)_3SMe$}$_2$(μ-S)$_2$] in section 3.2.4. The only difference between these two structures is that [Nb_2Cl_4{$MeS(CH_2)_3SMe$}$_2$(μ-S)(μ-S_2)] has one μ-S and one μ-S_2 bridge (Figure 4.11), while [Nb_2Cl_4{$MeS(CH_2)_3SMe$}$_2$(μ-S)$_2$] has two μ-S bridges. The Nb–Nb distance (2.862(1) Å) is consistent with other niobium(IV) dimer structures.[20] The distance S3–$S3^{ii}$ (1.991(6) Å) is corresponding to the literature reported the distance of fragment moiety unit of S^{2-}.[15, 17, 18] The core Nb_2Cl_4(μ-S)(μ-S_2) unit is similar to the crystal structure of [$Nb_2Cl_4(THT)_4$(μ-S)(μ-S_2)].[15] The observed reduction is probably due to the excess S^{2-} present and/or C–S cleavage of the free ligand.

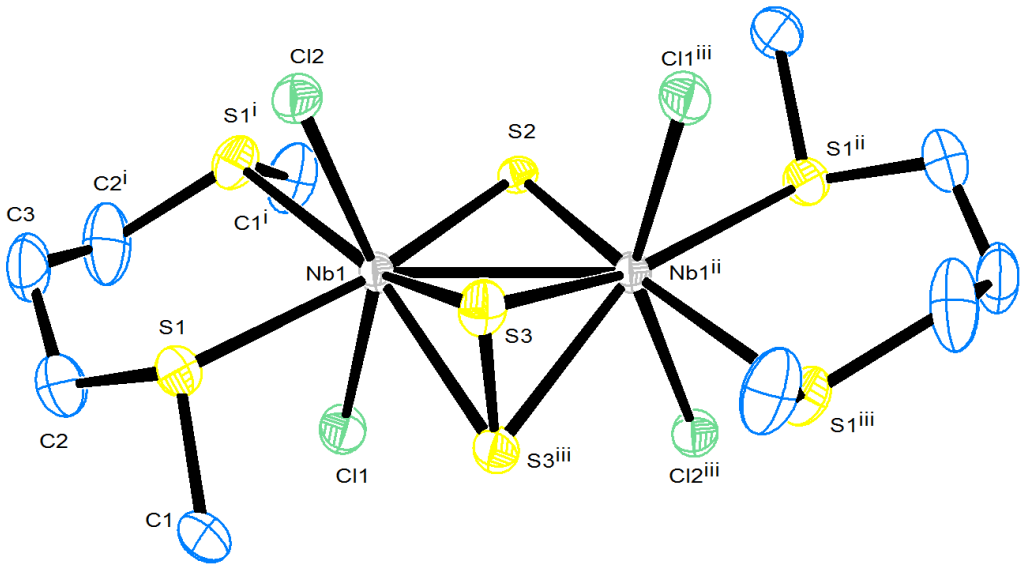

Figure 4.11 The structure of [Nb_2Cl_4{$MeS(CH_2)_3SMe$}$_2$(μ-S)(μ-S_2)] showing the atom numbering scheme and with ellipsoids drawn at the 50 % probability level. Hydrogen atoms are omitted for clarity.

Table 4.7 Selected bond lengths (Å) and angles (°) for $[Nb_2Cl_4\{MeS(CH_2)_3SMe\}_2(\mu\text{-}S)(\mu\text{-}S_2)]$

Bond lengths				**Bond Angles**	
Nb1–Cl1	**2.448(2)**	**Nb1–S3**	**2.529(2)**	**Cl1–Nb1–Cl2**	**149.77(6)**
Nb1–Cl2	**2.474(2)**	**Nb1–S3^{ii}**	**2.530(2)**	**Nb1–S2–Nb1^{ii}**	**76.16(9)**
Nb1–S1	**2.690(1)**	**Nb1–Nb1^{ii}**	**2.862(1)**	**Nb1–S3–Nb1^{ii}**	**68.92(7)**
Nb1–S2	**2.321(2)**	**S3–S3^{ii}**	**1.991(6)**	**S1–Nb1–S1^{i}**	**88.81(6)**

4.2.7 Chloride/selenide substitution

Preparation of $NbSCl_3$ using chloride/sulfide substitution by adding $S(SiMe_3)_2$ was successful (section 4.2.3–4.2.5). $[NbSeCl_3(NCCH_3)_2]$ was prepared using an analogous method to $[NbSCl_3(NCCH_3)_2]$, but adding $Se(SiMe_3)_2$. This resulted in a brown solid after removing the solvent under vacuum. The microanalysis result for C:H:N is satisfied by the formula $[NbSeCl_3(NCCH_3)_2]$. The infrared spectrum shows peaks from coordinated acetonitrile (2310 and 2281 cm^{-1}), Nb═Se (397 cm^{-1}) and Nb–Cl (377 and 344 cm^{-1}) (Figure A6.40). The ^{93}Nb NMR spectroscopic resonance at ambient temperature is found at δ = 923 ppm (Figure A7.18), which is significantly further downfield compared to the $NbSCl_3$ analogues reflecting the effect of the selenide coordination.[21]

Unfortunately, attempts to prepare dithio- or diselenoether complexes from $[NbSeCl_3(NCCH_3)_2]$ were unsuccessful, even when using excess ligand or increasing the reaction time. When reacting $[NbCl_5(Se^nBu_2)]$ with $Se(SiMe_3)_2/CH_2Cl_2$ solution, a black solid formed; the formula of this complex has been identified reproducibly from microanalysis, IR and ^{1}H NMR spectroscopy as $[NbSe_2Cl_3(Se^nBu_2)]$. Although recrystallization of the product was unsuccessful, the structure may be dimeric containing a bridged Se_2^{2-} group.[8, 11]

4.2.8 Thermogravimetric analysis of potential LPCVD precursors

Complexes $[NbSCl_3(S^nBu_2)]$, $[NbSCl_3\{^nBuS(CH_2)_3S^nBu\}]$ and $[NbSe_2Cl_3(Se^nBu_2)]$ were identified as possible candidates for use as single source LPCVD precursors for NbS_2 and $NbSe_2$ thin films, on the basis of their volatility and the presence of ^{n}Bu groups that could be readily eliminated. Thermogravimetric analyses were undertaken for these complexes (Figure A3.1–A3.3) in order to understand the decomposition pathways for each potential precursor for use in LPCVD.

The TGA profile of $[NbSCl_3(S^nBu_2)]$ shows two separate weight loss steps (*ca.* 114–195 ℃ and *ca.* 195–370 ℃) and a further gradual weight loss up to 600 ℃. The percentage weight loss for the first step is difficult to assign unambiguously due to the fact that it is followed immediately by the second weight loss step. After the second step, the sample left a residue with 45.3 wt%. NbS_2 would be expected to have a final residue mass of 41.6 %. This precursor was tested in LPCVD as a single source precursor and successfully deposited NbS_2 thin films (Section 4.2.9.1).

The TGA profile of [$NbSCl_3\{^nBuS(CH_2)_3S^nBu\}$] presents a single weight loss step occurring at *ca.* 200–300 ℃, leaving a black residue (43.4 wt%). The mass of the residue is significantly higher than that for the target material NbS_2 (34.8 wt%). The TGA does show that the complex is volatile. It was therefore tested under LPCVD conditions and successfully deposited NbS_2 thin films (Section 4.2.9.2).

The TGA profile of [$NbSe_2Cl_3(Se^nBu_2)$] shows two distinct weight loss steps (RT–*ca.* 235 ℃ and *ca.* 235–500 ℃ and gave a residue with 32.7 wt%. This is lower than that of the desired material $NbSe_2$ (45.5 wt%). This precursor was used in LPCVD and successfully deposited $NbSe_2$ thin films (Section 4.2.9.3).

Although TGA profiles for these three single source precursors do not all correspond to clean decomposition to give the desired materials, TGA experiments indicate the temperature at which each individual weight loss step occurs, providing an indication of the low temperature threshold. Therefore, LPCVD experiments were performed at a pressure of *ca.* 0.05 mmHg using a range of temperatures around 600−750 °C.

Table 4.8 TGA data for precursors in Chapter 4

Complexes	Onset Temperature (℃)	Step End Temperature (℃)	Remaining weight (wt%)
[$NbSCl_3(S^nBu_2)$] (Step 1)	*ca.* 114	*ca.*195	70.6
[$NbSCl_3(S^nBu_2)$] (Step 2)	*ca.*195	*ca.* 370	45.3
[$NbSCl_3\{^nBuS(CH_2)_3S^nBu\}$] (One Step)	*ca.* 200	*ca.* 300	43.4
[$NbSe_2Cl_3(Se^nBu_2)$] (Step 1)	RT	*ca.* 235	60.8
[$NbSe_2Cl_3(Se^nBu_2)$] (Step 2)	*ca.* 235	*ca.* 500	32.7

NbS_2 expected weight loss from precursor: 41.6 % ([$NbSCl_3(S^nBu_2)$]); 34.8 % ([$NbSCl_3\{^nBuS(CH_2)_3S^nBu\}$]

$NbSe_2$ expected weight loss from precursor: 45.5 % ([$NbSe_2Cl_3(Se^nBu_2)$]).

4.2.9 LPCVD application

Complexes $[NbSCl_3(S^nBu_2)]$, $[NbSCl_3\{^nBuS(CH_2)_3S^nBu\}]$, $[NbSCl_3(Se^nBu_2)]$ and $[NbSe_2Cl_3(Se^nBu_2)]$ were tested as potential single source low pressure chemical vapour deposition (LPCVD) precursors at a range of temperatures between 600−750 ℃ at a pressure *ca*. 0.05 mmHg. There is no significant deposition observed at lower temperature.

$NbSCl_3$ has also been tested as a single source LPCVD precursor. The experiments were performed at a range of temperatures (400−750 ℃), and unfortunately, no significant deposition was observed.

4.2.9.1 LPCVD using $[NbSCl_3(S^nBu_2)]$

Thin black films obtained by LPCVD from $[NbSCl_3(S^nBu_2)]$ at 700 ℃ show diffraction patterns consistent with NbS_2 in space group *R*3*mh* (3R-type NbS_2) (Figure 4.12). These NbS_2 films appear to be both air and moisture stable. Lattice parameters determined by Le Bail fitting of the grazing incidence XRD pattern are: a = 3.317(6) and c = 17.79(4) Å (R_{wp} = 6.61 %, R_p = 4.46 %). These are close to the literature values for bulk NbS_2 of a = 3.3303(3), c = 17.918(2) Å .[22] The grazing incidence and in-plane XRD patterns shows considerable variations in intensity considered with preferred orientation. The 0 0 3 (2θ = 14.97°) reflection is the strongest in the grazing incidence XRD pattern, whereas 1 0 1 (2θ = 31.4°), 0 1 2 (2θ = *ca.* 32.7°) and 1 1 0 (2θ = 54.9°) reflections are the strongest from the in-plane XRD pattern.

Pole figure measurements were undertaken on a NbS_2 film obtained from the $[NbSCl_3(S^nBu_2)]$ precursor to establish the film texture. Using 0 0 3 reflection, a single and sharp peak (FWHM ~ 5°) was observed at the centre of the figure with α = 90° (Figure 4.13 a). The figure, corresponding to the 1 0 1 reflection, exhibits a ring with α = 9° (Figure 4.13 b). These results are consistent with preferred orientation in the *ab* plane of the crystallites which is parallel with the substrate surface.

Scanning electron microscopy (SEM) images reveal that the NbS_2 films have a regular morphology formed of microcrystalline platelets, the majority of which are aligned with the ab plane parallel to the substrate agreeing with XRD data (Figure 4.14). EDX data measured at an accelerating voltage of 15 keV show significant amounts of Si and O from the substrate in addition to Nb and S peaks, indicating that the films are thin. EDX data also shows there is no evidence of any residual Cl in the films (Cl K_α = 2.621 keV).[23] Accurate quantification of the Nb:S ratio by EDX is difficult due to the Nb L_α and S K_α peaks overlapping (Figure 4.15).

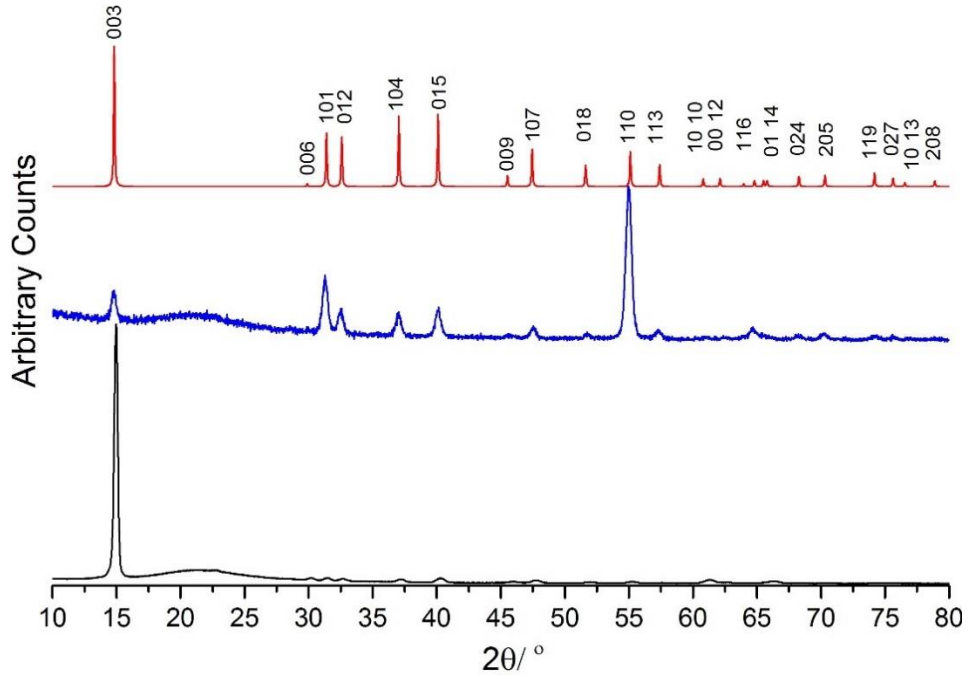

Figure 4.12 Grazing incidence XRD (black) and in plane XRD (blue) from the NbS_2 thin film deposited by LPCVD using [$NbSCl_3(S^nBu_2)$] at 700 °C; stick diagram of the XRD of bulk NbS_2 (red).[22] The broad feature at 2θ = *ca.* 22° is from the SiO_2 substrate.

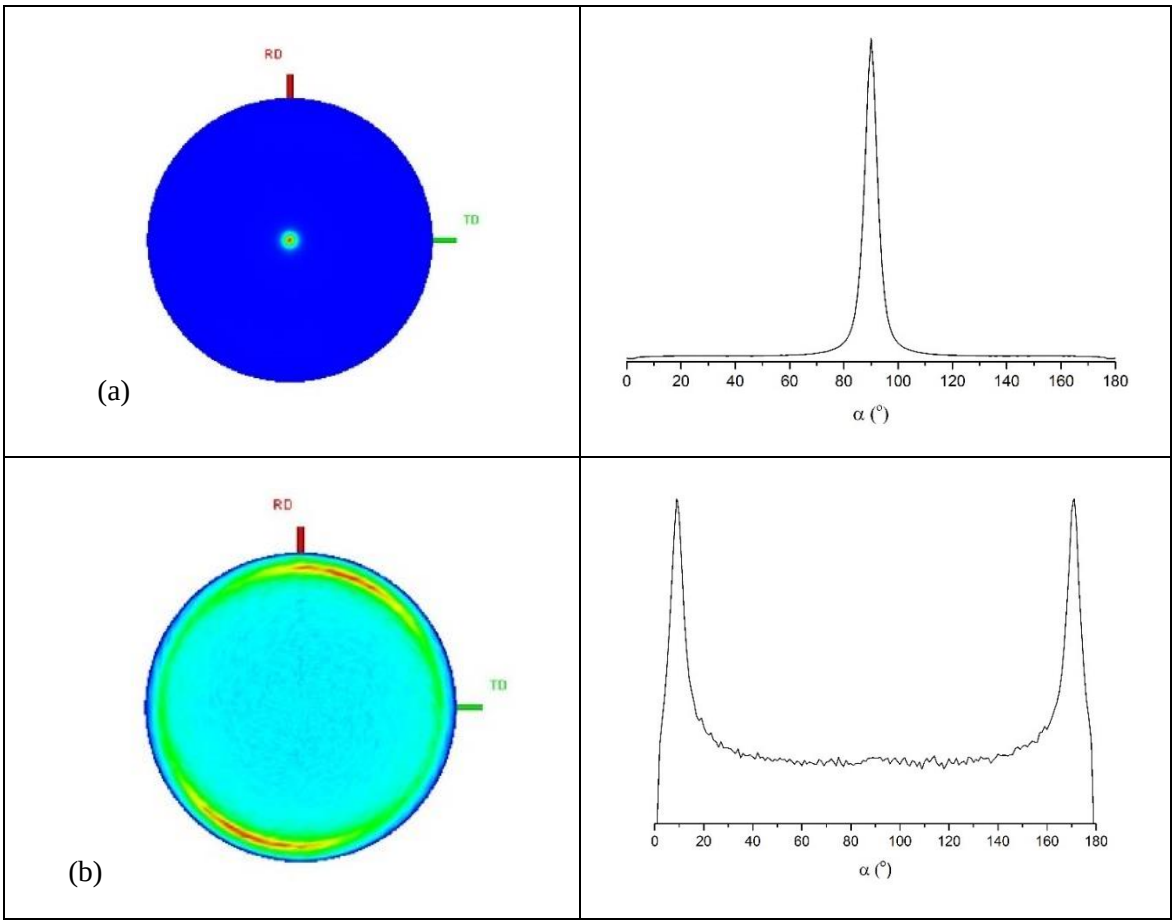

Figure 4.13 (a) Pole figures with cut line graphs for the 0 0 3 (2θ = 14.97°) and (b) 1 0 1 (2θ = 31.47°) reflection of NbS_2 deposited on a SiO_2 substrate.

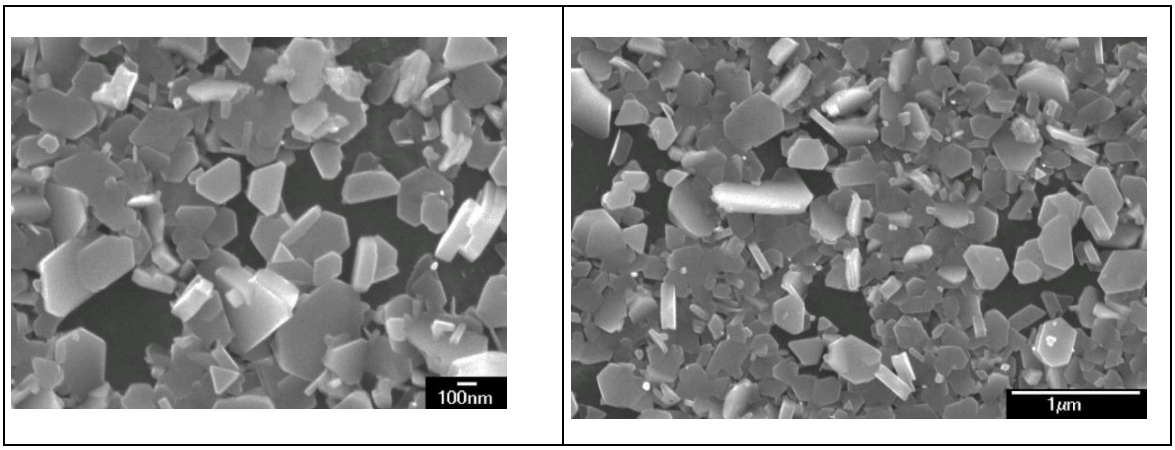

Figure 4.14 SEM images of NbS_2 thin film deposited by LPCVD from $[NbSCl_3(S^nBu_2)]$ at 700 °C.

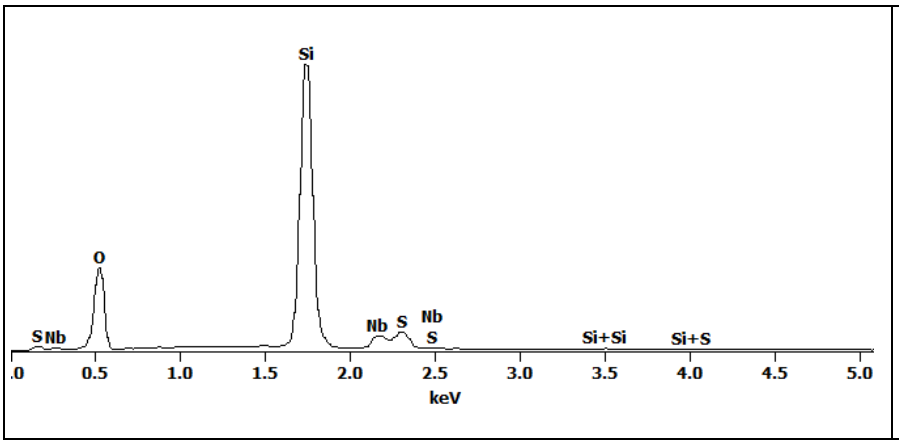

Elements	Atom %
Nb	42.56
S	57.44

Figure 4.15 EDX spectrum using accelerating voltage 15 kV from NbS_2 thin film deposited by LPCVD from $[NbSCl_3(S^nBu_2)]$ at 700 °C.

4.2.9.2 LPCVD using $[NbSCl_3\{^nBuS(CH_2)_3S^nBu\}]$

Films obtained from LPCVD using $[NbSCl_3\{^nBuS(CH_2)_3S^nBu\}]$ at 700 °C also present diffraction patterns consistent with *R*3*mh* (3R-type NbS_2) (Figure 4.16). Lattice parameters determined by Le Bail fitting of the grazing incidence XRD pattern are: a = 3.29(2) and c = 17.8(2) Å (R_{wp} = 5.54 %, R_p = 3.47 %). These NbS_2 films have the same preferred crystallite orientation (c-axis) with those NbS_2 films deposited using $[NbSCl_3(S^nBu_2)]$ as described in section 4.2.9.1.

SEM images of the NbS_2 film obtained from $[NbSCl_3\{^nBuS(CH_2)_3S^nBu\}]$ precursor show those microcrystalline grown across the ab plane parallel to the substrate (Figure 4.17), corresponding to the XRD data. The EDX data also shows no evidence of residual Cl and the ratio of Nb:S is about 2:3 due to the overlapping of Nb L_α and S K_α peaks (Figure 4.18).

$[NbSCl_3(S^nBu_2)]$ and $[NbSCl_3\{^nBuS(CH_2)_3S^nBu\}]$ are considered to be more effective single source precursors than $[NbCl_5(S^nBu_2)]$. This is because they have a better Nb:S ratio for the target material, NbS_2, and form a thicker film determined by the comparison of the intensities between substrate and

NbS_2 peaks using XRD technique. They also produce larger crystallites, as shown by SEM images. Whereas both EDX spectra of NbS_2 films in this chapter were collected using an accelerating voltage of 15 kV. This means the electron beam is penetrating deeper into the substrate, causing the intensity of the substrate related peaks to increase. Unfortunately, cross-section SEM images taken from all NbS_2 thin films (including the NbS_2 thin films obtained from $[NbCl_5(S^nBu_2)]$) were unsuccessful due to the charging effect from substrates (silica).

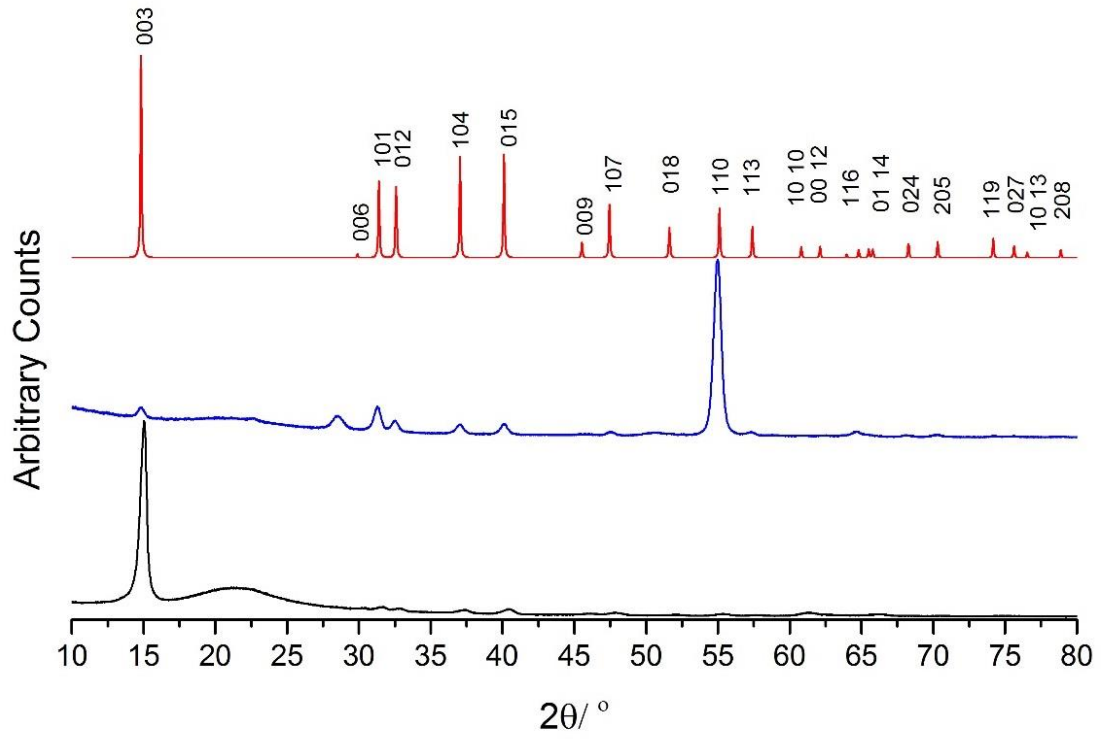

Figure 4.16 Grazing incidence XRD (black) and in plane XRD (blue) from the NbS_2 thin film deposited by LPCVD using $[NbSCl_3\{^nBuS(CH_2)_3S^nBu\}]$ at 700 °C; stick diagram of the XRD of bulk NbS_2 (red).[22] The broad feature at 2θ = *ca.* 22° is from the SiO_2 substrate.

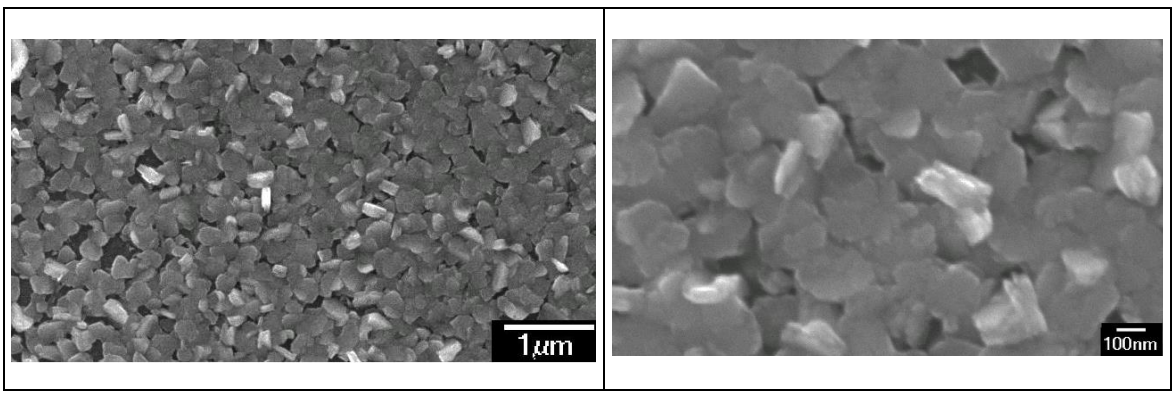

Figure 4.17 SEM images of NbS_2 thin film deposited by LPCVD from $[NbSCl_3\{^nBuS(CH_2)_3S^nBu\}]$ at 700 °C.

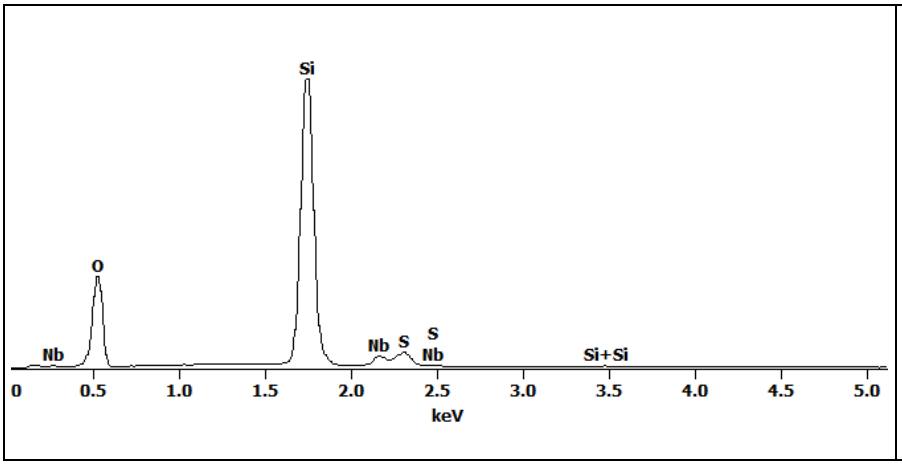

Elements	Atom %
Nb	39.7
S	60.3

Figure 4.18 EDX spectrum using accelerating voltage 15 kV from NbS_2 thin film deposited by LPCVD from $[NbSCl_3\{^nBuS(CH_2)_3S^nBu\}]$ at 700 ℃.

4.2.9.3 $NbSe_2$ films deposited using $[NbSe_2Cl_3(Se^nBu_2)]$

Films deposited by LPCVD using $[NbSe_2Cl_3(Se^nBu_2)]$ at 650 ℃ present diffraction patterns consistent with $NbSe_2$ in space group $P6_3/mmc$ (2H-type $NbSe_2$) (Figure 4.19). These $NbSe_2$ films appear to be air and moisture stable. The 0 0 2 (2θ = *ca.* 14°), 1 0 1 (2θ = *ca.* 30.5°) and 1 1 0 (2θ = *ca.* 53°) reflections are the strongest in both grazing incidence and in-plane XRD.

Lattice parameters determined by Le Bail fitting of the grazing incidence XRD pattern are: a = 3.434(7) and c = 12.53(3) Å (R_{wp} = 2.48 %, R_p = 1.87 %), compared to the literature values for bulk $NbSe_2$ (a = 3.4446(2), c = 12.5444(7) Å).[24] The precursor was also tested in LPCVD at 600 ℃, however, there was no deposition observed.

SEM images of the same $NbSe_2$ film show a polycrystalline film formed of hexagonal platelets with orientation with the c axis mostly parallel to the substrate, although the absence of significant preferred orientation from the XRD data suggests it is likely that there are different crystal orientations within the film. (Figure 4.20). EDX result from the same area give the ratio of Nb:Se of *ca.* 35.8:64.2 %, with no residual Cl (Figure 4.21).

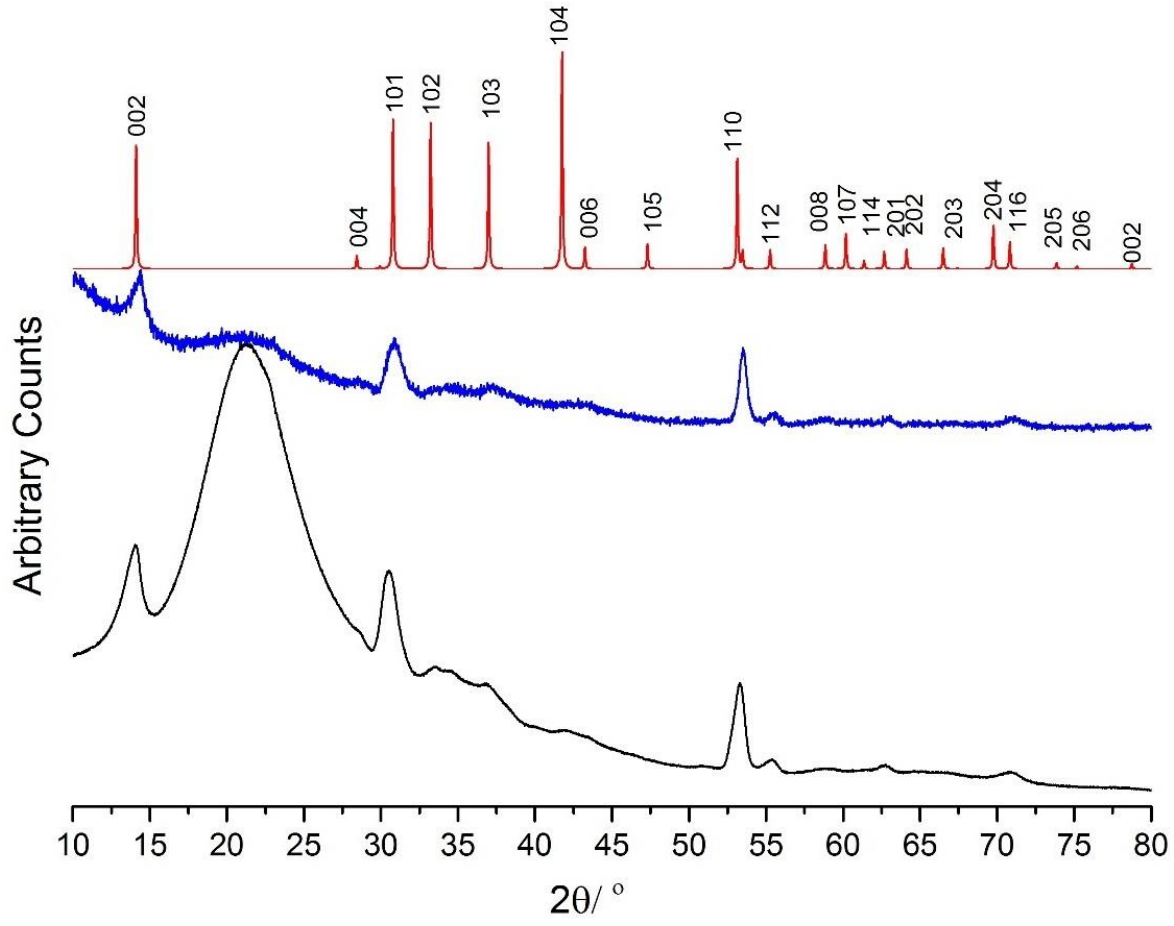

Figure 4.19 Grazing incidence XRD (black) and in plane XRD (blue) from the $NbSe_2$ thin film deposited by LPCVD using $[NbSe_2Cl_3(Se^nBu_2)]$ at 650 °C; stick diagram of the XRD of bulk $NbSe_2$ (red).[24]

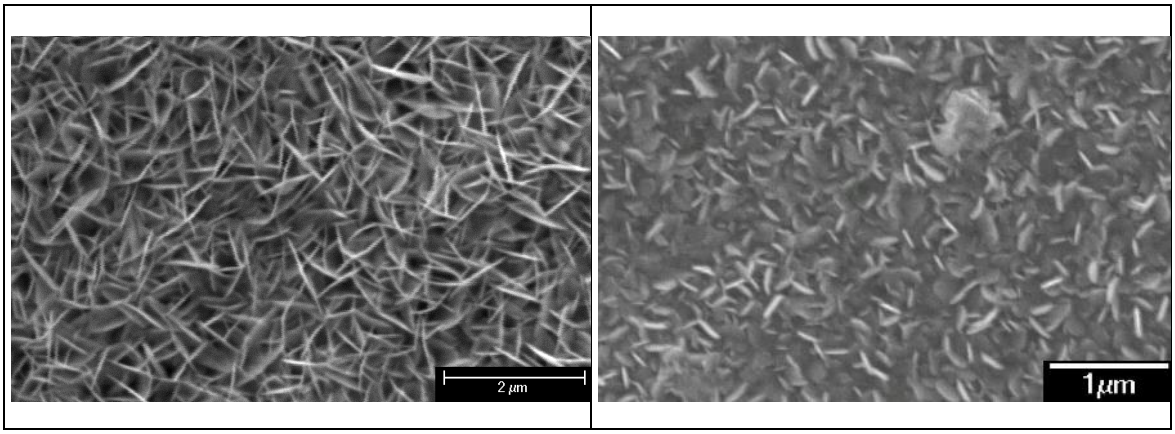

Figure 4.20 SEM images of $NbSe_2$ thin film deposited by LPCVD from $[NbSe_2Cl_3(Se^nBu_2)]$ at 650 °C.

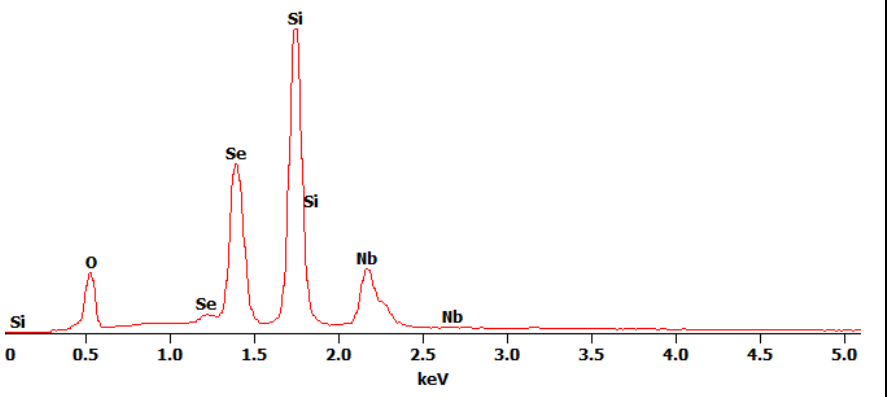

Elements	Atom %
Nb	35.8
Se	64.2

Figure 4.21 EDX spectrum using accelerating voltage 15 kV from $NbSe_2$ thin film deposited by LPCVD from $[NbSe_2Cl_3(Se^nBu_2)]$ at 700 ℃.

4.2.9.4 Attempted deposited using $[NbSCl_3(Se^nBu_2)]$

$[NbS_2Cl_3(Se^nBu_2)]$ was tested in LPCVD at 600–700 ℃. There was no deposition observed except elemental carbon/selenium films.

4.3 Conclusion

A series of six-coordinate $[NbSCl_3(L–L)]$ and dimeric $[Nb_2S_2Cl_2(ER_2)_2(\mu\text{-}Cl)_2]$ complexes featuring neutral thio- and seleno-ether ligands have been synthesised and characterised.

The monomeric complexes $[NbSCl_3(L–L)]$ (L–L = $MeS(CH_2)_2SMe$, $^{i}PrS(CH_2)_2S^{i}Pr$, $MeSe(CH_2)_3SeMe$) feature the *DL* ligand geometry. The isoelectronic S^{2-} and Cl^{-} are distinguished from solid state X-ray crystal data indicating S/Cl disorder is not significant with no clear evidence for disorder. The different chemical environment of the Nb–Cl and Nb═S bonds also impact the ^{1}H NMR spectra and this has been discussed. Structural differences in the chemical environment also lead to differences in multinuclear NMR spectra.

The dimeric $NbSCl_3$ complexes of formula $[Nb_2S_2Cl_2(ER_2)_2(\mu\text{-}Cl)_2]$ (ER_2 = Me_2S, $^{n}Bu_2S$ or $^{n}Bu_2Se$) possess ligands in *syn* positions. The multinuclear NMR spectra reflect the different chemical environments of those $NbSCl_3$ monomers.

The complex, $[NbSeCl_3(NCCH_3)_2]$, can be prepared using chloride/seleno- substitution, but further substitution of CH_3CN using chalcogenoethers was unsuccessful. $[NbSe_2Cl_3(Se^{n}Bu_2)]$ is made by using chloride/selenide substitution and the formulation agrees with spectroscopic data, although the solid-state geometry remains unclear.

$NbSCl_3$ and the niobium complexes, $[NbSCl_3(S^{n}Bu_2)]$, $[NbSCl_3(Se^{n}Bu_2)]$, $[NbSCl_3\{^{n}BuS(CH_2)_3S^{n}Bu\}]$ and $[NbSe_2Cl_3(Se^{n}Bu_2)]$ were tested as potential single source precursors for LPCVD. $[NbSCl_3(S^{n}Bu_2)]$ and $[NbSCl_3\{^{n}BuS(CH_2)_3S^{n}Bu\}]$ were found to deposit 3R-NbS_2 thin film successfully, while LPCVD using $[NbSCl_3(Se^{n}Bu_2)]$ was found to deposit a 2H-$NbSe_2$ thin film. The two novel 3R-NbS_2 single source LPCVD precursors are considered good single source precursors as they provide a thicker coverage of NbS_2 than has been achieved $[NbCl_5(S^{n}Bu_2)]$.[1] All of the films have XRD refinement with the selected phase and SEM images agree with the orientation observed from XRD. Although the elemental ratio of Nb:S in NbS_2 films is not clear due to the overlapping peaks in EDX results, the ratio of Nb:Se is close to 1:2 corresponding to the composition of $NbSe_2$.

4.4 Experimental

4.4.1 $NbSCl_3$

$NbCl_5$ (405 mg, 1.5 mmol) was suspended in CH_2Cl_2 (20 mL) in an ice bath (0 °C). A solution of $S(SiMe_3)_2$ (260 mg, 1.5 mmol) and CH_2Cl_2 (6 mL) was added with stirring. The solution immediately turned black and was stirred for 30 minutes at ambient temperature. The solvent was removed *in vacuo*, leaving a dark green powder. Yield: 295 mg, 83 %. IR (Nujol, cm^{-1}): 550 (Nb═S), 395, 356, 294 (Nb–Cl).

4.4.2 $[NbSCl_3(NCCH_3)_2]$

The complex was prepared by the modified literature method.[7] $NbCl_5$ (405 mg, 1.5 mmol) was dissolved in CH_3CN (30 mL) and the solution cooled in an ice bath. A solution of $S(SiMe_3)_2$ (260 mg, 1.5 mmol) and CH_3CN (20 mL) was added. The solution was removed from the ice bath, and the colour quickly changed from yellow to green after stirred for 1 hour. The solvent was removed *in vacuo* to afford a yellow-green solid. Yield: 337 mg, 72 %. Required for $C_4H_6N_2Cl_3NbS$ (313.33 g/mol): C, 15.33; H, 1.93; N, 8.94. Found: C, 15.26; H, 1.96; N, 8.82. IR (Nujol, cm^{-1}): 2287 (CH_3CN), 530s (Nb═S), 355sh, 343s, 319s (Nb–Cl). ^1H NMR (CD_2Cl_2, 298 K): δ = 1.97 (s, CH_3CN). ^{93}Nb NMR (CD_3CN, 298 K) δ = 414.

Alternative method: $NbSCl_3$ (83 mg, 0.35 mmol) was dissolved in CH_3CN (20 mL) and stirred for 30 minutes, resulting in a dark green solution. The solution was filtered and the filtrate taken to dryness *in vacuo* to afford a green powder. Yield: 100 mg, 90 %. The product was spectroscopically identical to $[NbSCl_3(CH_3CN)_2]$ on the basis of its IR.

4.4.3 $[NbSCl_3\{MeS(CH_2)_2SMe\}]$

$[NbSCl_3(NCCH_3)_2]$ (94 mg, 0.3 mmol) was dissolved in CH_2Cl_2 (10 mL) at ambient temperature. A solution of $MeS(CH_2)_2SMe$ (110 mg, 0.9 mmol) in CH_2Cl_2 (1 mL) was added and the solution stirred for 30 minutes to give green-yellow precipitate. After filtering, the green solution was dried *in vacuo* and washed with *n*-hexane (10 mL x 2). The green solid was dried *in vacuo*. Yield: 67 mg, 63 % Required for $C_4H_{10}Cl_3NbS_3$ (353.58 g/mol): C, 13.59; H, 2.85. Found: C, 13.64; H, 2.93. IR (Nujol, cm^{-1}): 526 (Nb═S), 361sh, 349, 319 (Nb–Cl). ^1H NMR (CD_2Cl_2, 298 K): δ = 2.22 (br, [5H], S<u>Me</u>), 2.77 (br, [5H], S<u>Me</u>) 3.03(s), 3.26(s) ([4H], CH_2) (detail in text). ^{93}Nb NMR (CD_2Cl, 298 K) δ = 507. Green crystals were grown by allowing the slow evaporation of CH_2Cl_2 under a nitrogen atmosphere.

4.4.4 [NbSCl$_3${^{i}PrS(CH$_2$)$_2$S^{i}Pr}]

Prepared in a similar fashion to [NbSCl$_3${MeS(CH$_2$)$_2$SMe}] and isolated as a green powder. Yield: 76 %. Required for $C_8H_{18}Cl_3NbS_3$ (409.69 g/mol): C, 23.45; H, 4.43. Found: C, 23.27; H, 4.41. IR (Nujol, cm^{-1}): 527 (Nb═S), 348, 318 (Nb–Cl). ^{1}H NMR (CD_2Cl_2, 298 K): δ = 1.32 (sbr, [6H], SCH$_2$<u>Me$_2$</u>), 1.59 (sbr, [6H], SCH$_2$<u>Me$_2$</u>), 3.01–3.28 (br, [4H], SCH$_2$), 3.46 (br, [2H], SCH$_2$). ^{93}Nb NMR (CD_2Cl_2, 298 K) δ = 522. Green crystals were grown by allowing CH_2Cl_2 solution to evaporate under a nitrogen atmosphere.

4.4.5 [NbSCl$_3${MeS(CH$_2$)$_3$SMe}]

Prepared in a similar fashion to [NbSCl$_3${MeS(CH$_2$)$_2$SMe}] and formed a green solid. Yield: 68 % Required for $C_5H_{12}Cl_3NbS_3$ (367.61 g/mol): C, 16.34; H, 3.29. Found: C, 16.48; H, 3.21. IR (Nujol, cm^{-1}): 524 (Nb═S), 369sh, 345, 323 (Nb–Cl). ^{1}H NMR ($CDCl_3$, 298 K): δ = 2.14 (br, [2H], SCH$_2$<u>CH$_2$</u>CH$_2$S), 2.45 (br, [6H], SCH$_3$), 2.96 (br, [4H], SCH$_2$). ^{93}Nb NMR (CD_2Cl_2, 298 K) δ = 530.

4.4.6 [NbSCl$_3${^{n}BuS(CH$_2$)$_3$S^{n}Bu}]

Prepared in a similar fashion to [NbSCl$_3${MeS(CH$_2$)$_2$SMe}] and formed a dark green oil after washing with *n*-hexane and drying *in vacuo*. Yield: 76 %. Required for $C_{11}H_{24}Cl_3NbS_3$ (451.77 g/mol): C, 29.24; H, 5.35. Found: C, 29.37; H, 5.45. IR (Nujol, cm^{-1}): 529 (Nb═S), 349, 322 (Nb–Cl). ^{93}Nb NMR (CD_2Cl_2, 298 K) δ = 534.

4.4.7 [NbSCl$_3${MeSe(CH$_2$)$_3$SeMe}]

Prepared in a similar fashion to [NbSCl$_3${MeS(CH$_2$)$_2$SMe}] to afford a yellow brown powder. Yield: 58 % Required for $C_5H_{12}Cl_3NbSSe_2$ (461.40 g/mol): C, 13.02; H, 2.62. Found: C, 13.17; H, 2.74. IR (Nujol, cm^{-1}): 521 (Nb═S), 342, 320 (Nb–Cl). ^{1}H NMR (CD_2Cl_2, 298 K): δ = 2.25 (br, [8H], SeMe & <u>CH$_2$</u>CH$_2$Se), 2.92 (br, [4H], <u>CH$_2$</u>Se). ^{77}Se{^{1}H} NMR (CD_2Cl_2, 298 K): no resonance; (223 K): δ = 163, 70. ^{93}Nb NMR (CD_2Cl_2, 298 K) δ = 547.

Yellow crystals were growth by allowing CH_2Cl_2 solution to evaporate under a nitrogen atmosphere. The Cl and terminal S atoms of the crystal structure of [NbSCl$_3${MeS(CH$_2$)$_2$SMe}] was disordered and therefore refined with split occupancies giving a 50:50 ratio.

4.4.8 [NbSCl$_3$(SMe$_2$)]

$NbCl_5$ (135 mg, 0.5 mmol) was suspended in CH_2Cl_2 (10 mL). Dimethyl sulfide (1 mL) was added with stirring for 30 minutes forming a dark brown solution. The solution was then cooled in an ice bath (0 ℃), and a solution of S(SiMe$_3$)$_2$ (90 mg, 0.5 mmol) in CH_2Cl_2 (*ca.* 1 mL) was added slowly with stirring for 30 minutes. The solution was removed from ice bath and stirred for another 5

minutes. The solvent and excess ligands were removed *in vacuo*, leaving a pale yellow green solid. Yield: 55 mg, 38 %. Required for $C_2H_6Cl_3NbS_2$ (293.46 g/mol): C, 9.19; H, 2.06. Found: C, 9.29; H, 2.37. IR (Nujol, cm^{-1}): 530 (Nb═S), 369, 356, 322 (Nb–Cl). ^1H NMR ($CDCl_3$, 298 K): δ = 2.32 (s, SMe_2). ^{93}Nb NMR (CD_2Cl_2, 298 K) δ = 651. Yellow green crystals were grown by allowing a CH_2Cl_2 solution to evaporate in a nitrogen atmosphere.

4.4.9 [$NbSCl_3(S^nBu_2)$]

$NbCl_5$ (270 mg, 1.0 mmol) was suspended in CH_2Cl_2 (10 mL). A solution of S^nBu_2 (147 mg, 1.0 mmol) and CH_2Cl_2 (3 mL) was added with stirring for 15 minutes. A CH_2Cl_2 (3 mL) solution of $S(SiMe_3)_2$ (179 mg, 1.0 mmol) was added to the orange stirring solution. The colour changed to dark green after stirring for 30 minutes. The solution was taken to dryness *in vacuo* and left a black sticky oil, which was washed with *n*-hexane (5 mL) and dried *in vacuo* to afford a sticky black oil. Yield: 331 mg, 88 %. Required for $C_8H_{18}Cl_3NbS_2$ (377.62 g/mol): C, 25.44; H, 4.8. Found: C, 25.58; H, 4.88. IR (Nujol, cm^{-1}): 554 (Nb═S), 387, 374, 359sh, 346sh (Nb–Cl). ^1H NMR ($CDCl_3$, 298 K): δ = 0.97 (t, [6H], Me), 1.48 (m, [4H], CH_2Me), 1.74 (m, [4H], $SCH_2\underline{CH_2}CH_2$), 2.94 (t, [4H], SCH_2). ^{93}Nb NMR (CD_2Cl_2, 298 K) δ = 654.

4.4.10 [$NbSCl_3(Se^nBu_2)$]

$NbCl_5$ (270 mg, 1.0 mmol) was suspended in CH_2Cl_2 (10 mL). A solution of Se^nBu_2 (193 mg, 1.0 mmol) in CH_2Cl_2 (3 mL) was added and formed a red solution after stirring for 1 hour. $S(SiMe_3)_2$ (0.21 mL, 1.0 mmol) was then added, with a dark green forming immediately. After stirring for 30 minutes, the solvent was removed *in vacuo* and left a black sticky oil, which was washed with *n*–hexane (5 mL), the residue was then dried *in vacuo* leaving a sticky black oil. Yield: 200 mg, 47 %. $C_8H_{18}Cl_3NbSSe$ (424.52 g/mol): C, 22.63; H, 4.27. Found: C, 22.52; H, 4.29 %. IR (Nujol, cm^{-1}): 530 (Nb═S), 380, 355, 346 (Nb–Cl). ^1H NMR ($CDCl_3$, 298 K): δ = 0.93 (t, [6H], Me), 1.42 (m, [4H], $\underline{CH_2}Me$), 1.66 (m, [4H], $SeCH_2\underline{CH_2}CH_2$), 2.61 (br, [4H], $SeCH_2$). ^{93}Nb NMR (CD_2Cl_2, 298 K) δ = 694.

4.4.11 [$NbSeCl_3(NCCH_3)_2$]

$NbCl_5$ (135 mg, 0.5 mmol) was dissolved in CH_3CN (10 mL), before a solution of $Se(SiMe_3)_2$ (113 mg, 0.5 mmol) and CH_3CN (5 mL) was then added to form a dark brown solution immediately. The solution was stirred for 30 minutes and no further change was observed. The solution was taken to dryness *in vacuo* to afford a brown solid. Yield: 150 mg, 83 %. Required for $C_4H_6N_2Cl_3NbSe$ (360.33 g/mol): C, 13.33; H, 1.68; N, 7.77. Found: C, 13.25; H, 1.65; N, 7.57. IR (Nujol, cm^{-1}): 2310, 2281 (CH_3CN), 397 (Nb═Se), 377, 344 (Nb–Cl). ^{93}Nb NMR (CD_2Cl_2, 298 K): δ = 923.

4.4.12 [$NbSe_2Cl_3(Se^nBu_2)$]

$NbCl_5$ (235 mg, 0.88 mmol) was suspended in CH_2Cl_2 (20 mL). A solution of $^nBu_2Se$ (177 mg, 0.88 mmol) in CH_2Cl_2 (*ca.* 1.5 mL) was added with stirring for 1 hour, the reaction mixture became a dark red solution. A solution of $Se(SiMe_3)_2$ (0.22 mL, 0.88 mmol) and CH_2Cl_2 (*ca.* 1.7 mL) was added, resulting in a colour change from dark red to black. The solution was stirred for 15 minutes before it was taken to dryness *in vacuo*. The resulting black solid was washed with *n*-hexane (15 mL) and dried *in vacuo*. Yield: 298 mg, 61 %. Required for $C_8H_{18}Cl_3NbSe_3$ (550.37 g/mol): C, 17.46; H, 3.3. Found: C, 17.59; H, 3.38. IR (Nujol, cm^{-1}): 344, 319, 272 (Nb–Cl). ^1H NMR ($CDCl_3$, 298 K): δ = 0.94 (t, [6H], Me), 1.44 (m, [4H], $\underline{CH_2}Me$), 1.70 (m, [4H], $SeCH_2\underline{CH_2}$), 2.71 (t, [4H], $SeCH_2$).

LPCVD experiments

4.4.13 Precursor $NbSCl_3$

This precursor (*ca.* 33 mg) was loaded in a LPCVD tube in a glovebox. Silica substrates were loaded after the precursor and placed end-to-end. The tube was place in a furnace and then linked to a vacuum pump (0.01 mmHg). The temperature in the furnace was increased to 300, 400 or 700 ℃ and stay for 10 minutes to allow the temperature to stabilize (three LPCVD tests). The precursor end was moved into the furnace gradually until at the edge of the furnace. The precursor did not change when moved it into the furnace in all the experiments. The furnace was cooled to ambient temperature and the substrates were unloaded under ambient conditions. No deposition was deposited observed on the substrates in each of the three experiments.

4.4.14 Precursor [$NbSCl_3(S^nBu_2)$]

This precursor (54 mg) was dissolved in CH_2Cl_2 (1 mL) and loaded into a LPCVD tube in a glovebox. Silica substrates were loaded after the precursor was loaded and placed end-to-end. The tube was placed in a furnace and then linked to a vacuum pump (0.01 mmHg) which removed the CH_2Cl_2. The temperature in the furnace was increased to 600 ℃ and left for 10 minutes to allow the temperature to settle. The precursor end was moved into the furnace's edge immediately. An orange film was grown through the open end of the tube. The precursor was stayed in the position for 30 minutes and no further change was observed. The furnace was then cooled to ambient temperature. Silica substrates were unloaded under ambient conditions. A continuous black thin film was found from tile 2 to 4, which corresponds to temperature profile *ca.* 570 ℃.

4.4.15 Precursor [$NbSCl_3(Se^nBu_2)$]

This precursor (30 mg) was dissolved in CH_2Cl_2 (1 mL) and loaded in a LPCVD tube in a glovebox. Silica substrates were loaded after the precursor had been loaded and placed end-to-end. The tube

was placed in a furnace and then linked to a vacuum pump (0.01 mmHg) which removed the CH_2Cl_2. The temperature in the furnace was increased to 600 ℃ and left for 10 minutes to allow the temperature to settle. The precursor end was moved into the furnace's edge immediately. An orange films was grown through the open end of the tube. The precursor remained in there for 30 minutes and no further change was observed. The furnace was then cooled to ambient temperature. Silica substrates were unloaded under ambient condition and no any deposition was observed on substrates.

4.4.16 Precursor [$NbSCl_3\{^nBuS(CH_2)_3S^nBu\}$]

This precursor (40 mg) was dissolved in CH_2Cl_2 (1 mL) and loaded in a LPCVD tube in a glovebox. Silica substrates were loaded after the precursor had been loaded and placed end-to-end. The tube was placed in a furnace and then linked to a vacuum pump (0.01 mmHg) which removed the CH_2Cl_2. The temperature in the furnace was increased to 700 ℃ and left for 10 minutes to allow the temperature to equilibrate. The precursor end was moved into the furnace's edge immediately. An orange films was grown through the open end of the tube. The precursor remained in the position for 30 minutes and no further change was observed. The furnace was then cooled to ambient temperature. Silica substrates were unloaded in ambient condition. A continuous black thin film was found from tile 4 to 6, which corresponds to temperature profile *ca.* 670 ℃.

4.4.17 Precursor [$NbSe_2Cl_3(Se^nBu_2)$]

This precursor (100 mg) was dissolved in CH_2Cl_2 (1 mL) and loaded in a LPCVD tube in a glovebox. Silica substrates were loaded after the precursor had been loaded and placed end-to-end. The tube was placed in a furnace and then linked to a vacuum pump (0.01 mmHg) which removed the CH_2Cl_2. The temperature in the furnace was increased to 650 ℃ and left for 10 minutes to allow the temperature to stabilize. The precursor end was moved into the furnace's edge immediately. A red films was grown through the open end of the tube. The precursor remained in the position for 30 minutes and no further change was observed. The furnace was then cooled to ambient temperature. Silica substrates were unloaded in ambient condition. A black thin film was found at tile 1, which corresponds to temperature profile *ca.* 625 ℃.

4.5 References

1. S. L. Benjamin, Y.-P. Chang, C. Gurnani, A. L. Hector, M. Huggon, W. Levason and G. Reid, *Dalton Trans.*, 2014, **43**, 16640.
2. Y.-P. Chang, M.Sc Thesis, University of Southampton, 2014.
3. S. L. Benjamin, Y.-P. Chang, M. Huggon, W. Levason and G. Reid, *Polyhedron*, 2015, **99**, 230.
4. U. Müller and P. Klingelhöfer, *Z. Anorg. Allg. Chem.*, 1984, **510**, 109.
5. M. G. B. Drew and R. J. Hobson, *Inorg. Chim. Acta*, 1983, **72**, 233.
6. K. Behzadi, A. O. Baghlaf and A. Thompson, *J. Less-Common. Met.*, 1987, **128**, 195.
7. V. C. Gibson, A. Shaw and D. N. Williams, *Polyhedron*, 1989, **8**, 549.
8. M. G. B. Drew, D. A. Rice and D. M. Williams, *J. Chem. Soc., Dalton Trans.*, 1984, 1087.
9. M. G. B. Drew, D. A. Rice and D. M. Williams, *J. Chem. Soc., Dalton Trans.*, 1985, 417.
10. M. G. B. Drew., I. B. Baba., D. A. Rice and D. M. Williams, *Inorg. Chim. Acta*, 1980, **44**, L217.
11. M. G. B. Drew, D. A. Rice and D. M. Williams, *Acta Cryst.*, 1984, **C40**, 1547.
12. I. Nowak, E. M. Page, D. A. Rice, A. D. Richardson, R. J. French, K. Hedberg and J. S. Ogden, *Inorg. Chem.*, 2003, **42**, 1296.
13. G. W. A. Fowles, R. J. Hobson, D. A. Rice and K. J. Shanton, *J. Chem. Soc., Chem. Commun.*, 1976, **14**, 552.
14. M. Jura, W. Levason, R. Ratnani, G. Reid and M. Webster, *Dalton Trans.*, 2010, **39**, 883.
15. M. G. B. Drew, D. A. Rice and D. M. Williams, *J. Chem. Soc., Dalton Trans.*, 1983, 2251.
16. D. J. Gulliver, E. G. Hope, W. Levason, S. G. Murray, D. M. Potter and G. L. Marshall, *J. Chem. Soc., Perkin Trans. II*, 1984, 429.
17. D. H. Evans, N. E. Gruhn, J. Jin, B. Li, E. Lorance, N. Okumura, N. A. Macias-Ruvalcaba, U. I. Zakai, S. Z. Zhang, E. Block and R. S. Glass, *J. Org. Chem.*, 2010, **75**, 1997.
18. S. Hayashi, K. Matsuiwa, N. Nishizawa and W. Nakanishi, *J. Org. Chem.*, 2015, **80**, 11963.
19. S. L. Benjamin, C. H. de Groot, C. Gurnani, A. L. Hector, R. Huang, K. Ignatyev, W. Levason, S. J. Pearce, F. Thomas and G. Reid, *Chem. Mater.*, 2013, **25**, 4719.
20. E. Babaian-Kibala, F. A. Cotton and P. A. Kibala, *Inorg. Chem.*, 1990, **29**, 4002.
21. V. P. Tarasov, S. M. Sinitsyna, V. D. Kopanev, V. G. Khlebodarov and Y. A. Buslaev, *Russ. J. Coord. Chem.*, 1980, **6**, 1568.
22. B. Morosin, *Acta Cryst.*, 1974, **B30**, 551.
23. A. C. Thompson and D. Vaughan, *X-ray data booklet*, Lawrence Berkeley National Laboratory, University of California, Berkeley, Calif., 2001.
24. B. E. Brown and D. J. Beerntsen, *Acta Cryst.*, 1965, **18**, 31.

Chapter 5: Niobium and tantalum pentahalide complexes as single source precursors for LPCVD application

5.1 Introduction

A series of single source precursors for the low-pressure chemical vapour deposition of NbE_2 (E = S, Se) thin films have been tested in this project. The precursors include $[NbCl_5(E^nBu_2)]$ (E = S, Se),[1] $NbCl_4$ compounds (Chapter 3), $NbCl_3$ dimers $[Nb_2Cl_4(S^nBu_2)_2(\mu\text{-}Cl)_2(\mu\text{-}S^nBu_2)]$[2] and $NbSCl_3$ complexes (Chapter 4). Both $[NbCl_5(E^nBu_2)]$ precursors deposited NbE_2 thin films as the 3R-polytype.[1] Additionally, $[NbSCl_3(S^nBu_2)]$ and $[NbSCl_3\{^nBu_2S(CH_2)_3S^nBu\}]$ also deposited 3R-NbS_2 films and $[NbSe_2Cl_3(Se^nBu_2)]$ deposited 2H-$NbSe_2$. In contrast, dimers and tetravalent organometallic niobium complexes are thought to be unsuitable as single source precursors due to their high molecular weight and the very stable metal halide polymer.[2]

It has been illustrated in Chapter 1 that TMD materials such as NbE_2 (E = S, Se) have many stacking sequences, 1T-(*P*-3*m*1), 2H-(*P*6$_3$/*mmc*), 3R-(*R*3*mh*) or 4H-(*P*-6*m*2) (T = Tetragonal, H = Hexagonal, R = Rhombohedral), which were all prepared by different techniques,[3-6] 2H- and 3R- are the two packing sequences which have been widely studied.

NbS_2 thin films are generally deposited with 3R-stacking sequences using CVD techniques, which includes APCVD[7-10] and LPCVD,[1, 11] whereas other reports show the deposition of 1T- and 2H-NbS_2 using APCVD[10, 12, 13] or AACVD[14] (for detail of each method please see Chapter 1). It is likely that the packing sequence of NbS_2 thin films depend on the deposition method and precursors using in each case of the conditions required for the CVD experiment.

Interestingly, the most commonly deposited $NbSe_2$ thin film is its 2H-stacking sequence, including chemical vapour transport[15, 16] and APCVD (for detail of each method please see Chapter 1).[17, 18] However, thus far, there is only one literature report of 3R-$NbSe_2$ thin film deposition,[1] and this 3R-$NbSe_2$ thin film is also only the second report of the material 3R-$NbSe_2$, which was grown by vapour transport methods.[3]

Precursors of the type $[TaCl_5(E^nBu_2)]$ (E = S, Se, Te) failed to deposit TaE_2 thin films,[1] and interestingly, there is only one literature report of TaS_2 thin films using AACVD,[14] whereas 2H-$TaSe_2$ is only reported from chemical vapour transport (for details of each methods, please see Chapter 1).[19, 20]

It is interesting that there is only one example of a 3R-$NbSe_2$ thin film using any deposition method.[1] The temperature used in this report (650 ℃) is also noticeably higher than in other CVD methods.[17, 18] Hence, this chapter aims to explore the effect of the temperature of deposition on thin film stacking sequences.

The other question emerges when a series of niobium based LPCVD precursors are considered. These complexes lose/eliminate halide ligands and alkyl substituents in the hot zone during a CVD process.[21] $NbBr_5$ is a weaker Lewis acid compared to its chloride analogue and the bond dissociation energy of M–Br is lower than that of M–Cl.[22] Therefore, it was considered that the bromide analogues, such as [$NbBr_5(E^nBu_2)$], may be preferable as single source precursors in LPCVD, despite their higher molecular weights.

This Chapter focuses on three topics. Firstly, the selected precursors [$MBr_5(E^nBu_2)$] (M = Nb, Ta; E = S, Se) will be prepared and tested under LPCVD conditions. Then, thermal decomposition of a series these precursors will be studied using thermogravimetric analysis (TGA). Finally, a range of temperatures for LPCVD will be tested to investigate any temperature effect for the same precursors.

5.2 Result and Discussion

5.2.1 Precursor synthesis and discussion

Complexes [$MBr_5(ER_2)$] (M = Nb, Ta; E = S, Se; R = ^{n}Bu) were prepared *via* the literature method to form either a deep red (M = Nb) or dark yellow oil (M = Ta) with good agreement with theoretical microanalysis data.[1] Far-infrared spectra of these bromide complexes (Figure A6.42–A6.45) indicate a shift to low wavenumbers by about 100 cm^{-1}, compared their chloride analogues and corresponding to a change in the ligand environment due to the presence of different halides.[1, 23-25] There are three bands, which is consistent with a pseudo octahedral geometry ($2A_1$ + E) (Table 5.1).[25] ^{1}H NMR spectra show significant chemical shifts from free ligand (Figure A7.19–A7.22). ^{93}Nb NMR spectra of $NbBr_5$ complexes show resonances at *ca.* 770 ppm (Figure A7.24–A7.25), consistent with other reported [$NbBr_5$(L)] species.[23] Therefore, it is agreed that the geometry of these bromide species are the same as that of the chloride species.

Table 5.1 Selected Nb–X absorption (cm^{-1})

Species	**X = Cl[1]**	**X = Br (This work)**
[$NbX_5(S^nBu_2)$]	**394sh, 371, 363sh**	**281sh, 270s, 253sh**
[$NbX_5(Se^nBu_2)$]	**394sh 371s, 340sh**	**281sh, 268s, 257sh**
[$TaX_5(S^nBu_2)$]	**392s, 364sh, 347s**	**250sh, 232s, 215sh**
[$TaX_5(Se^nBu_2)$]	**387s, 338sbr, 319sh**	**251sh, 231s, 221sh**

5.2.2 Thermogravimetric analysis of complexes

5.2.2.1 Precursors to niobium dichalcogenide thin films

The complexes [$NbCl_5(S^nBu_2)$], [$NbBr_5(S^nBu_2)$], [$NbCl_5(Se^nBu_2)$] and [$NbBr_5(Se^nBu_2)$] are potential candidates for use as single source LPCVD precursors for NbS_2 and $NbSe_2$ thin films due to their volatility and the presence of readily eliminated ^{n}Bu groups; [$NbCl_5(S^nBu_2)$] and [$NbCl_5(Se^nBu_2)$] have previously been shown to deposit NbE_2 thin films successfully.[1] Thermogravimetric analyses were undertaken on these complexes (Figure A3.4–A3.7 and Table A3.1), and EDX spectra for the residues from the TGA experiment are discussed below. Unfortunately, in all case the weight loss does not correspond with the residue being NbS_2 or $NbSe_2$. This is not surprising due to the different experimental conditions used in TGA and in typical low-pressure CVD experiments.

EDX spectra for the residues from the TGA experiment on [$NbBr_5(S^nBu_2)$] and [$NbCl_5(Se^nBu_2)$] have been collected. Very strong peaks of niobium and oxygen as well as weak bromine signal were

found for the former, suggesting that the ligand completely dissociated during the TGA experiment (Figure 5.1). The presence of oxygen in the sample is likely due to exposure to air when preparing the EDX samples. The EDX spectrum of the residues from sample [$NbCl_5(Se^nBu_2)$] contains carbon, chlorine, selenium and niobium (Figure 5.2), suggesting the Nb–Se bond is slightly more stable than Nb–S bond when the temperature increased in ambient pressure under inert gas atmosphere. This is consistent with the assertion that selenoethers are stronger donor than thioethers when coordinating to the highest oxidation state metal centres.[26] The significant carbon peak in the EDX spectrum is mainly from carbon tape used to mount the sample. Both EDX spectra show that all both the NbS_2 and $NbSe_2$ precursors mainly undergo ligand dissociation during typical TGA experiments under inert gas condition.

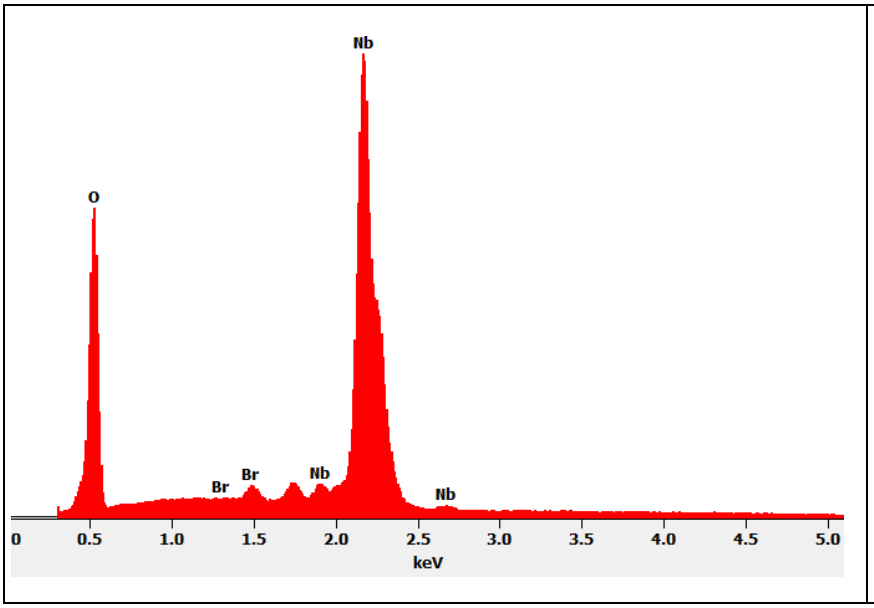

Elements	Atom %
Nb	40.5
O	58.8
Br	0.7

Figure 5.1 EDX spectrum of the TGA sample residue from [$NbBr_5(S^nBu_2)$] with accelerating voltage 10 kV.

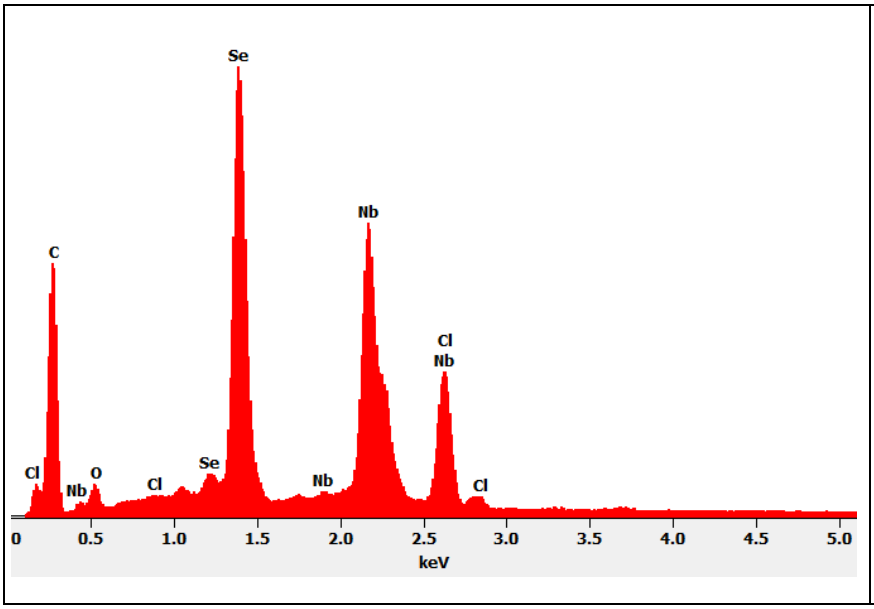

Elements	Atom %
O	27.2
Cl	22.7
Se	23.5
Nb	26.6

Table 5.2 EDX spectrum of the TGA sample residue from [$NbCl_5(Se^nBu_2)$] with accelerating voltage 10 kV.

5.2.2.2 Tantalum(V) halide chalcogenoether complexes

No deposition is observed from $[TaCl_5(S^nBu_2)]$ and $[TaCl_5(Se^nBu_2)]$ in LPCVD at a range of temperatures between 600–750 °C.[1] $[TaBr_5(Se^nBu_2)]$ has been tested in LPCVD and was also unsuccessful (Section 5.2.3.5). This section focuses solely on the analysis of thermal decomposition data relating to $[TaCl_5(Se^nBu_2)]$ and $[TaBr_5(Se^nBu_2)]$.

The TGA data for $[TaCl_5(Se^nBu_2)]$ shows a step mass loss to a black residue (*ca.* 51 weight %, Figure 5.3). The EDX spectrum from this residue shows the predominant elements are tantalum, oxygen with a small amount (< 1 %) of Se (L_α = 1.379 keV) and Cl (K_α = 2.621 keV) (Figure 5.4).[27] The TGA residue from $[TaCl_5(Se^nBu_2)]$ is likely a mixture of tantalum, selenium and chlorine.

The TGA data for $[TaBr_5(Se^nBu_2)]$ shows two weight loss steps (20–100 °C and 180–260 °C) and leaves a *ca.* 50 weight % residue with slow weight loss until 600 °C (final residual recorded 40 weight % at 600 °C) (Figure 5.5). The EDX spectrum from the TGA residue of $[TaBr_5(Se^nBu_2)]$ suggests tantalum is the predominant element. It is difficult to distinguish Se from Ta due to the overlap in peaks, while the Br peak (L_α = 1.480 keV) appears very weak (Figure 5.6). The TGA residue of $[TaBr_5(Se^nBu_2)]$ likely contains a mixture of Ta, Se and Br.

The TGA results for $[TaX_5(Se^nBu_2)]$ only show the possible decomposition route when temperature is increased in an argon environment, which is different to the conditions for the LPCVD application.

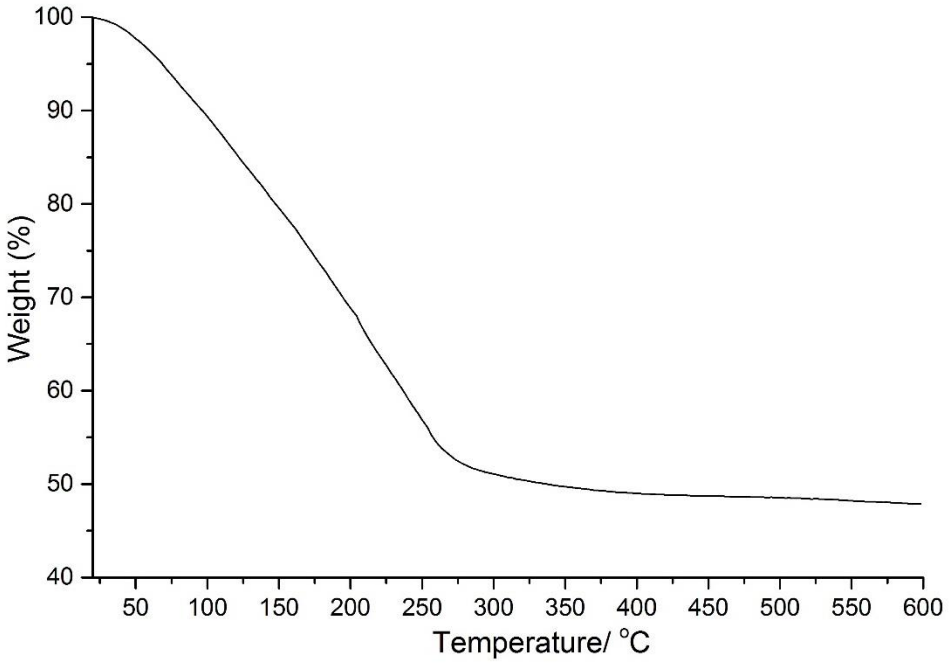

Figure 5.2 TGA profile of $[TaCl_5(Se^nBu_2)]$.

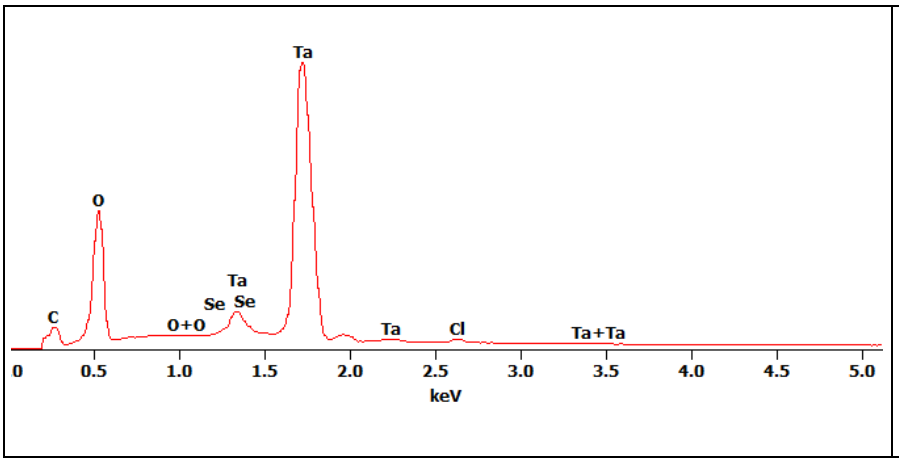

Elements	Atom %
C	15.1
O	55.5
Cl	1.1
Se	0.6
Ta	27.7

Figure 5.3 EDX spectrum of the TGA sample residue of [$TaCl_5(Se^nBu_2)$] with accelerating voltage 10 kV.

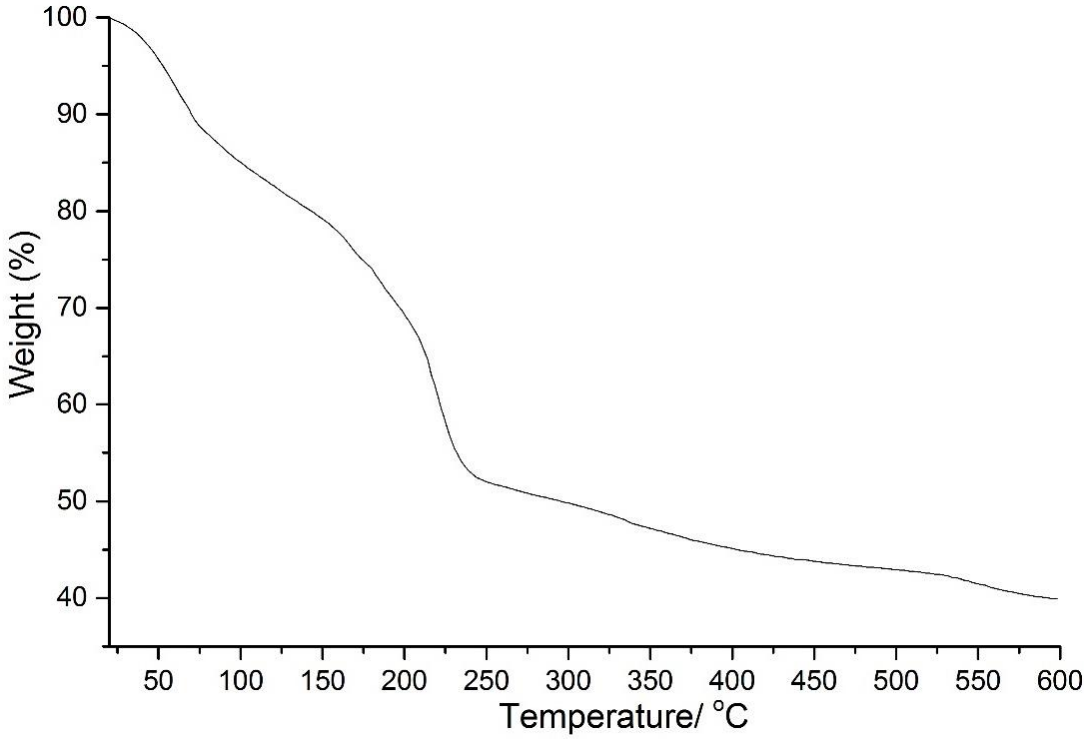

Figure 5.4 TGA profile of [$TaBr_5(Se^nBu_2)$].

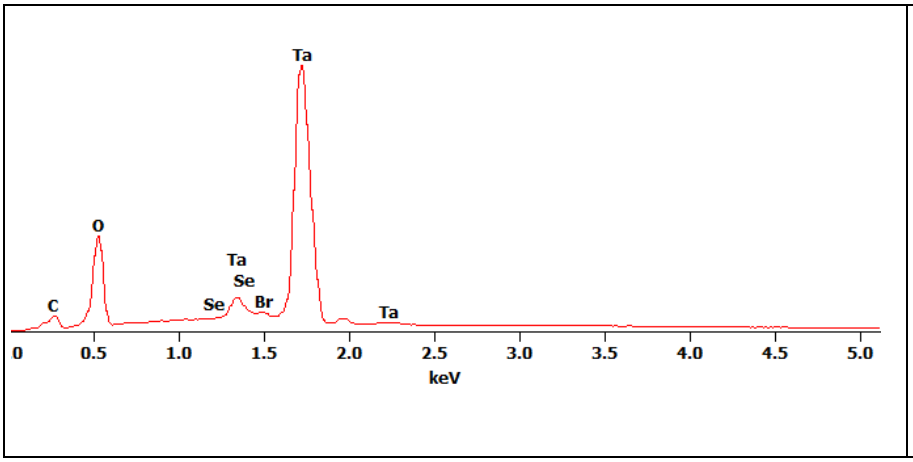

Elements	Atom %
C	21.8
O	46.8
Br	1.3
Se	2.1
Ta	28.0

Figure 5.5 EDX spectrum of the TGA sample residue of [$TaBr_5(Se^nBu_2)$] with accelerating voltage 10 kV.

5.2.3 LPCVD application

5.2.3.1 NbS_2 thin films obtained using [$NbBr_5(S^nBu_2)$]

Precursor [$NbBr_5(S^nBu_2)$] deposited a continuous black 3R-NbS_2 thin film on SiO_2 substrates using LPCVD at 750 ℃ of 0.05 mmHg. These films are oxygen and moisture stable. The grazing incidence X-ray diffraction pattern shows preferred orientation in 0 0 3 reflection whereas the 1 1 0 reflection presents the strongest diffraction in in-plane XRD (Figure 5.7). Lattice parameters determined by Le Bail fitting of the grazing incidence XRD pattern are: a = 3.3409(9), c = 17.859(7) Å (R_{wp} = 4.74 %, R_p = 3.4 %). These are similar to literature values for bulk 3R-NbS_2 (a = 3.3303(3), c = 17.918(2) Å).[4]

Pole figure measurements were undertaken on a NbS_2 film obtained from the [$NbBr_5(S^nBu_2)$] precursor to establish the film texture. Using 2θ = 14.90°, corresponding to the 0 0 3 reflection, resulted in a single sharp peak (FWHM ~ 5°) observed at the centre of the figure with α = 90° (Figure 5.8 a). The figure taken with 2θ = 31.33°, corresponding to the 1 0 1, exhibits a ring with α = 9 and 171° (Figure 5.8 b). These results confirmed the <0 0 *l*> preferred orientation, in which the *ab* planes of the crystallites lie parallel to the substrate.

Scanning electron microscopy (SEM) images reveal that the NbS_2 films are formed of microcrystalline platelets mainly lying flat on the substrate (Figure 5.9 top), consistent with the orientation inferred from the XRD data. An EDX spectrum was taken at an accelerating voltage of 10 keV and shows significant Si and O peaks in addition to peaks for Nb and S, indicating that the films are thin. The EDX spectrum also shows there is no evidence for any residual Cl in the films (Cl K_α = 2.621 keV).[27] Accurate quantification of the Nb:S ratio by EDX is difficult due to the Nb L_α and S K_α peaks overlapping (Figure 5.9 bottom).

The Raman spectrum of the NbS_2 film was collected using 785 nm excitation and shows broad bands at *ca*. 455, 385, 324 and 280 cm^{-1} (Figure 5.10). The peaks at 385 and 455 cm^{-1} were assigned as A modes, whereas the bands at 324 and 280 cm^{-1} were assigned to E modes of the 3R-NbS_2 film.[1, 9, 28-31] The low frequency peaks are thought to be a result of two-phonon scattering.[9, 28, 29]

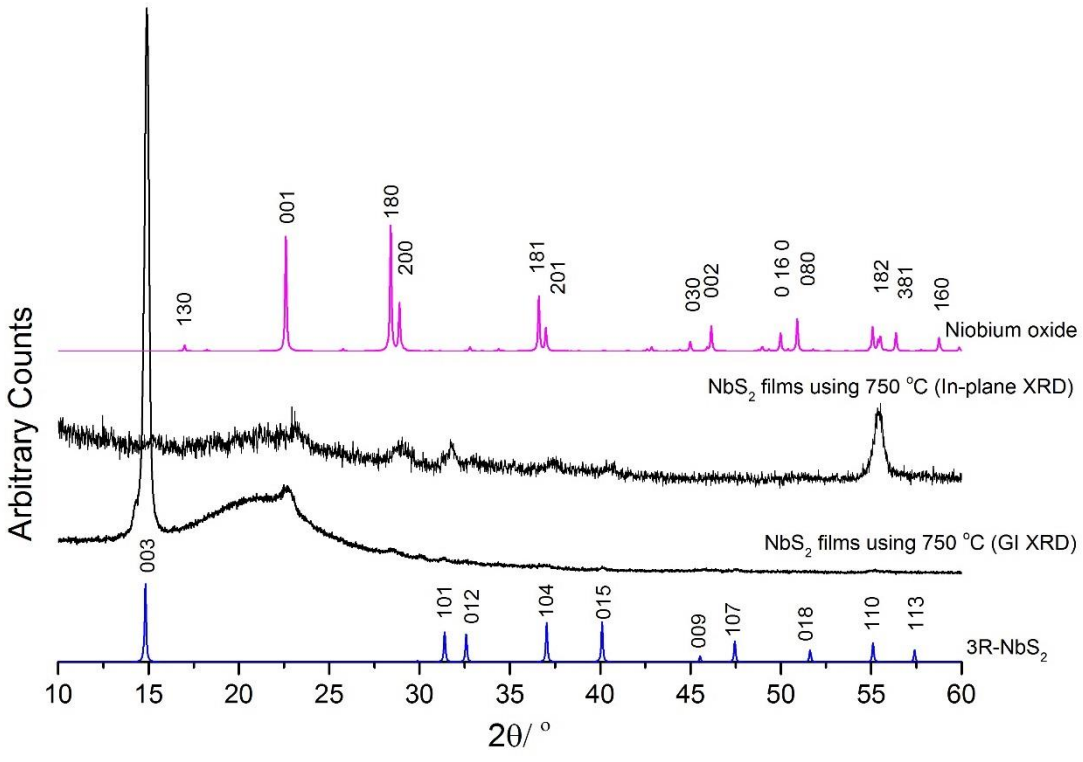

(a)

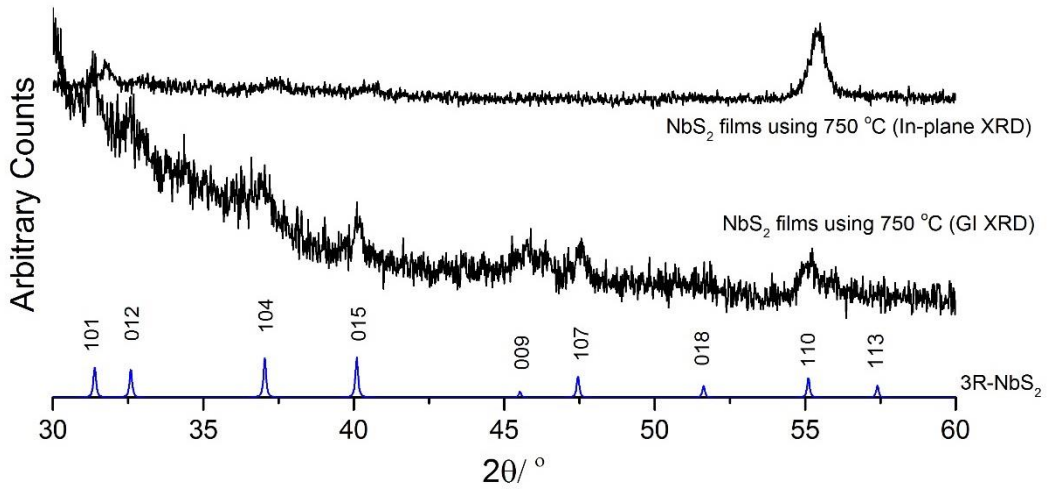

(b)

Figure 5.6 (a) Grazing incidence (θ_1 = 1°) and in-plane (θ_1 = 0.5°) XRD (black) from the NbS_2 thin film deposited by LPCVD using [$NbBr_5(S^nBu_2)$] at 750 °C; simulated XRD pattern from bulk 3R-NbS_2 (blue) and bulk niobium oxide (pink).[4, 32] The broad feature at 2θ = *ca.* 22° is from the SiO_2 substrate. (b) Expansion of selected range (2θ =30–60°).

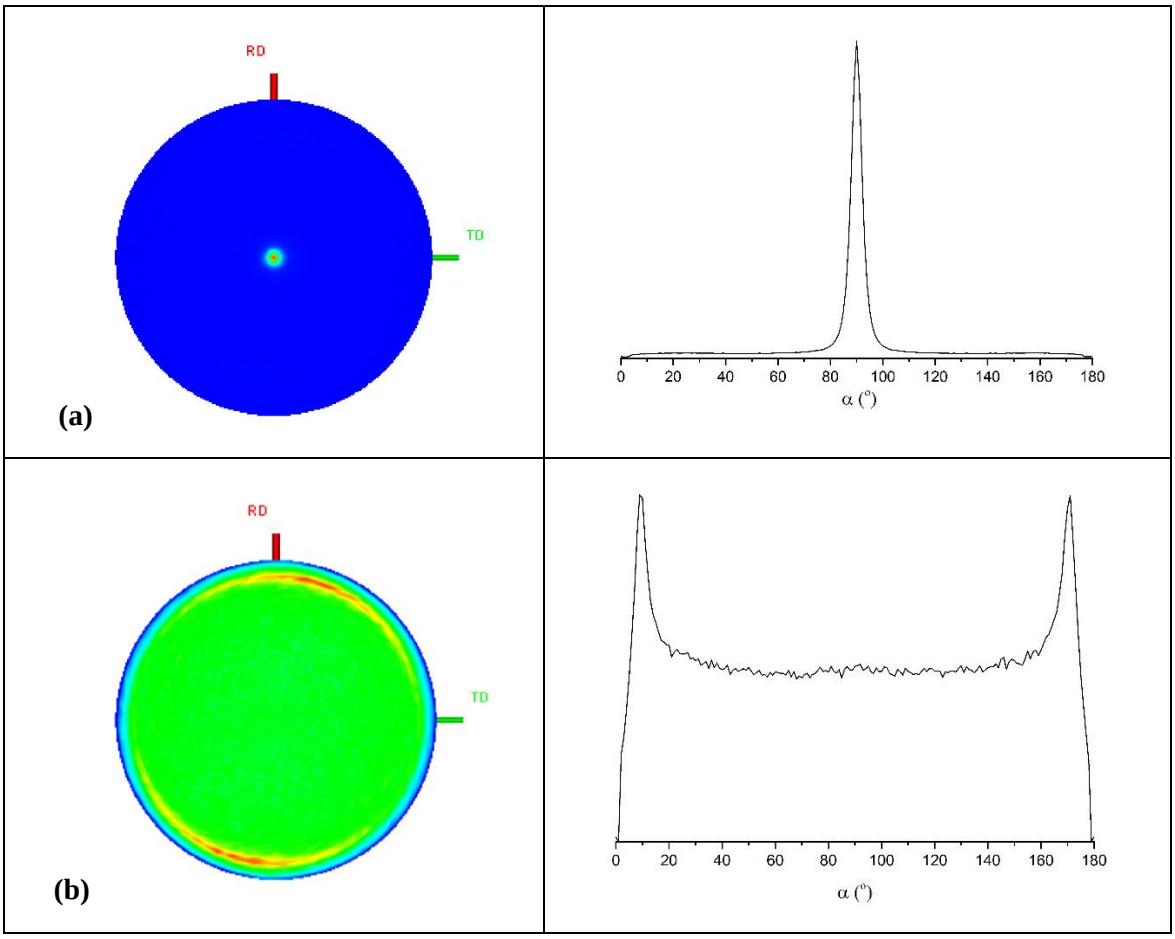

Figure 5.7 Pole Figures with cut line graphs for the (a) 0 0 3 (2θ = 14.90°) and (b) 1 0 1 (2θ = 31.33°) reflections of a film of NbS_2 deposited on a SiO_2 substrate.

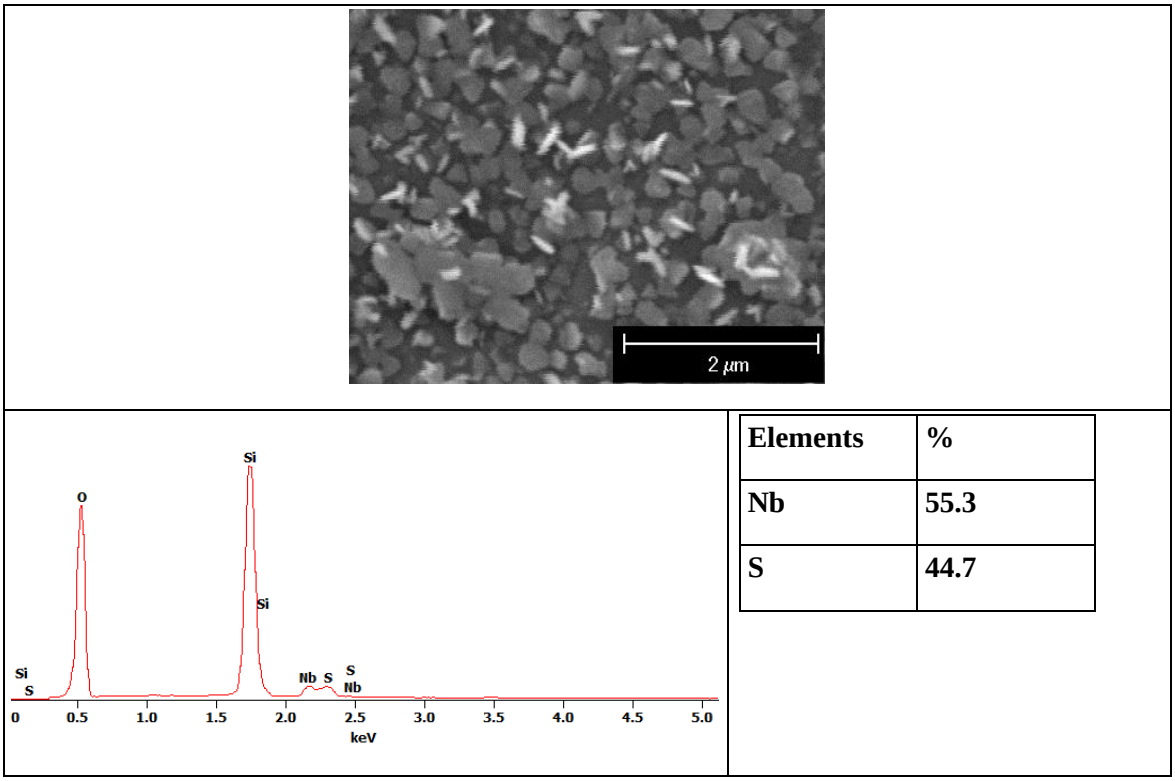

Elements	%
Nb	55.3
S	44.7

Figure 5.8 (top) SEM images and (bottom) EDX spectrum of a polycrystalline NbS_2 film deposited by LPCVD from $[NbBr_5(S^nBu_2)]$ at 750°C with accelerating voltage 10 kV.

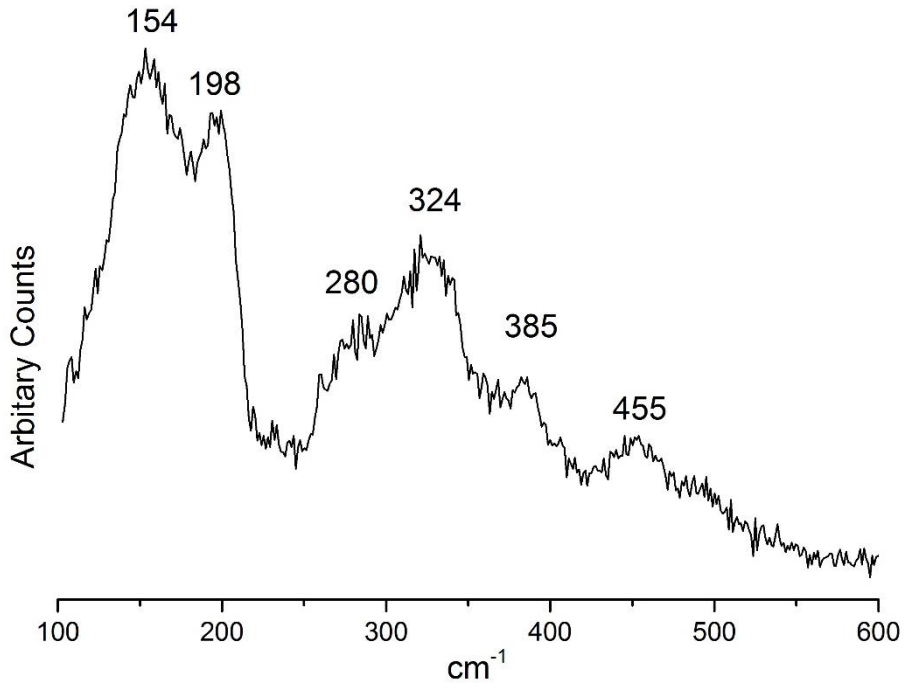

Figure 5.9 Raman spectrum of NbS_2 deposited by LPCVD from [$NbBr_5(^nBu_2S)$] at 750 ˚C

5.2.3.2 $NbSe_2$ thin films obtained using [$NbCl_5(Se^nBu_2)$]

$NbSe_2$ thin films were deposited successfully using [$NbCl_5(Se^nBu_2)$] as single source LPCVD precursor over a range of temperatures (550–650 ℃) (Figure 5.11–5.12). The films obtained at 650 ℃ have been reported as 3R-$NbSe_2$ (Space group *R*3*mh*, data supported in reference 1) whereas 2H-$NbSe_2$ (Space group $P6_3/mmc$) films were identified when using the same precursor in LPCVD at 550 ℃. Interestingly, $NbSe_2$ films obtained at 600 ℃ show both 2H- and 3R-$NbSe_2$ phase in the region 2θ = *ca.* 35–40° (Figure 5.13). Lattice parameters determined by Le Bail fitting of the grazing incidence XRD pattern are: a = 3.427(5), c = 12.44(5) Å (R_{wp} = 2.8 %, R_p = 2.09 %; 2H-$NbSe_2$ films from 550 ℃), compared to the literature values for bulk 2H-$NbSe_2$ of a = 3.4446(2), c = 12.5444(7) Å .[3] Rietveld refinement parameter of 3R-$NbSe_2$ thin film using 650 ℃ is reported in the literature.[1]

EDX spectra of films obtained from 550 ℃ (2H-$NbSe_2$ film) and 600 ℃ (2H- and 3R-$NbSe_2$) show the Nb : Se ratio as 1 : 2, corresponding to the composition $NbSe_2$ (Figure A4.1–A4.2 in Appendix 4)

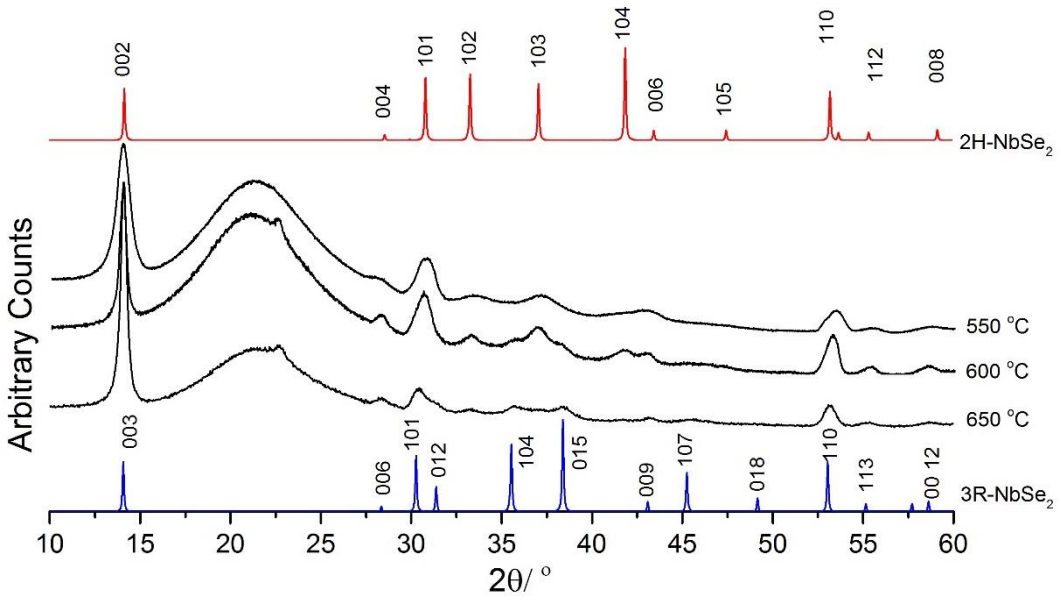

Figure 5.10 Grazing incidence XRD (black) from the $NbSe_2$ thin film deposited by LPCVD using $[NbCl_5(Se^nBu_2)]$ at 550–650 °C; simulated XRD pattern from bulk 2H-$NbSe_2$ (red) and 3R-$NbSe_2$ (blue).[3] The broad feature at 2θ = *ca.* 22° is from the SiO_2 substrate. The weak peak at 2θ = *ca.* 22° is from niobium oxide.[32]

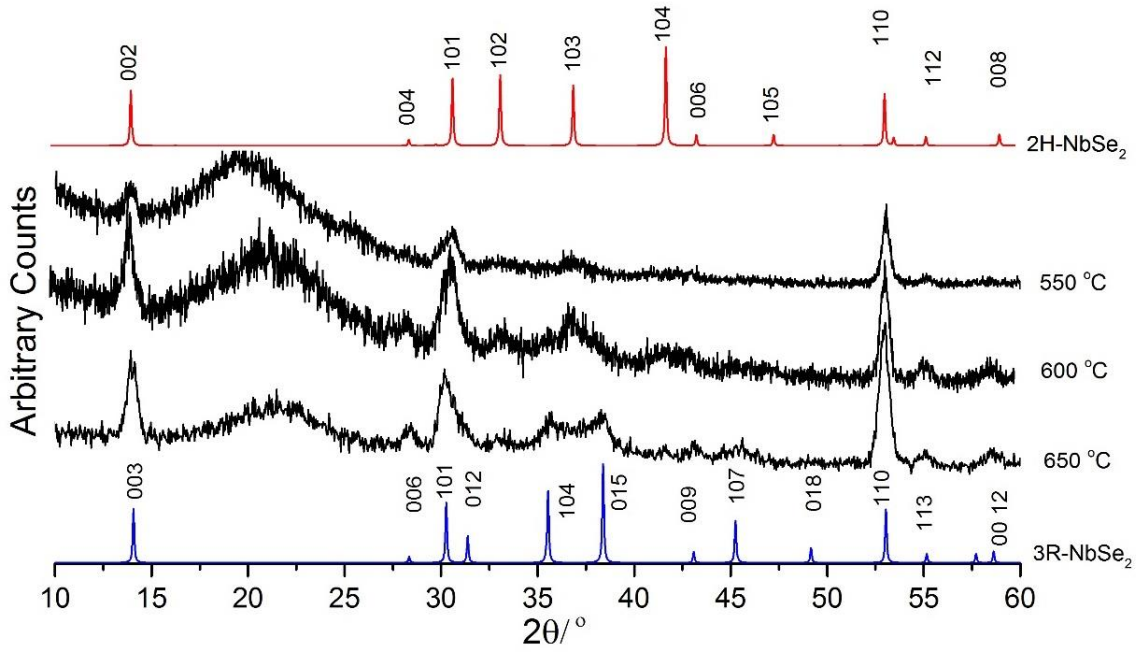

Figure 5.11 In-plane XRD (black) from the $NbSe_2$ thin film deposited by LPCVD using $[NbCl_5(Se^nBu_2)]$ at 550–650 °C; simulated XRD pattern from bulk 2H-$NbSe_2$ (red) and 3R-$NbSe_2$ (blue).[3] The broad feature at 2θ = *ca.* 22° is from the SiO_2 substrate.

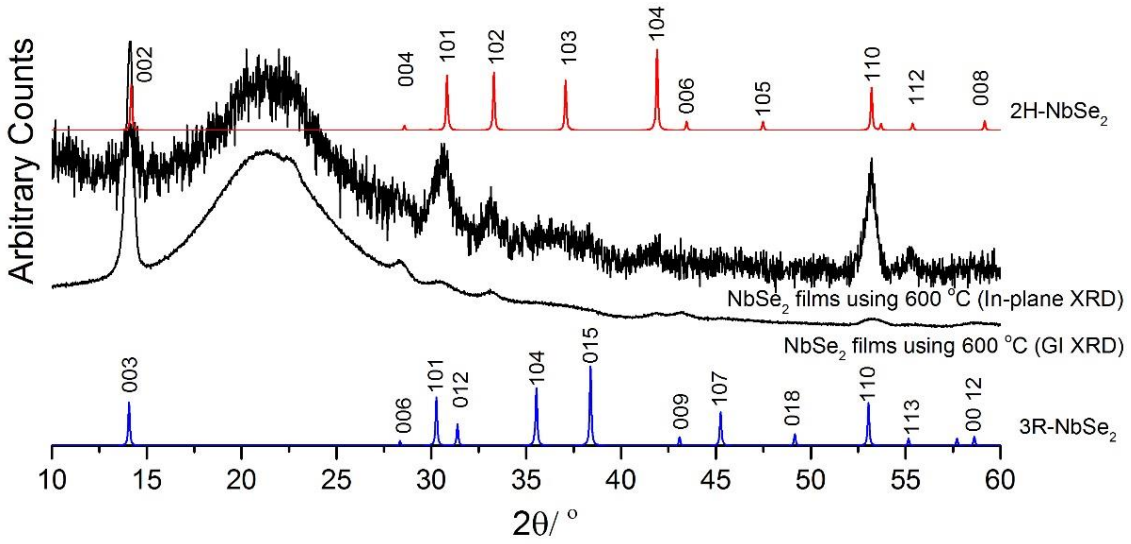

Figure 5.12 Grazing incidence and in-plane XRD (black) from the $NbSe_2$ thin film deposited by LPCVD using [$NbCl_5(Se^nBu_2)$] at 600 ℃; simulated XRD pattern from bulk 2H-$NbSe_2$ (red) and 3R-$NbSe_2$ (blue).[3] The broad feature at 2θ = *ca.* 22° is from the SiO_2 substrate.

5.2.3.3 $NbSe_2$ thin films obtained using [$NbBr_5(Se^nBu_2)$]

The $NbSe_2$ films using [$NbBr_5(Se^nBu_2)$] in LPCVD over temperatures ranging from 550–650 ℃. 2H-$NbSe_2$ thin films deposit at 550 ℃, whereas 3R-$NbSe_2$ films were found to deposit at 650 ℃ (Figure 5.14–5.15). Again, where deposition temperature is controlled at 600 ℃, the resulting $NbSe_2$ films show both 2H- and 3R- stacking (Figure 5.16).

Lattice parameters determined by Le Bail fitting of the grazing incidence XRD pattern are: a = 3.437(5), c = 12.60(7) Å (R_{wp} = 2.8 %, R_p = 2.09 %; 2H-$NbSe_2$ films from 550 ℃), compared to the literature values for bulk 2H-$NbSe_2$ of a = 3.4446(2), c = 12.5444(7) Å .[3] EDX spectra correspond to the formula $NbSe_2$ for the materials deposited onto these films (Figure A4.3–A4.5 in Appendix 4).

All the $NbSe_2$ thin films discussed in this chapter have preferred orientation <0 0 *l*> shown by grazing incidence X-ray pattern, whereas 1 0 1 and 1 0 2 are the strongest reflection in the in-plane X-ray data. Pole figure XRD of a 3R-$NbSe_2$ thin film using [$NbBr_5(Se^nBu_2)$] taken with 2θ = 14.03°, corresponding to the 0 0 3 reflection, exhibits a single sharp peak (FWHM ~ 5°), whereas pole figure diagram using 1 0 1 reflection (2θ = 30.34°) shows a ring with α = *ca.* 9° and 170° (Figure 5.17). These results are consistent with preferred orientation mostly with the *ab* plane of the crystallites, which are parallel to the substrate surface.

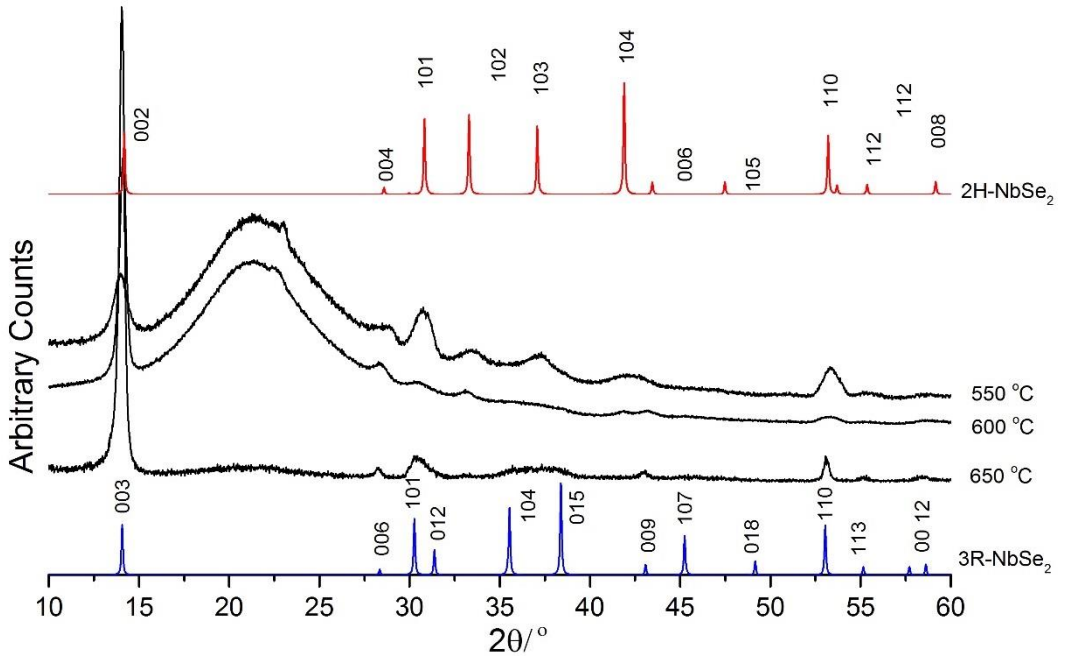

Figure 5.13 Grazing incidence XRD (black) from the $NbSe_2$ thin film deposited by LPCVD using $[NbBr_5(Se^nBu_2)]$ at 550–650 °C; simulated XRD pattern from bulk 2H-$NbSe_2$ (red) and 3R-$NbSe_2$ (blue).[3] The broad feature at 2θ = *ca.* 22° is from the SiO_2 substrate. The weak peak at 2θ = *ca.* 22° is from niobium oxide.[32]

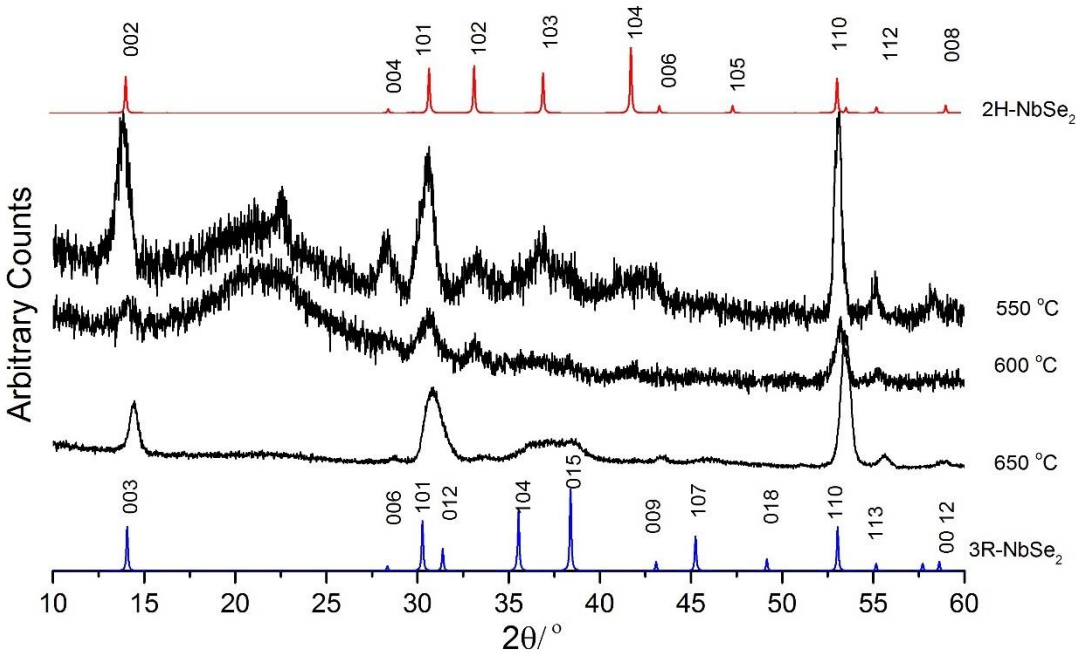

Figure 5.14 In-plane XRD (black) from the $NbSe_2$ thin film deposited by LPCVD using $[NbBr_5(Se^nBu_2)]$ at 550–650 °C; simulated XRD pattern from bulk 2H-$NbSe_2$ (red) and 3R-$NbSe_2$ (blue).[3] The broad feature at 2θ = *ca.* 22° is from the SiO_2 substrate. The weak peak at 2θ = *ca.* 22° is from niobium oxide.[32]

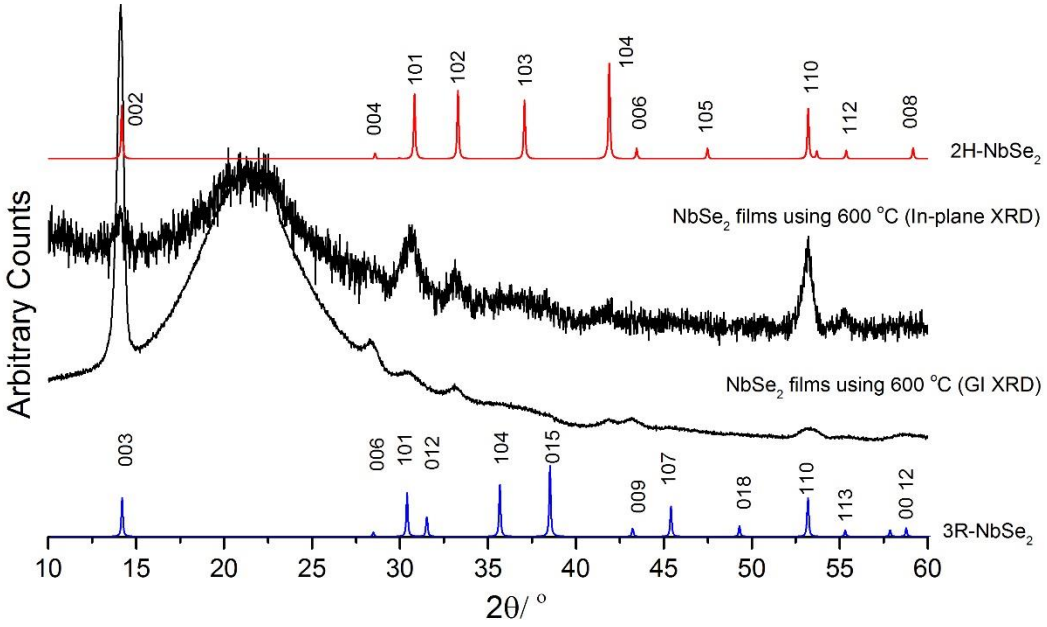

Figure 5.15 Grazing incidence and in-plane XRD (black) from the $NbSe_2$ thin film deposited by LPCVD using [$NbBr_5(Se^nBu_2)$] at 600 °C; simulated XRD pattern from bulk 2H-$NbSe_2$ (red) and 3R-$NbSe_2$ (blue).[3] The broad feature at 2θ = *ca.* 22° is from the SiO_2 substrate.

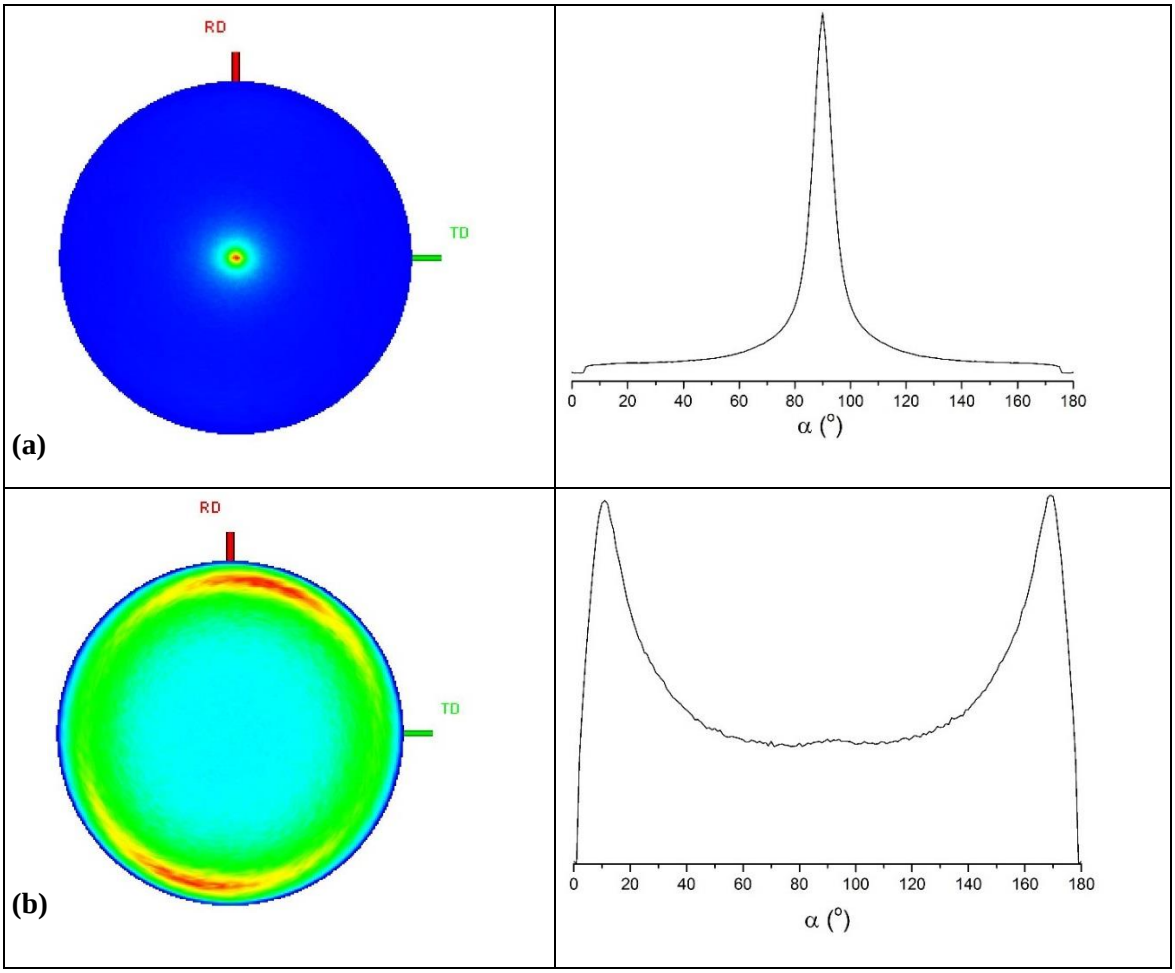

Figure 5.16 Pole Figures with cut line graphs for the 0 0 3 (2θ = 14.03°) (a) and 1 0 1 (2θ = 30.34°) (b) reflections of a film of 3R-$NbSe_2$ deposited on a SiO_2 substrate at 650 °C.

5.2.3.4 Raman spectra of 2H-/3R-NbSe2 thin films

The Raman spectra of 2H-$NbSe_2$ films, deposited at 550 °C, and 3R-$NbSe_2$, deposited at 650 °C, were obtained using 785 nm excitation and compared to the 3R-$NbSe_2$ Raman spectrum from the literature.[1, 31] There is no significant difference in the spectra of the 2H- and 3R-$NbSe_2$ films. The two overlapping peaks (228 and 237 cm^{-1}) can be assigned to be A_{1g} and E_{2g} mode respectively (Figure 5.18). The broad band at *ca.* 189 cm^{-1} has been assigned to a lattice distortion.[1, 17, 31, 33-38]

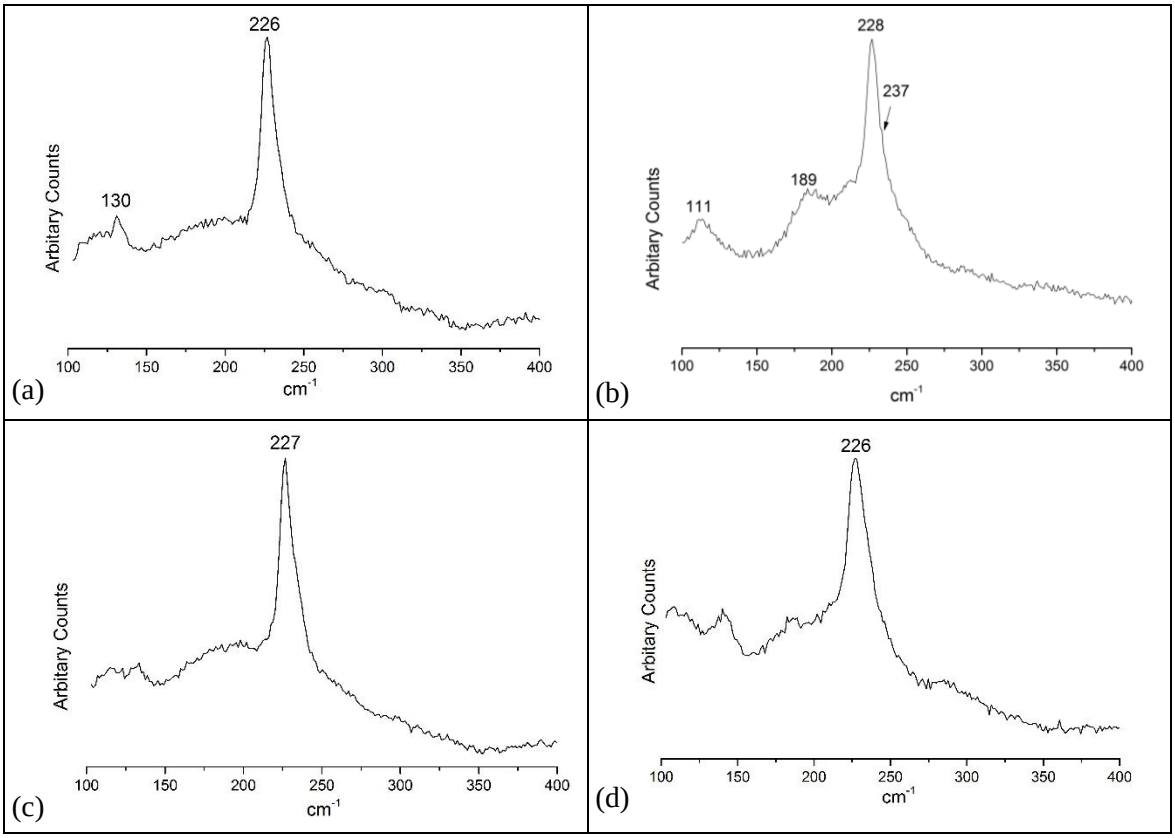

Figure 5.17 Raman spectra of 2H-/3R-$NbSe_2$ thin films deposited by LPCVD from $[NbX_5(^nBu_2Se)]$ at different deposition temperatures. (a) X = Cl, 550 °C; (b) X = Cl, 650 °C;[1] (c) X = Br, 550 °C; (d) X = Br, 650 °C.

5.2.3.5 Attempted deposition of $TaSe_2$ thin film using $[TaX_5(Se^nBu_2)]$ complexes

Attempts to use tantalum selenide precursors, $[TaCl_5(Se^nBu_2)]$ and $[TaBr_5(Se^nBu_2)]$, to deposit thin films of $TaSe_2$ using LPCVD were unsuccessful. Red films were observed at the open end of the tube and no deposition observed on the substrates. The red films are thought to be elemental selenium. There are many possible reasons for this failure.

These complexes are hard metal halides with soft neutral donor ligands, and the bond dissociation energy of Ta–E is low, so the ligands are easily lost. As tantalum (180 amu) is heavier than niobium (92 amu), the tantalum compounds are expected to be less volatile than the niobium analogues. TGA

results and EDX spectra from the TGA residues of both [$TaCl_5(Se^nBu_2)$] and [$TaBr_5(Se^nBu_2)$] support that the Ta–Se bonds are weak and broken at increased temperature, whereas the Se^nBu_2 in [$NbCl_5(Se^nBu_2)$] remains in TGA experiments and is observed in the EDX spectrum of its TGA residue. TGA, EDX spectra and attempted LPCVD applications using [$TaX_5(Se^nBu_2)$] (X = Cl, Br) all show that these complexes are too unstable to use in LPCVD.

5.3 Conclusion

A series of $[MBr_5(E^nBu_2)]$ (M = Nb, Ta; E = S, Se) complexes was prepared with full characterisation using IR and multinuclear NMR spectroscopies and with satisfactory microanalysis results of carbon to hydrogen ratio. Thermogravimetric analysis of $[NbX_5(S^nBu_2)]$, $[NbX_5(Se^nBu_2)]$ and $[TaX_5(Se^nBu_2)]$ were collected. In general, all of the complexes show weak bond energies between neutral soft chalcogenethers coordinated with hard metal such as Nb(V) and Ta(V) halides; all of them showed the decomposition under inert condition when the temperature increases.

The LPCVD application of $[NbBr_5(S^nBu_2)]$ successfully deposited black continuous 3R-NbS_2 thin films, which were identified *via* grazing incidence X-ray diffraction and in-plane X-ray diffraction. These NbS_2 films have preferred orientation in <0 0 *l*> direction which is consistent with pole figure XRD using the acute angle between 0 0 3 and 1 0 1. Scanning Electronic Microscopy images shown that the crystallites are parallel to the substrate surface, agreeing with the <0 0 *l*> preferred orientation. Although Energy-dispersive X-ray spectroscopy cannot give the ratio of Nb:S due to the respective peaks overlapping, EDX also demonstrates the exclusion of Cl.

LPCVD using $[NbCl_5(Se^nBu_2)]$ and $[NbBr_5(Se^nBu_2)]$ complexes deposited 2H-$NbSe_2$ thin films at 550 ℃, 2H-/3R- stacking $NbSe_2$ thin films at 600 ℃ and 3R-$NbSe_2$ thin films at 650 ℃. The 2H-$NbSe_2$ and 3R-$NbSe_2$ films were identified *via* grazing incidence XRD, in-plane XRD. EDX data are consistent with the formation of $NbSe_2$ with those films. The mechanism of 2H- and 3R-$NbSe_2$ phase change remains unclear. These $NbSe_2$ films all have preferred orientation in <0 0 *l*> reflections in their grazing incidence XRD pattern and 1 0 1 and 1 1 0 are the preferred orientations in in-plane XRD patterns. Pole figure XRD using 0 0 3 and 1 0 1 from a 3R-$NbSe_2$ thin film is consistent with the acute angle between these two planes.

5.4 Experimental

Precursor Preparation

5.4.1 $[NbCl_5(S^nBu_2)]$, $[NbCl_5(Se^nBu_2)]$ and $[TaCl_5(Se^nBu_2)]$

Were made *via* literature procedure.[1]

5.4.2 $[NbBr_5(S^nBu_2)]$

$NbBr_5$ (245 mg, 0.5 mmol) was suspended in CH_2Cl_2 (15 mL) before S^nBu_2 (0.09 mL, 0.5 mmol) was then added and the mixture stirred for 30 minutes. The mixture was filtered and the red filtrate was taken to dryness *in vacuo* leaving a red sticky oil. *n*-Hexane (3 mL) was added to wash the residual oil and removed *via* a syringe. The red oil was dried *in vacuo* to afford a red sticky oil. Yield: 238 mg, 74 %. Required for $C_8H_{18}Br_5NbS$ (638.72 g/mol): C, 15.04; H, 2.84. Found: C, 15.20; H, 2.94. IR (Nujol, cm^{-1}): 281sh, 270s, 253sh (Nb–Br). ^1H NMR ($CDCl_3$, 298 K): δ = 0.96 (t, [6H], Me), 1.47 (m, [4H], $\underline{CH_2}Me$), 1.70 (br, [4H], $SCH_2\underline{CH_2}$), 2.82 (br, [4H], SCH_2). ^{93}Nb NMR (CD_2Cl_2, 298 K) δ = 778 ($w_{½}$ = 2500 Hz).

5.4.3 $[NbBr_5(Se^nBu_2)]$

$NbBr_5$ (494 mg, 1.0 mmol) was suspended in CH_2Cl_2 (30 mL) before a solution of Se^nBu_2 (195 mg, 1.0 mmol) in CH_2Cl_2 (3 mL) was added and stirred for 30 minutes. The mixture was filtered and the red filtrate was pumped to dryness to leave red sticky oil. *n*-Hexane (3 mL) was added to wash the residual oil and removed *via* a syringe. The red oil was dried *in vacuo*. Yield: 523 mg, 76 %. Required for $C_8H_{18}Br_5NbSe$ (685.61 g/mol): C, 14.01; H, 2.65. Found: C, 15.20; H, 2.94. IR (Nujol, cm^{-1}): 281sh, 268s, 257sh (Nb–Br). ^1H NMR ($CDCl_3$, 298 K): δ = 0.97 (t, [6H], Me), 1.48(m, [4H], $\underline{CH_2}Me$), 1.80 (br, [4H], $SCH_2\underline{CH_2}$), 3.15 (br, [4H], SCH_2). $^{77}Se\{^1H\}$ NMR (CD_2Cl_2, 228 K) δ = 242. ^{93}Nb NMR (CD_2Cl_2, 298 K) δ = 760 ($w_{½}$ = 1500 Hz).

5.4.4 $[TaBr_5(S^nBu_2)]$

$TaBr_5$ (290 mg, 0.5 mmol) was suspended in CH_2Cl_2 (15 mL). S^nBu_2 (0.09 mL, 0.5 mmol) was then added and the mixture stirred for 30 minutes. The mixture was filtered and the yellow filtrate was pump to dryness leaving a sticky oil. *n*-Hexane (3 mL) was added to wash the residue and removed *via* a syringe. The oil was dried *in vacuo*. A yellow sticky oil. Yield: 226 mg, 62 %. Required for $C_8H_{18}Br_5TaS$ (726.76 g/mol): C, 13.22; H, 2.5. Found: C, 13.39; H, 2.33. IR (Nujol, cm^{-1}): 250sh, 232s, 215sh (Ta–Br).^1H NMR ($CDCl_3$, 298 K): δ = 0.98 (t, [6H], Me), 1.51 (m, [4H], $\underline{CH_2}Me$), 1.81 (br, [4H], $SCH_2\underline{CH_2}$), 3.28 (br, [4H], SCH_2).

5.4.5 [$TaBr_5(Se^nBu_2)$]

$TaBr_5$ (290 mg, 0.5 mmol) was suspended in CH_2Cl_2 (15 mL), before a solution of Se^nBu_2 (99 mg, 0.5 mmol) in CH_2Cl_2 (ca. 2 mL) was added and the mixture stirred for 30 minutes. The mixture was filtered and the dark yellow filtrate was then pump to dryness, leaving a sticky oil. *n*-Hexane (3 mL) was added to wash the residue and removed *via* a syringe. The oil was dried *in vacuo* to afford a yellow sticky oil remained. Yield 293 mg, 75 %. Required for $C_8H_{18}Br_5TaSe$ (773.66 g/mol): C, 12.42; H, 2.34. Found: C, 12.56; H, 2.28. IR (Nujol, cm^{-1}): 251sh, 231s, 221sh (Ta–Br). ^1H NMR ($CDCl_3$, 298 K): δ = 0.99 (t, [6H], Me), 1.51 (m, [4H], $\underline{CH_2}Me$), 1.84 (m, [4H], $SeCH_2\underline{CH_2}$), 3.33 (br, [4H], $SeCH_2$). $^{77}Se\{^1H\}$ NMR (CD_2Cl_2, 298 K): δ = 220.

LPCVD experiments

5.4.6 Precursor [$NbBr_5(S^nBu_2)$]

The precursor (54 mg for each applications) was loaded with CH_2Cl_2 (1 mL) in a glovebox. Silica substrates were loaded after the precursor was loaded and placed end-to-end. The tube was placed in a furnace and then linked to a vacuum pump (0.01 mmHg). The temperature in the furnace was increased to 750 ℃ and left for 10 minutes to allow the temperature to stabilise. The precursor end was moved into the furnace immediately until the edge of the furnace. An orange film grown through the open end of the tube. After 30 minutes, the furnace was cooled to ambient temperature and the substrates were unload in ambient condition. Black films were observed on the substrates.

5.4.7 Precursor [$NbCl_5(Se^nBu_2)$] using temperature 550 ℃, 600 ℃ and 650 ℃

The precursor (*ca.* 50 mg for each applications) was loaded with CH_2Cl_2 (1 mL) in a glovebox. Silica substrates were loaded after the precursor was loaded and placed end-to-end. The tube was placed in a furnace and then linked to a vacuum pump (0.01 mmHg). The temperature in the furnace was increased to 550 or 600 ℃ (two LPCVD experiments) and left for 10 minutes to allow the temperature to stabilise. The precursor end was moved into the furnace immediately until the edge of the furnace. A red film grown through the open end of the tube. After 30 minutes, the furnace was cooled to ambient temperature and the substrates were unload in ambient condition.

5.4.8 Precursor [$NbBr_5(Se^nBu_2)$] using temperature 550 ℃, 600 ℃ and 650 ℃

The precursor (*ca.* 50 mg for each applications) was loaded with CH_2Cl_2 (1 mL) in a glovebox. Silica substrates were loaded after the precursor was loaded and placed end-to-end. The tube was placed in a furnace and then linked to a vacuum pump (0.01 mmHg). The temperature in the furnace was increased to 550, 600 or 650 ℃ (two LPCVD experiments) and left for 10 minutes to allow the temperature to stabilise. The precursor end was moved into the furnace immediately until the edge

of the furnace. A red film grown through the open end of the tube. After 30 minutes, the furnace was cooled to ambient temperature and the substrates were unload in ambient condition. In all experiments, black films were observed on the substrates.

5.5 References

1. S. L. Benjamin, Y.-P. Chang, C. Gurnani, A. L. Hector, M. Huggon, W. Levason and G. Reid, *Dalton Trans.*, 2014, **43**, 16640.
2. S. L. Benjamin, Y.-P. Chang, M. Huggon, W. Levason and G. Reid, *Polyhedron*, 2015, **99**, 230.
3. B. E. Brown and D. J. Beerntsen, *Acta Cryst.*, 1965, **18**, 31.
4. B. Morosin, *Acta Cryst.*, 1974, **B30**, 551.
5. F. Jellinek, G. Brauer and H. Müller, *Nature*, 1960, **185**, 376.
6. Z. L. Liu, L. C. Cai and X. L. Zhang, *J. Alloys Compd.*, 2014, **610**, 472.
7. S. Zhao, T. Hotta, T. Koretsune, K. Watanabe, T. Taniguchi, K. Sugawara, T. Takahashi, H. Shinohara and R. Kitaura, *2D Materials*, 2016, **3**, 025027.
8. T. Yanase, S. Watanabe, M. Weng, M. Wakeshima, Y. Hinatsu, T. Nagahama and T. Shimada, *Cryst. Growth Des.*, 2016, **16**, 4467.
9. W. Ge, K. Kawahara, M. Tsuji and H. Ago, *Nanoscale*, 2013, **5**, 5773.
10. C. J. Carmalt, E. S. Peters, I. P. Parkin, T. D. Manning and A. L. Hector, *Eur. J. Inorg. Chem.*, 2004, 4470.
11. P. J. McKarns, M. J. Heeg and C. H. Winter, *Inorg. Chem.*, 1998, **37**, 4743.
12. C. J. Carmalt, T. D. Manning, I. P. Parkin, E. S. Peters and A. L. Hector, *J. Mater. Chem.*, 2004, **14**, 290.
13. C. J. Carmalt, T. D. Manning, I. P. Parkin, E. S. Peters and A. L. Hector, *Thin Solid Films*, 2004, **469**, 495.
14. E. S. Peters, C. J. Carmalt, I. P. Parkin and D. A. Tocher, *Eur. J. Inorg. Chem.*, 2005, 4179.
15. E. Hitz, J. Wan, A. Patel, Y. Xu, L. Meshi, J. Dai, Y. Chen, A. Lu, A. V. Davydov and L. Hu, *ACS Appl. Mater. Interfaces*, 2016, **8**, 11390.
16. Y. H. Huang, R. S. Chen, J. R. Zhang and Y. S. Huang, *Nanoscale*, 2015, **7**, 18964.
17. N. D. Boscher, C. J. Carmalt and I. P. Parkin, *Eur. J. Inorg. Chem.*, 2006, 1255.
18. N. D. Boscher, C. J. Carmalt and I. P. Parkin, *Appl. Surf. Sci.*, 2010, **256**, 3178.
19. J. Renteria, R. Samnakay, C. Jiang, T. R. Pope, P. Goli, Z. Yan, D. Wickramaratne, T. T. Salguero, A. G. Khitun, R. K. Lake and A. A. Balandin, *J. Appl. Phys.*, 2014, **115**, 034305.
20. D. C. Papageorgopoulos, V. Saltas, C. A. Papageorgopoulos, D. Tonti, C. Pettenkofer and W. Jaegermann, *Appl. Surf. Sci.*, 2000, **161**, 347.
21. S. L. Benjamin, C. H. de Groot, C. Gurnani, A. L. Hector, R. Huang, K. Ignatyev, W. Levason, S. J. Pearce, F. Thomas and G. Reid, *Chem. Mater.*, 2013, **25**, 4719.
22. T. L. Allen, *J.Chem. Phys.*, 1957, **26**, 1644.
23. M. Jura, W. Levason, R. Ratnani, G. Reid and M. Webster, *Dalton Trans.*, 2010, **39**, 883.
24. S. L. Benjamin, A. Hyslop, W. Levason and G. Reid, *J. Fluorine Chem.*, 2012, **137**, 77.

25. K. Nakamoto, *Infrared and Raman Spectra of Inorganic and Coordination Compounds*, Wiley, New York, 1986.

26. W. Levason and G. Reid, *Comprehensive Coordination Chemistry II*, ed. J. A. McCleverty and T. J. Meyer, Elsevier, Oxford, 2003, **1**, 391.

27. A. C. Thompson and D. Vaughan, *X-ray data booklet*, Lawrence Berkeley National Laboratory, University of California, Berkeley, Calif., 2001.

28. S. Onari, T. Arai, R. Aoki and S. Nakamura, *Solid State Commun.*, 1979, **31**, 577.

29. W. G. McMullan and J. C. Irwin, *Solid State Commun.*, 1983, **45**, 557.

30. J. K. Dash, L. Chen, P. H. Dinolfo, T.-M. Lu and G.-C. Wang, *J. Phys. Chem. C*, 2015, **119**, 19763.

31. Y.-P. Chang, M.Sc Thesis, University of Southampton, 2014.

32. K. Kato and S. Tamura, *Acta Cryst.*, 1975, **B31**, 673.

33. C. S. Wang and J. M. Chen, *Solid State Commun.*, 1974, **14**, 1145.

34. J. Tsang, J. Smith and M. Shafer, *Phys. Rev. Lett.*, 1976, **37**, 1407.

35. M. Klein, *Phys. Rev. B*, 1981, **24**, 4208.

36. C. M. Pereira and W. Y. Liang, *J. Phys. C Solid. State Physi.*, 1982, **15**, L991.

37. C. M. Pereira and W. Y. Liang, *J. Phys. C Solid. State Physi.*, 1985, **18**, 6085.

38. A. Leblanc-Soreau, P. Molinié and E. Faulques, *Physica C: Superconductivity*, 1997, **282-287**, 1937.

Chapter 6: Chemical vapour deposition of MoE_2 films from chalcogenoether complexes of $MoCl_4$

6.1 Introduction

The LPCVD applications of niobium halide complexes with neutral donors is well established in previous chapters. This chapter is using the successful experience of designing LPCVD single source precursors onto the new materials, MoS_2 and $MoSe_2$.

2D-molybdenum dichalcogenide (MoS_2 and $MoSe_2$) thin films are highly promising candidates for a variety of applications such as spintronics,[1] electrocatalysts for hydrogen evolution,[2, 3] high performance materials for optoelectronics[4] and as sensors for environmental applications.[5] Very recently, MoS_2 has been studied for its thermoelectric properties.[6]

The preparations of thin MoE_2 films were described in Chapter 1. Although the synthesis by reaction MoO_3 with elemental S/Se powder at high temperature under vacuum could deposit very thin 2D films (*ca.* 0.7 nm ~ monolayer),[7-10] the method used requires high temperature (usually 700 ℃ or higher) and two or more process setps,[7-29] which are disadvantages when considering manufacturing processes. Other MoE_2 precursors reported in the literature were dual source precursors. Reduction of $[NH_4]_2[MoS_4]$ with dihydrogen gas in the gas-phase[30, 31] or APCVD application using $MoCl_5$ and Se^tBu_2.[32] One special preparation is using $MoSe_2$ powder in chemical vapour transport method to deposit $MoSe_2$ thin films.[33] Therefore, the deposition method for MoE_2 thin films is relatively uncommon. It would be advantageous to develop a convenient preparation for MoE_2 thin films and to develop new single source CVD precursors for these.

Molybdenum halide complexes with soft neutral donors are unusual,[34, 35] but have recently been studied by Marchetti and co-workers who synthesised a series of molybdenum complexes with differing numbers of N-, O- and S-ligands.[36-40] Density functional theory calculations of $[MoCl_5L]$ (L = ligands) indicate the compounds are energetically favourable.[37, 40] It is reported that $MoCl_5$ is reduced to $MoCl_4$ when using an excess of ligand or solvent.[36, 41, 42] $[MoCl_4(SR_2)_2]$ was also prepared,[43, 44] however, there is no literature data on $MoCl_4$ with coordinated seleno- or telluroethers. The complex, $[MoCl_3L_n]$ could be prepared *via* reduction of $[MoCl_4L_2]$ (L = THF, THT or SMe_2) using excess ligands or zinc powder.[43, 45]

$[MoCl_4L_2]$ complexes, which are reported to be monomers, contain the desired 1:2 Mo:E ratio, and therefore do not require a change in oxidation state when depositing MoE_2 materials suggesting they might be suitable CVD precursors. $[MoCl_3(SR_2)_3]$ (L = THT and SMe_2) complexes form dimeric structures and therefore are unsuitable as single source LPCVD precursors.[43] Although $[MoCl_3([9]aneS_3)]$ is reported as a monomer,[46, 47] macrocyclic ligands are less unsuitable ligands in

LPCVD. [$MoCl_5L$] complexes have only been simulated from density functional theory under extreme conditions.[37, 40] Therefore, [$MoCl_4L_2$] species are chosen to enter this research.

This chapter focuses on the preparation of suitable single source LPCVD MoE_2 precursors by the coordination of molybdenum tetrachloride with neutral chalcogenoethers. The preparation of $MoCl_4$ species with neutral chalcogenoethers will be described with infrared and UV-visible spectra and providing solid state structures. The candidates β-hydride elimination will be studied in terms of their thermal decomposition pathway *via* TGA and assessed in LPCVD.

6.2 Result and Discussion

6.2.1 Molybdenum tetrachloride with monodentate ligands

$[MoCl_4(NCCH_3)_2]$ and $[MoCl_4(THT)_2]$ were prepared using literature methods.[36, 41] Some examples $[MoCl_4L_2]$ (L = CH_3CN, SMe_2 or S^nBu_2) are prepared directly from $MoCl_5$ by adding an excess of the monodentate ligands, whereas all the $[MoCl_4(chalcogenoether)_n]$ species in this Chapter are accessed *via* ligand substitutions of $[MoCl_4(NCCH_3)_2]$ (Scheme 1). Crystals of $[MoCl_4(NCCH_3)_2]$ and $[MoCl_4(SMe_2)_2]$ were grown by allowing CH_2Cl_2 solution to evaporate to dryness in a nitrogen environment. Crystals of $[MoCl_5(SMe_2)][MeSCH_2SMe_2]$ were obtained from $[MoCl_4(SMe_2)_2]$ crystals as a minor product.

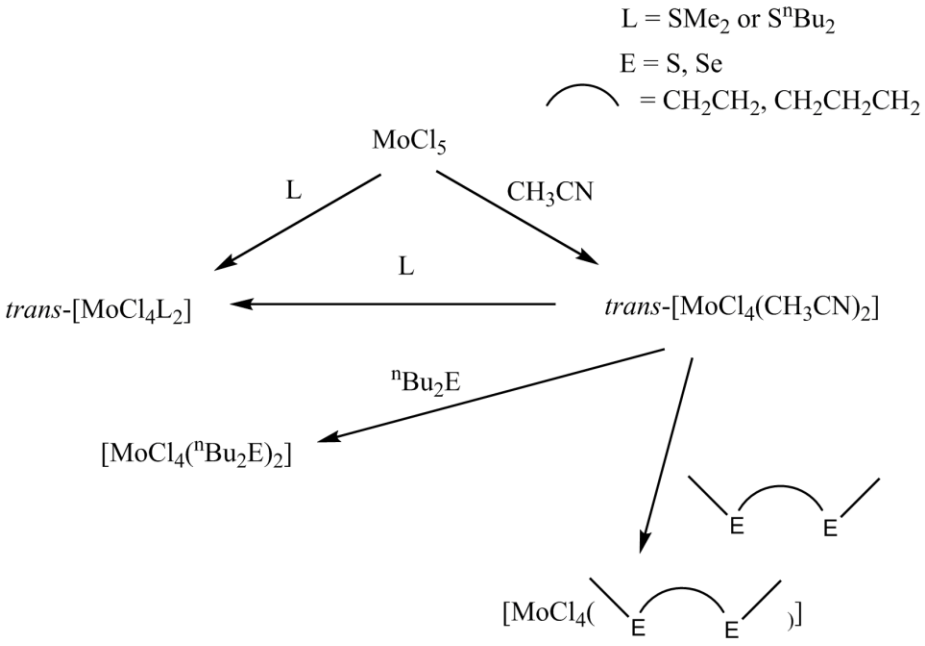

Scheme 6.1 The preparation of $MoCl_4$ species

The geometry of two chalcogenoether ligands in all $[MoCl_4L_2]$ complexes are assigned as *trans* because all of them have one broad infrared absorption (E_u), which corresponds to the structure of known examples, such as $[MoCl_4(NCCH_3)_2]$ and $[MoCl_4(SMe_2)_2]$ (discuss below) (Figure A6.46–A6.51 and Table 6.1).

Table 6.1 Selected Mo–Cl absorption(cm^{-1})

Complexes	ν(Mo–Cl)	Complexes	ν(Mo–Cl)
$[MoCl_4(NCCH_3)_2]$	335	$[MoCl_4(S^nBu_2)_2]$	334
$[MoCl_4(THT)_2]$	338	$[MoCl_4(SeMe_2)_2]$	306
$[MoCl_4(SMe_2)_2]$	332	$[MoCl_4(Se^nBu_2)_2]$	342

The solid state molecular structure of $[MoCl_4(NCCH_3)_2]$ is octahedral and $[MoCl_4(SMe_2)_2]$ is a distorted octahedron with the two neutral ligands disposed *trans* to each other. (Figure 6.1and Table 6.2–6.3) There is no significant difference in the Mo–Cl distance between these two structures. The bond distance of Mo–S in $[MoCl_4(SMe_2)_2]$ is longer than Mo–N in $[MoCl_4(NCCH_3)_2]$ because the sulfur atom is bigger than a nitrogen atom. The reason for the ligands adopting a *trans* position is most likely due to the *trans* effect. Both compounds have previously been reported without solid state data.[41, 43]

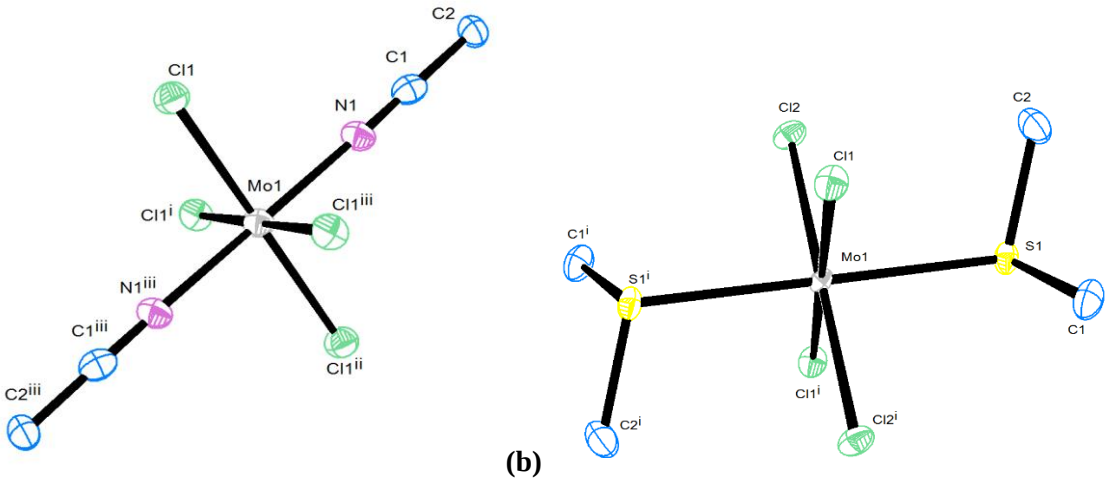

Figure 6.1 (a) The structure of $[MoCl_4(NCCH_3)_2]$ showing the atom numbering scheme and with ellipsoids drawn at the 50 % probability level. Hydrogen atoms are omitted for clarity. Symmetry operation: i = x, -y, z; ii = 1 - x, -y, 1 - z; iii = 1 - x, y, 1 - z. (b) The structure of $[MoCl_4(SMe_2)_2]$ showing the atom numbering scheme and with ellipsoids drawn at the 50 % probability level. Hydrogen atoms are omitted for clarity.

Table 6.2 Selected bond lengths (Å) for $[MoCl_4(NCCH_3)_2]$

Bond length			
Mo1–Cl1	**2.336(1)**	**Mo1–N1**	**2.113(3)**

Table 6.3 Selected bond lengths (Å) angles (°) for $[MoCl_4(SMe_2)_2]$

Bond length		**Bond Angles**			
Mo1–Cl1	**2.3457(5)**	**Cl1–Mo1–Cl2**	**89.39(2)**	**$Cl1^i$–Mo1–S1**	**88.65(2)**
Mo1–Cl2	**2.3323(5)**	**Cl1–Mo1–$Cl2^i$**	**90.61(2)**	**$Cl1^i$–Mo1–$S1^i$**	**91.35(2)**
Mo1–S1	**2.5297(6)**	**Cl1–Mo1–S1**	**91.35(2)**	**Cl2–Mo1–S1**	**90.51(2)**
		Cl1–Mo1–$S1^i$	**88.65(2)**	**Cl2–Mo1–$S1^i$**	**89.49(2)**
		$Cl1^i$–Mo1–Cl2	**90.62(2)**	**$Cl2^i$–Mo1–S1**	**89.49(2)**
		$Cl1^i$–Mo1–$Cl2^i$	**89.39(2)**	**$Cl2^i$–Mo1–$S1^i$**	**90.51(2)**

Table 6.4 Selected bond distance (Å) in [$MoCl_4$(monodentate)$_2$] crystals structures

Complexes	**Mo–Cl$_{trans\mathbf{Cl}}$**	**Mo–L**	**Mo–Cl$_{trans\mathbf{L}}$**
[$MoCl_4(NCCH_3)_2$]	**2.336(1)**	**2.113(3)**	**none**
[$MoCl_4(Me_2S)_2$]	**2.3390(5)**	**2.5297(6)**	**None**
[$MoCl_5(Me_2S)$][Me_2SCH_2SMe]	**2.3573(2)**	**2.552(2)**	**2.385(2)**

Crystals of [$MoCl_5(SMe_2)$][Me_2SCH_2SMe] were isolated from the recrystallization of [$MoCl_4(SMe_2)_2$] (Figure 6.2 and Table 6.5), where Mo is in its +4 oxidation state. Mo–Cl length in the [$MoCl_5(SMe_2)$]$^-$ anion is slightly longer than that in both [$MoCl_4(SMe_2)_2$] and [$MoCl_4(NCCH_3)_2$]; the Mo–Cl$_{transS}$ in [$MoCl_5(SMe_2)$]$^-$ is slightly longer than other Mo–Cl bonds in [$MoCl_5(SMe_2)$]$^-$ due to the *trans* influence (Table 6.4).

The reduction of Mo(V) to Mo(IV) in the reaction using chalcogenoethers is likely to be due to the chalcogenoether being oxidised. In similar systems, Marchetti and co-workers explain that Mo^vCl_5 is reduced by receiving one electron from one of the five Cl^- ligands. The evidence is the released chlorine gas during a test reaction (Cl(-1) → Cl(0)).[36,39] The isolation of crystals of [$MoCl_5(SMe_2)$][Me_2SCH_2SMe] suggests there might be another explanation, such as the metal centre may be undergoing reduction by ligands or solvents (*i.e.* CH_3CN, SMe_2 or CH_2Cl_2). The cation [Me_2SCH_2SMe)]$^+$ is evidence for oxidation of Me_2S. It is postulated that one of the C–H bond is cleaved, releasing H^+ and probably forming hydrogen chloride, released rapidly as a gas (Scheme 6.2).[48-51] ^{1}H NMR spectrum of [$MoCl_4(SMe_2)_2$] in CD_2Cl_2 solution at room temperature confirms the existence of [Me_2SCH_2SMe)]$^+$ (see Section 6.2.4 for detail). The next step of this reaction might be the formation of [$MoCl_4(SMe_2)_2$], the major product, and $MeSCH_2Cl$/Me_2S. Both $MeSCH_2Cl$ and Me_2S are volatile and therefore easily removed under vacuum.

This is not the first record of $MoCl_5$ being reduced by solvents. $MoCl_5$ has been shown to reduce to $MoCl_4$ when excess C_2Cl_4 or CH_3CN is added, with literature suggesting the formation of chlorinated organic products forming in the reaction.[41, 42] Sometime volatile byproducts can be pumped off in experiments (for CH_3CN, SMe_2, THT, S^nBu_2, $SeMe_2$) (see experimental for detail). However, removal of byproducts could be a problem when the ligands are heavy such as Se^nBu_2 or bidentate ligands (next section).

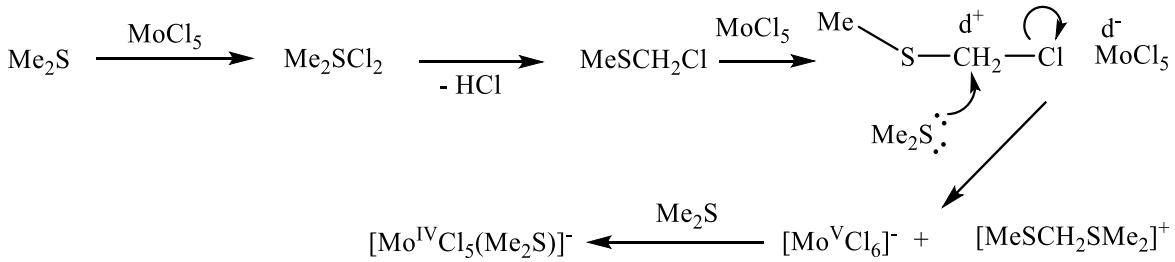

Scheme 6.2 The proposal mechanism of Mo^VCl_5 reduction by dimethyl sulfide in excess.[48-50]

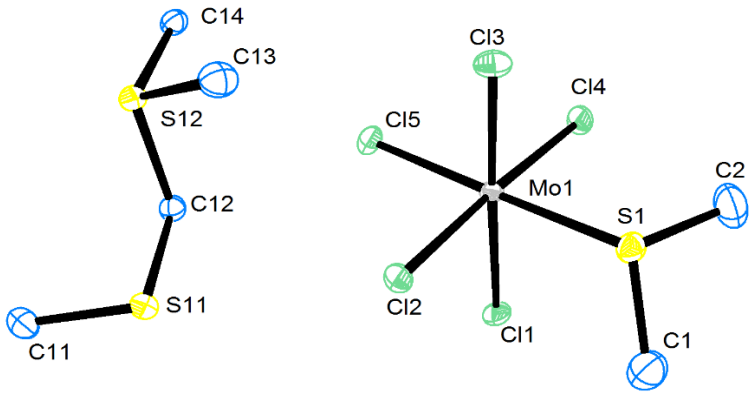

Figure 6.2 The structure of $[MoCl_5(SMe_2)][Me_2SCH_2SMe)]$ showing the atom numbering scheme and with ellipsoids drawn at the 50 % probability level. Hydrogen atoms are omitted for clarity.

Table 6.5 Selected angles (°) and bond lengths (Å) for $[MoCl_5(SMe_2)][Me_2SCH_2SMe)]$

Bond length		**Bond Angles**			
Mo1–Cl1	**2.351(2)**	**Cl1–Mo1–Cl2**	**88.10(6)**	**Cl2–Mo1–S1**	**85.05(6)**
Mo1–Cl2	**2.389(2)**	**Cl1–Mo1–Cl4**	**91.33(6)**	**Cl3–Mo1–Cl4**	**91.48(7)**
Mo1–Cl3	**2.363(2)**	**Cl1–Mo1–Cl5**	**92.11(7)**	**Cl3–Mo1–Cl5**	**92.87(7)**
Mo1–Cl4	**2.325(2)**	**Cl1–Mo1–S1**	**91.74(6)**	**Cl3–Mo1–S1**	**83.14(6)**
Mo1–Cl5	**2.385(2)**	**Cl2–Mo1–Cl3**	**88.80(6)**	**Cl4–Mo1–Cl5**	**91.15(6)**
Mo1–S1	**2.554(2)**	**Cl2–Mo1–Cl5**	**92.13(6)**	**Cl4–Mo1–S1**	**91.70(6)**

6.2.2 Molybdenum tetrachloride with dichalcogenoether ligands

$MoCl_4$ complexes with bidentate ligands are usually made by the substitution of coordinated solvent in $[MoCl_4(NCCH_3)_2]$ using an excess of ligand (Scheme 1). The crystals were grown by allowing slow evaporation of a CH_2Cl_2 solution under nitrogen atmosphere.

As mentioned in the previous section, the metal chloride may react with ligands resulting in Mo(V) → Mo(IV) reduction, and form chlorinated ligands as a byproduct. When using much less volatile ligands such as $MeS(CH_2)_2SMe$, $^{i}PrS(CH_2)_2S^{i}Pr$, $MeS(CH_2)_3SMe$ and $MeSe(CH_2)_3SeMe$, the impurity could not be removed by vacuum or by washing with a non-coordinating solvent. Therefore, direct substitution from $[MoCl_4(NCCH_3)_2]$ could reduce the likelihood of oxidation.

Studies of $[MoCl_4(L–L)]$ crystals reveal a typical pseudo octahedral geometry with deviation from ideal 90° and 180° (Figure 6.3–6.4 and Table 6.6–6.8). Ligands with ethylene backbone ($MeS(CH_2)_2SMe$ and $^{i}PrS(CH_2)_2S^{i}Pr$) adopt *DL* geometry upon coordination to the metal chloride. There is no significant *trans* influence in these two compounds. In contrast, the ligand in

[$MoCl_4${$MeS(CH_2)_3SMe$}] displays *meso* orientation and Mo–$Cl_{trans\ to\ Cl}$ is shorter than Mo–$Cl_{trans\ to\ S}$ by *ca*. 0.03 Å (see Table 6.9).

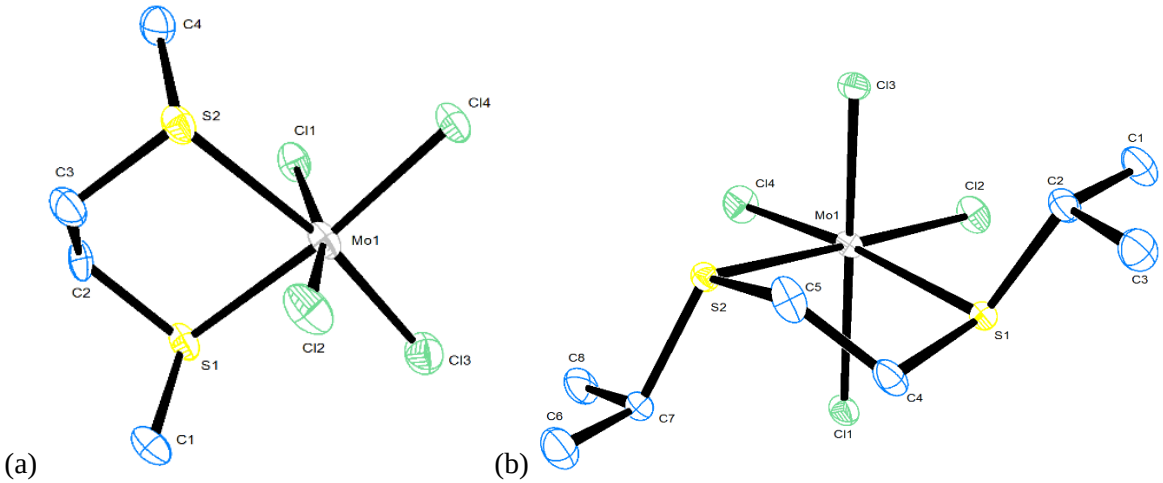

Figure 6.3 (a) The structure of [$MoCl_4${$MeS(CH_2)_2SMe$}] showing the atom numbering scheme and with ellipsoids drawn at the 50 % probability level. Hydrogen atoms are omitted for clarity. (b) The structure of [$MoCl_4${$^iPrS(CH_2)_2S^iPr$}] showing the atom numbering scheme and with ellipsoids drawn at the 50 % probability level. Hydrogen atoms are omitted for clarity.

Table 6.6 Selected bond lengths (Å) and angles (°) for [$MoCl_4${$MeS(CH_2)_2SMe$}]

Bond length		**Bond Angles**			
Mo1–Cl1	**2.305(3)**	**Cl1–Mo1–Cl3**	**97.6(1)**	**Cl2–Mo1–S1**	**91.1(1)**
Mo1–Cl2	**2.305(3)**	**Cl1–Mo1–Cl4**	**92.47(1)**	**Cl2–Mo1–S2**	**77.7(1)**
Mo1–Cl3	**2.247(3)**	**Cl1–Mo1–S1**	**82.2(1)**	**Cl3–Mo1–Cl4**	**96.8(1)**
Mo1–Cl4	**2.339(3)**	**Cl1–Mo1–S2**	**85.3(1)**	**Cl3–Mo1–S1**	**87.8(1)**
Mo1–S1	**2.519(3)**	**Cl2–Mo1–Cl3**	**98.4(1)**	**Cl4–Mo1–S2**	**91.1(1)**
Mo1–S2	**2.591(3)**	**Cl2–Mo1–Cl4**	**92.95(1)**	**S1–Mo1–S2**	**83.62(9)**

Table 6.7 Selected bond lengths (Å) and angles (°) for [$MoCl_4${$^iPrS(CH_2)_2S^iPr$}]

Bond length		**Bond Angles**			
Mo1–Cl1	**2.3203(7)**	**Cl1–Mo1–Cl2**	**96.14(3)**	**Cl2–Mo1–S1**	**89.61(2)**
Mo1–Cl2	**2.3295(7)**	**Cl1–Mo1–Cl4**	**96.60(3)**	**Cl3–Mo1–Cl4**	**97.30(3)**
Mo1–Cl3	**2.3135(7)**	**Cl1–Mo1–S1**	**78.40(2)**	**Cl3–Mo1–S1**	**87.01(2)**
Mo1–Cl4	**2.3016(7)**	**Cl1–Mo1–S2**	**86.63(2)**	**Cl3–Mo1–S2**	**79.16(2)**
Mo1–S1	**2.5872(7)**	**Cl2–Mo1–Cl3**	**96.57(3)**	**Cl4–Mo1–S2**	**92.81(3)**
Mo1–S2	**2.5730(7)**	**Cl2–Mo1–Cl4**	**93.37(3)**	**S1–Mo1–S2**	**84.52(2)**

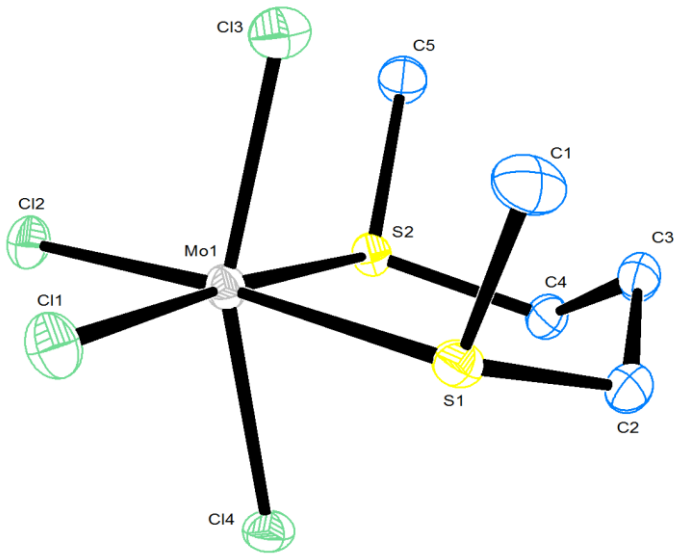

Figure 6.4 The structure of $[MoCl_4\{MeS(CH_2)_3SMe\}]$ showing the atom numbering scheme and with ellipsoids drawn at the 50 % probability level. Hydrogen atoms are omitted for clarity.

Table 6.8 Selected bond lengths (Å) and angles (°) for $[MoCl_4\{MeS(CH_2)_3SMe\}]$

Bond length		**Bond Angles**			
Mo1–Cl1	**2.3143(6)**	**Cl1–Mo1–Cl2**	**92.82(2)**	**Cl2–Mo1–S2**	**85.94(2)**
Mo1–Cl2	**2.3486(6)**	**Cl1–Mo1–Cl3**	**98.40(2)**	**Cl3–Mo1–S1**	**87.41(2)**
Mo1–Cl3	**2.2686(6)**	**Cl1–Mo1–Cl4**	**97.61(2)**	**Cl3–Mo1–S2**	**86.13(2)**
Mo1–Cl4	**2.3380(6)**	**Cl1–Mo1–S1**	**83.61(2)**	**Cl4–Mo1–S1**	**79.79(2)**
Mo1–S1	**2.5282(6)**	**Cl2–Mo1–Cl3**	**96.29(2)**	**Cl4–Mo1–S2**	**78.20(2)**
Mo1–S2	**2.5390(6)**	**Cl2–Mo1–Cl4**	**97.58(2)**	**S1–Mo1–S2**	**97.37(2)**

Table 6.9 Selected bond distance (Å) in $[MoCl_4(L–L)]$ crystals structures

	Mo–Cl$_{trans\ to\ Cl}$	**Mo–Cl$_{trans\ to\ S}$**	**Mo–S**
$[MoCl_4\{MeS(CH_2)_2SMe\}]$	**2.305(3)**	**2.293(3)**	**2.555(3)**
$[MoCl_4\{^iPrS(CH_2)_2S^iPr\}]$	**2.3169(7)**	**2.3156(7)**	**2.5801(7)**
$[MoCl_4\{MeS(CH_2)_3SMe\}]$	**2.3033(6)**	**2.3315(6)**	**2.5336(6)**

6.2.3 Attempted preparation of $[MoCl_4(TeMe_2)_2]$

The synthesis of $[MoCl_4(TeMe_2)_2]$ has been attempted using the $TeMe_2$ substitution of CH_3CN in $[MoCl_4(NCCH_3)_2]$ in a CH_2Cl_2 solution at 0 ℃. A dark purple solution formed after stirring for 30 minutes. After isolation, a dark powder remained but could not be identified from its infrared or microanalysis data. Recrystallization was achieved by the slow evaporation of CH_2Cl_2 under a nitrogen atmosphere, however only colourless crystals of $[Me_2TeCl_2]$ were analysed (Figure 6.5 and Table 6.10). The X-ray crystal structure of $[Me_2TeCl_2]$ has been reported previously in the literature.[52, 53] The ^1H NMR spectrum in $CDCl_3$ solution (3.17, s) agrees with the literature value for a CD_2Cl_2 solution (3.12, s).[54] This shows the reaction redox chemistry; the dimethyl tellurium(II) is oxidised to dimethyldichlorotellurium(IV).

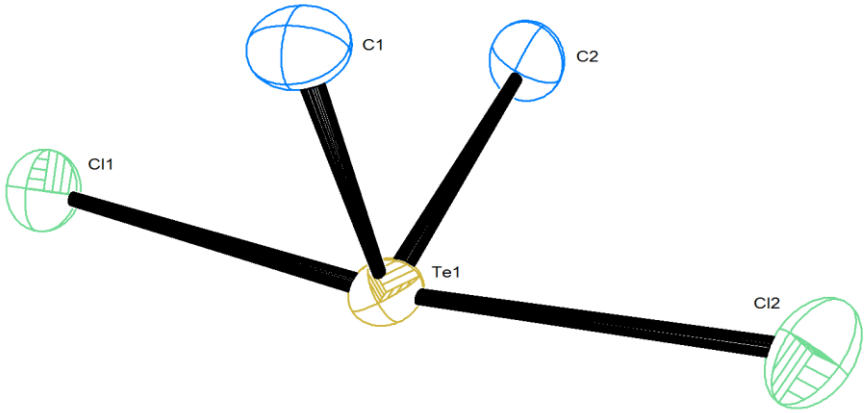

Figure 6.5 The structure of $[Me_2TeCl_2]$ showing the atom numbering scheme and with ellipsoids drawn at the 50 % probability level. Hydrogen atoms are omitted for clarity.

Table 6.10 Selected bond lengths (Å) and angles (°) for $[Me_2TeCl_2]$

Bond length		Bond Angles			
Te1–C1	**2.117(3)**	**C1–Te1–C2**	**96.7(1)**	**C2–Te1–Cl1**	**87.6(1)**
Te1–C2	**2.119(3)**	**C1–Te1–Cl1**	**89.3(1)**	**C2–Te1–Cl2**	**86.5(1)**
Te1–Cl1	**2.4942(9)**	**C1–Te1–Cl2**	**86.6(1)**	**Cl2–Te1–Cl2**	**172.33(3)**
Te1–Cl2	**2.5446(9)**				

6.2.4 Magnetic moment and UV-visible spectra

The magnetic moment of $MoCl_4$ complexes ($[MoCl_4(SMe_2)_2]$, $[MoCl_4(SeMe_2)_2]$, $[MoCl_4\{MeS(CH_2)_2SMe\}]$, $[MoCl_4\{^iPrS(CH_2)_2S^iPr\}]$ and $[MoCl_4\{MeS(CH_2)_3SMe\}]$) with both mono- and bidentate ligands are lower than the spin-only value for two unpaired electrons (found μ_{eff} = 2.1–2.6 B.M.; theory μ_{eff} = 2.83 B.M.). These values do, however, correspond with Mo(IV) coordination complexes already reported.[37, 55-57] The main reason for the discrepancy between the experimental and theoretic value is the presence of spin-orbit coupling for the triplet ground state derived from pseudo-t_{2g}^2 configuration.

Paramagnetic complexes generally do not exhibit NMR resonances due to line broadening, and any observed resonances are often shifted. However, literature reports of the ^{1}H NMR resonances for $[MoCl_4(SEt_2)_2]$ are not too far from expected (δ = -18.5 and +12.9 ppm),[44] which showing the possibility to collect ^{1}H NMR spectrum. $[MoCl_4(SMe_2)_2]$ was selected as model system for ^{1}H NMR spectroscopy due to its solubility and similarity to $[MoCl_4(SEt_2)_2]$ and its minimal proton environments.

The ^{1}H NMR spectrum (CD_2Cl_2, 298 K) of a sample of $[MoCl_4(SMe_2)_2]$, made *via* direct reaction from $MoCl_5$, contains three major resonances at δ = 2.52 (s), 3.14 (s), 4.01 (s), which are assigned to $[Me_2SCH_2SMe]^+$ from the byproduct $[MoCl_5(SMe_2)][Me_2SCH_2SMe]$ mentioned in section 6.2.1 (Figure 6.6). Apart from this impurity, there are two broad resonances at δ = -28.93 and -2.59 ppm, which could be assigned to Mo^{IV} complexes $[MoCl_4(SMe_2)_2]$ and $[MoCl_5(SMe_2)]^-$ (Figure 6.7).

A pure sample of $[MoCl_4(SMe_2)_2]$ was made *via* the substitution of CH_3CN from $[MoCl_4(NCCH_3)_2]$ in order to eliminate the resonance spectroscopic attributed to the Mo(IV) anion. The ^{1}H NMR spectrum of $[MoCl_4(SMe_2)_2]$ shows a single resonance at δ = *ca.* -28.73 ppm (Figure 6.8). Therefore, the signal at δ = -2.59 ppm is attributed to $[MoCl_5(SMe_2)]^-$. The relative difference in chemical shift nature of these complexes is called the 'Knight shift', which is explained in Chapter 1.[58, 59]

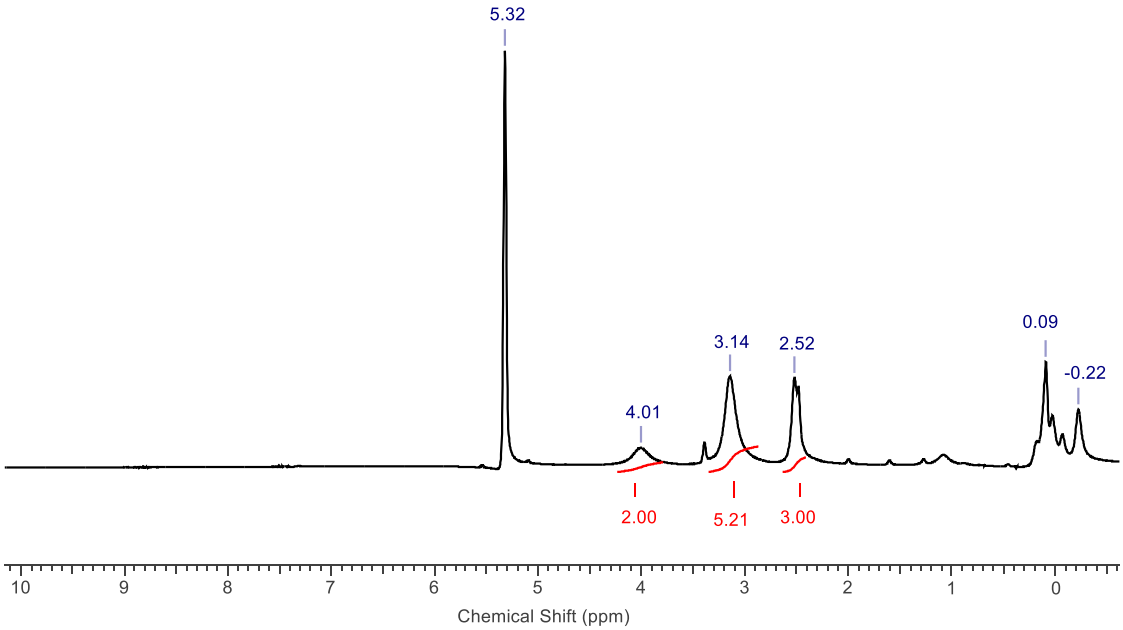

Figure 6.6 ^{1}H NMR (CD_2Cl_2, 298 K) spectrum of [$MoCl_4(SMe_2)_2$] obtained from preparation in CH_2Cl_2 in region 0–10 ppm.

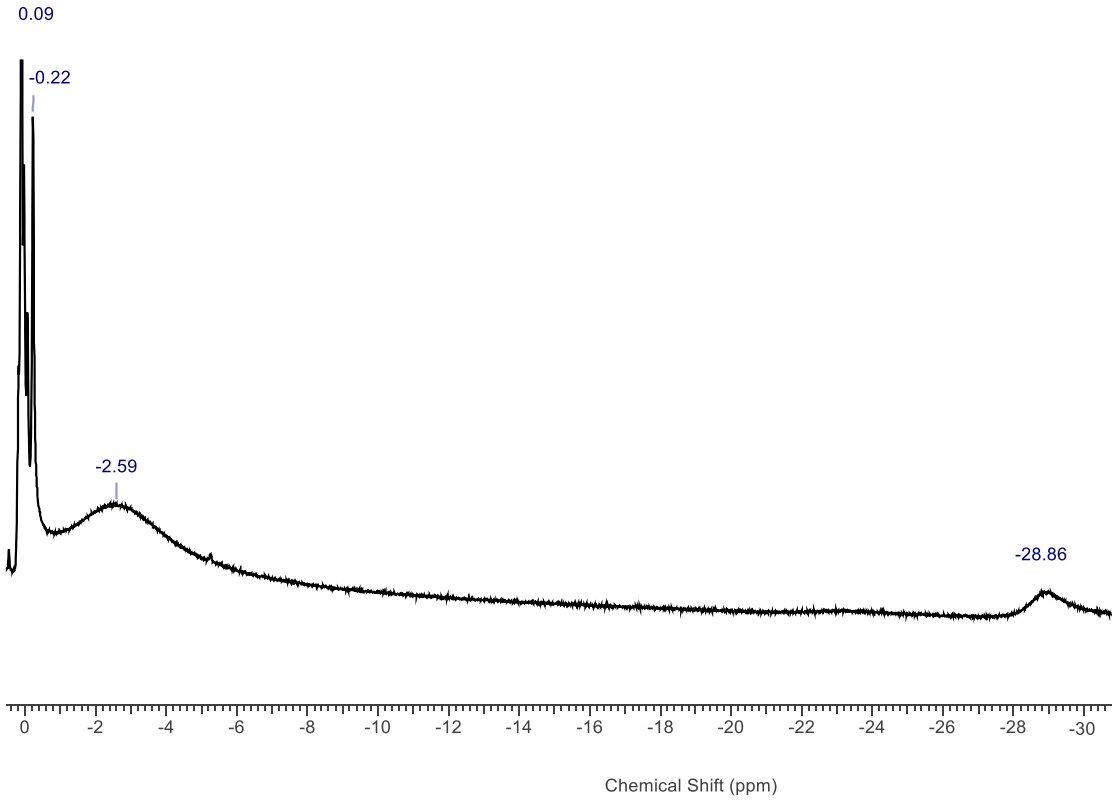

Figure 6.7 ^{1}H NMR (CD_2Cl_2, 298 K) spectrum of [$MoCl_4(SMe_2)_2$] obtained from preparation in CH_2Cl_2 in region -30–10 ppm.

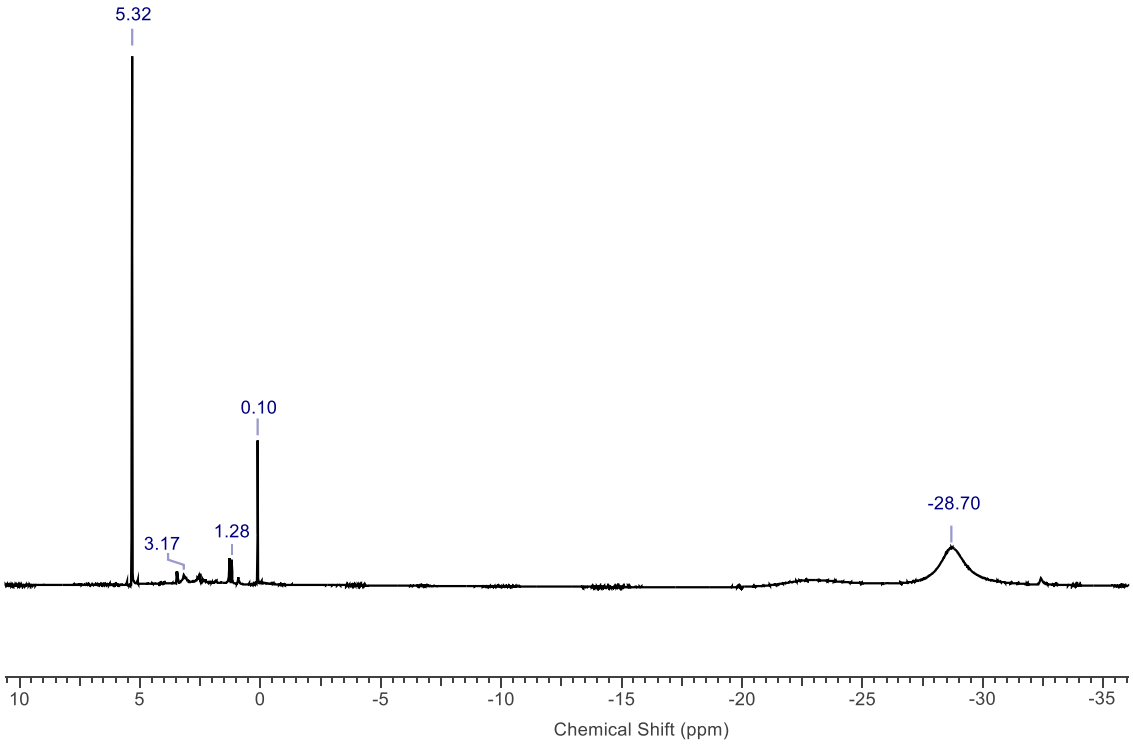

Figure 6.8 ^{1}H NMR (CH_2Cl_2, 298 K) spectrum of clean $[MoCl_4(SMe_2)_2]$ obtained from CH_3CN substitution in region -35 to 10 ppm.

The UV-visible spectra of all $[MoCl_4(chalcogenoether)_n]$ complexes present two strong absorptions in the region of 200–400 nm, which could be assigned to charge transfer from Cl(π) → Mo and S(π)/Se(π) → Mo. These spectra are usually two bands at *ca.* 450–600 nm, which could be assigned as $^{3}T_{1g} \rightarrow {}^{3}T_{1g}(P)$ and $^{3}T_{1g} \rightarrow {}^{3}T_{2g}$ (Figure 6.9–6.10), and match the literature data.[57, 60]

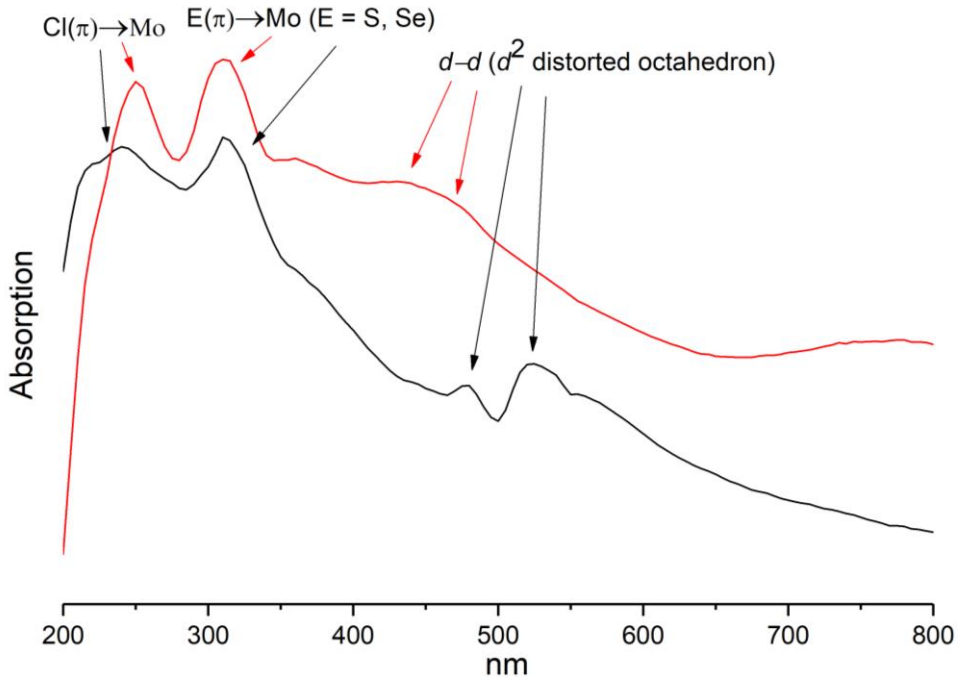

Figure 6.9 UV-visible spectra of $[MoCl_4(S^nBu_2)_2]$ (black) and $[MoCl_4(Se^nBu_2)_2]$ (red) diluted with $BaSO_4$.

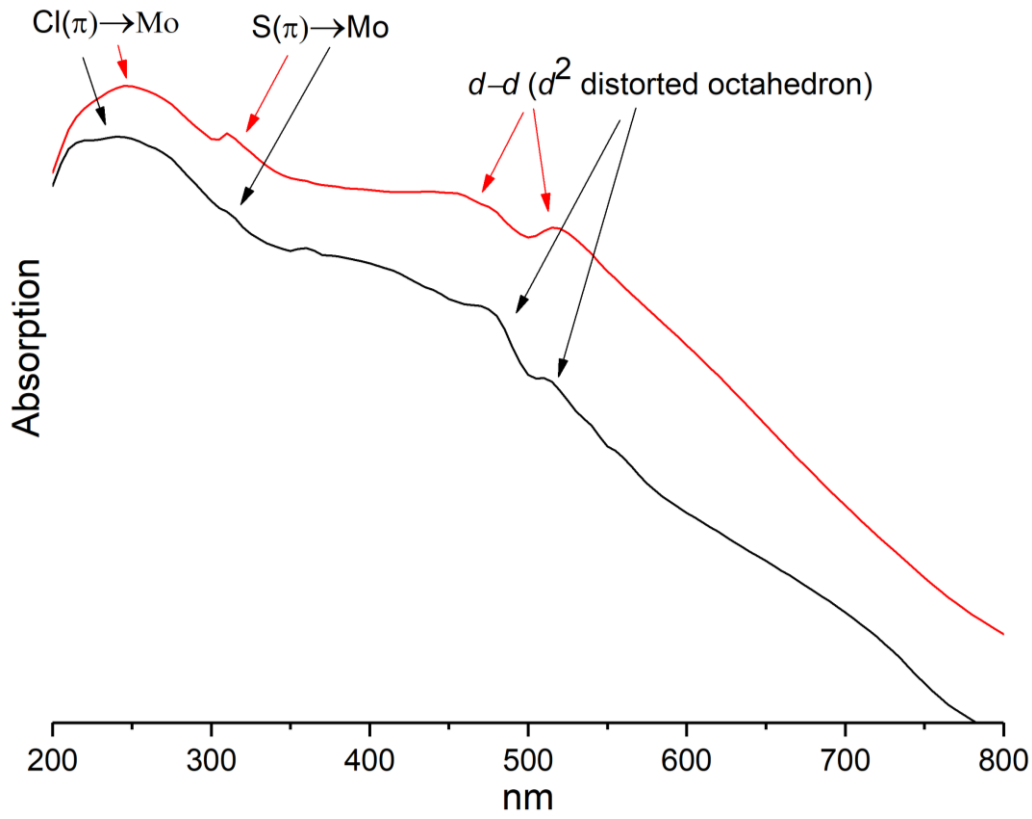

Figure 6.10 UV-visible spectra of solid [$MoCl_4(MeSCH_2CH_2SMe)$] (black) and [$MoCl_4(MeSCH_2CH_2CH_2SMe)$] (red).

6.2.5 Thermogravimetric analysis of potential LPCVD precursors

Thermogravimetric analysis (TGA) of [$MoCl_4(S^nBu_2)_2$] shows mass loss in three steps over the temperature ranges 25–160 ℃, 170–200 ℃ and 210–300 ℃, leaving a residual mass of *ca.* 44.9 % which remains unchanged up to 600 ℃ (Figure 6.11). The percentage weight of the residue is higher than that expected for MoS_2 (30.0 %). It appears that dibutyl sulfide was distilled off upon increasing the temperature leaving $MoCl_4$ only (44.7%). Data for each weight loss step can be found in Table 6.11.

TGA of [$MoCl_4(Se^nBu_2)_2$] shows three step mass loss occurring around 75–125 ℃, 180–200 ℃ and 200–280 ℃ leaving a residual mass of *ca.* 39.4 % which is slowly decreasing up to 600 ℃ (Figure 6.12). This result likely presents a complex decomposition pathway to $MoCl_4$ (38.0 %) as the final residue. Data for each weight loss step can be found in Table 6.11.

The TGA results present the evidence of weak bonding energy in a hard metal–soft donor pair in HSAB theory (Hard and Soft Acids and Bases). TGA experiments were performed under argon flowing atmosphere, which is very different to typical low-pressure chemical vapour deposition. [$MoCl_4(S^nBu_2)_2$] and [$MoCl_4(Se^nBu_2)_2$] have been tested in LPCVD and deposited MoE_2 (E = S, Se) thin film successfully (detail in next section).

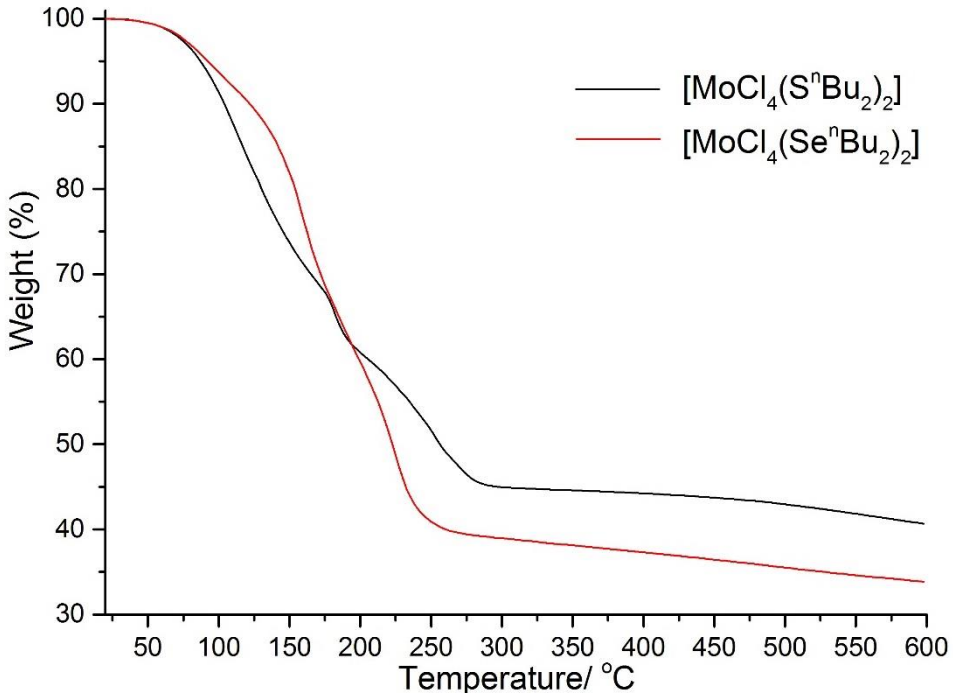

Figure 6.11 TGA profiles of $[MoCl_4(S^nBu_2)_2]$ (black) and $[MoCl_4(Se^nBu_2)_2]$ (red).

Table 6.11 TGA Data for precursors

Complexes	Onset Temperature (℃)	Step End Temperature (℃)	Remaining weight (wt%)
$[MoCl_4(S^nBu_2)_2]$ (Step 1)	*ca.* 25	*ca.* 160	71.1
$[MoCl_4(S^nBu_2)_2]$ (Step 2)	*ca.* 170	*ca.* 200	60.7
$[MoCl_4(S^nBu_2)_2]$ (Step 3)	*ca.* 210	*ca.* 280	44.9
$[MoCl_4(Se^nBu_2)_2]$ (Step 1)	*ca.* 75	*ca.* 125	89.3
$[MoCl_4(Se^nBu_2)_2]$ (Step 2)	*ca.* 160	*ca.* 200	59.6
$[MoCl_4(Se^nBu_2)_2]$ (Step 3)	*ca.* 200	*ca.* 270	38.9

MoS_2 expected weight loss from precursor: 30.0 %.

$MoSe_2$ expected weight loss from precursor: 40.4 %.

6.2.6 LPCVD application

6.2.6.1 CVD application using $[MoCl_4(Se^nBu_2)_2]$

LPCVD from $[MoCl_4(Se^nBu_2)_2]$ using *ca.* 30-70 mg resulted in the deposition of a reflective golden film on tiles positioned in the hotter region of the furnace at 400–550 ℃ (Figure 6.12). Once the deposition temperature is higher than 550 ℃, a MoO_2 thin film was deposited. Those films are air and moisture stable, however, they are easily scratched with a metal spatula. Lattice parameters determined by Le Bail fitting of the grazing incidence XRD pattern are: a = 3.266(1) and c = 13.17(2) Å (R_{wp} = 1.8 %, R_p = 1.3 %), which compare favourably with to the literature values for bulk 2H-$MoSe_2$ (a = 3.290(2), c = 12.930(6) Å).[61]

Parkin and co-workers have successfully deposited mixed stacking of 2H- and 3R-type $MoSe_2$ films using multi source precursors *via* APCVD.[32] The $MoSe_2$ films obtained using $[MoCl_4(Se^nBu_2)_2]$ in this work are more likely to be 2H-$MoSe_2$ from comparison to both grazing incidence and in-plane XRD patterns and with standard powder X-ray diffraction pattern (Figure 6.12).

A preferred orientation of 0 0 2 is revealed in grazing incidence XRD whereas (Figure 6.12, sharp broad peak at 2θ = *ca.* 13.5°), 1 0 0 and 1 1 0 are the strongest reflections in in-plane XRD (Figure 6.13, 2θ = *ca.* 31° and 56°). The pole figure taken with 2θ = 13.54°, corresponding to the 0 0 2 reflection, exhibits a single sharp peak (FWHM ~ 10°) at the centre of the figure with α = 90° and consistent with <0 0 *l*> crystallite orientation. Pole figure taken with 2θ = 56.10°, corresponding to the 1 1 0, exhibits a ring with α = *ca.* 0 and 180° (Figure 6.13). Pole figure using 1 0 3 reflection (2θ = *ca.* 37.82°) was attempted but was unfortunately featureless, which suggests some stacking faults may be reducing the intensity of the reflection.

The crystallite size from the Williamson-Hall method is 6.6(9) nm, which agrees with the scanning electron microscopy (SEM) images for the thickness of the crystallites. SEM images show that the $MoSe_2$ films have morphology formed of microcrystalline platelets, which are mostly aligned with the ab plane parallel to the substrate, although the absence of significant preferred orientation from the XRD data suggests it is likely that there are different crystal orientations within the film. The crystallite size is *ca.* 10 nm thick with a width of *ca.* 100 nm (Figure 6.14). The SEM image shows those crystallites are oriented approximately orthogonal to platelet growth on the surface. This is different to the observation from grazing incidence and in plane XRD patterns, which suggest the crystallites are parallel to the surface. Comparing both results, it is possible that the bulk of the $MoSe_2$ film has the crystallites lying flat, dominating the diffraction, with a small amount of crystallites grown vertical to the surface.

EDX data measured at an accelerating voltage of 15 kV show significant Si and O peaks from the SiO_2 substrates, indicating that the films are thin. EDX data also shows there is no evidence for any residual Cl in the films (Cl K_α = 2.621 keV).[62] Accurate quantification of the Mo:Se ratio by EDX is

1:2, consistent with the formation of $MoSe_2$ (Figure 6.15). Using a larger amount of precursor (*ca.* 200 mg) resulted in thicker films, but the optical quality of the films decreased. SEM images (Figure A4.6 in Appendix 4) showed that some crystallites continued to grow preferentially and thus the film thickness was less consistent over the area of the film.

The Raman spectrum from the $MoSe_2$ film was collected using 785 nm excitation and shows three peaks at 140, 241 and 290 cm^{-1} due to E_{1g}, A_{1g} and E_{2g} vibration modes of 2H-$MoSe_2$ respectively. There were additional peaks observed at *ca.* 317, 455 and 595 cm^{-1},[7, 11, 32, 63, 64] which can be attributed to contribution from acoustic phonons to the Raman scattering spectrum.[65]

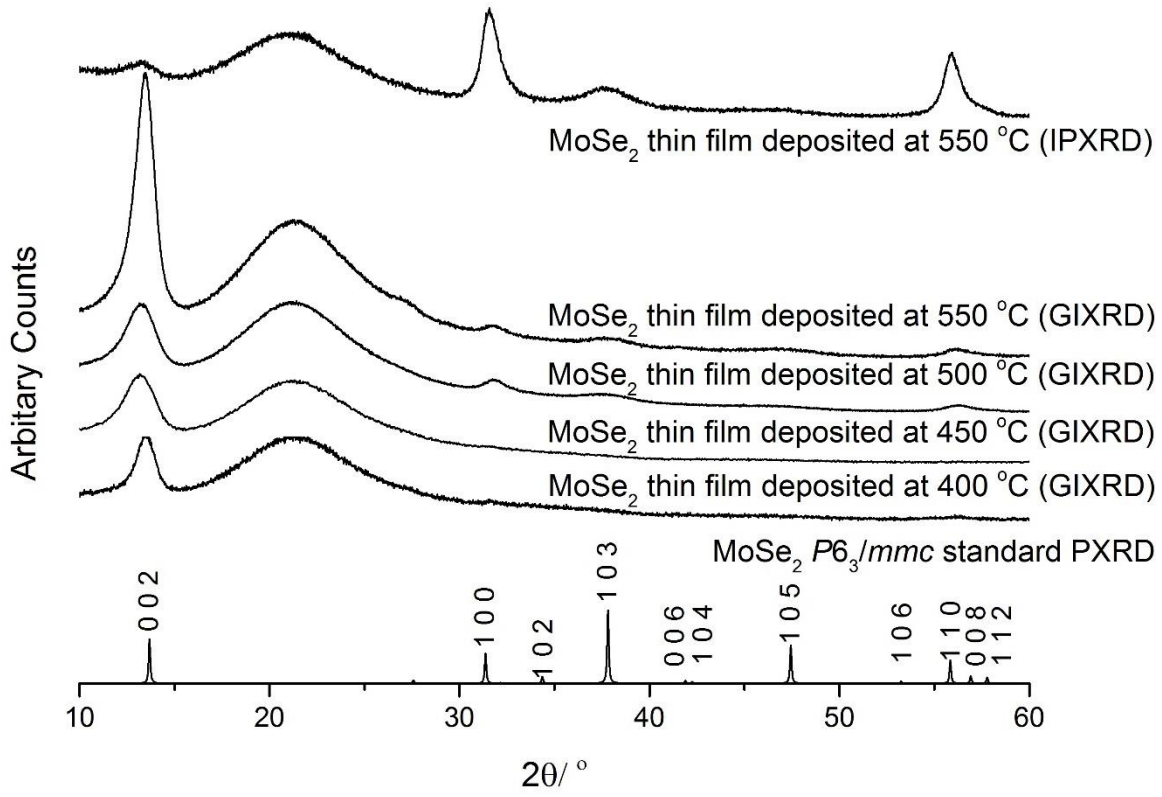

Figure 6.12 Grazing incidence XRD from $MoSe_2$ thin film deposited by LPCVD using $[MoCl_4(^nBu_2Se)_2]$ at 400–550 °C; In-Plane XRD from $MoSe_2$ thin film deposited by LPCVD using $[MoCl_4(^nBu_2Se)_2]$ at 550 °C; stick diagram of the XRD of bulk 2H-$MoSe_2$ ($P6_3/mmc$).[61] The broad feature at $2\theta \sim 22°$ is from the SiO_2 substrate.

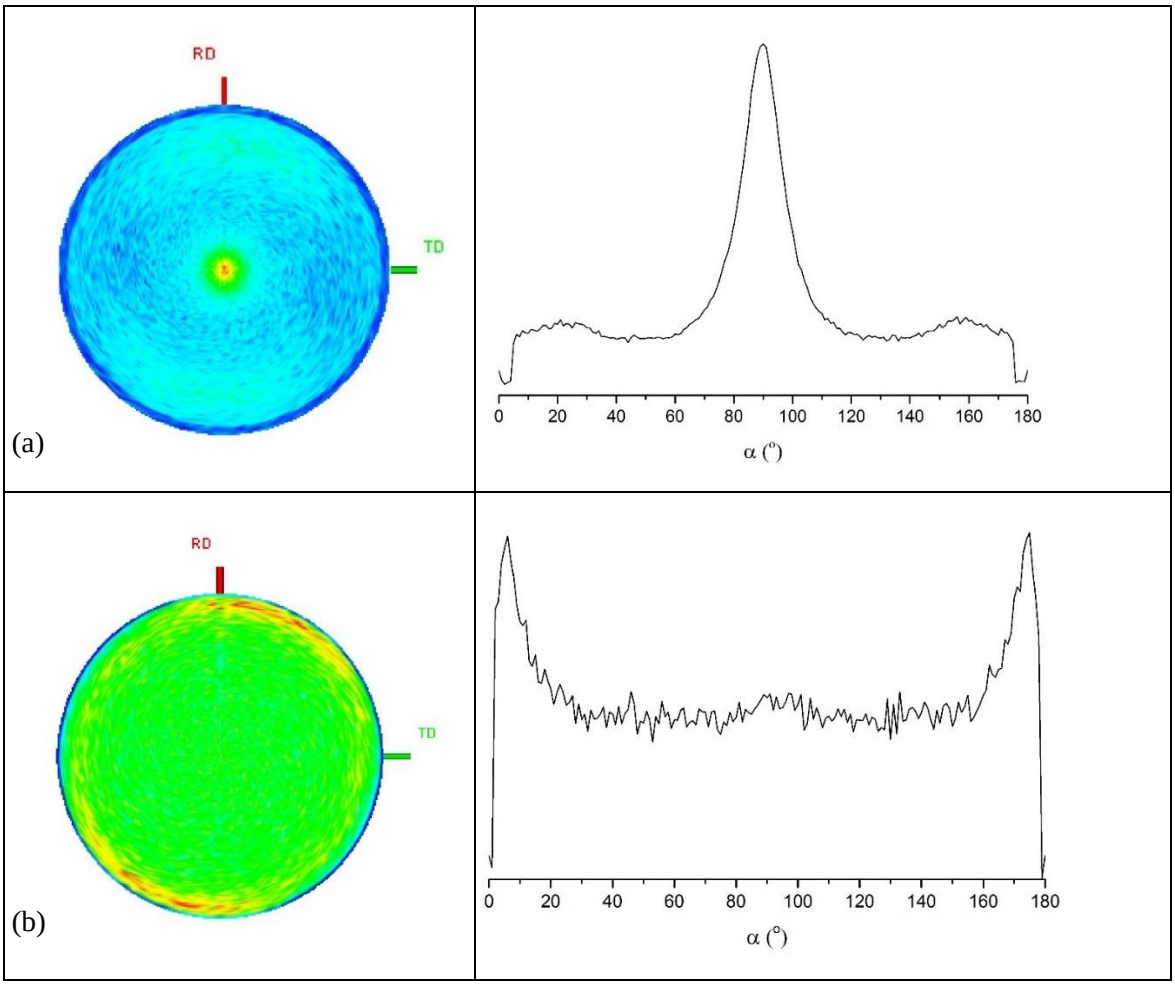

Figure 6.13 (a) Pole Figures with cut line graphs for the 0 0 2 (2θ = 13.45°) and (b) 1 1 0 (2θ = 56.10°) reflection of an array of $MoSe_2$ deposited on a SiO_2 substrate.

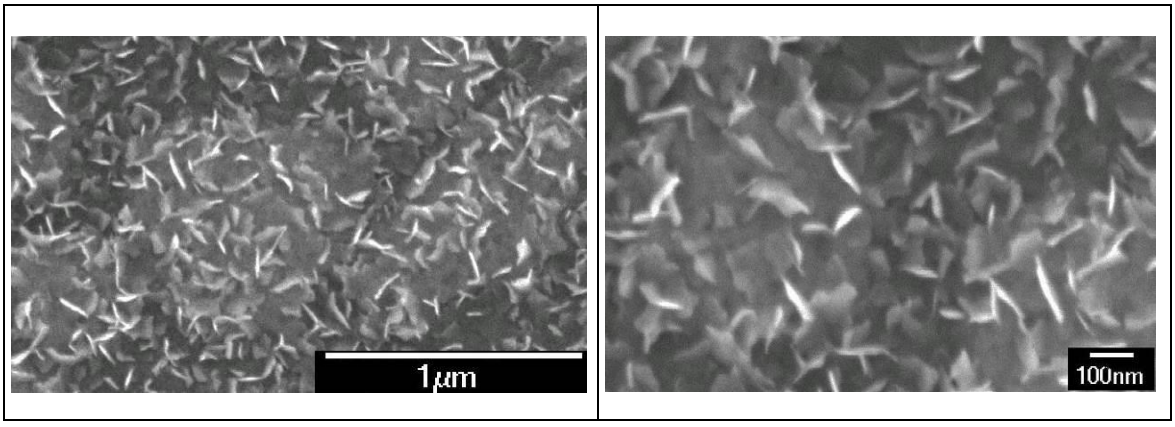

Figure 6.14 SEM images of $MoSe_2$ thin film deposited by LPCVD from $[MoCl_4(Se^nBu_2)_2]$ at 550 °C.

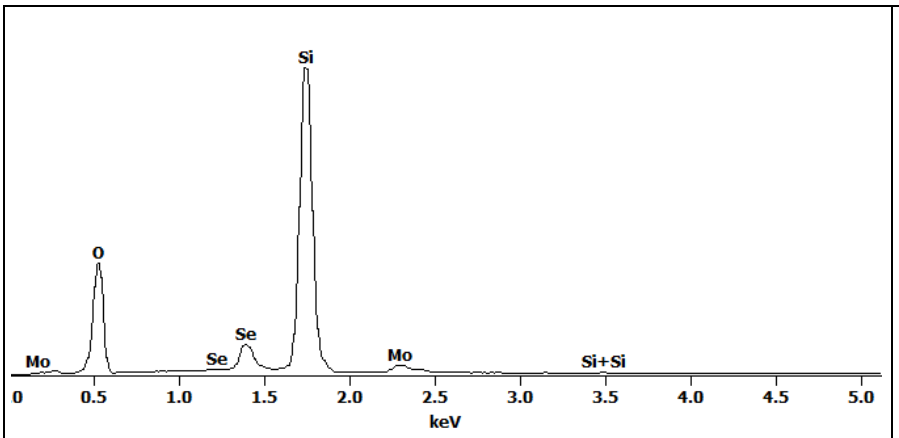

Elements	Atom %
Mo	34.88
Se	65.12

Figure 6.15 EDX result using accelerating voltage 15 kV from $MoSe_2$ thin film deposited by LPCVD from $[MoCl_4(Se^nBu_2)_2]$ at 550 ℃.

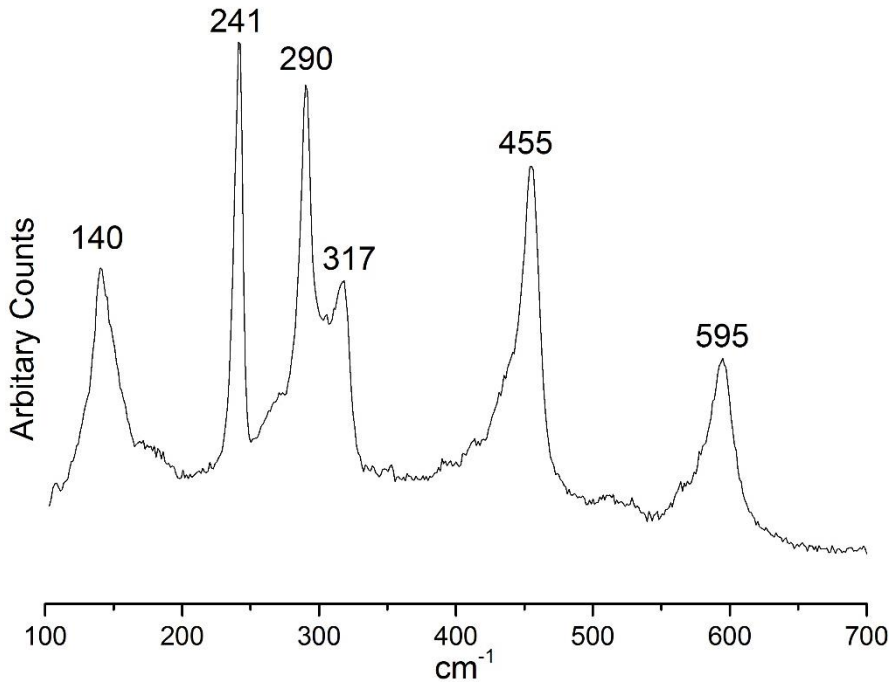

Figure 6.16 Raman spectrum of $MoSe_2$ deposited by LPCVD from $[MoCl_4(Se^nBu_2)_2]$ at 550 ˚C

6.2.6.2 CVD application using $[MoCl_4(S^nBu_2)_2]$

Using a small amount of precursor $[MoCl_4(S^nBu_2)_2]$ (*ca.* 30–70 mg) in LPCVD on SiO_2 substrates at 750 ℃, resulted in yellow films which were too thin to generate any X-ray diffraction using grazing incidence or in plane measurement. The crystallites were too small to produce scanning electronic microscopy (SEM) images and failed to provide energy-dispersive X-ray (EDX) spectra.

Silver reflective films were obtained by using a large amount of precursor (*ca.* 200 mg) in LPCVD at 750 ℃ on SiO_2 substrates. Grazing incidence and in-plane XRD measurements on these silver films show the crystals are really small and likely have has preferred orientation in the 0 0 2 direction (Figure 6.17). The lattice parameters were refined as a = 3.13(5) and c = 13.7(8) Å , although there is

significant uncertainty in these results due to the weak, broad peaks, compared to the literature values for bulk 2H-MoS_2 of a = 3.15(2), c = 12.30(7) Å (Figure 6.17).[66]

SEM images confirm that the crystallites on the MoS_2 film are very small. Unfortunately, due to significant Mo (L_α = 2.293 keV) and S (K_α = 2.307 keV) peak overlap, the Mo: S ratio is difficult to quantify. The EDX spectrum also shows there is no evidence of any residual Cl in the films (Cl K_α = 2.621 keV) (Figure 6.18–6.19).[62] The Raman spectrum from the MoS_2 film was collected using 785 nm excitation, however, weak intensity bands were observed in the spectrum due to the poor signal/noise ratio as the film is very thin. Two weak, broad bands at *ca.* 373 and 406 cm^{-1}, were tentatively assigned as E_{2g} and A_{1g} vibrational modes in 2H-MoS_2.[22, 30, 31, 63] There are two peaks observed at *ca.* 185 and 230 cm^{-1}, which could can be attributed to contribution from acoustic phonons.[67-69] The band at 143 cm^{-1} remains unidentified.

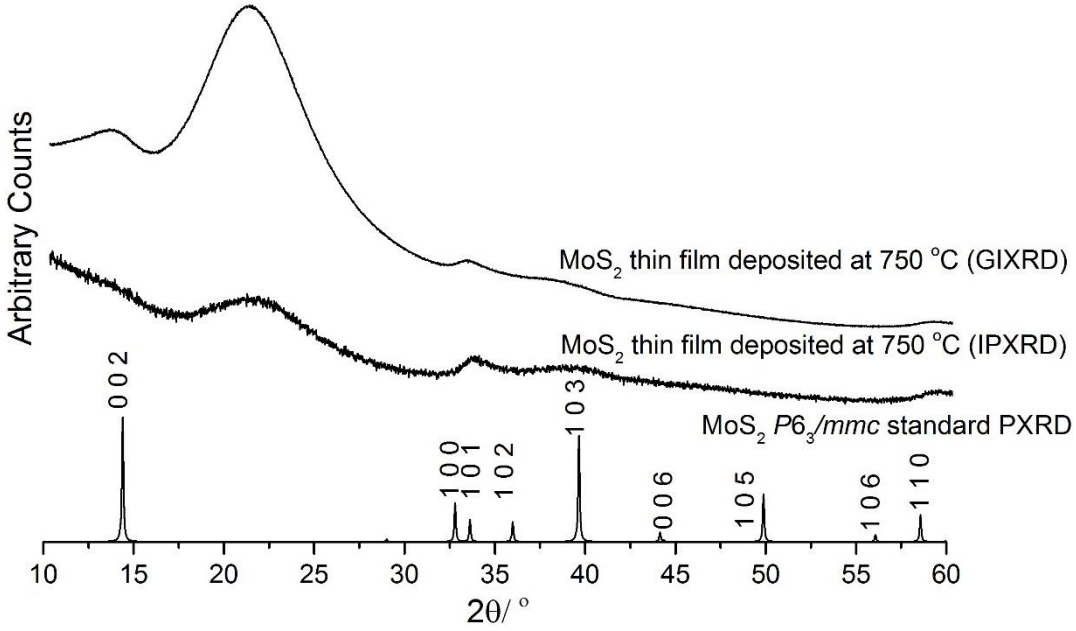

Figure 6.17 Grazing incidence and in-plane XRD from a thin film of MoS_2 deposited by LPCVD using [$MoCl_4(^nBu_2Se)_2$] at 750 °C; stick diagram of the XRD of bulk 2H-MoS_2.[66] The broad feature at 2θ ~ 22° is from the SiO_2 substrate.

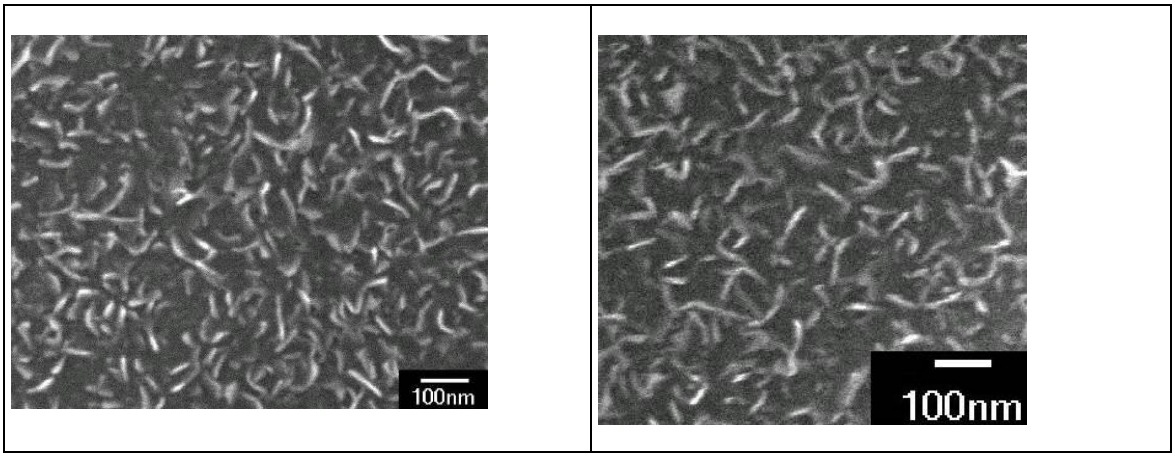

Figure 6.18 SEM images of MoS_2 thin film deposited by LPCVD from [$MoCl_4(S^nBu_2)_2$] at 750 °C.

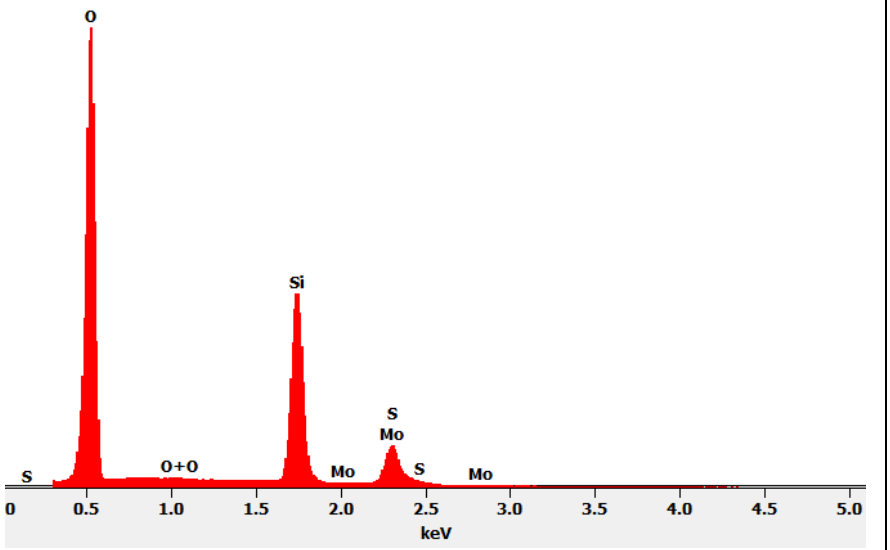

Elements	Atom %
O	46.2
Si	39.8
S	7.6
Mo	6.4

Figure 6.19 EDX result using accelerating voltage 5 kV from MoS_2 thin film deposited by LPCVD from $[MoCl_4(S^nBu_2)_2]$ at 750 ℃.

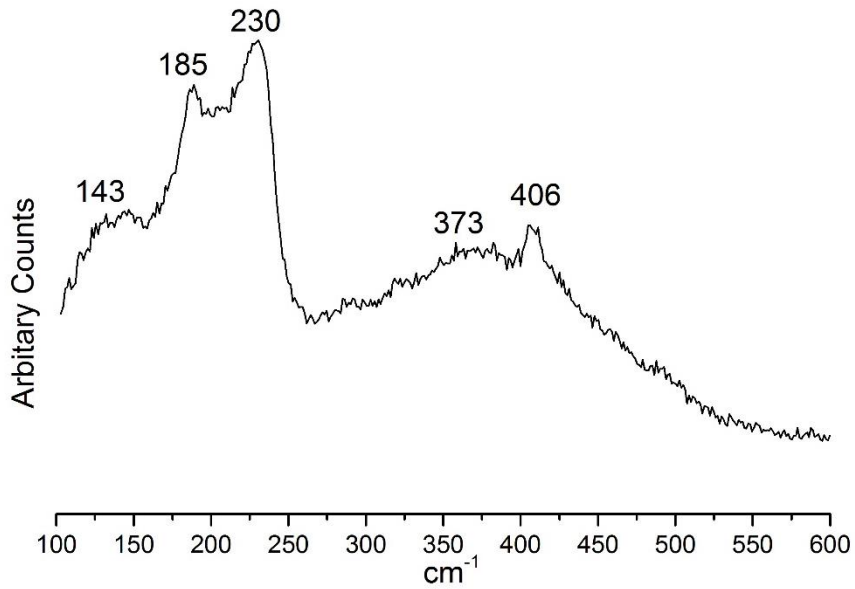

Figure 6.20 Raman spectrum of $MoSe_2$ deposited by LPCVD from $[MoCl_4(S^nBu_2)_2]$ at 750 ℃

6.3 Conclusion

A series of unusual $MoCl_4$ complexes with thio- or selenoether ligands have been synthesised and fully characterised. Compounds $[MoCl_4(ER_2)_2]$ ($ER_2 = SR_2$ or SeR_2) form six-coordinated octahedral complexes with the two chalcogen ligands occupying in *trans* positions. Complexes $[MoCl_4(L–L)]$ (L–L = $MeS(CH_2)_2SMe$, $^{i}PrS(CH_2)_2S^{i}Pr$, $MeS(CH_2)_3SMe$ and $MeSe(CH_2)_3SeMe$) are pseudo octahedral, with the crystal structure for $[MoCl_4(MeS(CH_2)_2SMe)]$ and $[MoCl_4(^{i}PrS(CH_2)_2S^{i}Pr)]$ showing the ligands are orientated in *DL* configuration.

The formation of the byproduct $[MoCl_5(SMe_2)][Me_2SCH_2SMe]$ has been proven *via* its solid state X-ray structure and ^{1}H NMR spectrum. This compound is the result of $MoCl_5$ undergoing self-reduction and reflects the fragile nature of the Mo–Cl bond in $MoCl_5$.

Two LPCVD candidates $[MoCl_4(S^{n}Bu_2)_2]$ and $[MoCl_4(Se^{n}Bu_2)_2]$ have been studied by TGA in order to establish their thermal decomposition route and, unfortunately, the data only show ligand dissociation when temperature is increased under inert atmosphere in ambient pressure, reflecting the weak bond energy of hard metal-soft donor pairs.

The two LPCVD candidates $[MoCl_4(S^{n}Bu_2)_2]$ and $[MoCl_4(Se^{n}Bu_2)_2]$ successfully deposited molybdenum dichalcogenide films onto SiO_2 substrates successfully at a temperature range 400–600 ℃. $[MoCl_4(Se^{n}Bu_2)_2]$ deposited thin 2H-$MoSe_2$ continuous golden films based on grazing incidence X-ray diffraction data. In-plane and pole figure XRD and SEM images show the crystals lie parallel to the substrate and the preferred orientation is in the <0 0 *l*> directions. EDX data agrees with the formula $MoSe_2$ and confirms the lack of CL impurity.

Very thin silver MoS_2 films were obtained *via* LPCVD using a large amount of $[MoCl_4(S^{n}Bu_2)_2]$ at 750 ℃. Grazing incidence XRD shows a very weak diffraction patterns for these thin MoS_2 films. In-plane XRD suggests it is likely to have preferred orientation. SEM images confirm crystallite sizes are tiny. Unfortunately, the EDX spectrum cannot be used to determine the ratio of Mo to S due to the fact that emission energies of both are coincident, however, it does confirm the absence of any Cl impurity into the films.

6.4 Experimental

6.4.1 *trans*-[$MoCl_4(NCCH_3)_2$]

Was made by a modified literature method.[41] $MoCl_5$ (270 mg, 1.0 mmol) was dissolved in CH_3CN (20 mL) with stirring for 30 minutes. to give a dark brown solution. The solvernt was evaporated *in vacuo* and the resulting dark brown solid was washed with *n*-hexane (5 mL), and the solid dried *in vacuo*. Yield: 249 mg, 78 %. Required for $C_4H_6N_2Cl_4Mo$ (319.56 g/mol): C, 15.02; H, 1.89; N, 8.76. Found: C, 14.84; H, 1.81; N, 8.61. IR (Nujol/cm^{-1}): 2314, 2283 (CH_3CN), 335 (Mo–Cl).

6.4.2 *trans*-[$MoCl_4(THT)_2$]

$MoCl_5$ (250 mg, 0.915 mmol) was dissolved in CH_2Cl_2 (10 mL) before the addition of THT (0.26 mL, 2.97 mmol). The resulting orange solution was taken to dryness *in vacuo,* to afford a dark orange solid. Yield: 296 mg, 78 %. Required for $C_8H_{16}Cl_4MoS_2$ (414.0 g/mol): C, 23.20; H, 3.89. Found: C, 23.28; H, 3.73. IR (Nujol/cm^{-1}): 338 (Mo-Cl). UV-vis/cm^{-1}: 22 700, 19 400, 16 600(sh).

6.4.3 *trans*-[$MoCl_4(SMe_2)_2$]

$MoCl_5$ (200 mg, 0.75 mmol) was dissolved in CH_2Cl_2 (15 mL). Anhydrous SMe_2 (1 mL) was then added with stirring for 30 minutes to afford a red-orange solution. The solution was filtered and dried *in vacuo*. *n*-Hexane (10 mL) was added to wash the solid and then removed with a syringe. The dark orange solid was dried *in vacuo*. Yield: 206 mg, 75.8%. Required for $C_4H_{12}Cl_4MoS_2$ (360.02 g/mol): C, 13.27; H, 3.34. Found: C, 13.36; H, 3.48. IR (Nujol/cm^{-1}): 332 (Mo–Cl). ^1H NMR (CD_2Cl_2, 298 K) δ = -28 (Detail in text). UV-vis/cm^{-1}: 22 000, 19 400, 16 800. μ_{eff}: 2.22 B.M. Orange crystals were grown by allowing a CH_2Cl_2 solution to evaporate in a nitrogen atmosphere.

Alternative method:

$MoCl_5$ (150 mg, 0.55 mmol) was dissolved in ca. 10 mL of CH_3CN with stirring to give a dark brown solution. The solution was stirred for an additional 10 minutes, before the solvent was removed to afford a dark brown solid. The solid was suspended in 10 mL CH_2Cl_2 before the addition of Me_2S (3 mL). The solid dissolved immediately to give a red brown solution. The solution was stirred for another 10 minutes before the solvent was removed to yield a dark orange solid. This orange solid was dissolved in CH_2Cl_2 (3 mL) before the addition of *n*-hexane (3 mL). The orange solution was filtered away from the white precipitate and taken to dryness by slow evaporation in nitrogen atmosphere to grow dark orange crystals. The product was spectroscopically identical with the product made from $MoCl_5$ in CH_2Cl_2.

Crystals of [$MoCl_5(SMe_2)$][Me_2SCH_2SMe]

The orange red crystals were obtained by crystallisation from a CH_2Cl_2 solution of [$MoCl_4(SMe_2)_2$] *via* direct reaction of $MoCl_5$ with SMe_2 in CH_2Cl_2. ^1H NMR (CD_2Cl_2, 298 K) δ = 2.52 (s, [3H], SMe), 3.14 (s, [6H], Me_2S^+), 4.01 (s, [2H], CH_2), 2.6 ([$MoCl_5(SMe_2)$], detail in text).

6.4.4 *trans*-[$MoCl_4(S^nBu_2)_2$]

$MoCl_5$ (205 mg, 0.75 mmol) was dissolved in CH_2Cl_2 (10 mL) before a solution of S^nBu_2 (274 mg., 2.5 mmol) and CH_2Cl_2 (ca. 3 mL) was then added with stirring for 30 minutes to afford a red-orange solution. The solution was filtered and evaporated to dryness *in vacuo*. The resulting solid was washed with *n*-hexane (10 mL), and the dark orange liquid dried *in vacuo*. Yield: 250 mg, 62 %. Required for $C_{16}H_{36}Cl_4MoS_2$ (526.31 g/mol): C, 36.51; H, 6.13. Found: C, 36.15; H, 6.72. IR (Nujol/cm^{-1}): 334, 305sh (Mo–Cl). UV-vis/cm^{-1}: 41 700, 20 900, 19 100, 18 500.

Alternative method:

$MoCl_5$ (136 mg, 0.5 mmol) was dissolved in CH_3CN (10 mL) with stirring for 30 minutes to give a dark brown solution. The solution was taken to dryness *in vacuo* and left a dark brown solid. CH_2Cl_2 (15 mL) was added, followed by a solution of S^nBu_2 (0.4 mL, 2.0 mmol) in CH_2Cl_2 (2 mL). The dark solution changed to red-orange immediately. The solution was then stirred for 15 minutes then evaporated *in vacuo* to afford a dark orange oil. The product was spectroscopically identical with the product made from $MoCl_5$ in CH_2Cl_2.

6.4.5 *trans*-[$MoCl_4(SeMe_2)_2$]

$MoCl_5$ (200 mg, 0.75 mmol) was dissolved in CH_2Cl_2 (15 mL). $SeMe_2$ (196 mg. 1.96 mmol) was then added with stirring for 30 minutes and produced an orange-red solution. The solution was filtered and taken to dryness *in vacuo*. The solid was washed with *n*-hexane (10 mL) with the washings removed with a syringe, and the residual dark orange powder dried *in vacuo*. Yield: 283 mg, 77 %. Required for $C_4H_{12}Cl_4MoSe_2$ (455.81 g/mol): C, 10.54; H, 2.65. Found: C, 10.69; H, 2.43. IR (Nujol/cm^{-1}): 306 (Mo–Cl). UV-vis/cm^{-1}: 37 000, 33 300, 26 800, 21 800, 19 000. μ_{eff}: 2.59 B.M.

Alternative method:

[$MoCl_4(CH_3CN)_2$] (100 mg, 0.31 mmol) was dissolved in 10 mL CH_2Cl_2 with stirring. A solution of $SeMe_2$ (73 mg, 0.65 mmol) and CH_2Cl_2 (5 mL) was then added and the solution stirred for 1 hour resulting in a red-orange solution. Evaporation *in vacuo* afforded dark orange powder. Yield: 99 mg, 70 %. Required for $C_4H_{12}Cl_4MoSe_2$ (455.81 g/mol): C, 10.54; H, 2.65. Found: C, 10.61; H, 2.54. The product was spectroscopically identical with *trans*-[$MoCl_4(SeMe_2)_2$] made from $MoCl_5$ in CH_2Cl_2.

6.4.6 *trans*-[$MoCl_4(Se^nBu_2)_2$]

$MoCl_5$ (136 mg, 0.5 mmol) was dissolved in CH_3CN (15 mL) with stirring for 30 minutes to give a dark brown solution. The solution was taken to dryness *in vacuo* to leave a dark brown solid. CH_2Cl_2 (25 mL) was added, followed by a solution of Se^nBu_2 (193 mg, 1.0 mmol) in CH_2Cl_2 (2 mL), the dark solution changed immediately to red-orange. The solution was then stirred for 15 minutes then evaporated *in vacuo* to afford a dark red-orange oil. Yield: 292 mg, 94 %. Required for $C_{16}H_{36}Cl_4MoSe_2$ (624.13 g/mol): C, 30.79; H, 5.81. Found: C, 30.23; H, 6.00. IR (Nujol/cm^{-1}): 342s, 305sh (Mo–Cl). UV-vis/cm^{-1}: 40 000, 32 000, 28 000, 22 900, 21 000.

6.4.7 [$MoCl_4\{MeS(CH_2)_2SMe\}$]

$MoCl_5$ (205 mg, 0.75 mmol) was dissolved in CH_2Cl_2 (10 mL). A solution of $MeS(CH_2)_2SMe$ (92 mg, 0.75 mmol) in CH_2Cl_2 (ca. 3 mL) was added and the mixture stirred overnight. More CH_2Cl_2 (10 mL) was added and the orange solution was filtered away from the brown precipitate. The filtrated was evaporated to dryness *in vacuo*. *n*-Hexane (10 mL) was added to wash the solid and was subsequently removed by a syringe. The solid was dried *in vacuo* to afford a dark orange solid. Yield 157 mg, 58 %. Required for $C_4H_{10}Cl_4MoS_2$ (360.00 g/mol): C, 13.35; H, 2.80. Found: C, 14.76; H, 2.84. IR (Nujol/cm^{-1}): 356, 319, 293 (Mo–Cl). UV-vis/cm^{-1}: 41 500, 27 300, 21 000, 19 600. μ_{eff}: 2.66 B.M.

Orange crystals grew on allowing a CH_2Cl_2 solution to evaporate in a nitrogen atmosphere.

Alternative method:

$MoCl_5$ (136 mg, 0.5 mmol) was dissolved in CH_3CN (10 mL) with stirring for 10 minutes to give a dark brown solution. The solution was taken to dryness *in vacuo* and left a dark brown solid. CH_2Cl_2 (10 mL) was added, followed by a solution of $MeS(CH_2)_2SMe$ (180 mg, 1.5 mmol) in CH_2Cl_2 (2 mL). The dark solution immediately changed to bright orange-green with a brown precipitate. Additional CH_2Cl_2 (10 mL x 3) was added but the brown solid not dissolve. The solution was filtered away from the brown solid and the brown residue was pumped to dryness and washed with Et_2O (5 mL), then CH_2Cl_2 (5 mL). The final residue was dried *in vacuo* to afford a brown solid. Yield: 60 mg, 33 %. Required for $C_4H_{10}Cl_4MoS_2$ (360.00 g/mol): C, 13.35; H, 2.80. Found: C, 14.38; H, 3.02 (sample containing *ca.* 10 % Et_2O from wash solvent and identified *via* ^1H NMR spectroscopy).

6.4.8 [$MoCl_4\{^iPrS(CH_2)_2S^iPr\}$]

$MoCl_5$ (136 mg, 0.5 mmol) was dissolved in CH_3CN (10 mL) forming a dark brown solution. The solution was stirring for 10 minutes and then evaporated *in vacuo*, affording a dark brown solid. The solid was dissolved in CH_2Cl_2 (15 mL) and a solution of $^iPrS(CH_2)_2S^iPr$ (133 mg, 0.75 mmol) in CH_2Cl_2 (2 mL) was added. The colour changed to orange and solid formed immediately. The solution

was stirred for 30 minutes and then evaporated *in vacuo*. The solid was washed with *n*-hexane (5 mL), the *n*-hexane removed via a syringe, and the solid was dried *in vacuo* to yield on orange powder. Yield: 160 mg, 77 %. Required for $C_8H_{18}Cl_4MoS_2$ (416.11 g/mol): C, 23.09; H, 4.36. Found: C, 24.33; H, 4.49. IR (Nujol/cm^{-1}): 371sh, 350, 309 (Mo–Cl). UV-vis/cm^{-1}: 41 300, 26 800, 25 000, 21 000, 18 700. μ_{eff}: 2.18 B.M. Orange red crystals were grown by allowing a CH_2Cl_2 solution to evaporate under a nitrogen atmosphere.

6.4.9 [$MoCl_4${$MeS(CH_2)_3SMe$}]

$MoCl_5$ (205 mg, 0.75 mmol) was suspended in CH_2Cl_2 (20 mL) and a solution of $MeS(CH_2)_3SMe$ (109 mg, 0.8 mmol) in CH_2Cl_2 (ca. 3 mL) was added, and stirred overnight to give an orange solution and some orange solid. The solution was removed by a syringe, and the solid washed with *n*-hexane (10 mL). The solid was subsequently dried *in vacuo*. Yield: 83 mg, 30 %. Required for $C_5H_{12}Cl_4MoS_2$ (374.03 g/mol): C, 16.06; H, 3.23. Found: C, 16.22; H, 3.35. IR (Nujol/cm^{-1}): 362, 342, 327 (Mo-Cl). UV-vis/cm^{-1}: 40 500, 22 070, 19 500. μ_{eff}: 2.21 B.M. Orange crystals were grown by allowing a CH_2Cl_2 solution to evaporate under a nitrogen atmosphere.

6.4.10 [$MoCl_4${$MeSe(CH_2)_3SeMe$}]

This complexes was made as described for [$MoCl_4(^iPrS(CH_2)_2S^iPr)$] and obtained as a light orange powder. Yield: 59%. Required for $C_5H_{12}Cl_4MoSe_2$ (467.82 g/mol): C, 12.84; H, 2.59. Found: C, 13.01; H, 2.57. IR (Nujol/cm^{-1}): 332, 308 (Mo-Cl). UV/vis (diffuse reflectance)/cm^{-1}: 41 100, 26 800, 21 000, 18 700.

LPCVD experiments

6.4.11 Precursor [$MoCl_4(S^nBu_2)_2$]

The precursor (42 mg) was loaded with CH_2Cl_2 (1 mL) in a glovebox. Silica substrates were loaded after the precursor was loaded and placed end-to-end. The tube was placed in a furnace and then linked to a vacuum pump (0.01 mmHg). The temperature in the furnace was increased to 750 ℃ and left for 10 minutes to allow the temperature to stabilise. The precursor end was moved into the furnace gradually until at the edge of the furnace. An orange film grew through the open end of the tube. After 30 minutes, the furnace was cooled to ambient temperature and the substrates were unload under ambient condition. Pale yellow films were observed on the substrates. The resulting films are too thin to characterise using grazing incidence XRD, in-plane XRD and SEM/EDX techniques.

The above technique was repeated with a large amount of precursor (193 mg) leading to the same observations during the LPCVD experiment. The substrates were unloaded under ambient condition and silver films were observed on the first two substrates, which corresponds to the temperature 735

℃ *via* temperature profiles data. The silver films are identical using grazing incidence and in-plane XRD and SEM/EDX spectroscopy. For further detail, please see Section 6.2.6.2.

6.4.12 Precursor [$MoCl_4(Se^nBu_2)_2$]

The precursor (*ca.* 50 mg) was loaded with CH_2Cl_2 (1 mL) in a glovebox. Silica substrates were loaded after the precursor was loaded and placed end-to-end. The tube was placed in a furnace and then linked to a vacuum pump (0.01 mmHg). The temperature in the furnace was increased to 400, 450, 500 and 500 ℃ (four LPCVD experiments) and left for 10 minutes to allow the temperature to stabilise stable. The precursor end was moved into the furnace gradually until the edge of the furnace. A red film grown through the open end of the tube. After 30 minutes, the furnace was cooled to ambient temperature and the substrates were unload in ambient condition. In all experiments, golden/brown films were observed on the substrates. Temperature profiled for the best $MoSe_2$ thin film position is 535 ℃ with the furnace monitor displayed 550 ℃.

The above technique was repeated with a large amount of precursor (200 mg) leading to the same observations during the LPCVD experiment. The substrates were unloaded under ambient conditions and golden films were observed on the first two substrate tiles. The golden films were thicker than the $MoSe_2$ films obtained using less precursor (as described above), they show higher resolution SEM images, but lower quality XRD data. For further discussion, please see Section 6.2.6.1.

6.5 References

1. H. Zeng, J. Dai, W. Yao, D. Xiao and X. Cui, *Nat. Nanotechnol.*, 2012, **7**, 490.
2. Q. Xiang, J. Yu and M. Jaroniec, *J. Am. Chem. Soc.*, 2012, **134**, 6575.
3. I. Roger, M. A. Shipman and M. D. Symes, *Nature Reviews Chemistry*, 2017, **1**, 0003.
4. J. Pu, Y. Yomogida, K.-K. Liu, L.-J. Li, Y. Iwasa and T. Takenobu, *Nano. Lett.*, 2012, **12**, 4013.
5. K. Lee, R. Gatensby, N. McEvoy, T. Hallam and G. S. Duesberg, *Adv. Mater.*, 2013, **25**, 6699.
6. G. Zhang and Y.-W. Zhang, *J. Mater. Chem. C*, 2017, **5**, 7684.
7. Y.-H. Chang, W. Zhang, Y. Zhu, Y. Han, J. Pu, J.-K. Chang, W.-T. Hsu, J.-K. Huang, C.-L. Hsu, M.-H. Chiu, T. Takenobu, H. Li, C.-I. Wu, W.-H. Chang, A. T. S. Wee and L.-J. Li, *ACS Nano*, 2014, **8**, 8582.
8. X. Lu, M. I. Utama, J. Lin, X. Gong, J. Zhang, Y. Zhao, S. T. Pantelides, J. Wang, Z. Dong, Z. Liu, W. Zhou and Q. Xiong, *Nano Lett.*, 2014, **14**, 2419.
9. X. Wang, Y. Gong, G. Shi, W. L. Chow, K. Keyshar, G. Ye, R. Vajtai, J. Lou, Z. Liu, E. Ringe, B. K. Tay and P. M. Ajayan, *ACS Nano*, 2014, **8**, 5125.
10. J. Krustok, T. Raadik, R. Jaaniso, V. Kiisk, I. Sildos, M. Marandi, H. P. Komsa, B. Li, X. Zhang, Y. Gong and P. M. Ajayan, *Appl. Phys. Lett.*, 2016, **109**, 253106.
11. A. Bachmatiuk, R. F. Abelin, H. T. Quang, B. Trzebicka, J. Eckert and M. H. Rummeli, *Nanotechnology*, 2014, **25**, 365603.
12. C. Jung, S. M. Kim, H. Moon, G. Han, J. Kwon, Y. K. Hong, I. Omkaram, Y. Yoon, S. Kim and J. Park, *Sci. Rep.*, 2015, **5**, 15313.
13. J. C. Shaw, H. Zhou, Y. Chen, N. O. Weiss, Y. Liu, Y. Huang and X. Duan, *Nano Research*, 2015, **7**, 511.
14. W. Zhang, X. Li, T. Jiang, J. Song, Y. Lin, L. Zhu and X. Xu, *Nanoscale*, 2015, **7**, 13554.
15. A. A. Mitioglu, K. Galkowski, A. Surrente, L. Klopotowski, D. Dumcenco, A. Kis, D. K. Maude and P. Plochocka, *Phys. Rev. B*, 2016, **93**, 165412.
16. M. O'Brien, N. McEvoy, D. Hanlon, T. Hallam, J. N. Coleman and G. S. Duesberg, *Sci. Rep.*, 2016, **6**, 19476.
17. A. S. Pawbake, M. S. Pawar, S. R. Jadkar and D. J. Late, *Nanoscale*, 2016, **8**, 3008.
18. B. B. Wang, K. Ostrikov, T. van der Laan, K. Zheng, R. Shao, M. K. Zhu and S. S. Zou, *RSC Adv.*, 2016, **6**, 37236.
19. J. Chen, X. Zhao, S. J. Tan, H. Xu, B. Wu, B. Liu, D. Fu, W. Fu, D. Geng, Y. Liu, W. Liu, W. Tang, L. Li, W. Zhou, T. C. Sum and K. P. Loh, *J. Am. Chem. Soc.*, 2017, **139**, 1073.
20. S. Umrao, J. Jeon, S. M. Jeon, Y. J. Choi and S. Lee, *Nanoscale*, 2017, **9**, 594.
21. B. B. Wang, K. Zheng, X. X. Zhong, D. Gao and B. Gao, *J. Alloys Compd.*, 2017, **695**, 27.
22. W. Park, J. Baik, T. Y. Kim, K. Cho, W. K. Hong, H. J. Shin and T. Lee, *ACS Nano*, 2014, **8**, 4691.

23. Y. H. Lee, X. Q. Zhang, W. Zhang, M. T. Chang, C. T. Lin, K. D. Chang, Y. C. Yu, J. T. Wang, C. S. Chang, L. J. Li and T. W. Lin, *Adv. Mater.*, 2012, **24**, 2320.

24. A. M. van der Zande, P. Y. Huang, D. A. Chenet, T. C. Berkelbach, Y. You, G.-H. Lee, T. F. Heinz, D. R. Reichman, D. A. Muller and J. C. Hone, *Nat. Mater.*, 2013, **12**, 554.

25. H. Schmidt, S. Wang, L. Chu, M. Toh, R. Kumar, W. Zhao, A. H. Neto, J. Martin, S. Adam, B. Ozyilmaz and G. Eda, *Nano Lett.*, 2014, **14**, 1909.

26. J. Wu, H. Schmidt, K. K. Amara, X. Xu, G. Eda and B. Ozyilmaz, *Nano Lett.*, 2014, **14**, 2730.

27. A. Zafar, H. Nan, Z. Zafar, Z. Wu, J. Jiang, Y. You and Z. Ni, *Nano Research*, 2016, **10**, 1608.

28. S. Hao, B. C. Yang and Y. L. Gao, *Appl. Phys. Lett.*, 2017, **110**, 153105.

29. M. Chhowalla, H. S. Shin, G. Eda, L. J. Li, K. P. Loh and H. Zhang, *Nat. Chem.*, 2013, **5**, 263.

30. K. K. Liu, W. Zhang, Y. H. Lee, Y. C. Lin, M. T. Chang, C. Y. Su, C. S. Chang, H. Li, Y. Shi, H. Zhang, C. S. Lai and L. J. Li, *Nano Lett.*, 2012, **12**, 1538.

31. Y. Shi, W. Zhou, A. Y. Lu, W. Fang, Y. H. Lee, A. L. Hsu, S. M. Kim, K. K. Kim, H. Y. Yang, L. J. Li, J. C. Idrobo and J. Kong, *Nano Lett.*, 2012, **12**, 2784.

32. N. D. Boscher, C. J. Carmalt, R. G. Palgrave, J. J. Gil-Tomas and I. P. Parkin, *Chem. Vap. Dep.*, 2006, **12**, 692.

33. J. S. Rhyee, J. Kwon, P. Dak, J. H. Kim, S. M. Kim, J. Park, Y. K. Hong, W. G. Song, I. Omkaram, M. A. Alam and S. Kim, *Adv. Mater.*, 2016, **28**, 2316.

34. Y.-P. Chang, W. Levason and G. Reid, *Dalton Trans.*, 2016, **45**, 18393.

35. C. G. Young, *Comprehensive Coordination Chemistry II*, ed. J. A. McCleverty and T. J. Meyer, Elsevier, Oxford, 2004, **4**, 415.

36. L. Favero, F. Marchetti, G. Pampaloni and S. Zacchini, *Dalton Trans.*, 2014, **43**, 495.

37. E. Ferretti, M. Hayatifar, F. Marchetti, G. Pampaloni and S. Zacchini, *Polyhedron*, 2015, **100**, 400.

38. M. Hayatifar, F. Marchetti, G. Pampaloni, C. Pinzino and S. Zacchini, *Polyhedron*, 2013, **61**, 188.

39. F. Marchetti, G. Pampaloni and S. Zacchini, *Dalton Trans.*, 2013, **42**, 2477.

40. M. Bortoluzzi, E. Ferretti, M. Hayatifar, F. Marchetti, G. Pampaloni and S. Zacchini, *Eur. J. Inorg. Chem.*, 2016, 3838.

41. J. R. Dilworth and R. L. Richards, *Inorg. Synth.*, 1990, **28**, 33.

42. E. L. McCann III and T. M. Brown, *Inorg. Synth.*, 1970, **12**, 181.

43. K. J. Moynihan, X. Gao, P. M. Boorman, J. F. Fait, G. K. W. Freeman, P. Thornton and D. J. Ironmonger, *Inorg. Chem.*, 1990, **29**, 1648.

44. P. Dierkes, G. Frenzen, S. Wocadlo, W. Massa, S. Berger, J. Pebler and K. Dehnicke, *Z. Naturforsch., B: Chem. Sci.*, 1995, **50**, 159.

45. M. W. Anker, J. Chatt, G. J. Leigh and A. G. Wedd, *J. Chem. Soc., Dalton Trans.*, 1975, **23**, 2639.

46. S. A. Bartlett, P. P. Wells, M. Nachtegaal, A. J. Dent, G. Cibin, G. Reid, J. Evans and M. Tromp, *J. Catal.*, 2011, **284**, 247.

47. D. Sellmann and L. Zapf, *J. Organomet. Chem.*, 1985, **289**, 57.

48. G. H. Robinson and S. A. Sangokara, *J. Am. Chem. Soc.*, 1988, **110**, 1494.

49. G. H. Robinson, H. Zhang and J. L. Atwood, *Organometallics*, 1987, **6**, 887.

50. H. Bock and U. Lechner-Knoblauch, *J. Organomet. Chem.*, 1985, **294**, 295.

51. K. George, M. Jura, W. Levason, M. E. Light and G. Reid, *Dalton Trans.*, 2014, **43**, 3637.

52. R. F. Ziolo and J. M. Troup, *J. Am. Chem. Soc.*, 1983, **105**, 229.

53. G. D. Christofferson, R. A. Sparks and J. D. McCullough, *Acta Cryst.*, 1958, **11**, 782.

54. A. L. Hector, A. Jolleys, W. Levason and G. Reid, *Dalton Trans.*, 2012, **41**, 10989.

55. F. Stoffelbach, D. Saurenz and R. Poli, *Eur. J. Inorg. Chem.*, 2001, 2699.

56. B. N. Figgis and J. Lewis, *Prog. Inorg. Chem.*, 1964, **6**, 37.

57. W. M. Carmichael, D. A. Edwards and R. A. Walton, *J. Chem. Soc. (A)*, 1966, **1**, 97.

58. W. D. Knight, *Phys. Rev.*, 1949, **76**, 1259.

59. K. E. Schwarzhans, *Angew. Chem. Int. Ed.*, 1970, **9**, 946.

60. A. B. P. Lever, *Inorganic Electronic Spectroscopy*, Elsevier, New York, 1984.

61. B. L. Evans and R. A. Hazelwood, *Physica Status Solidi (A)*, 1971, **4**, 181.

62. A. C. Thompson and D. Vaughan, *X-ray data booklet*, Lawrence Berkeley National Laboratory, University of California, Berkeley, Calif., 2001.

63. S. Sugai and T. Ueda, *Phys. Rev. B*, 1982, **26**, 6554.

64. A. Roy, H. C. Movva, B. Satpati, K. Kim, R. Dey, A. Rai, T. Pramanik, S. Guchhait, E. Tutuc and S. K. Banerjee, *ACS Appl. Mater. Interfaces*, 2016, **8**, 7396.

65. P. Soubelet, A. E. Bruchhausen, A. Fainstein, K. Nogajewski and C. Faugeras, *Phys. Rev. B*, 2016, **93**, 155407.

66. R. G. Dickinson and L. Pauling, *J. Am. Chem. Soc.*, 1923, **45**, 1466.

67. G. L. Frey, R. Tenne, M. J. Matthews, M. S. Dresselhaus and G. Dresselhaus, *Phys. Rev. B*, 1999, **60**, 2883.

68. S. Mignuzzi, A. J. Pollard, N. Bonini, B. Brennan, I. S. Gilmore, M. A. Pimenta, D. Richards and D. Roy, *Phys. Rev. B*, 2015, **91**, 195411.

69. G. L. Frey, R. Tenne, M. J. Matthews, M. S. Dresselhaus and G. Dresselhaus, *J. Mater. Res.*, 2011, **13**, 2412.

Chapter 7: General conclusions

This work has two major themes, the study of several series of early d-block metal complexes containing chalcogenoether ligands, their characterisation by X-ray crystallography and various spectroscopic techniques, and an exploration of selected complexes as potential LPCVD precursors for metal dichalcogenide films.

7.1 Coordination chemistry studies

This work develops the coordination chemistry of three series of niobium halides in a range of oxidation states with soft neutral chalcogenoether ligands, and in addition similar complexes of molybdenum(IV) chloride. Some brief studies of TaX_5 complexes are also included.

Previous work described in my MSc thesis explored the synthesis of thio- and selenoether complexes of $NbCl_5$ and the successful LPCVD of NbS_2 and $NbSe_2$ films.[1] In that work, attempts to use Nb(III) dimer complexes $[Nb_2Cl_4(SR_2)(\mu\text{-}Cl)_2(\mu\text{-}SR_2)]$ (R = Me, ^{n}Bu) were unsuccessful with the complexes decomposing on heating *in vacuo* without evaporation or any film deposition. In this thesis I describe complexes of niobium(IV) chloride, niobium(V) thiochloride and niobium(V) bromide with various chalcogenoethers and deposition studies on selected examples.

One reason for the scarcity of research using NbX_4 (X = Cl, Br) is likely to be the difficult of preparing pure starting materials. The usual synthetic route to NbX_4 is very difficult to repeat as there is limited experimental detail available.[2] Our work developed a much more reliable preparation for NbX_4, a reduction using NbX_5 and elemental Nb powder and defined the successful experimental conditions. An alternative synthesis of $NbBr_5$ from $NbCl_5$ and BBr_3 was also established. There are other reduction routes using Na/Hg, Na/K or Mg/Et_2O which worked well with $[NbCl_5(\text{phosphine})]$ complexes. However, using these reducing agents with $[NbCl_5(\text{thioether})]$ only results in dimeric Nb(III) complexes.[3-5] There are no commercial sources for oxygen-free Nb(IV) compounds, and this makes researching NbX_4 complexes more difficult.

A range of six-coordinate $[NbCl_4(SR_2)_2]$, $[NbCl_4(SeR_2)_2]$, $[NbCl_4(L\text{–}L)]$ (L–L = dithioether or diselenoether) and eight-coordinate $[NbCl_4\{MeS(CH_2)_2SMe\}_2]$ complexes were obtained and fully characterised by X-ray crystallography and various spectroscopies. The six-coordinate M–M bonded dimers $[Nb_2Cl_6(EMe_2)_2(\mu\text{-}Cl)_2]$ and the unique eight-coordinate $[Nb_2Cl_4(EMe_2)_4(\mu\text{-}Cl)_4]$ (also with a single Nb–Nb bond) were also characterised. The Nb(IV) complexes proved to be very sensitive to moisture and oxygen, and readily oxidise to Nb(V) species, whilst in some cases the chalcogenoether undergoes C-E bond fission to generate compounds with S or Se bridges. Prior to this study only a few literature reports had explored the coordination of NbX_4 with neutral chalcogenoether ligands and contained very little data. This contrasts with the large amount of data on niobium-phosphines.[6-9]

As little data were available for diphosphine complexes, a study of NbX_4 (X = Cl or Br) complexes of diphosphines was also carried out. This revealed the major complex types were eight-coordinate $[NbX_4(diphosphine)_2]$ and unstable $[NbX_4(diphosphine)]$ which are likely to be dimers with Nb–Nb bonds as they are diamagnetic both in the solid and in solution. Generally, the diphosphine complexes are much more stable than the chalcogenoether complexes.

Alternative possible precursors to NbE_2 films were the thio- and seleno- halides $[NbECl_3]$, which already contain a Nb–E bond. The ideal synthesis of $[NbSCl_3(dichalcogenoether)]$ uses the substitution of acetonitrile from $[NbSCl_3(NCCH_3)_2]$.[10] The successful preparation of $[NbSCl_3(SR_2)]$ and $[NbSCl_3(L–L)]$ was achieved and these new complexes have been fully characterised. Attempts to prepare complexes from $NbSeCl_3$ had limited success.

Although MoS_2 and $MoSe_2$ are amongst the most intensively studied dichalcogenides,[11-13] very few attempts have been made to obtain them from molybdenum coordination complexes by CVD.

One reason for the lack of molybdenum(V) or molybdenum(IV) chloride complexes with chalcogenoethers is likely to be due to the fragile Mo–Cl bonds and the ease of reduction to Mo(III). $Mo^{VI}Cl_6$ decomposes to $Mo^{V}Cl_5$ at temperature above -10 °C,[14] and $Mo^{V}Cl_5$ undergoes facile redox reaction with solvents or ligands (Chapter 6). Mo^{IV}–Cl bonds are also rather weak and $[Mo^{IV}Cl_4(ER_2)_2]$ can be easy reduced to $[Mo^{III}Cl_3L_3]$, for example by excess ligands or Sn powder.[15] During this work, a series of $MoCl_4$ complexes with thioether or selenoether ligands, $[MoCl_4(ER_2)_2]$ or $[MoCl_4(L–L)]$, have been prepared. Telluroether ligands instead undergo redox reactions with $[MoCl_4(NCCH_3)_2]$ resulting in the formation of for example $[Me_2TeCl_2]$.

In conclusion, the ER_2 ligand binding strength follows the order with donor S < Se >> Te when coordinated with a transition metal in its higher oxidation states *i.e.* $[Nb^{V}Cl_5(ER_2)]$, $[Nb^{V}SCl_3(ER_2)]$, $[Nb^{IV}Cl_4(ER_2)_2]$, although all complexes appear less stable than those with phosphorus or arsenic donor ligands. These behaviours of neutral chalcogenoethers as σ-donors agree with the trends for acyclic chalcogenoether ligands reported in other systems (see Comprehensive Coordination Chemistry II).[9]

7.2 Chemical vapour deposition studies

Selected complexes were tested as LPCVD reagents for the deposition of ME_2 films. Decomposition of the complexes was explored by heating under inert gas using a TGA instrument. However, the precursors' decomposition temperatures, as measured by TGA, do not always correlate to the temperature of the furnace used during LPCVD. This is because TGA experiments are performed at ambient pressure under flowing argon gas; these are different conditions to those employed in typical low pressure CVD application. The only CVD application process, which will correspond directly to the TGA, is atmospheric pressure CVD which was not used in this work. The precursors in this work are typically described as 'hard metal halides' coordinated with 'soft neutral ligands', accordingly HSAB theory would describe the M–E bonds as relatively weak bonds. This means ligand dissociation is the common degradation pathway shown in TGA.

This work has investigated a number of compounds as single source precursors for LPCVD. Ideal single source precursors are typically thought to include a direct intermolecular A–B bond (where A and B are elements of the target materials), to be volatile *in vacuo* and requiring minimal synthetic steps. Candidates containing alkyl groups, in order to enable β-hydride elimination (*i.e.* not Me groups) are preferred, and they should ideally contain the appropriate A:B ratio (1:2 for M:E). The quality of the ME_2 film produced is also a key consideration - for example the absence of oxide or chloride in the film is essential for some applications. This work has shown that there are several additional aspects that should be considered when designing a new single source LPCVD precursor. One key point is to avoid complexes containing M–M bonds or compounds which are highly likely to form M–M bonds.

Both $NbCl_4$ complexes (Chapter 3) and Nb(III) dimeric complexes have been tested as single source LPCVD precursors.[5] The failure of Nb(III) dimeric complexes to form thin films is attributed to these species being too stable and non-volatile, and so require very high temperatures to evaporate. The unsuccessful attempts using $NbCl_4$ complexes are explained because these complexes are likely to reform a dimer or polymer with strong M–M bonds and evaporate off the chalcogenoether. This tendency to lose ligand is demonstrated by the recrystallized, thioether and selenoether analogues of $[NbCl_4(ER_2)_2]$ which are shown by X-ray crystal structure data to form dimeric complexes (Section 3.2.5). Although $[NbSCl_3(S^nBu_2)]$ is thought to be dimeric, based upon the similarity of the spectroscopic data to that of dimeric $[NbSCl_3(SMe_2)]$, these dimeric species do not contain a M–M bond because they are Nb(V) complexes, and appear to vaporise successfully. This is a major reason why all Nb(V) single source precursors, $[NbCl_5(S^nBu_2)]$, $[NbCl_5(Se^nBu_2)]$, $[NbSCl_3(S^nBu_2)]$, $[NbSCl_3\{^nBu_2S(CH_2)_3S^nBu_2\}]$ and $[NbSe_2Cl_3(Se^nBu_2)]$, deposit NbE_2 thin film successfully using LPCVD.[1, 16] In the same way, when selecting precursors for the deposition of MoE_2 thin films, $[MoCl_3L_3]$ compounds are not generally considered, since the lower oxidation state will probably lead to weaker Mo–E bonds, resulting in easily lost ligands. In contrast, as $[MoCl_4L_2]$ species are

only reported to exist as monomers and the M:E ratio matches the target material, precursors of this form have been shown to deposit MoE_2 thin films successfully.

7.3 Outlook

This thesis has described new chemistry of niobium and molybdenum with chalcogenoethers. An obvious topic for further work is the investigation of similar systems containing tantalum or tungsten. There is some work on TaF_5, $TaCl_5$ and $TaBr_5$ complexes,[16, 17] but TaX_4 chemistry remains largely unexplored.[18] There is very little work describing tungsten coordination chemistry with chalcogen ligands,[18] and so there is much scope for a detailed study. For tantalum, an investigation of complexes derived from $TaSCl_3$ should be of particular interest. Although some success has been achieved in this work using telluroethers, the number of complexes is quite limited, although more may form if suitable ligand types are used. One possibility of stabilising Te–M bonds is to use hybrid ligands such as $R_2NCH_2CH_2CH_2TeR$ where the amine functionality may stabilise the M–Te bond.

There remains significant scope to develop new reagents as single source precursors for LPCVD (or AACVD) of ME_2 films. This thesis has described the use of niobium(V) chloride and niobium(V) thiochloride complexes. Some work on changing the halide (using $[NbBr_5(E^nBu_2)]$) has also been carried out. Complexes of the type $[NbF_5(ER_2)]$ can be sublimed *in vacuo* and therefore may be suitable for LPCVD.[19] They are extremely moisture sensitive and pyrolysis may yield corrosive HF, but this is not necessarily a barrier to using them.

At present there are very few LPCVD precursors for TaE_2 films and as described in previous chapters, $TaCl_5$ complexes do not work (in contrast to the niobium systems). However $TaSCl_3$ complexes[20, 21] are certainly worthy of study and possibly $[TaF_5(ER_2)]$. The other possible single source LPCVD precursor route is from $[Ta(ER)_nCl_{5-n}]$ complexes. Additionally, $[M(SR)_n(NMe_2)_{5-n}]$ (M = Nb, Ta) were reported to deposit MS_2 films using AACVD or LPCVD.[22, 23] It is likely that the species $[M(ER)_2L_3]$ (L = any suitable ligands) are ideal single source precursors for NbE_2 and TaE_2.

MTe_2 materials are also of great potential for electronic applications but at present there are no single source precursors for Group 5 or 6 metal tellurides. The instability of the telluroether complexes is a significant problem, but rather than use a LPCVD approach, an AACVD method may be more successful, as thermal stability during vapourisation is not required in AACVD.

An alternative approach would be to use a CVD reactor which has more control of the temperature and which might yield higher quality films, or lead to better control of film thickness. Finally, in order to take the applications of this work forward, it will be necessary to obtain electrical or magnetic measurements on the thin films, and hence attempt to improve the film quality.

7.4 References

1. Y.-P. Chang, M.Sc Thesis, University of Southampton, 2014.
2. R. E. McCarley and B. A. Torp, *Inorg. Chem.*, 1963, **2**, 540.
3. A. D. Allen and S. Naito, *Can. J. Chem.*, 1976, **54**, 2948.
4. M. Matsuura, T. Fujihara, M. Kakeya, T. Sugaya and A. Nagasawa, *J. Organomet. Chem.*, 2013, **745-746**, 288.
5. S. L. Benjamin, Y.-P. Chang, M. Huggon, W. Levason and G. Reid, *Polyhedron*, 2015, **99**, 230.
6. J. B. Hamilton and R. E. McCarley, *Inorg. Chem.*, 1970, **9**, 1333.
7. J. B. Hamilton and R. E. McCarley, *Inorg. Chem.*, 1970, **9**, 1339.
8. Y.-P. Chang, W. Levason, M. E. Light and G. Reid, *Dalton Trans.*, 2016, **45**, 16262.
9. W. Levason and G. Reid, *Comprehensive Coordination Chemistry II*, ed. J. A. McCleverty and T. J. Meyer, Elsevier, Oxford, 2003, **1**, 391.
10. A. Bashall, V. C. Gibson, T. P. Kee, M. McPartlin, O. B. Robinson and A. Shaw, *Angew. Chem. Int. Ed.*, 1991, **30**, 980.
11. M. Chhowalla, H. S. Shin, G. Eda, L. J. Li, K. P. Loh and H. Zhang, *Nat. Chem.*, 2013, **5**, 263.
12. B. B. Wang, K. Zheng, X. X. Zhong, D. Gao and B. Gao, *J. Alloys Compd.*, 2017, **695**, 27.
13. D. Nam, J. U. Lee and H. Cheong, *Sci. Rep.*, 2015, **5**, 17113.
14. F. Tamadon and K. Seppelt, *Angew. Chem. Int. Ed.*, 2013, **52**, 767.
15. J. R. Dilworth and R. L. Richards, *Inorg. Synth.*, 1990, **28**, 33.
16. S. L. Benjamin, Y.-P. Chang, C. Gurnani, A. L. Hector, M. Huggon, W. Levason and G. Reid, *Dalton Trans.*, 2014, **43**, 16640.
17. S. L. Benjamin, A. Hyslop, W. Levason and G. Reid, *J. Fluorine Chem.*, 2012, **137**, 77.
18. Y.-P. Chang, W. Levason and G. Reid, *Dalton Trans.*, 2016, **45**, 18393.
19. F. Fairbrother, K. H. Grundy and A. Thompson, *J. Chem. Soc.*, 1965, 765.
20. M. G. B. Drew, G. W. A. Fowles and R. J. R. Hobson, D. A., *Inorg. Chim. Acta*, 1976, **20**, L35.
21. M. G. B. Drew, D. A. Rice and D. M. Williams, *J. Chem. Soc., Dalton Trans.*, 1984, 845.
22. C. J. Carmalt, C. W. Dinnage, I. P. Parkin, A. J. White and D. J. Williams, *Inorg. Chem.*, 2002, **41**, 3668.
23. E. S. Peters, C. J. Carmalt, I. P. Parkin and D. A. Tocher, *Eur. J. Inorg. Chem.*, 2005, 4179.

Appendix 1: General experimental techniques

General preparation and characterisation

Syntheses were performed by using standard Schlenk and glove-box techniques to ensure a dry nitrogen atmosphere.[1] $MoCl_5$, $NbCl_5$, $NbBr_5$, SMe_2, $SeMe_2$, S^nBu_2, THT, $[NbCl_4(THF)_2]$ and $S(SiMe_3)_2$ were obtained from Sigma-Aldrich and stored in a glovebox. $[NbCl_4(THF)_2]$ was stored in a freezer under a nitrogen atmosphere and $S(SiMe_3)_2$ and Se $(SiMe_3)_2$ (Fluorochem) were stored in the glovebox in ampoules under a nitrogen atmosphere.

$TaBr_5$ and diphosphine ligands, $Me_2P(CH_2)_2PMe_2$, $Et_2P(CH_2)_2PEt_2$, *o*-$C_6H_4(PPh_2)_2$, $Cy_2P(CH_2)_2PCy_2$ and $Ph_2P(CH_2)_3PPh_2$, were purchased from Strem Chemicals and stored in a glovebox. Ligands, *o*-$C_6H_4(PMe_2)_2$,[2] $MeS(CH_2)_nSMe$ (n = 2 or 3),[3] $^iPrS(CH_2)_2S^iPr$,[3], *o*-$C_6H_4(CH_2SEt)_2$,[3, 4] Se^nBu_2,[5] $MeSe(CH_2)_nSeMe$ (n = 2 or 3),[6] *o*-$C_6H_4(CH_2SeMe)_2$,[6] $^nBuSe(CH_2)_3Se^nBu$,[7] $^tBuTe(CH_2)_3Te^tBu$,[8, 9] $TeMe_2$ and Te^nBu_2,[8, 9] were prepared *via* literature methods. $^nBuS(CH_2)_3S^nBu$ was prepared *via* modified literature methods (see experimental below).[3, 4]

Solvents were dried by distillation from CaH_2 (CH_2Cl_2 or CH_3CN) or Na/benzophenone ketyl (diethyl ether, *n*-hexane, toluene, benzene).

Ligands preparation:

$^nBuS(CH_2)_3S^nBu$

$HS(CH_2)_2SH$ (6.048 g, *ca.* 5.7 mL, 56 mmol) was mixed in dried EtOH (60 mL) before slowly adding sodium pieces (2.8 g, 112 mmol). The system was linked with a condenser and refluxed for one hour after all sodium dissolved in solution. After the solution was cooled to ambient temperature, ^{n}BuBr (15.344 g, *ca.* 12.03 mL, 112 mmol) was added slowly with formation of a white solid. The solution was taken to refluxed for one hour. Saturated $NaCl/H_2O$ and $NaHCO_3/H_2O$ solutions were added in with stirring after the solution was cooled to ambient temperature. The clean supernatant solution was separated and the product was extracted with Et_2O (50 mL x 4 times). The Et_2O solution was dried using Na_2SO_4 and stirred overnight. The remained dried Et_2O solution was taken to dryness under vacuum to give a colourless liquid. Yield: 6 g, 48 %. ^{1}H NMR ($CDCl_3$, 298 K): δ = 0.92 (t, [6H], $S(CH_2)_3\underline{CH_2}$), 1.41 (m, [4H], $S(CH_2)_2\underline{CH_2}CH_3$), 1.57 (m, [4H], $SCH_2\underline{CH_2}CH_2CH_3$), 1.86 (m, [2H], $SCH_2\underline{CH_2}CH_2S$), 2.52 (t, [4H], $S\underline{CH_2}CH_2CH_2S$), 2.62 (t, [4H], $S\underline{CH_2}(CH_2)_2CH_3$). $^{13}C\{^1H\}$ NMR ($CDCl_3$, 298 K): δ = 13.65, 21.98, 29.43, 30.96, 31.74, 31.81.

LPCVD general procedure

The single source precursor (*ca.* 50 mg, or otherwise stated in the discussion) was loaded into the end of silica tubes in a nitrogen purged glove box with *ca.* 1 mL CH_2Cl_2. Silica substrates were obtained from UQG Optics Ltd as silica sheet and cut to size (~1 × 8 × 20 mm^3). The silica substrates were dried in an oven (70 ℃) overnight before transferred into a glovebox. The substrates were subsequently loaded in the tube and placed end-to-end (Figure A1). The tube was positioned in a furnace so that the substrates were in the heated zone and the precursor was *ca.* 2 cm away from the start of the heated zone. The tube was evacuated to 0.05 mmHg. After the precursor solvent had evaporated, the furnace was heated to the requisite temperature (400-750 ℃). The tube was then moved into the furnace. The position of the sample was maintained until the all the precursor had evaporated. The tube was then cooled to room temperature and the tiles were unloaded under ambient conditions. Temperature profiling of the deposition region was carried out using a temperature probe.

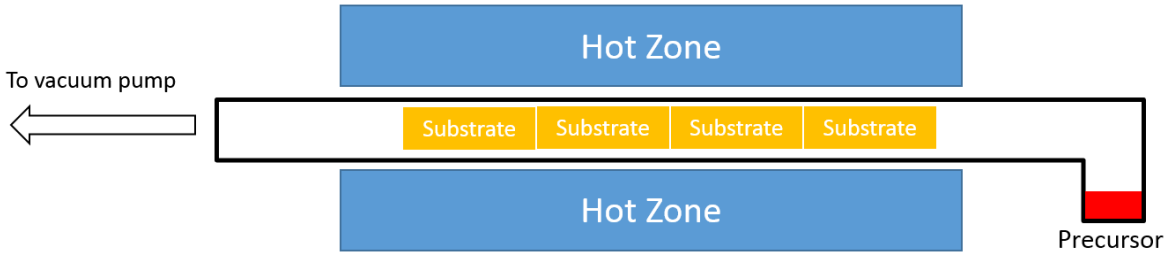

Figure A1 General setup for LPCVD experiments

Physical Measurements

Infrared spectra were recorded on a Perkin-Elmer Spectrum 100 spectrometer in the range 4000-200 cm^{-1}. Samples were prepared as Nujol mulls as thin films between two CsI plates. UV-visible spectra were recorded as neat powdered solid or diluted with $BaSO_4$ using the diffuse reflectance attachment of a Perkin Elmer 750S spectrometer.

Multinuclear (^1H, $^{13}C\{^1H\}$, $^{31}P\{^1H\}$, $^{77}Se\{^1H\}$, $^{125}Te\{^1H\}$ and ^{93}Nb) NMR spectra were recorded from $CDCl_3$, CD_2Cl_2 or CD_3CN solutions using a Bruker AV II 400 spectrometer at 298 K unless otherwise stated. ^1H and $^{13}C\{^1H\}$ NMR spectra are referenced to the residual proton-solvent resonance. $^{31}P\{^1H\}$ NMR spectra are referenced to external 85 % H_3PO_4. $^{77}Se\{^1H\}$, $^{125}Te\{^1H\}$ and ^{93}Nb NMR spectra are referenced to external neat $SeMe_2$, $TeMe_2$ or $[Et_4N][NbCl_6]$ in CH_3CN ($\delta = 0$), respectively.

Thermogravimetric analysis (TGA) used a NETZSCH TG209 F1 Libra analyser under a flow of argon at 65 mL/minutes, contained within a dry, nitrogen purged glovebox. Samples were loaded in aluminium sample cups. Magnetic susceptibility measurements were carried out on a Johnson

Matthey magnetic susceptibility balance. Microanalyses on new compounds were undertaken by London Metropolitan University or Medac Ltd.

X-ray Diffraction

PXRD data were collected using a Bruker D2 diffractometer (Cu-K_α) and a sealed aluminium sample holder with a hemicylindrical Kapton window. Phase matching, lattice parameter refinement and Rietveld refinement ($NbCl_4$ and $NbBr_4$ PXRD data) were all performed using the PDXL2 software package and diffraction patterns from ICSD.[10-12]

Single crystal X-ray data was collected using a Rigaku AFC12 goniometer equipped with an enhanced sensitivity (HG) Saturn724+ detector mounted at the window of an FR-E+ SuperBright molybdenum ($\lambda = 0.71073$) rotating anode generator with VHF Varimax optics (70 micron focus) with the crystal held at 100 K (nitrogen cryostream). Structure solutions and refinements were performed using SHELX(S/L)97, SHELX-2014/7 and were generally straightforward.[13-17] H atoms were added and refined with a riding model.

Film characterisation:

X-ray diffraction patterns were collected in grazing incidence mode ($\theta_1 = 1°$), in-plane mode ($\theta_1 = 0.5°$, $2\theta\chi$ scan with the detector scanning in the film plane) or pole-figure mode ($\theta_1 = 0.5°$, α scan with the detector scanning rotation) using a Rigaku SmartLab diffractometer (Cu-K_α) with parallel X-ray beam and a DTex Ultra 250 1D detector. Phase matching, lattice parameter refinement and Le Bail fitting (3R-NbS_2, 2H-$NbSe_2$, 3R-$NbSe_2$, 2H-$MoSe_2$ thin films) were all performed using the PDXL2 software package and diffraction patterns from ICSD.[10-12]

Scanning electron microscopy (SEM) was performed using a Philips XL30 ESEM instrument with an acceleration voltage of 10 kV or 15 kV or a JEOL JSM6500 and an accelerating voltage of 10 kV. Energy dispersive X-ray (EDX) data were obtained at accelerating voltage of 5–15 kV with a Thermofisher Ultradry NSS 3 (XL30) detector or at an accelerating voltage of 5–15 kV with an Oxford INCA x-act X-ray detector (JSM6500). Raman spectra were collected by a Renishaw InVia Raman Microscope with a 100 mW He-Ne 785 nm Laser.

References for general experimental

1. C. M. Davis and K. A. Curran, *J. Chem. Educ.*, 2007, **84**, 1822.
2. E. P. Kyba, S.-T. Liu and R. L. Harris, *Organometallics*, 1983, **2**, 1877.
3. F. R. Hartley, S. G. Murray, W. Levason, H. E. Soutter and C. A. McAuliffe, *Inorg. Chim. Acta*, 1979, **35**, 265.
4. W. Levason, M. Nirwan, R. Ratnani, G. Reid, N. Tsoureas and M. Webster, *Dalton Trans.*, 2007, 439.
5. N. Kuhn, P. Faupel and E. Zauder, *J. Organomet. Chem.*, 1986, **302**, C4.
6. D. J. Gulliver, E. G. Hope, W. Levason, S. G. Murray, D. M. Potter and G. L. Marshall, *J. Chem. Soc., Perkin Trans. II*, 1984, 429.
7. C. H. de Groot, C. Gurnani, A. L. Hector, R. Huang, M. Jura, W. Levason and G. Reid, *Chem. Mater.*, 2012, **24**, 4442.
8. E. G. Hope, T. Kemmitt and W. Levason, *Organometallics*, 1988, **7**, 78.
9. K. George, C. H. de Groot, C. Gurnani, A. L. Hector, R. Huang, M. Jura, W. Levason and G. Reid, *Chem. Mater.*, 2013, **25**, 1829.
10. S. Grazulis, D. Chateigner, R. T. Downs, A. F. Yokochi, M. Quiros, L. Lutterotti, E. Manakova, J. Butkus, P. Moeck and A. Le Bail, *J. Appl. Cryst.*, 2009, **42**, 726.
11. Inorganic Crystal Structure Database accessed August 2017.
12. *PDXL2*, Rigaku Corporation, Tokyo, Japan, 2012.
13. G. M. Sheldrick, *Acta Cryst.*, 2015, **C71**, 3.
14. *CrysAlis PRO*, Agilent Technologies Ltd, Yarnton, Oxfordshire, England, 2017.
15. *CrystalClear*, Rigaku Corporation, Tokyo, Japan, 2012.
16. G. M. Sheldrick, *SHELXS-97, Program for crystal structure solution*, University of Göttingen, Germany, 1997.
17. G. M. Sheldrick, *SHELXS-97, Program for crystal sturcture refinement*, University of Göttingen, Germany, 1997.

Appendix 2: **X-ray crystallographic data**[a]

X-ray crystal data from Chapter 2

Compound	$NbBr_4$	$[NbCl_4\{Me_2P(CH_2)_2PMe_2\}_2]$
Formula	Br_4Nb	$C_{12}H_{32}Cl_4NbP_4$
Formula weight	412.55	534.96
Crystal system	Monoclinic	Orthorhombic
Space group	*I*2/*m* (No. 12)	$P2_12_12$ (No. 18)
a/ Å	9.2587(6)	10.7216(9)
b/ Å	7.1856(8)	11.289(1)
c/ Å	8.6314(7)	9.4711(9)
α/deg	90	90
β/ deg	92.540(7)	90
γ/ deg	90	90
U/ Å ^{3}	543.68(9)	1146.4(2)
Z	4	2
μ(Mo-K_α)/mm^{-1}	29.794	1.263
F(000)	724	546
Total no. reflections	1833	9661
Unique reflections	610	2248
R_{int}	0.0304	0.0364
No. of Parameters, restraints	27, 0	100, 0
R_1[b] [$I_o>2\sigma(I_o)$]	0.0497	0.0209
R_1 (all data)	0.0522	0.0223
wR_2[b] [$I_o>2\sigma(I_o)$]	0.1304	0.0453
wR_2 (all data)	0.1337	0.0457

[a]Common items: temperature =100 K; wavelength (Mo-K_α) = 0.71073 Å; θ(max)= 27.5°.
[b]$R_1 = \Sigma||F_o|-|F_c||/\Sigma|F_o|$. $\omega R_2=[\Sigma\omega(Fo^2-Fc^2)^2/\Sigma\omega Fo^4]^{1/2}$.

Compound	$[NbCl_4\{Et_2P(CH_2)_2PEt_2\}_2]$	$[NbBr_4\{Me_2P(CH_2)_2PMe_2\}_2]$
Formula	$C_{20}H_{48}Cl_4NbP_4$	$C_{12}H_{32}Br_4NbP_4$
Formula weight	647.17	712.80
Crystal system	Monoclinic	Orthorhombic
Space group	$P2_1$ (No. 4)[c]	$Pca2_1$ (No. 29)
a/ Å	10.5571(5)	13.3974(9)
b/ Å	11.6652(5)	12.4285(9)
c/ Å	11.9053(8)	14.181(1)
α/deg	90	90
β/ deg	95.008(7)	90
γ/ deg	90	90
U/ Å ^{3}	1460.6(1)	2361.2(3)
Z	2	4
μ(Mo-K_α)/mm^{-1}	1.005	7.543
F(000)	674	1380
Total no. reflections	12265	18564
Unique reflections	4819	4641
R_{int}	0.0190	0.0426
No. of Parameters, restraints	280, 1	199, 1
R_1[b] [$I_o>2\sigma(I_o)$]	0.0166	0.0221
R_1 (all data)	0.0170	0.0250
wR_2[b] [$I_o>2\sigma(I_o)$]	0.0402	0.0424
wR_2 (all data)	0.0404	0.0435

[c]Flack parameter = -0.039(17).

Compound	$[NbCl_4\{o\text{-}C_6H_4(PMe_2)_2\}_2]$	$[NbBr_4\{o\text{-}C_6H_4(PMe_2)_2\}_2]$
Formula	$C_{20}H_{32}Cl_4NbP_4$	$C_{20}H_{32}Br_4NbP_4$ *
Formula weight	631.04	808.88
Crystal system	Tetragonal	Tetragonal
Space group	*I*-42*m* (No. 121)	*I*-42*m* (No. 121)
a/ Å	8.9876(7)	9.0690(3)
b/ Å	8.9876(7)	9.0690(3)
c/ Å	16.148(1)	16.330(1)
α/deg	90	90
β/ deg	90	90
γ/ deg	90	90
U/ Å ^{3}	1304.4(2)	1343.1(1)
Z	2	2
μ(Mo-K_α)/mm^{-1}	1.124	3.313
F(000)	642	708
Total no. reflections	2204	2680
Unique reflections	754	650
R_{int}	0.0346	0.0355
No. of Parameters, restraints	43, 0	45, 42
R_1[b] [$I_o>2\sigma(I_o)$]	0.0477	0.0434
R_1 (all data)	0.0523	0.0460
wR_2[b] [$I_o>2\sigma(I_o)$]	0.1111	0.0915
wR_2 (all data)	0.1149	0.0930

*Crystal examined appear to contain chloride impurity (see cif file for detail)

Compound	[{{$Cy_2P(CH_2)_2PCy_2$}$NbCl_3$}$_2${μ-$Me_2C_2N_2$}]
Formula	$C_{56}H_{102}Cl_6N_2Nb_2P_4$
Formula weight	1325.79
Crystal system	Orthorhombic
Space group	$P2_12_12$ (No. 18)
a/ Å	15.7288(4)
b/ Å	18.6228(5)
c/ Å	24.7255(7)
α/deg	90
β/ deg	90
γ/ deg	90
U/ Å ^{3}	7242.5(3)
Z	4
μ(Mo-K_α)/mm^{-1}	0.658
F(000)	2784
Total no. reflections	30880
Unique reflections	14198
R_{int}	0.0453
No. of Parameters, restraints	633, 634
$R_1{}^b$ [I_o>2σ(I_o)]	0.0563
R_1 (all data)	0.0795
$wR_2{}^b$ [I_o >2σ(I_o)]	0.1267
wR_2 (all data)	0.1360

X-ray crystal data from Chapter 3

Compound	$[Nb_2Cl_4(THF)_2(\mu\text{-}Cl)_2(\mu\text{-}SMe_2)][C_6H_6]_2$	$[NbCl_4\{MeS(CH_2)_2SMe\}_2]$
Formula	$C_{10}H_{22}Cl_6Nb_2O_2S$, C_6H_6	$C_8H_{20}Cl_4NbS_4$
Formula weight	682.96	479.19
Crystal system	Triclinic	Tetragonal
Space group	*P*-1 (No. 2)	$P4_32_12$ (No. 96)
a/ Å	8.250(1)	9.1410(1)
b/ Å	8.561(1)	9.1410(1)
c/ Å	18.031(2)	20.574(2)
α/deg	78.774(8)	90
β/ deg	83.671(8)	90
γ/ deg	84.085(7)	90
U/ Å ^{3}	1237.2(3)	1719.1(2)
Z	2	4
μ(Mo-K_α)/mm^{-1}	1.669	1.786
F(000)	680	964
Total no. reflections	20053	7720
Unique reflections	4867	1691
R_{int}	0.0406	0.0620
No. of Parameters, restraints	264, 0	80, 0
R_1[b] [$I_o>2\sigma(I_o)$]	0.0252	0.0266
R_1 (all data)	0.0288	0.0326
wR_2[b] [$I_o>2\sigma(I_o)$]	0.0614	0.0558
wR_2 (all data)	0.0631	0.0577

Compound	$[NbCl_4\{MeS(CH_2)_2SMe\}]$	$[NbCl_4\{^iPrS(CH_2)_2S^iPr\}]$
Formula	$C_4H_{10}Cl_4NbS_2$	$C_8H_{18}Cl_4NbS_2$
Formula weight	365.95	413.05
Crystal system	Monoclinic	Monoclinic
Space group	$P2_1$ (No. 4)[c]	$P2_1/c$ (No. 14)
a/ Å	7.2443(3)	8.7424(4)
b/ Å	11.2723(4)	9.2175(3)
c/ Å	7.9616(3)	19.6381(9)
α/deg	90	90
β/ deg	116.177(5)	98.649(4)
γ/ deg	90	90
U/ Å ^{3}	583.46(4)	1564.5(1)
Z	2	4
μ(Mo-K$_\alpha$)/mm^{-1}	2.248	1.690
F(000)	350	828
Total no. reflections	3485	10862
Unique reflections	2002	4029
R_{int}	0.0137	0.0530
No. of Parameters, restraints	102, 1	140, 0
R_1[b] [$I_o>2\sigma(I_o)$]	0.0177	0.0614
R_1 (all data)	0.0178	0.1053
wR_2[b] [$I_o>2\sigma(I_o)$]	0.0450	0.1221
wR_2 (all data)	0.0452	0.1403

[c]Flack parameter = 0.03(6).

Compound	$[NbCl_4\{MeS(CH_2)_3SMe\}]$	$[NbCl_4\{o\text{-}C_6H_4(CH_2SEt)_2\}]$
Formula	$C_5H_{12}Cl_4NbS_2$	$C_{12}H_{18}Cl_4NbS_2$
Formula weight	370.98	461.09
Crystal system	Tetragonal	Orthorhombic
Space group	*I*-42*d* (No. 122)	*Pnma* (No. 62)
a/ Å	9.964(3)	19.407(9)
b/ Å	9.964(3)	12.502(6)
c/ Å	25.11(1)	7.084(3)
α/deg	90	90
β/ deg	90	90
γ/ deg	90	90
U/ $Å^3$	2493(2)	1719(1)
Z	8	4
μ(Mo-K_α)/mm^{-1}	2.108	1.549
F(000)	1464	924
Total no. reflections	3934	8916
Unique reflections	1225	1768
R_{int}	0.0743	0.0746
No. of Parameters, restraints	58, 0	92, 0
R_1[b] [$I_o>2\sigma(I_o)$]	0.0521	0.0328
R_1 (all data)	0.0821	0.0486
wR_2[b] [$I_o>2\sigma(I_o)$]	0.1205	0.0681
wR_2 (all data)	0.1338	0.0738

Compound	$[NbCl_4\{MeSe(CH_2)_3SeMe\}]$	$[Nb_2Cl_6(SMe_2)_2(\mu\text{-}Cl)_2]$
Formula	$C_5H_{12}Cl_4NbSe_2$	$C_4H_{12}Cl_8Nb_2S_2$
Formula weight	464.78	593.68
Crystal system	Tetragonal	Monoclinic
Space group	$I4_1/a$ (No. 88)	$P2_1/n$ (No. 14)
a/ Å	9.9381(2)	6.4589(2)
b/ Å	9.9381(2)	10.1598(4)
c/ Å	26.265(1)	13.1644(5)
α/deg	90	90
β/ deg	90	94.499(4)
γ/ deg	90	90
U/ Å ^{3}	2594.1(2)	861.20(5)
Z	8	2
μ(Mo-K$_\alpha$)/mm^{-1}	7.317	2.787
F(000)	1752	572
Total no. reflections	8738	5264
Unique reflections	1281	1690
R_{int}	0.0831	0.0199
No. of Parameters, restraints	58, 0	75, 0
$R_1{}^b$ [$I_o>2\sigma(I_o)$]	0.0281	0.0205
R_1 (all data)	0.0302	0.0233
$wR_2{}^b$ [$I_o>2\sigma(I_o)$]	0.0689	0.0509
wR_2 (all data)	0.0697	0.0521

Compound	$[Nb_2Cl_6(SeMe_2)_2(\mu\text{-}Cl)_2]$	$[Nb_2Cl_4(TeMe_2)_4(\mu\text{-}Cl)_4]$
Formula	$C_4H_{12}Cl_8Nb_2Se_2$	$C_8H_{24}Cl_8Nb_2Te_4$
Formula weight	687.48	1100.09
Crystal system	Orthorhombic	Tetragonal
Space group	*Cmca* (No. 64)	$P4_22_12$ (No. 94)
a/ Å	10.4725(8)	10.4835(1)
b/ Å	7.2592(5)	10.4835(1)
c/ Å	22.501(1)	12.0612(2)
α/deg	90	90
β/ deg	90	90
γ/ deg	90	90
U/ Å ^{3}	1710.6(2)	1325.57(3)
Z	4	2
μ(Mo-K_α)/mm^{-1}	6.818	5.979
F(000)	1288	996
Total no. reflections	5388	8870
Unique reflections	888	1315
R_{int}	0.0657	0.0302
No. of Parameters, restraints	44, 0	54, 0
$R_1{}^b$ [$I_o>2\sigma(I_o)$]	0.0291	0.0119
R_1 (all data)	0.0391	0.0120
$wR_2{}^b$ [$I_o>2\sigma(I_o)$]	0.0603	0.0295
wR_2 (all data)	0.0638	0.0295

Compound	$[Nb_2Cl_4\{MeS(CH_2)_3SMe\}_2(\mu\text{-}S)_2]$	$[Nb_2Cl_4\{o\text{-}C_6H_4(CH_2)_2Se\}_4(\mu\text{-}Se)_x]$
Formula	$C_{10}H_{24}Cl_4Nb_2S_6$	$C_{32}H_{32}Cl_4Nb_2Se_{4+x}$
Formula weight	664.27	1060+79x
Crystal system	Orthorhombic	Monoclinic
Space group	*Pnnm* (No. 58)	$P2_1/c$ (No. 14)
a/ Å	10.8359(6)	10.6850(5)
b/ Å	10.0475(7)	12.3759(5)
c/ Å	10.1149(6)	14.1909(7)
α/deg	90	90
β/ deg	90	106.821(5)
γ/ deg	90	90
U/ Å ^{3}	1101.3(1)	1796.3(2)
Z	2	2
μ(Mo-K$_\alpha$)/mm^{-1}	2.087	7.039
F(000)	660	1156
Total no. reflections	8409	18891
Unique reflections	1149	4644
R_{int}	0.0919	0.0761
No. of Parameters, restraints	58, 0	205, 0
$R_1{}^b$ [$I_o>2\sigma(I_o)$]	0.0330	0.0498
R_1 (all data)	0.0431	0.0854
$wR_2{}^b$ [$I_o>2\sigma(I_o)$]	0.0812	0.0939
wR_2 (all data)	0.0850	0.1052

X-ray crystal data from Chapter 4

Compound	$[NbSCl_3\{MeS(CH_2)_2SMe\}]$	$[NbSCl_3\{^iPrS(CH_2)_2S^iPr\}]$
Formula	$C_4H_{10}Cl_3NbS_3$	$C_8H_{18}Cl_3NbS_3$
Formula weight	353.56	409.66
Crystal system	Monoclinic	Monoclinic
Space group	$P2_1$ (No. 4)[c]	$P2_1/c$ (No. 14)
a/ Å	7.2010(3)	8.7791(2)
b/ Å	11.3494(4)	9.1658(2)
c/ Å	7.8693(5)	19.6825(5)
α/deg	90	90
β/ deg	115.502(7)	98.753(2)
γ/ deg	90	90
U/ Å ^{3}	580.47(6)	1565.36(6)
Z	2	4
μ(Mo-K_α)/mm^{-1}	2.209	1.652
F(000)	348	824
Total no. reflections	5010	14369
Unique reflections	2251	5181
R_{int}	0.0164	0.0322
No. of Parameters, restraints	102, 2	140, 0
R_1[b] [$I_o>2\sigma(I_o)$]	0.0175	0.0375
R_1 (all data)	0.0179	0.0504
wR_2[b] [$I_o>2\sigma(I_o)$]	0.0423	0.0839
wR_2 (all data)	0.0425	0.0907

[c]Flack parameter = -0.06(4).

Compound	$[NbSCl_3\{MeSe(CH_2)_3SeMe\}]$	$[Nb_2S_2Cl_2(SMe_2)_2(\mu\text{-}Cl)_2]$
Formula	$C_5H_{12}Cl_3NbSSe_2$	$C_4H_{12}Cl_6Nb_2S_4$
Formula weight	461.39	586.9
Crystal system	Tetragonal	Monoclinic
Space group	$I4_1/a$ (No. 88)	$P2_1$ (No. 4)[c]
a/ Å	10.0061(1)	7.2513(5)
b/ Å	10.0061(1)	13.0295(6)
c/ Å	26.1100(8)	9.8715(7)
α/deg	90	90
β/ deg	90	108.075(7)
γ/ deg	90	90
U/ Å ^{3}	2614.2(1)	886.6(1)
Z	8	4
μ(Mo-K_α)/mm^{-1}	7.216	2.641
F(000)	1744	568
Total no. reflections	11648	7662
Unique reflections	2242	3468
R_{int}	0.0454	0.0342
No. of Parameters, restraints	60, 0	149, 1
R_1[b] $[I_o>2\sigma(I_o)]$	0.0302	0.0360
R_1 (all data)	0.0423	0.0424
wR_2[b] $[I_o>2\sigma(I_o)]$	0.0634	0.0725
wR_2 (all data)	0.0679	0.0745

[c]Flack parameter = -0.14(6).

Compound	$[Nb_2Cl_4\{MeS(CH_2)_3SMe\}_2(\mu\text{-}S)(\mu\text{-}S_2)]$
Formula	$C_{10}H_{24}Cl_4Nb_2S_7$
Formula weight	696.33
Crystal system	Orthorhombic
Space group	*Pnnm* (No. 58)
a/ Å	10.5305(4)
b/ Å	10.8226(4)
c/ Å	10.1712(3)
α/deg	90
β/ deg	90
γ/ deg	90
U/ Å ^{3}	1159.19(7)
Z	2
μ(Mo-K$_\alpha$)/mm^{-1}	2.075
F(000)	692
Total no. reflections	5741
Unique reflections	1205
R_{int}	0.0238
No. of Parameters, restraints	67, 0
$R_1{}^b$ [$I_o>2\sigma(I_o)$]	0.0348
R_1 (all data)	0.0361
$wR_2{}^b$ [$I_o>2\sigma(I_o)$]	0.0784
wR_2 (all data)	0.0789

X-ray crystal data from Chapter 6

Compound	$[MoCl_4(NCCH_3)_2]$	$[MoCl_4(SMe_2)_2]$
Formula	$C_4H_6Cl_4MoN_2$	$C_4H_{12}Cl_4MoS_2$
Formula weight	319.85	362.00
Crystal system	Monoclinic	Orthorhombic
Space group	*C*2/*m* (No. 12)	*Pbca* (No. 61)
a/ Å	11.622(9)	10.7754(4)
b/ Å	7.507(4)	8.6531(4)
c/ Å	5.825(4)	13.0339(7)
α/deg	90	90
β/ deg	102.28(2)	90
γ/ deg	90	90
U/ Å ^{3}	496.6(6)	1215.3(1)
Z	2	4
μ(Mo-K$_\alpha$)/mm^{-1}	2.336	2.248
F(000)	308	712
Total no. reflections	5422	5273
Unique reflections	534	1195
R_{int}	0.0637	0.0325
No. of Parameters, restraints	34, 0	54, 0
R_1[b] [$I_o>2\sigma(I_o)$]	0.0231	0.0208
R_1 (all data)	0.0256	0.0270
wR_2[b] [$I_o>2\sigma(I_o)$]	0.0570	0.0439
wR_2 (all data)	0.0579	0.0457

Compound	$[MoCl_5(SMe_2)][Me_2SCH_2SMe]$	$[MoCl_4\{MeS(CH_2)_2SMe\}]$
Formula	$C_6H_{17}Cl_5MoS_3$	$C_4H_{10}Cl_4MoS_2$
Formula weight	458.57	359.98
Crystal system	Orthorhombic	Monoclinic
Space group	*Pna*2$_1$ (No. 33)	*P*2$_1$ (No. 4)[c]
a/ Å	11.1611(3)	7.1386(6)
b/ Å	23.676(1)	11.1622(6)
c/ Å	12.6813(3)	7.8033(7)
α/deg	90	90
β/ deg	90	115.91(1)
γ/ deg	90	90
U/ Å^3	3351.1(2)	559.27(9)
Z	8	2
μ(Mo-K$_\alpha$)/mm^{-1}	1.925	2.442
F(000)	1824	352
Total no. reflections	14898	5766
Unique reflections	6472	2142
R_{int}	0.0340	0.0603
No. of Parameters, restraints	281, 184	103, 1
R_1[b] [$I_o>2\sigma(I_o)$]	0.0340	0.0471
R_1 (all data)	0.0431	0.0556
wR_2[b] [$I_o>2\sigma(I_o)$]	0.0700	0.1177
wR_2 (all data)	0.0735	0.1223

[c]Flack parameter = -0.13(16).

Compound	$[MoCl_4\{^iPrMeS(CH_2)_2S^iPr\}]$	$[MoCl_4\{MeS(CH_2)_3SMe\}]$
Formula	$C_8H_{18}Cl_4MoS_2$	$C_5H_{12}Cl_4MoS_2$
Formula weight	416.08	374.01
Crystal system	Monoclinic	Triclinic
Space group	$P2_1/c$ (No. 14)	P-1 (No. 2)
a/ Å	8.6773(2)	6.9578(3)
b/ Å	9.1092(2)	7.3230(2)
c/ Å	19.7049(4)	12.5840(5)
α/deg	90	77.457(3)
β/ deg	98.465(2)	81.727(3)
γ/ deg	90	72.082(3)
U/ Å ^{3}	1504.57(6)	593.49(4)
Z	4	2
μ(Mo-K$_\alpha$)/mm^{-1}	1.786	2.305
F(000)	832	368
Total no. reflections	12891	12279
Unique reflections	3018	2335
R_{int}	0.0215	0.0223
No. of Parameters, restraints	140, 0	111, 0
$R_1{}^b$ [$I_o>2\sigma(I_o)$]	0.0256	0.0194
R_1 (all data)	0.0259	0.0218
$wR_2{}^b$ [$I_o>2\sigma(I_o)$]	0.0575	0.0516
wR_2 (all data)	0.0577	0.0528

Compound	$[Me_2TeCl_2]$
Formula	$C_2H_6Cl_2Te$
Formula weight	228.57
Crystal system	Monoclinic
Space group	$P2_1/c$ (No. 14)
a/ Å	9.4821(3)
b/ Å	6.1123(2)
c/ Å	11.0931(4)
α/deg	90
β/ deg	98.365(3)
γ/ deg	90
U/ Å ^{3}	636.09(4)
Z	4
μ(Mo-K_α)/mm^{-1}	5.372
F(000)	416
Total no. reflections	5280
Unique reflections	1259
R_{int}	0.0226
No. of Parameters, restraints	48, 0
R_1[b] [$I_o>2\sigma(I_o)$]	0.0258
R_1 (all data)	0.0283
wR_2[b] [$I_o>2\sigma(I_o)$]	0.0653
wR_2 (all data)	0.0669

Appendix 3: **Thermogravimetric Analysis data**

TGA data from Chapter 4

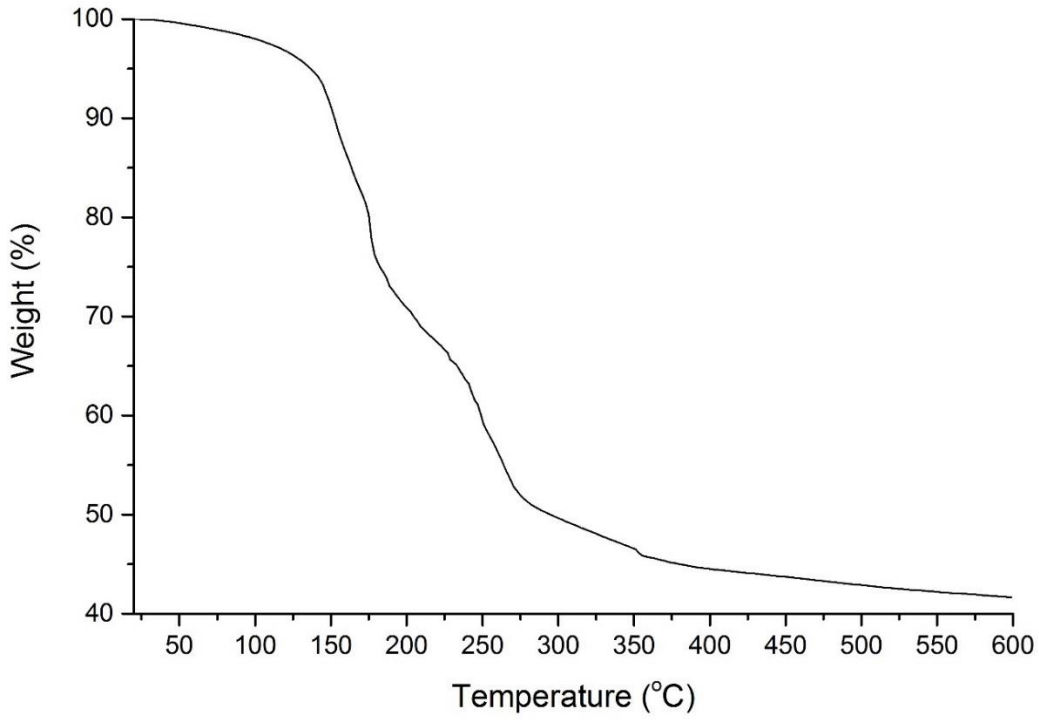

Figure A3.1 TGA profile of [$NbSCl_3(S^nBu_2)$].

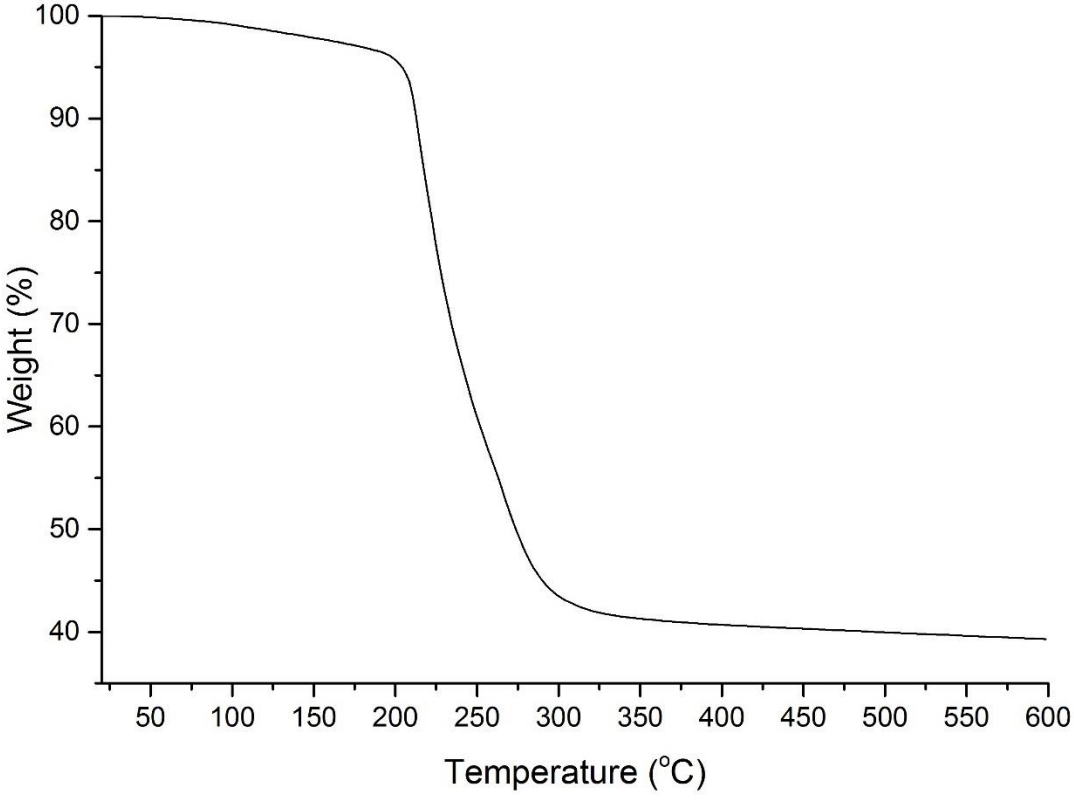

Figure A3.2 TGA profile of [$NbSCl_3\{^nBuS(CH_2)_3S^nBu\}$].

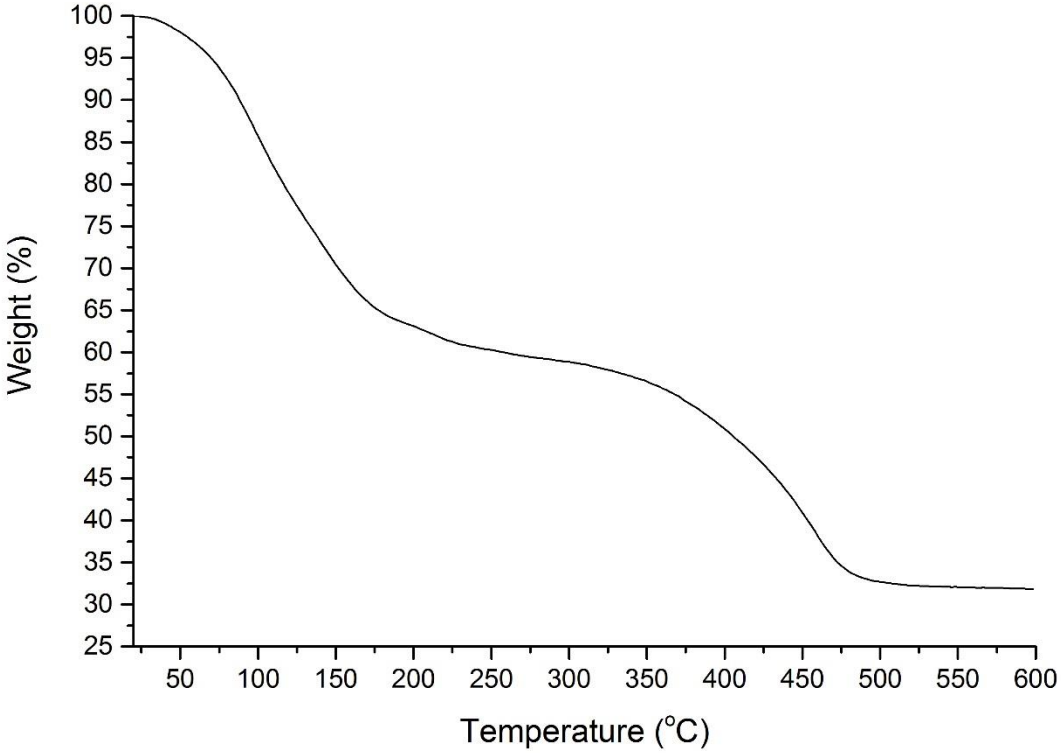

Figure A3.3 TGA profile of [$NbSe_2Cl_3(Se^nBu_2)$].

TGA data from Chapter 5

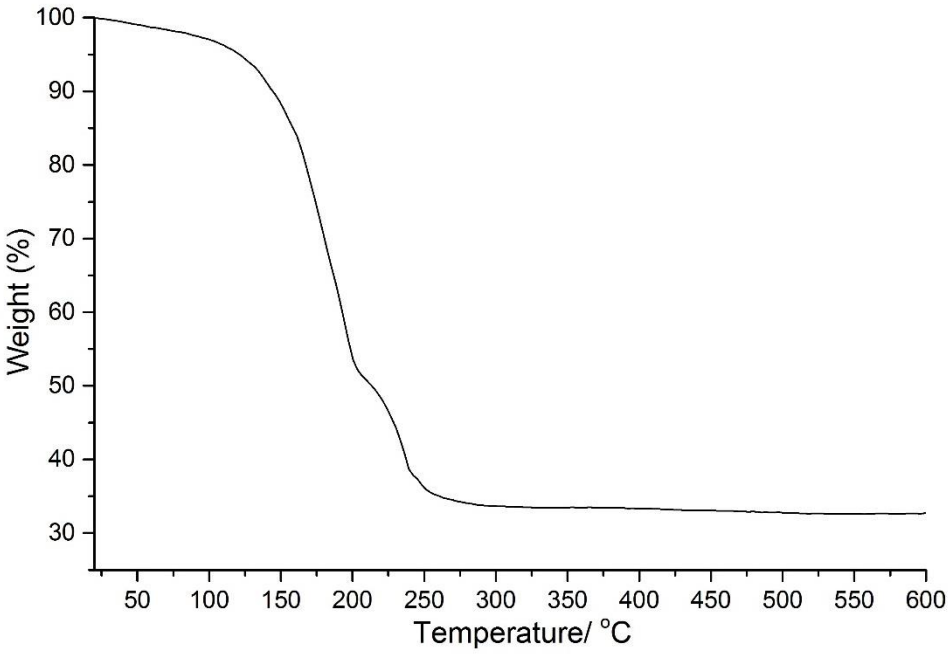

Figure A3.4 TGA profile of [$NbCl_5(S^nBu_2)$].

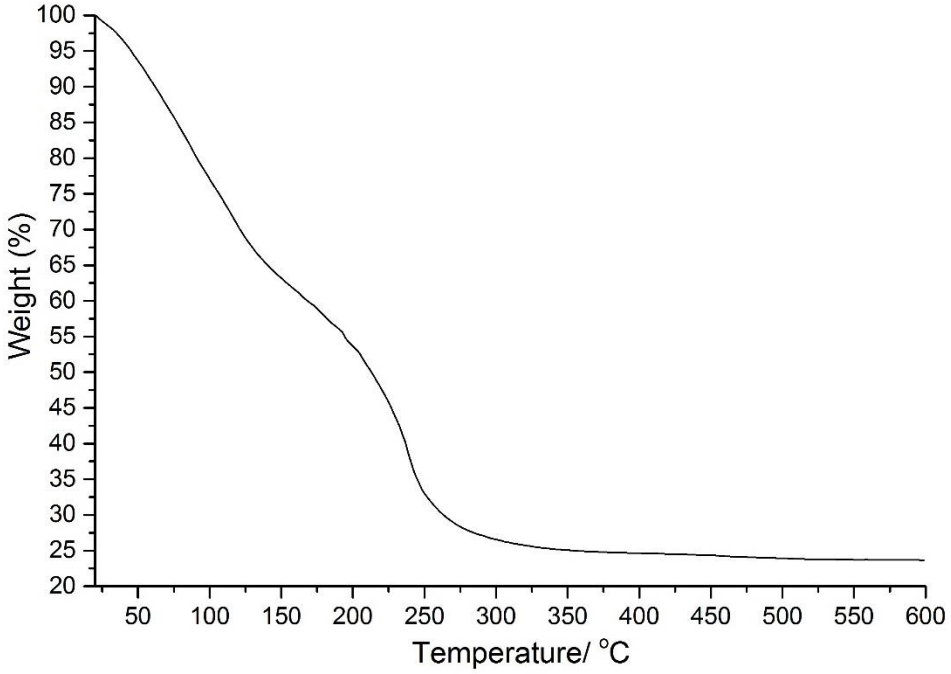

Figure A3.5 TGA profile of [$NbBr_5(S^nBu_2)$].

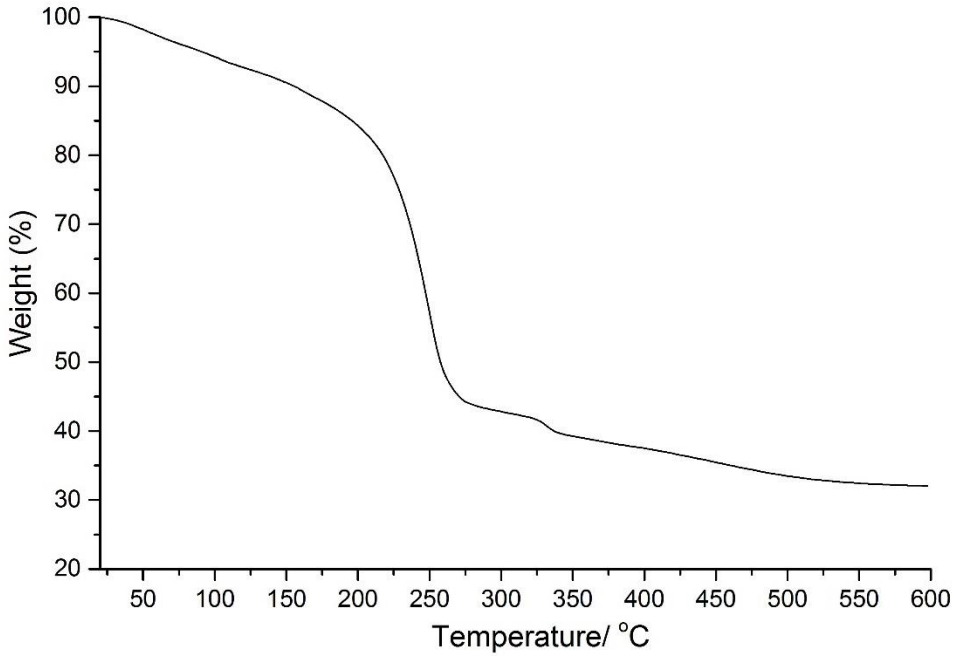

Figure A3.6 TGA profile of [$NbCl_5(Se^nBu_2)$].

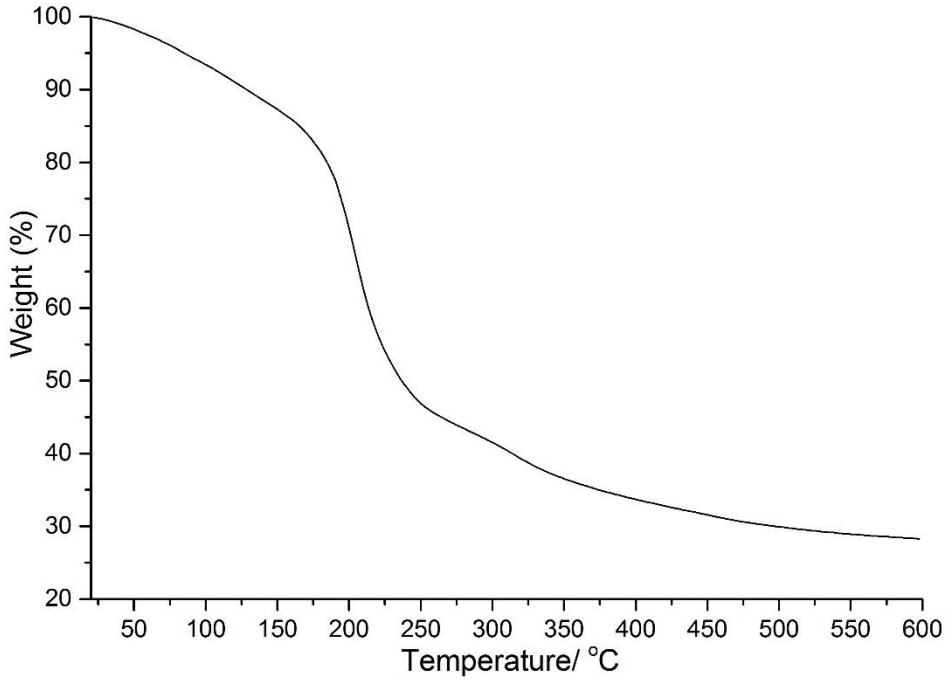

Figure A3.7 TGA profile of [$NbBr_5(Se^nBu_2)$].

Table A3.1 TGA data for precursors in Chapter 5

Complexes	Onset Temperature (℃)	Step End Temperature (℃)	Remaining weight (wt%)
$[NbCl_5(S^nBu_2)]$ (Step 1)	*ca.* 100	*ca.* 200	34.1
$[NbCl_5(S^nBu_2)]$ (Step 2)	*ca.* 200	*ca.* 270	33.7
$[NbBr_5(S^nBu_2)]$ (Step 1)	RT	*ca.* 160	61.4
$[NbBr_5(S^nBu_2)]$ (Step 2)	*ca.* 160	*ca.* 300	26.5
$[NbCl_5(Se^nBu_2)]$ (Step 1)	*ca.* 170	*ca.* 270	43.3
$[NbCl_5(Se^nBu_2)]$ (Step 2)	*ca.* 315	*ca.* 330	39.2
$[NbBr_5(Se^nBu_2)]$ (Step 1)	*ca.* 125	*ca.* 250	44.4
$[NbBr_5(Se^nBu_2)]$ (Step 2)	*ca.* 275	*ca.* 350	33.6
$[TaCl_5(Se^nBu_2)]$	*ca.* RT	*ca.* 325	50.3
$[TaBr_5(Se^nBu_2)]$	*ca.* RT	*ca.* 250	51.3

NbS_2 expected weight loss from precursor: 35.0 % ($[NbCl_5(S^nBu_2)]$); 23.4 % ($[NbBr_5(S^nBu_2)]$).

$NbSe_2$ expected weight loss from precursor: 46.2.0 % ($[NbCl_5(Se^nBu_2)]$); 32.8 % ($[NbBr_5(Se^nBu_2)]$).

Appendix 4: Scanning Electron Microscopy and Energy-dispersive X-ray spectroscopy

SEM and EDX data from Chapter 5

LPCVD precursor [$NbCl_5(Se^nBu_2)$]

The SEM and EDX results of 3R-$NbSe_2$ films obtained from [$NbCl_5(Se^nBu_2)$] at 650 °C are published in *Dalton Trans.*, 2014, **43**, 16640.

$NbSe_2$ film obtained at 550 °C

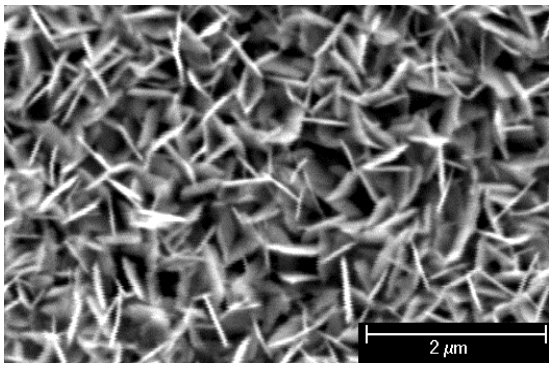

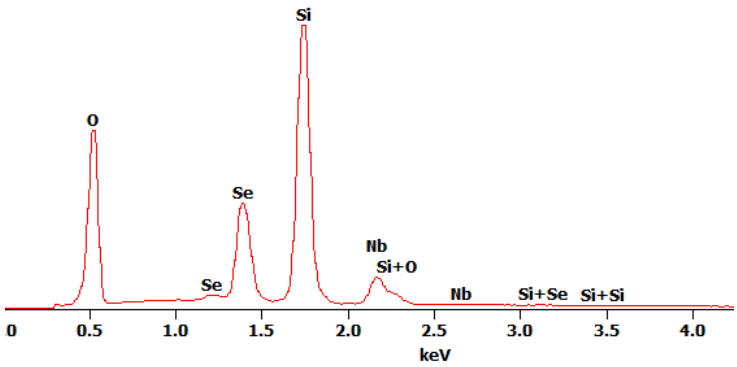

Elements	Atom %
Nb	31.1
Se	68.9

Figure A4.1 (top) SEM images and (bottom) EDX spectrum with accelerating voltage 10 keV.

$NbSe_2$ film obtained at 600 °C

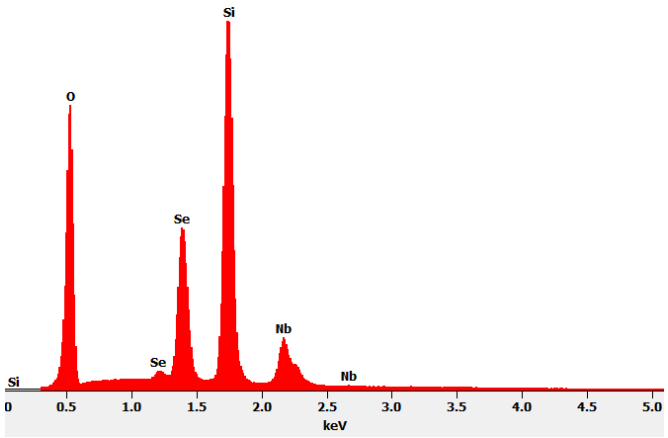

Elements	Atom %
Nb	32.9
Se	67.1

Figure A4.2 EDX spectrum with accelerating voltage 10 keV.

LPCVD precursor using [$NbBr_5(Se^nBu_2)$]

$NbSe_2$ film obtained at 550 °C

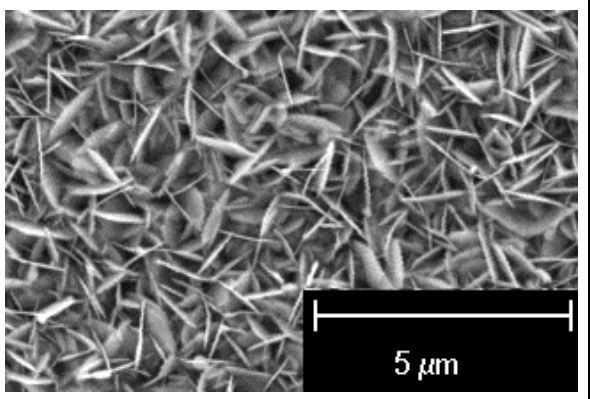

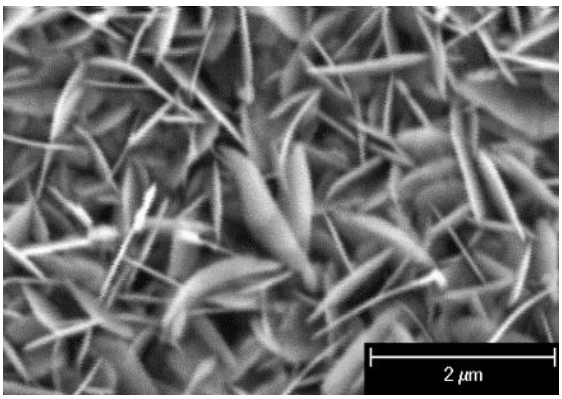

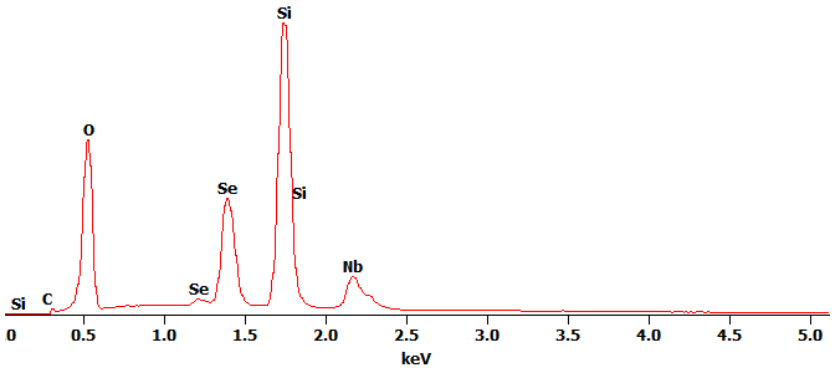

Elements	Atom %
Nb	33.7
Se	66.3

Figure A4.3 (top) SEM images and (bottom) EDX spectrum with accelerating voltage 10 keV.

$NbSe_2$ film obtained at 600 °C

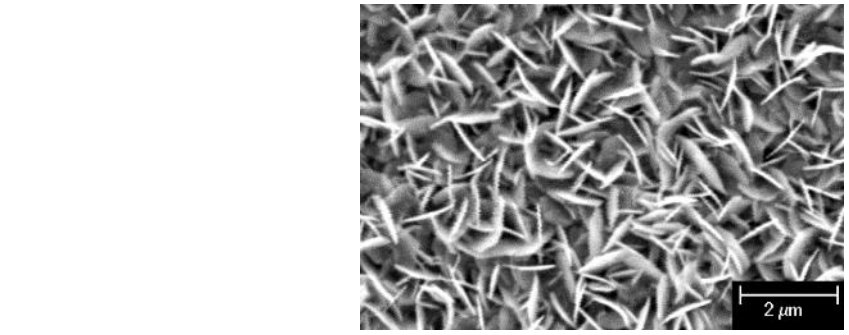

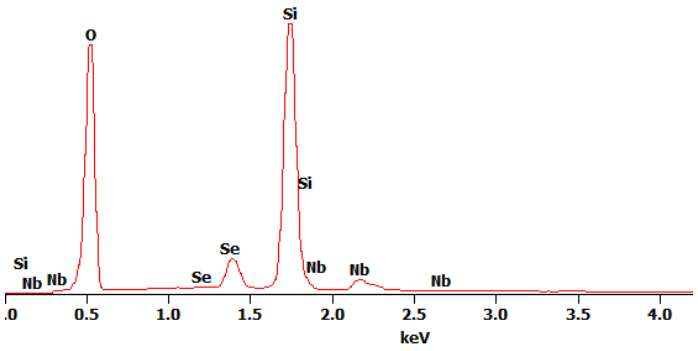

Elements	Atom %
Nb	33.5
Se	66.5

Figure A4.4 (top) SEM images and (bottom) EDX spectrum with accelerating voltage 10 keV.

$NbSe_2$ film obtained at 650 °C

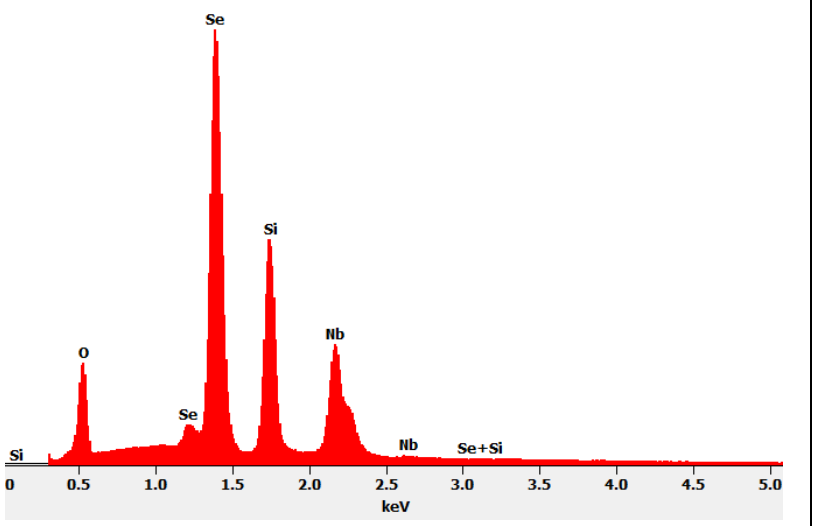

Elements	Atom %
Nb	32.8
Se	67.2

Figure A4.5 EDX spectrum with accelerating voltage 10 keV.

SEM/EDX result in Chapter 6

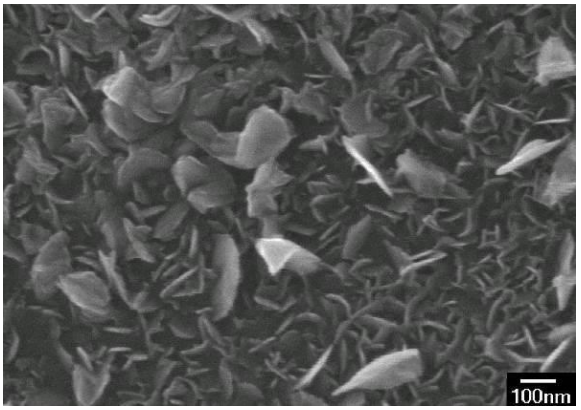

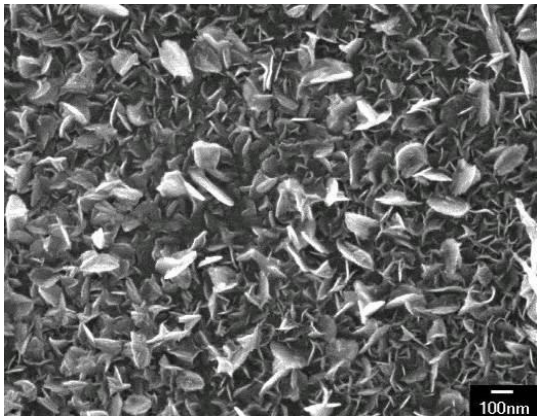

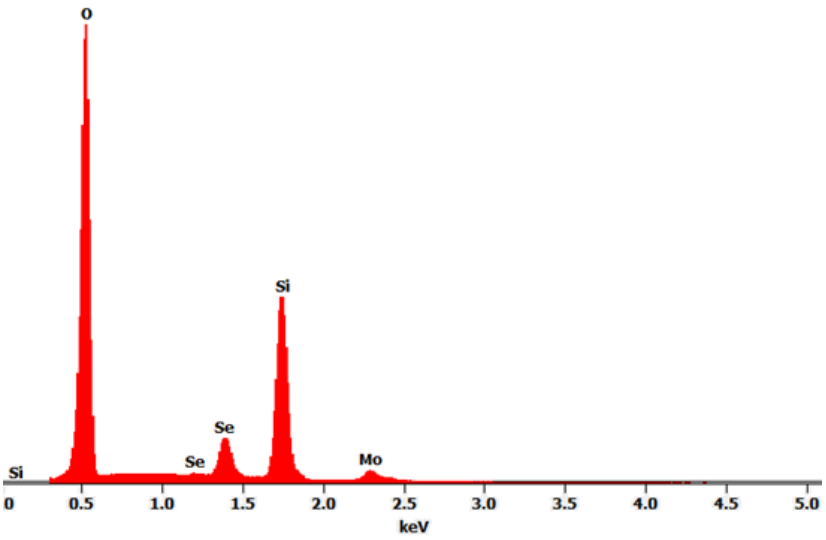

Elements	Atom %
Mo	33.13
Se	66.87

Figure A4.6 (top) SEM images and (bottom) EDX spectrum with accelerating voltage 5 kV.

Appendix 5: **The preparation of [$NbOCl_3(SMe_2)$]**

[$NbOCl_3(SMe_2)$]

$NbCl_5$ (135 mg, 0.5 mmol) was placed in a Schlenk tube before a solution of CH_2Cl_2 (8 mL) and excess of Me_2S (1 mL) added with stirring. A dark red solution formed immediately. A solution of $O(SiMe_3)_2$ (87 mg, 0.5 mmol) and CH_2Cl_2 (*ca*. 2 mL) was added. The solution was heated to 40 ^oC and stirring for *ca.* 10 minutes. The dark red solution slowly turned to yellow. The solution was then dried in *vacuo* to afford a green yellow powder left. Yield: 79 mg, 57%. Required for $C_2H_6Cl_3NbOS$ (277.40): C, 8.66; H, 2.18. Found: C, 8.84; H, 2.03. IR (Nujol, cm^{-1}): 840, 807, 381, 362, 347. ^1H NMR ($CDCl_3$, 295K): $\delta = 2.37$ (s, SMe_2).

Appendix 6: **Infrared Spectra of complexes in each chapters**

Chapter 2

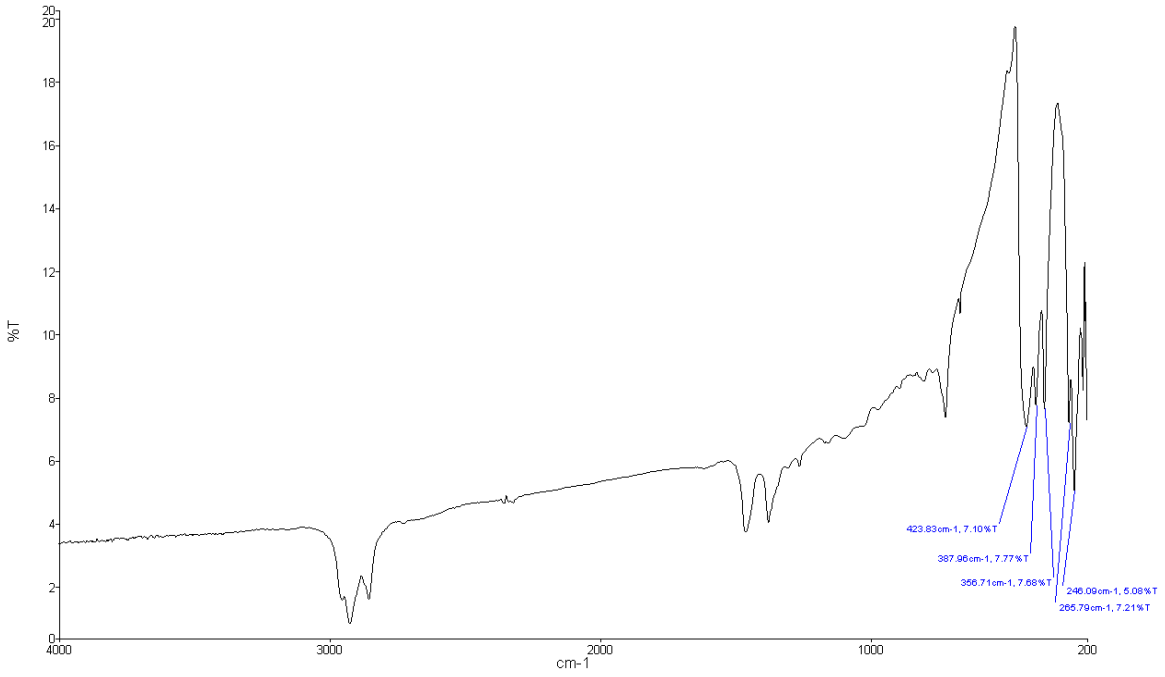

Figure A6.1 IR spectrum of $NbCl_4$

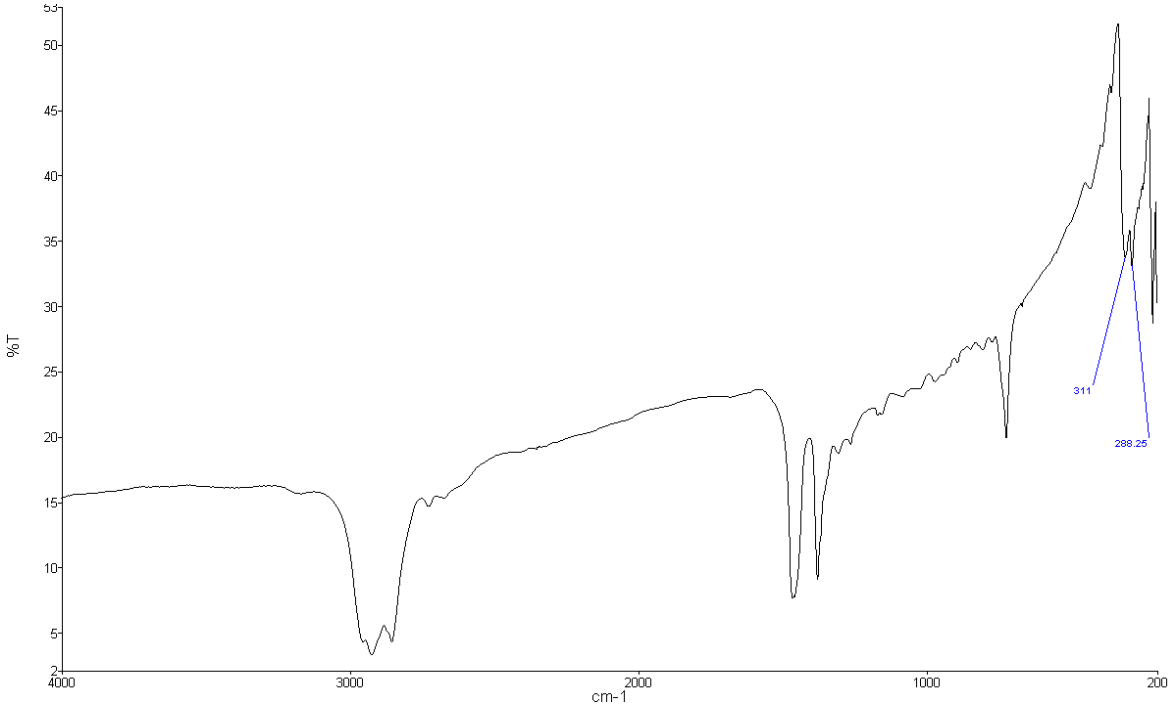

Figure A6.2 IR spectrum of $NbBr_4$

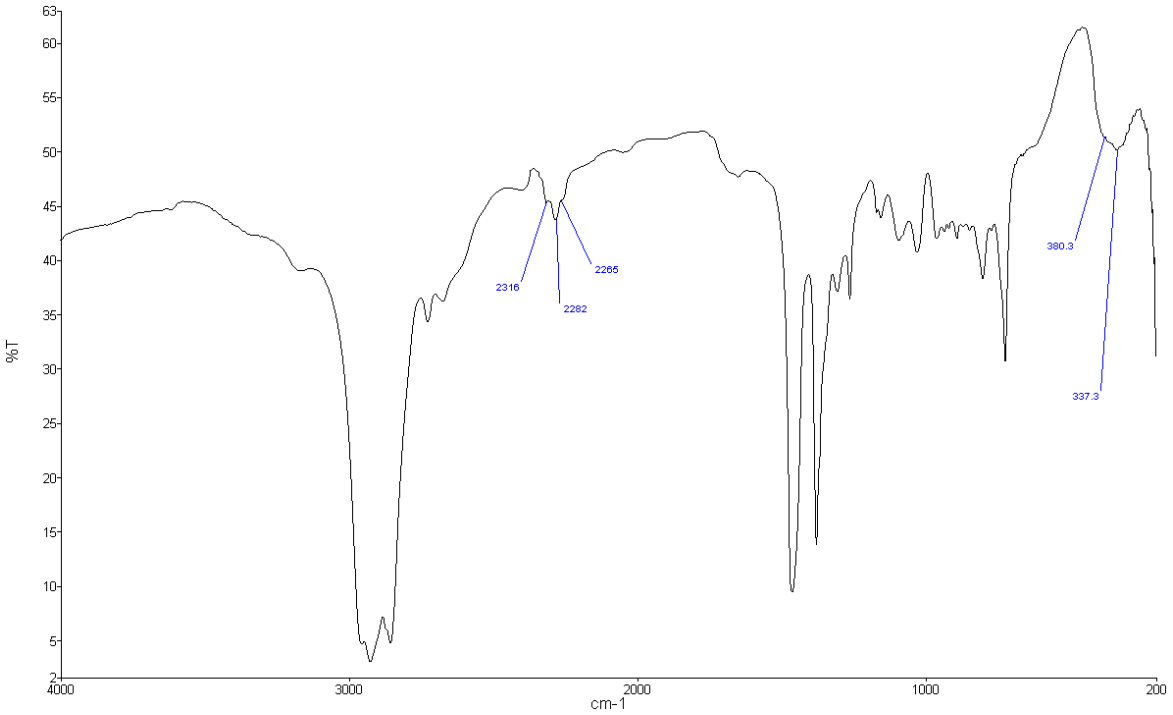

Figure A6.3 IR spectrum of $[NbCl_4(NCCH_3)_2]$

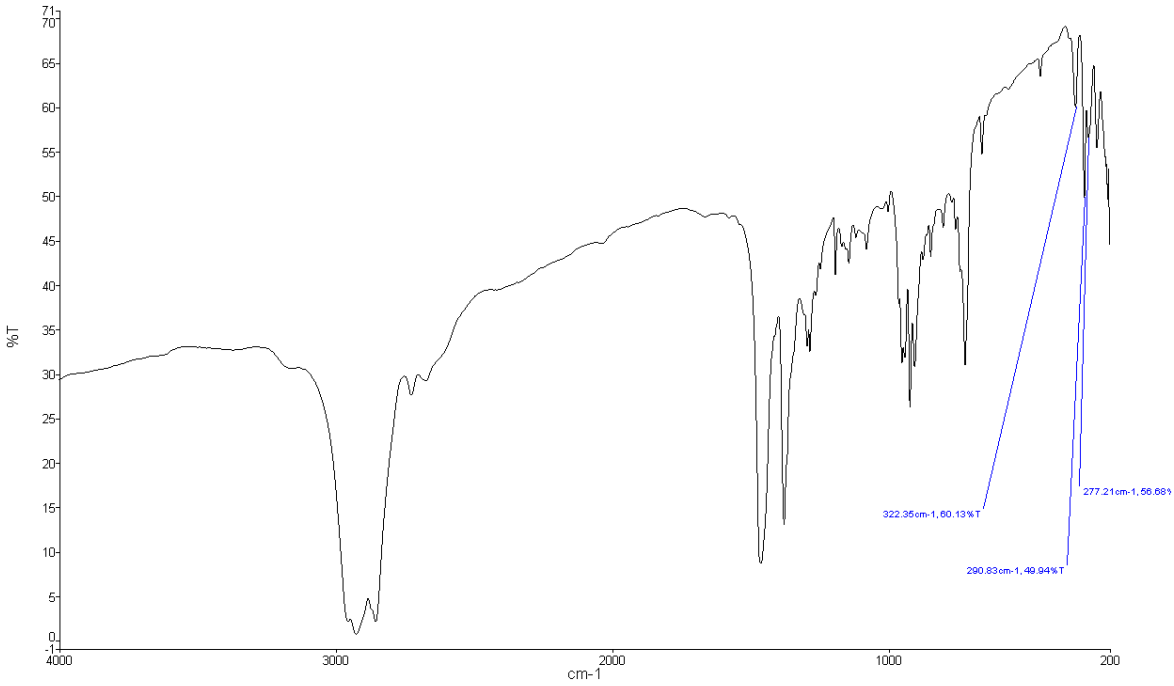

Figure A6.4 IR spectrum of $[NbCl_4\{MeP(CH_2)_2PMe\}_2]$

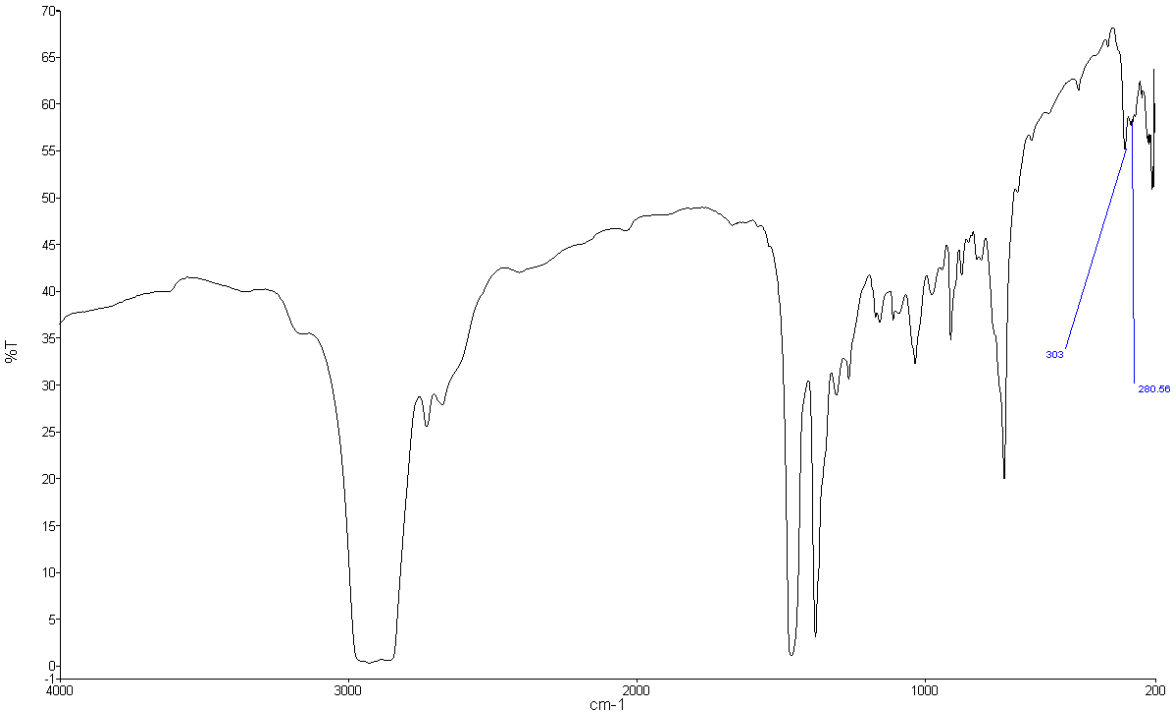

Figure A6.5 IR spectrum of $[NbCl_4\{EtP(CH_2)_2PEt\}_2]$

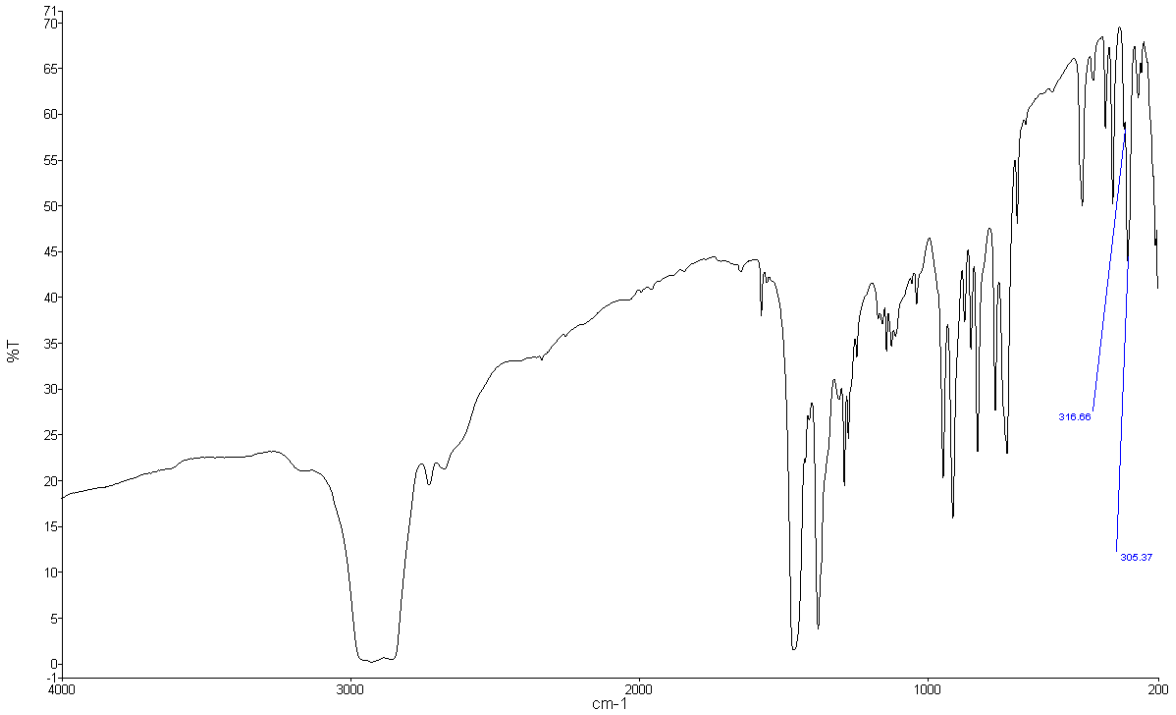

Figure A6.6 IR spectrum of $[NbCl_4\{o\text{-}C_6H_4(PMe_2)_2\}_2]$

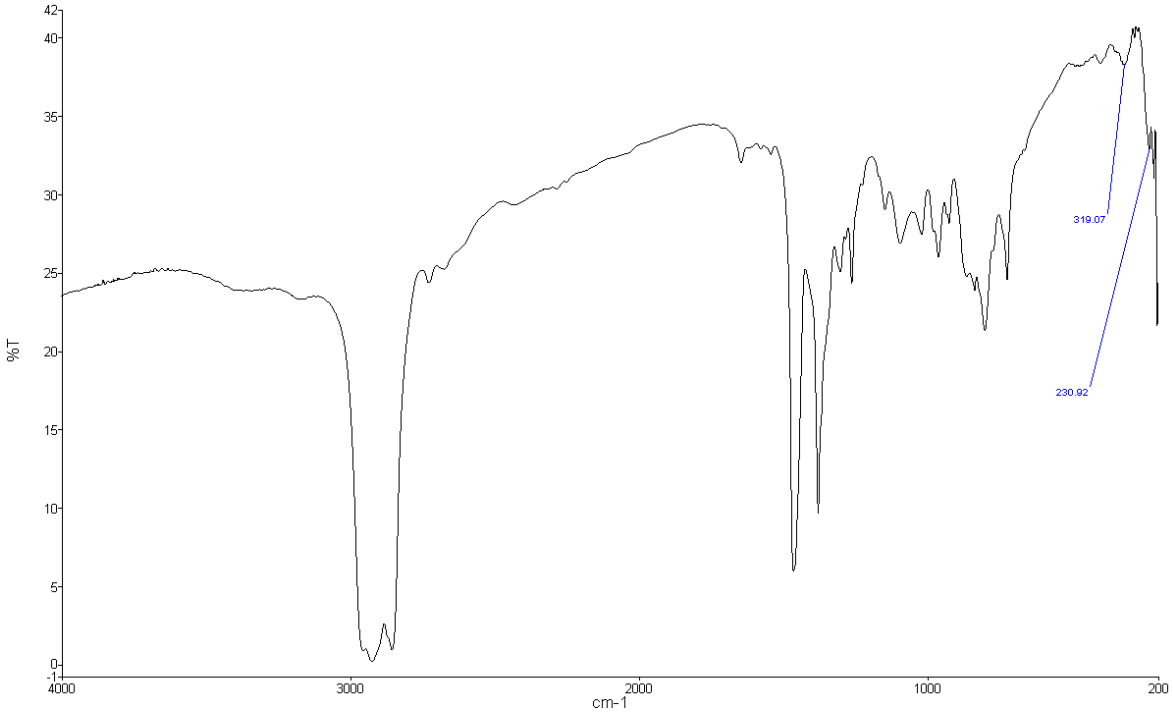

Figure A6.7 IR spectrum of [$NbBr_4${$MeP(CH_2)_2PMe$}$_2$]

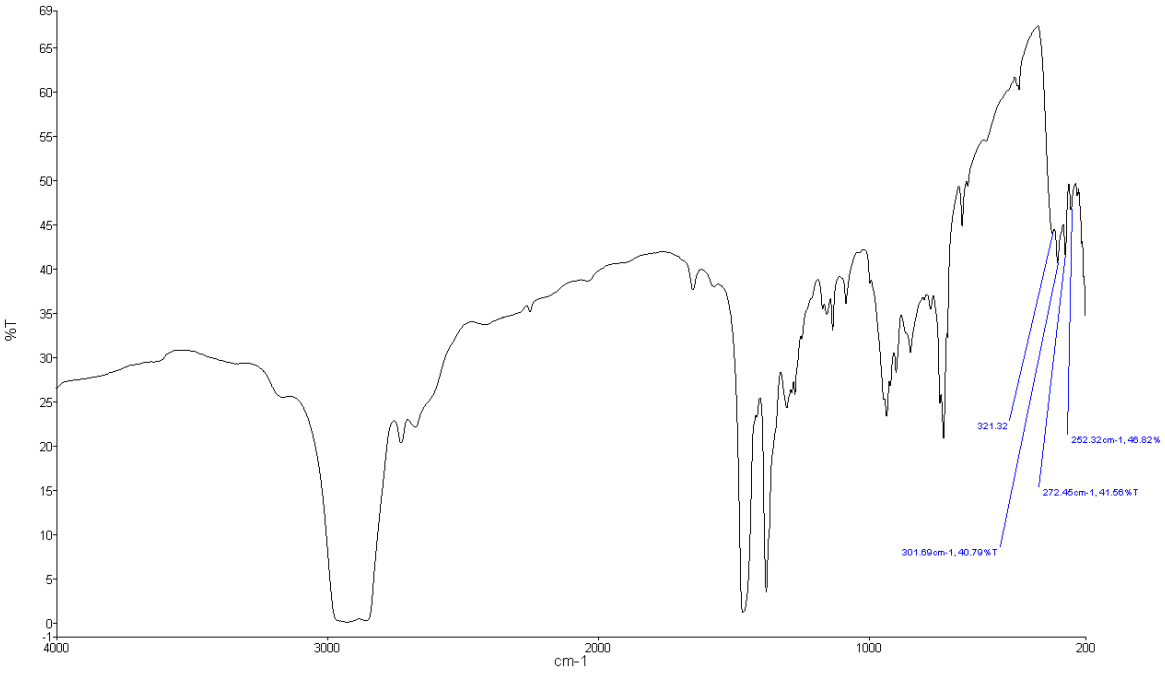

Figure A6.8 IR spectrum of [$NbCl_4${$MeP(CH_2)_2PMe$}]

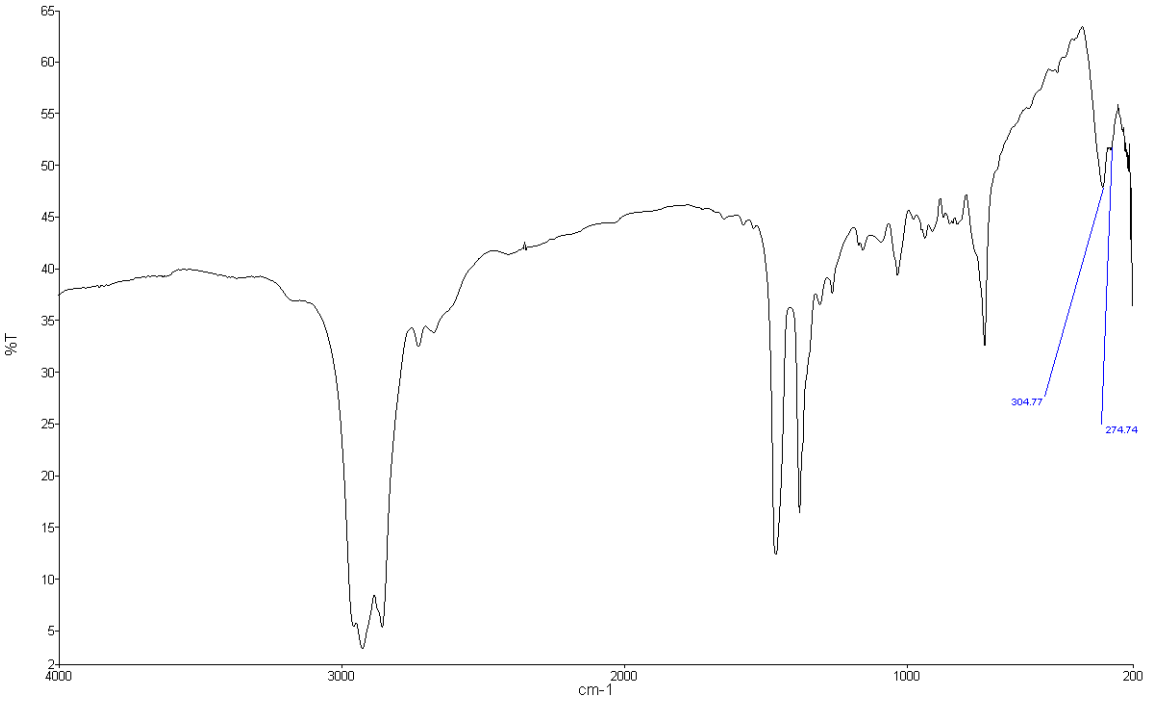

Figure A6.9 IR spectrum of [$NbCl_4${$EtP(CH_2)_2PEt$}]

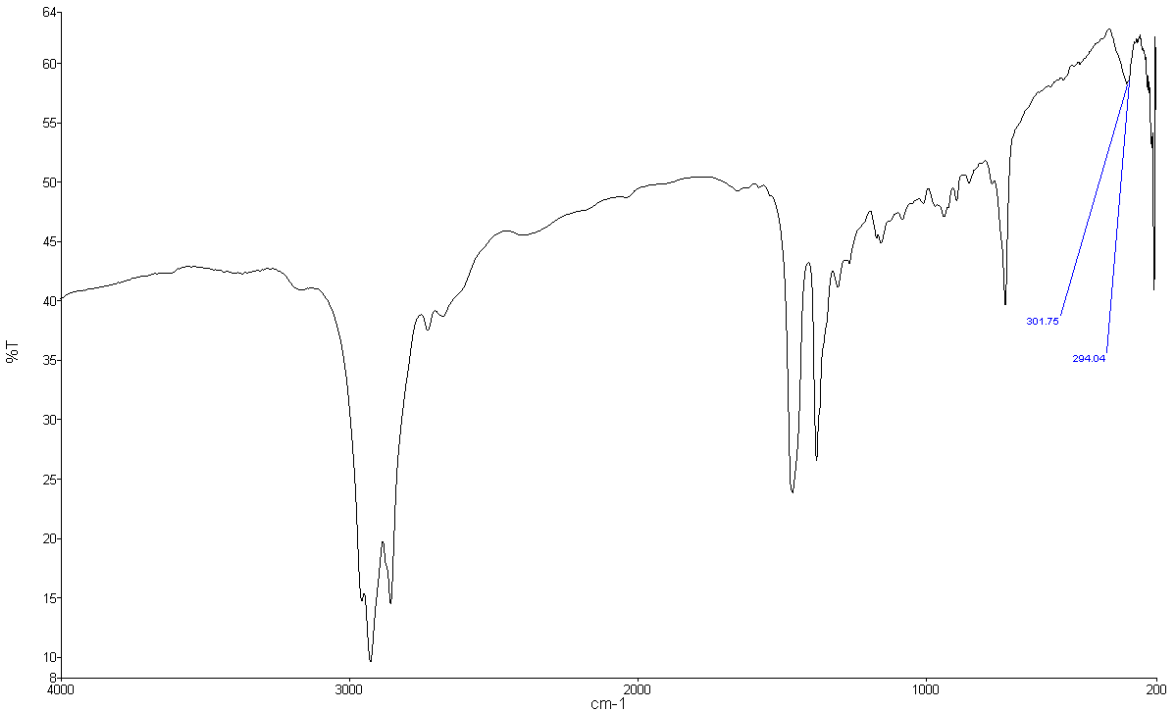

Figure A6.10 IR spectrum of [$NbCl_4${$CyP(CH_2)_2PCy$}]

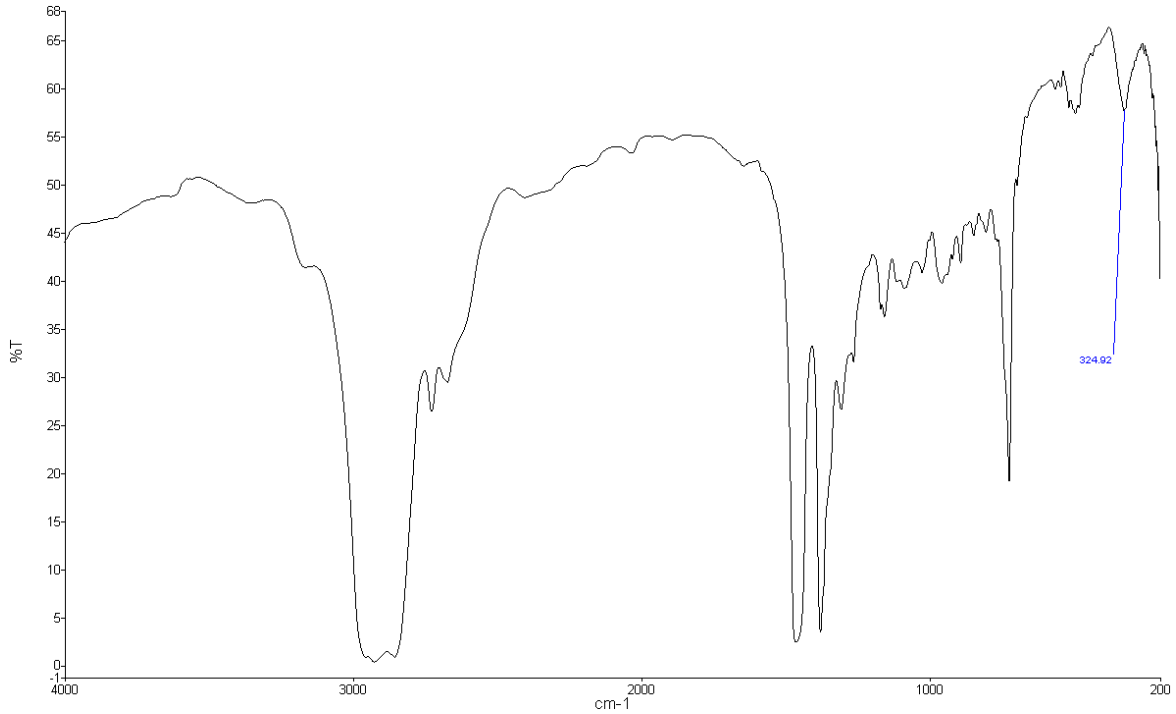

Figure A6.11 IR spectrum of [$NbCl_4${*o*-$C_6H_4(PPh_2)_2$}]

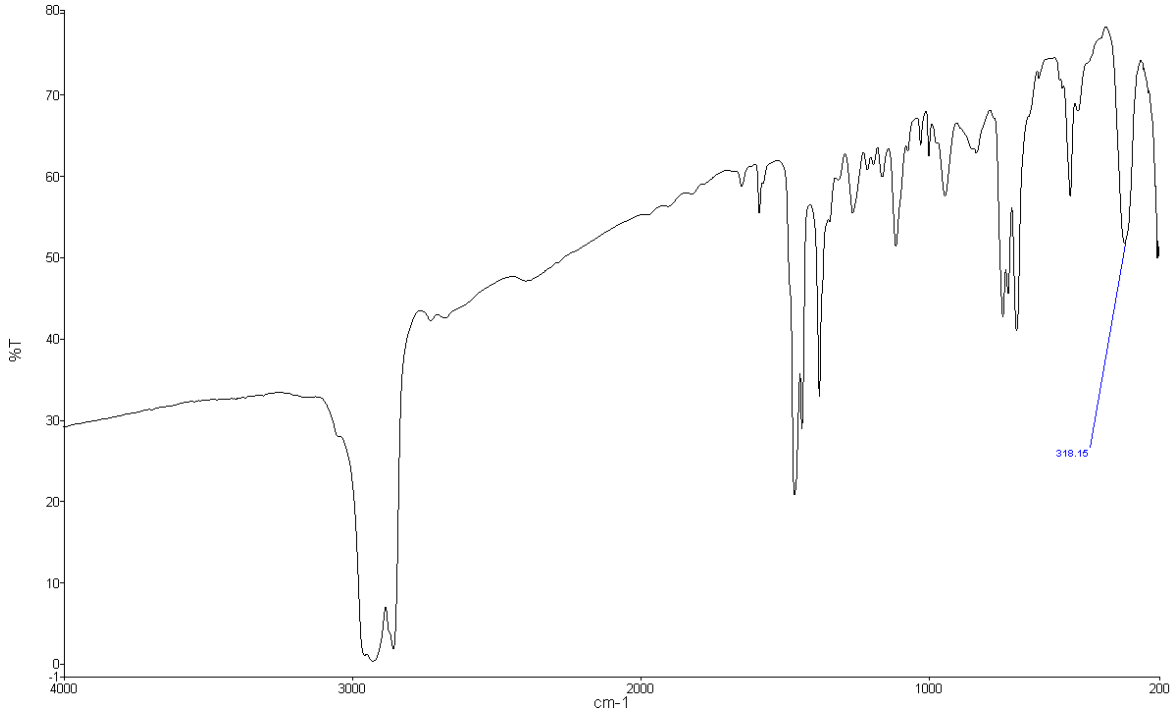

Figure A6.12 IR spectrum of [$NbCl_4${$PhP(CH_2)_3PPh$}]

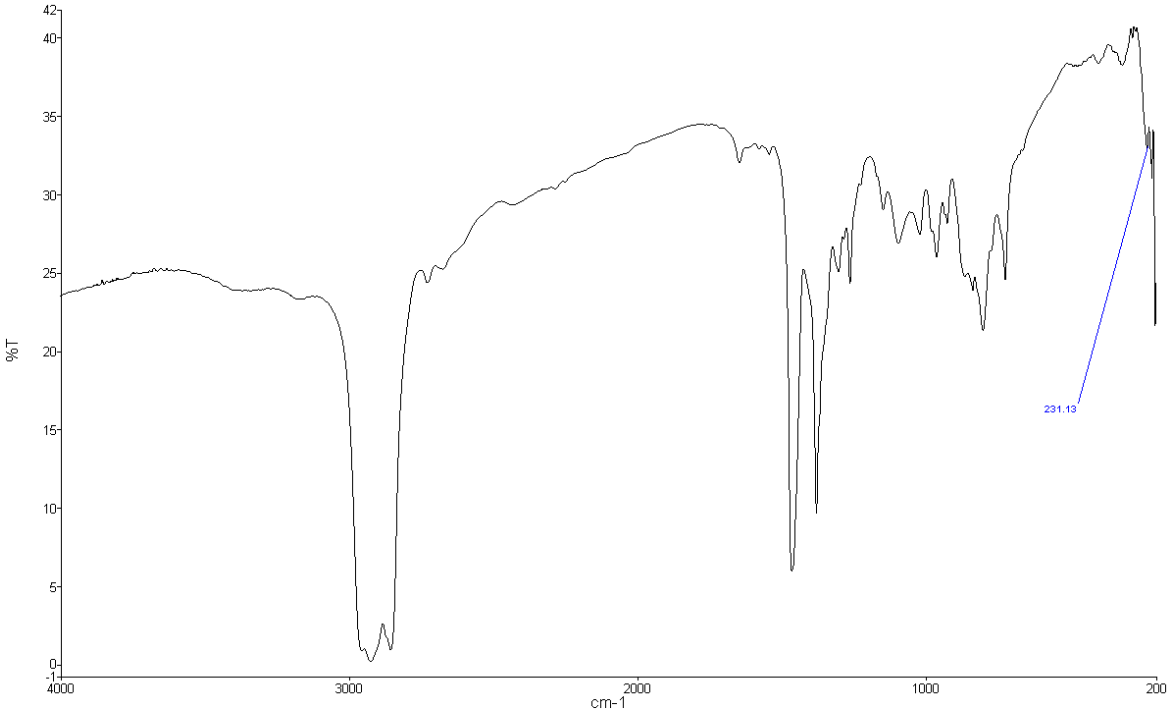

Figure A6.13 IR spectrum of [$NbBr_4${$MeP(CH_2)_2PMe$}]

Chapter 3

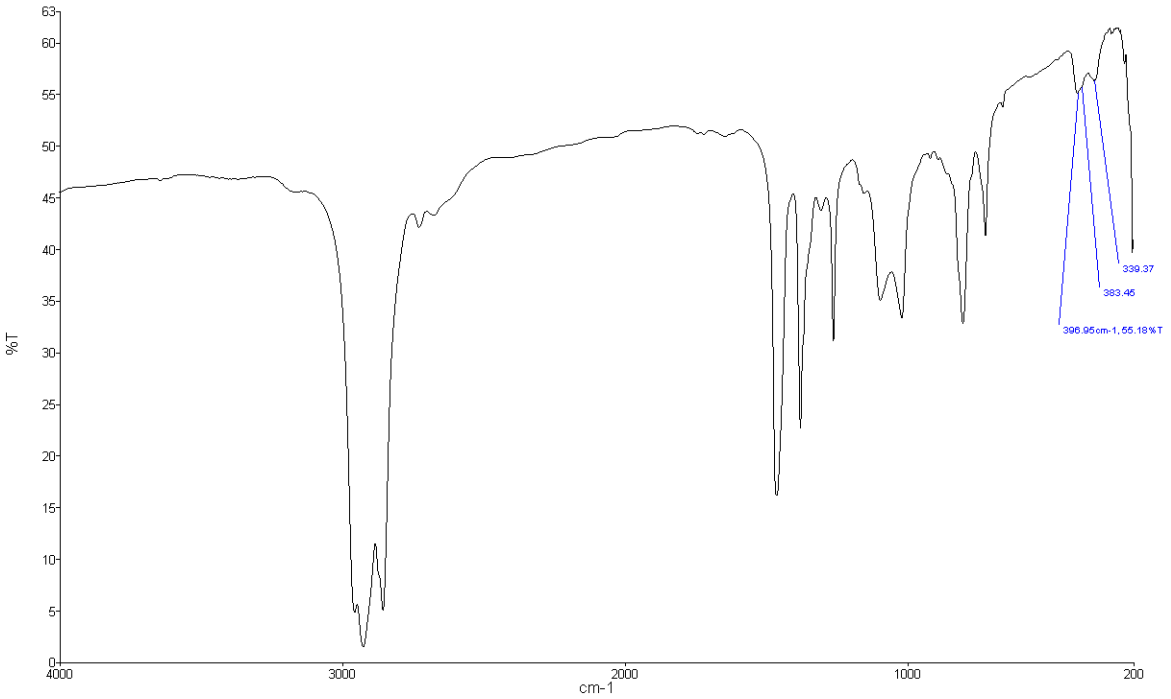

Figure A6.14 IR spectrum of $[Nb_2Cl_4(THF)_2(\mu\text{-}Cl)_2(\mu\text{-}SMe_2)]$

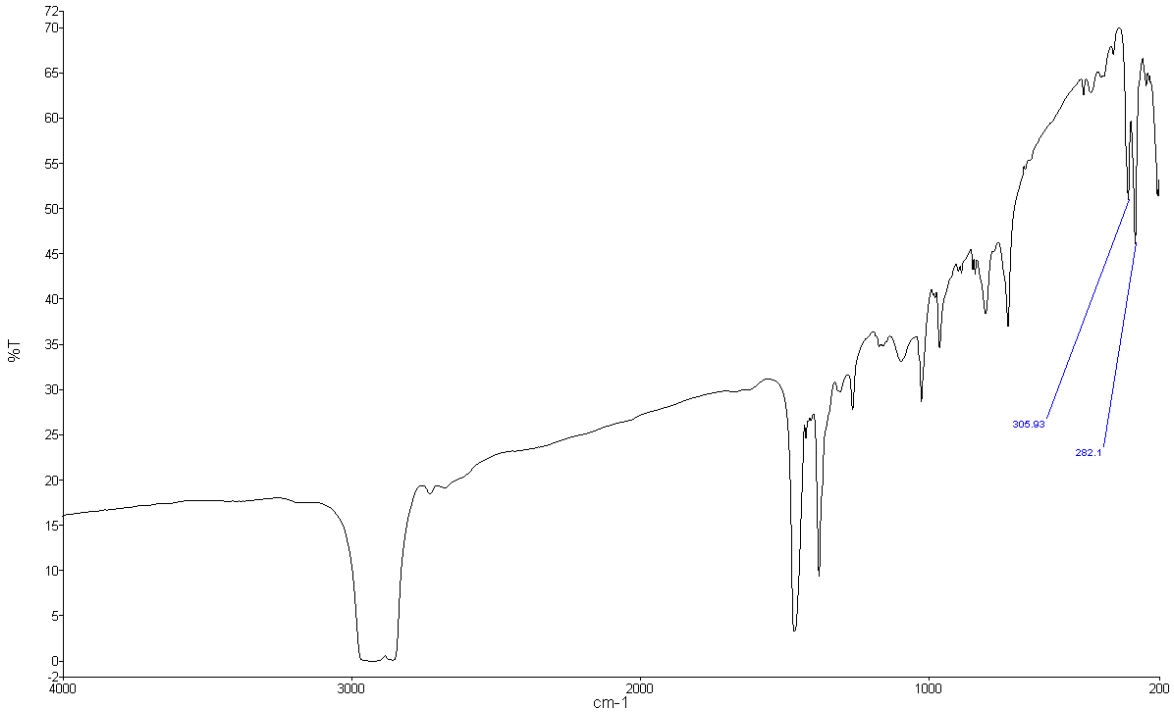

Figure A6.15 IR spectrum of $[NbCl_4\{MeS(CH_2)_2SMe\}_2]$

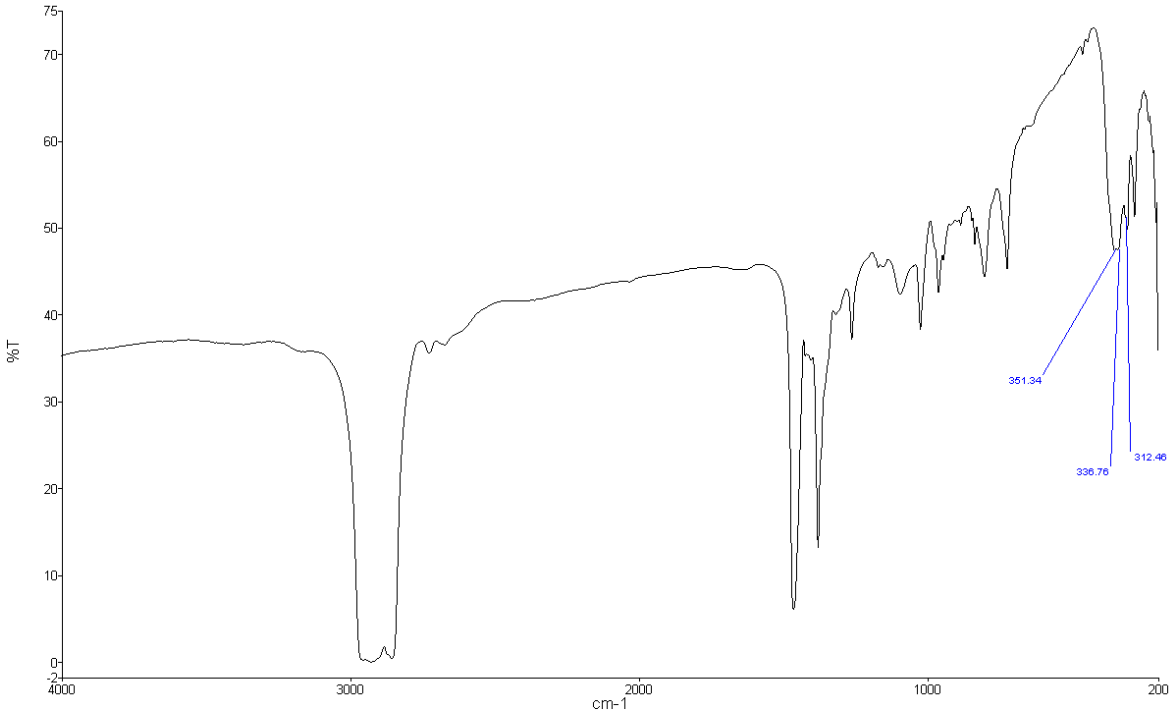

Figure A6.16 IR spectrum of $[NbCl_4\{MeS(CH_2)_2SMe\}]$

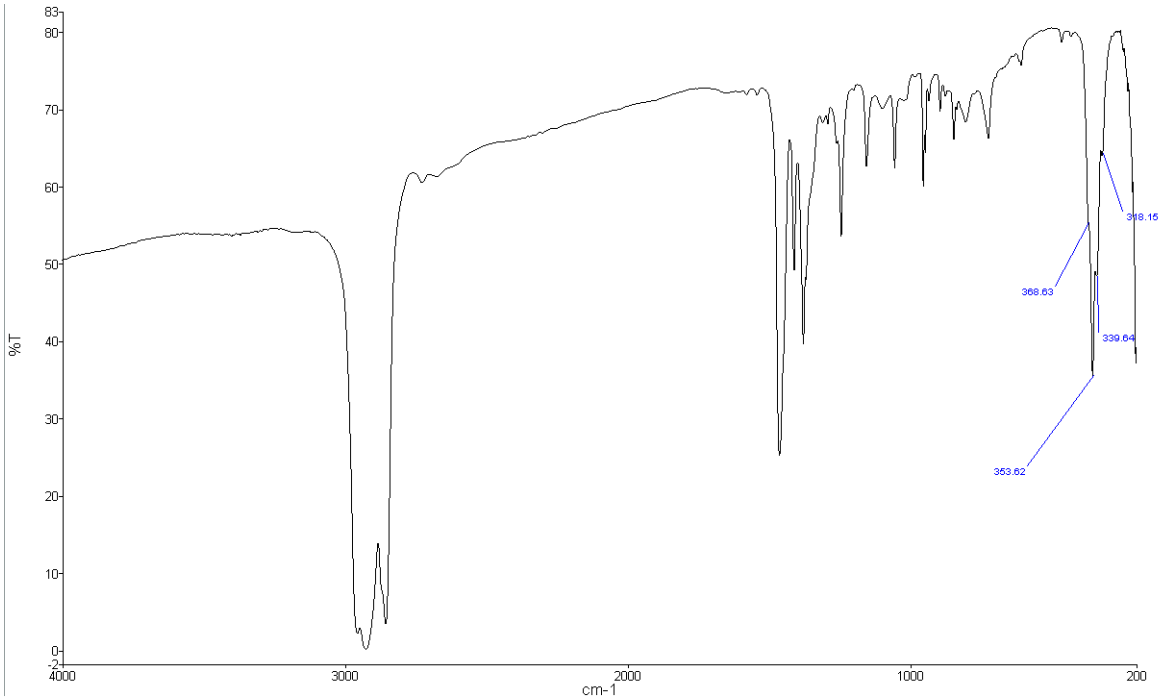

Figure A6.17 IR spectrum of $[NbCl_4\{^{i}PrS(CH_2)_2S^{i}Pr\}]$

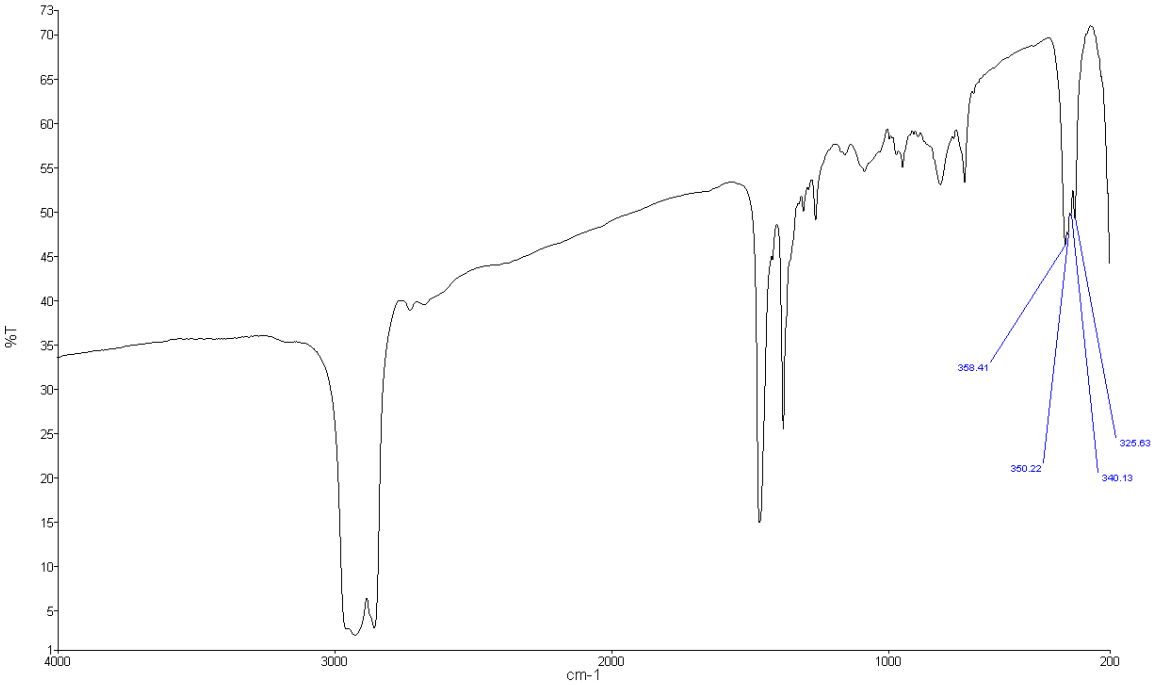

Figure A6.18 IR spectrum of [$NbCl_4${$MeS(CH_2)_3SMe$}]

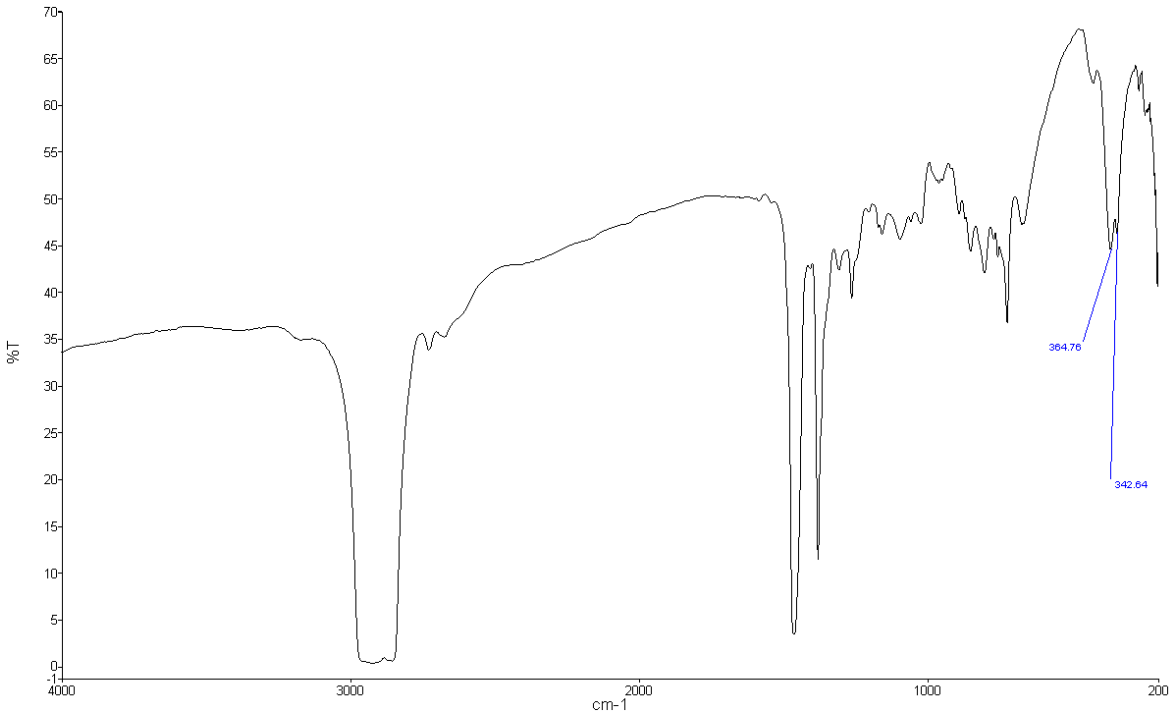

Figure A6.19 IR spectrum of [$NbCl_4${o-$C_6H_4(CH_2SEt)_2$}]

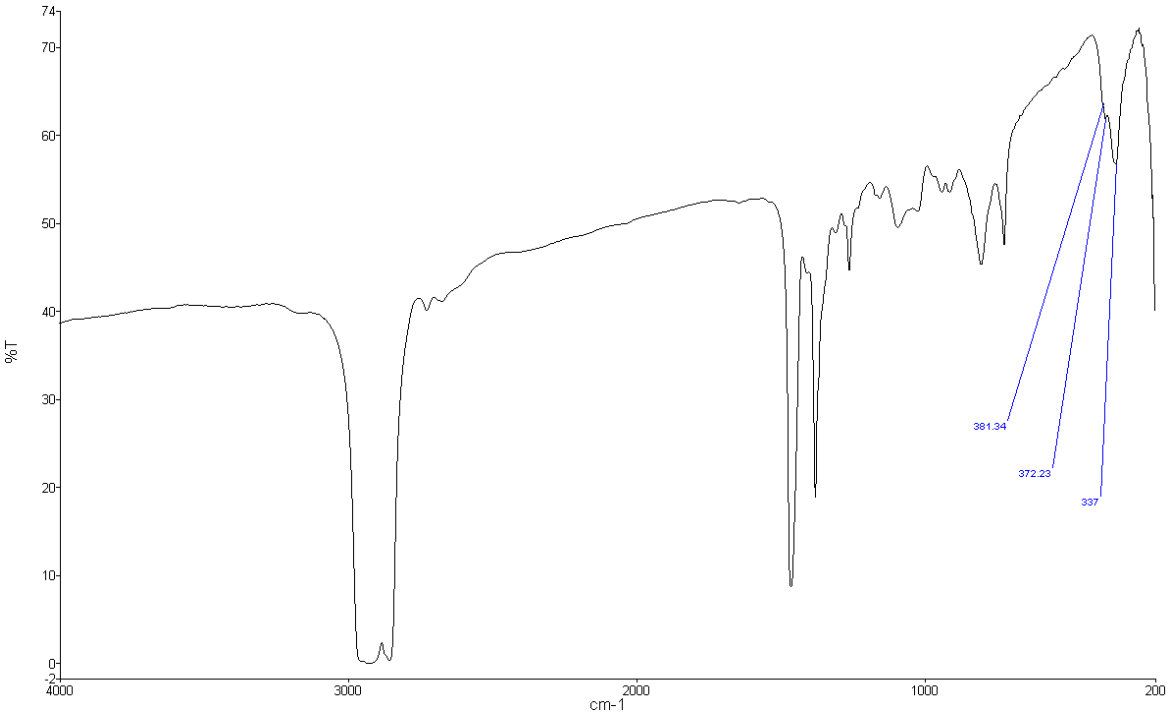

Figure A6.20 IR spectrum of [$NbCl_4${$MeSe(CH_2)_2SeMe$}]

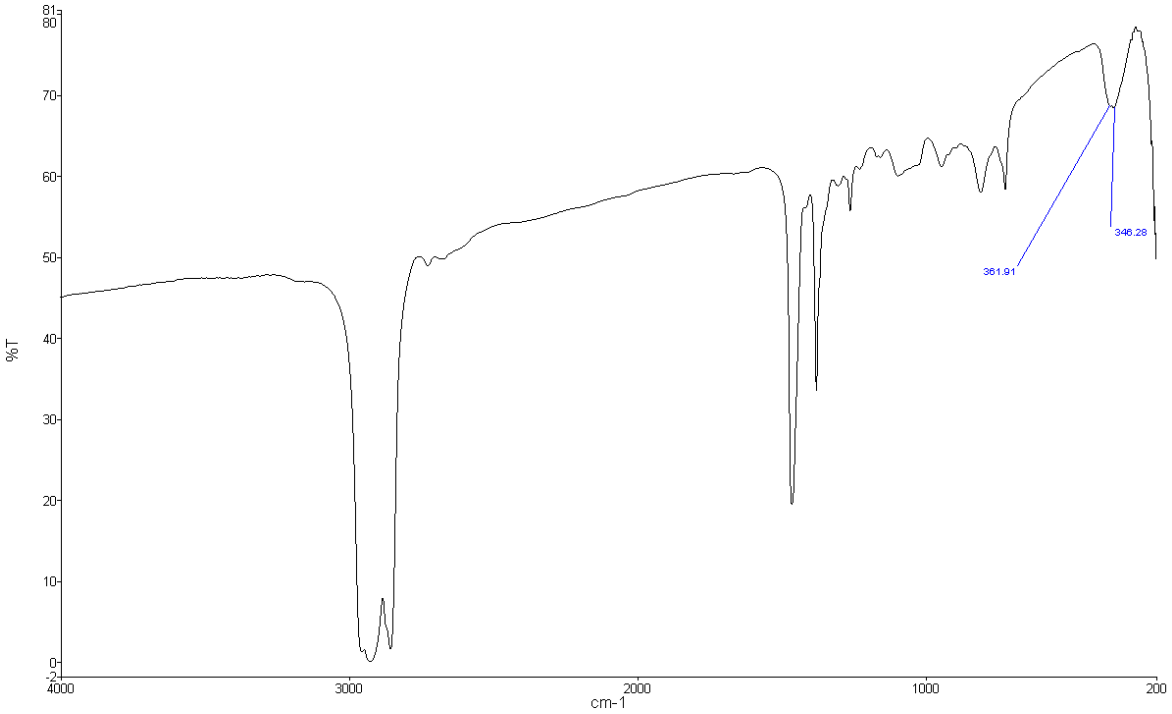

Figure A6.21 IR spectrum of [$NbCl_4${$MeSe(CH_2)_3SeMe$}]

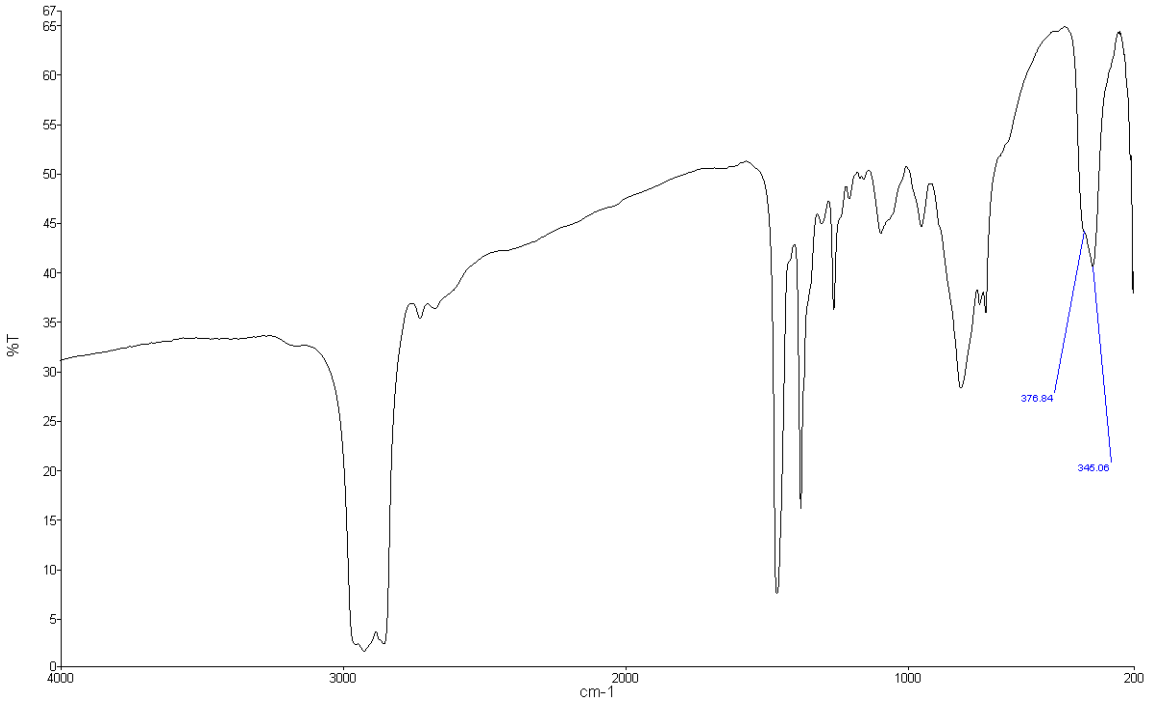

Figure A6.22 IR spectrum of [$NbCl_4$\{^{n}BuSe$(CH_2)_3$Se^{n}Bu\}]

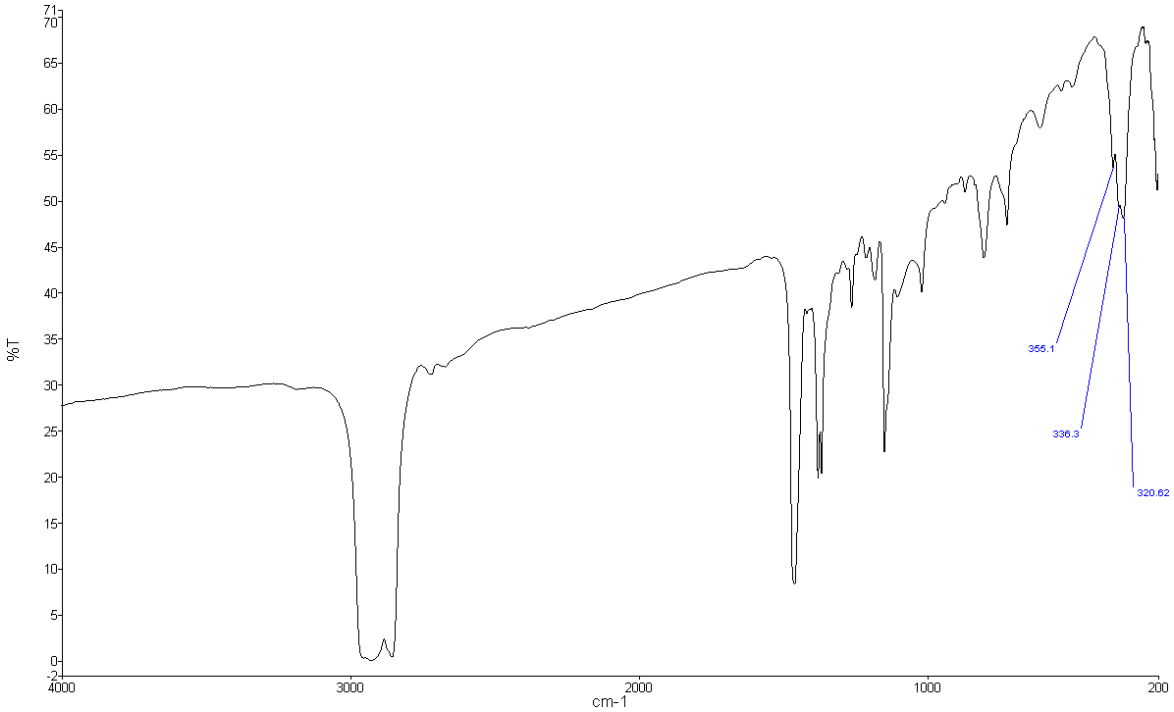

Figure A6.23 IR spectrum of [$NbCl_4$\{^{t}BuTe$(CH_2)_3$Te^{t}Bu\}$_2$]

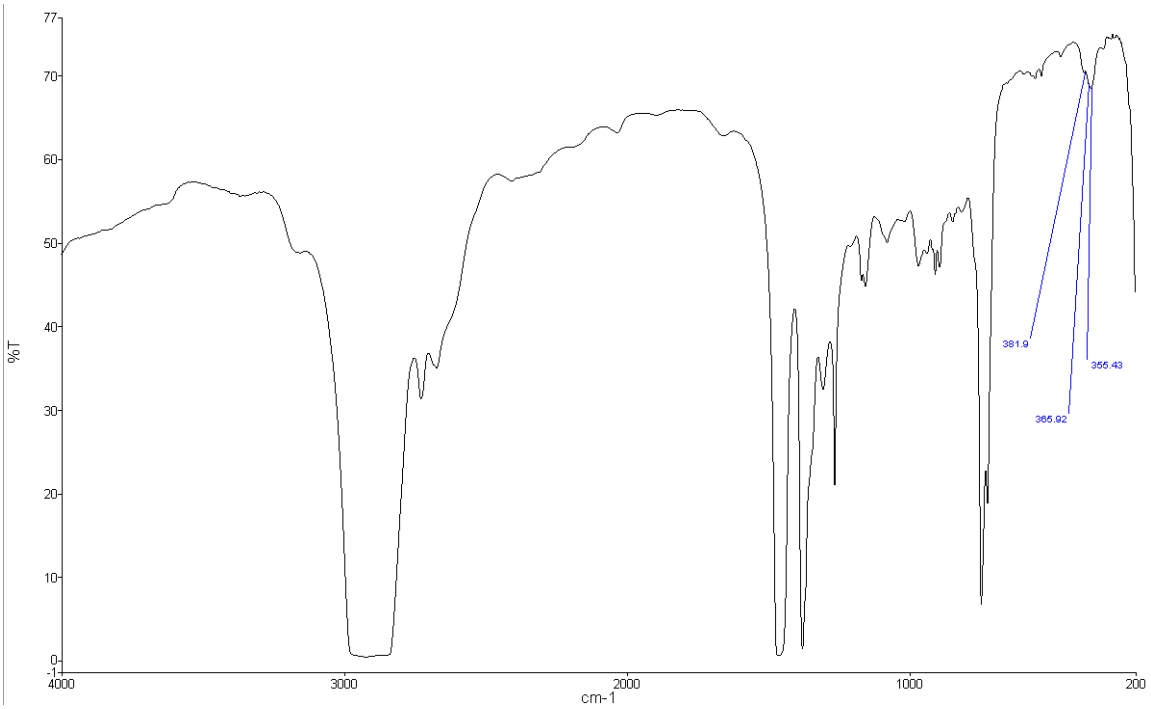

Figure A6.24 IR spectrum of $[NbCl_4(SMe_2)_2]$

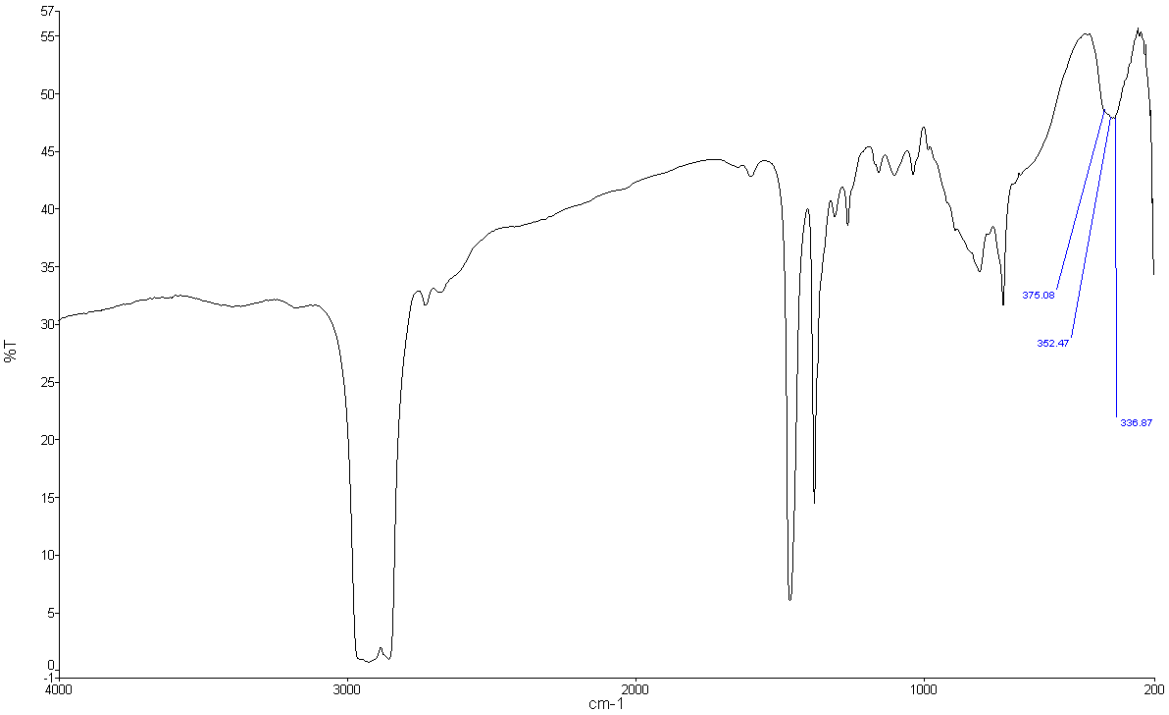

Figure A6.25 IR spectrum of $[Nb_2Cl_6(SMe_2)_2(\mu\text{-}Cl)_2]$

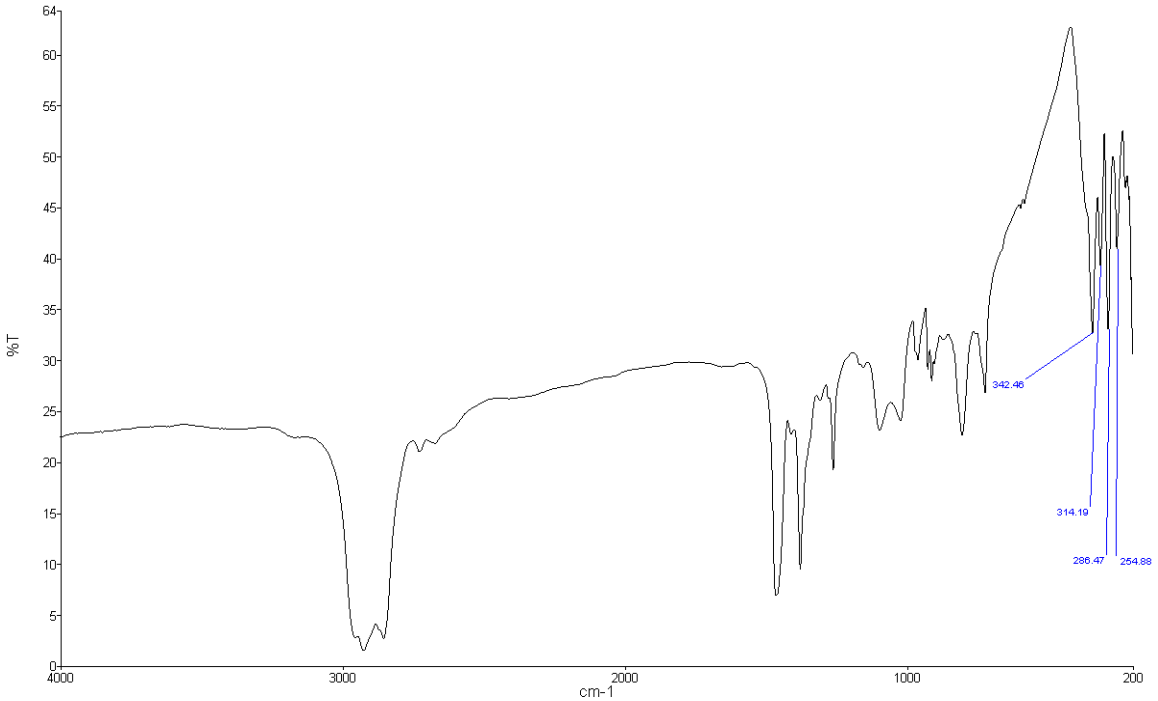

Figure A6.26 IR spectrum of $[NbCl_4(SeMe_2)_2]$

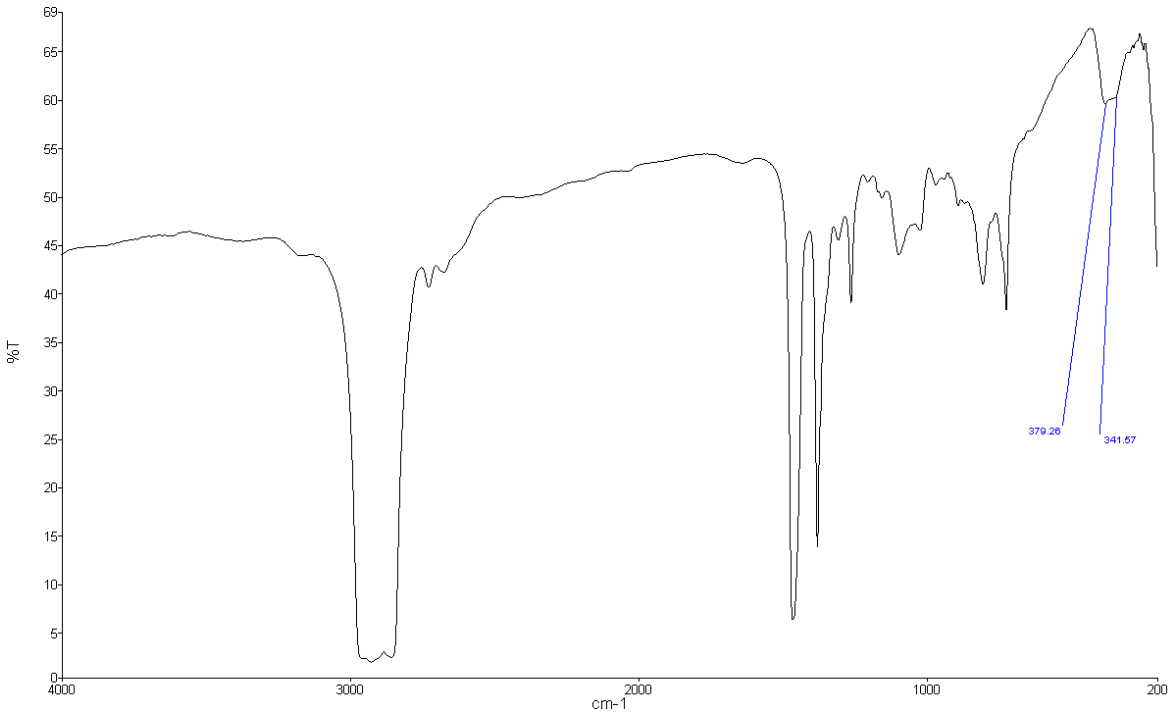

Figure A6.27 IR spectrum of $[NbCl_4(Se^nBu_2)_2]$

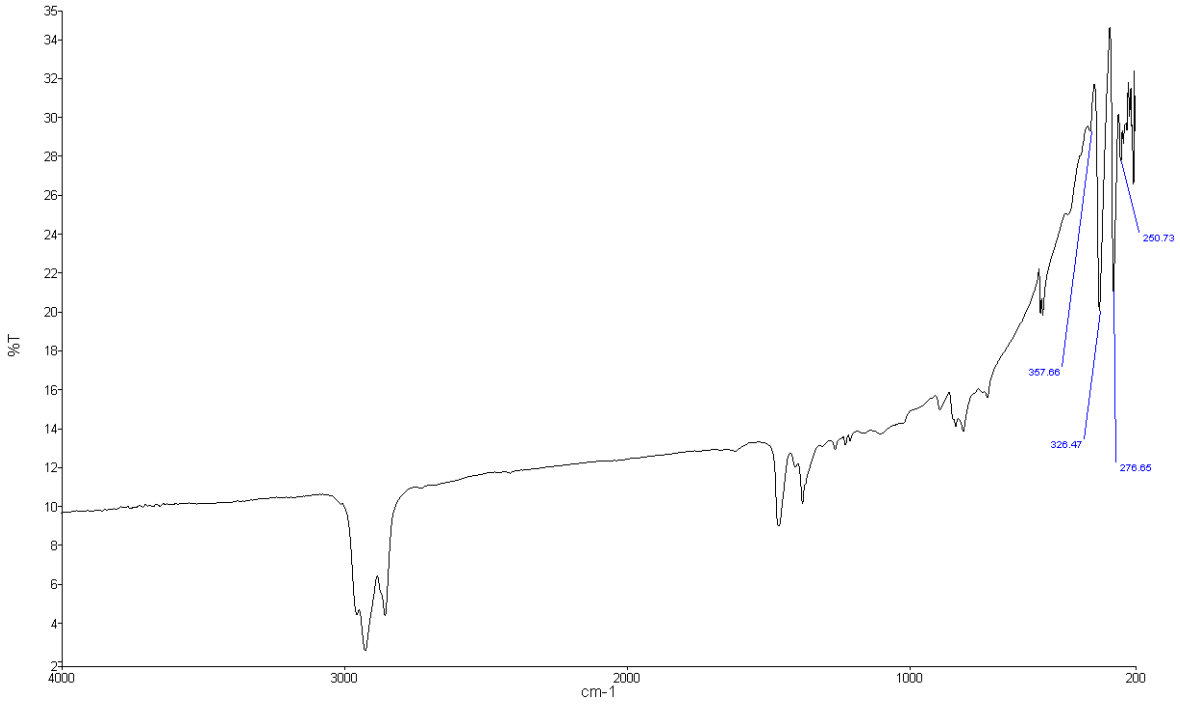

Figure A6.28 IR spectrum of $[Nb_2Cl_4(TeMe_2)_4(\mu\text{-}Cl)_4]$

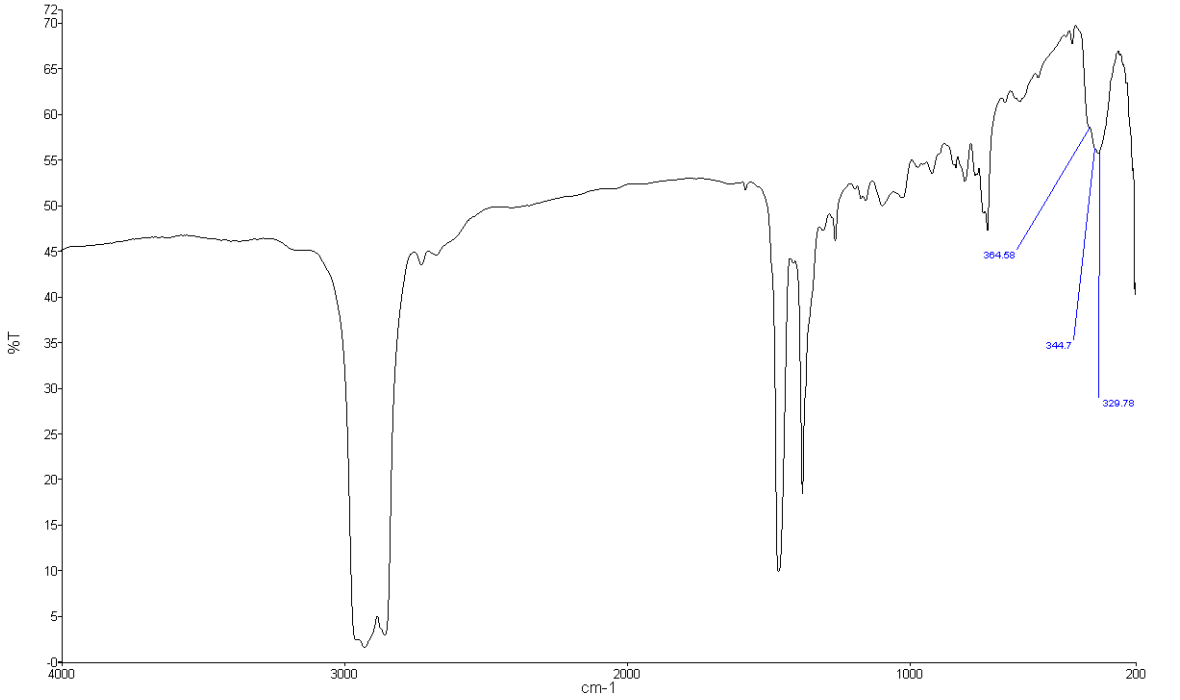

Figure A6.29 IR spectrum of $[Nb_2Cl_4\{o\text{-}C_6H_4(CH_2)_2Se\}_4(\mu\text{-}Se_n)(\mu\text{-}Se)]$ (n = 1 or 2, please see text)

Chapter 4

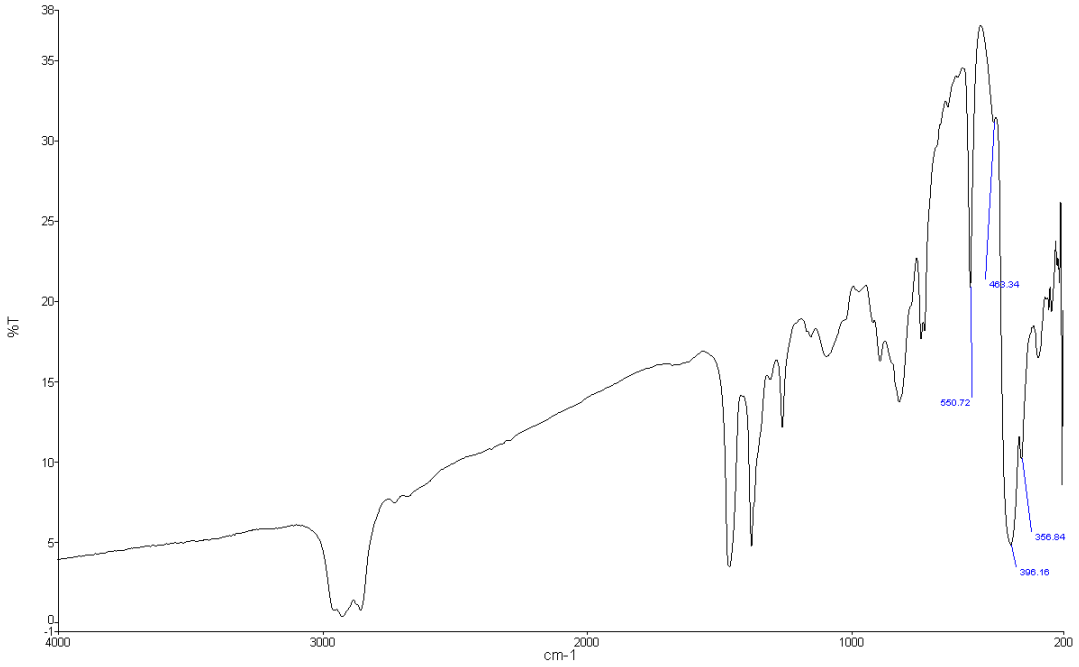

Figure A6.30 IR spectrum of $NbSCl_3$

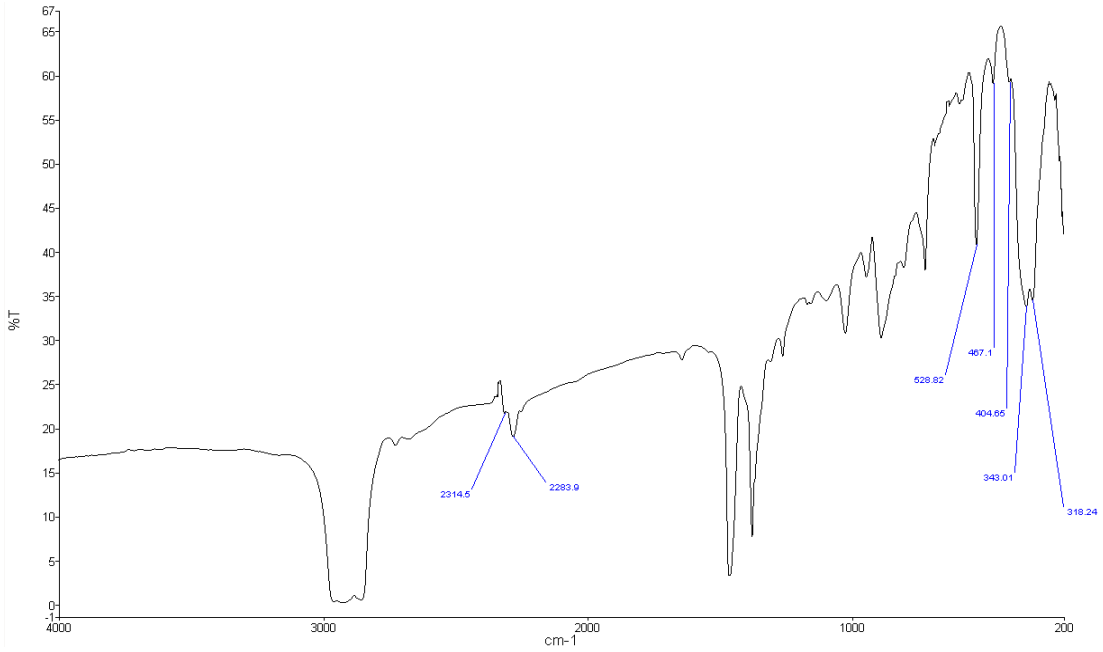

Figure A6.31 IR spectrum of $[NbSCl_3(NCCH_3)_2]$

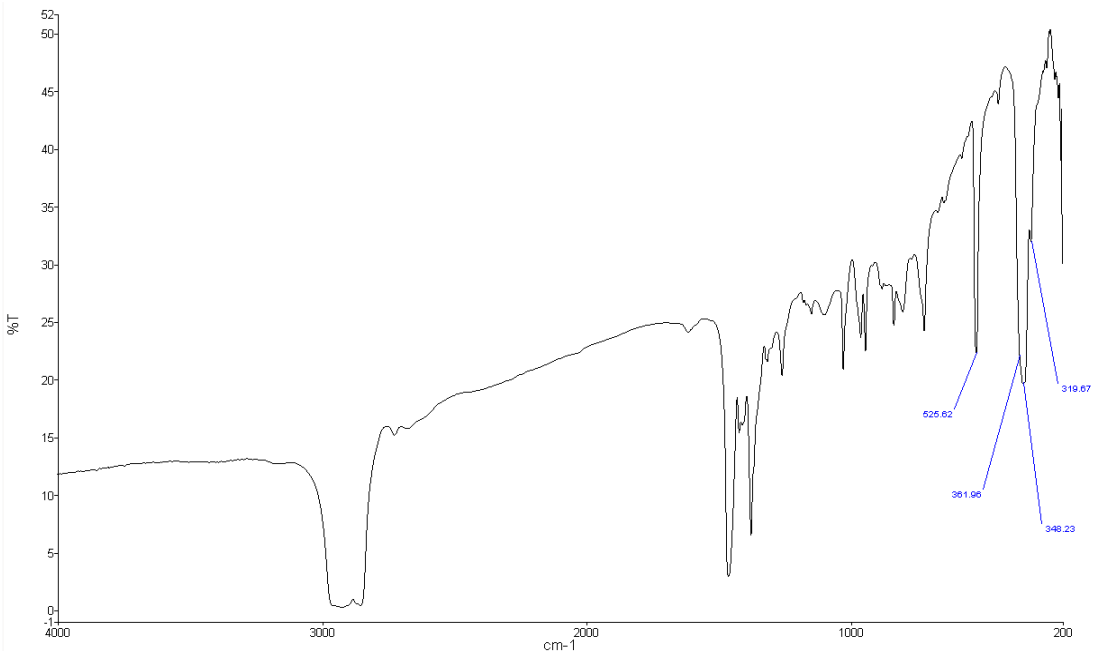

Figure A6.32 IR spectrum of [$NbSCl_3${$MeS(CH_2)_2SMe$}]

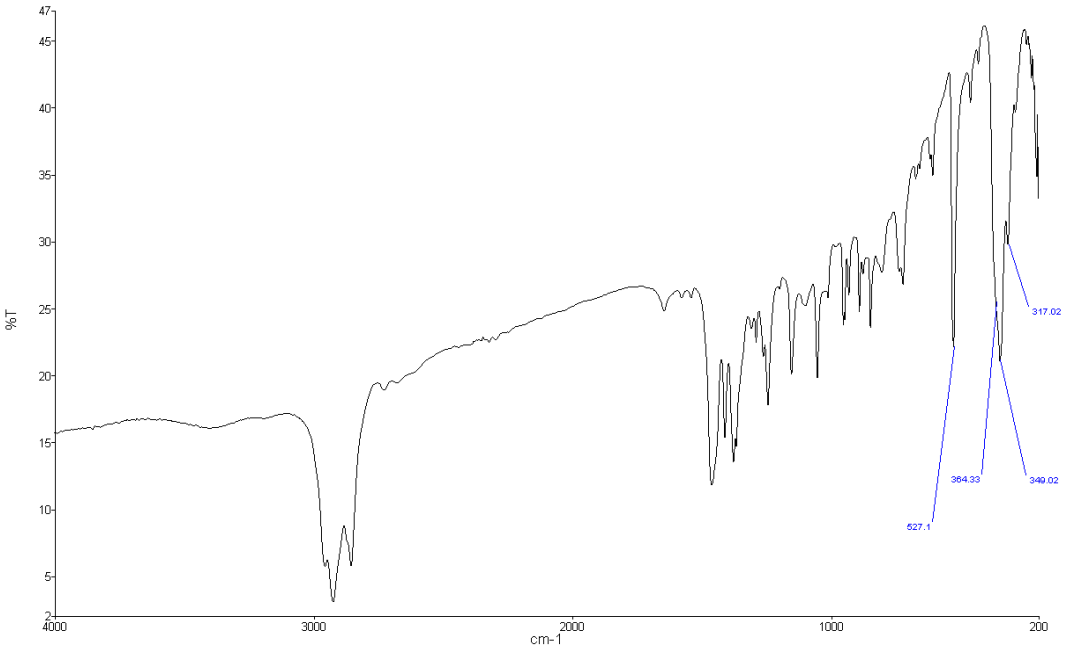

Figure A6.33 IR spectrum of [$NbSCl_3${$^iPrS(CH_2)_2S^iPr$}]

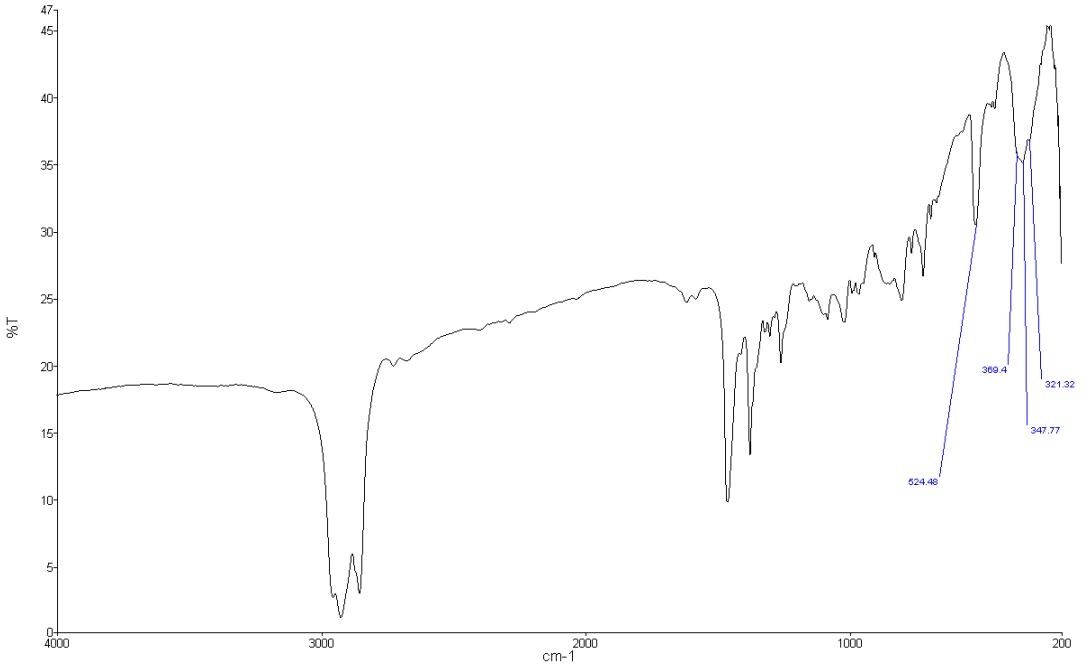

Figure A6.34 IR spectrum of [$NbSCl_3${$MeS(CH_2)_3SMe$}]

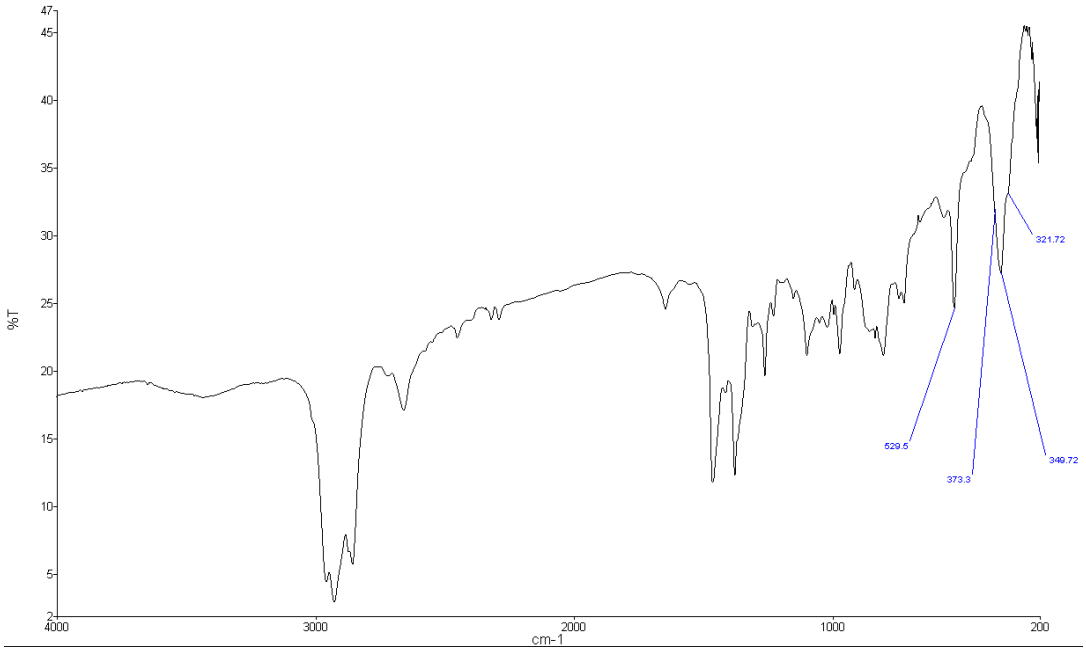

Figure A6.35 IR spectrum of [$NbSCl_3${$^nBuS(CH_2)_3S^nBu$}]

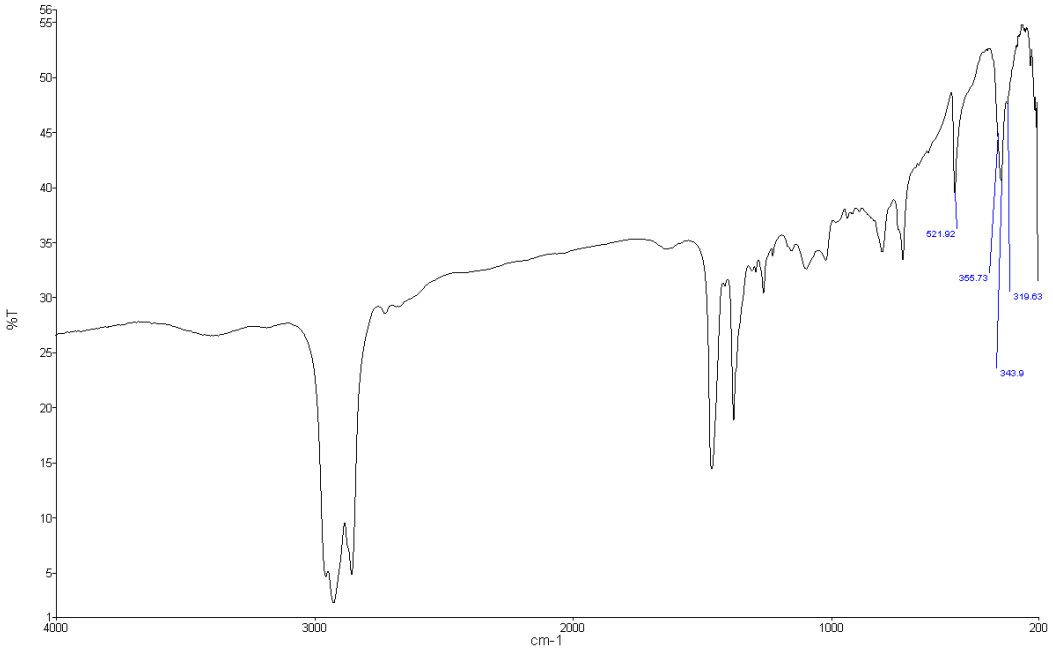

Figure A6.36 IR spectrum of [$NbSCl_3${$MeSe(CH_2)_3SeMe$}]

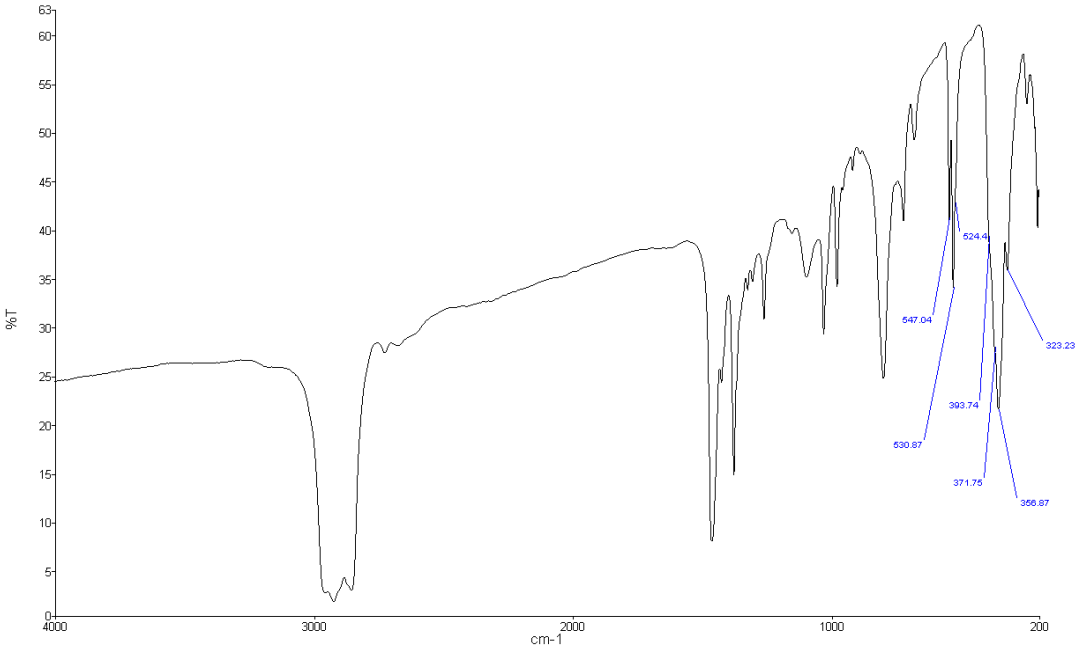

Figure A6.37 IR spectrum of [$NbSCl_3(SMe_2)$]

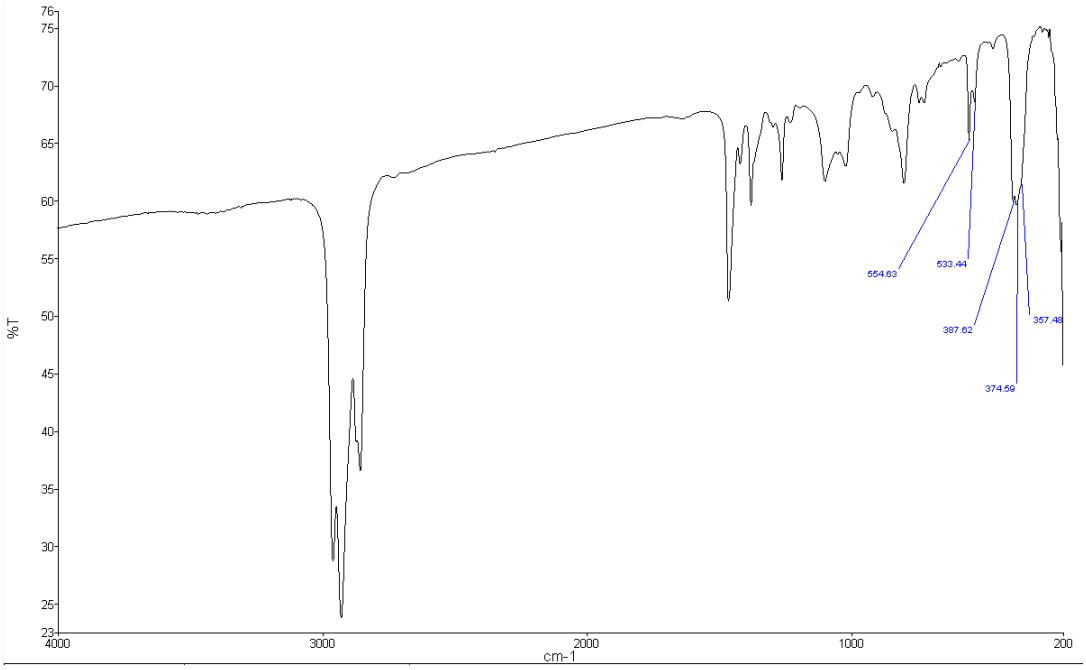

Figure A6.38 IR spectrum of [$NbSCl_3(S^nBu_2)$]

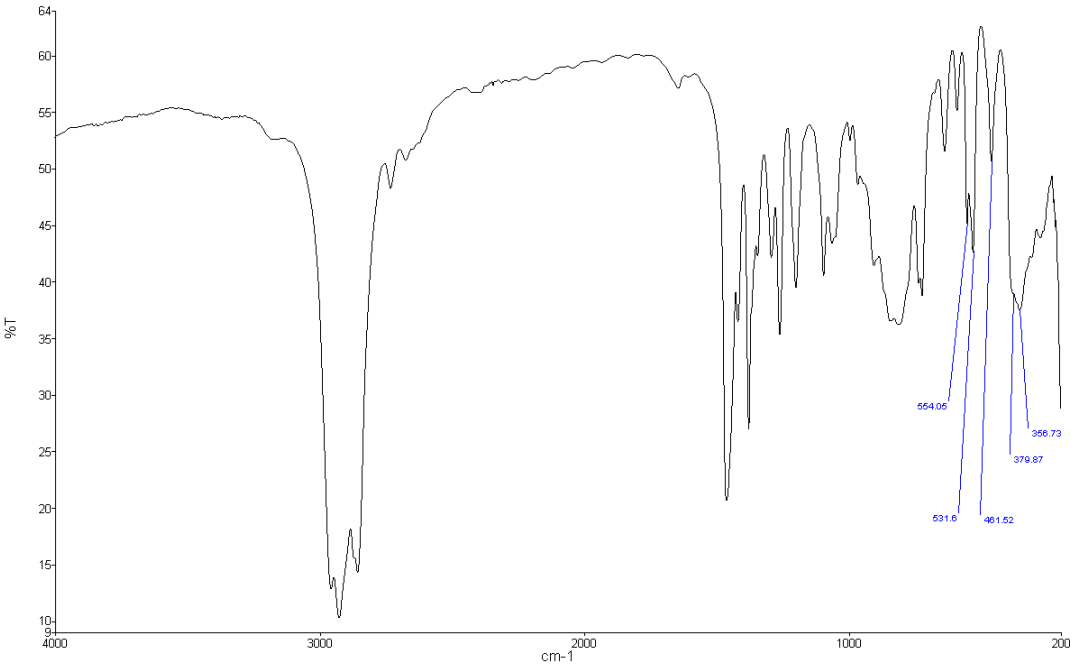

Figure A6.39 IR spectrum of [$NbSCl_3(Se^nBu_2)$]

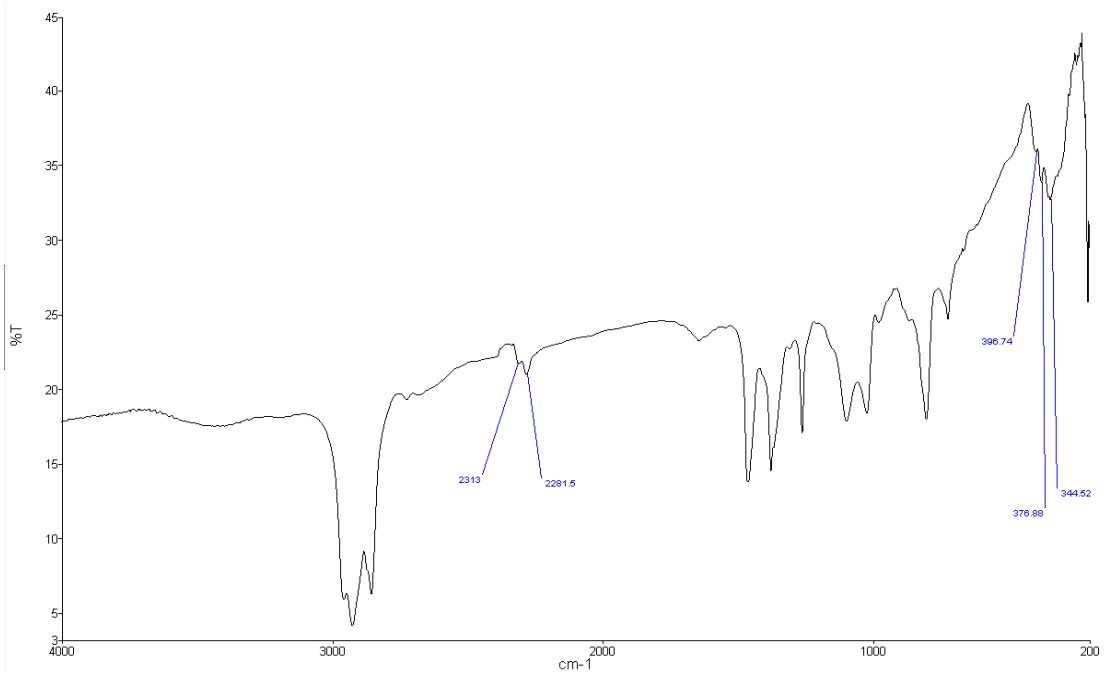

Figure A6.40 IR spectrum of $[NbSeCl_3(NCCH_3)_2]$

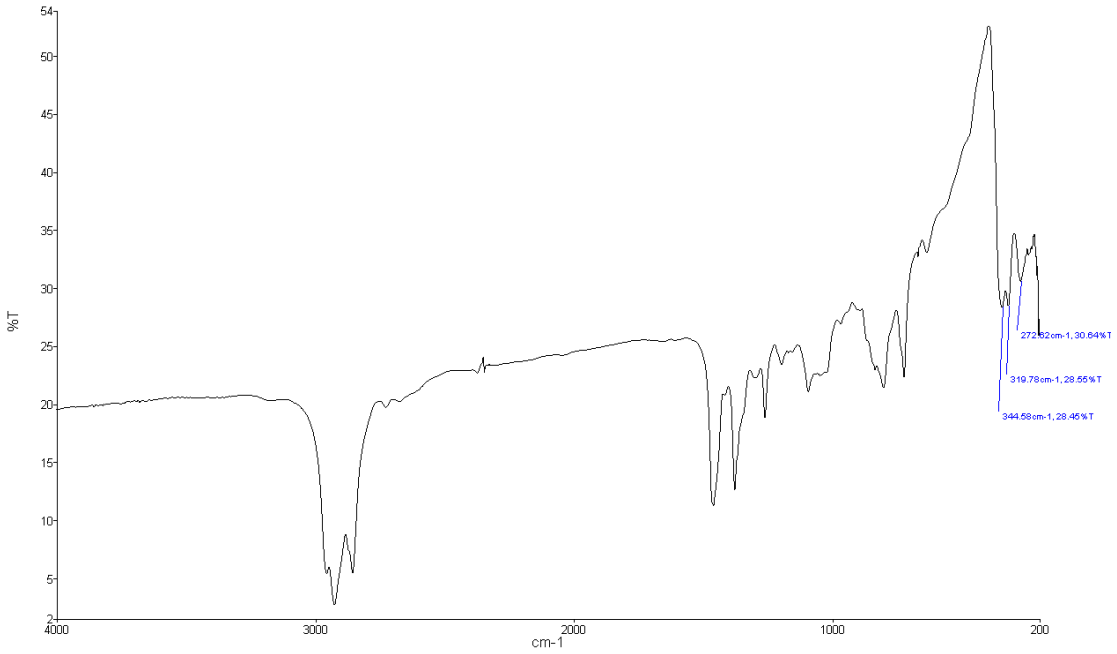

Figure A6.41 IR spectrum of $[NbSe_2Cl_3(Se^nBu_2)]$

Chapter 5

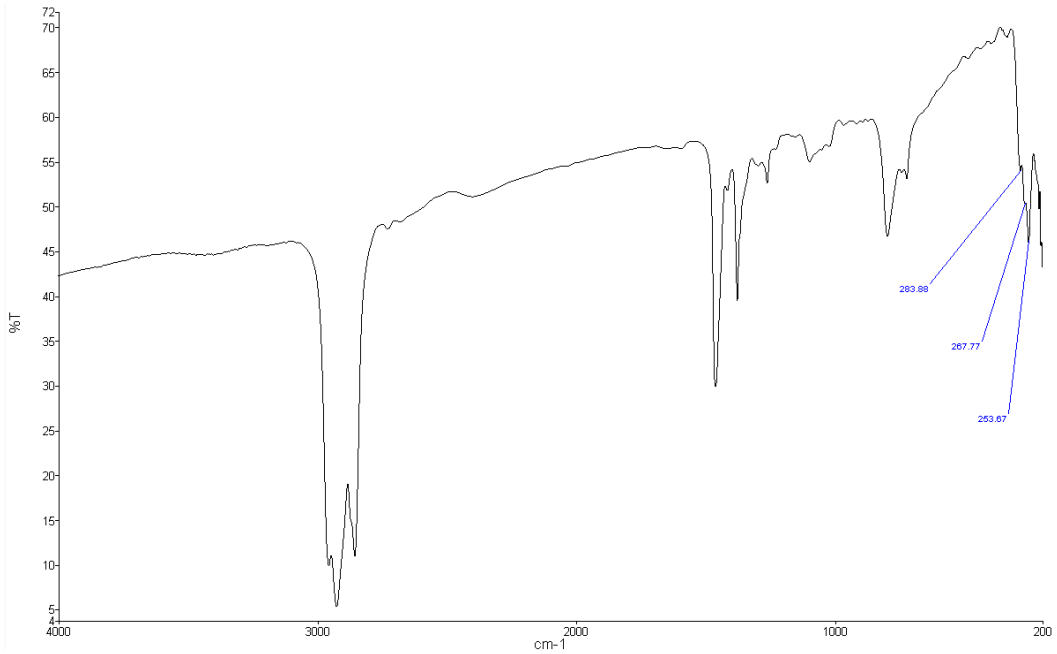

Figure A6.42 IR spectrum of [$NbBr_5(S^nBu_2)$]

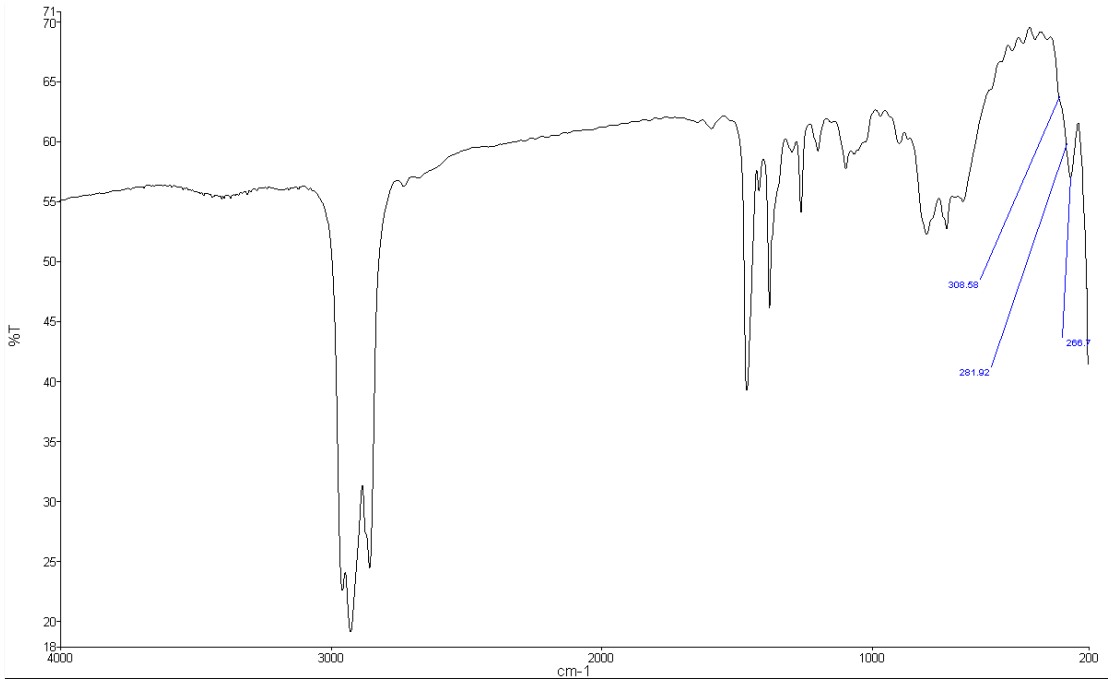

Figure A6.43 IR spectrum of [$NbBr_5(Se^nBu_2)$]

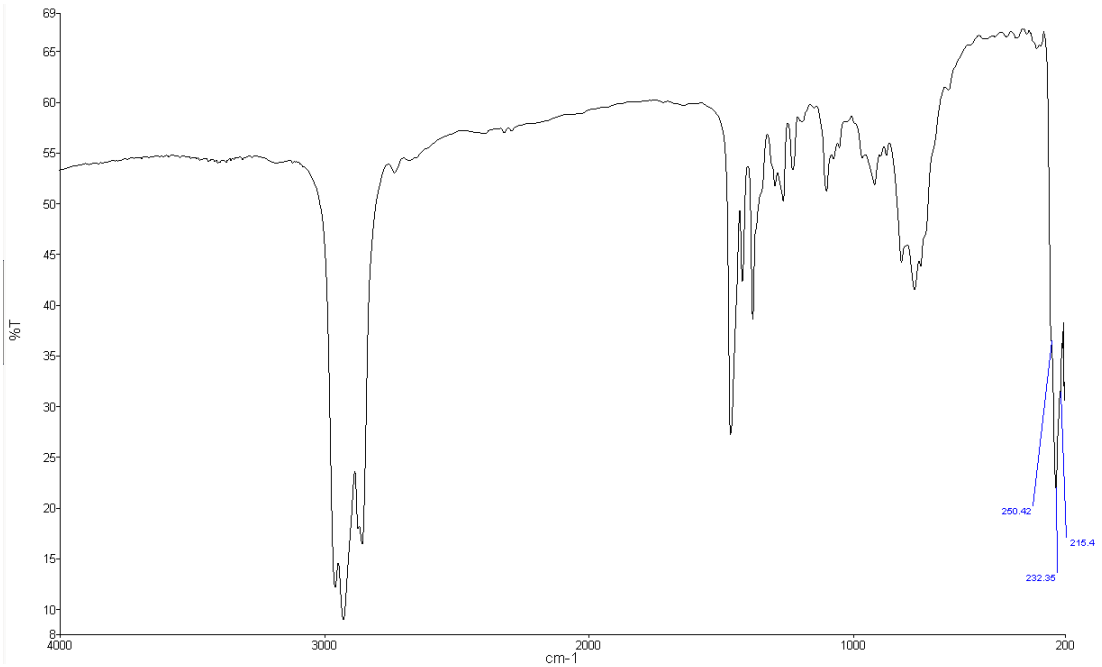

Figure A6.44 IR spectrum of [$TaBr_5(S^nBu_2)$]

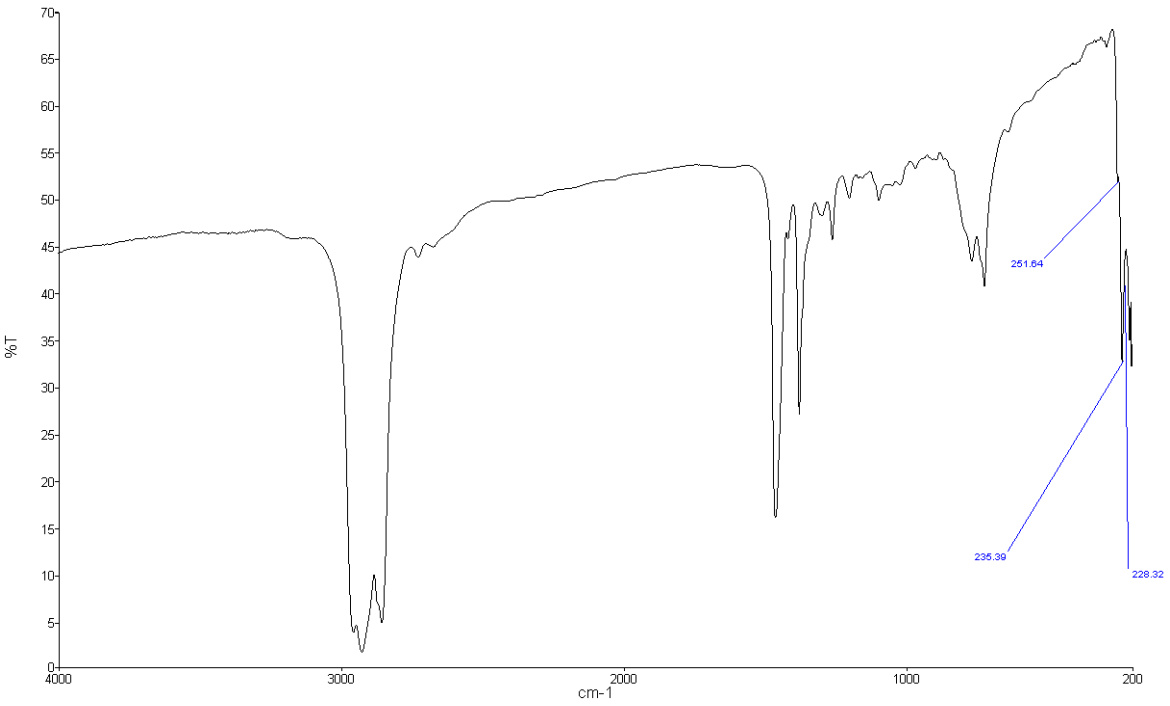

Figure A6.45 IR spectrum of [$TaBr_5(Se^nBu_2)$]

Chapter 6

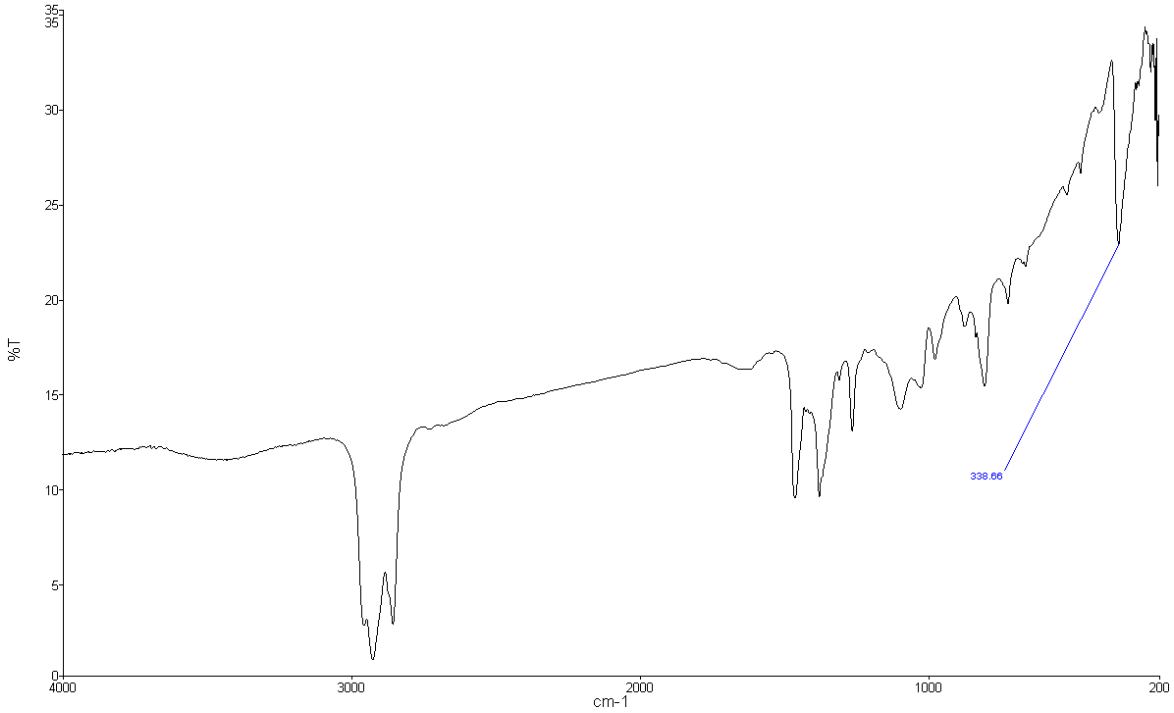

Figure A6.46 IR spectrum of *trans*-[$MoCl_4(NCCH_3)_2$]

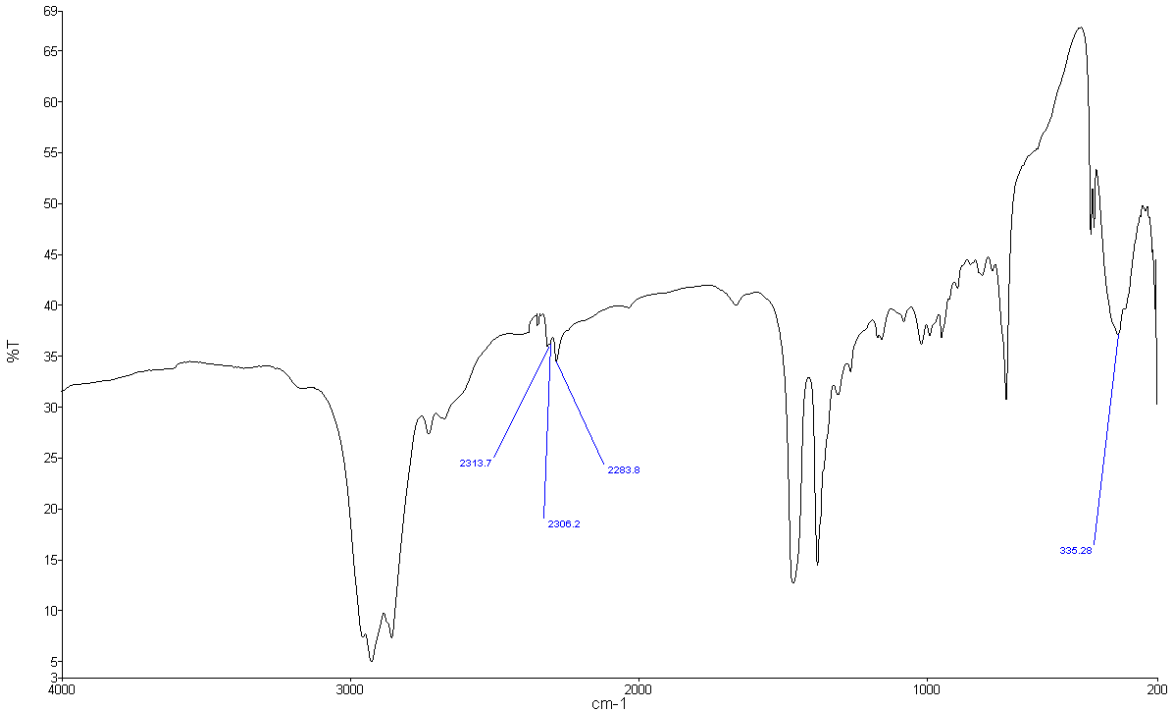

Figure A6.47 IR spectrum of *trans*-[$MoCl_4(THT)_2$]

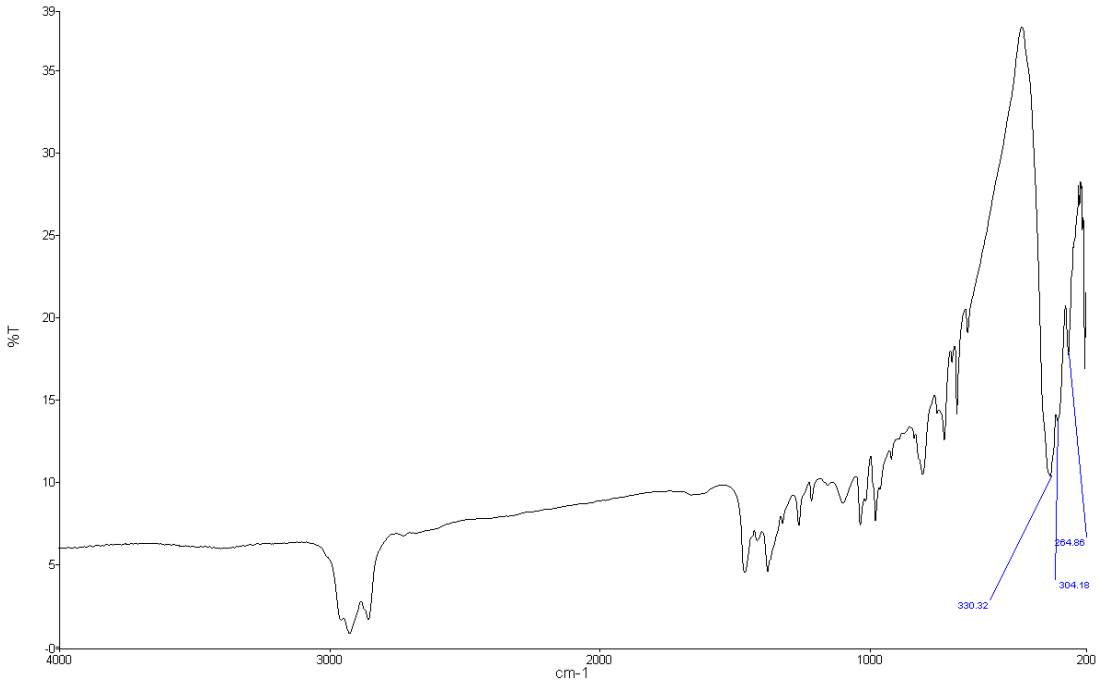

Figure A6.48 IR spectrum of *trans*-[$MoCl_4(SMe_2)_2$]

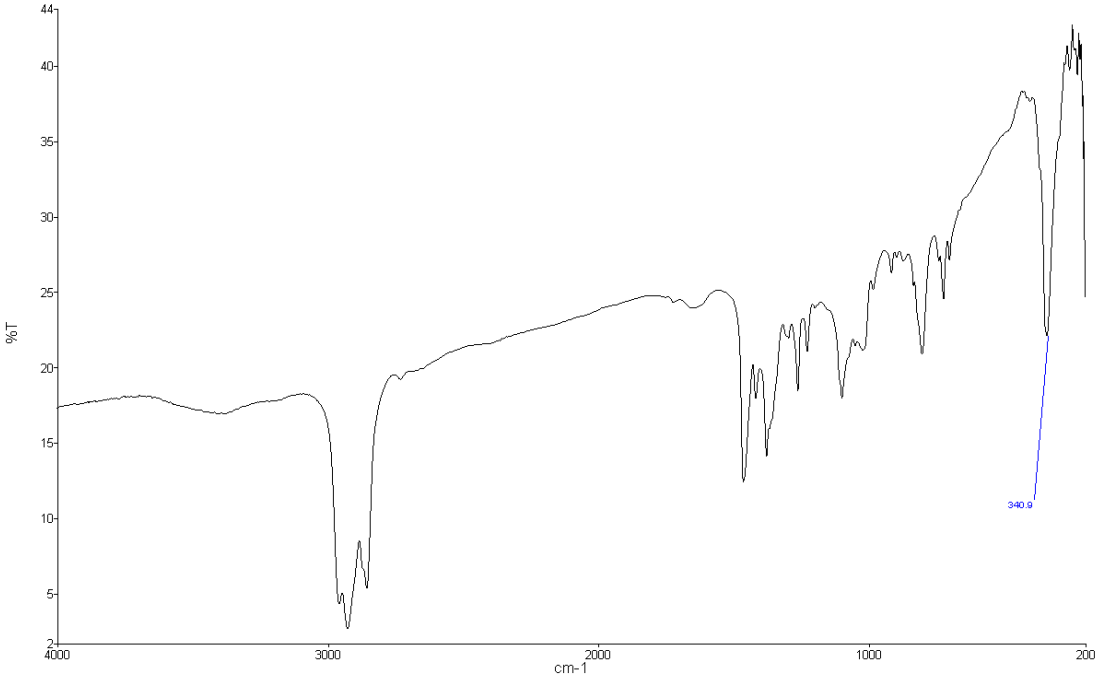

Figure A6.49 IR spectrum of *trans*-[$MoCl_4(S^nBu_2)_2$]

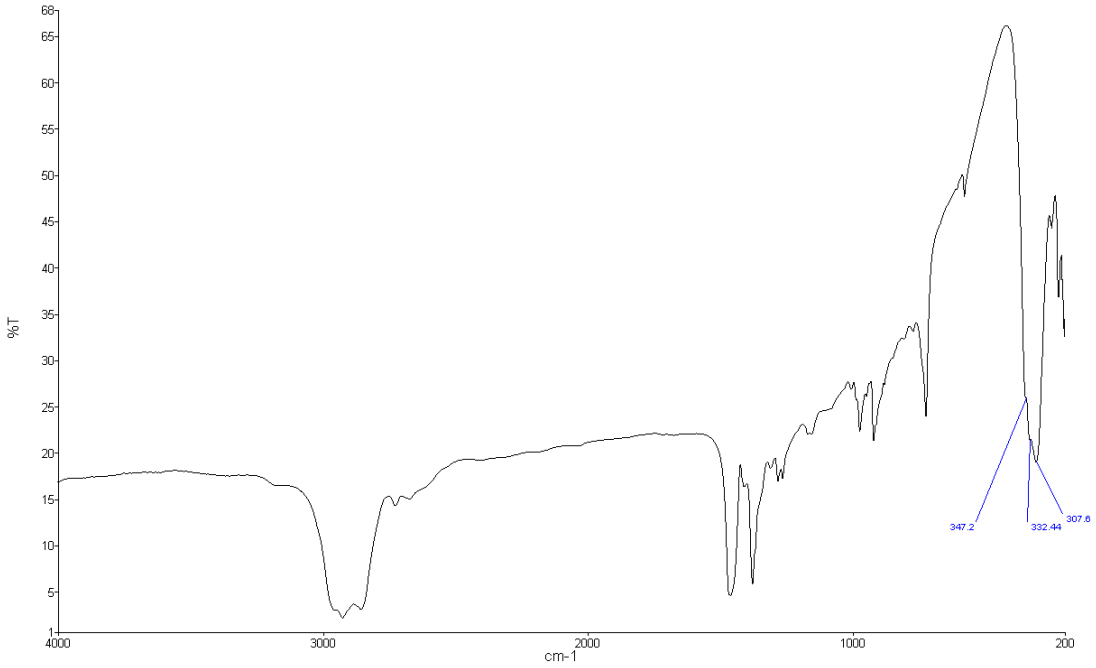

Figure A6.50 IR spectrum of *trans*-[$MoCl_4(SeMe_2)_2$]

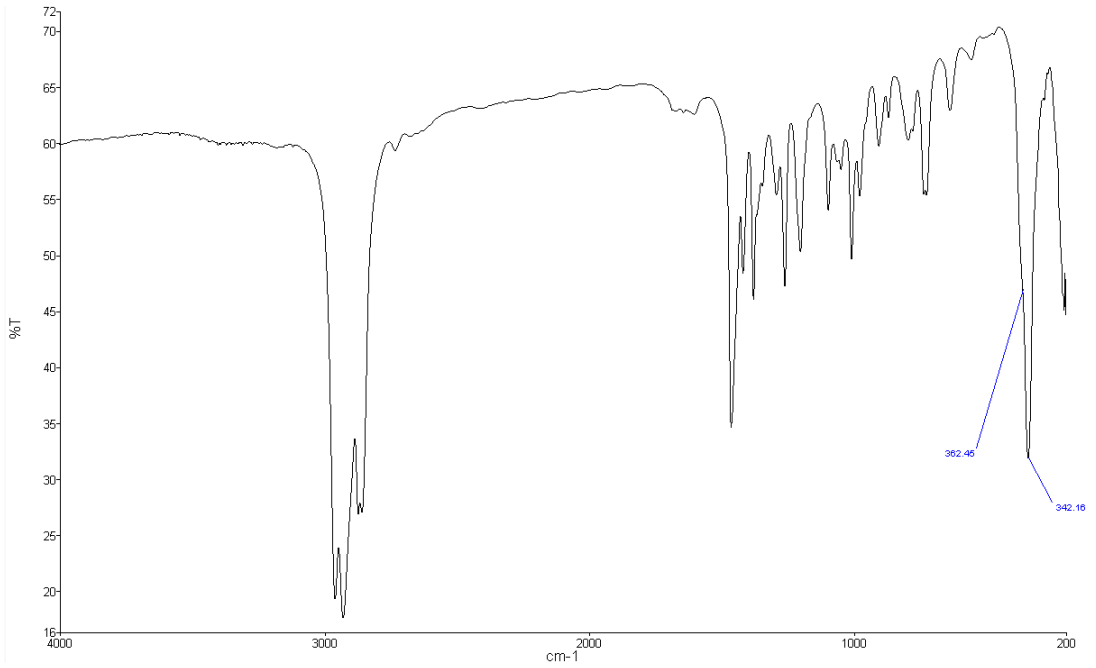

Figure A6.51 IR spectrum of *trans*-[$MoCl_4(Se^nBu_2)_2$]

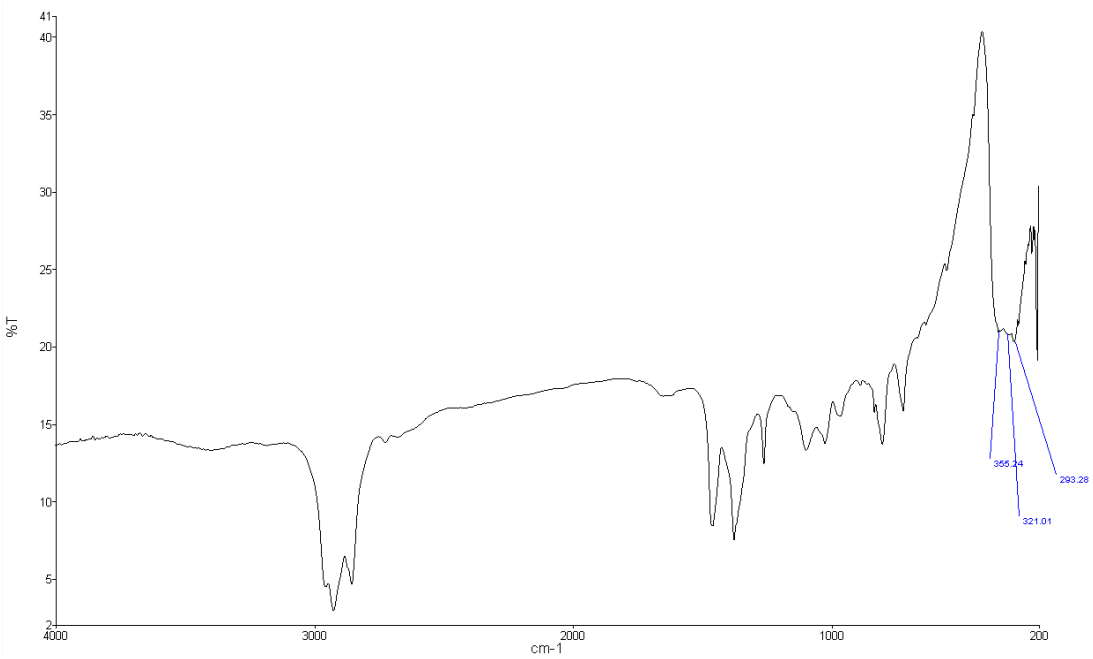

Figure A6.52 IR spectrum of $[MoCl_4\{MeS(CH_2)_2SMe\}]$

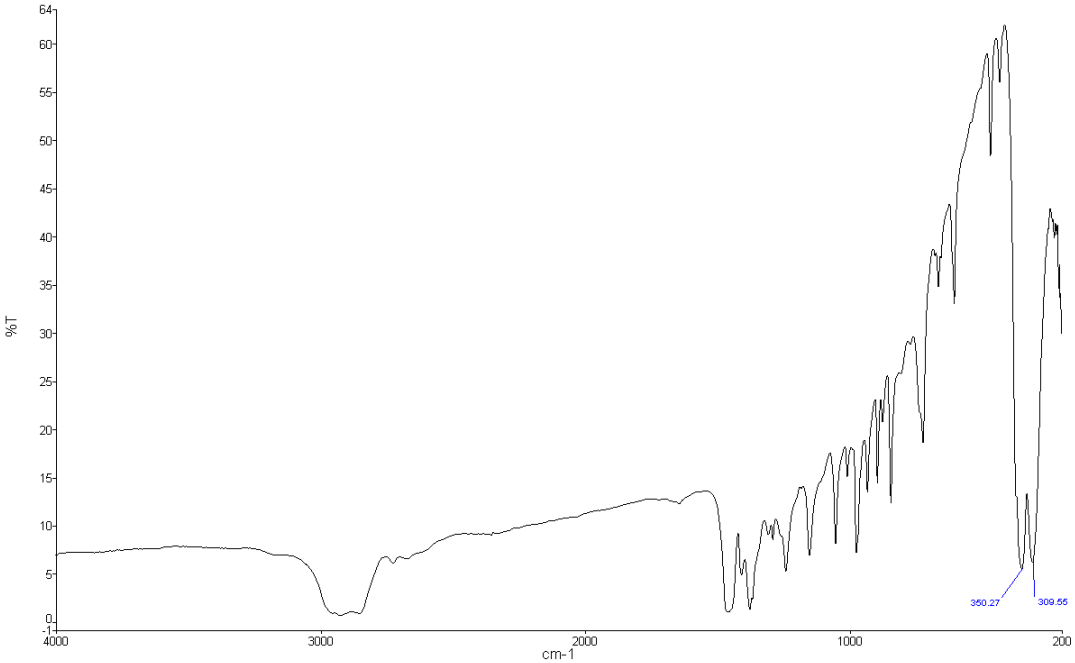

Figure A6.53 IR spectrum of $[MoCl_4\{^iPrS(CH_2)_2S^iPr\}]$

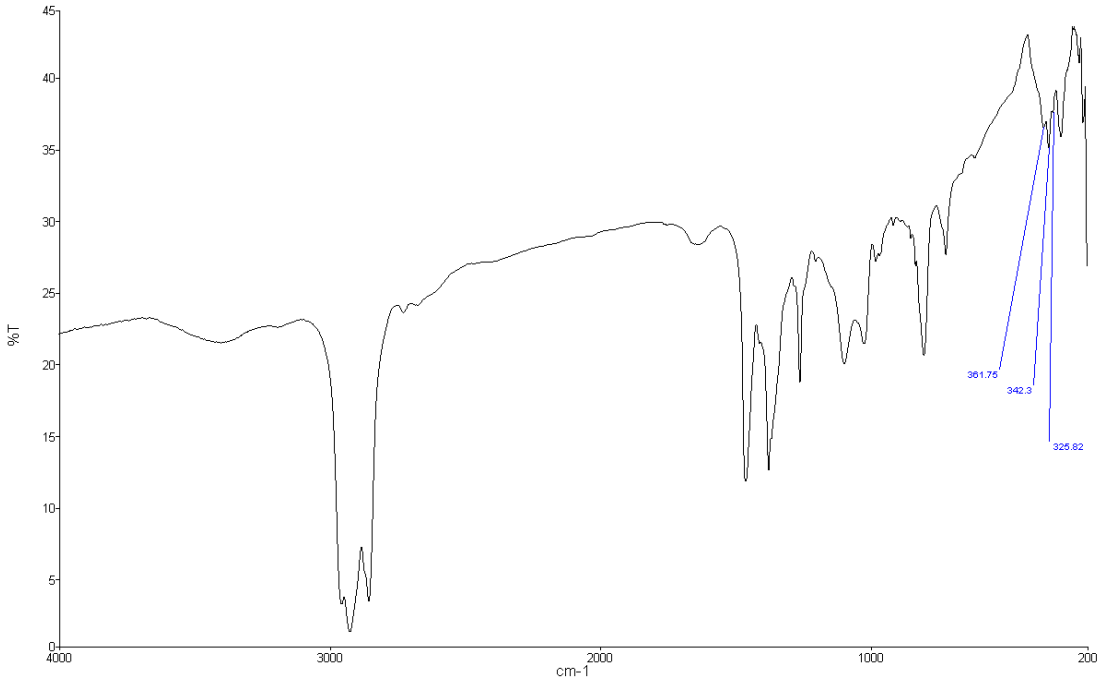

Figure A6.54 IR spectrum of [$MoCl_4${$MeS(CH_2)_3SMe$}]

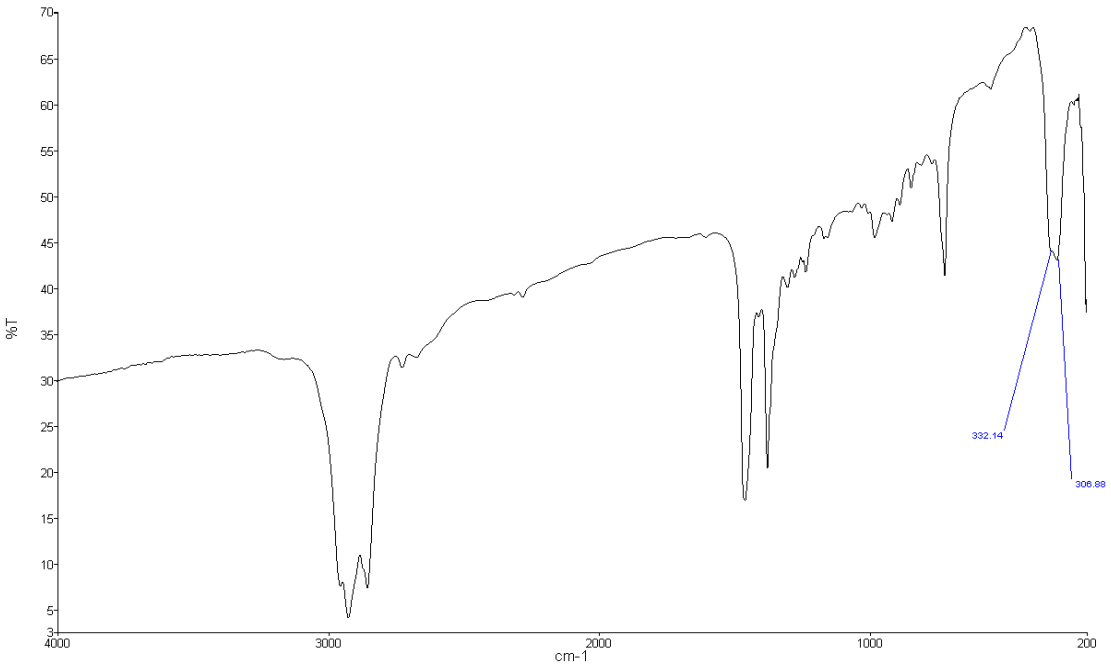

Figure A6.55 IR spectrum of [$MoCl_4${$MeSe(CH_2)_3SeMe$}]

Appendix 7: **Multi-nuclear NMR spectra in Chapter 4 & 5**

Chapter 4

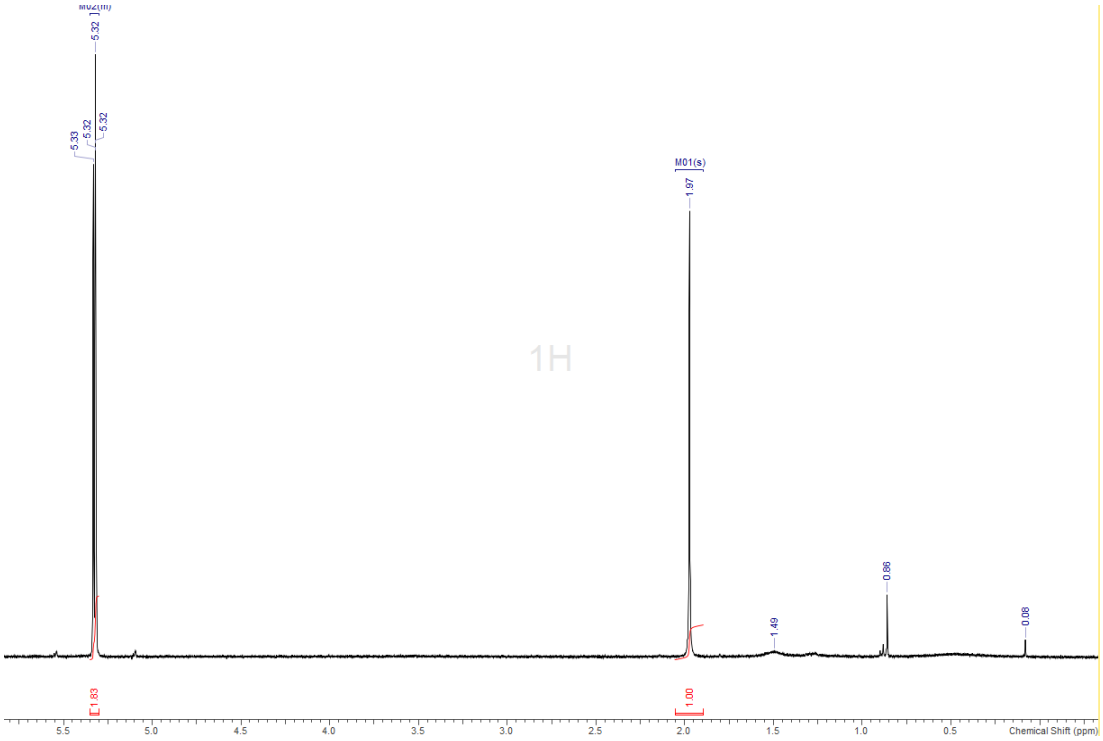

Figure A7.1 ^{1}H NMR spectrum of $[NbSCl_3(NCCH_3)_2]$(400 MHz, CD_2Cl_2, 298 K)

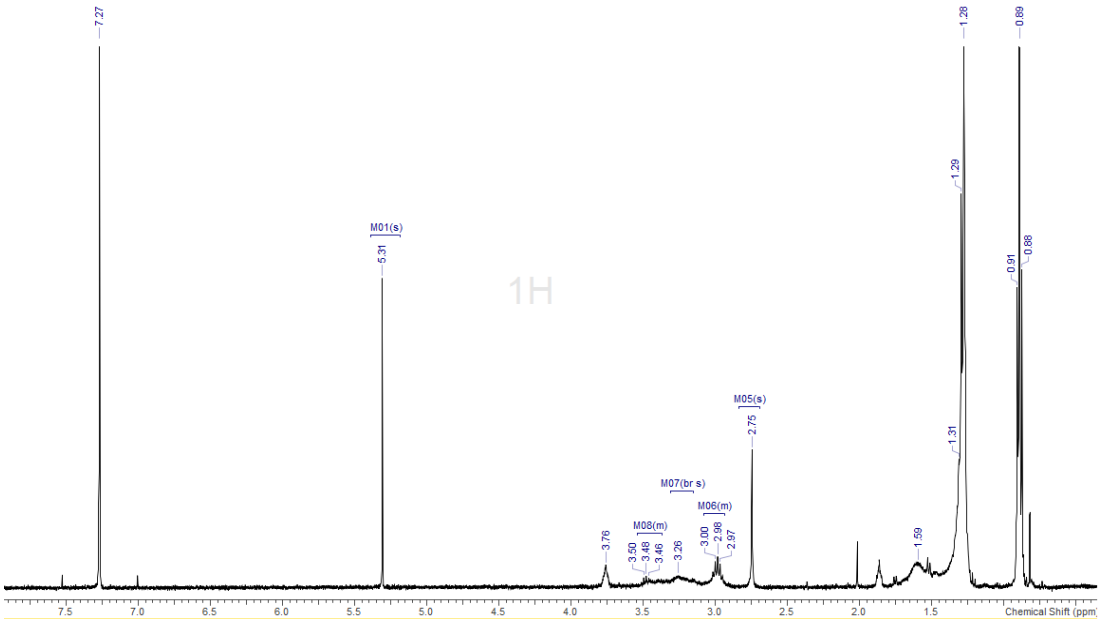

Figure A7.2 ^{1}H NMR spectrum of $[NbSCl_3\{^{i}PrS(CH_2)_2S^{i}Pr\}]$ (400 MHz, $CDCl_3$, 298 K)

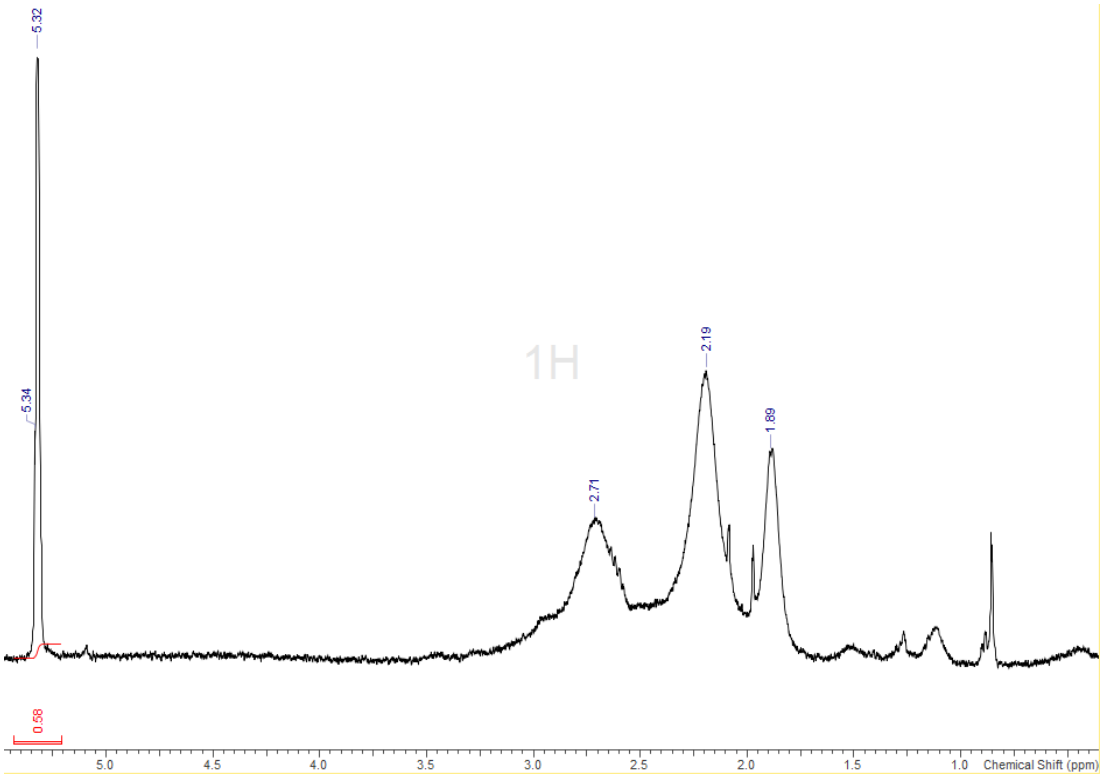

Figure A7.3 ^{1}H NMR spectrum of [$NbSCl_3${$MeS(CH_2)_3SMe$}](400 MHz, CD_2Cl_2, 298 K)

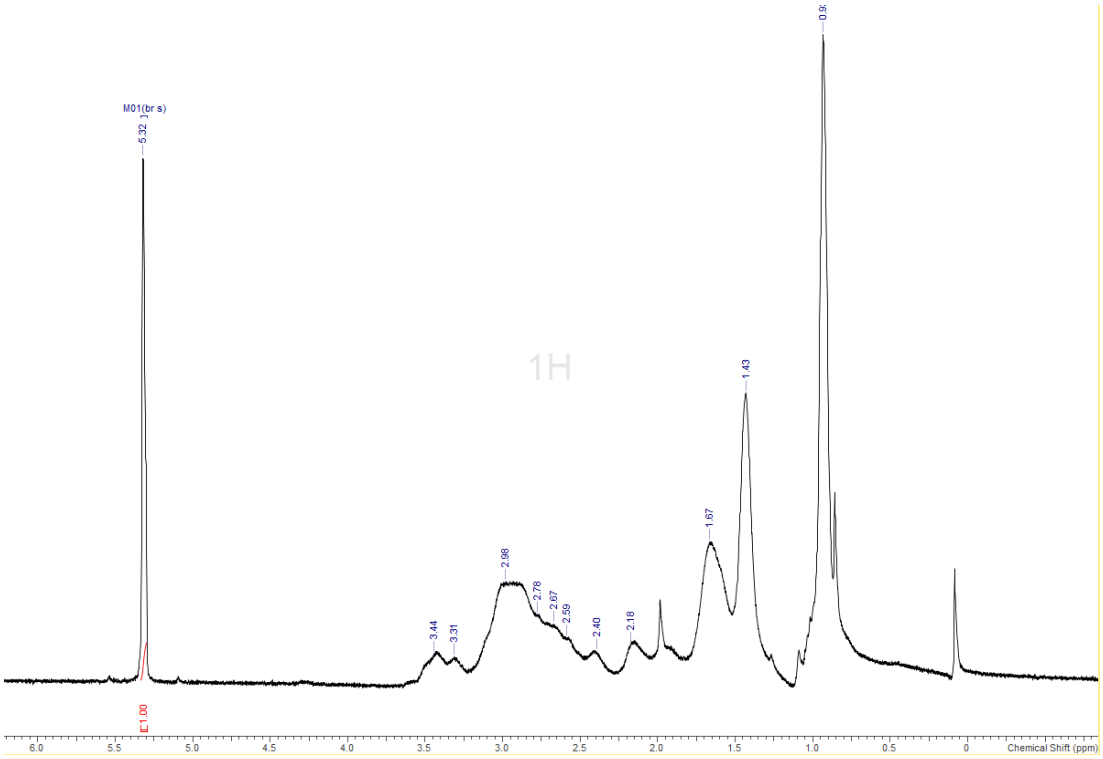

Figure A7.4 ^{1}H NMR spectrum of [$NbSCl_3${$^{n}BuS(CH_2)_3S^{n}Bu$}]((400 MHz, CD_2Cl_2, 298 K)

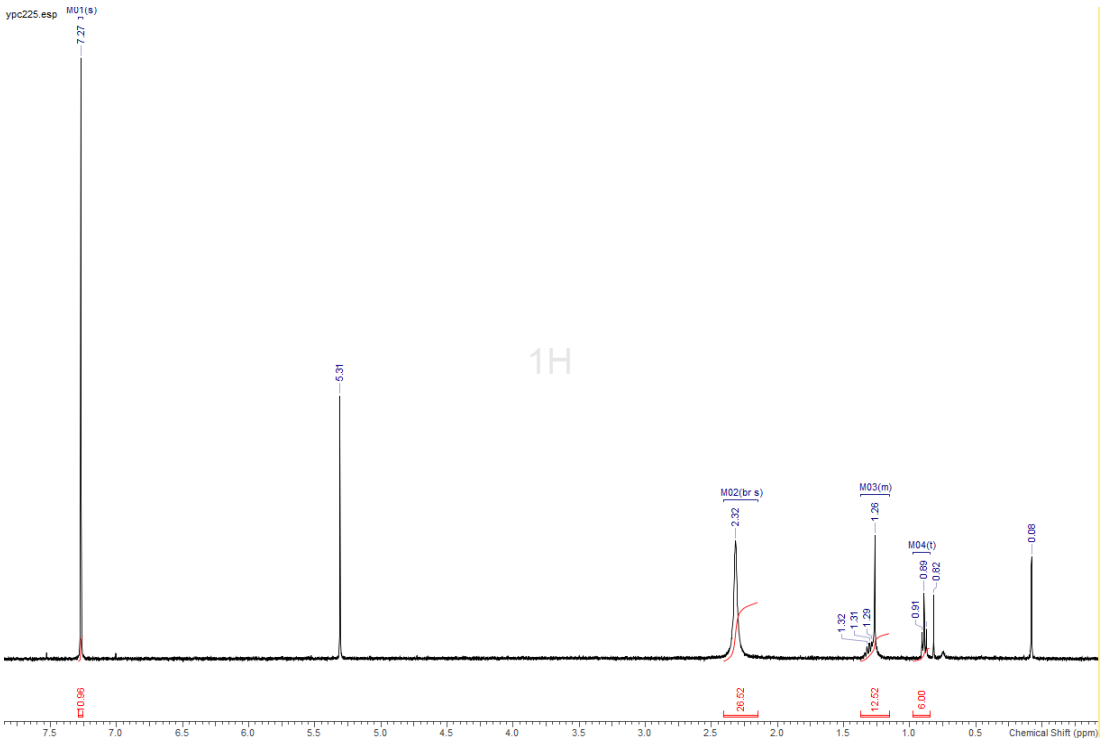

Figure A7.5 ^{1}H NMR spectrum of [$NbSCl_3(SMe_2)$]((400 MHz, CD_2Cl_2, 298 K)

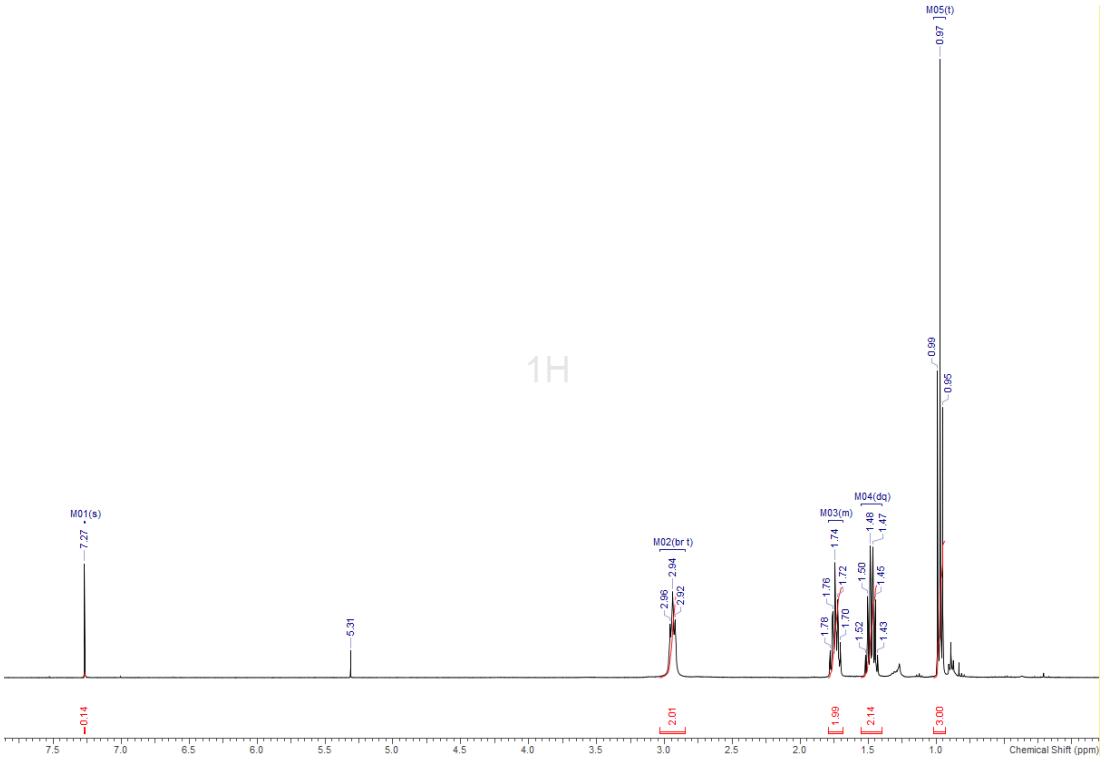

Figure A7.6 ^{1}H NMR spectrum of [$NbSCl_3(S^nBu_2)$] (400 MHz, $CDCl_3$, 298 K)

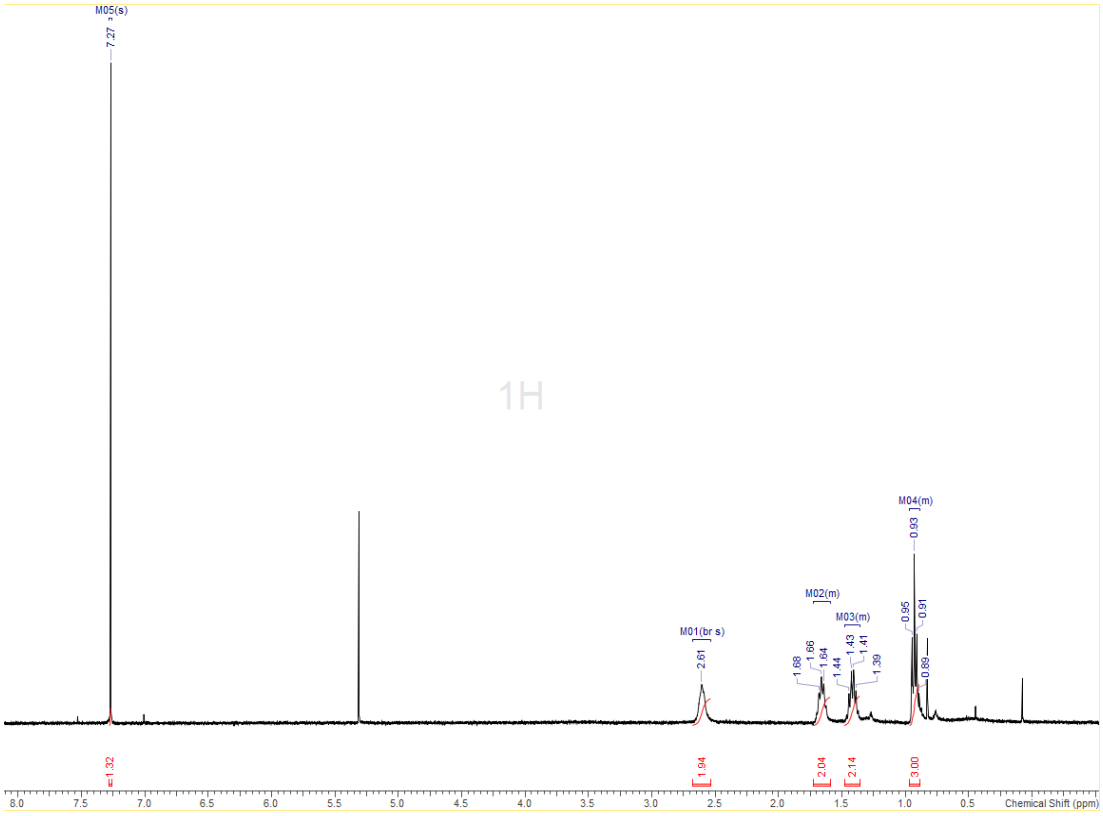

Figure A7.7 ^{1}H NMR spectrum of [$NbSCl_3(Se^nBu_2)$] (400 MHz, $CDCl_3$, 298 K)

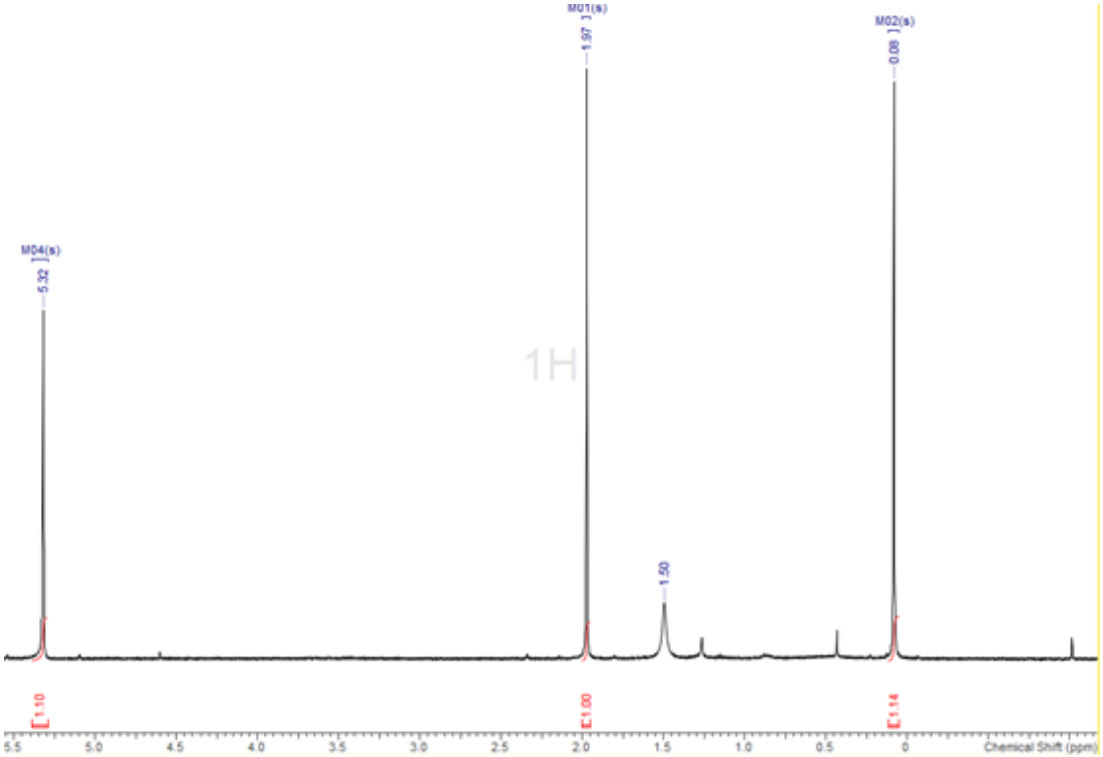

Figure A7.8 ^{1}H NMR spectrum of [$NbSCl_3(NCCH_3)_2$] (400 MHz, CD_2Cl_2, 298 K)

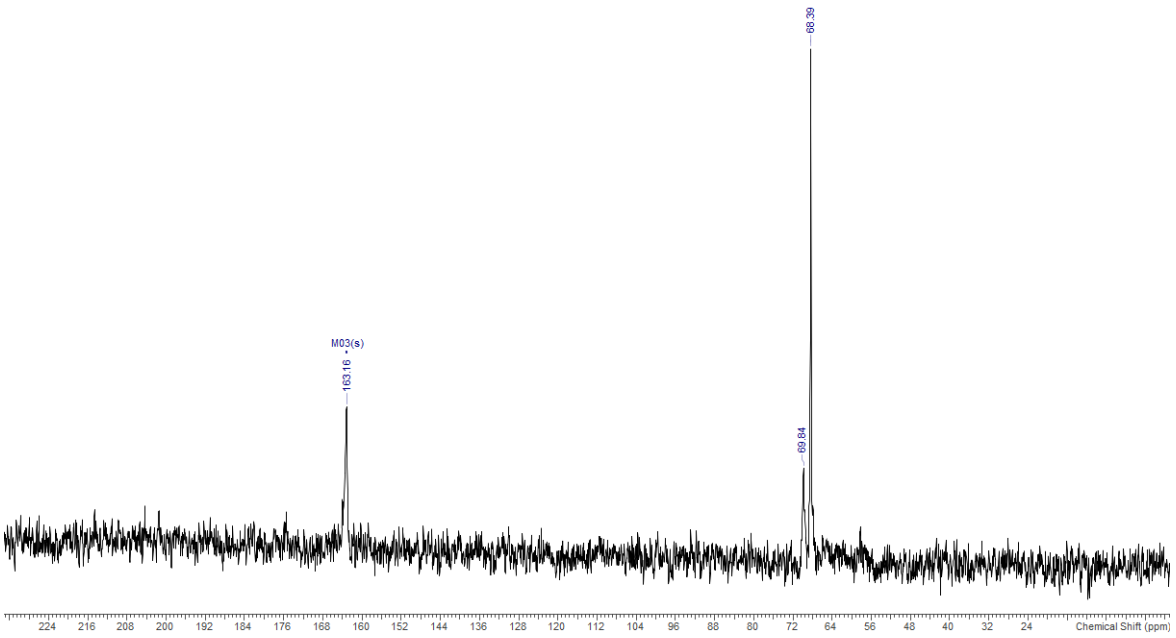

Figure A7.9 $^{77}Se\{^{1}H\}$ NMR spectrum of $[NbSCl_3\{MeSe(CH_2)_3SeMe\}]$ (400 MHz, CH_2Cl_2/CD_2Cl_2, 183 K)

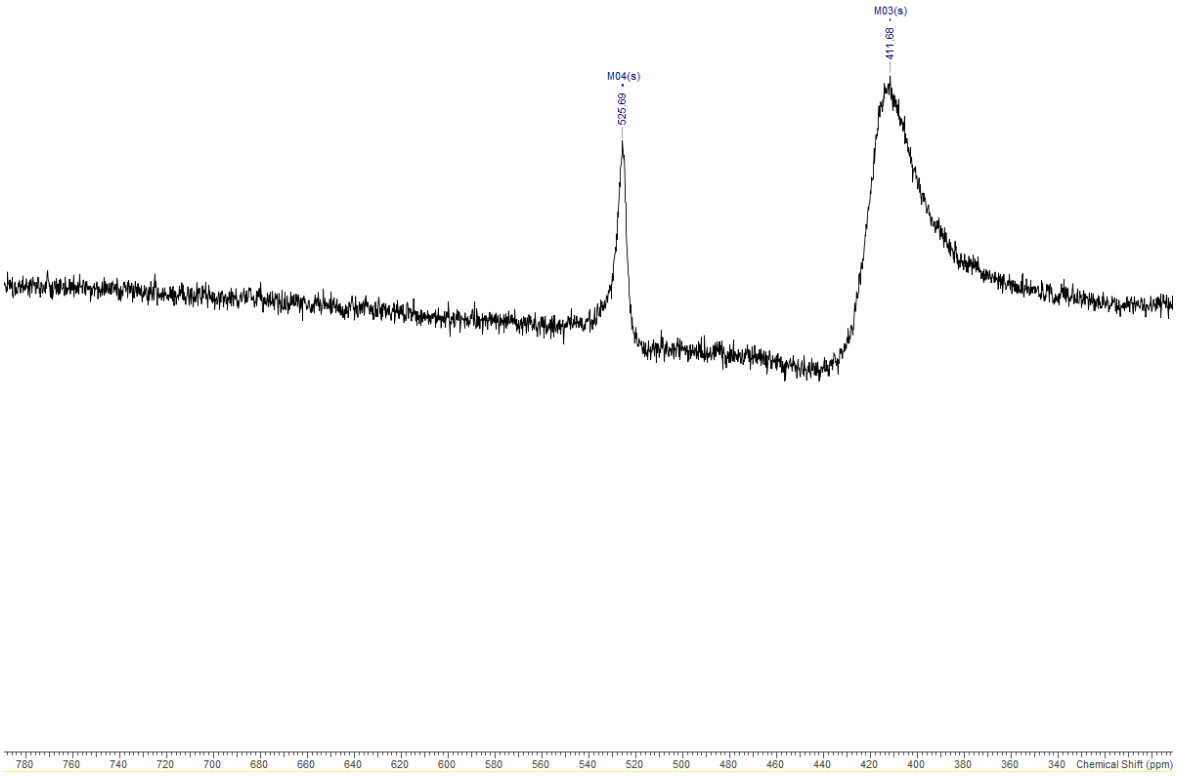

Figure A7.10 ^{93}Nb NMR spectrum of $[NbSCl_3(NCCH_3)_2]$ (400 MHz, CH_3CN/CD_3CN, 298 K)

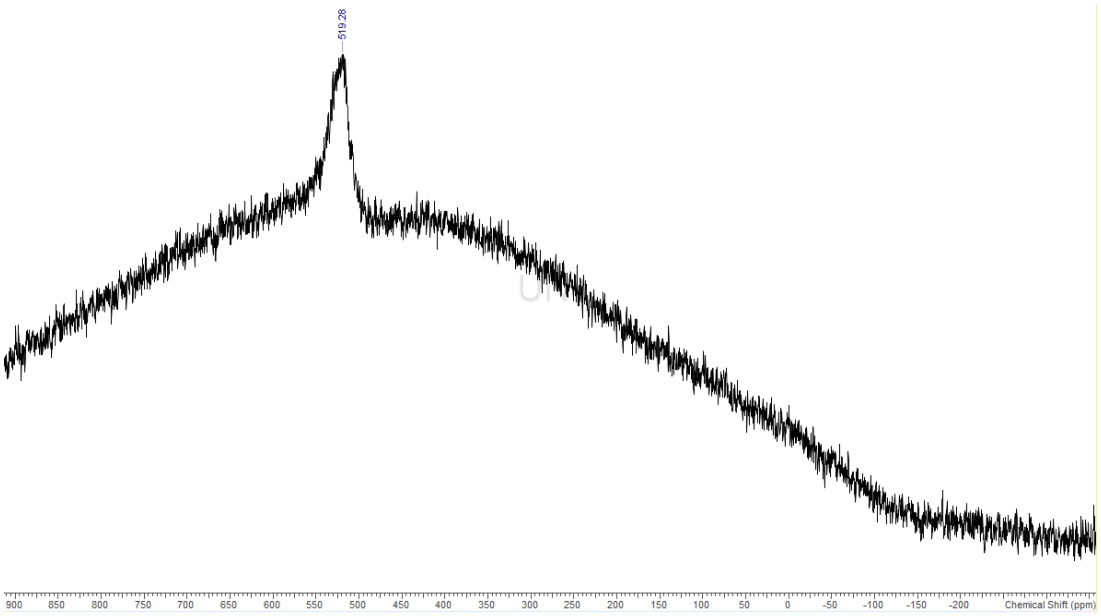

Figure A7.11 ^{93}Nb NMR spectrum of [$NbSCl_3${$^{i}PrS(CH_2)_2S^{i}Pr$}] (400 MHz, CD_2Cl_2, 293K)

Figure A7.12 ^{93}Nb NMR spectrum of [$NbSCl_3${$MeS(CH_2)_3SMe$}] (400 MHz, CH_2Cl_2/CD_2Cl_2, 298 K)

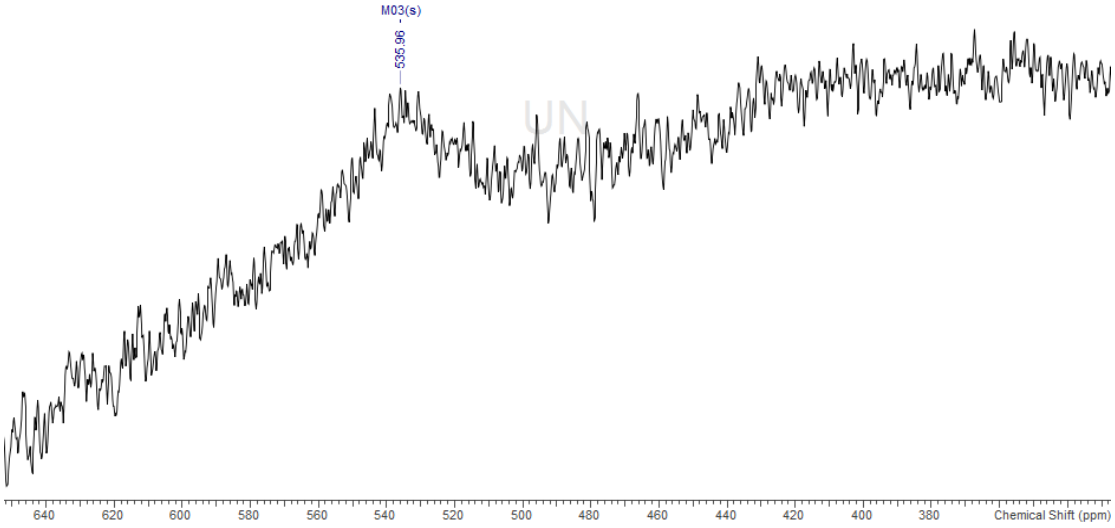

Figure A7.13 ^{93}Nb NMR spectrum of [$NbSCl_3${$^nBuS(CH_2)_3S^nBu$}] (400 MHz, CH_2Cl_2/CD_2Cl_2, 298 K)

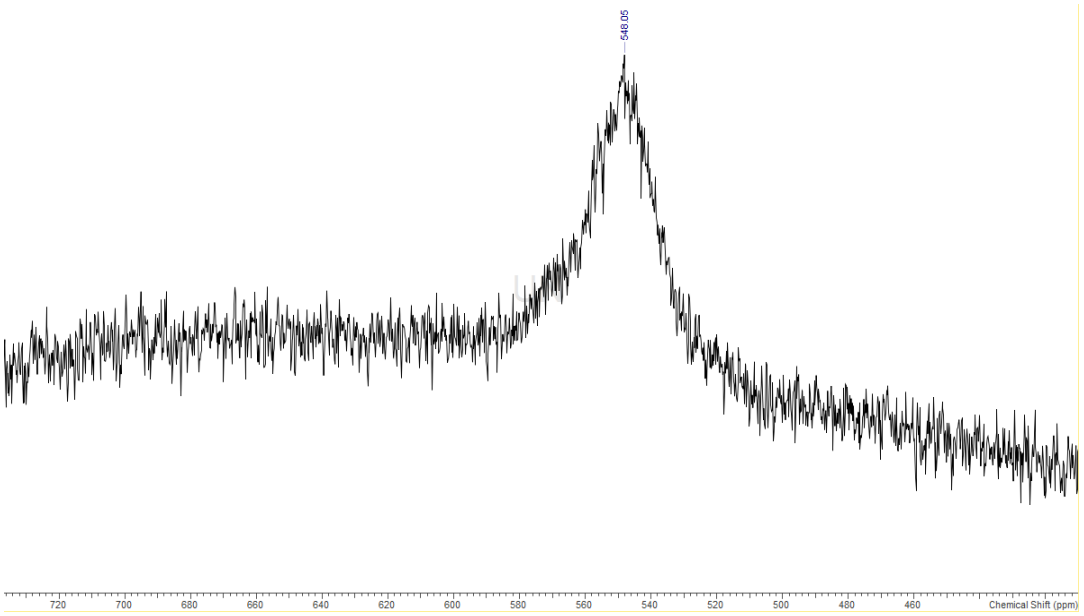

Figure A7.14 ^{93}Nb NMR spectrum of [$NbSCl_3${$MeSe(CH_2)_3SeMe$}] (400 MHz, CH_2Cl_2/CD_2Cl_2, 183 K)

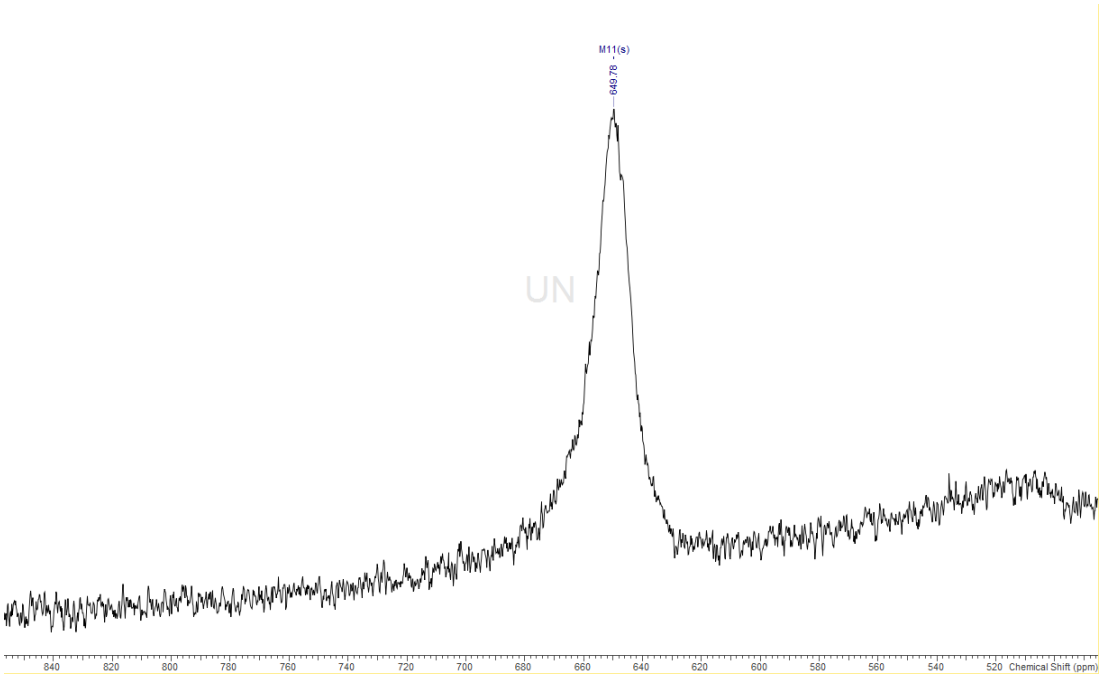

Figure A7.15 ^{93}Nb NMR spectrum of [$NbSCl_3(SMe_2)$] (400 MHz, CH_2Cl_2/CD_2Cl_2, 298K)

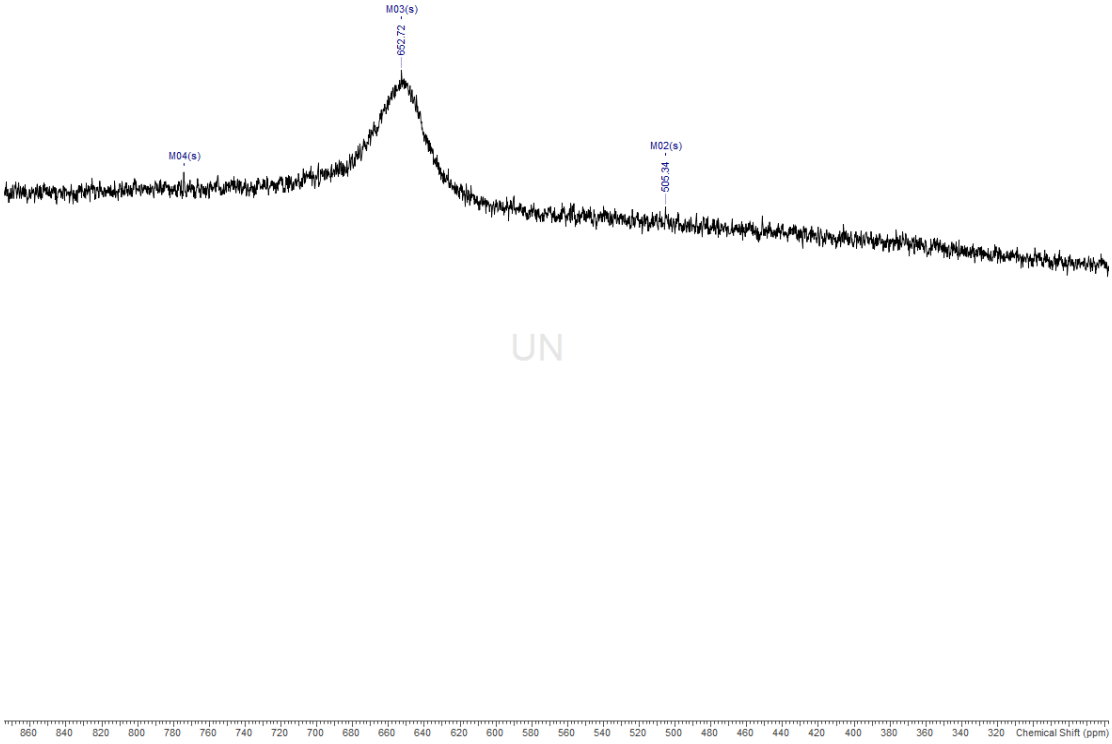

Figure A7.16 ^{93}Nb NMR spectrum of [$NbSCl_3(S^nBu_2)$] (400 MHz, CH_2Cl_2/CD_2Cl_2, 298K)

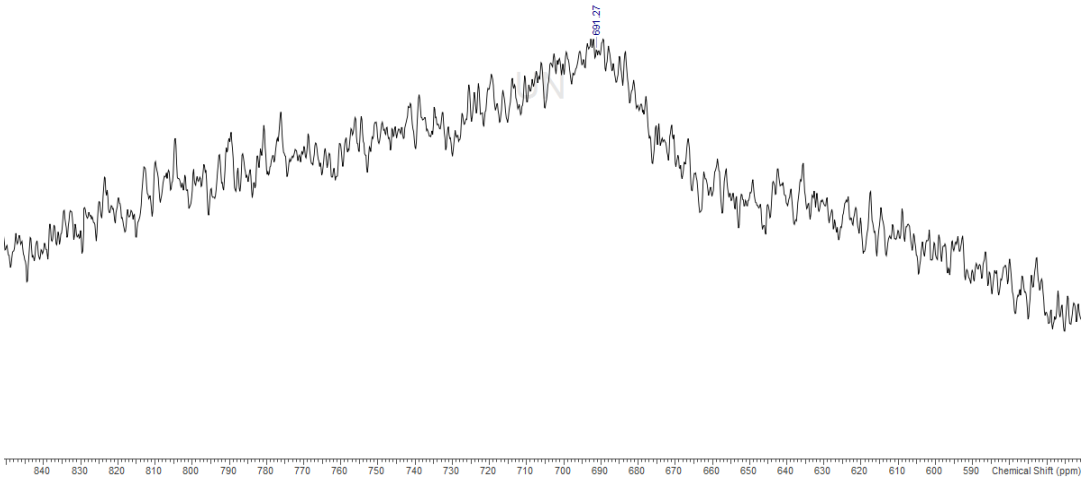

Figure A7.17 ^{93}Nb NMR spectrum of [$NbSCl_3(Se^nBu_2)$] (400 MHz, CH_2Cl_2/CD_2Cl_2, 298K)

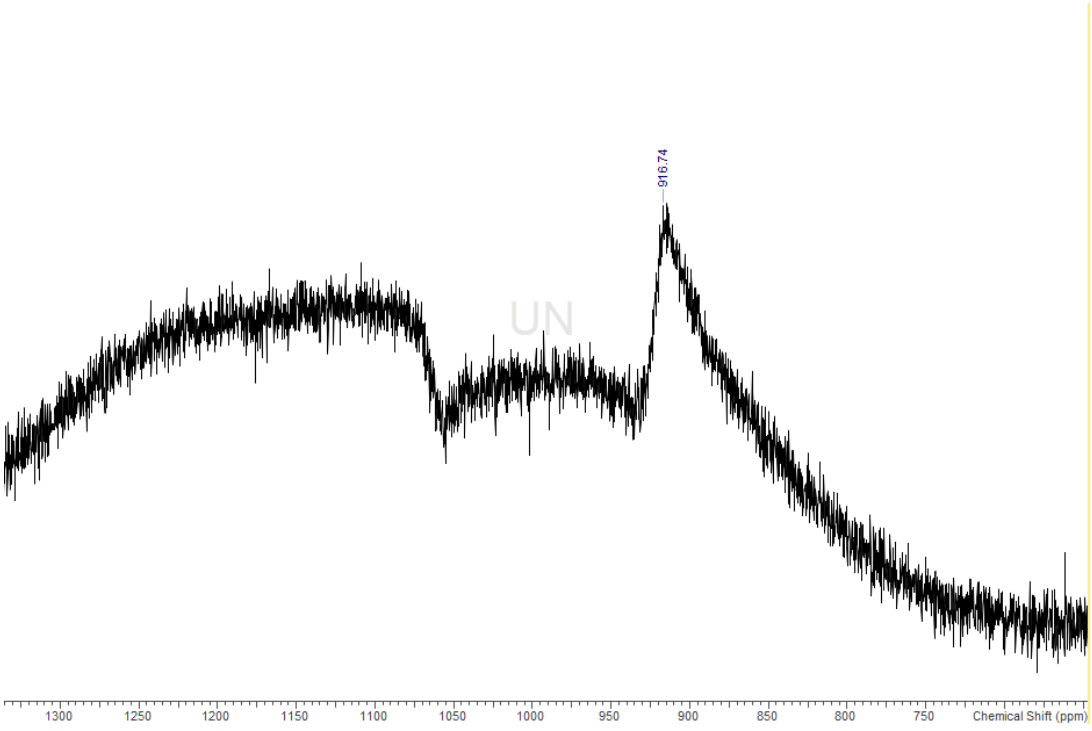

Figure A7.18 ^{93}Nb NMR spectrum of [$NbSCl_3(NCCH_3)$] (400 MHz, CH_2Cl_2/CD_2Cl_2, 298K)

Chapter 5

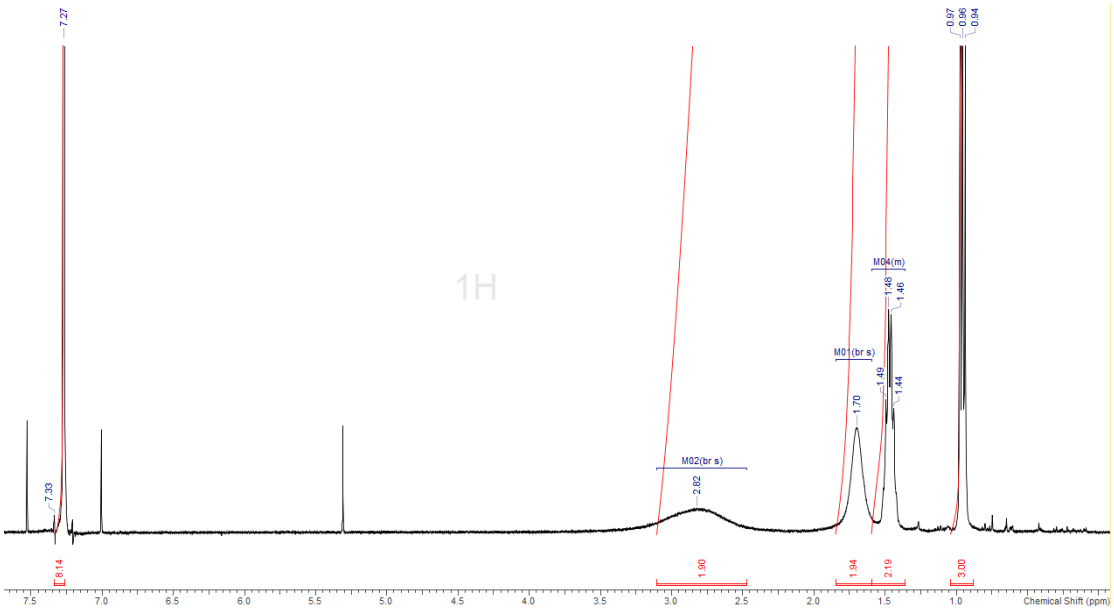

Figure A7.19 ^{1}H NMR spectrum of [$NbBr_5(S^nBu_2)$] (400 MHz, $CDCl_3$, 298 K)

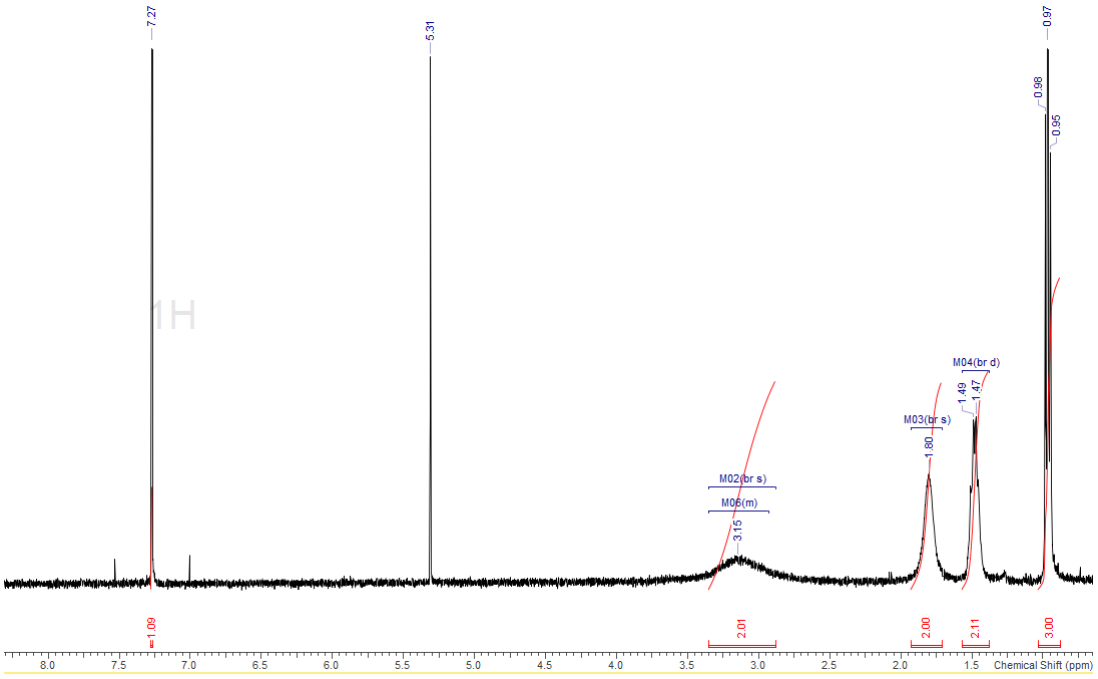

Figure A7.20 ^{1}H NMR spectrum of [$NbBr_5(Se^nBu_2)$] (400 MHz, $CDCl_3$, 298 K)

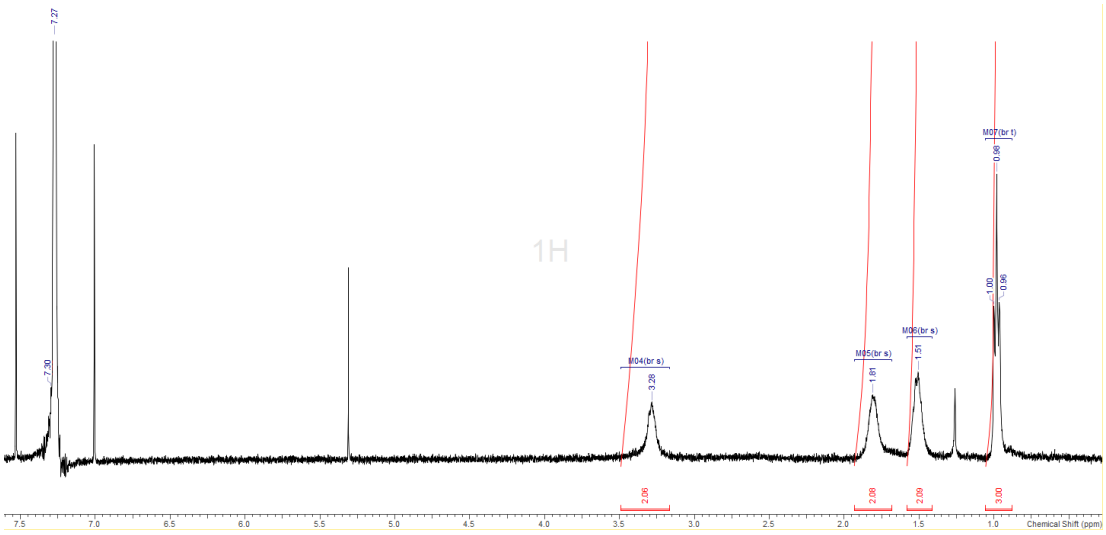

Figure A7.21 ^{1}H NMR spectrum of [$TaBr_5(S^nBu_2)$] (400 MHz, $CDCl_3$, 298 K)

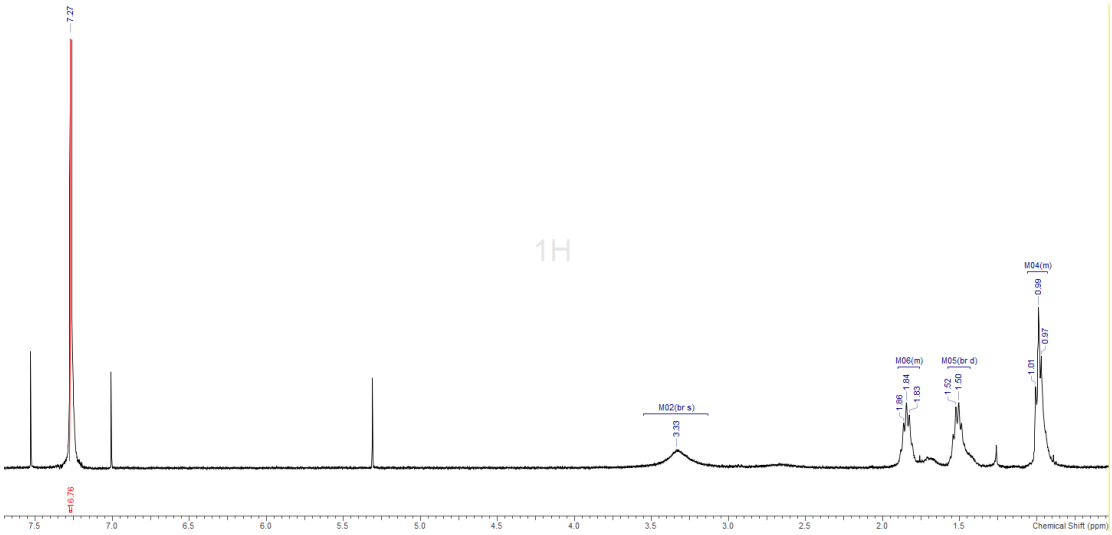

Figure A7.22 ^{1}H NMR spectrum of [$TaBr_5(Se^nBu_2)$] (400 MHz, $CDCl_3$, 298 K)

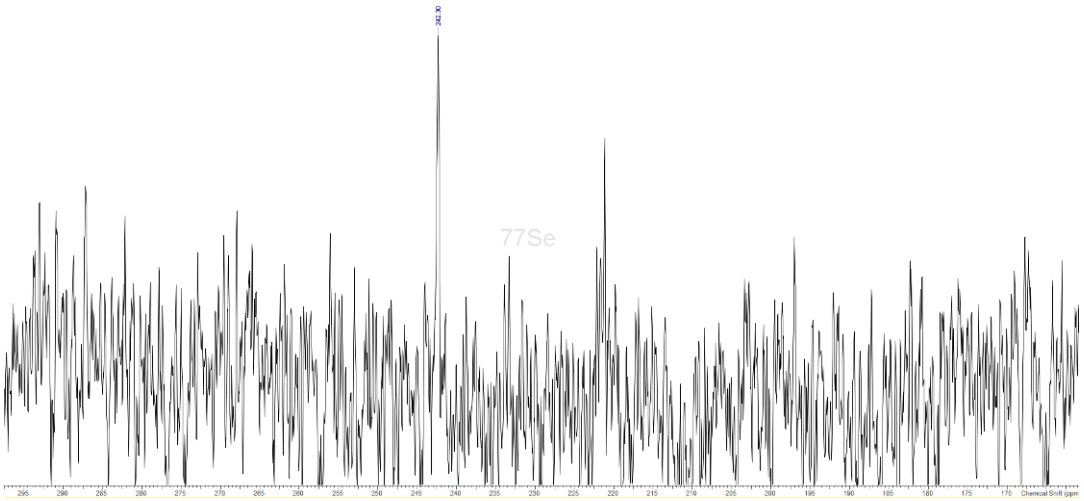

Figure A7.23 $^{77}Se\{^{1}H\}$ NMR spectrum of [$NbBr_5(Se^nBu_2)$] (400 MHz, CD_2Cl_2, 298 K)

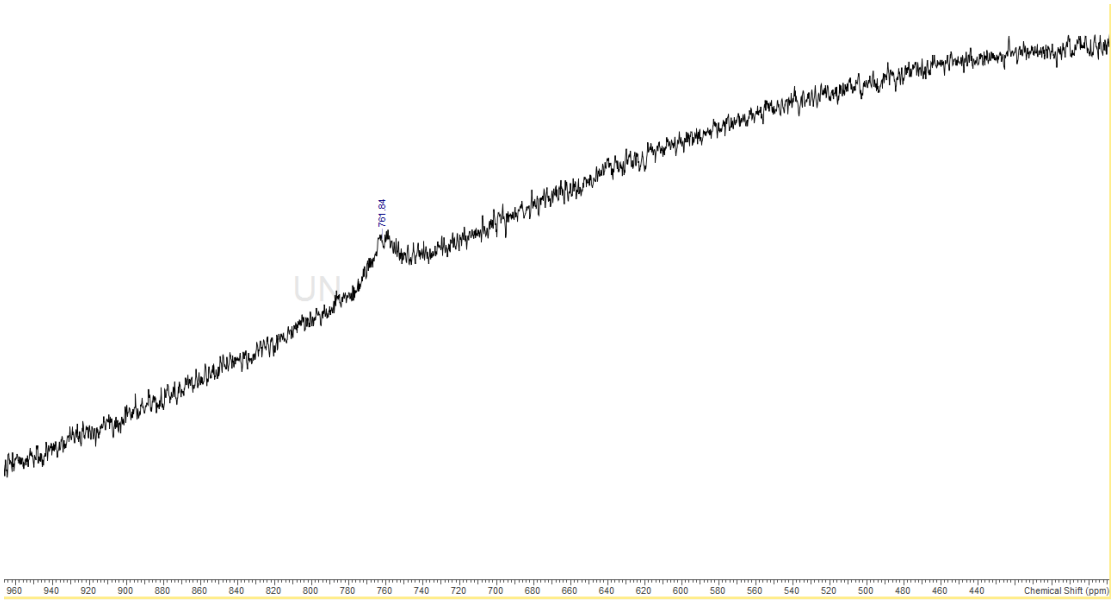

Figure A7.24 ^{93}Nb NMR spectrum of [$NbBr_5(Se^nBu_2)$] (400 MHz, CD_2Cl_2, 228 K)

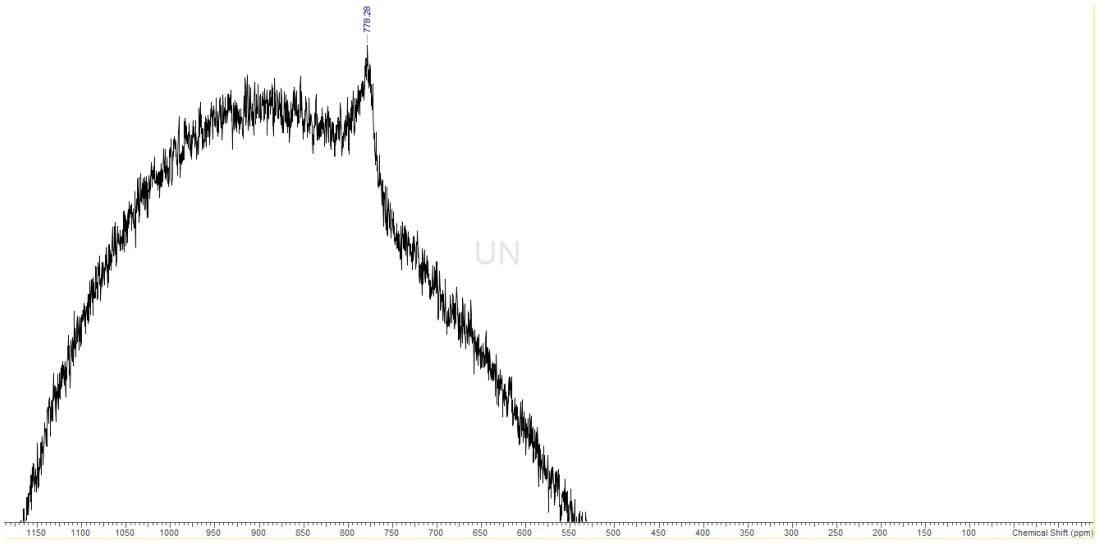

Figure A7.25 ^{93}Nb NMR spectrum of [$NbBr_5(S^nBu_2)$] (400 MHz, CH_2Cl_2/CD_2Cl_2, 298K)